ΠΑΝΕΠΙΣΤΗΜΙΟ ΚΡΗΤΗΣ
UNIVERSITY OF CRETE

H.Giessen

F.H. da Jornada
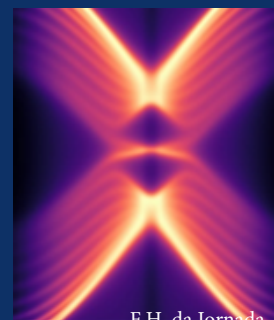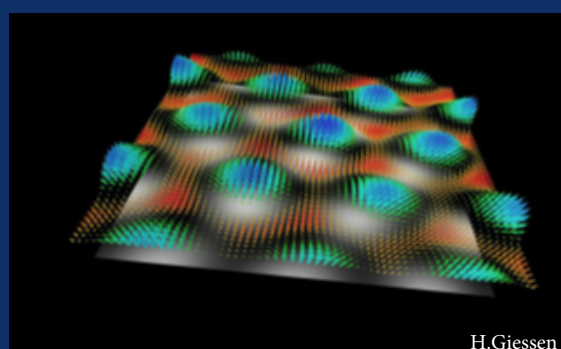
Abstract Proceedings

DYNAMICS of NONEQULIBRIUM

XIII Symposium

2025

Michael K.Rafailov
Symposium Chair

Abstract Proceedings comprising summaries of research papers prepared for two closely related to research of nonequilibrium states in condenced matter – Ultrafast Bandgap Photonics and Ultrafast Dynamics and Metastability which forming the Symposium. The Symposium builds a bridge between cutting edge modern physics and emerging applications which are desperately in need. Symposium is vertically integrated, covering the area of interaction of high intensity and relatively low energy pulses with condensed matter, from fundamental physics to practically applicable energy sources, devices and technologies.

This workshop is the 13th in a series of International symposia, conferences and workshops on *Ultrafast Dynamics, Metastability* and closely related while mostly technology application driven *Ultrafast Bandgap Photonics* which we are running from 2011. University of Crete and Foundation for Research and Technology - FORTH are hosting the 13th Symposium on the island of Crete

---

The Symposium is organized by sections that are focused either on research field or on phenomena. The division is pretty much conditional, while providing direct access to general topics of interest for the research community and applications as well. Phenomenology topics, like ultrafast dynamic in heterostructures and spin-and orbital ultrafast phenomena may overlap areas of studies like noneqilibrium high temperature superconductivity and ultrafast magnetism, creating multiple entries into the Proceedings   General reviews of Ultrafast Dynamics and Ultrafast Bandgap Photnics progresss as well as the most interesting recent discoveries are presented here as the keynote papers. Material oranized in sections and each section divided by sessions. Each section has the keynote papers, where results and considerations of most common interest topics are presented, while the Astract Proceedings is compiled based on generally alphabetic list of the speakers in Program -as it was presented at the Symposium. Plus to Table of Contents the Abstract Prosceeding has list of authors where the authors of submitted papers are listed with their papers associated page numbers.

The Abstract Proceeding is actually a snapshot of most interesting and noticeable research results in *Dynamics of Nonequilibrium* that one can get in 2025. a snapshot of up to date research results and progress in *Ultrafast Dynamics and Metastability* and the applications in *Ultrafast Bandgap Photonics***.** It is an Encyclopedia of *Ultrafast Dynamics, Metastability and Ultrafast Bandgap Photonics* that presents the status quo in the disciplines ranging from Theoretical Physics to Ultrafast Laser and covering practically all phenomena of interests in interaction of light with complexly organized condensed matter in form of low dimentional structures of different origins as well as bulk materials in different ambient contitions including temperature, pressure, electric and magnetic potentials, biased irradience or current and so on.

In Loving Memory of Elena

Crete 2025
Content

Lightwave electronics in quantum materials –from Band-structure engineering to attosecond microscopy

R. Huber[1], J. Repp[1], M. Kira[2], U. Höfer[3]
[1] University of Regensburg, 93040 Regensburg, Germany
[2] University of Michigan, Ann Arbor, MI 48109, USA
[3]Philipps-Universität, 35032 Marburg, Germany

Lightwave electronics. Intense light pulses in the infrared spectral window have enabled a disruptive development at the interface between electronics and strong-field optics known as 'lightwave electronics' [1]. The key idea is to employ the oscillating carrier field of tailor-made infrared pulses as an alternating voltage to ballistically accelerate electrons through solids. By driving electrons faster than a cycle of light and thus also faster than typical scattering times, lightwave electronics can unlock an intriguing coherent quantum world with exciting perspectives for future quantum technologies [1]. Prominent aspects of lightwave-driven electron dynamics in solids range from dynamical Bloch oscillations and high-harmonic generation [2] to quasiparticle collisions [3,4], all-optical reconstruction of band structures [5] and Bloch wavefunctions [6] as well as first lightwave electronic device functionalities [7]. Here, we will review some of the recent unexpected discoveries in our quest to shape electronic quantum trajectories with tailored terahertz and infrared field transients.

Lightwave electronics meets topology and correlations. In the first step, we explore the unusual quantum pathways of lightwave-driven electrons in topologically non-trivial materials. A prototypical example is given by the topological surface state on bulk Bi_2Te_3. Owing to the linear energy-momentum relation and the rigid spin-momentum locking of these surface states, terahertz light fields can accelerate electrons like relativistic particles to cover large distances without scattering and heating. This motion leads to a new quality of non-integer high-harmonic generation, whose polarization reveals topologically non-trivial electron trajectories [8]. By advancing angle-resolved photoelectron spectroscopy (ARPES) to subcycle time scales, we can even visualize the lightwave-driven acceleration of Dirac electrons [9], the transient formation of Floquet-Bloch states (Fig. 1) and the non-perturbative interplay of inter- and intraband dynamics in actual subcycle band-structure movies [10]. Moreover, we leverage spin-momentum locking in the topological surface state to demonstrate subcycle switching of magnetization [11]. Our results shed new light on the process of high-harmonic generation and open novel possibilities for ultrafast band-structure engineering and lightwave spintronics.
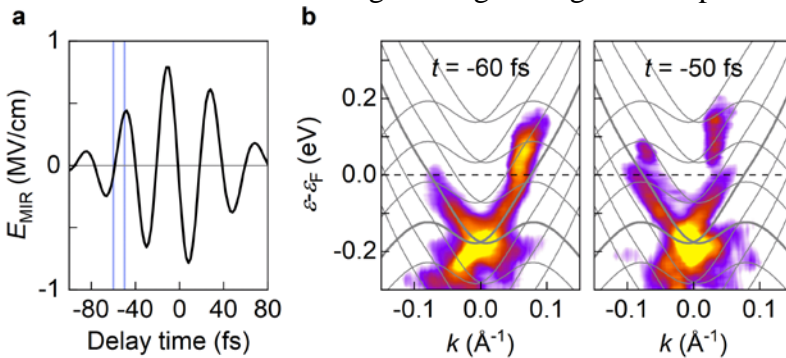
Fig. 1. Birth of a Floquet-Bloch band structure. a, *Phase-locked mid-infrared driving field.* **b,** *Subcycle band-structure videography captures how band replica of the topological surface state of Bi_2Te_3 emerge within one oscillation cycle of the carrier wave of an intense mid-infrared light pulse [9].*

Going beyond dominantly single-particle dynamics, we also show how Coulomb correlations manifest directly in the time domain [12]. Photogenerated electron–hole pairs can be accelerated and collided by lightwaves, giving rise to high-order sideband generation [3-6]. By clocking electron-hole recollisions with attosecond precision, we find that strong Coulomb correlations in atomically thin WSe_2 shift the optimal timing of recollisions by up to 1.2 ± 0.3 fs compared to the bulk material [12]. Such attosecond chronoscopy of delocalized electrons could thus become a powerful tool in exploring unexpected phase transitions and emergent many-body quantum-dynamic phenomena.

Subcycle band-structure videography of the entire Brillouin zone. The above advances in angle-resolved photoemission spectroscopy have allowed us to directly visualize the buildup of Floquet-Bloch band structures, the emergence of intraband currents, and interband transitions with subcycle time resolution. Yet hemispherical photoelectron detectors in combination with near-UV probe pulses (photon energy, 3 to 6 eV) have accessed electron dynamics only along specific directions near the Brillouin zone center. In many quantum materials, however, critical phenomena occur at the Brillouin zone boundaries. By combining electron momentum microscopes with femtosecond EUV pulses, the photoemission horizon

of ultrafast ARPES has been extended beyond the first Brillouin zone of key quantum materials [13,14,15,16]. We combine this breakthrough with strong-field control of electrons, for the first time [17]. Utilizing atomically strong 1.5-cycle mid-infrared (MIR) driving fields together with sub-10-fs EUV probe pulses (photon energy, 21.7 eV) and state-of-the-art photoemission momentum microscopy, we explore lightwave electronics throughout the entire first Brillouin zone. To reach good measurement statistics within short acquisition times, we develop a laser system that operates at a high repetition rate of 50 kHz while still reaching MIR peak electric fields above 200 MV/cm, corresponding to an average MIR power as high as 1 W. The new laboratory allows us to drive electrons in a monolayer of graphene with MIR pulses (center frequency, 27 THz) while EUV pulses probe the dynamics with subcycle time resolution (Fig. 2). Observing the full 2D carrier distribution with sub-fs temporal resolution, we uncover the fundamental microscopic processes at play. In particular, the dynamics of intraband currents and interband transitions as well as the subsequent interplay between different scattering channels are revealed. Our approach provides key insights into the conditions necessary for achieving fully coherent, field-driven electronic dynamics and opens new avenues for exploring rich phenomena in the strong-field regime, including Landau-Zener tunneling, dynamical Bloch oscillations, optical band-structure engineering and light-induced phase transitions.
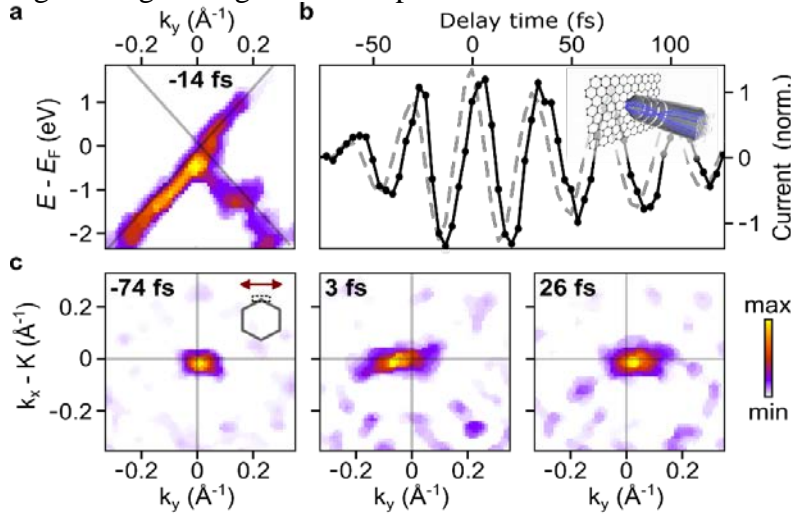
Fig. 2. a, A subcycle snapshot of the band structure at the Dirac point of graphene visualizes how a MIR field accelerates the electron distribution away from the Fermi level and shifts it along the Dirac cone (delay time, t = -14 fs). *b,* The current extracted from the photoemission maps trails after the MIR waveform (grey dashed curve, peak field, 1.5 MV/cm), indicating a partly ballistic electron motion. *c,* The full 2D carrier distribution at the K-point, captured for selected delay times, holds key information about the nature of lightwave-driven currents and the mechanisms of the relevant scattering processes [17].

Lightwave electronics with atomic resolution. Finally, we merge the idea of lightwave electronics with the sub-Ångström spatial resolution of low-temperature scanning tunneling microscopy (STM) to capture the elementary building blocks of matter in direct ultrafast atom-scale slow-motion videography. Starting with first femtosecond movies of individual vibrating molecules [18], our approach is widely tunable to visualize structural and electronic dynamics as well as atomically localized electromagnetic fields on their intrinsic length and time scales. These fields can also act as femtosecond atomic forces to selectively choreograph a coherent structural motion of a single-molecule switch in its electronic ground state [19]. By combining atomic forces with energy-selective tunneling in the first-ever lightwave scanning tunneling spectroscopy, we resolve how spin-orbit-split energy levels of an isolated selenium vacancy in a WSe_2 monolayer continuously evolve under controlled excitation of lattice vibrations (Fig. 3a) [20]. Moreover, we utilize ultrafast tunneling currents as ultimately small emitters of electromagnetic radiation to push all-optical microscopy to atomic spatial and femtosecond temporal resolution [21]. This novel kind of near-field optical tunneling emission (NOTE) microscopy (Fig. 3b) allows for atomic resolution ultrafast nanoscopy even of insulating samples [21]. Finally, we show how lightwave-driven STM can be scaled from terahertz to near-infrared driving fields [22]. In principle, this step could improve the temporal resolution from ~100 fs down to attoseconds. Yet, competing multi-photon processes and thermal instabilities pose severe challenges in this spectral domain. Therefore, we introduce an attosecond STM concept that is immune against thermal artifacts. By pulse synthesis, we periodically vary the waveform of single-cycle near-infrared pulses to drive tunneling currents while keeping the thermal load on the tip constant. In a non-degenerate pump-probe scheme, we observe clear attosecond features in the subcycle currents and demonstrate atomic resolution by taking snapshot images of a single Cu adatom on a silver surface (Fig. 3c).
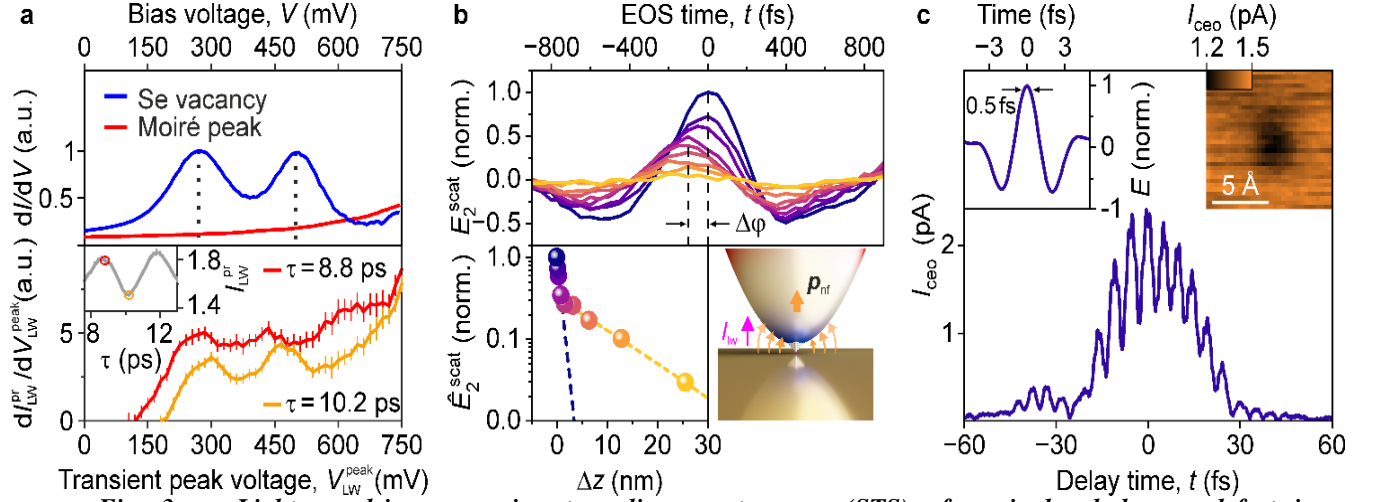
Fig. 3. a, Lightwave-driven scanning tunneling spectroscopy (STS) of a single chalcogen defect in a monolayer of WSe₂ [20]. *The local density of states measured with d.c. STS (top panel) indicates two spin-orbit split states (vertical broken lines) of the single selenium vacancy (blue curve) located inside the gap of the pristine monolayer (red curve). Ultrafast STS (lower panel) captures a periodic energy shift of the defect levels as a function of the delay time t between terahertz excitation of a drum mode of the monolayer and STS probing.* **b, Near-field optical tunneling emission microscopy (NOTE) [21].** *When the tip of an ultra-high vacuum near-field microscope is approached within atomic distance of a metal substrate the amplitude of the scattered terahertz waveform (top panel) suddenly increases while its phase shifts by p/2. This behavior is caused by a new contrast mechanism where lightwave-driven atomically-confined tunneling currents between tip and sample lead to coherent light emission (inset).* **c, Attosecond STM [22].** *Biasing the junction of a low-temperature STM with phase-locked single-cycle near-infrared waveforms (left inset) while keeping the optical power strictly constant allows us to observe attosecond tunneling currents. These currents can be used to spatially resolve a single Cu adatom on a silver surface (**right inset**).*

Our results pave the way to recording the fastest relevant dynamics of electrons within atoms, molecules and quantum materials in actual attosecond atomic videography.

References

[1] M. Borsch, M. Meierhofer, R. Huber, M. Kira, *Nature Reviews Materials* **8**, 668 (2023).
[2] M. Hohenleutner F. Langer, O. Schubert, M. Knorr, U. Huttner, S.W. Koch, M. Kira, R. Huber, *Nature* **523**, 572 (2015).
[3] F. Langer, M. Hohenleutner, C. Schmid, C. Poellmann, P. Nagler, T. Korn, C. Schüller, M. S. Sherwin, U.Huttner, J. T. Steiner, S. W. Koch, M. Kira R. Huber, *Nature* **533**, 225 (2016).
[4] F. Langer, C. P. Schmid, S. Schlauderer, M. Gmitra, J. Fabian, P. Nagler, C. Schüller, T. Korn, P. G. Hawkins, J. T. Steiner, U. Huttner S. W. Koch, M. Kira, R. Huber, *Nature* **557,** 76 (2018).
[5] M. Borsch , C.P. Schmid, L. Weigl, S. Schlauderer, N. Hofmann, C. Lange, J. T. Steiner, S. W. Koch, R. Huber, M. Kira, *Science* **370**, 1204 (2020)
[6] J. B. Costello, S.D. O'Hara, Q. Wu, D.C. Valovcin, L.N. Pfeiffer, K.W. West, M.S. Sherwin, *Nature* **599**, 57 (2021).
[7] T. Boolakee, C. Heide, A. Garzón-Ramírez, H.B. Weber, I. Franco, P. Hommelhoff, *Nature* **605**, 251 (2022).
[8] C. P. Schmid, L. Weigl, P. Grössing , V. Junk , C. Gorini, S. Schlauderer, S. Ito, M. Meierhofer, N. Hofmann, D. Afanasiev, J. Crewse K. A. Kokh, O. E. Tereshchenko, J. Güdde, F. Evers, J. Wilhelm, K. Richter, U. Höfer, R. Huber, *Nature* **593,** 385 (2021).
[9] J. Reimann, S. Schlauderer, C. P. Schmid, F. Langer, S. Baierl, K. A. Kokh, O. E. Tereshchenko, A. Kimura, C. Lange, J. Güdde, U. Höfer R. Huber, *Nature* **562**, 396 (2018).
[10] S. Ito, M. Schüler, M. Meierhofer, S. Schlauderer, J. Freudenstein, J. Reimann, D. Afanasiev, K. A. Kokh, O. E. Tereshchenko, J. Güdde M. A. Sentef, U. Höfer, R. Huber, *Nature* **616**, 696 (2023).
[11] J. Riepl, *to be submitted* (2025).
[12] J. Freudenstein, M. Borsch, M. Meierhofer, D. Afanasiev, C. P. Schmid, F. Sandner, M. Liebich, A. Girnghuber, M. Knorr, M. Kira, R. Huber *Nature* **610**, 290 (2022).
[13] M. Aeschlimann, J. P. Bange, M. Bauer, U. Bovensiepen, H.- J. Elmers, T. Fauste, L. Gierster, U. Höfer, R. Huber, A. Li, X. Li, S. Mathias K. Morgenstern, H. Petek, M. Reutzel, K. Rossnagel, G. Schönhense, M. Scholz, B. Stadtmüller, J. Stähler, S. Tan, B. Wang, Z. Wang M. Weinelr, *Surface Science* **753**, 122631 (2025).
[14] R. Wallauer, R. Perea-Causin, L. Münster, S. Zajusch, S. Brem, J. Güdde, K. Tanimura, K.- Q. Lin, R. Huber, E. Malic, U. Höfer, *Nano Letters* **21**, 5867 (2021).
[15] M. Merboldt, M. Schüler, D. Schmitt, J. P. Bange, W. Bennecke, K. Gadge, K. Pierz, H. W. Schumacher, D. Momeni, D. Steil, S. R. Manmana M. Sentef, M. Reutzel, S. Mathias, *Nature Physics* (2025). arXiv:2404.12791
[16] D. Choi, M. Mogi, U. De Giovannini, D. Azoury, B. Lv, Y. Su, H.Hübener, A. Rubio, N. Gedik. arXiv:2404.14392. (2024).
[17] V. Eggers, *to be submitted* (2025).
[18] T. L. Cocker, D. Peller, P. Yu, J Repp, R. Huber, *Nature* **539**, 263 (2016).
[19] D. Peller,, L.Z. Kastner, T. Buchner, C. Roelcke, F. Albrecht, N. Moll, R. Huber, J. Repp,. *Nature* **585**, 58 (2020).
[20] C. Roelcke, L. Z. Kastner, M. Graml, A. Biereder, J. Wilhelm, J. Repp, R. Huber, Y. A. Gerasimenko, *Nature Photonics* **18**, 595 (2024).
[21] T. Siday, J. Hayes, F. Schiegl, F. Sandner, P. Menden, V. Bergbauer, M. Zizlsperger, S. Nerreter, S. Lingl, J. Repp, J. Wilhelm, M. A. Huber Y. A. Gerasimenko, R. Huber, *Nature* **629**, 329 (2024).
[22] S. Maier, *to be submitted* (2025).

Conductivity dynamics in THz driven spin-ladders

J. Dössegger[1], P. Puphal[2], E. Pomjakushina[3], T. Suter[1], Z. Macdermid[1], Z. Chen[1], S. L. Johnson[1], E. Abreu[1]

[1]ETH Zürich, 8093 Zürich, Switzerland
[2] Max-Planck Institute for Solid State Research, 70569 Stuttgart, Germany
[3]Paul Scherrer Institut, 5232 Villigen, Switzerland

The nature of the superconducting state in unconventional superconductors, in particular high temperature superconducting cuprates, remains to be fully understood. The fundamental building blocks in cuprates are two-dimensional CuO_2 layers. One approach to simplifying the problem consists in lowering the dimensionality of the system. $Sr_{14-x}Ca_xCu_{24}O_{41}$ (SCCO) compounds have a quasi-one-dimensional structure characterized by alternating layers of Cu_2O_3 ladders and CuO_2 chains. These spin-ladder systems exhibit a rich phase diagram, where conductivity, charge order and magnetic order can be controlled by varying temperature, external pressure and the level of Sr substitution by Ca, x. In particular, a superconducting phase arises for temperatures below 15 K, an applied pressure of 3-10 GPa and x > 11.5. The conductivity in these inherently hole doped materials, and in particular the superconducting phase, is believed to be controlled by the distribution of holes between the chains and the ladders. [1] We investigate the low frequency response of bulk single crystal SCCO samples with Ca contents x = 0, 7 and 12. In the first part of my talk I will discuss the ultrafast nonlinear conductivity transient that arises following excitation by a strong THz field pulse, and how this behavior depends on the intensity and polarization of the pump and on the temperature and doping level of the sample. In a second part I will discuss our efforts to combine THz spectroscopy with the application of high pressure in a diamond anvil cell [2].
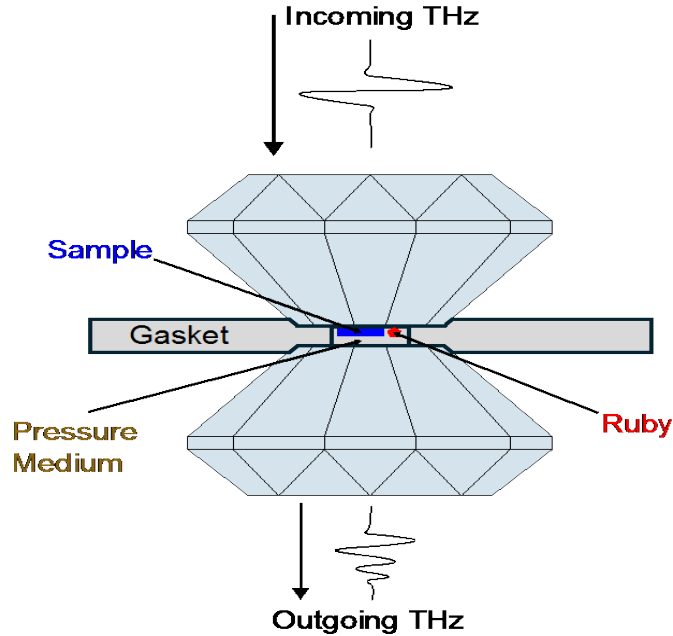
Fig. 1. Schematic of a diamond anvil cell showing the two diamonds and the gasket. *The sample chamber includes the sample, a pressure medium and a ruby crystal used as a pressure gauge. The THz spot size being larger than the gasket hole, the THz beam is truncated by the gasket [2].*

While pressure has been used extensively to draw phase diagrams in equilibrium, it has been applied only to some extent in ultrafast measurements and very seldom in combination with THz time-domain spectroscopy. Combining high pressure, low temperature and time-resolved THz spectroscopy is of great interest in condensed matter, in particular for the study of quantum materials such as spin-ladder compounds and Mott insulators.

References
[1] T. Vuletić, B. Korin-Hamzić, T. Ivek, S. Tomić, B. Gorshunov, M. Dressel, J. Akimitsu, *Physics Reports* **42**, 169 (2006).
[2] T. Suter, Z. Macdermid, Z. Chen, S. L. Johnson, E. Abreu, *arXiv:2504.18493* (2025).

Ultrafast magnetism across magnetic material classes

M. Aeschlimann

RPTU Kaiserslautern-Landau, 67663 Kaiserslautern, Germany

Ultrafast magnetism - the exploration of magnetic dynamics on femtosecond to picosecond timescales - offers profound insights into the fundamental processes that govern spin behavior in different classes of magnetic materials. A key distinction emerges between metallic and dielectric magnetic systems, rooted in their contrasting electronic structures and excitation mechanisms. In metallic ferromagnets, such as transition metals and their alloys, ultrafast demagnetization is primarily mediated by strong electron-electron and electron-phonon interactions, made possible by the high density of free charge carriers [1]. These interactions enable efficient energy redistribution, leading to demagnetization on sub-picosecond timescales - often within a few hundred femtoseconds. The dense electronic environment facilitates rapid angular momentum transfer, contributing to the remarkably fast magnetic response.

Metallic antiferromagnets, by contrast, are predicted to exhibit even swifter magnetization dynamics. Here, spin-flip scattering between antiparallel sublattices can drive ultrafast magnetic responses without requiring significant angular momentum exchange with the lattice. This intrinsic mechanism points toward magnetization changes on timescales potentially shorter than those observed in ferromagnets, highlighting their promise for ultrafast spintronic applications.

Dielectric antiferromagnets - including magnetic insulators and garnet systems - exhibit fundamentally different behavior due to the absence of free electrons. In these materials, the ultrafast magnetic response is not governed by electron scattering, but instead emerges from spin-lattice coupling, magnon excitation, and spin-orbit interactions [2,3]. As a result, their magnetization dynamics tend to unfold over longer timescales, often involving coherent spin wave phenomena and nonthermal pathways. The complexity of these processes provides rich opportunities for the manipulation of collective spin excitations in insulating environments.

In our comprehensive study, we investigated the ultrafast magnetic response of representative systems from various magnetic classes - including metallic ferromagnets, metallic and dielectric antiferromagnets (see Fig. 1), as well as emerging altermagnetic materials [4]. By employing direct optical excitation to drive magnetic dynamics, we aim to uncover the characteristic timescales, mechanisms, and interplay of spin, charge, and lattice degrees of freedom in each system.
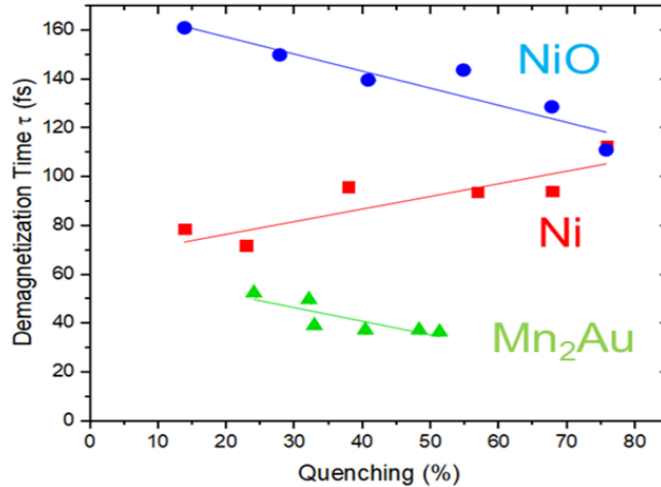
Fig. 1: Demagnetization time as a function of the quenching of the magnetic order parameter induced by direct optical excitation with ultrashort laser pulses. A clear contrast emerges between antiferromagnetic (AFM) and ferromagnetic (FM) materials: in AFMs, the demagnetization dynamics accelerate with increasing excitation strength, reflecting an enhanced efficiency of spin angular momentum redistribution under strong perturbation. In contrast, for ferromagnetic nickel, a pronounced slowdown of demagnetization is observed as the quenching deepens, suggesting a bottleneck in angular momentum dissipation at higher excitation levels. Across the examined systems, metallic compounds exhibit consistently shorter demagnetization times relative to their dielectric counterparts, underscoring the pivotal role of free carriers in facilitating ultrafast spin dynamics.

Understanding these fundamental differences is essential not only for the design of next-generation spintronic devices and ultrafast magnetic memory technologies, but also for accessing novel nonequilibrium phenomena that are uniquely accessible in the ultrafast regime.

References
[1] B. Koopmans, G. Malinowski, F., Dalla Longa, F., D. Steiauf, M. Fähnle, T. Roth, M. Cinchetti, M. Aeschlimann, *Nature Materials*, **9**, 259 (2010).
[2] S. Wust, C. Seibel, H. Meer, P. Herrgen, C. Schmitt, L. Baldrati, R. Ramos, T. Kikkawa, E. Saitoh, O. Gomonay, J. Sinova, Y. Mokrousov H. C. Schneider, M. Kläui, B. Rethfeld, B. Stadtmüller, M. Aeschlimann, *arXiv* 2205.02686 (2022).
[3] H. Meer, S. Wust, C. Schmitt, P. Herrgen, F. Fuhrmann, S. Hirtle, B. Bednarz, A. Rajan, R. Ramos, M. A. Niño, M. Foerster, F. Kronast A. Kleibert, B. Rethfeld, E. Saitoh, B. Stadtmüller, M. Aeschlimann, M. Kläui, *Advanced Functional Materials* **33**, 2213536, (2023).
[4] M. Weber, S. Wust, L. Haag, A. Akashdeep, K. Leckron, C. Schmitt, R. Ramos, T. Kikkawa, E. Saitoh, M. Kläui, L. Šmejkal, J. Sinova M. Aeschlimann, G. Jakob, B. Stadtmüller, H. C. Schneider, *arXiv* 2408.05187 (2024).

Unveiling photoinjection dynamics

M. Agarwal, V.S. Yakovlev

Max-Planck-Institut für Quantenoptik, 85748 Garching, Germany

Strong-field ionization, leading to the formation of electron wave packets, is central to attosecond science. In solids, valence electrons can be promoted to conduction bands via multiphoton absorption or interband tunnelling induced by a strong laser field. The highly nonlinear nature of this process confines photoinjection to sub-half-cycle time intervals (for linearly polarized fields). Furthermore, for few-cycle pulses, photoinjection can be largely confined to a single half-cycle of the electric field [1]. These properties are central to ultrafast techniques such as nonlinear photoconductive sampling [2] and solid-state TIPTOE [3], which enable optical-field-resolved measurements with a petahertz bandwidth [4]. Advancing these techniques requires a deeper understanding of photoinjection dynamics. Key questions remain: What is the duration of a sub-half-cycle photoinjection event? How many carriers are photoinjected by each half-cycle? And what are the optimal conditions for single subfemtosecond photoinjection within feasible optical waveforms?

Answering these questions hinges on the availability of reliable strong-field photoinjection rates. However, calculating non-adiabatic (diabatic) rates from first principles is challenging due to the lack of a rigorous definition of instantaneous ionization probability in the presence of a strong electric field [5]. Because of this, the precise rate of carrier generation during the laser pulse remained elusive, and many researchers resorted to using rates based on crude approximations. At the same time, the concentration of photoinjected carriers *after* the interaction with a laser pulse is unambiguously defined and easily calculated.
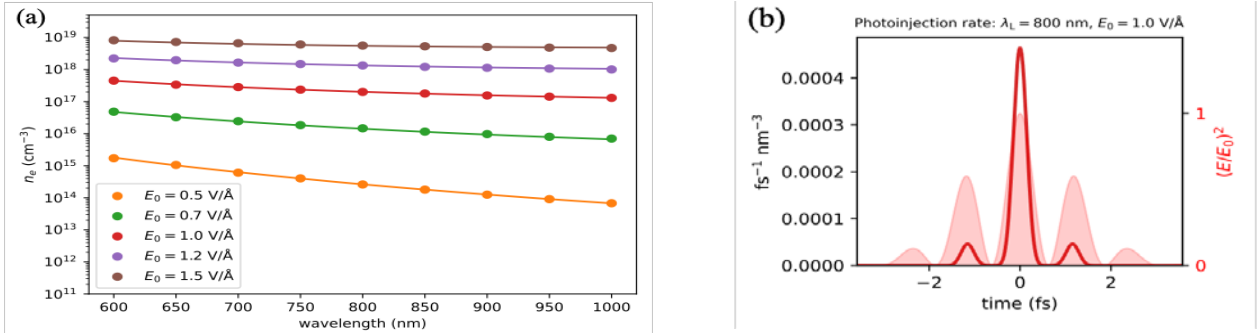
Fig. 1 An illustration of GASFIR performance for SiO$_2$ (*Left-a*) *The input data, represented by the full circles, consists of concentrations of conduction-band electrons, n_e, obtained in 45 ab initio simulations, where photoinjection by a single-cycle pulse was calculated for various values of the pulse's central wavelength, λ_L, and peak electric field, E_0. With 9 adjustable parameters, GASFIR accurately reproduces all the input data. (**Right-b**) Photoinjection rate for $\lambda_L = 800$ nm and $E_0 = 1$ V/Å. The shaded region represents the squared electric field of the pulse.*

We re-examine the problem of defining and calculating photoinjection rates by asking: "Can we reconstruct ionization dynamics from photoinjection probabilities obtained for a set of different laser pulses?" We demonstrate that this is possible, but it requires an ionization model that is not limited by the quasistatic approximation and combines the flexibility required for matching ab initio input data with constraints imposed by the physics of nonlinear light-matter interaction. We present such a model, which we call a General Approximator for Strong-Field Ionization Rates (GASFIR). We have validated its performance across diverse materials (α-quartz, diamond, silicon) and ionization regimes (few-photon, multiphoton, tunneling). By revealing accurate photoinjection dynamics, this new method may find many applications in lightwave (petahertz) electronics.

References
[1] A. Sommer, E. M. Bothschafter, S. A. Sato, C. Jakubeit, T. Latka, O. Razskazovskaya, H. Fattahi, M. Jobst, W. Schweinberger, V. Shirvanyan V. S. Yakovlev, R. Kienberger, K. Yabana, N. Karpowicz , M. Schultze, F. Krausz., *Nature* **534**, 86 (2016).
[2] S. Sederberg, D. Zimin, S. Keiber, F. Siegrist, M.S. Wismer, V.S. Yakovlev, I. Floss, C. Lemell, J. Burgdörfer, M. Schultze, F. Krausz, N. Karpowicz *Nature Communications* **11**, 430 (2020).
[3] Y. Liu, S. Gholam-mirzaei, J.E. Beetar, J. Nesper, A.Yousif, M. Nrisimhamurty, M. Chini, *Photonics Research* **9**, 929 (2021).
[4] C. Heide, P. D. Keathley, M. F. Kling, *Nature Reviews Physics* **6**, 648 (2024).
[5] A. Karamatskou, S. Pabst, R. Santra, *Physical Review* A **87**, 043422 (2013).

Photocurrent-induced harmonics in nanostructures

I. Babushkin[1], A. Husakou[2], A. Demircan[1], M. Kovacev[1], U.Morgner[1]

[1]Gottfried Wilhelm Leibniz Universität Hannover, 30167 Hannover, Germany
[2]Max-Born- Institut für Nichtlineare Optik und Kurzzeitspektroskopie, 12489 Berlin, Germany

Photoionization in strong optical fields of atoms and molecules, as well as analogous processes of transitions from valence to conduction band in solids, are at the heart of attosecond science. In a similar way, under the action of the strong fields electrons leave the surface of metallic nanostructures (NS) [1,2]. In the last decade this process has attracted strong and growing interest in the context of attosecond science. Most of the attention is paid to the dynamics of electrons themselves, which is of high importance in the context of generation of on-chip petahertz electronics [3-5], as well as several other applications. Here we consider, in contrast, a photoinduced current mechanism. Electrons which emerge in the continuum and are subsequently accelerated by the field, also emit radiation, which does not depend on their return to the parent ion [6-8]. This radiation, typically located at lower frequencies than high harmonic generation (HHG), attracted much less attention, with an exception of the lowest-order (0th) harmonic [9], which is typically located in terahertz (THz) range.
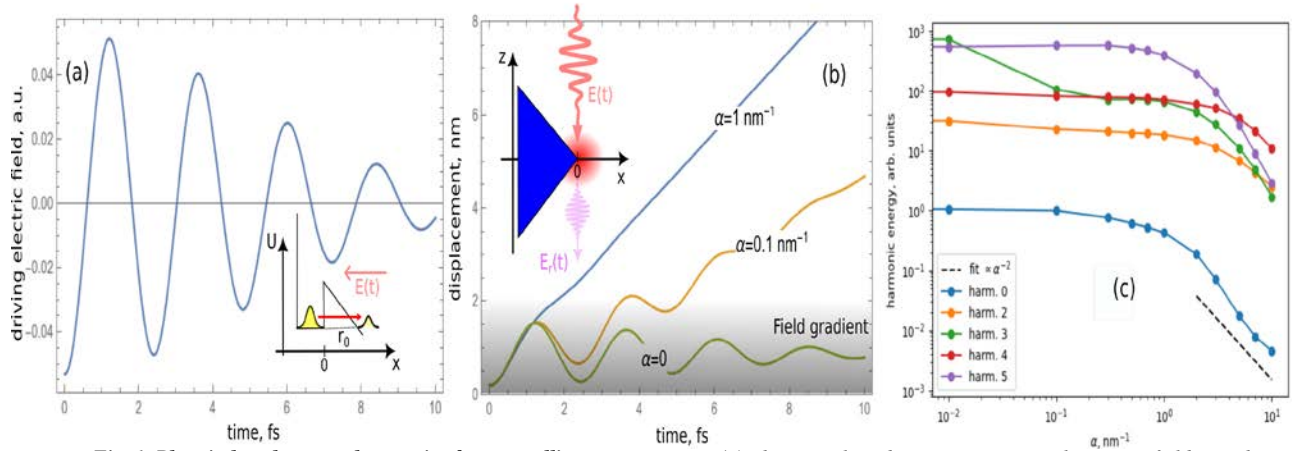
Fig. 1. Photoinduced current harmonics from metallic nanostructures. (**a**) *The exemplary driving strong electric field. The inset shows the rectangular modeling potential, deformed by the electric field, and the tunneling of the electron.* (**b**) *The exemplary classical trajectories, showing the influence of the field gradient α near the nanostrcture. The inset shows the geometry, including the nanostructure (**blue**) and the field gradient (**red shading**), as well as the external field E(t) and the emitted harmonics $E_r(t)$.* (**c**) *Dependence of the harmonic strength on the field gradient.*

Here, we study the emission of harmonics, emitted by the photoinduced mechanism in metallic NSs at THz and higher frequencies [10]. We use the single-particle Schrödinger equation with the modeling potential [3,4] (see insets to Fig. 1a,b) to model the ionization dynamics. We predict that the same mechanisms which acts in gases and solids will also create the photocurrent-based harmonics in the case of NSs. One of the distinctive features of the nanostructures is the presence of the extremely strong local field gradients due to the field enhancement [1,2] (see Fig. 1b). We show (see Fgi. 1b,c) that the field gradient can significantly reduce the harmonic emission efficiency in the case if the gradient is large enough. We also show that the scaling of harmonic energy with the field gradient can shed light on the dynamics of the electron wavepacket at the exit of the tunneling barrier.

References
[1] G. Vampa, H. Fattahi, J. Vučković, F. Krausz, *Nature Photonics* **11**, 210 (2017).
[2] P. Dombi, Z. Pápa, J. Vogelsang, S. V. Yalunin, M. Sivis, G. Herink, S. Schafer, P. Groß, C. Ropers, C. Lienau, *Review of Modern Physics* **92** 025003 (2020).
[3] L. Shi, I. Babushkin, A. Husakou, O. Melchert, B. Frank, J.Yi, G.Wetzel, A.Demircan, C. Lienau, H. Giessen, M. Ivanov, U. Morgner, M. Kovacev Laser Photonics Review **15**, 2000475 (2021).
[4] J. Schoetz, Z. Wang, E. Pisanty, M. Lewenstein, M. F. Kling, M. Ciappina, *ACS Photonics* **6**, 3057 (2019).
[5] A. Schiffrin, T. Paasch-Colberg, N. Karpowicz, V. Apalkov, D. Gerster, S.Mühlbrandt, M. Korbman, J. Reichert, M.Schultze, S.Holzner,J. V. Barth R. Kienberger, R. Ernstorfer, V.S. Yakovlev, M. I. Stockman, F. Krausz, *Nature* **493**, 70 (2013).
[6] F. Brunel, *Journal of Optical Society of America* B **7**, 521 (1990).
[7] I. Babushkin, C. Brée, C. M. Dietrich, A. Demircan, U. Morgner, A. Husakou, Journal of Modern Optics **64**, 1078 (2017).
[8] P. Jürgens, B. Liewehr, B. Kruse, C. Peltz, D. Engel, A. Husakou, T. Witting, M. Ivanov, M. J. J. Vrakking, T. Fennel,A. Mermillod-Blondin *Nature Physics* **16**, 1035 (2020).
[9] K. Y. Kim, A. J. Taylor, J. H. Glownia, G. Rodriguez, *Nature Photonics* **2**, 605 (2008).
[10] I. Babushkin, A. Husakou, L. Shi, A. Demircan, M. Kovacev, U. Morgner, *Nanophotonics* **14**, 853 (2025).

Dark-field photoelectron momentum microscopy and Electric field gated 2D semiconductors

J. P. Bange[1], B. van Wingerden[1], J. Pöhls[1], W. Bennecke[2], P. Werner[1], D. Schmitt[1], A. AlMutairi[2]
D. Steil[1], R. T. Weitz[1], G. S. M. Jansen[1], S. Hofmann[2], G. Meneghini[3], S. Brem[3], E. Malic[3]
M. Reutzel[1], S. Mathias[1]

[1] *Georg-August-Universität Göttingen, 37077Göttingen, Germany*
[2] *University of Cambridge, Cambridge, CB3 0HE, U.K.*
[3] *Philipps Universität Marburg, 35032 Marburg, Germany*

Two-dimensional (2D) transition metal dichalcogenide semiconductors exhibit correlated phenomena that can lead to emergent quantum phases, making them highly promising for next-generation electronic and optoelectronic devices. A possibility to tune the many-body interactions is *in-situ* electric field gating, which allows precise and reversible control of the filling of states in a moiré potential. In combination with angle-resolved photoemission spectroscopy (ARPES) for static band structure measurements, this approach has been shown to be a powerful experimental probe [1]. However, the study of excited states in gated 2D material structures, such as hybrid excitons [2], interlayer excitons [3, 4] and trions, has so far remained elusive, due to the limited real-space resolution of ultrafast time- and momentum-resolved spectroscopy techniques.

Here we combine time-resolved momentum microscopy with dark-field imaging techniques to gain access to many-body interactions on femtosecond time and nanometer length scales [5].
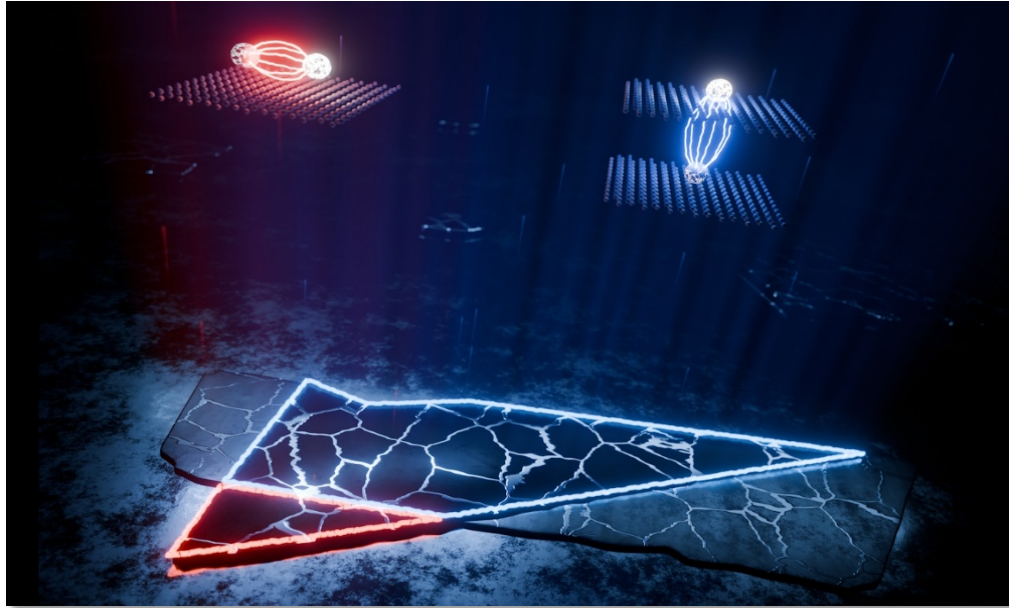
Fig. 1. *Ultrafast dark-field momentum microscopy images the formation of dark intra- and interlayer excitons at the nanoscale [5].*

This approach enables the direct observation of spatio-temporal and spatio-spectral dynamics of bright and dark excitons at the nanoscale, providing unprecedented insight into the locally varying excited state energy landscape. We further extend this method to study electric field gated homo-bilayer WSe_2 and report the ultrafast formation of quasiparticles as a function of applied gate voltage.

References
[1] P. V. Nguyen, N. C. Teutsch, N. P. Wilson, J. Kahn, X. Xia, A. J. Graham, V. Kandyba, A. Giampietri, A. Barinov, G. C. Constantinescu N. Yeung, N. D. M. Hine, X. Xu, D. H. Cobden, N. R. Wilson, *Nature* **572**, 220 (2019).
[2] J. P. Bange, P. Werner, D. Schmitt, W. Bennecke, G. Meneghini, A. Al-Mutairi, M. Merboldt, K. Watanabe, T. Taniguchi, S. Steil, D. Steil R. T. Weitz, S. Hofmann, G. S. M. Jansen, S. Brem, E. Malic, M. Reutzel, S. Mathias, *2D Materials* **10**, 035039 (2023).
[3] J. P. Bange, D. Schmitt, W. Bennecke, G. Meneghini, A. AlMutairi, K. Watanabe, T. Taniguchi, D. Steil, S. Steil, R. T.Weitz, G. S. M. Jansen S. Hofmann, S. Brem, E. Malic, M. Reutzel, S. Mathias, *Science Advances* **10**, eadi1323 (2024).
[4] D. Schmitt, J. P. Bange, W. Bennecke, A. Al-Mutairi, G. Meneghini, K. Watanabe, T. Taniguchi, D. Steil, D. R. Luke, R. T. Weitz, S. Steil G. S. M. Jansen, S. Brem, E. Malic, S. Hofmann, M. Reutzel, S. Mathias, *Nature* **608**, 499 (2022).
[5] D. Schmitt, J. P. Bange, W. Bennecke, G. Meneghini, A. Al-Mutairi, M. Merboldt, J. Pöhls, K. Watanabe, T. Taniguchi, S. Steil, D. Steil R. T. Weitz, S. Hofmann, S. Brem, G. S. M. Jansen, E. Malic, S. Mathias, M. Reutzel, *Nature Photonics* **19**, 187 (2025).

Control-based variational quantum algorithms and minimal Evolution time

E. Barnes

Virginia Tech, Blacksburg, VA 24061, USA

Quantum simulation on noisy intermediate-scale quantum devices is severely limited by short qubit coherence times. We developed a pulse-based variational quantum algorithm known as ctrl-VQE to address this issue by eliminating the need for parameterized quantum circuits, which lead to long state preparation times [1]. We use this algorithm to find the fastest possible pulses that prepare target molecular wave functions for a given device Hamiltonian describing coupled transmon qubits using simulations [2]. We find that the resulting time-optimal pulses develop a bang-bang form consistent with Pontryagin's maximum principle. We further investigated how the minimal state preparation time is impacted by the number of energy levels active in the transmon simulations. We find that leakage outside the computational subspace (something that is usually considered problematic) speeds up the state preparation, further reducing device coherence time demands. Our analysis reveals that this speedup is due to both an enlarged solution space of target wave functions and the appearance of additional channels connecting initial and target states.
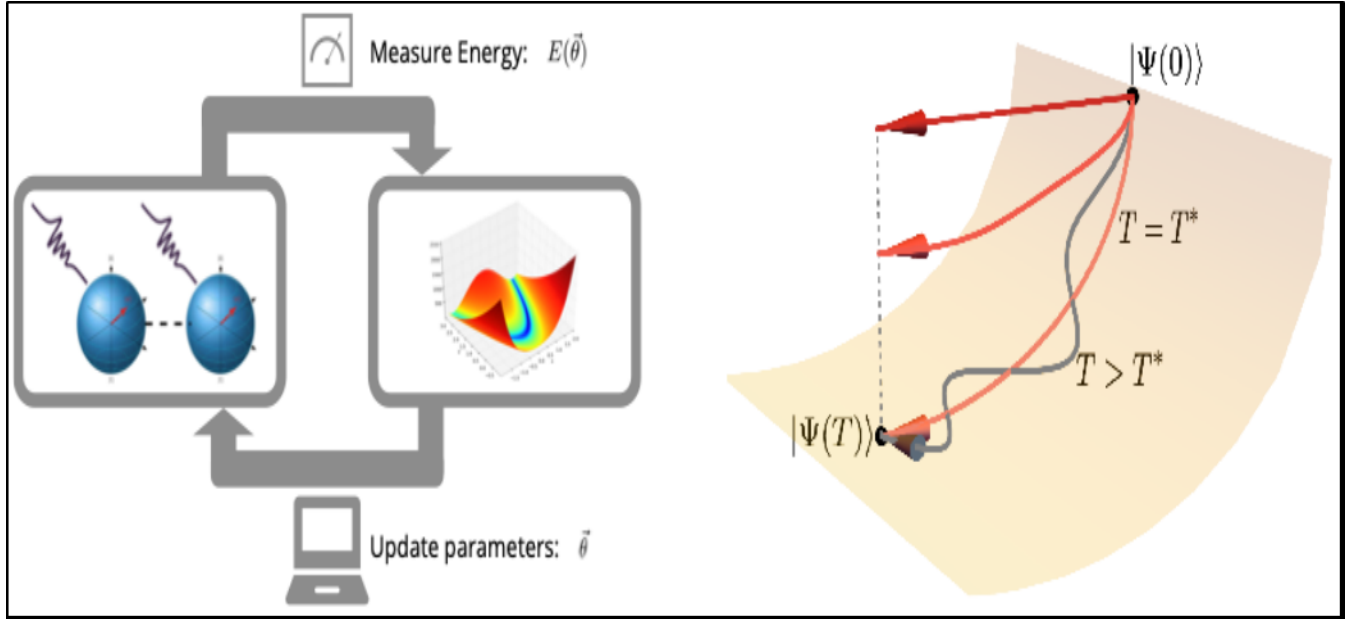
Fig. 1. (Left) Schematic of pulse-based variational quantum algorithms. *Pulses are applied to qubits on a quantum processor to prepare many-body quantum states. Measurements of the energy on the quantum processor are fed into a classical computer, which uses this data to determine updated pulse parameters. The quantum-classical feedback loop is iterated until the energy is minimized and the target state is prepared on the quantum processor.*
(Right) Qualitative depiction of state evolution in the Hilbert space of qudits with two or more levels. *The time-optimal path in the computational subspace (yellow surface) is shown as the path with evolution time $T = T^*$. Many paths are possible to reach the solution $\Psi(T)$ when $T > T^*$ (**gray curvy line**). Access to leakage states provides new paths (**shown by darker red paths**) that reach the solution faster than T^* when the final state is projected onto the computational subspace.*

In addition, we find that the performance of the algorithm can be enhanced by making a judicious choice of pulse parameterization [3]. Even shorter state preparation times are possible on other hardware, such as semiconductor spin qubit devices [4].

References

[1] O. R. Meitei, B. T. Gard, G. S. Barron, D. P. Pappas, S. E. Economou, E. Barnes, N. J. Mayhall, *npj Quantum Inf0rmation* **7**, 155 (2021).

[2] A. Asthana, C.Liu , O.R.Meitei, S.E. Economou,E.Barnes,N.J. Mayhall, *Physical Review Applied* **19**, 064071 (2023).

[3] K. M. Sherbert, H.Amer,S.E. Economou, E.Barnes, N. J. Mayhall, *Physical Review Applied* **23**, 024036 (2025).

[4] C. K.Long, N.J Mayhall, S. E. Economou, E. Barnes, C. H. W. Barnes, F. Martins, D. R. M. Arvidsson-Shukur, N. Mertig, *arXiv:*2406.10913 (2024)

Terahertz-driven parametric excitation of Raman-active Phonons in LaAlO$_3$

M. Basini[1], V. Unikandanunni [2,], F. Gabriele[3], M. Cross[4], A. M. Derrico[6], A. X. Gray[5], M. C. Hoffmann[4]
F. Forte[3], M. Cuoco[3], S. Bonetti[7]
[1]ETH Zürich, 8093 Zürich, Switzerland
[2] Bern University, 3012 Bern, Switzerland
[3]Universit´a di Salerno,84084 Fisciano, Italy
[4]SLAC National Accelerator Laboratory, Menlo Park, CA 94025, USA
[5]Temple University, Philadelphia, PA 19122, USA
[6]University of California Berkeley, Berkeley, CA 94720, USA
[7]Ca' Foscari University of Venice, 30172 Venice, Italy

Parametric excitation and associated devices play a crucial role in enhancing weak electromagnetic signals, facilitating the conversion of collective modes between different frequencies, generating and measuring squeezed and entangled states, and enabling the development of innovative information processing architectures. When brought to the realm of sound waves, the parametric control, generation, and manipulation of phonons have long been sought after, presenting unparalleled opportunities to advance the field of phononics. In this framework, the attention has been mostly devoted to the realization of materials platforms and devices for the amplification of phonons in low-frequency range (e.g. trapped ions, optical tweezers and nanomechanical resonators), as well as for terahertz phonons in semiconductor superlattices and by means of pump-probe experiments in SiC. Although significant advancements have been made, parametric controlling of collective excitations like phonons remains a challenge. In this work, we present evidence of a yet unexplored mechanism for a coherent parametric excitation of low-energy Raman-active phonon in the centrosymmetric lanthanum aluminate, LaAlO$_3$ (LAO), which makes use of an intense THz electric field [1]. So far, the excitation of Raman-active modes in solids have been achieved via Impulsive Stimulated Raman Scattering (ISRS) [2], via Sum Frequency Generation (SFG) [3], or, via Ionic Raman Scattering (IRS) [4,5,6]. Here, we demonstrate that an intense terahertz pulse, with central frequency in the range of 1-2 THz, not only has the ability to coherently stimulate, by ISRS and SFG, the Raman-active Eg phonon at about 1 THz but also generates significant subharmonic spectral components, which are distinct signatures of an underlying parametric-driving mechanism. This mechanism is based on the absorption of photons through an optical transition involving a pair of acoustic vibrational modes.
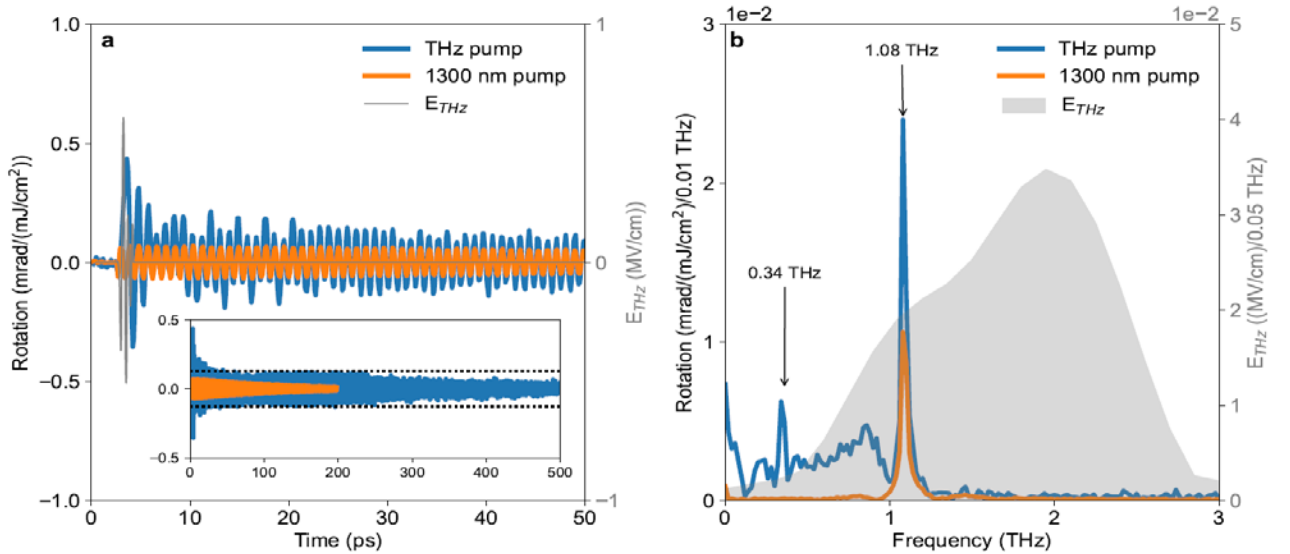
Fig. 1 Experimentally detected polarization rotation in LaAlO3 following near-infrared or broad band THz pumps. Polarization rotation of a transmitted 800 nm probe through a LaAlO3 crystal, following the excitation by a near-infrared (1300nm) (**orange curve**) or a broadband THz excitation (**blue curve**), in (**a**) time and (**b**) frequency domains. Measurements are performed at 8K. The FFT is evaluated in the range of 0-50 ps. The sample response is normalized by the pump fluence. Inset in panel (a): time-domain dynamics at longer timescales.

Here, we demonstrate that an intense terahertz pulse, with central frequency in the range of 1-2 THz, not only has the ability to coherently stimulate, by ISRS and SFG, the Raman-active Eg phonon at about 1 THz but also generates significant subharmonic spectral components, which are distinct signatures of an underlying parametric-driving mechanism. This mechanism is based on the absorption of photons through an optical transition involving a pair of acoustic vibrational modes.
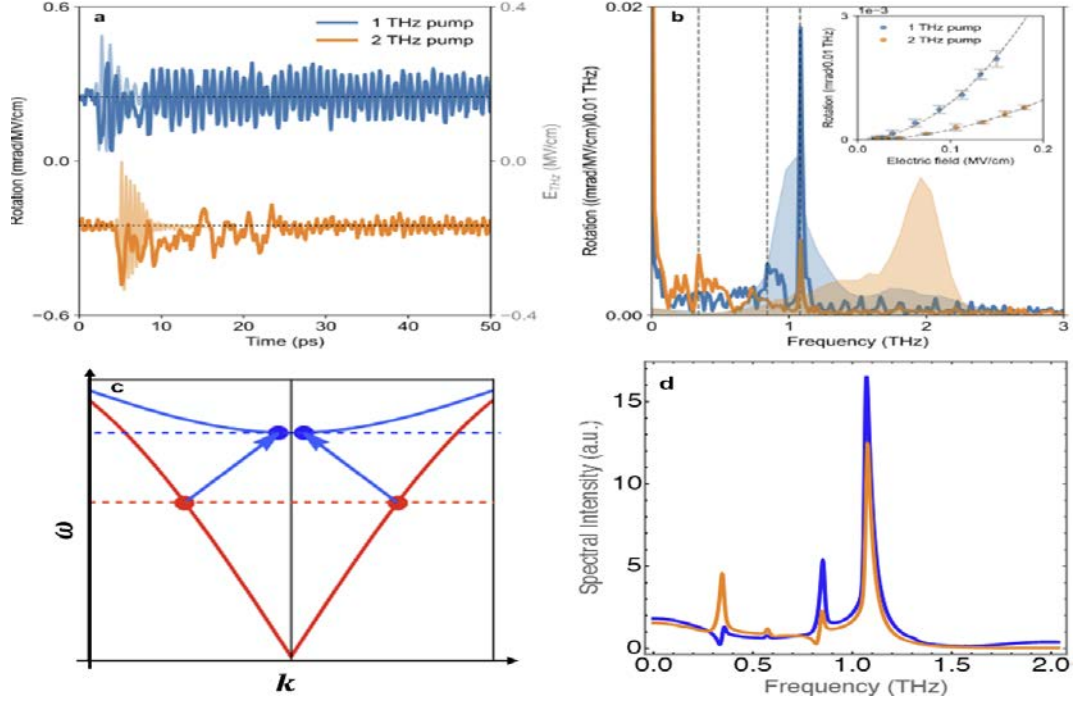
Fig. 2. *LAO [100] Probe polarization rotation in time (**a**) and frequency domain (**b**) following narrowband THz excitation (with central frequencies of 1 THz and 2 THz). The light blue and orange traces in panel (**a**), as well as the light blue and orange shaded regions in panel (**b**), show electro-optical sampling of the incident narrowband THz pulses in the time and frequency domains, respectively. Inset of panel (**b**) shows Eg amplitude vs electric field amplitude. The dashed **gray** lines in the inset show the best fit. figure (**c**) is a schematic of the Eg Raman-active phonon dispersion (blue) and the acoustic phonons dispersion (**red**) and illustrates the up-conversion mechanism where two acoustic phonons (**red dots**) convert into Raman-active phonons (**blue dots**). (**d**) shows the calculated spectral intensity of the Raman amplitude $|Q_R|$ (**solid black line**) as a function of the frequency. The calculation was made assuming parametric phonon dynamics in LaAlO3, driven by narrowband 1THz (**blue**) and 2THz excitation.*

The interaction between the Raman-active and the acoustic modes results in a parametric excitation of the Raman-active phonon, leading to the emergence of dynamical components at subharmonic frequencies.

References
[1] M. Basini, V. Unikandanunni, F. Gabriele, M. Cross, A. M. Derrico, A. X. Gray, M. C. Hoffmann, F. Forte, M. Cuoco, S. Bonetti *arXiv:2410.06748* (2024).
[2] M. V. Klein, Electronic Raman scattering pp. 147–204 *Springer*, (2005).
[3] S. Maehrlein, A. Paarmann, M. Wolf, T. Kampfrath, *Physical Review Letters* **119**, 127402 (2017).
[4] A. Maradudin, R. Wallis, *Physical Review* B **2**, 4294 (1970).
[5] R. Wallis, A. Maradudin, *Physical Review* B **3**, 2063 (1971).
[6] L. Humphreys, *Physical Review* B **6**, 3886 (1972).

Ultrafast charge transfer and band renormalization in bilayer Graphene/monolayer Ag/SiC

E. Moos[1], Z. Y. Deng[1], H. Bever[1], A. Jain[2], C. Dong[2], J. A. Robinson[2], M. Bauer[1]

[1]*Christian-Albrechts-Universität zu Kiel, 24098 Kiel, Germany*
[2]*Pennsylvania State University, University Park, PA 16802, USA*

Barnal stacked bilayer graphene is a promising material for electronic and optoelectronic applications since it supports an interlayer asymmetry band gap, which can be manipulated, for example, by applying an external electric field or by changing the carrier concentration [1, 2]. Even more and as shown more recently, charge carrier injection can also induce cascades of correlated phases at sufficiently low temperatures, such as metallic Stoner phases or electronic Wigner crystals [3]. The question arises whether such changes in the electronic properties of bilayer graphene are also possible on ultrashort time scales. Previous work by various groups has shown that ultrafast charge transfer processes in different types of 2D heterostructures enable the necessary charge injection on the relevant time scales [4, 5]. However, the effect of such charge injection on electronic structure changes in bilayer graphene and the associated time scales have not yet been investigated.

In this contribution, we present results of a time- and angle-resolved photoemission study on ultrafast band renormalization effects in bilayer graphene following laser-induced injection of charge carriers at densities in the order of a few 10^{-3} electrons per unit cell from an intercalated silver monolayer on SiC. The experimental data indicate band shifts on different time scales ranging from 10 fs to several 100 fs that we associate with transient changes in the chemical potential, in the size of the band gap and in the splitting of the π-band (see Fig. 1).
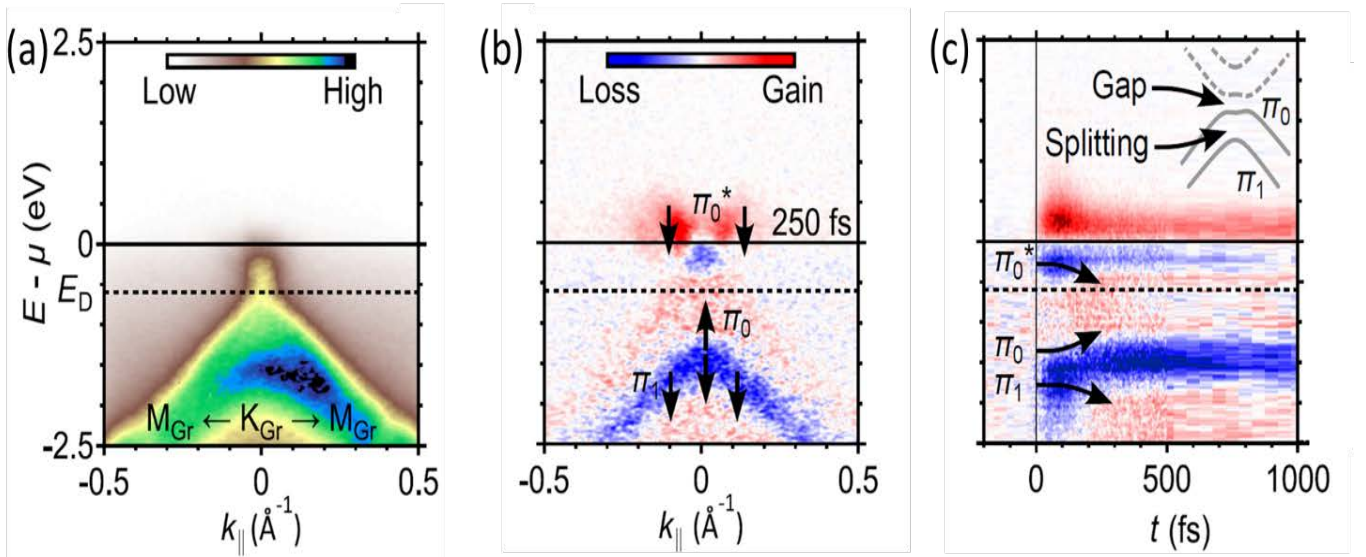
Fig. 1. *(a):ARPES data auf bilayer graphene/monolayer Ag/SiC along the M-K-M direction of the bilayer graphene Brillouin zone; (b) ARPES difference intensity map highlighting transient band structure changes 250 fs after excitation, arrows indicate band shifts associated with the observed changes in spectral weight; (c)ARPES difference intensity transient at K; **the inset** illustrated the bandstructure of bilayer graphene near K.*

The various effects can be attributed to a complex interplay between the global change in charge carrier density and to transient changes in the interlayer asymmetry of bilayer graphene due to changes in the potential difference and dimer coupling between the graphene layers. The results demonstrate the possibility of efficient band engineering of bilayer graphene on ultra-short time scales.

References
[1] T. Ohta, A. Bostwich, T. Seyller, K. Horn, E. Rotenberg, *Science* **313,** 951, (2006).
[2] K. F. Mak, C. H. Lui, J. Shan, T. F. Heinz, *Physical Review Letters* **102.** 256405 (2009).
[3] A. M. Seiler, F. R. Geisenhof, F. Winterer, K. Watanabe, T. Taniguchi, T. Xu, F. Zhang, R. T. Weitz, R. Thomas, *Nature* **608**, 298 (2022).
[4] X. Hong, J. Kim, S. F. Shi, Y. Zhang, C. Jin, Y. Sun, S. Tongay, J. Wu, Y. Zhang, F. Wang, *Nature Nanotechnology* **9**, 682 (2014).
[5] S. Aeschlimann, A. Rossi, M. Chávez-Cervantes, R. Krause, B. Arnoldi, B. Stadtmüller, M. Aeschlimann, S. Forti, F. Fabbri, C. Coletti, I. Gierz *Science Advances* **6**, eaay0761 (2020).

Exciton-polariton formation and propagation in semiconducting Transition metal dichalcogenides

M. Bauer

Christian-Albrechts-Universität zu Kiel, 24098 Kiel, Germany

Excitons are the focus of numerous experimental and theoretical research efforts due to their promising potential for light-driven energy harvesting. From the many semiconducting materials exhibiting excitonic resonances, transition-metal dichalcogenides (TMDC) have garnered special interest in recent years since they exhibit excitons with large binding energies [1]. Embedding TMDC films within micrometer-sized cavities creates a suitable environment for a strong interaction between excitons and photons facilitating the formation of light-matter quasiparticles termed exciton-polaritons [2]. Its hybrid nature promises new avenues for the energy exchange between light and matter and thus new technological developments. The transfer of energy via the propagation of such a quasiparticle is especially interesting. Therefore, the interaction of excitons with propagating light modes rather than spatially confined cavity photons may provide another suitable environment for exciton-polaritons. Essentially, thin films of TMDC materials themselves host the necessary waveguiding modes, which are able to interact with the intrinsic exciton resonances [3].

In this contribution I will give an introduction to the formation of propagating exciton-polaritons and the conditions under which such modes form in thin TMDC films. I will further explain how we detect and characterize these quasiparticle modes using the technique of photoemission electron microscopy (PEEM) (see Fig. 1) [4].
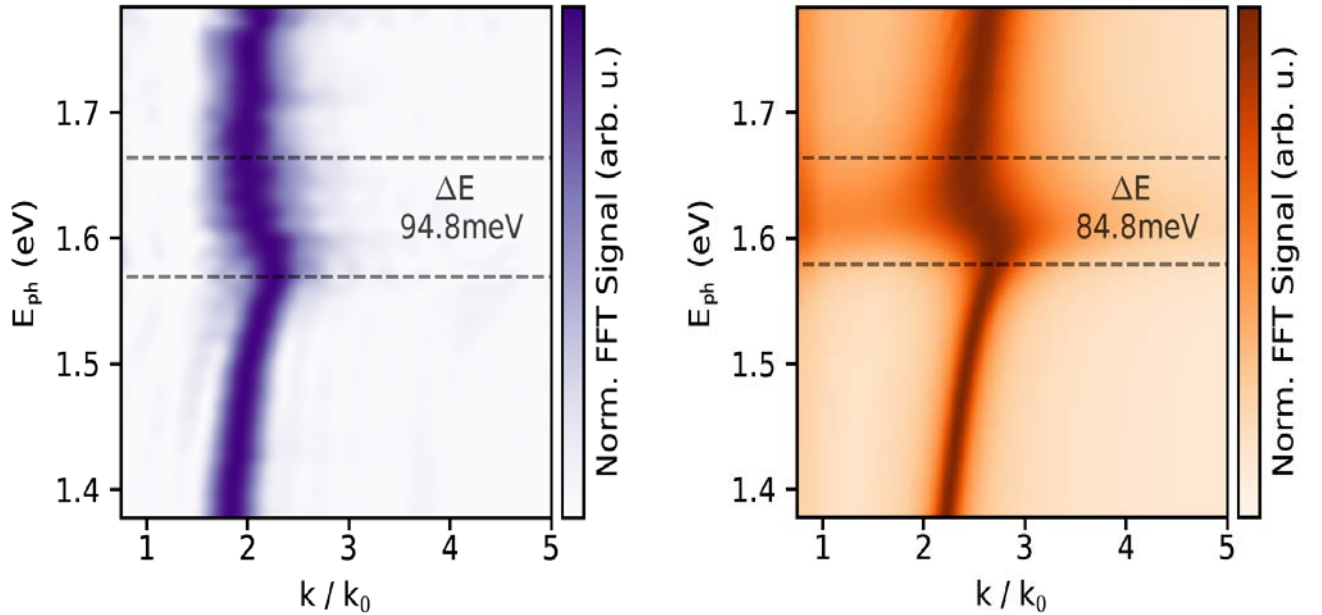
Fig. 1. Exciton-polariton dispersion relation in a 30 nm thick WSe$_2$ flake: PEEM data (left) in comparison to results of a Finite Difference Time Domain (FDTD) simulation (right). The deviation from the linear polariton dispersion near the energy of the A exciton in WSe$_2$ of about 1.6 eV is the spectral signature for exciton-polariton coupling. ΔE indicates the value for the characteristic energy splitting of the dispersion relation due to exciton-polariton coupling as determined from the PEEM data and FDTD data, respectively.

Finally, I will show in a first example that we can even track the propagation of these modes in real time under broadband excitation using time-resolved PEEM.

References
[1] G. Wang, A. Chernikov, M. M. Glazov, T. F. Heinz, X. Marie, T. Amand, B. Urbaszek, *Review of Modern Physics* **90**, 021001 (2018).
[2] N. Lundt, S. Klembt, E. Cherotchenko, S. Betzold, O. Iff, A. V. Nalitov, M. Klaas, C. P. Dietrich, A.V. Kavokin, S. Höfling, C. Schneider *Nature Communications* **7**. 13328 (2016).
[3] X. Zong, L. Li, L. Li, K. Yu, Y. Liu, *Optics Express* **31**, 18545 (2023)
[4] T. Eul, M. Sabir, V. de Manuel-Gonzales, F. Diekmann, K. Rossnagel, M. Bauer, *arXiv:2502.03361*(2025).

Exciton photoemission orbital tomography from 2D semiconductor materials

W. Bennecke[1], I. Gonzalez Oliva[2], J. P. Bange[1], P. Werner[1], M. Merboldt[1], A. M. Seiler[1], D. Steil[1]
R. T. Weitz[1], P. Puschnig[3], C. Draxl[2], G. S. M. Jansen[1], M. Reutzel[1], S. Mathias[1]

[1] Georg-August-Universität Göttingen, 37073 Göttingen, Germany
[2] Humboldt-Universität zu Berlin, 10177 Berlin, Germany
[3] Universität Graz, 8010 Graz, Austria

Excitons are realizations of a correlated many-body wavefunction, consisting of a Coulomb-bound electron and hole pair. They are the dominant excitations in semiconducting organic and low-dimensional quantum materials and, thus, govern their optoelectronic response. To unlock the full optoelectronic potential and to harvest and control exciton-mediated energy conversion pathways, a microscopic understanding of excitons is crucial. Ultimately, this relies on access to the correlated exciton wavefunction, which has hardly been realized in experiments. A powerful technique to access quantum mechanical wavefunctions is photoemission orbital tomography (POT). POT provides direct access to the single-electron wavefunctions, i.e., the molecular orbitals, of well-oriented organic molecules using angle-resolved photoemission spectroscopy (ARPES) [1]. Our work expands on the concepts of POT to gain unprecedented insight into the correlated wavefunction of excitons in organic semiconductors [2], 2D transition metal dichalcogenides (TMDs) [3], and 2D-organic hybrid interfaces [4]. This includes exciton localization, hybridization, charge and energy transfer, as well as ultrafast exciton formation and relaxation dynamics. In this presentation, I will introduce the concept of exciton photoemission orbital tomography and demonstrate the power of this technique to investigate the exciton landscape of a hybrid 2D-organic interface [4].
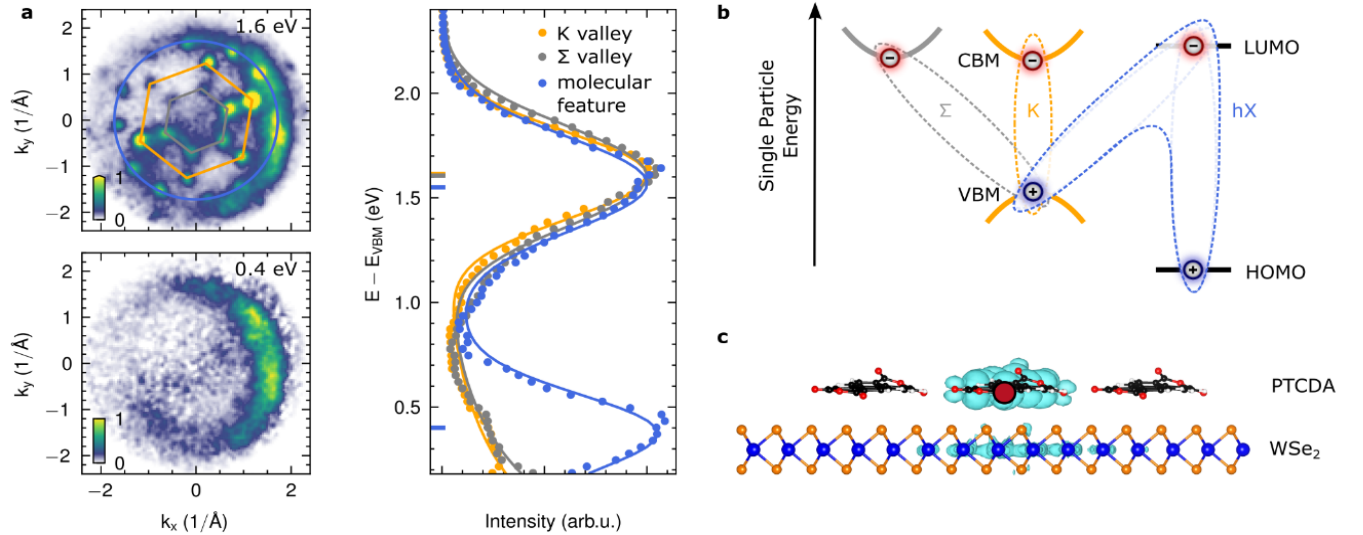
Fig. 1. Exciton landscape of the hybrid WSe_2/PTCDA interface *[4]. **a** Photoemission signatures of the different excitons, which can directly be attributed to the K (orange), Σ (gray) and the hybrid (hX) (blue) excitons shown in **b**. Here, the hX is characterized by a two-peak structure in energy, which can be traced back to the different hole contributions, and a LUMO-like momentum distribution. **c.** Exemplary hole probability density isosurface (cyan) for the hX for fixed electron position (red dot) on the molecule. Notably, the hole has a significant probability to be found on the PTCDA molecule as well as on the WSe_2 layer.*

Notably, our findings reveal a hybrid exciton state characterized by concomitant intra- and interlayer electron-hole transitions within the molecular layer and across the 2D-organic interface, respectively, which gives rise to an exciton wavefunction with a mixed Frenkel-Wannier character.

References
[1] P. Puschnig, S. Berkebile, A. J. Fleming, G. Koller, K. Emtsev, T. Seyller, J. D. Riley, C. Ambrosch-Draxl, F. P. Netzer, M. G. Ramsey, *Science* **326** 702 (2009)
[2] W. Bennecke, A. Windischbacher, D. Schmitt, J. P. Bange, R. Hemm, C. S. Kern, G. D'Avino, X. Blase, D. Steil, S. Steil, M. Aeschlimann B. Stadtmueller, M. Reutzel, P. Puschnig, G. S. M. Jansen, S. Mathias, *Nature Communications* **15**, 1804 (2024)
[3] D. Schmitt, J. P. Bange, W. Bennecke, A. Al-Mutairi, K. Watanabe, T. Taniguchi, D. Steil, D. R. Luke, R. T. Weitz, S. Steil, G. S. M. Jansen S. Hofmann, M. Reutzel, S. Mathias, *Nature* **608**, 499 (2022)
[4] W. Bennecke, I. Gonzalez Oliva, J. P. Bange, P. Werner, M. Merboldt, A. M. Seiler, K. Watanabe, T. Taniguchi, D. Steil, R. T. Weitz, P. Puschnig C. Draxl, G. S. M. Jansen, M. Reutzel, S. Mathias, *arxiv:2411.14993* (2024)

Energy scaling of nanosecond fiber amplifiers at 2.8 microns

M. Bernier[1], Q.Perry-Auger[1], S. Leonov[1], D. Zhang[2], Y.O.Aydin[1], D.Kraemer[2], R.Vallée[1]
[1]Université Laval, Québec, QC G1V 0A6 Canada
[2]Light Matter Interaction Inc., Toronto, ON M8Z 2T7 Canada

High-energy nanosecond pulsed sources near 2.8 µm are gaining considerable attention due to their strong absorption by water-rich biological tissues, making them highly effective for precise laser ablation in surgical and biomedical applications. While short pulse durations, typically in the nanosecond range, help limit thermal damage in soft tissues, high pulse energy and average power remain essential for effective ablation of less water-rich materials such as bone or dental enamel [1,2].The laser sources are energy-limited in this wavelength region and fluoride fibers offer a promising solution for the efficient amplification of 2.8 µm pulses with their broad mid-infrared transparency, favorable absorption band properties and high rare-earth doping capacity. Recently, the potential of such amplifiers has been demonstrated at the millijoule-level in various configurations, including two-stage amplification with multimode output seeded by an optical parametric generator (OPG) and single-mode output using coiled low-NA Er:ZrF$_4$ fibers seeded by a Qswitched laser [3,4]. We also proposed a simple design which eliminates isolators and complex free space optics used in previous works and demonstrated 2 mJ output at 10 W average power with a peak power of 10 MW, using a hybrid architecture [5]. This system consists of an OPG as the seed and two amplification stages made of large-core Er:ZrF$_4$ fibers and home-made pump combiners as shown in the Fig.1 below.
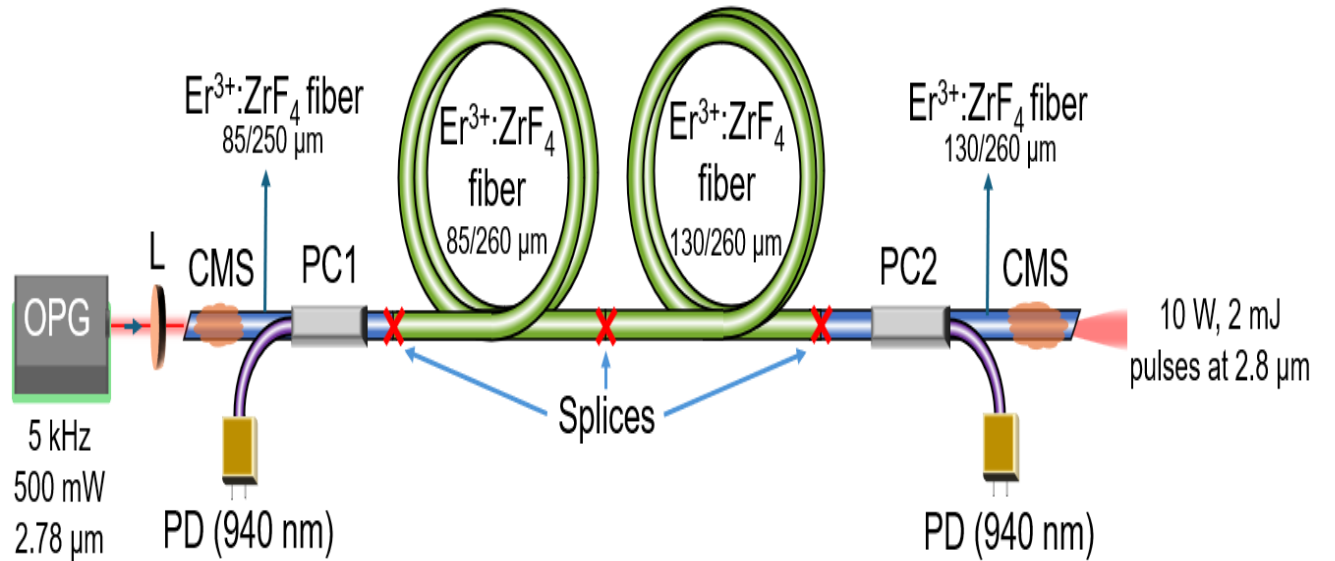
Fig. 1 Experimental setup of an isolator-free fluoride fiber amplifier based on custom home-made combiners.
CMS: Cladding mode stripper, L: lens, PC: pump combiner, PD: pump diode.

These recent advances demonstrate the capability of fluoride fiber amplifiers to combine energy scalability with architectural simplicity and their strong potential for achieving multi-millijoule output. In this talk, we will present the steps required to scale up to 10 mJ-level pulse energy and beyond near 2.8 µm by using fluoride fiber amplifiers. These include optimized fiber fabrication and gain distribution, improved thermal handling and component-level improvements such as ultra-low splicing techniques and more efficient pump combining strategies. Such developments could enable a new class of mid-infrared laser systems suitable for demanding applications in biomedical surgery and advanced material processing

References
[1] M. H. Niemz, *Laser-Tissue Interactions* (Springer, 2007).
[2] C. Apel, R. Franzen, J. Meister, H. Sarrafzadegan, S. Thelen, N. Gutknecht, *Lasers in Medical Sciences* **17**, 253 (2002).
[3] Y. O. Aydin, S. Magnan-Saucier, D. Zhang, V. Fortin, D. Kraemer, R. Vallée, M. Bernier, *Optics Letters* **46**, 4506 (2021).
[4] Y. Bai, B. Zhou, W. Du, Y. Cui, A. Galvanauskas, *Optics Letters* **50**, 1140 (2025).
[5] S. Leonov, Q. Perry-Auger, A. Karim, D. Zhang, D. Kraemer, R. Vallée, M. Bernier, *Optics Letters* **49**, 6169 (2024).

Gapless-to-gapped transition in the fluctuation mode spectra of Semiconductor lasers

R. Binder[1], N.H. Kwong[1], M. Spotnitz[2]
[1]*University of Arizona, Tucson, AZ 85721, USA*
[2]*Sandia National Laboratories, Albuquerque, NM 87123, USA*

Semiconductor lasers have become ubiquitous, with examples ranging from laser diodes in optical communications networks to surface-emitting lasers (VCSELs) used in facial recognition in smart phones. There is also a wide variety of lasing mechanisms, ranging from optical gain provided by electron-hole recombination without Coulomb interaction effects (this simple model is found in many engineering textbooks), to exotic macroscopic quantum states such as Bose-Einstein condensates of excitons. One would assume that the physics of the simple (and robust) electron-hole recombination model is well understood. But generally, in physics, understanding a system implies understanding its linear response to external probes (in lasers and other systems undergoing spontaneous symmetry breaking, linear response is analyzed in terms of the system's fluctuation modes). It turns out that the linear excitations and fluctuation modes of semiconductor lasers are not well understood, not even for the simplest case of electron-hole recombination without Coulomb interaction. Formally, a semiconductor quantum well (QW) microcavity laser is microscopically a highly coherent, driven-dissipative phase of electrons, holes, and the cavity light field. Electrons and holes, being charged particles, interact via the attractive Coulomb interaction, but also via the cavity light field. If the incoherent pump source is above a certain threshold and the laser is 'switched on', the laser light, being coherent, can be called the system's order parameter. There are useful formal analogies between semiconductor lasers and Bardeen-Cooper-Schrieffer (BCS) superconductors, with electrons and holes corresponding to Cooper pairs. An important concept in the original BCS theory for superconductors in thermal equilibrium is that of an energy gap in the excitation spectrum of the superconducting state. However, in some superconductors, e.g., those with dilute magnetic impurities, there is a gapless regime in which the order parameter is finite, and the system is superconducting, but the energy gap is zero [1]. In previous work, we have demonstrated that polariton lasers can indeed operate in the so-called polaritonic BCS regime (in contrast to the regime where the polaritons are almost like ideal bosons and exhibit Bose-Einstein condensation) [2]. We have analyzed the fluctuation spectra of polariton lasers triggered by interband probes, and found that these spectra contain exceptional points, which form continua in the plane of the parameters cavity decay rate and pump density [3]. We have also analyzed fluctuation spectra triggered by terahertz (THz) probes [4,5], and found that the gap energy can be extracted from THz absorption/gain spectra by tracing out absorption extrema as a function of pump density [5]. This work shows that, in analogy to gapless superconductivity, a gapless lasing parametric regime, in which the frequency gap in the fluctuation spectrum is closed, exists for steady-state semiconductor lasers [6]. The gap opens when the laser intensity exceeds a threshold. This gapless-to-gapped transition occurs at a third-order exceptional point. The transitions are schematically summarized in Fig.1.
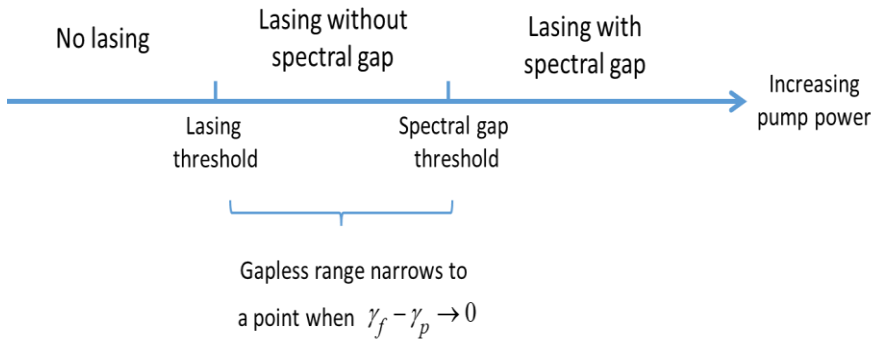
Fig. 1: Schematic of gapless and gapped regime as a function of pump power (which determines the strength of the condensate, usually represented by the order parameter Δ); γ_f and γ_P are the decay rates of the carrier occupation and the interband polarization (related to the order-parameter), respectively.

This figure holds for lasers with and without Coulomb interaction between the charge carriers.

The energy eigenvalues of the THz fluctuation modes of a laser in which the Coulomb interaction between charge carriers is neglected are shown in Fig.2:
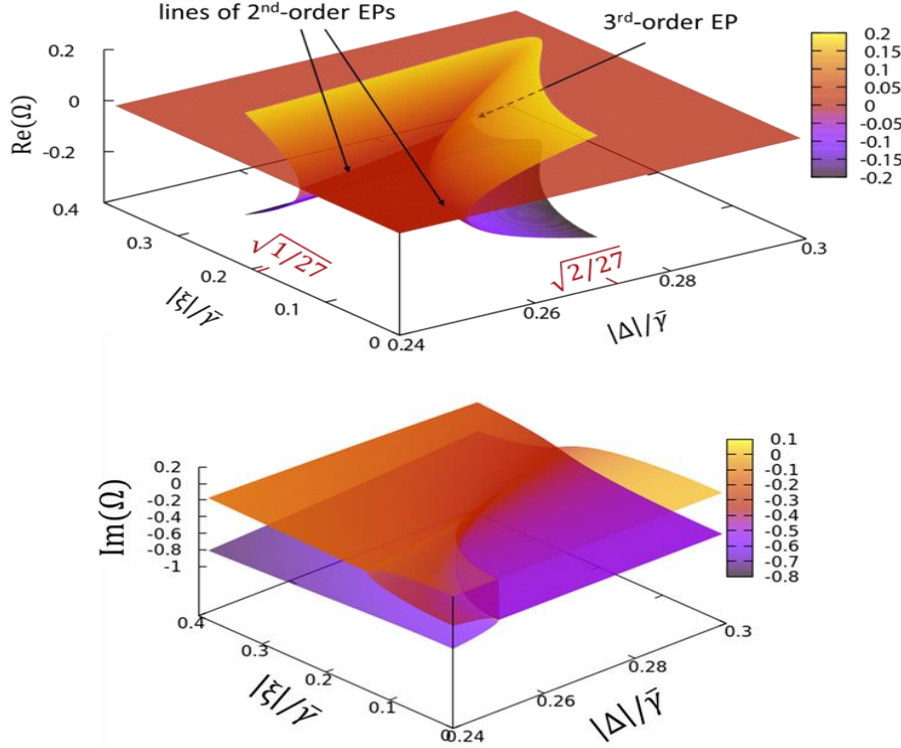
Fig. 2. Example of real (top) and imaginary (bottom) parts of the fluctuation spectrum (complex energy eigenvalues λ, here parametrized as $\Omega = (\lambda + i\gamma_P)/\bar{\gamma}$), as a function of the steady state order parameter Δ, which is related to the laser intensity, and the electron-hole energy measured from the laser frequency, ξ, with $\bar{\gamma} = \gamma_f - \gamma_P$ being the difference between the decay rates of the carrier occupation and the interband polarization (related to the order-parameter). A gap exists for fixed Δ when the upper (yellowish) solution of $Re(\Omega)$ is not zero for any ξ. For details, see Ref. [6].

In Fig.3 we present the information from Fig.1 in a quantitative way for the case of lasers without Coulomb interaction. It is seen that the gapless regime collapses to a single point when the relaxation rates of the decay rates of the carrier occupation and the interband polarization are equal.
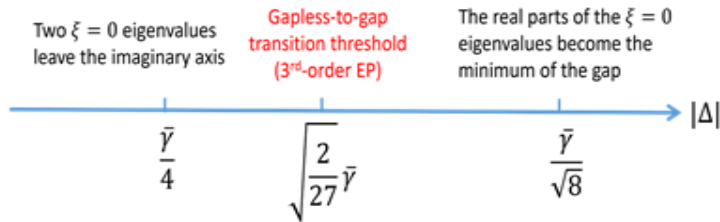
Fig.3. Schematic drawing, analogous to Fig.1, showing several threshold values of the order parameter $|\Delta|$ in the photon laser model (i.e. Coulomb interaction between charge carriers is neglected). ξ is the electron-hole energy measured from the laser frequency. $\xi = 0$ is the value at which the sum of the electron and hole band energies is in resonance with the laser frequency. See the caption of Fig.2 for the definition of $\bar{\gamma}$.

This is formally analogous to the case of magnetically doped BCS superconductors, where the gapless regime exists only if the decay rates of the single-particle distribution and that of the order parameter are different [1].

References
[1] A. A. Abrikosov, L. P. Gor'kov, *Journal of Experimental and Theoretical Physics* **39**, 1781 (1960).
[2] J. Hu, Zh. Wang, S. Kim, H. Deng, S. Brodbeck, Ch. Schneider, S. Hoefling, N.H. Kwong, R. Binder, *Physical Review* X **11** 011018 (2021).
[3] R. Binder, N.H. Kwong, *Physical Review* B **103**, 085304 (2021).
[4] M. Spotnitz, N.H. Kwong, R. Binder, *Physical Review* B **104**, 115305 (2021).
[5] M. Em. Spotnitz, N. H. Kwong, R. Binder, *Physical Review* B **107,** 125309 (2023).
[6] N. H. Kwong, M. Em. Spotnitz, R. Binder, *Physical Review* B **109**, 045306 (2024).

Terahertz control of angular momentum in solids

S. Bonetti

Ca' Foscari University, 30172 Venice, Italy

The interaction between light and matter is at the heart of the understanding of condensed matter physics. Historically, the development of previously unavailable light sources, extending both the achievable wavelength and brightness ranges, has greatly impacted fundamental research and eventually technology, such as for the case of the laser. In this talk, I will focus on coherent terahertz radiation of large amplitude, i.e. with electric fields of the order of 1 MV/cm and corresponding magnetic fields in the 0.1 – 1 Tesla range. Such combination of relatively low-frequency radiation (as compared to the frequency of the visible range) and strong fields, has paved the way for a new understanding and control of the spin and orbital angular momentum in solids. In fact, thanks to these light sources, we have recently been able to experimentally discover two novel and elusive phenomena in condensed matter. First, the evidence of magnetic "nutation", predicted over 10 years ago, and second, the observation of dynamical multiferroicity, i.e. of magnetic order coexisting with an electric polarization. Nutation is the rocking motion of an object going on a precession around and axis, common to spinning tops and planets. It is a consequence of the conservation of angular momentum, and can be described knowing the tensor of the inertia of the object. Surprisingly, since the discovery, almost a century ago, of the ferromagnetic resonance, i.e. the precession of the magnetization vector around a magnetic field, nutation was ignored by physical models of such phenomenon. Instead, an unphysical inertia tensor was assumed in the phenomenological Landau – Lifshitz – Gilbert (LLG) equation used to describe the precession of the magnetization. Such an unphysical inertial tensor was anticipated by Gilbert himself in the footnote of a widely cited paper [1], but was left undiscussed until recently. In 2011, the group of Wegrowe et al. published a paper [2] introducing a variation of the LLG equation with a physically correct inertial tensor and where, indeed, nutation could be described. It was immediately obvious that the detection of such nutation required performing experiments at frequencies above the typical gigahertz range of ferromagnetic resonance. With the recent development of intense terahertz sources, the time was ripe to attempt the experimental detection. We succeeded in such endeavor both at the TELBE facility [3] as well as in table-top experiments [4], revealing many details that the phenomenological theory had left out. Finally, recent experiments performed at cryogenic temperature suggest that nutation is just one of the many consequences of a non-Markovian behavior (i.e. the presence of "memory effects") of spins in ferromagnets [5]. I will show some unpublished data which confirms the predictions of the non-Markovian description of the phenomenon.
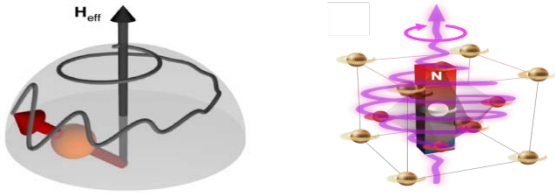
Fig. 1.Left: Schematic representation of inertial spin dynamics in ferromagnets, showing a damped nutation on top of a damped precession. Adapted from Ref. [3]. Right: Schematic mechanism of the dynamical multiferroicity effect: a circularly polarized terahertz pulse, resonant with an infrared-active phonon mode in the material, induces a circular motion of the ions in the material. Such circular motion induces a magnetic moment.

In the second part of the talk, I will present our recent results [6] on the observation of a large magnetization induced in an archetypal dielectric perovskite, strontium titanate, by means of strong, circularly polarized terahertz electric fields. The results confirm the existence of dynamical multiferroicity, i.e. of the induction of a magnetization following a time-varying polarization in a materials owing to a large phonon displacement, predicted in a recent paper [7]. However, our experiments show that the effect is four orders of magnitude larger than what the theory predicts, revealing that the induced magnetization is of the order of the electronic Bohr magneton, and not the nuclear one. Our results suggest that the *mechanical* angular momentum is efficiently transferred from the phononic to the electronic system, thus boosting the *magnetic* angular momentum by a factor similar to the ratio of the nuclei to electron masses. Our results have soon been reproduced by independent groups in several other material systems [8], and much theoretical effort has been put into towards understanding the microscopic mechanisms for such enhancement [9]. Such induced magnetization is large enough to cause switching of ferrimagnetic metals used in data storage [10], and opens up for creating large magnetization in virtually any materials, in particular insulating ones, which occur very rarely in nature.

References
[1] T. L. Gilbert. *IEEE Transections on Magnetics* **40**, 3443 (2004)
[2] M.-C. Ciornei,J. M. Rubi,J.-E. Wegrowe, *Phyical Reiew* B **83**, 020410 (2011).
[3] K. Neeraj, A. Nilesh, S. Kovalev, D. Polley, N. Zhou Hagström, S. S. P K. Arekapudi, A. Semisalova, K. Lenz, B. Green, J. - C. Deinert, I. Ilyakov M. Chen, M. Bawatna, V. Scalera, M. d'Aquino,   C. Serpico,   O. Hellwig,   J. - E. Wegrowe, M. Gensch, S. Bonetti, *Nature Physics* **17**, 245 (2021).
[4] V. Unikandanunni, M.Rajasekhar,M.Asa, E. Albisetti,D.Petti,R.Bertacco,E.E. Fullerton, S.Bonetti,*Physical Review Letters* **129**, 237201 (2022).
[5]   J. Anders,, C.R.J. Sait, S.A.R. Horsley, *New Journal Physics* **24**, 033020 (2020).
[6] M. Basini, M. Pancaldi. B. Wehinger. M. Udina. T. Tadano, M. C. Hoffmann, A. V. Balatsky, S. Bonetti, *Nature* **628**, 534 (2024).
[7] D. M. Juraschek, M. Fechner, A.V. Balatsky, N.A. Spaldin, *Physical Review Materials* **1**, 014401 (2017).
[8] H. Mustafa, C. Nnokwe, G. Ye, M. Fang, S. Chaudhary, J.- A. Yan, K. Wu, C. J. Cunningham, C. M. Hemesath, A. J. Stollenwerk, P. M. Shand, E.- H. Yang G. A. Fiete, R. He, W. Jin, *ACS Nano* **19**, 11241 (2025).
[9] R. Merlin, *PNAS Nexus* **4**, pgaf002 (2025).
[10] C. S. Davies F.G.N. Fennema, A.Tsukamoto, I.Razdolski, A.V. Kimel, A.Kirilyuk, *Nature* **628**, 540 (2024).

Ultrafast electronic structure engineering in 1*T*-TaS$_2$: Effects of chemical doping and the amplitude mode

J. Jayabalan[1], J. Chen[2], L. Pätzold[3], F. Petocchi[4], F. K. Diekmann[5], N. Najafianpour[1], P. Zhou[1], W. Schnelle[6]
G.-R. Siemann[7], P. Hofmann[7], K. Roßnagel[8], T. Wehling[3], M. Eckstein[3], P. Werner[2]
U. Bovensiepen[1]

[1]*Universität Duisburg-Essen, 47048 Duisburg, Germany*
[2]*University of Fribourg, 1700 Fribourg, Switzerland*
[3]*Universität Hamburg, 20355 Hamburg, Germany*
[4]*University of Geneva, 1211 Geneva, Switzerland*
[5]*Christian-Albrechts-Universität zu Kiel, 24098 Kiel, Germany*
[6]*Max Planck Institute for Chemical Physics of Solids, 01187 Dresden, Germany*
[7]*Aarhus University, 8000 Aarhus C, Denmark*
[8]*Deutsches Elektronen-Synchrotron DESY, 22607 Hamburg, Germany*

In strongly correlated transition metal dichalcogenides, an intricate interplay of polaronic distortions, stacking arrangement, and electronic correlations determines the nature of the insulating state [1,2]. Here, we study the response of the electronic structure to optical excitations to reveal the effect of electron doping in 1*T*-Ta$_{(1-x)}$Mo$_x$S$_2$ on this complex interplay. Transient changes in pristine and electron-doped 1*T*-TaS$_2$ are measured by femtosecond time-resolved photoelectron spectroscopy and compared to theoretical modeling based on non-equilibrium dynamical mean-field theory and density functional theory, see Fig. 1. The fine changes in the oscillatory signal of the charge density wave amplitude mode indicate phase-dependent modifications in the Coulomb interaction and the hopping for the parent compound, see Fig. 1 (a-d). A detailed comparison of experiment and theory, reported in [3], shows that the experimental observation for the parent compound requires to consider coexisting mono- and bilayers on the surface probed by photoemission. The strong changes observed in the experiment for the doped compound indicate a dominant monolayer contribution, see Fig. 1 (e-h).
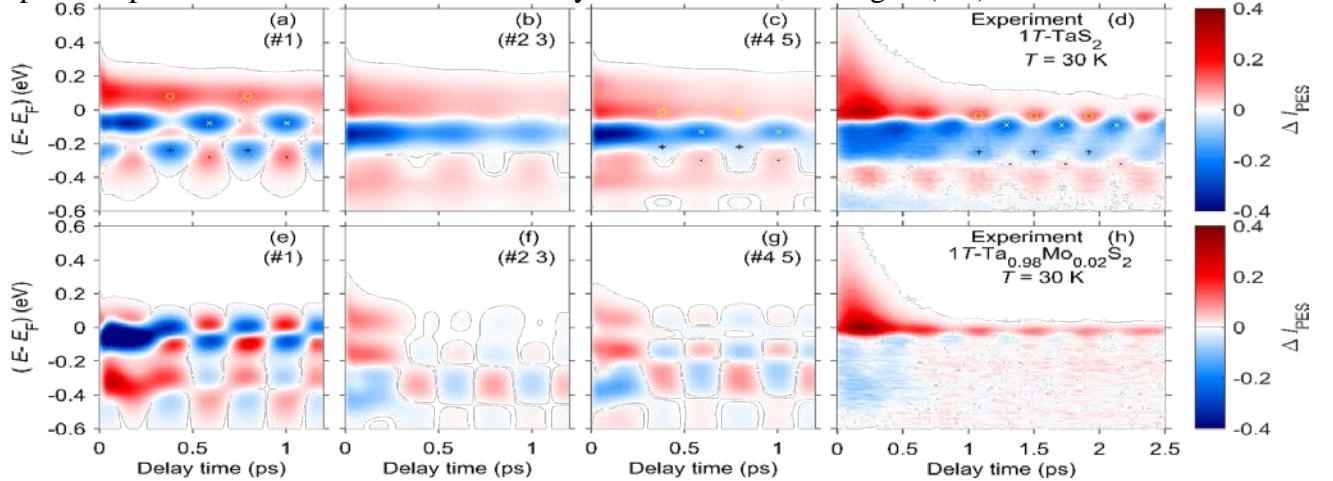
Fig. 1. False color representation of the calculated (a-c, e-g) transient spectral changes *for the monolayer at the surface #1, the 1st bilayer #2 3, and the 2nd bilayer #4 5, respectively. Panels (**d,h**) show the spectral changes observed in photoemission at hv=6 eV . Top and bottom panels contain x = 0 and 0.02, respectively. Figure is reproduced from Ref. 3.*

Our work demonstrates how the combination of time-resolved spectroscopy and advanced theoretical modeling provides insights into the physics of correlated transition metal dichalcogenides. Our analysis of dynamic changes of the electronic structure combined with electronic structure engineering through chemical doping sheds light onto the fundamental electronic interactions governing complex materials with considerable potential for future analysis.

References
[1] B. Sipos, A. F. Kusmartseva, A. Akrap, H. Berger, L. Forró, E. Tutiš, *Nature Materials* **7**, 960 (2008).
[2] H. Yang, S. Kim, M. Chhowalla, Y. H. Lee, *Nature Physics* **13**, 931 (2017).
[3] J. Jayabalan et al., arXiv:2504.19961.

Detecting new quasi-particles in 2D materials

K.S. Burch

Boston College, Chestnut Hill, MA 0246, USA

In materials, new quasi-particles can emerge as collective excitations of ordered states. Detecting these modes and their associated properties is an essential step to understanding how the properties of materials combine to create these new phases. I will discuss why 2D materials are particularly promising in this regard and then explain why Raman is the perfect tool for this effort. I will demonstrate how we have detected fractional excitations in the 2D magnet $RuCl_3$, and then focus on our discovery of a new Higgs Boson from a charge density wave. These modes were always scalar, or just massive particles. I will discuss our discovery an unconventional axial Higgs mode of the charge density wave in the GdTe3. The Axial Higgs mode is revealed using the interference of excitation quantum pathways in Raman scattering.
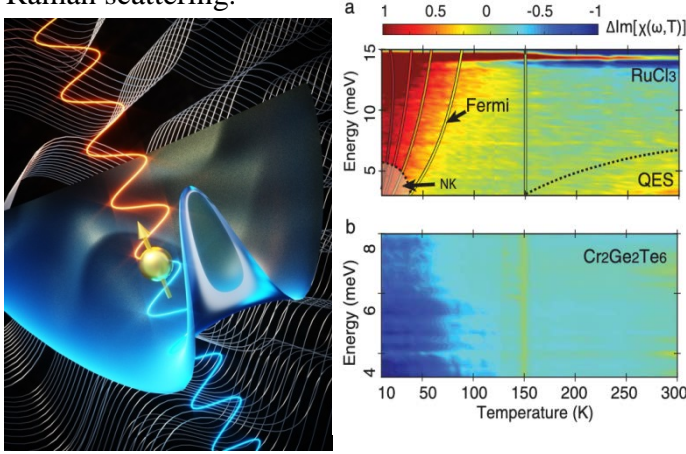
Fig. 1. Left :Quantum interference revealing the axial higgs in Raman [1] Right: a) The temperature and energy dependence of Raman from fractional, fermionic particles in $RuCl_3$ versus the trivial bosonic response of a standard 2d magnet ($Cr_2Ge_2Te_6$)[2].

I will also show direct evidence that this results from a previously hidden orbital order in the system, likely due to the unique quantum geometry combined with the CDW. Time permitting I will discuss our efforts to combine Raman and quantum optics to better probe correlations and entanglement in these systems [1, 2].

References
[1] Y. Wang, I. Petrides, G. McNamara, M. M. Hosen, S. Lei, Y.-C. Wu, J. L Hart, H. Lv, J. Yan, D. Xiao, J. J. Cha, P. Narang, L.M Schoop K.S Burch, *Nature* **606**, 896 (2022).
[2] Y. Wang, G.B. Osterhoudt, Y.Tian, P. Lampen-Kelley, A. Banerjee, T. Goldstein, J. Yan, J. Knolle, H. Ji, R.J. Cava, J. Nasu, Y. Motome, S. E. Nagler D. Mandrus, K. S. Burch, *Npj Quantum Materials* **5,** 14 (2020)

Light-induced Lifshitz transition in High Tc Superconductor $Bi_2Sr_2CaCu_2O_{8+\delta}$

J. Dai1[1], L. Hellbrück[1], M. Puppin[1], A. Crepaldi[1], E. Martino[1], L. Yong[1], A. Magrez[1]
L. Forró[1], M. Grioni[1], F. Carbone[1], S. Benhabib[2]
[1] *École Fédérale de Lausanne (EPFL), CH-1015 Lausanne, Switzerland*
[2]*Université Paris-Saclay, 91400 Orsay, France*

One of the strengths of out-of-equilibrium processes lies in their ability to generate long-lived states with lifetimes exceeding the inverse of the laser system's repetition rate. These states are particularly intriguing due to the presence of long-lived quasiparticles, which enable the emergence of distinctive electronic states that cannot be reached through thermodynamic equilibrium. Commonly described as hidden phases or new states of matter, these phenomena are characterized by photostationary signals observed in steady-state spectra. In this work, we present the observation of a photostationary state in high Tc superconductor cuprates (Bi2212) and its significant influence on the Fermi surface topology.

Fig. 1. *Ultrafast photodoping of Bi2212 by 1.6 eV pulses, promoting a Lifshitz transition*
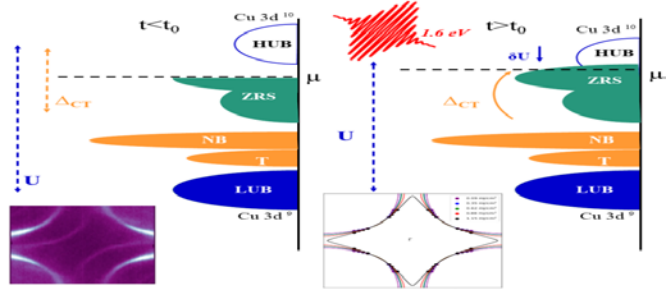
We demonstrate a light-induced metastable Lifshitz transition, enabled by effective photodoping. This photodoping is attributed to cooperative mechanisms, including charge transfer excitations and the renormalization of effective electronic correlations. These findings offer new insights into previously inaccessible electronic states in cuprates, opening promising pathways for further research in photostationary states and hidden phases in strongly correlated system.

Reference
L. Hellbrück, J. Dai, S. Benhabib, M. Puppin, A. Crepaldi, M. Grioni, H. Rønnow, F. Carbone, *International Atomic Energy Agency-IAEA* **1**, (2021).

Giant resonant enhancement of Photoinduced Cooper pairing, far above T_c

S. Chattopadhyay[2], M. H. Michael[3], E. A. Demler[1]
[1]*ETH Zürich, 8093 Zürich, Switzerland*
[2]*Harvard University, Cambridge, MA 02138, USA*
[3] *Max-Planck-Institut für Struktur und Dynamik der Materie, 22761 Hamburg, Germany*

Pump-probe experiments performed on K_3C_{60} have unveiled both optical and transport signatures of metastable photoinduced superconductivity up to room temperature, far above T_c [1, 2, 3, 4]. Recent experiments have uncovered that excitation in the vicinity of 50 meV enables the observation of high temperature photoinduced superconductivity at significantly lower fluences [3]. Inspired by the microscopic insight that such a discovery enables, we develop a mechanism which can explain such a giant resonant enhancement of photoinduced superconductivity. First, within a minimal non-linear Holstein model, we show that resonantly driving optical Raman modes leads to a time-dependent electron-phonon coupling. Such a coupling then modulates the effective electron-electron attraction, with the strongest modulations occurring when the drive is resonant with the phonon frequency. As shown in Fig.1, dynamical modulations of the pairing interactions lead to Floquet-BCS instabilities [5] at temperatures far exceeding equilibrium T_c, as observed in experiments.
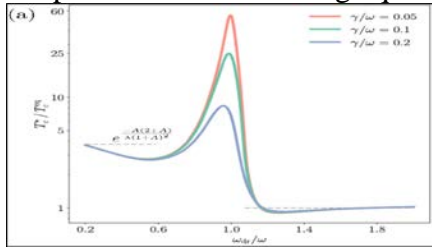
Fig 1. Non - equilibrium critical temperature as a function of frequency exemplifying a giant resonant enhancement in the vicinity of the phonon resonance, evaluated as a function of the phonon Q-factor

We conclude by discussing the implications of our general analysis on the K_3C_{60} experiments specifically, suggesting not only experimental signatures of our mechanism but also features whose plausibility can be verified using *ab initio* methods.

References
[1] M. Mitrano, A. Cantaluppi, D. Nicoletti, S. Kaiser, A. Perucchi, S. Lupi, P. Di Pietro, D. Pontiroli, M Riccò, S.R. Clark, D. Jaksch, A.Cavalleri *Nature* **530**, 461 (2016).
[2] M. Budden, T. Gebert, M. Buzzi, G. Jotzu, E. Wang, T. Matsuyama, G. Meier, Y. Laplace, D. Pontiroli, M. Riccò, F. Schlawin, D. Jaksch A. Cavalleri. *Nature Physics* **17**, 611 (2021).
[3] E. Rowe, B. Yuan, M. Buzzi, G. Jotzu, Y. Zhu, M. Fechner, M. Först, B. Liu, D. Pontiroli, M. Riccò,A. Cavalleri, *Nature Physics* **19**, 1821(2023).
[4] E. Wang, J. Adelinia, M.Chavez-Cervantes, T. Matsuyama, M. Fechner, M. Buzzi, G.Meier , A.Cavalleri, *Nature Communications* **14**, 7233 (2023).
[5] M. Knap, M.Babadi, G.Refael, I.Martin,E. Demler, *Physical Review B, 94*(21), 214504 (2016).

Phonon-driven magnetization rectification and reversal

D. Bustamante[1], D. M. Juraschek[2]
[1]*Boston University, Boston, MA 02215, USA*
[2]*Eindhoven Technische Universiteit Eindhoven, 5612 Eindhoven, the Netherlands*

The coherent control of lattice vibrations via ultrafast light–matter interactions has opened powerful avenues for manipulating quantum materials far from equilibrium. Among the most promising developments is the emerging field of chiral phononics, where circularly polarized phonon modes carry well-defined angular momentum that couples to spin, orbital, and valley degrees of freedom [1–3]. These chiral vibrations can be selectively excited by circularly polarized light, acting as microscopic sources of dynamical magnetic fields on the tesla scale [4–10]. This capability has led to growing recognition that phonons are not merely passive carriers of heat but can serve as active agents in modifying magnetic order on ultrafast timescales. In particular, the angular momentum of chiral phonons can couple to spin systems in magnetic materials through interactions that are both strong and symmetry-dependent [11,12]. Recent theoretical and experimental advances demonstrate that phonon angular momentum can influence magnetization, induce nonthermal switching, and even generate quasistatic magnetic moments in nominally nonmagnetic or antiferromagnetic materials [13,14]. These findings suggest that lattice-driven spin dynamics may offer a low-dissipation, high-speed alternative to conventional electronic control mechanisms. In this work, we present theoretical predictions of two related mechanisms by which coherently driven chiral phonons can induce and control magnetization in different classes of magnetic materials:*1. Nonlinear magnonic rectification: light-induced quasistatic magnetization.* We introduce a fundamental process whereby an oscillating spin precession is rectified into a quasistatic magnetization component via nonlinear coupling with driven magnon modes in antiferromagnetic materials. Specifically, the coherent excitation of infrared-active chiral phonon modes transiently cants spins, generating an effective magnetic field that rectifies spin dynamics. This mechanism—termed *nonlinear magnonic rectification*—is broadly applicable across antiferromagnets hosting chiral phonon modes. It enables light-induced weak ferromagnetism and the creation of dynamic, nonequilibrium spin textures inaccessible under equilibrium conditions. *2. Phonon-induced magnetization reversal in two-dimensional ferromagnets*. Extending the concept of magnonic rectification to ferromagnets, we demonstrate that phonon-driven effective magnetic fields can drive permanent magnetization reversal. Focusing on two-dimensional chromium-based ferromagnets such as CrI_3, $CrGeTe_3$, and $CrCl_3$, we investigate reversal pathways mediated by damping-induced switching and precessional dynamics.
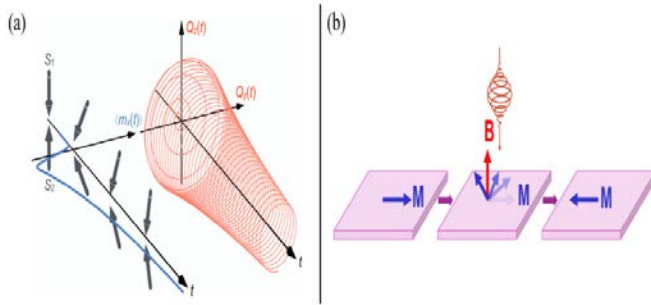
Fig. 1 Phonon-Driven Magnetization Rectification and Reversal.(a) Magnonic rectification by chiral phonons. Time evolution of the two orthogonal components of a laser-excited chiral phonon mode, $Q_\perp(t)$ and $Q_\parallel(t)$, and the corresponding average magnetization component $\langle m(t) \rangle$ of a coupled magnon mode. The transient tilting of the spin precession axis results in a light-induced canted antiferromagnetic state and the emergence of a quasistatic magnetization. (b) Phonon-induced magnetization reversal. In layered ferromagnetic crystals, applying the pulsed effective magnetic field of a chiral phonon mode perpendicular to the initial magnetization enables precessional switching. This mechanism may drive robust, ultrafast reversal of magnetization.

Our results show that circularly polarized phonon driving can achieve robust, ultrafast magnetization reversal within nanoseconds, offering a purely phononic route to nonthermal magnetic control.

References
[1] H. Zhu, J. Yi, M. Y. Li, J . Xiao, L. Zhang, C. W. Yang, R. A. Kaindl, L. J. Li, Y. Wang, X. Zhang, *Science* **359**, 579 (2018).
[2] H. Ueda, M. García-Fernández, S. Agrestini, C. P. Romao, J. van den Brink, N. A. Spaldin, K.-J. Zhou, U. Staub, *Nature* **618**, 946 (2023)
[3] D. M. Juraschek, N. A. Spaldin, *Physical Review Materials* **3**, 064405 (2019).
[4] D. M. Juraschek, M. Fechner, A. V. Balatsky, N. A. Spaldin, *Physical Review Materials* **1**, 014401 (2017).
[5] D. M. Juraschek, T. Neuman, P. Narang, *Physical Review Research* **4**, 013129 (2022).
[6] S. Chaudhary, D. M. Juraschek, M. Rodriguez-Vega, G. A. Fiete, *Physical Review* B **110**, 094401 (2024).
[7] T. Nova, A. Cartella, A.Cantaluppi, M Först, D. Bossini, R. V.Mikhaylovskiv, A V.Kimel, R.Merlin, A.CavallerI, *Nature Physics* **13**, 132 (2017)
[8] J. Luo, T. Lin, J. Z. Zhang, X.Chen, E. R. Blackert, R. Xu , B. I. Yakobson, H. Zhu , *Science* **382**, 698 (2023).
[9] M. Basini, M. Pancaldi, B. Wehinger,M. Pancaldi, B. Wehinger, M. Udina, V. Unikandanunni, T. Tadano, M. C. Hoffmann, A. V. Balatsky S. Bonetti, *Nature* **628**, 534 (2024).
[10] C. S. Davies, F. G. N. Fennema, A. Tsuka moto,,I. Razdolski, A. V. Kimel, A. Kirilyuk, *Nature* **628**, 540 (2024).
[11] B. Ma, Z. D. Wang,G. V. Chen, *Physical Review Letters* **133**, 246604 (2024).
[12] S. G. Jeong, J. Kim, A. Seo, S. Park, H. Y. Jeong, Y. - M. Kim, V. Lauter, T. Egami, J.H. Han, W.S. Choi, *Science Advances* **8**, 4005 (2022).
[13] T. Kahana, D. A. Bustamante Lopez, D. M. Juraschek, *Sciience Advances* **10**, 0722 (2024).
[14] C. Paiva, M. Fechner, D. M. Juraschek, *arXiv:2404.16234* (2024).

Indirect excitons in heterostructures

L.V. Butov

University of California San Diego, La Jolla, CA 92093

Spatially indirect excitons (IXs), also known as interlayer excitons, are formed by electrons and holes confined in separated layers in a semiconductor heterostructure (HS). IX lifetimes are orders of magnitude longer than lifetimes of spatially direct excitons (DXs). Due to their long lifetimes, IXs can thermalize below the temperature of quantum degeneracy that gives an opportunity to create quantum excitonic states. We present recent results in quantum IX systems: the Cooper-pair-like excitons [1] and the excitonic Bose polarons [2,3] in GaAs/AlGaAs HS and the long-range IX transport [4] and the IX mediated long-range spin transport [5] in MoSe$_2$/WSe$_2$ HS. *The Cooper-pair-like excitons* [1]. In neutral dense electron-hole systems at low temperatures, theory predicted Cooper-pair-like excitons at the Fermi edge. Optical excitations create electron-hole systems with the density controlled via the excitation power. The separation of electron and hole layers enables the realization of a dense and cold electron-hole system. We found a strong enhancement of photoluminescence (PL) intensity at the Fermi edge of the neutral dense ultracold electron-hole system that demonstrates the emergence of Cooper-pair-like excitons at the Fermi edge. We found a crossover from the hydrogen-like excitons to the Cooper-pair-like excitons with increasing density, consistent with the theoretical prediction of a smooth transition. *The excitonic Bose-polarons* [2,3]. Bose polarons are mobile impurities dressed by excitations of a surrounding degenerate Bose gas. We found that Bose polarons are formed by DXs immersed in Bose gases of IXs in electron-hole bilayers. We detected both attractive and repulsive Bose polarons and observed an enhancement of the energy splitting between attractive and repulsive Bose polarons with increasing IX density, in agreement with our theoretical calculations [2]. We found the Mott transition and measured the Mott transition parameter $n_M^{1/2}a_B$ (n_M is the density of the Mott transition, a_B the Bohr radius of the pair) in 2D excitonic Bose polarons [3]. For the Mott transition in polarons, the polaron states vanish with increasing density of the surrounding gas.
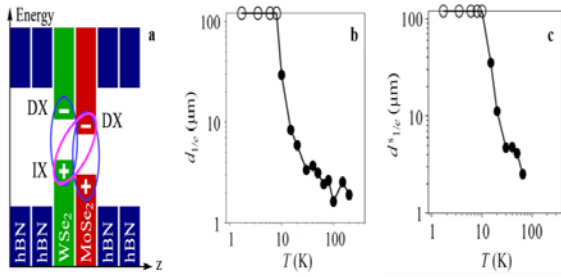
Fig. 1. a. *Energy band diagram of a heterostructure (HS) with separated electron and hole layers. Indirect excitons (IXs), also known as interlayer excitons, are formed by electrons and holes confined in separated layers. Direct excitons (DXs) are formed by electrons and holes confined in the same layer. **b**. The IX transport 1/e decay distance $d_{1/e}$ vs. temperature in MoSe$_2$/WSe$_2$ HS. The data with the fit indicating diverging $d_{1/e}$ are presented by points on the edge. The IX long-range transport vanishes above ~ 10 K [4]. **c**. The 1/e decay distance $d^s_{1/e}$ of IX mediated spin density transport vs. temperature in MoSe$_2$/WSe$_2$ HS. The data with the fit indicating diverging $d^s_{1/e}$ are presented by points on the edge. The IX mediated long-range spin transport vanishes above ~ 10 K [5].*

The long-range IX transport in TMD HS [4]. Van der Waals HS composed of atomically thin layers of transition-metal dichalcogenides (TMD) offer the opportunity to explore IXs in moiré superlattices. Diffusive IX transport in TMD HS is characterized by 1/e decay distances up to ~ 4 μm, as measured in earlier studies. We found the IX long-range transport with 1/e decay distances reaching and exceeding 100 μm in a MoSe$_2$/WSe$_2$ HS. The IX long-range transport vanishes at temperatures above ~ 10 K (Fig. 1b). The IX transport is in qualitative agreement with the Bose-Hubbard theory prediction for superfluid and insulating phases in periodic potentials of moiré superlattices. We measured transport kinetics of IXs in MoSe$_2$/WSe$_2$ HS in the regime of the IX long-range transport. *The IX mediated long-range spin transport in TMD HS* [5]. The spin relaxation caused by scattering of the particles carrying the spin, limits the spin transport. Diffusive IX mediated spin transport in TMD HS is characterized by 1/e decay distances up to ~ 4 μm, as measured in earlier studies. Due to the coupling of the spin and valley indices in TMD HS, the spin transport is coupled to the valley transport, therefore, for simplicity, we use the term 'spin' also for 'spin-valley'. We found the IX mediated long-distance spin transport with the decay distances reaching and exceeding 100 μm (Fig. 1c). The emergence of long-distance spin transport is observed at the densities and temperatures where the IX transport decay distances and, in turn, scattering times are strongly enhanced. The suppression of IX scattering suppresses the spin relaxation and enables long-distance spin transport. This mechanism of protection against spin relaxation makes IXs a platform for the realization of long-distance decay-less spin transport.

References
[1] D. J. Choksy, E.A. Szwed, L.V. Butov, K.W. Baldwin, L.N. Pfeiffer, *Nat. Phys.* **19**, 1275 (2023).
[2] E. A. Szwed, B. Vermilyea, D. J. Choksy, Z. Zhou, M. M. Fogler, L. V.Butov, D.K. Efimkin, K.W. Baldwin, L.N. Pfeiffer, *Nano Letters* **24** 13219(2024)
[3] E. A. Szwed, B. Vermilyea, D. J. Choksy, Zhiwen Zhou, M. M. Fogler, L. V. Butov, K. W. Baldwin, L.N. Pfeiffer, *arXiv*:2504.07227 (2025)
[4] L. H. Fowler-Gerace, Zhiwen Zhou, E.A. Szwed, D.J. Choksy, L.V. Butov, *Nature Photonics* **18**, 823 (2024).
[5] Zhiwen Zhou, E. A. Szwed, D. J. Choksy, L. H. Fowler-Gerace, L.V. Butov, *Nature Communications* **15**, 9454 (2024)

Coherent dynamic in model 2D structures

F. Schäfer[1], H. Mittenzwey[2], M., O. Voigt[2], L, Greten[2], D. Anders[1], I. Müller[1], F. Dobener[1], M. Cuccu[3]
C. Fuchs[4], K. Watanabe[5], T. Taniguchi[5], K. Volz[4], A. Chernikov[3], A. Knorr[2], S. Chatterjee[1]

[1]*Justus-Liebig Universität Giessen, 35392 Giessen, Germany*
[2]*Technische Universität Berlin, 10623 Berlin, Germany*
[3]*Technische Universität Dresden, 01062 Dresden, Germany*
[4]*Philipps-Universität Marburg, 35032 Marburg, Germany*
[5]*National Institute for Materials Science, Tsukuba 305-0044, Japan*

Rabi splitting is a fundamental concept in light matter interaction. It occurs if photons interact intensely enough with electronic transitions and form new quantum states. In model two-level systems the absorption spectrum splits into (two) different bands, an effect sometimes amongst others referred to as to as Autler-Townes effect, Stark splitting or Rabi splitting. The magnitude of the splitting depends on the magnitude of the transition dipole moment and strength of the external driving field. This phenomenon was first observed in gas molecules. It is more challenging to observe in condensed matter due to its immanent many-body nature. Intrinsic effects like carrier-carrier scattering or structural strain as well as defects and impurities render the observation of Rabi splitting challenging. We examine Rabi splitting under cryogenic conditions in prototypical two-dimensional structures: a TMDC monolayers and (Ga,In)As quantum wells. We compare exciton binding energies, to the Rabi energies in these systems and apply a microscopic many-body theory to identify the underlying mechanisms. The TMDC monolayer has exciton binding energies much larger than its Rabi energy. In contrast, the exciton and Rabi energies in quantum wells are about comparable. The experimental setup uses a 850 fs pump pulses paired with a short, broad-spectrum white-light supercontinuum probe, which enables detailed observations of the dynamics. We capture the complete temporal evolution of excitonic resonances by varying the delay between pump and probe pulses. Fig.1 shows exemplary experimental data (left) and the results from a corresponding microscopic calculation.
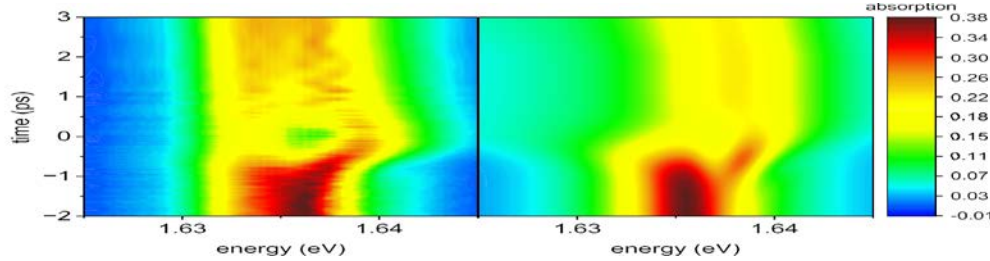
Fig. 1. Left*:2D false-color plots of the nonlinear absorption of $MoSe_2$ as function of time delay for an excitation energy density of 16 $\mu J/cm^2$* **Right***: corresponding simulated results.*

The theoretical model utilizes the exciton Bloch equations of motion, accounting for optical field-induced blocking, Coulomb-mediated dephasing related to excitation, excitation-induced energy shifts, incoherent population formation due to optical interactions, and exciton-phonon coupling [3].We identify three distinct experimental features corresponding to different ratios of Rabi energy to exciton binding energy, explicated by our microscopic theory: Rabi oscillations, coherent gain, and spectral shifts and splitting. In the quantum wells (QWs), the Rabi to exciton binding energy ratio is approximately 10^{-1}, which is significantly larger compared to a 10^{-3} ratio in the transition metal dichalcogenide (TMDC) samples. Consequently, Coulomb many-body effects dominate the TMDC features, whereas light-matter interactions predominantly influence the QW characteristics. In (Ga,In)As QWs, the observed Rabi oscillations are attributed to changes in coherent and incoherent exciton densities, driven by Coulomb-enhanced blocking and the formation of incoherent exciton populations. The monolayer $MoSe_2$, on the other hand, lacks temporal Rabi oscillations due to the presence of spin-unlike biexcitons and transitions from excitons to biexcitons, which accelerate coherence decay. Our findings conclude that (Ga,In)As MQWs behave like a modified two-level system due to their relatively weak Coulomb interactions, while monolayer $MoSe_2$ displays sublinear splitting behavior attributable to spin-unlike exciton-to-biexciton transitions. This underscores the pronounced influence of Coulomb correlations on the optical properties of these materials. The observed narrowing of linewidths associated with splitting peaks further substantiates these interpretations.

References
[1] F. Katsch, M. Selig, A. Knorr, *Physical Review Letters* **124**, 257402 (2020).
[2] D. Anders, F. Dobener, F. Schäfer, S. Chatterjee, M. Stein, *Physical Review Letters* **132**, 106901 (2024).
[3] F. Katsch, M. Selig, A. Carmele, A. Knorr, *Physica Status Solidi* b **255**, 1800185 (2018).

Probe of topological materials using terahertz emission spectroscopy

E. E. M. Chia

Nanyang Technological University, Singapore 637371, Singapore

In this talk I will explain how terahertz (THz) emission spectroscopy has been used as a probe of the interesting properties of some topological materials. In the ferromagnetic (FM)/topological insulator (TI) bilayer Co/Bi_2Se_3, we observe a giant THz emission that is predominantly spin-mediated and dominated by the topological surface states, and identify a 0.12-picosecond timescale that sets a technological speed limit of spin-to-charge conversion processes in TIs [1]. Replacing Bi_2Se_3 by a monolayer semiconductor MoS_2, in Co/MoS_2, we demonstrate a giant spin injection from a ferromagnet into a semiconductor that is orders of magnitude larger than state-of-the-art, that is a consequence of the strongly out-of-equilibrium character of the injected spins, thus overcoming the crippling problem of impedance mismatch [2]. A follow-up question is: can this spintronic THz emitter architecture be integrated with silicon? Our data shows the formation of silicide layer at the Co/Si interface that also shows large spin-to-charge conversion [3]. In thin polycrystalline films of the centrosymmetric Dirac semimetal $PtSe_2$, we observe a giant and highly tunable THz emission that is rapidly turned on at oblique incidence, locked to both the in-plane photon momentum and polarization state of the incident pump beam, and whose polarization-state-locked THz emission is strong evidence of the central role played by quantum geometry [4]. A follow-up question is: can we tune the THz emission of this (or similar) Dirac semimetal, by electrical means, via the control its quantum geometry? The answer is yes. We first demonstrate piezoelectric strain control of THz emission in the simpler PMN-PT/NiFe/Pt stack [5].
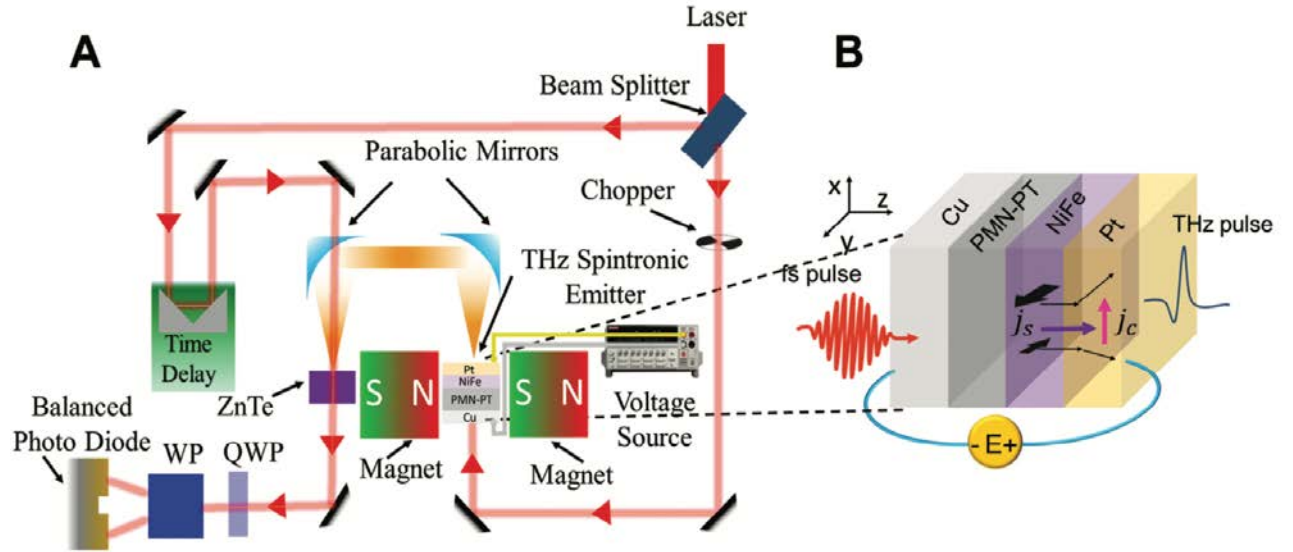
Fig. 1 *(A) Schematic of the setup for measurement and generation of THz radiation. (B) Schematic of the artificial multiferroic spintronic emitter with piezoelectric strain control [6].*

Moving on to $PMN-PT/NiFe/PtTe_2$, we electrically modulate the Fermi level and Berry curvature, thereby controlling its spin Hall conductivity and yielded a 20% modulation of the THz emission amplitude, performed under a constant magnetic field without field cycling-permanent magnetization [6].

References
[1] X. Wang, L. Cheng, D. Zhu, Y. Wu, M. Chen, Y. Wang, D. Zhao, C. B. Boothroyd, Y.M. Lam, J.-X. Zhu, M. Battiato, J. C. W. Song, H. Yang E. E. M. Chia, *Advanced Materials* **30,** 1802356 (2018).
[2] L. Cheng, X. Wang, W. Yang, J. Chai, M. Yang, M. Chen, Y. Wu, X. Chen, D. Chi, K.E. Johnson Goh, J.-X. Zhu, H. Sun, S. Wang, J. C.W. Song M. Battiato, H. Yang, E. E. M. Chia, *Nature Physics* **15,** 347 (2019).
[3] J. Liu, Y. Yang, K. Lee, R. Sharma, H. Yang, M. Battiato, E. E. M. Chia. *Physical Review Applied* **18,** 034056 (2022).
[4] L. Cheng, Y. Xiong, L. Kang, Q. Chang, M. Chen, J. Qi, H. Yang, Z. Liu, J. C. W. Song, E. E. M. Chia, *Science Advances* **9,** eadd7856 (2023).
[5] A. Chaurasiya, Z. Li, R. Medwal, S. Gupta, J R. Mohan, Y. Fukuma, H. Asada, E. E.M. Chia, R. S. Rawat, *Advanced Optical Materials* **10** 2201929 (2022).
[6] Z. Li, D. Yang, F. Wang, Y. Yang, Y. Guo, D. Bao, T. Yin, C. S. Tang, T. Salim, L. Xi, C. Boothroyd, Y. M. Lam, B. Peng, M. Battiato, H. Yang E. E. M. Chia. *Nano Letters* (under review).

On the light-induced rotated CDW phase in Tri-telluride compounds

F. Cilento

Elettra – Sincrotrone Trieste, 34149 Trieste, Italy

The RTe_3 (R=rare earth) tri-tellurides charge-density-wave materials display a rich phenomenology of charge-density wave (CDW) states, governed by the small ($\approx$0.3%) anisotropy of the in-plane lattice constants [1]. All RTe_3 systems display at least one (high-temperature) unidirectional CDW state, aligned along the in-plane c axis. Surprisingly, recent experiments showed that an orthogonal (rotated) CDW state, aligned along the in-plane a axis, can be light-induced in some family members [2,3]. Importantly, this rotated CDW state differs from the equilibrium low-temperature a-axis CDW state. On a complementary side, very recently it has been proved that the 1D CDW can rotate after the application of suitable strain, that reverses the relative magnitude of the in-plane a & c lattice constants [4,5]. Here I will report on the results from polarization-resolved broadband time resolved optical spectroscopy (TR-OS) experiments performed on the compound $LaTe_3$, that indicate the formation of a light-induced symmetry breaking CDW state. Thanks to the high time-resolution of TR-OS experiments, as compared to that presently attainable in time-resolved UED (Ultrafast Electron Diffraction) experiments [2], the early stages of formation of this light induced transient CDW state could be disclosed. Moreover, the amplitude mode of the light-induced rotated CDW state has been measured for the first time. The results from polarized TR-OS, as reported in Fig. 1 [6], show that the time-resolved signal along the a & c crystal axes display markedly different decay times, although the coherent response associated to the AM of the CDW shows the same frequency.
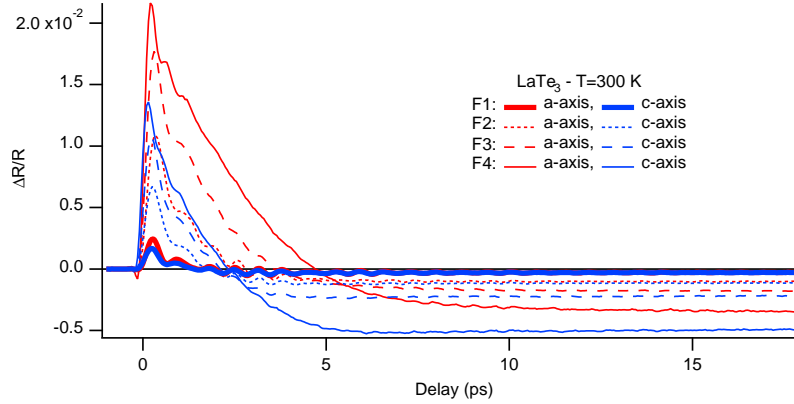
Fig. 1. Time-Resolved Reflectivity on $LaTe_3$ performed at T=300 K. *Curves at four fluences are shown, with F1<F2<F3<F4. The $\Delta R/R$ signal has been acquired on both in-plane crystal axes, **a** and **c**. The signal is very similar along the two directions at low fluence, showing clearly the excitation of the AM at $\approx$2.2 THz. Upon increasing the fluence, the signal starts to become different along the two axes, and displays markedly different relaxation timescales, much slower for the a-axis.*

We also used TR-XPS as a complementary probe to study the precursor states of the rotated CDW phase, and propose, as a possible origin of this state, an anisotropic lattice expansion. In conclusion, our experiments disclose a complex phenomenology of the rotated CDW phase in RTe_3 compounds, where a well-formed transient CDW state emerges after photoexcitation. Future experiments will aim at extending this protocol to several RTe_3 family members, in order to disclose the phase-diagram of the light-induced rotated CDW state. Moreover, a key tool to reveal the microscopic origin of the rotated CDW phase will be the application of uniaxial strain, to tune selectively the ratio among the a & c lattice constants and verify to what extent the rotated CDW state can be achieved.

References
[1]   K. Yumigeta, Y. Qin, H. Li, M. Blei, Y. Attarde, C. Kopas, S. Tongay, *Advanced Science* **8**, 2004762 (2021)
[2]   A. Kogar, A. Zong, P. E. Dolgirev, X. Shen, J. Straquadine, Y.- Q. Bie, X. Wang, T. Rohwer, I.-C. Tung, Y. Yang, R. Li, J. Yang, S. Weathersby S. Park, M. E. Kozina. E. J. Sie. H. Wen. P. Jarillo-Herrero. I. R. Fisher. X. Wang. N. Gedik,: *Nature Physics* **16**, 159 (2020)
[3]   F. Zhou, J. Williams, S. Sun, C.D. Malliakas, M. G. Kanatzidis, A.F. Kemper, C.-Y. Ruan, *Nature Communications* **12**, 566 (2021)
[4]   A. Gallo-Frantz, A. A. Sinchenko, D. Ghoneim, L. Ortega, P. Godard, P.- O. Renault, P. Grigoriev, A. Hadj - Azzem, P. Monceau D. D. Thiaudiere, E. Bellec, V. L. R. Jacques, D. Le Bolloc'h, *arXiv*:2306.15712 (2023).
[5]   A. G. Singh, M. D. Bachmann , J. J. Sanchez, A. Pandey , A. Kapitulnik, J. W. Kim , P. J. Ryan, S.A. Kivelson, I. R. Fisher, *Science Advances* **10** eadk3321 (2024)
[6]   F. Silento *to be submitted* (2025)

Ultrafast modulation of proximity-enhanced functionalities in Hybrid nano-scale systems

M. Cinchetti[1], M.Benini[1], U.Parlak[1], S.Bork[1], J.Strohsack[2], R. Leven[1], D. Gutnikov[1], F. Mertens[1], E. Zhukov[1]
R.K.Rakshit[3], I.Bergenti[3], A. Droghetti[4], T.Mertelj[3], V.A. Dediu[3]
[1]TU Dortmund University, 44227 Dortmund, Germany
[2]Jozef Stefan Institute, 1000 Ljubljana, Slovenia
[3]ISMN-CNR, 40129 Bologna, Italy
[4]Universitá Ca' Foscari Venezia, 30123 Venezia, Italy

In the pursuit of advancing quantum information and communication technology (qICT) through smaller and faster components, a key research focus is the development of quantum- based devices with new, actively controllable functionalities. In this work, we present a novel strategy for modulating the magnetic properties of materials by harnessing proximity effects that can be dynamically controlled using light. Our results demonstrates that not only the modulation is strong but also localized at the nanoscale, as it originates from complex quantum behaviors. Moreover, we propose that the underlying physics is universal, potentially allowing for the optical tuning of any proximity-induced physical property, beyond just magnetic ones. We demonstrate this universal concept using hybrid nanoscale systems composed of molecules in close proximity to metallic ferromagnetic surfaces, where proximity effects are extremely strong. In particular, we have chosen the metallic ferromagnet cobalt interfaced with C60 molecules as model system [1,2], schematically depicted in Fig. 1.
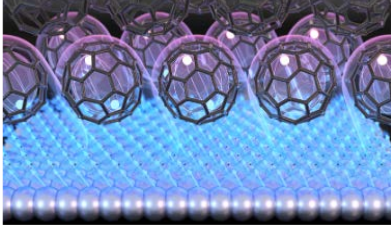
Fig. 1. *Schematic representation of the cobalt/C60 system used in our experiments to demonstrate the possibility of optically tuning proximity-enhanced magnetic properties.*

Our findings show that by inducing excitons in C60 molecules with resonant ultrashort light pulses [3], we can significantly modify the interaction between a thin cobalt film and the C60 molecules deposited on it. This results in a substantial 60% change in the spin precession frequency, detected in a specifically designed time-resolved magneto-optical Kerr effect (trMOKE) experiment [4]. This physical observable is linked to the anisotropy field—an essential parameter for technological applications, demonstrating that light can be used as an active stimulus for tuning magnetic properties at the nanoscale.

References
[1] M.Benini, A. Shumilin, R. Rakshit, A.Sahoo, A. Halder, A. Droghetti, F. Cugini, M.Solzi, D.Bisero, P. Graziosi, A. Riminucci, I. Bergenti, M. Singh L. Gnoli, S. Sanna,T.Mertelj,V.Kabanov, S. Sanvito, V. Dediu, *Nature Portfolio*, Preprint: *https://doi.org/10.21203/rs.3.rs-4540787/v1* (2025).
[2] J. Strohsack, A. Shumilin, H. Zhao, G. Jecl, V.V. Kabanov, M. Benini, R. Rakshit, V.A. Dediu, M. Rogers, S. Ozdemir, O.Cespedes, U. Parlak M.Cinchetti, T. Mertelj *arXiv:2412.08677* (2024).
[3] B. Stadtmüller, S. Emmerich, D. Jungkenn, N. Haag, M. Rollinger, S. Eich, M. Maniraj, M. Aeschlimann, M. Cinchetti, S. Mathias, *Nature Communications* **10**, 1470 (2019).
[4] F. Mertens, M. Terschanski,D. Mönkebüscher,S. Ponzoni,D. Bossini,M. Cinchetti, *Review of Sciientific Instruments* **91**. 113001 (2020).
* *Acknoledgment:* we acknowledge support by the EC H2020 programme under grant agreement No. 965046, FET-Open project INTERFAST (Gated interfaces for fast information processing).

Temperature dependence of conductivity and mobility and Electron-phonon coupling strength in graphene determined from Electron relaxation rates

I. Chatzakis, S. Sharma
Texas Tech University, 79409 Lubbock, Texas U.S.A

We report the determination of the electron-phonon coupling strength extracted from the relaxation rates of the electrons' energy using ultrafast pump-probe spectroscopy. The energy transferred from electrons to the lattice depends on the coupling strength between the two subsystems and the temperatures of electrons and lattice, as described by the Two-Temperature Model. Allen's theory related the relaxation time to electronic temperature T_e and the coupling strength $\lambda\langle\omega^n\rangle$ (the second moment of the Eliashberg function). We found that the dimensionless parameter $\lambda= (1.36 \pm 0.13) \times 10^{-2}$, which agrees with
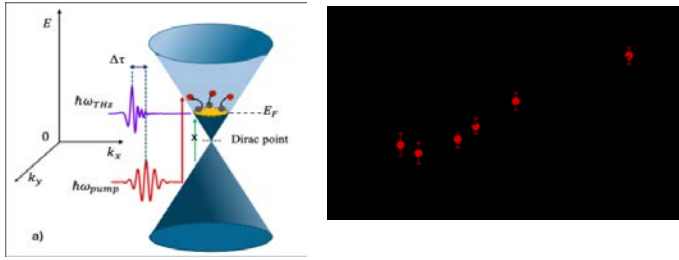
Fig. 1. Left : *The excitation scheme*. *The green arrow depicts a forbitten transition due to the Pauli principle as the THz photon energy is lower $\hbar\omega_{THz} < 2E_F$; **Right: The relaxation time** extracted from the fit of the transient transmission plotted as a function of the maximum pump-induced temperature of electrons (submitted Chatzakis et.al., APL 2025).*

previous studies [1], and the deformation potential of the E_g phonon mode $6.4\ eV/\text{Å}$, which is consistent with the value obtained in previous works [2,3,4].

References
[1] E. Pomarico, M. Mitrano, H. Bromberger, M. A Sentef, A. Al-Temimy, C. Coletti, A. Stöhr, S. Link, U. Starke, C.Cacho, R. Chapman E. Springate , A. Cavalleri, I. Gierz, *Physical Review* B **95,** 024304 (2017).
[2] A. H. Castro Neto, F. Guinea, *Physical Review* B **75**, 045404 (2007).
[3] M. Lazzeri, S. Piscanec, F. Mauri, A.C. Ferrari, J. Robertson, *Physical Review* **73**, 155426 (2006).
[4] S. Pisana, M. Lazzeri, C. Casiraghi, K.S. Novoselov, A.K. Geim, A.C. Ferrari, F. Mauri, *Nature Materials* **6**, 198 (2007).

Probing light and matter dynamics with ultrafast Transmission electron microscopy

L. Ciorciaro, J. Kuttruff, D. Kazenwadel, J. Holder, M. Mattes, N. Neathery, P. Baum
Universität Konstanz, 78457 Konstanz, Germany

Technological advances in the generation of ultrashort laser pulses have pushed the limit of the experimentally achievable temporal resolution to ever-smaller time scales. These improvements have been initially transferred to electron beams in the form of ultrafast electron diffraction, where optical excitation pulses are combined with a spatially extended pulsed electron-beam probe. Such experiments have been used, among other things, to study structural dynamics in solids [1]. In ultrafast transmission electron microscopy (UTEM), we bring together the temporal resolution of optical systems and the spatial resolution of a fully-fledged electron microscope, resulting in a device capable of measuring dynamics on attosecond time and nanometer length scales. Due to the versatility of the electron microscope, a variety of systems can be studied, ranging for example from magnetization dynamics and structural transitions in solids to the propagation of electromagnetic modes in nanostructured devices.In this talk, I will give an overview of selected research topics in our group. In the first part, I will review the interactions of electron beams with terahertz and optical fields and the different techniques employed in ultrafast electron microscopy that make use of these interactions. I will show how terahertz pulses are used to compress electron pulses to < 20 fs duration and as a diagnostic tool in optical streaking [Fig. 1a)] [2-4]. I will explain how electron pulse trains generated by an optical field are used to image surface plasmon-polaritons propagating in a nanostructure [Fig. 1b)] [5].
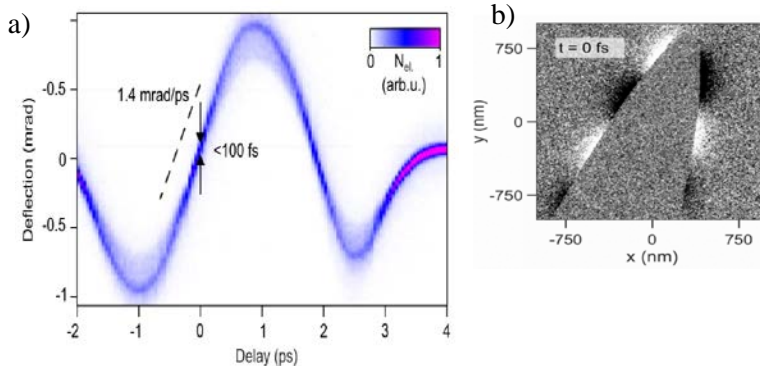
Fig. 1: a) *Measurement of the electron pulse duration via THz streaking [4]. The electron beam is deflected by the electric field of a THz pulse. The slope of the trace serves as calibration to calculate the electron pulse duration from its angular width on the detector.* **b)** *Energy-filtered attosecond TEM image showing the instantaneous longitudinal electric field of the surface plasmon-polariton on a tungsten needle. [5]*

In the second part, I will show examples of experiments on the ultrafast dynamics in solid state systems and finally discuss our recent results on selected topics [6].

References
[1] D.-S. Yang, P. Baum, A. H. Zewail, *Structural Dynamics* **3**, 034304 (2016),
[2] C. Kealhofer, W. Schneider, D. Ehberger, A. Ryabov, F. Krausz, P. Baum, *Science* **352**, 429 (2016),
[3] J. Kuttruff, D. Nabben, A.-C. Zimmermann, A. Ryabov, P. Baum, *Science Advances* **10**, eadl6543 (2024).
[4] M. Mattes, M. Vokov, P. Baum, *Nature Communications* **15**, 1743 (2024),
[5] D. Nabben, J. Kuttruff, L. Stolz, A. Ryabov, P. Baum, *Nature* **619**, 63 (2023),
[6] J. Holder, D. Kazenwadel, P. Nielaba, P. Baum, *Physical Review Research* **5**, 043272 (2023).

Quantum-geometric and cavity quantum-electrodynamical approaches for Controlling matter with light

M. Claassen

University of Pennsylvania, Philadelphia, PA 19104, USA

The coherent manipulation of macroscopic quantum systems with light is a frontier for accessing new materials properties, ranging from the ultrafast control of quantum states with strong fields to harnessing the strong-coupling regime of interacting electrons and photons confined in an optical cavity. In this talk, I will provide a perspective on achieving and probing strong interactions of light and matter, with potential applications ranging from steering electronic orders with ultrafast THz pulses to generating entangled photon pair sources from cavity-confined quantum materials. I will first show that the low-frequency optical conductivity in correlated metals generically acquires a quantum geometric contribution that originates from the structure of Bloch wave functions at the Fermi surface, leading to sharply enhanced THz absorption near a topological band inversion [1]. This effect arises from integrating out Coulomb-scattering-assisted interband processes, demonstrating how quantum geometry and electronic interactions can enrich Fermi liquid physics and unlock novel optical processes. I will argue that such quantum geometric interactions of light and matter can enable the coupling of competing electronic orders with ultrafast light pulses [2] and provide a route towards the strong coupling regime for electrons and photons by placing materials inside optical cavities. I will then discuss how cavity-photon-induced changes in materials can lead to pronounced antibunching of light transmitted through the cavity, observable via the second-order photon coherence $g^{(2)}(t)$ that measures the statistical correlation of photon pairs.
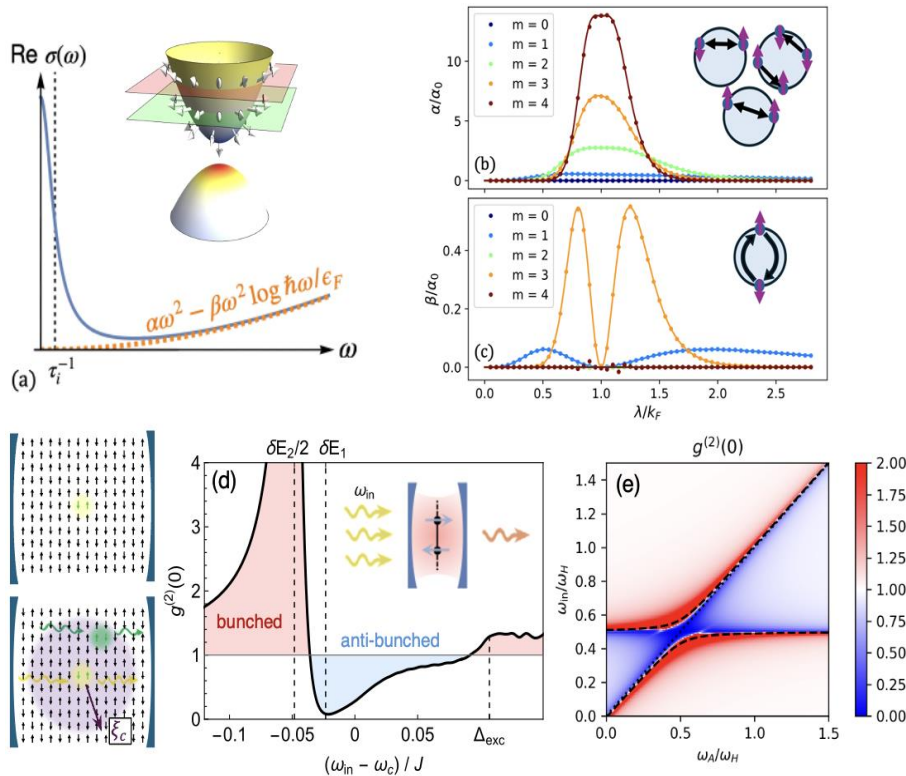
Fig. 1. (a) Quantum-geometric optical conductivity of correlated metals in two dimensions near a topological band inversion. Inset depicts the orbital pseudospin texture at the Fermi surface $k=k_F$ (red) and at momenta $k=\lambda$ of maximal orbital admixture (green). (b) Power-law and (c) logarithmic scaling contributions for the low-frequency incoherent background in clean correlated metals, as a function of angular momentum m of the band inversion, showing strong light matter coupling as a function of the change of Bloch wave functions at the Fermi surface. (d) Antibunching of photons from a cavity with an embedded quantum magnet as a function of the detuning of a weak classical input field ω_{in} [Left: photon nonlinearity due to magnetic fluctuations near a quantum critical point can realize a many-body photon blockade regime]. (e) Second-order photon coherence $g^{(2)}(t)$ at coincidence for Higgs polaritons in superconductors integrated with a THz cavity.

Near a quantum critical point [3] or at ultrastrong coupling [4], such systems can realize a many-body photon blockade regime, enabling the generation of single photons or Einstein-Podolsky-Rosen pairs via leveraging strong matter fluctuations.

References

[1] D. P. Carmichael, M. Claassen, *arXiv: 2504.11428* (2025)**.**

[2] S. Gassner, C. Weber, M. Claassen, *Nature Communications* **15**, 1776 (2024).

[3] B. Kass, S. Talkington, A. Srivastava, M. Claassen, *arXiv:2411.08964* (2024).

[4] S. Talkington, B. Kass, M. Claassen, *in preparation* (2025).

Towards time-momentum-energy resolved Electron diffraction and spectroscopy

R. Claude[1], F.Barantani[2], M. Puppin[1], B.Weaver[3], C. Missaglia[1], T. LaGrange[1], F. Carbone[1]

[1] *École Polytechnique Fédérale de Lausanne (EPFL), CH-1015 Lausanne, Switzerland*
[2] *The University of Texas at Austin, Austin, Texas 78712, USA*
[3] *Rutherford Appleton Laboratory, Harwell Campus, Didcot OX11 0QX, UK*

In condensed matter systems, the interplay between lattice, electronic, and spin degrees of freedom leads to a diverse range of quantum phases. When considered as an ensemble, these particles can give rise to collective modes such as phonons, plasmons, or magnons, which manifest as quasiparticles that carry energy and momentum. Inelastic electron scattering provides a direct means to probe the population of these modes with energy and momentum resolution. When combined with time-resolved techniques, this approach enables measurement of the coupling strength between particles and quasiparticles. Using ultrafast electron diffraction (UED) with a high signal-to-noise ratio [1], we measured the phonon population throughout reciprocal space, integrated over energy. In contrast, time- and momentum-resolved electron energy loss spectroscopy (tr-q-EELS) allowed us to probe along a selected axis in reciprocal space, while retaining energy resolution (see Fig. 1).
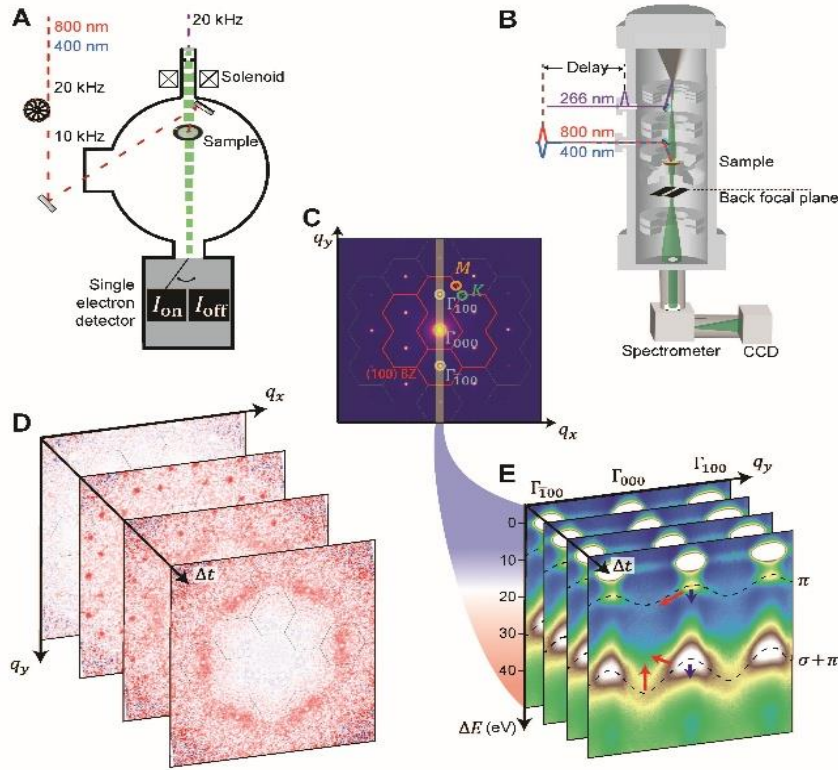
Fig. 1. (A) UED setup with shot-to-shot acquisition method. (B) tr-q-EELS setup where the slit selects the momentum dispersion along the $\Gamma \rightarrow M$ direction as shown on the graphite diffraction pattern in panel (C). (D) Snapshots of the normalized diffraction pattern at selected delays after photoexcitation. (E) Electron energy loss spectra along the $\Gamma \rightarrow M$ direction revealing the π and $\sigma + \pi$ plasmons dispersion. The blue and red arrows show the dynamics of the plasmons after 3.1 and 1.55 eV photoexcitation, respectively. Fig.1 adapted from [2]

We combined both techniques to investigate the interaction between low- and high-energy collective modes—phonons and plasmons, respectively—in graphite [2]. By photoexciting with two different photon energies, we varied the initial dispersion of excited electrons, leading to distinct phonon populations. Coupled to the electronic degrees of freedom, the resulting lattice dynamics modulate the plasmon dispersion, as observed in the tr-q-EELS measurements. The combination of UED and tr-qEELS paves the way for understanding the coupling between single-particle photoexcitation and, more importantly, the subsequent interactions among collective modes that give rise to elusive quantum phases of matter. We apply this approach to nearly optimally doped BSCCO-2212. Our preliminary results reveal signatures of magnetic resonance, charge density waves, and phonon populations, all of which exhibit distinct behavior between the strange metal and superconducting phases.

References
[1] R. Claude, M. Puppin, B. Weaver, P. Usai, T. La Grange, F. Carbone, *arXiv:2502.02540* (2025).
[2] F. Barantani, R. Claude, F Barantani, R. Claude, F. Iyikanat, I. Madan, A. A. Sapozhnik, M. Puppin, B. Weaver, T. LaGrange F. J. García de Abajo, F. Carbone, *Science Advances* **11**, eadu1001 (2025).

Coherent control of photoconductivity in graphene nanoribbons

H. P. Ojeda Collado, L. Broers, L. Mathey
Universität Hamburg, 20148 Hamburg, Germany

Inspired by recent experimental demonstration of coherent control of electron dynamics in graphene [1,2], we study the photoconductivity response of graphene nanoribbons with armchair edges in the presence of dissipation using a Lindblad–von Neumann master equation formalism [3,4,5]. We propose to control the transport properties by illuminating the system with light that is linearly polarized along the finite direction of the nanoribbon while probing along the extended direction. We demonstrate that the largest steady-state photocurrent occurs for a driving frequency that is slightly blue detuned to the electronic band gap proportional to the width of the nanoribbon (Fig.1 left). We compare the photoconductivity in the presence of coherent and incoherent light and conclude that the enhancement of the photoconductivity for blue-detuned driving relies on the coherence of the driving term. Based on this result, we propose a switching protocol for fast control of the photocurrent on a timescale of a few picoseconds.
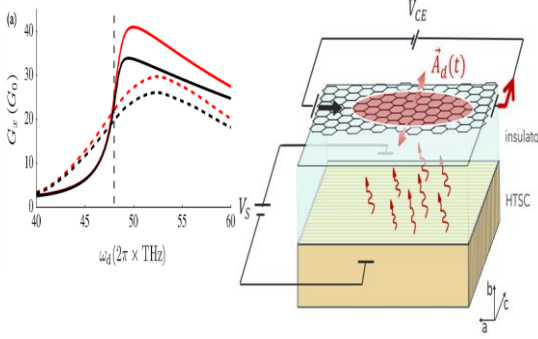
Fig.1. Left:*steady-state longitudinal photoconductivity as a function of the driving frequency in units of the onductance quantum $G_0 = 2e^2/h$. Solid and dashed lines correspond to the photoconductivity produced by coherent and noisy drives, respectively. **Red lines** indicate photoconductivities that are evaluated by using the master equation formalism, whereas the black lines correspond to a calculation using a semi-classical Boltzmann-like analysis. The vertical dashed line marks the electronic band gap. **Right**: transistor design, based on a heterostructure of a graphene nano-ribbon, an insulating layer (**transparent slab**), and a layered high-Tc superconductor (**ochre**), from top to bottom. By means of a switching voltage Vs, the high-Tc superconductor (HTSC) emits light in the THz range that controls the current passing through the graphene nano-ribbon. The latter is probed by applying a collector-emitter voltage V_{CE}.*

Furthermore, we suggest a design for a heterostructure of a graphene nano-ribbon and a high-T_C superconductor that is operated as a transistor as a step towards next-generation coherent electronics.

References
[1] T. Higuchi, C. Heide, K. Ullmann, H. B. Weber, P. Hommelhoff, *Nature* **550,** 224 (2017).
[2] T. Chlouba, R. Shiloh, S. Kraus, L. Brückner, J. Litzel, P. Hommelhoff, *Nature* **622,** 476 (2023).
[3] M. Nuske, L. Broers, B.Schulte, G.Jotzu, S. A. Sato, A. Cavalleri, A. Rubio, J. W. McIver, L. Mathey, *Physical Review Research* **2,** 043408, (2020).
[4] L. Broers, L. Mathey, *Physical Review Research* **4,** 013057(2022).
[5] H. P. Ojeda Collado, L. Broers, L. Mathey, *Physical Review* B **111,** 104304 (2025).

Optical control of coherent electronic currents in Patterned graphene nanoribbons

R. H. Rüstemeier, H. P. O. Collado, L. Mathey
Universität Hamburg, 20148 Hamburg, Germany

Coherent electronics is a promising, emerging field that relies on the coherent excitation of electrons in solids [1,2, 3]. To advance this field, we demonstrate a viable and versatile methodology of optically controlling electronics, by addressing a key issue. In particular, the issue is that a curved band structure makes the excitations momentum-dependent, which prevents coherence. We propose to flatten the band structure of graphene nanoribbons by using periodically arranged control gates (Fig. 1).
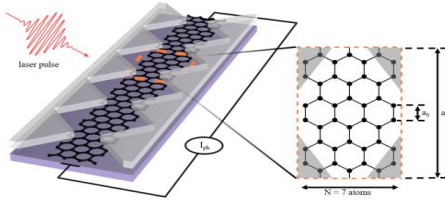
Fig. 1. Segment of the armchair graphene nanoribbon with control gates [4]: *The nanoribbon has a hexagonal structure with an atom-atom distance of 1.42 Å. There is a one-dimensional superlattice with lattice constant $= 3/2(N-1)a_0$ imposed by the periodically arranged control gates (**gray**). A zoom-in of the unit cell of the superlattice is shown in the **dashed box**. We use the control gates to flatten the band structure enabling coherent control over the electronic state of the nanoribbon and the photocurrent via laser pulses.*

We demonstrate coherent optical control over the electronic states of the graphene nanoribbons paving the way towards coherent electronic devices [4].

References
[1] H. P. O. Collado, L. Broers, L. Mathey, *Physical Review* B **111,** 104304 (2025).
[2] T. Higuchi, C. Heide, K. Ullmann, H. B. Weber, P. Hommelhoff, *Nature* **550**, 224 (2017).
[3] C. Heide, T. Eckstein, T. Boolakee, C. Gerner, H. B. Weber, I. Franco, P. Hommelhoff, *Nano Letters* **21**, 9403 (2021)
[4] R. H. Rüstemeier, H. P. O. Collado, L. Mathey, *to be submitted* (2025).

High power electro-optical frequency combs in the mid-IR

A. Monzani[1], P. Planche[1], E. Freysz[1], J. Didierjean[2], A. Bendahmane[1], G. Santarelli[1], E. Cormier[1]

[1]Université Bordeaux, 33400 Talence, France
[2]Bloom Lasers, 33600 Pessac, France

The recent years have seen growing a sharp interest in sources providing sequences of ultrashort pulses with extreme repetition rates at the GHz level. Beyond obvious telecommunication concerns, micro-machining with NIR bursts of GHz pulses became a hot topic [1]. Converted to UV or DUV, such sources are unavoidable tools in the context of X-band photo-injectors [2]. There is however very little work reporting on GHz sources in the midIR where many applications are also requesting such systems such as for instance pollutant detection or astronomical spectrograph calibration [3].

During the last decade, the group has developed a versatile technology based on electro-optic modulation able to generate ps (0.8 to 2 ps) pulses at adjustable repetition rate between 1 and 18 GHz. The systems implement Yb-doped fiber amplifiers and therefore allow to achieve very high power at the wavelength of 1030 nm [4]. The advantage of operating at the Yb wavelength allows to easily convert the temporal/spectral properties of the GHz electro-optical comb (EO-comb) to various spectral ranges through non-linear processes. In particular, we were able to produce bursts of pulses in visible and DUV by frequency doubling and quadrupling with a pulse repetition rate of 12 GHz [2]. Here, we report on a transfer of the EO-comb towards longer wavelengths in the midIR. The architecture involves, here as well, a non-linear process based on a second order susceptibility material. The midIR radiation is generated via difference frequency generation (DFG) between the strong GHz pump source at 1 µm and a wavelength tunable continuous wave signal around 1.5 µm. As depicted on Fig. 1, it results in an idler in the vicinity of 3 µm.
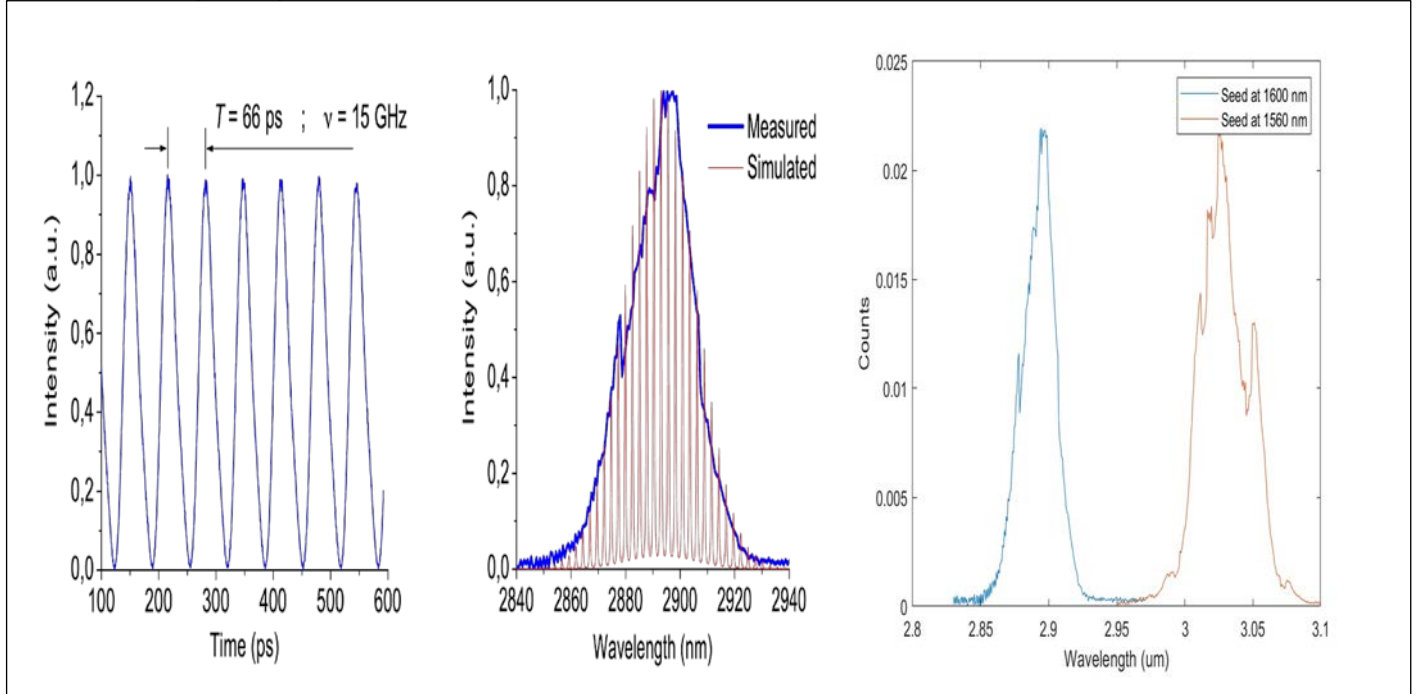
Fig.1*.(**Center**)ps pump pulses at 15 GHz (**left**) and transient frequency comb at the idler wavelength around 3 µm Tunability around 3 µm for 2 different signal wavelengths (**right**).*

The mid-IR central wavelength being adjusted by scanning the CW signal wavelength. Power scaling is further achieved by additional non-linear stages only limited by the available pump power.

References
[1] C. Kerse, H. Kalaycıoğlu, P. Elahi, B. Çetin, D. K. Kesim, Ö. Akçaalan, S. Yavaş, M. D. Aşık, B. Öktem, H. Hoogland, R. Holzwarth, F. Ö. Ilday *Nature* **537**, 84 (2016).
[2] H. Ye, L. Pontagnier, C. Dixneuf, G. Santarelli, E. Cormier, *Optics Express* OE **28**, 37209 (2020).
[3] P. Sekhar, M. K. Kreider, C. Fredrick, J. P. Ninan, C. F. Bender, R. Terrien, S. Mahadevan, S. A. Diddams, *Optics Letters* **49**, 6257 (2024)
[4] H. Ye, F. Leroi, L. Pontagnier, G. Santarelli, J. Boullet, E. Cormier, *Optics Express OE* **30**, 10605 (2022).

Charge density waves fluctuations and collective modes in Cuprates revealed by ultrashort X-ray probes

G. Coslovich

SLAC National Accelerator Laboratory, Menlo Park, California 94720, USA

Ultrashort X-ray pulses offer new opportunities to study charge fluctuations and collective modes in materials exhibiting unconventional quantum states, such as high-temperature superconductivity. To provide microscopic insight on charge fluctuations and excitations, a probe capable of studying their natural length, energy and time scales is necessary. In this talk, I will present results on high temperature superconductors obtained at the LCLS using ultrafast x-ray scattering techniques, including time-resolved Resonant Inelastic X-ray Scattering (RIXS), Resonant Energy-integrated X-ray Scattering (REXS) and X-ray Diffraction (XRD). These experiments build upon previous results from ultrafast resonant soft x-ray scattering which allowed tracking the dynamical interaction between Charge Density Waves (CDW) and superconductivity in $YBa_2Cu_3O_{6+x}$ (YBCO) [1]. In our more recent investigations at LCLS, we focused on two problems: 1) uncovering CDW fluctuations via transient melting of quasi-static CDW studied via ultrafast REXS, and 2) studying the coherent response of lattice distortions associated with CDW via XRD. I will present results addressing both these topics. An exemplary result from the latter study is shown in Fig.1 below. Here the CDW peak in YBCO is probed by scattering of 8.8 keV photons and it is shown in a false color scale as a function of time delay with an 800nm pump pulse.
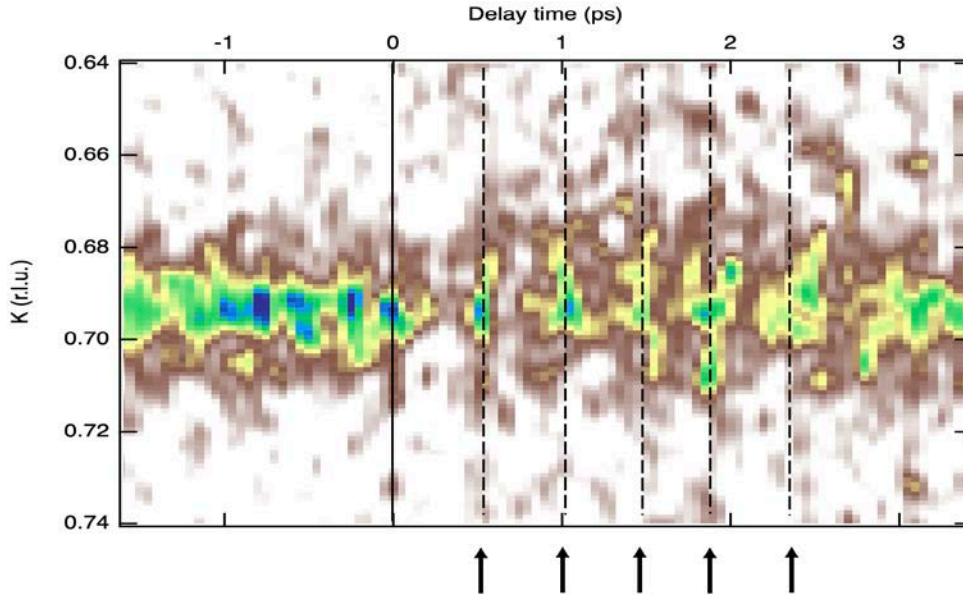
*Fig. 1. X-ray scattering profile of the CDW integrated along the H direction and shown here along the K direction in reciprocal space and as a function of delay time with the 800nm pump pulse (fluence ≈ 1 mJ/cm^2) at 65 K. **The arrows i**ndicate the time points where the CDW reappears in conjunction with its amplitude coherent oscillations.*

Following an initial drop in intensity at time overlap, we observe clear oscillations in the response, directly uncovering the amplitude mode in YBCO. The period of oscillation is discernible directly in the data with a frequency of the order of ≈ 2.2 THz and can be compared to previously reported coherent oscillations in the ultrafast optical response on this material [2,3]. We repeated such optical measurements in the same YBCO sample as our LCLS experiment and in similar experimental conditions (with both 800nm and THz pump) and concluded that the coherent oscillations observed optically are distinct from the amplitude mode observed with the hard x-ray probe. Finally, I will present very recent results from the qRIXS instruments enabling time-resolved RIXS experiments on solid state samples at high repetition rates, using LCLS-II. Results will include early studies on cuprate superconductors using this new instrument at LCLS.

References
[1] S. Wandel, F. Boschini, E. H. da Silva Neto, L. Shen, M. X. Na, S. Zohar, Y. Wang, S. B. Welch, M. H. Seaberg, J. D. Koralek, G. L. Dakovski, W. Hettel, M.-F. Lin, S. P. Moeller, W. F. Schlotter, A. H. Reid, M. P. Minitti, T. Boyle, F. He, R. Sutarto, Ruixing. Liang, D. Bonn, W. Hardy, R. A. Kaindl, D. G. Hawthorn, J.- S. Lee, A. F. Kemper, A. Damascelli, C. Giannetti, J. J. Turner, G. Coslovich, *Science* **376**, 860 (2022).
[2] J. P. Hinton, J. D. Koralek, Y. M. Lu, A Vishwanath, J. Orenstein, D. A. Bonn, W. N. Hardy, R. Liang, *Physical Review* B **88**, 060508 (2013)
[3] G. L. Dakovski, W.-S. Lee, D.G.Hawthorn, N.Garner, D. A.Bonn, W.N.Hardy, R.Liang, M. C. Hoffmann, J. J. Turner, *Physical Review* B **91**, 220506 (2015)

Dynamic phase transition into a mixed-CDW state in 1T-TaS$_2$ via a Thermal quench

A. de la Torre

Northeastern University, Boston, MA 02115, USA

Ultrafast light-matter interaction has emerged as a new mechanism to exert control over the macroscopic properties of quantum materials toward novel functionality. To date, technological applications of non-thermal phases are limited by their ultrashort lifetimes and low-ordering temperatures. The hidden metallic charge density wave (H-CDW) in 1T-TaS$_2$ is among the most studied photoinduced metastable phases because of its technological promise [1,2]. However, despite active study, the nature of the photoinduced H-CDW remains the subject of debate and potential applications have been limited because it has so far only been stabilized at cryogenic temperatures. Here, we stabilize the H-CDW phase at thermal equilibrium by accessing a mixed CDW order regime via thermal quenching [3]. Using x-ray high dynamic range reciprocal space mapping (HDRM) and scanning tunneling spectroscopy (STS), we reveal the coexistence of commensurate (C) CDW and H-CDW domains up to 210 K..
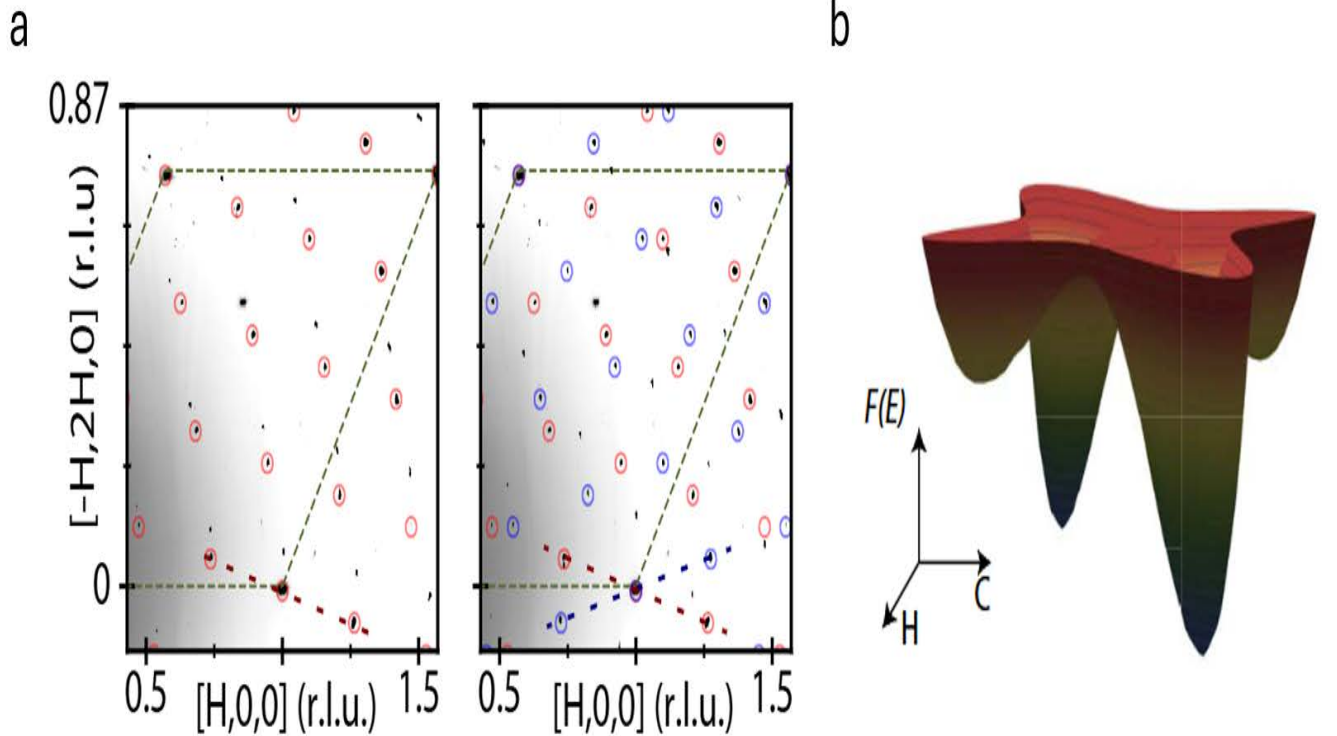
Fig. 1. a: *Reciprocal space maps parallel to the [HK0] plane for an as-grown sample (**left**) and after a quench (**righ**t). Red and blue markers highlight the C-CDW and H-CDW-like satellite peaks, respectively. Green dashed lines highlight the a* and b* directions. **b:** Meanfield-only free energy functional for the two competing CDW order*

.

Our findings show that each order parameter breaks basal plane mirror symmetry with different chiral orientations and induces out-of-plane unit cell tripling in the H-CDW phase. Despite metallic domain walls and a finite density of states at zero bias observed via STS, bulk resistance remains insulating due to CDW stacking disorder. By comparing our data to Landau-Ginzburg theory calculations of the free energy functional, our study establishes the H-CDW as a thermally stable phase. It introduces a new mechanism for switchable metallic behavior in thin flakes of 1T-TaS$_2$ and similar materials with competing phases

References
[1] Q. Stahl, M. Kusch, F. Heinsch, G. Garbarino, N. Kretzschmar, K. Hanff, K. Rossnagel, J. Geck, T.Ritschel, *Nature Communications* **11**, 1247 (2020)
[2] L. Stojchevska, I. Vaskivskyi, T. Mertelj, P. Kusar, D. Svetin, S. Brazovskii, D. Mihailovic, *Science* **344**, 177 (2014).
[3] A de la Torre, Q Wang, Y Masoumi, B Campbell, J. V. Riffle, D. Balasundaram, P. M. Vora, J.P.C. Ruff, G.A. Fiete, S.M. Hollen, K.W. Plumb *arxiv: 2407.07953* (2024).

Dispersive dark excitons in van der Waals ferromagnet CrI₃

W. He[1], J. Sears[1], F. Barantani[2], T. Kim[3], J. W. Villanova[3], T. Berlijn[3], M. Lajer[1], M. A. McGuire[3]
J. Pelliciari[1], V. Bisogni[1], S. Johnston[4], E. Baldini[2], M. Mitrano[5], M. P. M. Dean[1]

[1]*Brookhaven National Laboratory, Upton, NY 11973, USA*
[2]*The University of Texas at Austin, Austin, TX 78712, USA*
[3]*Oak Ridge National Laboratory, Oak Ridge, TN 37831, USA*
[4]*The University of Tennessee, Knoxville, TN 37966, USA*
[5]*Harvard University, Cambridge, MA 02138, USA*

Excitons are central to understanding the optical properties of solids. While bright excitons have been widely explored, their optically inactive counterparts—dark excitons—offer unique advantages for quantum information technologies due to their extended lifetimes and magnetic tunability. In this work, we report the observation of dark excitons in the ferromagnetic van der Waals material CrI₃ , utilizing high-resolution resonant inelastic x-ray scattering (RIXS). We identify two distinct dark excitons near 1.7 eV, as shown in Fig. 1, exhibiting much narrower linewidths than the previously known bright excitons, indicating long-lived quasiparticle behavior.We find that these dark excitons display momentum-dependent dispersion with bandwidths on the order of 10 meV—comparable to the magnetic exchange interactions in CrI₃—suggesting a strong coupling to the material's ferromagnetic order. Their intensities and energies show pronounced changes across the ferromagnetic transition temperature (T_c = 61 K), further highlighting their sensitivity to magnetic order. Through detailed modeling using an Anderson impurity model and exact diagonalization, we
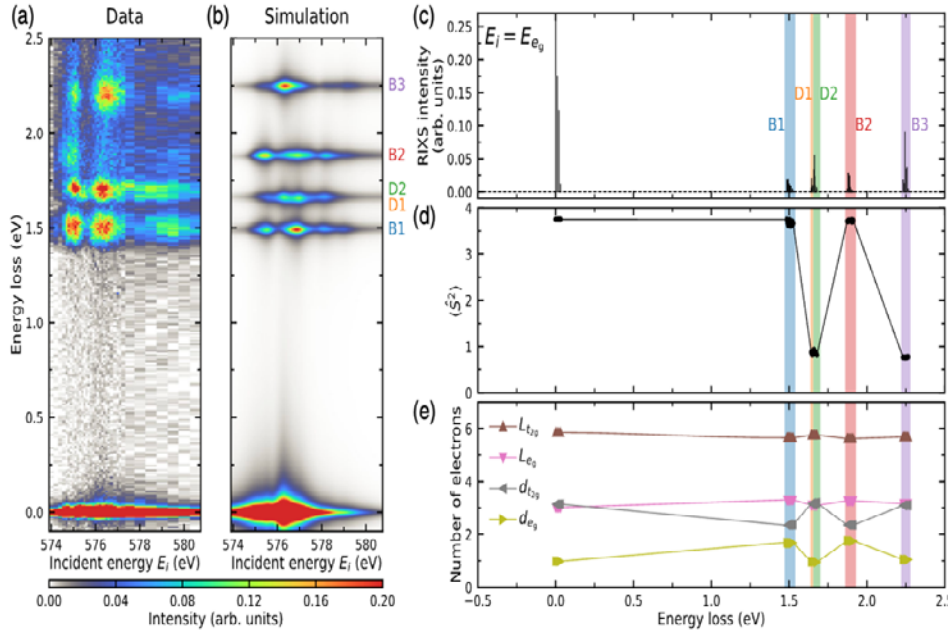
Fig. 1. *Electronic character of the dark excitons. (a) RIXS intensity map as a function of incident photon energy through the Cr L_3 resonance. (b) RIXS calculations that reproduce the energy and resonant profile of the five lowest-energy excitons in the material B1, B2, B3 are the bright excitons and D1 and D2 are the dark excitons. (c) Calculated RIXS stick diagram at the main resonant energy E_{eg}. (d),(e) Analysis of the ground and excited states for the calculated RIXS spectrum. (d) Expectation value of the total spin operator squared$\langle \hat{S}^2 \rangle$. (e) Electron occupations of Cr 3d (denoted by d) and ligand (denoted by L) orbitals.*

demonstrate that these excitons possess spin-flip character predominantly governed by Hund's coupling, and involve ligand orbitals due to a small charge-transfer energy. Our findings establish RIXS as a powerful technique for probing dark excitons and their interactions with magnetism, and open new avenues for magneto-optical applications in layered materials. We anticipate that our results will inform future efforts to optically access and control dark excitons in CrI₃ and related systems.

Reference
[1] W. He, J. Sears, F. Barantani, T. Kim, J. W. Villanova, T. Berlijn, M. Lajer, M. A. McGuire, J. Pelliciari, V. Bisogni, S. Johnston, E. Baldini M. Mitrano, M. P. M. Dean, *Physical Review* X **15**, 011042 (2025).

Spin dynamics and anisotropic spin Seebeck effect in Low-dimensional materials

A. Delin

KTH Royal Institute of Technology,10691 Stockholm, Sweden

Magnons, i.e., quanta of spin waves, enable pure spin-current transport in magnetic insulators. The application of magnon transport instead of electric charge transport offers intriguing and compelling opportunities for low-energy consumption, nanoscale wavelengths, miniaturization, and wave-based computing [1]. The dynamics of magnons are governed by the interactions between neighboring spins, typically described by the predominant Heisenberg exchange couplings. Since the spin–spin interactions hinge with the crystal symmetry, which determines the electronic hopping pathway, magnon transport is also intrinsically connected to the crystal symmetry. A particularly interesting situation arises when vdW magnets possess in-plane crystal anisotropy, i.e., the absence of in-plane rotation symmetries except for C2, as recently reported for the antiferromagnet CrPS4, opening the door for anisotropic spin transport under a thermal gradient and a magnetic field.
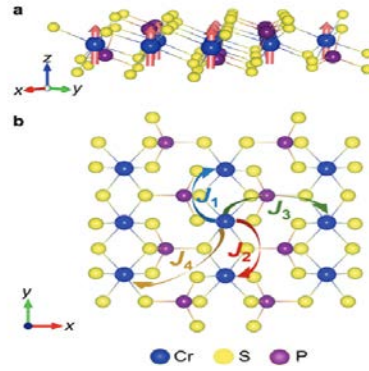
Fig. 1. Crystal structure of CrPS4 and the four Cr-Cr Heisenberg Exchange interactions used in the present work.
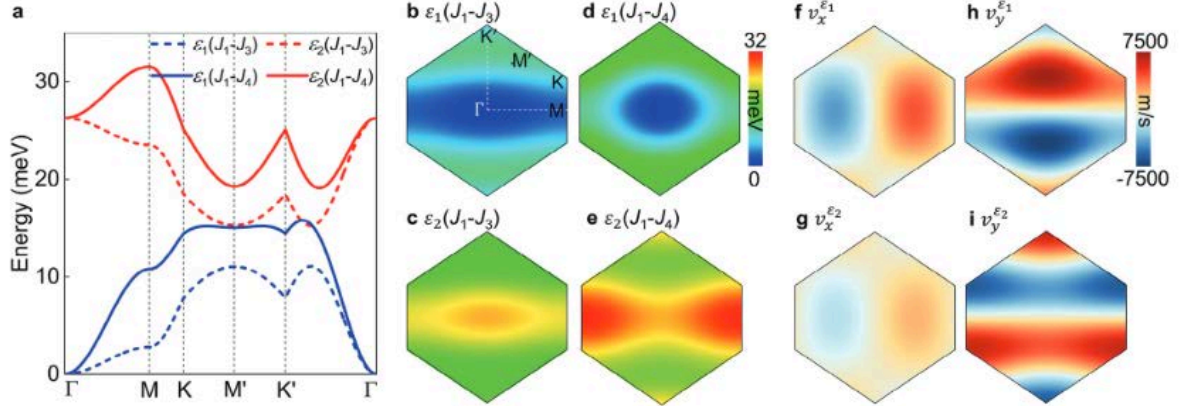
Fig. 2. a) Magnon dispersion along the high-symmetry direction Γ-M-K-M'-K'-Γ. The dashed and solid lines I ndicate eigenvalues from the J1-J3 and J1-J4 models, respectively. The acoustic (blue lines) and optical (red lines) modes split in the energy scale. The eigenvalue spectrum in the Brillouin zone, is based on (b, c) the J1-J3 model, and (d, e). the J1-J4 model. f–h) The magnon group velocity spectrum in the Brillouin zone deduced from the J1-J4 model.

In this talk, I will elaborate on how the anisotropic magnon dispersion contributes to longitudinal and transverse magnon currents and how this in turn relates to various spin transport phenomena such as the anisotropic spin Seebeck effect (ASSE), the thermal Hall effect-THE and the spin Nernst effect-SNE [2]

References
[1] K. Uchida, S. Takahashi, K. Harii, J. Ieda, W. Koshibae, K. Ando, S. Maekawa, E. Saitoh, *Nature* **455**, 778 (2008).
[2] Q. Cui, X. Bai, A. Delin, *Advanced Functional Materials* **35**, 2407469 (2025).

Controlling light-driven correlated phases in complex oxides with Atomic layer engineering

A. Disa

Cornell University, Ithaca, NY 14853 USA

Complex oxides exhibit a host of competing electronic, magnetic, and structural interactions, which lead to emergent macroscopic phases with enormous technological potential such as high-temperature superconductivity and multiferroicity. A variety of techniques, such as chemical doping and epitaxial strain, have been utilized over the past decades to engineer these systems in equilibrium creating rich phase diagrams with tunable ground states [1]. An alternative pathway to control correlated phases has been to use excitation with optical pulses, which can dynamically induce non-equilibrium properties on ultrafast time scales [2,3]. While many novel phenomena have been discovered through this approach – including ferroelectricity, magnetism, superconductivity, and more – little is understood about whether and how we can *control* the dynamic, non-equilibrium behavior of these systems through materials engineering. Here, I will highlight our ongoing experiments combining tailored light pulses and atomically layered oxide heterostructures, which demonstrate the ability to manipulate ultrafast charge, spin, and structural dynamics and stabilize "hidden" non-equilibrium phases, which cannot be accessed otherwise. First, I will discuss our studies of the optically driven phase transition in the prototypical correlated oxide $NdNiO_3$, which features coexistant metal-insulator, paramagnetic-antiferromagnetic, and charge ordering transitions. Using time-resolved soft x-ray scattering and optical reflectivity, we measure the ultrafast dynamics of these intertwined orders in $NdNiO_3$ heterostructures with controlled layer thickness, demonstrating that the interfacial reconstructions and dimensional confinement have a drastic effect on the susceptibility and lifetimes of the electronic and phononic degrees of freedom. This atomic layer engineering leads to a decoupling of charge and spin order, a suppression of the structural phase transition, and the formation of a non-equilibrium metastable magnetic phase.
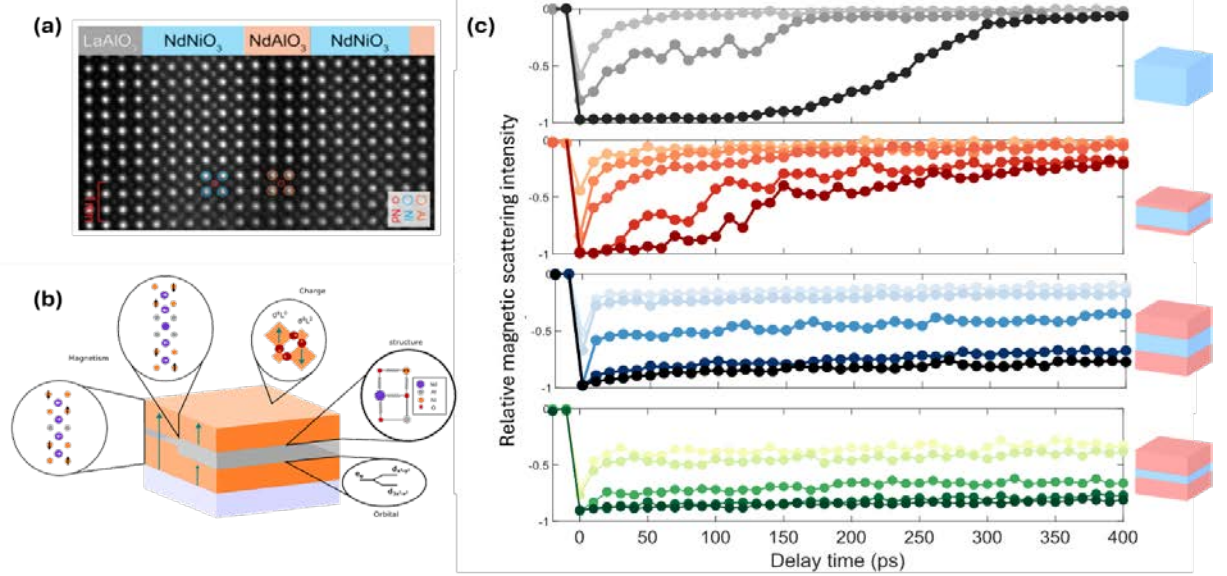
Fig. 1. Engineering non-equilibrium phases in atomically layered heterostructures. *(a) Scanning transmission electron micrograph of $NdNiO_3$ heterostructures. (b) Schematic of the reconstruction of magnetism, charge order, orbital configuration, and structure due to confinement and interfacial reconstructions. (c) Time-resolved resonant soft x-ray scattering measuring the change in antiferromagnetic order after optical excitation for different layer thicknesses.*

I will also show how we are extending this methodology to engineer a new room-temperature ferroelectric-ferromagnet with strong magnetoelectric coupling. This work sets the stage for the development of a new paradigm for "non-equilibrium materials design" for next-generation quantum and ultrafast technologies.

References
[1] Z. Huang, Ariando, X. R. Wang, A. Rusydi, J. Chen, H. Yang, T. Venkatesan, *Advanced Materials* **30,** 1802439 (2018).
[2] A. de la Torre, D.M. Kennes, M. Claassen, S. Gerber, J.W. McIver, M. Sentef, *Reviews of Modern Physics* **93**, 041002 (2021).
[3] A. S. Disa, T. F. Nova, A. Cavalleri, *Nature Physics* **17**, 1087 (2021).

Pair-breaking features of Raman spectra

J. Dolgner[1], S. Tian[1], T. Glier[2], M. Rübhausen[2], D. Manske[1]

[1] *Max Planck Institute for Solid State Research, 70569 Stuttgart, Germany*

[2] *Universität Hamburg, 20148 Hamburg, Germany*

Due to their direct coupling with electromagnetic radiation pair-breaking or quasi particle (QP) excitation features are ubiquitous in the spectroscopy of superconductors (SC). In contrast to the conventional s-wave materials, QP features in gapless superconductors, e.g., high-T_C superconductors such as the cuprates, are broad and not gapped. Because of this, pair-breaking peaks provide a background, which often dominates more interesting collective mode signals. As such, even when quasi-particles are not the focus of investigation, a solid understanding of them is often necessary to be able to disentangle the single particle channel from collective modes e.g. Higgs- , Bardasis-Schrieffer-, Legget- and more exotic modes. We review the basic characteristics of pair-breaking features in s- and d-wave materials, that is, their energies, symmetries and vertex corrections due to Coulomb screening. Furthermore, we discuss a phenomenological fitting scheme of pair-breaking peaks in Raman spectra based on a Fermi-surface harmonics expansion in the BCS model, which was introduced in [1] and recently adapted in [2]
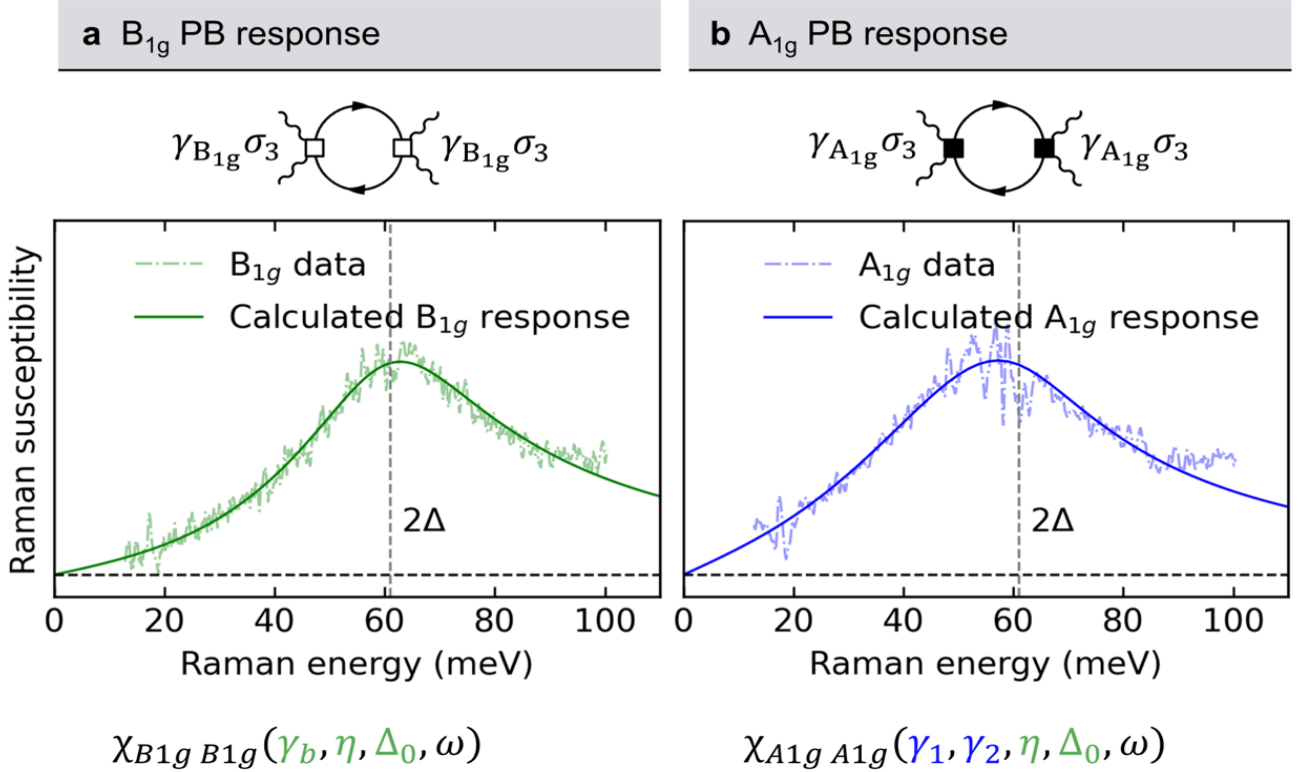
Fig. 1. Comparison between NEARS data of Bi-2212 and BCS model calculations. (a) *The experimental B_{1g} electronic Raman susceptibility on the Stokes side (**dash-dotted line**) is extracted by parameterization and phonon subtraction. The B_{1g} PB Raman response is depicted diagrammatically in the upper part of panel. We find the parameters $\gamma_b = 0.1116 \pm 0.0003$, $\eta = 0.225 \pm 0.003$, and $\Delta_0 = 30.50 \pm 0.05$ meV from the B_{1g} fit (**green**). **(b)** The A_{1g} PB Raman response is depicted diagrammatically with filled squares representing the Coulomb-screened vertices. We keep η and Δ_0 from the B_{1g} fit, and fit γ_1 and γ_2 to the A_{1g} experimental data (**blue**, $\gamma_1 = 0.117\pm0.001$, $\gamma_2 = 0.054\pm0.001$ with $\eta = 0.225$, $\Delta_0 = 30.50$ meV.). Adapted from [2].*

We show how perturbatively accounting for particle-hole asymmetry in our adaption allows to model both the A_{1g} and B_{1g} curves more accurately than in the past.

References

[1] T. P. Devereaux, R. Hackl, *Review of Modern Physics* **79**, 175 (2007).

[2] T. E. Glier, S.Tian, M.Rerrer, L.Westphal, G. Lullau, L. Feng, J. Dolgner, R. Haenel, M. Zonno, H. Eisaki, M. Greven, A. Damascelli, S. Kaiser D. Manske, M. Rübhausen, *arXiv.*2310.08162 (2024).

Strong-field nano-optics

P.Dombi

HUN-REN Wigner Research Centre for Physics, 1121 Budapest, Hungary

An exciting non-perturbative regime of light-matter interactions is reached when the amplitude of the external electromagnetic fields that are driving a material approach or exceed the field strengths that bind the electrons inside the medium. In this strong-field regime, light-matter interactions depend on the amplitude and phase of the field, rather than its intensity, as in more conventional perturbative nonlinear optics. Traditionally, such strong-field interactions have intensely been investigated in atomic and molecular systems and this resulted in the generation of high harmonic radiation and laid the foundations for contemporary attosecond science. During the last decade, however, a new field of research has emerged, the study of strong-field interactions in solid-state nanostructures [1]. By using nanostructures, specifically those made out of metals, external electromagnetic fields can be localized on length scales of just a few nanometers, resulting in greatly enhanced field amplitudes that can exceed those of the external field by orders of magnitude in the vicinity of the nanostructures. This not only leads to dramatic enhancements of perturbative nonlinear optical effects but also significantly increases photoelectron yields.   In particular, I will review our recent results on ultrafast strong-field photoemission from nanoplasmonic structures including the non-adiabatic tunneling of photoelectrons [2] and photoelectron rescattering in the multi-photon-induced photoemission regime [3]. The carrier-envelope phase (CEP) is a powerful knob to steer interactions of laser light with matter in the strong-field regime, as evidenced by numerous studies of ultrafast electron dynamics in atomic, molecular and solid-state media. Precise characterization of CEP or CEP changes in time or space is a key ingredient in applying electric-field sensitive techniques to study and control ultrafast electron processes in matter. Thus, characterizing and controlling CEP in space can support strong-field nanooptics experiments [1] or PHz optoelectronics. I will also present a novel, on-chip scanning CEP probe that is capable of measuring 3D CEP maps in the vicinity of a few-cycle laser beam focus for laser pulses having only ~pJ-nJ pulse energy without having to use vacuum equipment for this purpose [4]. The measurement principle and some results are depicted in Fig. 1 from [5].
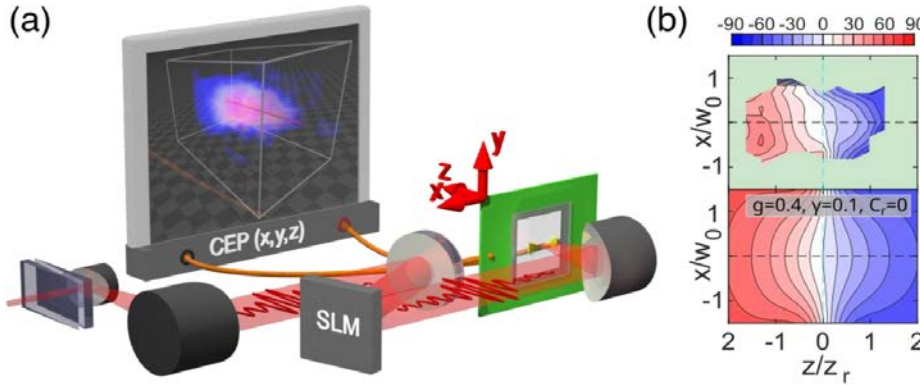
Fig. 1. (a) Measurement setup with a false-color cloud showing measured values of the 3D CEP(x,y,z) distribution in the beam focus. Pink, white and blue color show positive, zero and negative CEP values respectively. (b) Measured CEP spatial distribution of a focused few-cycle laser beam (top panel). (bottom panel) Respective CEP distribution calculated with an analytical formula.

I will also feature recent results on how to use dielectric-metal heterostructures to enhance CEP dependent signal levels significantly. In addition, experiments on revealing the mechanisms of the ultrafast current generation process will also be presented. We also demonstrate a method to sculpt the CEP of few-cycle pulses in the vicinity of the focal volume. In addition, I will also review our recent experimental results on our novel free space pump/plasmon probe experiments with which (in addition to the investigation of hot electron dynamics), we could also realize an ultrafast nano-optical signal switching scheme [6].

References
[1] P. Dombi, Z. Pápa, J. Vogelsang, S. V. Yalunin, M. Sivis, G. Herink, S. Schafer, P. Groß, C. Ropers, C. Lienau, *Review of Modern Physics* **92** 025003 (2020).
[2] B. Lovász, P. Sándor, G.-Z. Kiss, B. Bánhegyi, P. Rácz, Z. Pápa, J. Budai, C. Prietl, J. R. Krenn, P. Dombi, *Nano Letters* **22**, 2303 (2022).
[3] B Bánhegyi, G.Z Kiss, Z Pápa, P .Sándor, L Tóth, L Péter, P Rácz, P Dombi, *Physical Review Letters* **133**, 033801 (2024).
[4] V. Hanus, V.Csajbók, Z. Pápa, J.Budai, Z. Márton, G.Z.Kiss, P.Sándor, P. Paul, A. Szeghalmi, Z. Wang ,B. Bergues,M.F.Kling, G.Molnár, J. Volk P. Dombi, *Optica* **8**, 570 (2021).
[5] V. Hanus, B. Fehér, V. Csajbók, P. Sándor, Z. Pápa, J. Budai, Z. Wang, P. Paul, A. Szeghalmi, P. Dombi, *Nature Communications* **14**, 5068 (2023).
[6] P Sándor, B Lovász, J Budai, Z Pápa, P Dombi, *Nano Letters* **24**, 8024 (2024).

Broadband phase-locked cw optical parametric oscillators

M. Ebrahim-Zadeh

ICFO-Institut de Ciencies Fotoniques, 08860 Castelldefels, Spain

A novel approach for frequency comb generation based on bulk degenerate $\chi^{(2)}$ OPOs presented. Driven by a continuous-wave laser and using intracavity dispersion control, coherent broadband spectral output with corresponding to transform-limited femtosecond pulses in the time domain is obtained. Optical frequency combs have had a remarkable impact on photonics, paving the way for many new applications from frequency metrology and spectroscopy to remote sensing and astronomy. The established techniques for comb generation are based on the direct use of mode-locked femtosecond laser oscillators such as Ti:sapphire and fiber lasers [1,2], their combination with photonic fibers [3], or the use of $\chi^{(3)}$ Kerr microcavities pumped by mode-locked or continuous-wave (cw) lasers [4]. These approaches have resulted in tremendous advances in frequency combs, enabling remarkable progress in photonics. Nevertheless, it remains the case that these techniques rely on relatively complex and costly femtosecond lasers, or sophisticated fabrication methods for advanced microstructures. It would be desirable to explore potential alternative approaches to frequency comb generation offering reduced complexity and cost, increased flexibility, practical powers, and wider accessibility for continually evolving applications. Optical parametric oscillators (OPOs) based on bulk $\chi^{(2)}$ nonlinear materials are now widely established as flexible sources of tunable radiation across broad spectral regions from the UV to mid-IR. Using ultrafast femtosecond laser oscillators, in combination with synchronous pumping, femtosecond OPOs can provide broadband radiation in non-degenerate [5,6] or degenerate [7,8] operation, offering another approach to comb generation. However, the need for a mode-locked pump laser (to provide the input comb), together with synchronous pumping, similarly result in high complexity and cost. Broadband generation can also be achieved using cw OPOs in *singly resonant oscillator* (*SRO*) configuration by exploiting large parametric gain bandwidth [9] or cascaded $\chi^{(2)}$ nonlinearity [10]. However, both these techniques are strictly limited to specific phase-matching conditions and do not generally provide a coherent phase-locked output spectrum characteristic of a frequency comb. An alternative approach to optical frequency comb generation is active phase modulation based on $\chi^{(2)}$ cw OPOs in degenerate *doubly resonant oscillator* (*DRO*) configuration. This technique has been previously demonstrated in MgO:LiNbO$_3$ pumped at 532 nm, generating an output spectrum over a bandwidth of 20 nm (5.4 THz) centered at ~1064 nm [11]. In the time domain, operation of such a degenerate phase-modulated cw OPO corresponds to mode-locked output pulses, where using a degenerate cw OPO based on MgO:sPPLT pumped at 532 nm, we demonstrated the generation of ~500 ps output pulses [12]. In a recent report, we further theoretically investigated the process of spectral formation and pulse generation in degenerate cw OPO based on MgO:PPLN pumped at 532 nm subjected to intracavity phase modulation [13]. Using an intracavity electro-optic modulator synchronized to the free-spectral-range of the cavity, in combination with spectral filtering, we showed that a stable, uniform, and periodic train of picosecond pulses of <5 ps with FWHM spectral bandwidth of 0.4 THz could be generated (Fig. 1). Our simulations confirmed that the intracavity phase modulator enables spectral broadening accompanied by uniform period pulse train formation at degeneracy.
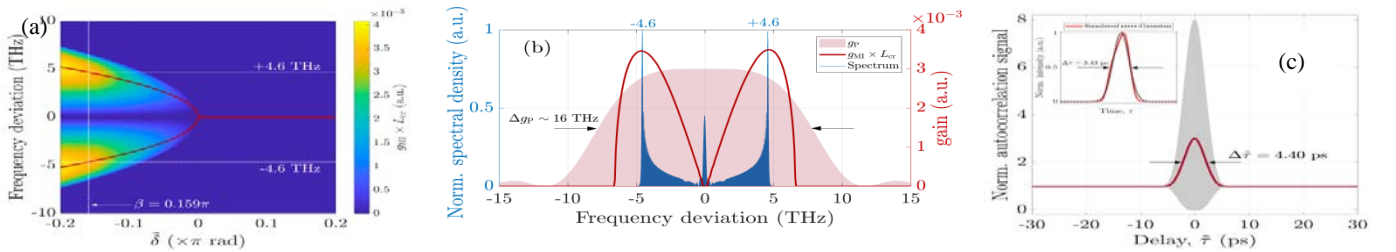
Fig. 1. (a) Modulation instability (MI) gain profile (g$_{MI}$). *The red curve corresponds to the spectral peak for net cavity detuning (d), while for positive detuning degeneracy is maintained, as shown by the single red line. The red curve is well-matched with the g$_{MI}$ maxima. (b) Output spectrum and the corresponding parametric and MI gain profiles. The spectrum exhibiting two peaks at the position of g$_{MI}$ maxima at ±4.6 THz. (c) Normalized interferometric and intensity autocorrelations (grey and red curves, respectively). Inset: the last pulses (red solid) in the final round-trip with a Gaussian fit (black dashed) showing a pulse FWHM=3.43 ps.*

On the other hand, in the context of frequency comb generation, the spectral and temporal coherence of phase-modulated cw OPOs are strictly limited due to the dispersion characteristics of the DRO configuration. In normal operation, cw DROs are over-constrained by the requirements of phase-matching ($k_p=k_s+k_i$), energy conservation ($\omega_p=\omega_s+\omega_i$), and simultaneous cavity resonance at both signal and idler frequencies ($m_s\omega_s=c/2n_sL$; $m_i\omega_i=c/2n_iL$, L is the optical cavity length). In conventional schemes widely deployed to date, cw DROs can only be reliably operated at a single (or very few) signal-idler frequency pairs nearest the peak of parametric gain [14]. This is an intrinsic property of DRO due to the *Vernier* effect arising from cavity dispersion. As such, the generation of broadband multi-axial-mode radiation is fundamentally precluded in cw DROs at any wavelength. To overcome this fundamental limitation and thus enable broadband generation from degenerate cw OPOs, a parameter of critical importance is thus the *control of cavity dispersion*. We previously demonstrated the generation of broadband radiation from a degenerate cw OPO based on MgO:sPPLT pumped at 532 nm [15]. By deploying chirped mirrors for dispersion compensation of the cavity, we generated broadband radiation over 34 nm (9 THz) about ~1064 nm, limited by unoptimized dispersion characteristics of the mirror coatings. Under this condition, we also observed signature of the frequency comb generation by recording the RF spectrum of the output spectrum under passive conditions. At the same time, we have also recently theoretically studied the feasibility of broadband frequency comb generation in degenerate cw OPOs using active phase modulation in combination with full dispersion control of the cavity [16,17]. Our simulations show that under this condition, it is possible to achieve coherent broadband phase-locked output spectrum characteristic of a frequency comb, with a temporal output corresponding to transform-limited femtosecond pulses, irrespective dispersion regime (normal or anomalous). Using a degenerate cw OPO based on MgO:PPLN pumped at 532 nm, in the presence of intracavity dispersion compensation, we confirm spectral generation with a FWHM bandwidth of $\Delta\nu \approx 6.9$ THz centred at 1064 nm, with stable pulses of duration as short as $\Delta\tau \approx 65$ fs in the normal dispersion regime, corresponding to a transform-limited time-bandwidth product of $\Delta\tau\Delta\nu \approx 0.45$, can be achieved (Fig. 2).
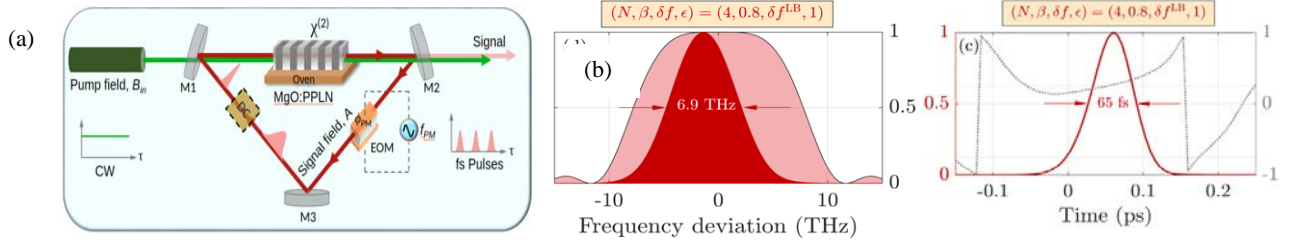
Fig. 2. (a) Generic design of the phase-locked degenerate cw OPO with intracavity dispersion control. *In the normal dispersion regime, optimum detuning together with dispersion compensation result in (b) spectral output with a FWHM bandwidth of 6.9 THz, and (c) transform-limited pulses of 65 fs duration with flat temporal phase.*

Our results point to the feasibility of generating broadband phase-locked degenerate cw OPOs under optimum compensation of cavity dispersion. The approach could pave the way for the realization of a new class of comb sources in different spectral regions based on bulk $\chi^{(2)}$ OPOs pumped by cw pump lasers.

References
[1] T. Udem, R. Holzwarth, T. W. Hänsch, *Nature* **416**, 233 (2002).
[2] S. A. Diddams, *Journal of Optical Society of America* B **17**, 51(2010).
[3] S. A. Diddams, D. J. Jones, J. Ye, S. T. Cundiff, J. L. Hall, J. K. Ranka, R. S. Windeler, R. Holzwarth, T. Udem, T. W. Hänsch, *Physical Review Letters* **84**, 5102 (2000).
[4] P. Del'Haye, A. Schliesser, O. Arcizet, T. Wilken, R. Holzwarth, T. J. Kippenberg, *Nature* **450**, 1214 (2007).
[5] F. Adler, K. C. Cossel, M. J. Thorpe, I. Hartl, M. E. Fermann, J. Ye, *Optics Letters* **34**, 1330 (2009).
[6] S. Chaitanya Kumar, A. Esteban-Martin, T. Ideguchi, M. `Yan, S. Holzner, T. W. Hänsch, N. Picqué, M. Ebrahim-Zadeh, *Laser and Photonics Review* **8**, L 86 (2014).
[7] T. Wong, T. Plettner, K. L. Vodopyanov, K. Urbanek, M. Digonnet, R. L. Byer, *Optics Letters* **33**, 1896 (2008).
[8] V. R. Badarla, A. Esteban-Martin, M. Ebrahim-Zadeh, *Laser and Photonics Review* **7**, L55 (2013).
[9] R. Das, S. Chaitanya Kumar, G. K. Samanta, M. Ebrahim-Zadeh, *Optics Letters* **34**, 3836 (2009).
[10] V. Ulvila, C. R. Phillips, L. Halonen, M. Vainio, *Optics Letters* **38**, 4281 (2013).
[11] S. A. Diddams L. S. Ma, J. Ye, J. L. Hall, *Optics Letters* **24**, 1747 (1999).
[12] K. Devi, S. Chaitanya Kumar, M. Ebrahim-Zadeh, *Optics Express* **21**, 23365 (2013).
[13] A. D. Sanchez, S. Chaitanya Kumar, M. Ebrahim-Zadeh, *IEEE Journal of Selected Topics Quantum Electronics* **29**, 1(2023).
[14] R. C. Eckardt, C. D. Nabors, W. J. Kozlovsky, R. L. Byer, *Journal of Optical Society of America* B **8**, 646 (1991).
[15] K. Devi, S. Chaitanya Kumar, M. Ebrahim-Zadeh, *Advanced Solid-State Lasers*, Nagoya, Japan (2017).
[16] A. D. Sanchez, S. Chaitanya Kumar, M. Ebrahim-Zadeh, *Physical Review Research* **6**, 013263 (2024).
[17] A. D. Sanchez, S. Chaitanya Kumar, M. Ebrahim-Zadeh, *Physical Review Research* **7**, 023110 (2025).

Subcycle band-structure videography of graphene

V. Eggers[1], G. Inzani[1], M. Meierhofer[1], J. Helml[1], L. Münster[1], R. Wallauer[2], S. Zajusch[2], S. Ito[2], L.Machtl[1]
H.Yin[3], C. Kumpf[3], F. C. Bocquet[3], C. Bao[1], J. Güdde[2], F. S. Tautz[3] R. Huber[1], U. Höfer[2]
[1] Universität Regensburg, 93040 Regensburg, Germany
[2] Philipps-Universität Marburg, 35037 Marburg, Germany
[3] Forschungszentrum Jülich, 52428 Jülich, Germany

Lightwave electronics [1] leverages the carrier wave of light pulses to accelerate electrons faster than a single optical cycle. Its potential for technological advancement [2] hinges on our ability to precisely control the interaction between ultrafast light transients and emerging quantum materials. To truly understand how light and matter interact at these extremely short time scales, it is essential to observe electron dynamics in momentum space and directly correlate them with the driving light waveform. Recent breakthroughs in angle-resolved photoemission spectroscopy revealed the emergence of intraband currents [3] and Floquet-Bloch states [4] within a fraction of an optical cycle, but only along specific directions near the Brillouin zone center. Yet, in many quantum materials, critical phenomena occur at the Brillouin zone boundaries.

Here, we present the next generation of subcycle band-structure videography. Utilizing strong few-cycle mid-infrared (MIR) driving fields combined with sub-10-femtosecond extreme-ultraviolet (XUV) probe pulses and a state-of-the-art photoemission momentum microscope, we explore electron dynamics across the full Brillouin zone. In a photoemission momentum microscope, the electron detection rate is constrained to roughly one electron per laser shot, as both the electron's position on the detector and its time of flight must be measured simultaneously. To maintain reasonable acquisition durations and achieve reliable statistical outcomes, operating at a high repetition rate is essential. However, this introduces the technical challenge of developing extremely strong, few-cycle MIR pulses within a compact tabletop setup. The newly developed system addresses this by producing phase-stable MIR pulses that, to the best of current knowledge, achieve unprecedented levels of average power and peak electric field strength reaching up to 1 W and exceeding 200 MV/cm at a repetition rate of 50 kHz. In this work, we drive a monolayer of graphene with s-polarized MIR pulses at 27 THz, while 21.7-eV XUV pulses generated from high-harmonic generation probe the dynamics with subcycle time resolution.
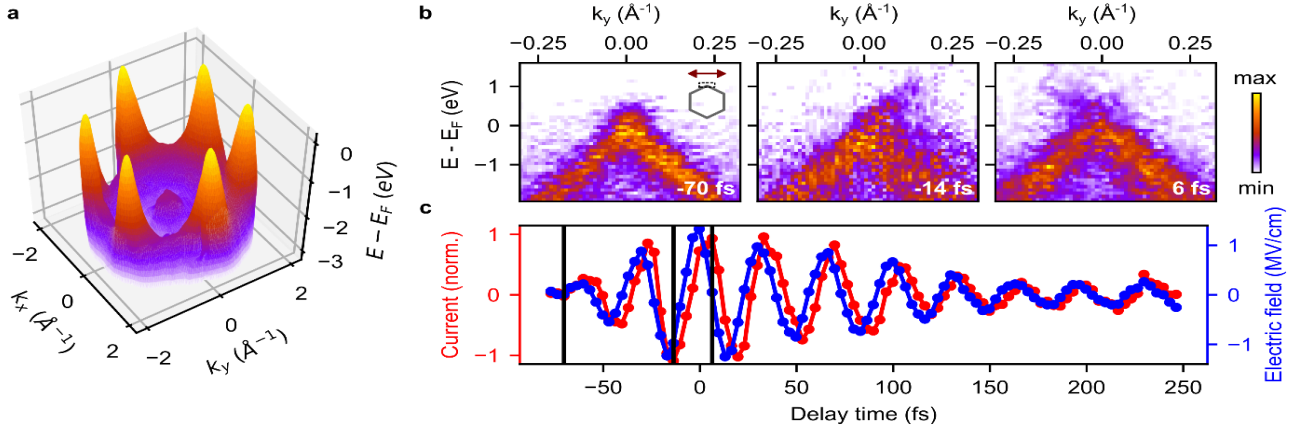
Fig. 1. a, Measured occupied band structure of a monolayer of graphene. b, *View into the band structure at the Dirac point before the arrival of the MIR pulse (t = −70 fs) and for selected delay times, t = -14 fs and t = 6 fs. The latter two show how the electron distribution is accelerated away from the Fermi level and shifted along the Dirac cone. The inset indicates the position of the evaluated window in momentum space, and the arrow marks the MIR polarization.* ***c,*** *Current extracted from the photoemission maps (**red data points**) and the MIR waveform reconstructed from the momentum streaking (blue data points, peak amplitude of 1.5 MV/cm). Vertical lines highlight the temporal positions of the photoemission cuts in **b**.*

A view of the band structure of graphene (Fig. 1a) provides insight into the subcycle dynamics triggered by mid-infrared excitation. Figure 1b presents snapshots of photoemission spectra at the K-point before the MIR transient arrives and at selected delay times shortly after a negative and a positive field crest. Before the arrival of the MIR field (t = −70 fs), we observe the linearly dispersing Dirac cone. Closer to the peak field (t = −14 and 6 fs), the carrier distribution changes: electrons accelerate along the Dirac

cone, moving away from the Fermi level. This redistribution flips direction with the field polarity, indicating a rapid displacement of the Fermi circle in momentum space. The asymmetric electron
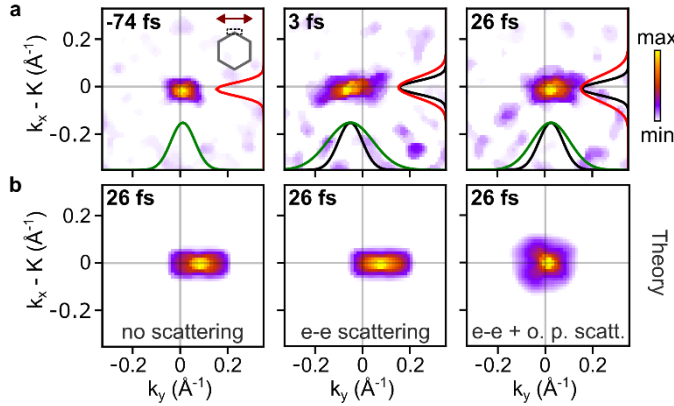
Fig. 2. a, Curvature filtered 2D carrier distribution at the K-point for selected delay times. The inset indicates the position of the evaluated window in momentum space, and the arrow marks the MIR polarization. The Gaussian fits illustrate the width of the projection of the carrier distribution on the k_x axis (red) and the k_y axis (green). The width of the carrier distribution before the pulse (t = −74 fs) is shown in black in the later snapshots. b, Snapshots of the carrier distribution at t = 26 fs calculated with the SBE accounting for different scattering types (left: no scattering, center: electron-electron scattering, right: electron-electron scattering + scattering with optical phonons). The broadening along k_x can only be reproduced when scattering with phonons is included.

distribution at each instant reflects a field-induced current [3]. The trajectory of this current can be directly linked to the shape of the MIR field transient by analyzing how the band structure is streaked in momentum space. This comparison reveals a temporal offset of 4.85 ± 0.21 fs between the current and the driving field (Fig. 1b), highlighting the influence of ultrafast scattering events in setting the pace for lightwave electronics. Repeating the experiment for monolayer graphene samples with varying rotational alignments relative to the SiC substrate, we retrieve a sizable variation of the subcycle delay. An unconventional twist configuration, in which the monolayer is aligned parallel to the substrate [5], was found to enhance coherent charge carrier motion more effectively than the standard growth orientation. This approach points to a promising route for optimizing graphene-based lightwave electronic devices. Recording the full 2D charge distribution allows us to distinguish hallmarks of electron-electron and electron-phonon scattering (Fig. 2a). Initially, the applied driving field stretches the carrier distribution along the k_y axis, resulting in an elliptical shape ($t = -3$ fs). For later delays ($t = 26$ fs) scattering processes lead to a broadening of the distribution also along the k_x direction. Interactions with Γ-LO and TO phonons leads to an isotropic redistribution of hot carriers, while the pseudospin favors collinear electron-electron scattering towards the Dirac point [6]. By comparing these experimentally observed 2D distributions with simulations based on the semiconductor Bloch equations (SBE) [7] that incorporate various scattering mechanisms, we can identify the distinct signatures associated with each type of scattering (Fig. 2b). Analyzing the broadening of the carrier distribution in the direction perpendicular to the field, reveals that scattering with optical phonons primarily drives the rapid decay of coherence in the current. Meanwhile, electron-electron interactions are mainly responsible for thermalizing the excited carriers. Subcycle access to 2D momentum space with attosecond precision proves essential in elucidating these dynamics before relaxation and thermalization. In conclusion, we report an angle-resolved photoemission approach that, for the first time, combines subcycle temporal precision with full 2D Brillouin zone coverage. Its power is demonstrated through the investigation of lightwave-driven currents in graphene, where subcycle analysis reveals ultrafast scattering dynamics that determine the limits of lightwave-driven technologies. Comparing currents across different graphene orientations with sub-femtosecond temporal resolution identifies twist angles optimized for coherent carrier control. Observing the 2D carrier distribution allows us to uncover the fundamental microscopic processes at play, highlighting the interaction between different scattering channels. This method provides key insight into the conditions necessary for achieving fully coherent, field-driven electronic dynamics. It also opens new avenues for exploring rich phenomena in the strong-field regime, including interband and intraband transitions, Landau-Zener tunneling, dynamical Bloch oscillations, and the formation of Floquet-Bloch states.

References
[1] M.Borsch, M. Meierhofer, R. Huber, M. Kira, *Nature Reviews Materials* **8**, 668 (2023).
[2] F. Krausz, M. Stockman, *Nature Photonics* **8**, 205-213 (2014).
[3] J. Reimann, S. Schlauderer, C. P. Schmid, F. Langer, S. Baierl, K. A. Kokh, O. E. Tereshchenko, A. Kimura, C. Lange, J. Güdde, U. Höfer R Huber, *Nature* **562**, 396 (2018).
[4] S. Ito, M. Schüler, M. Meierhofer, S. Schlauderer, J. Freudenstein, J. Reimann, D. Afanasiev, K. A. Kokh, O. E. Tereshchenko, J. Güdde M. A. Sentef, U. Höfer, R. Huber, *Nature* **616**, 696-701 (2023).
[5] F. C. Bocquet,Y.-R.Lin, M. Franke,N. Samiseresht, S.Parhizkar, S.Soubatch, T.-L.Lee, C.Kumpf, F.Tautz, *Physical Review Letters* **125**, 106102 (2020)
[6] E. Malic, T. Winzer, A. Knorr, *Applied Physics Letters* **101**, 213110 (2012).
[7] J. Wilhelm, P. Grössing, A. Seith, J. Crewse, M. Nitsch, L. Weigl, C. Schmid, F. Evers, *Physical Review B* **103**, 125419 (2021).

Short-time dynamics in pair-density-wave superconductor: THG signatures of the elusive many-body state

P. Derendorf[1], P. Choubey[2], I.M. Eremin[1]

[1]*Ruhr-Universität Bochum, 44801 Bochum, Germany*
[2]*Indian Institute of Technology Roorkee, Roorkee 247667, Uttarakhand, India*

A pair density wave superconductor (PDW) is an exotic form of superconducting state in which Cooper pairs carry finite center-of-mass momentum in the absence of the external magnetic field [1]. There are multiple experimental signatures of PDW order in correlated electronic systems including the observation of unidirectional PDW order in high-Tc superconductors [2,3]. At the same time, there are no direct experimental evidence of PDW order obtained so far and the PDW state remains elusive. Here, we investigate the signatures of a unidirectional pair-density wave state in the third harmonic generation (THG) using an effective microscopic model, motivated by the cuprate superconductors. The system possesses a unidirectional PDW Larkin-Ovchinnikov (LO) state with d-wave symmetry in thermodynamic equilibrium ground state without extra need for an additional perturbation such as external Zeeman field or leading charge density wave order. The PDW state is characterized by the breaking of rotational symmetry and the presence of the residual Bogoliubov Fermi surfaces, as shown in the left panel of Fig. 1. We extend this model under the non-equilibrium by including a periodic driving in the form of external ac-field. The signatures of the emerging massive modes on the THG are derived via a gauge-invariant effective action approach. We discuss the emerging signatures in the third harmonic generation and their origin with and without coexisting with uniform d-wave superconducting state.
.
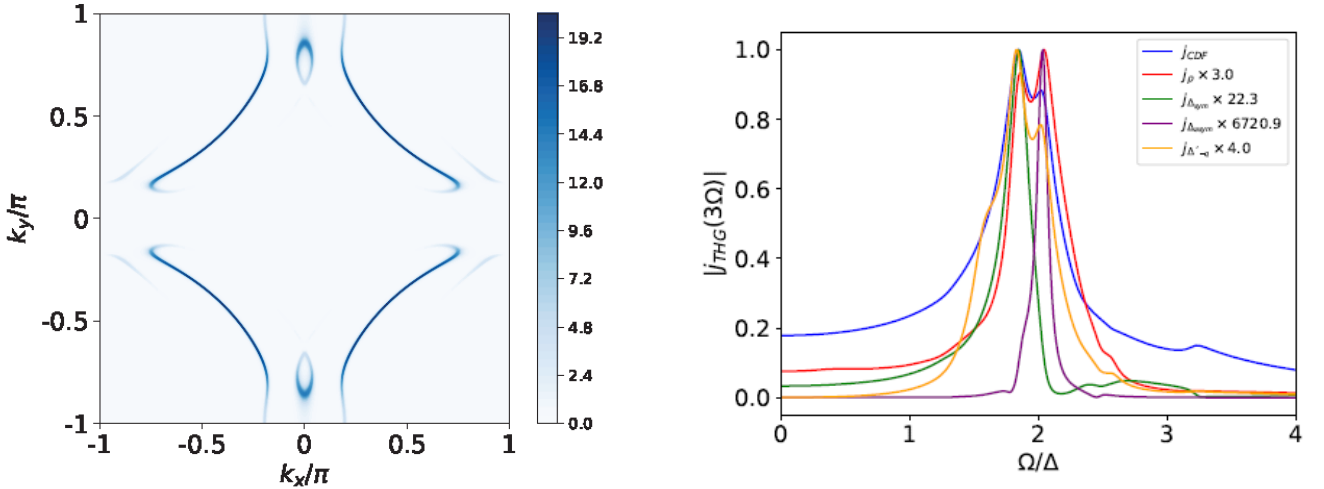
Fig.1. Left :*Calculated spectral function A(k,ω=0) in the PDW Larkin-Ovchinnikov state with Q_x=(π/4,0) ordering wavevector;* **Right**: *Calculated contributions to the third harmonic generation current from the charge density fluctuations (CDF), amplitude fluctuations of the antisymmetric and symmetric modes and the relative phase mode. Note the global phase mode becomes the plasma mode, like it is the case for the uniform superconducting order parameter.*

In particular, in the right panel of Fig.1 we show various contributions to the third harmonic generation current from charge density fluctuations (CDF), collective modes of the antisymmetric and symmetric combinations of the Δ_{+q} and Δ_{-q}, as well as relative phase fluctuations between them. As one could see the THG currents is characterized by the presence of three peaks related to the amplitude modes of the symmetric and antisymmetric channels and the relative phase mode at the energies above 2 Δ. I will discuss further details of the model and results in the talk.

References
[1] D. F. Agterberg, J. S. Davis, S. D. Edkins, E. Fradkin, D. J. Van Harlingen, S. A. Kivelson, P. A. Lee, L. Radzihovsky, J. M. Tranquada, Y. Wang *Annual Review of Condensed Matter Physics* **11**, 231 (2020).
[2] S. D. Edkins, A. Kostin, K. Fujita, A. P. Mackenzie, H. Eisaki, S. Uchida, M. Sachdev, M. J. Lawler, E.-A. Kim, J. C. S. Davis, M. H. Hamidian *Science* 364, 976 (2019).
[3] Z. Du, H. Li, S. H. Joo, E. P. Donoway, J. Lee, J. C. S. Davis, G. Gu, P. D. Johnson, K. Fujita, *Nature* **580**, 65 (2020).
[4] J. Wårdh, M. Granath, *Physical Review* B **96**, 224503 (2017).

Dynamics and fundamental spatial limits in all-optical Magnetic switching

S. Eisebitt

Max-Born- Institut für Nichtlineare Optik und Kurzzeitspektroskopie, 12489 Berlin, Germany

Magnetic structures on the nanometer scale are the basis for current data storage technology in hard drives. In contrast to the conventional use of external magnetic fields, ultrashort laser pulses allow to manipulate magnetization via nonequilibrium states, fueling the hope that more energy efficient process can be realized. Given that the magnetic structures need to be on the order of 10 nm small to be of technological interest, processes on the few-nm scale such as energy transport via hot electrons become relevant when trying to understand the limitations of nonequilibrium pathways to generate and ultimately stabilize desired structures. I will report on studies with ultrashort laser and soft x-ray pulses which explore fundamental physics of nanometer-size magnetic structures, exploiting the short pulse duration and nm-wavelength to address some of the temporal and spatial limitations in this context. [1,2,3]. A dimension that is mostly terra incognita is the development of the magnetization profile along the *depth* of the sample, although the magnetization dynamics along this direction may be pivotal for switching processes, formation of topological non-trivial structures or memory effects, in conjunction with in-plane dynamics. This is also true in in thin-film-based samples, where in addition to the actual magnetic (multi)layers additional layers such as seed-layers for growth or capping for chemical inertness are often present and may influence the behavior. At the same time, the dynamics over spatial scales on the order of one to a few nanometers is ultrafast even when considering the speed of magnons or phonons. Nevertheless, the depth dimension has been explored little in time-resolved experiments due to lack of suitable methods.I will report on substantial progress toward obtaining time-resolved magnetization depth profiles on the femto-and picosecond time scale. This has become possible via pump-probe experiments at broadband high harmonic generation (HHG) sources at photon energies corresponding to the giant absorption resonances of rare earth metals of about 150 eV photon energy. In conjunction with simulations of the x-ray scattering response of the thermal, structural, and magnetic dynamics after laser excitation, [4] time-resolved magnetization depth profiles can be extracted. All-optical switching (or its failure under unsuitable conditions) is observed to depend on dynamic processes along the depth of the sample.[5,6]

References
[1] F. Steinbach, N. Stetzuhn, D. Engel, U. Atxitia, C. von Korff Schmising, S. Eisebitt, *Applied Physics Letters* **120**, 112406 (2022).
[2] F. Steinbach, U. Atxitia, K. L. Yao, M. Borchert, D. Engel, F. Bencivenga, L. Foglia, R. Mincigrucci, E. Pedersoli, D. De Angelis, M. Pancaldi D. Fainozzi, J. S. P. Cresi, E. Paltanin, F. Capotondi, C. Masciovecchio, S. Eisebitt, C. von Korff Schmising, *Nano Letters* **24**, 6865 (2024).
[3] T. Sidiropoulos, P. Singh, T. Noll, M. Schneider, D. Engel, D. Sommer, F. Steinbach, I. Will, B. Pfau, C. von Korff Schmising, S. Eisebitt *Nano Letters* **25**, 4645 (2025).
[4] D. Schick, *Computer Physics Communications* **266**, 108031 (2021).
[5] M.Hennecke, D. Schick, T. Sidiropoulos, F. Willems, A . Heilmann, M. Bock, L. Ehrentraut, D. Engel, P. Hessing, B. Pfau, B.M. Schmidbauer A. Furchner, M. Schnuerer, C von Korff Schmising, S. Eisebitt, *Physical Review Research* **4**, L022062 (2022).
[6] M. Hennecke, D. Schick, T. P.H. Sidiropoulos, J.-X. Lin, Z. Guo, G. Malinowski, M. Mattern, L. Ehrentraut, M. Schmidbauer, M. Schnuerer C. von Korff Schmising, S. Mangin, M. Hehn, S. Eisebitt, *Transient domain boundary drives ultrafast magnetisation reversal*, (submitted).
  * *Acknowledgement:* I would like to explicitly acknowledge all coworkers that have contributed to the research results that are part of this overview presentation, as indicated by the author lists in references [1-6].

Hund excitons and singlet polarons in 2-D van der Waals magnets

A. Feiguin[1], C. Hellman[2], L. Manuel[3], I. Hamad[3], A. Aligia[2]
[1] *Northeastern University, MA 02115 Boston, USA*
[2] *Centro Atómico Bariloche, 8400 Bariloche, Argentina*
[3] *Universidad Nacional de Rosario, 2000 Rosario, Argentina*

We construct a theory that explains the low-energy optical excitations at 1.476 eV and 1.498 eV observed by photoluminiscence, optical absorption, and RIXS in the van der Waals antiferromagnet NiPS3. Using ab initio methods, we construct a two-band Hubbard model for two effective Ni orbitals of the original lattice. The dominant hopping corresponds to third-nearest neighbors. This model exhibits two triplet-singlet excitations of energy near two times the Hund exchange. From perturbation theory, we obtain an effective model for the movement of the singlets in an antiferromagnetic background. We calculate the dynamics of the singlet polarons for the first time through an advanced adaptation of the state-of-the-art self-consistent Born approximation (SCBA) method. These triplet-to-singlet excitations, dressed by a cloud of magnons, move coherently as polaronic-like quasi-particles.
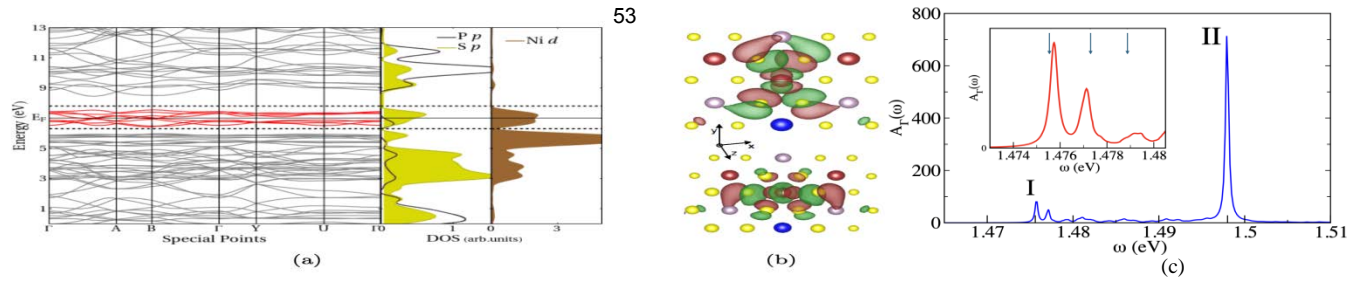
Fig. 1 **(a) Band structure of NiPS$_3$ for the non-magnetic case,** with a unit cell that contains four unit formulae. In red, fit of the bands using the MLWFs. Projected density of states on different atom types are shown on the side of the band structure. **(b)** Representation of the Wannier functions centered on the Ni atoms (depicted as **blue/red spheres**). The top/bottom panels display the odd/even Maximally Localized Wannier Functions (MLWFs), respectively. It is noteworthy that in both cases, the wave functions extend from the S atoms (**yellow spheres**) to the P atoms (**violet spheres**), indicating a strong bonding among them and displaying the mixed nature of each wave function. **(c)** Total spectral function of the singlets at the Γ point as a function of energy. Two quasiparticle peaks can be observed at 1.4757 and 1.498 eV, together with several satellite peaks of the first. The position of the experimentally observed peaks is marked as I and II (see text for details). Inset: detail of the low energy peak and first satellites. The position of the experimentally observed main peak (**peak I**) and satellites is marked with arrows.

Our semi-quantitative treatment explains the key characteristics of the remarkably narrow excitations observed below the gap in various optical experiments and accurately predict their dispersion relation.

References
[1] I. J. Hamad, C. S. Helman, L. O. Manuel, A. E. Feiguin, A. A. Aligia; *Physical Review Letters* **133**, 146502 (2024).

Photo-induced chirality

Z. Zeng[1], M. Först[1], M. Buzzi[1], E. Amuah[1], C. Putzke[1], P.J.W. Moll[1]
D. Prabhakaran[2], P.G. Radaelli[2], A. Cavalleri[2]
[1]Max-Planck-Institut für Struktur und Dynamik der Materie,22761 Hamburg, Germany
[2]University of Oxford, Oxford OX1 3PU, UK

Optically induced functional phenomena in condensed matter require that spatial or temporal symmetries are lowered through interaction with an oscillatory dipolar field. Especially challenging is the search for optically induced chirality in a non-chiral solid, because it requires that all mirrors and all roto-inversions be simultaneously broken. On the other hand, chirality is a pervasive form of symmetry that is intimately connected to the physical properties of solids as well as to chemical and biological activity, making it an attractive target. Here, we use nonlinear phononics to show that chirality of either handedness can be induced in the non-chiral solid BPO$_4$. At equilibrium, two compensated sub-structures of opposite handedness coexist within the unit cell. By resonantly driving either one of two orthogonal, doubly degenerate infrared-active phonon modes with intense mid-infrared light pulses, we displace a second lattice distortion with a positive or negative amplitude, uncompensating the staggered chirality and creating a picosecond-lived structure with either handedness.
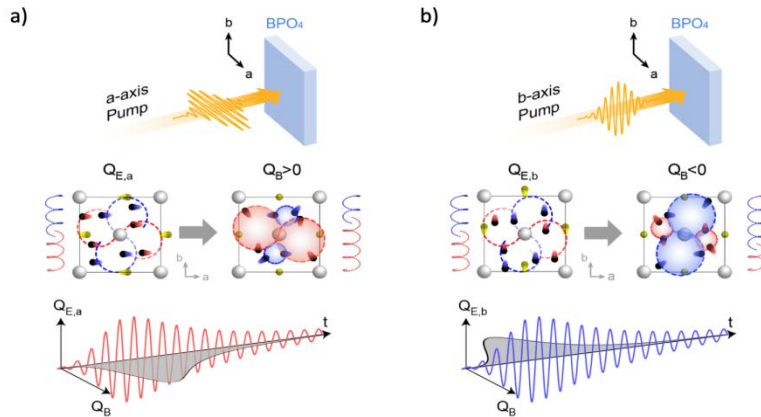
Fig.1. Sketch of the nonlinear phononic interaction used to induce the chiral state. (a) A mid-infrared pump electric field polarized along the a axis induces coherent oscillations of the mode $Q_{E,a}$ about its equilibrium position. A positive transient displacement along the coordinates Q_B of a B-symmetry mode is induced via anharmonic phonon coupling, driving the system into the non-equilibrium chiral state with left handedness. (b)Exciting the generate E-symmetry phonon along the b axis induces coherent oscillations of the $Q_{E,b}$ mode about its equilibrium position. In this case, a negative transient displacement is induced along the Q_B mode coordinates, driving the system into a chiral state with right handedness.

The rotary power of the transient photo-induced chiral state, currently limited by the strength of the mid-infrared excitation pulse, is comparable to the static value of prototypical chiral α-quartz.

Reference
Z. Zeng, M. Först, M. Fechner, M. Buzzi, E. Amuah, C. Putzke, P. J. W. Moll, D. Prabhakaran, P. Radaelli, A. Cavalleri, *Science* **387**, 431 (2025)

Fingerprints of superconducting collective modes in Nonlinear THz spectroscopies

J.Fiore[1], N.Sellati[1], M.Udina[2,3], G.Seibold[4], C. Castellani[1], L.Benfatto[1]

[1]*Universite Sapienza Rome, 00185 Rome, Italy*
[2]*Université de Strasbourg,67081 Strasbourg, France*
[3]*Université Paris Cité,75006 Paris, France*
[4]*Brandenburgische Technische Universität,03046 Cottbus, Germany*

Time-resolved nonlinear THz spectroscopies have experienced tremendous success in recent years in characterizing and controlling the various phases of quantum materials [1,2]. In this talk, we will present an in-depth analysis of the nonlinear optical response in superconductors exposed to intense THz pulses, using a quasi-equilibrium approach rooted in many-body perturbation theory. By establishing connections between nonlinear response functions and experimentally measurable quantities, we investigate how superconducting systems respond to single-pulse and two-pulse multidimensional protocols. Two-dimensional spectroscopy at THz frequencies (2D-THz) has been used to detect collective excitations in solid-state systems [3,4,5], with very recent applications to superconductors [6-8]. While a theoretical understanding of 2D spectroscopy is well established for molecular-like cases [9], many-body systems hosting a continuum of excitations present several complications [10-11]. Here, we propose a perturbative scheme that allows us to compute the contributions of superconducting collective excitations to the 2D signal, taking into account experimental geometries to disentangle the genuine signatures of nonlinear processes from linear response effects. We benchmark this approach on the fingerprint of the Higgs mode in superconducting NbN [8] and on the nonlinear excitation of c-axis Josephson plasmons in cuprates [7].
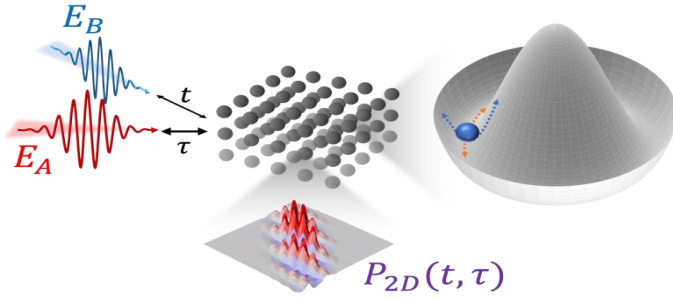
Fig. 1. In the typical 2D experimental setup *two time-delayed electric fields impinge on a superconductor and generate a nonlinear signal. Studying the 2D map as a function of the two times (t, τ) one can track fingerprints of superconducting collective modes.*

In the first case, we reveal how it is possible to detect signatures of amplitude fluctuations in the nonlinearly generated first harmonic of the incoming narrowband electric fields. This enhancement, linked to the nonadiabatic nature of the light-matter interaction when the field resonates with the superconducting spectral gap, allows us to draw a parallel between the excitation of the Higgs mode and the so-called displacive excitation of a coherent phonon (DECP) [12]. In the second case, we investigate the c-axis response of single-layer cuprates, extending insights from previous analyses of third harmonic generation (THG) [13]. A key challenge in this case is disentangling contributions from two-plasmon processes—characteristic nonlinear pathways in these systems—from simpler, instantaneous processes due to screening effects. These examples underscore the challenges and critical refinements needed for the effective analysis of 2D spectra in superconducting materials. In perspective, the developed framework could be applied to distinguish among the various excitation channels of quantum materials characterized by a complex interplay of collective modes [14].

References
[1] D. Nicoletti, A. Cavalleri, *Advances in Optics and Photonics* **8**, 401 (2016).
[2] C. J. Yang, J. Li, M. Fiebig, S. Pal, *Nature Reviews Materials* **8**, 518 (2023).
[3] C. L. Johnson, B. E. Knighton, J. A. Johnson, *Physical Review Letters* **122**, 073901 (2019).
[4] F. Mahmood, D. Chaudhuri, S. Gopalakrishnan, R. Nandkishore , N. P. Armitage, *Nature Physics* **17**, 627 (2021).
[5] T. G. H. Blank, K. A. Grishunin, K. A. Zvezdin, N. T. Hai, J. C. Wu, S. H. Su, J. C. A. Huang, A. K. Zvezdin, A. V. Kimel, *Physical Review Letters* **131**, 026902 (2023)
[6] L. Luo, M. Mootz, J. H. Kang, C. Huang, K. Eom, J. W. Lee, C. Vaswani, Y. G. Collantes, E. E. Hellstrom, I. E. Perakis, C. B. Eom, J. Wang *Nature Physics* **19**, 201 (2023).
[7] A. Liu, D. Pavicevic, M. H. Michael, A. G. Salvador, P. E. Dolgirev, M. Fechner, A. S. Disa, P. M. Lozano, Q. Li, G. D. Gu, E. Demler A. Cavalleri, *Nature Physics* **20**, 1751 (2024)
[8] K. Katsumi, J. Fiore, M. Udina, R. Romero, D. Barbalas, J. Jesudasan, P. Raychaudhuri, G. Seibold, L. Benfatto, N. P. Armitage, *Physical Review Letters* **132** (2024).
[9] S. T. Cundiff, S. Mukamel, *Physics Today* **66**, 44(2013).
[10] O. Hart and R. Nandkishore, *Physical Review B* **107**, 205143 (2023).
[11] A. Gómez Salvador, P. E. Dolgirev, M. H. Michael, A. Liu, D. Pavicevic, M. Fechner, A. Cavalleri, E. Demler, *Physical Review* B **110**, 09451 (2024)
[12] T. E. Stevens, J. Kuhl and R. Merlin, *Physical Review* B **65**, 144304 (2002).
[13] J. Fiore, N. Sellati, F. Gabriele. G. Seibold, C. Castellani, M. Udina, L. Benfatto, *Physical Review* B **110**, L060504 (2024)
[14] J. Fiore, *Ph. D. thesis, Universite Sapienza Rome* (2025).

Coherent phononics in a Rashba semiconductor

P. Fischer[1], J. Bär[1], M. Cimander[1], L. Feuerer[1], V. Wiechert[1], O. Tereshchenko[2]
D. Bossini[1]
[1]Universität Konstanz, D-78457 Konstanz, Germany
[2] Rzhanov Institute of Semiconductor Physics, Novosibirsk 630090, Russia

Optically driven lattice excitations have recently been the subject of intensive investigation as a means to control the macroscopic properties of quantum materials [2–5]. In opaque solids, it is well established that coherent phonons can be excited by laser pulses with photon energies exceeding the electronic band-gap energy [6,7]. However, the dominant microscopic mechanism remains unresolved: Neither experimental nor theoretical approaches [8] have succeeded in disentangling the effects of a photo-induced change in carrier density from an increase in carrier temperature. In this study, we employ time-resolved pump-probe spectroscopy on the Rashba semiconductor BiTeI. By tuning the pump-photon energy from the visible to the mid-infrared, we selectively excite both electronic interband and scarcely accessible intraband transitions. As shown in Fig. 1(a)–(d), coherent phonons with a central frequency of 2.7 THz are generated in both excitation regimes, despite the absence of a charge-carrier density increase in the intraband regime.
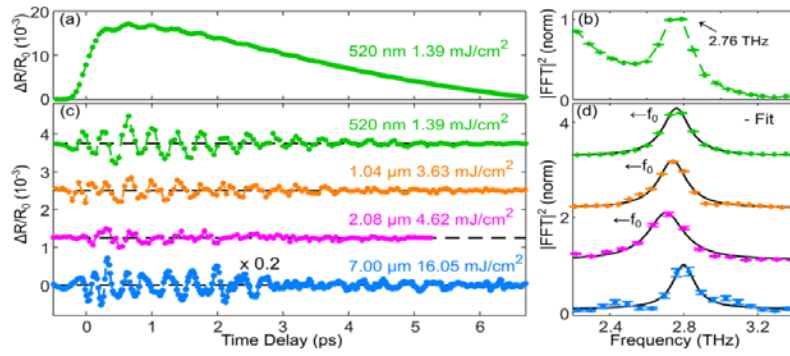
Fig. 1: *(a) Temporal evolution of the normalized reflectivity of BiTeI following excitation by 520-nm laser pulses at a fluence of 1.39 mJ/cm². (b) Fourier-transformed power spectrum of the time trace in panel (a). (c) Oscillatory component of the transient reflectivity for pump wavelengths spanning the visible to mid-infrared range, obtained after subtracting the incoherent background. The 7.00-μm time trace (blue) was scaled by a factor of 0.2 for visualization. (d) Power spectra of the time traces in panel (c), normalized to their respective peak values at the central frequency f_0. Solid black lines represent Lorentzian fits. For interband excitation (520 nm to 2.08 μm), f_0 exhibits a redshift with increasing fluence. Adapted from [1].*

This observation indicates that lattice dynamics are predominantly driven by an elevated carrier temperature. Moreover, in contrast to analogous experiments on other semiconductors relying on interband transitions [9–12], we find that for BiTeI in the intraband regime (Fig. 2), the phonon coherence time remains robust against increasing laser fluence.

Fig. 2. Coherence time τ_c as a function of excitation density. *The value determined from spontaneous Raman spectroscopy is indicated by the* *dashed* *line [13]. For interband excitation (* *green (520 nm),* *orange (1.04 μm),* *purple (2.08 μm))* *τ_c decreases for excitation densities larger than $1x10^{21}$ cm^{-3}. For intraband excitation (* *blue (7 μm))* *we observe no density dependent variations of τ_c. Adapted from [1]*
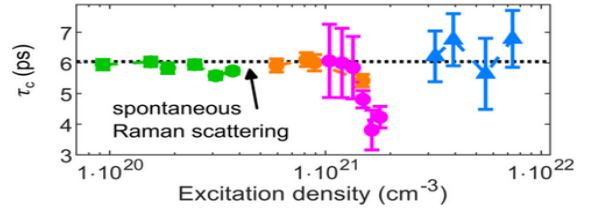
These findings offer new perspectives on the coherent structural manipulation of solids exhibiting the Rashba effect [14-19].

References
[1] P. Fischer, J. Bär, M. Cimander, L. Feuerer, V. Wiechert, O. Tereshchenko, D. Bossini, *Physical Review* B **111**, L081201 (2025).
[2] K.W. Kim, A. Pashkin, H Schäfer, M. Beyer, M. Porer, T. Wolf, C Bernhard, J. Demsar, R. Huber, A. Leitenstorfer, *Nature Materials* **11**, 497 (2012)
[3] T. F. Nova, A. Cartella, A. Cantaluppi, M. Först, D. Bossini, R. V.Mikhaylovskiy, A. V. Kimel, R. Merlin, A. Cavalleri, *Nature Physics* **13**, 132 (2017)
[4] T. F. Nova, A. S. Disa, M. Fechner, A. Cavalleri, Metastable ferroelectricity in optically strained SrTiO3, Science **364**, 1075 (2019).
[5] D. Fausti, R. I. Tobey, N. Dean, S. Kaiser, A. Dienst, M.C. Hoffmann, S. Pyon, T. Takayama, H. Takagi, A. Cavalleri, *Science* **331**, 189 (2011)
[6] T. K. Cheng, S. D. Brorson, A. S. Kazeroonian, J. S. Moodera, G. Dresselhaus, M. S. Dresselhaus, E. P. Ippen, *Applied Physics Letters* **57**, 1004 (1990)
[7] G.C. Cho, W. Kütt, H. Kurz, *Physical Review Letters* **65**, 764 (1990).
[8] H. J. Zeiger, J. Vidal, T. K. Cheng, E. P. Ippen, G. Dresselhaus, M. S. Dresselhaus, *Physical Review* B **45**, 768 (1992).
[9] W.Kutt, G. C. Cho, T. Pfeifer, H. Kurz, *Semiconductor Science and Technology* **7**, B77 (1992).
[10] O. V. Misochko, *Journal of Experimental and Theoretical Physics* **92**, 246 (2001).
[11] K. J. Yee, K. G. Lee, E. Oh, D. S. Kim, Y. S. Lim, *Physical Review Letters* **88**, 105501 (2002).
[12] M. Hase, S.-I. Nakashima, K. Mizoguchi, H. Harima, K. Sakai, *Physical Review* **B** 60, 16526 (1999)
[13] I. Y. Sklyadneva, R. Heid, K .- P. Bohnen, V. Chis, V. A. Volodin, K. A. Kokh, O. E. Tereshchenko, P. M. Echenique, E. V. Chulkov, *Physical Review* B 86, 094302 (2012).
[14] A. Crepaldi, L. Moreschini, G. Autès, C. Tournier - Colletta, S. Moser, N. Virk, H. Berger, P. Bugnon, Y. J. Chang, K. Kern, A. Bostwick E. Rotenberg, O. V. Yazyev, M. Grioni, *Physical Review Letters* **109**, 096803 (2012).
[15] L. Cheng, L. Wei, H. Liang, Y. Yan, G. Cheng, M. Lv, T. Lin, T. Kang, G. Yu, J. Chu, Z . Zhang, C. Zeng, *Nano Letters* **17**, 6534 (2017).
[16] G. Kremer, J. Maklar, L. Nicolaï, C. W. Nicholson, C. Yue, C. Silva, P. Werner, J. H. Dil, J. Krempaský, G. Springholz, R. Ernstorfer, J. Minár L. Rettig, C. Monney, *Nature Communicatios* **13**, 6396 (2022).
[17] S. T. Ciocys, N. Maksimovic, J. G. Analytis, A. Lanzara, *npj Quantum Materials* **7**, 79 (2022).
[18] M. Michiardi, F. Boschini, H. - H. Kung, M. X. Na, S. K. Y. Dufresne, A. Currie, G. Levy, S. Zhdanovich, A. K. Mills, D. J. Jones, J. L. Mi B. B. Iversen, P. Hofmann, A. Damascelli, *Nature Communications* **13**, 3096 (2022).
[19] J. Qu, E. F. Cuddy, X. Han, J. Liu, H. Li, Y.- J. Zeng, B. Moritz, T. P.Devereaux, P. S.Kirchmann, Z.-X. Shen, J. A. Sobota, *Physical Review Letters* **133** 106401 (2024)

Nonequilibrium dynamics of a disordered binary alloy

H. F. Fotso

State University of New York Buffalo, Buffalo, NY14260, USA

We study the nonequilibrium dynamics of a disordered correlated binary alloy, described by the Anderson-Hubbard model with binary disorder. The system is subjected to an interaction quench whereby the interaction is abruptly switched from one initial value to another. Our nonequilibrium solution uses the recently formulated nonequilibrium DMFT+CPA [1, 2]. While CPA is known to not capture a localization effect arising from disorder with the so-called "box" disorder, it does effectively describe the disorder-induced metal-to-insulator transition with binary disorder. Thus, the present study examines the interplay between the disorder-induced metal-to-insulator transition and the interaction-induced metal-to-Mott insulator transition, with a focus on how this interplay affects the nonequilibrium dynamics. Our solution is first used to examine the equilibrium density of states of the system and its dependence on both the interaction and the disorder strength. We find that disorder delays the opening of the Mott gap to stronger interactions in agreement with previous results. Vice-versa, the interaction delays the opening of the disorder gap to stronger disorder. Next we examine the dynamics of the system across the interaction quench. Across the interaction quench, we find that disorder plays a non-trivial role on the dynamics and on the long-time state of the system. For weak interaction, we observe that the final kinetic energy is increased with the disorder strength. As the interaction increases, we observe at moderate interactions, a reversal in the initial trend for the kinetic energy, with increased disorder strength leading to lower kinetic energy. The possibility of both the disorder and the Mott gap in the Anderson-Hubbard model for a random binary alloy gives rise in the DMFT+CPA calculation to a more complex behavior of the density of states. Figs. 1 (a) and (b) show the density of states for the noninteracting system ($U = 0$) and for $U = 1.5$ respectively, with disorder strengths varying between $W = 0$ and $W = 0.7$.
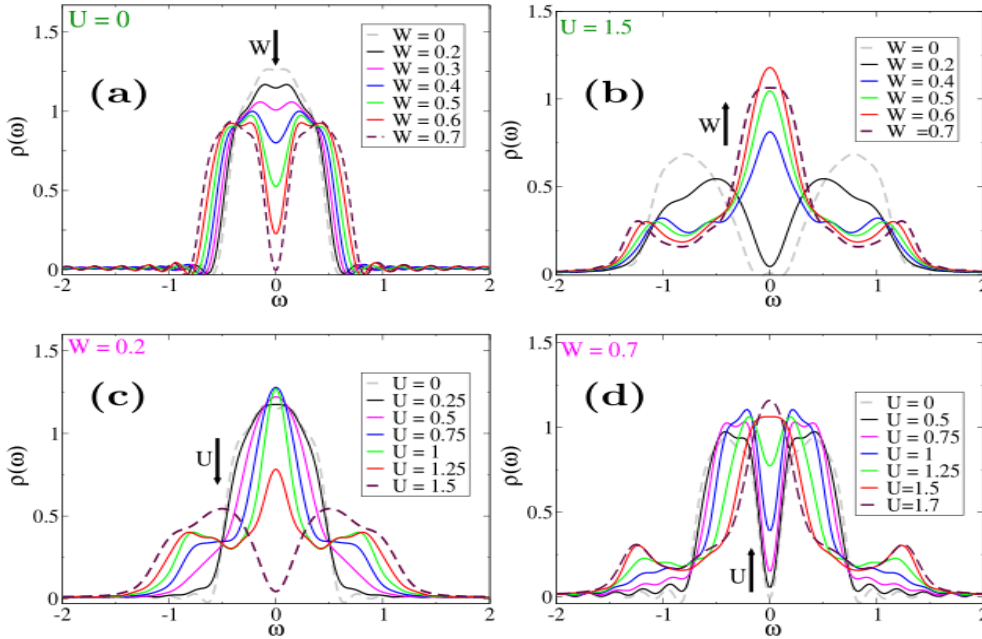
*Fig. 1: Equilibrium density of states of the Anderson-Hubbard model with $U = 0$ (Anderson model) (**a**), $U = 1.5$ (**b**) for disorder strength W varying from 0 to 0.7. Equilibrium density of states of the Anderson-Hubbard model with $W = 0.2$ (**c**) and $W = 0.7$ (**d**) for interaction strength U varying from 0 to 1.5 and from 0 to 1.7 respectively. The arrows indicate increasing disorder strength in (**a**) and (**b**), and increasing interaction strength in (**c**) and (**d**) [3].*

For the noninteracting system, in the absence of disorder, we recover the semi-elliptical density of states, despite the Gibbs phenomenon arising from the truncation of the time axis. Increasing the disorder strength on this noninteracting system gradually splits the spectral weight into two symmetric peaks centered around $+W/2$ and $-W/2$. At finite but small disorder, these are two small bumps and they eventually form a fully gaped spectrum at $W \sim 0.7$ (Fig.1 (a)). A weak but finite interaction strength delays the formation of the disorder gap (not shown). When the interaction is above the critical value of the Mott metal-to-insulator transition for the clean system, as shown in Fig.1 (b) for $U = 1.5$, increasing the disorder strength gradually increases the spectral weight around the Fermi energy and eventually closes the gap. Figs.1 (c) and (d) show the density of states for the $W = 0.2$ (c) and for $W = 0.7$ (d)

respectively, with interaction strength varying between U = 0 and U = 1.7. For W=0.2, the density of states is similar to that of the clean system with the opening of the Mott gap delayed to a slightly stronger interaction. This delayed opening of the gap is more apparent for W= 0.7 where increasing the interaction strength, is seen to fill the disorder gap. Continuing to increase the interaction eventually leads to the opening of the Mott gap with two Hubbard bands that are each additionally split into two parts due to the presence of the strong binary disorder (not shown). To probe the interplay of interaction and disorder in the nonequilibrium dynamics, we track the time dependence of the kinetic and potential energy in the system across the interaction quench whereby, with the system initially in equilibrium at a given temperature and with a fixed disorder strength, the interaction is abruptly switched from $U_1 = 0$ to a finite value U_2 at which it is subsequently kept constant. We also evaluate the total energy in the system. It is obtained by summing up the kinetic energy and the potential energy. Fig. 2 presents the relaxation of the potential (blue), kinetic (red), and total (black) energy as a function of time when the system is quenched at time t = 0 from $U_1 = 0$ to $U_2 = t^*$ (a), $U_2 = 1.5\, t^*$ (b), $U_2 = 2\, t^*$ (c), $U_2 = 2.5\, t^*$ (d).
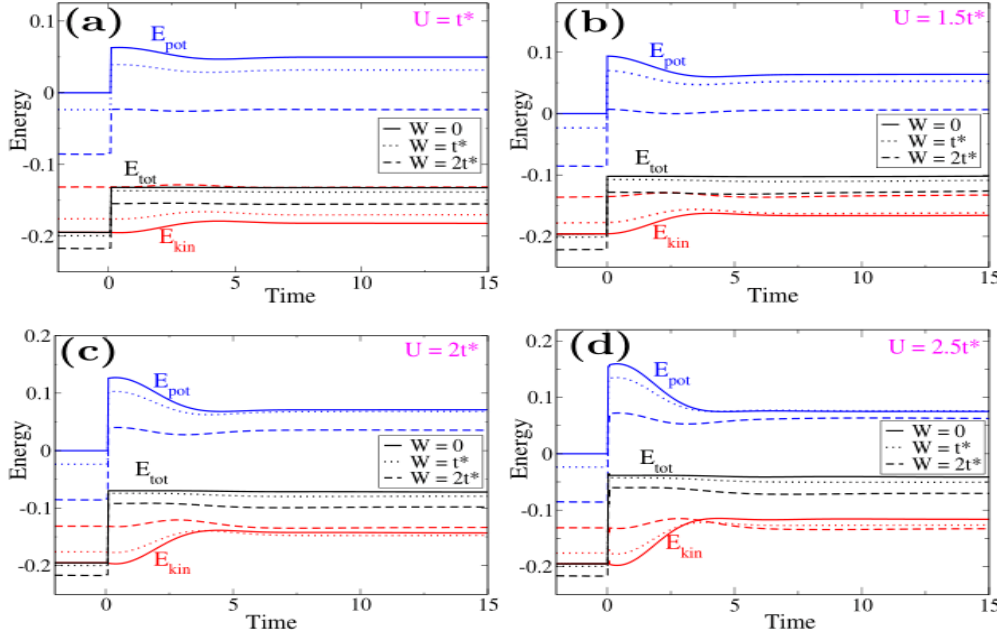
Fig. 2. Relaxation of the potential (blue), kinetic (red) and total (black) energy as a function of time when the system is quenched at time t = 0 from $U_1 = 0$ to $U_2 = t^*$ (a), $U_2 = 1.5\, t^*$ (b), $U_2 = 2\, t^*$ (c), $U_2 = 2.5\, t^*$ (d). Each panel shows the time evolution of the three types of energy for disorder strength W = 0 (solid line), W = t* (dotted line) and W = 2t* (dashed line) [3]

Each panel shows the time evolution of the three types of energy for disorder strengths W = 0 (solid line), W = t* (dotted line) and W = 2t* (dashed line). After the interaction quench, the total energy changes from an initial value to another value at which it is subsequently kept constant since the system is isolated. This total energy decreases with increased disorder strength. During the transient, the kinetic energy and the potential energy evolve in a complementary manner so as to keep the total energy constant. Immediately across the interaction quench, the change in potential energy for a clean system increases with the final interaction strength. As the disorder strength is increased, this change in potential energy is decreased. After the short-time transient, both the kinetic energy and the potential energy settle into their long-time values. For weak interaction, the long-time value of the kinetic energy increases with the disorder strength. At moderate interaction (Fig. 2 (d)), this trend is reversed and the long-time value of the kinetic energy decreases with increasing disorder strength. Altogether, using the nonequilibrium DMFT+CPA on a disordered binary alloy enable the characterization of the nontrivial interplay between disorder and interaction on the density of states and on the relaxation of the system away from equilibrium.

References
[1] E. Dohner, H. Terletska, K.-M. Tam, J. Moreno, H. F. Fotso, *Physical Review* B **106,** 195156 (2022).
[2] E. Dohner, H. Terletska, H. F. Fotso, *Physical Review* B **108**, 144202 (2023).
[3] A. Aubelmaged, E. Dohner, S. Liou H. F. Fotso, *arXiv:2503.23505* (2025).
 * We acknowledge support from the Department of Energy under grant number DE-SC0024139.

Floquet-Bloch valleytronics

S. Fragkos[1], B. Fabre[1], O.Tkach[2,3], S.Petit[1], D. Descamps[1], G.Schonhense[2], Y. Mairesse[1], M. Schuler[4]
S.Beaulieu[1]

[1]*Universite de Bordeaux, F33405 Talence, France*
[2]*Johannes Gutenberg-Universitat,D-55099 Mainz, Germany*
[3]*Sumy State University, 40007 Sumy, Ukraine*
[4]*University of Fribourg, CH-1700 Fribourg, Switzerland*

Driving quantum materials out-of-equilibrium makes it possible to generate states of matter inaccessible through standard equilibrium tuning methods [1-3]. Upon time-periodic coherent driving of electrons using electromagnetic fields, the emergence of Floquet-Bloch states enables the creation and control of exotic quantum phases [4-7]. In transition metal dichalcogenides, broken inversion symmetry within each monolayer results in a non-zero Berry curvature at the K and K' valley extrema, giving rise to chiroptical selection rules that are fundamental to valleytronics [8-12]. Here, we bridge the gap between these two concepts and introduce Floquet-Bloch valleytronics. Using time- and polarization-resolved extreme ultraviolet momentum microscopy (Fig. 1a,b) combined with state-of-the-art ab initio theory, we demonstrate the formation of valley-polarized Floquet-Bloch states in 2H-WSe2 upon below-bandgap coherent electron driving with chiral light pulses (Fig. 1c). We investigate quantum path interference between Floquet-Bloch and Volkov states [13-16], showing that this interferometric process depends on the valley pseudospin and light polarization-state. Conducting extreme ultraviolet photoemission circular dichroism in these nonequilibrium settings reveals the potential for controlling the orbital character of Floquet-engineered states (Fig. 1d).
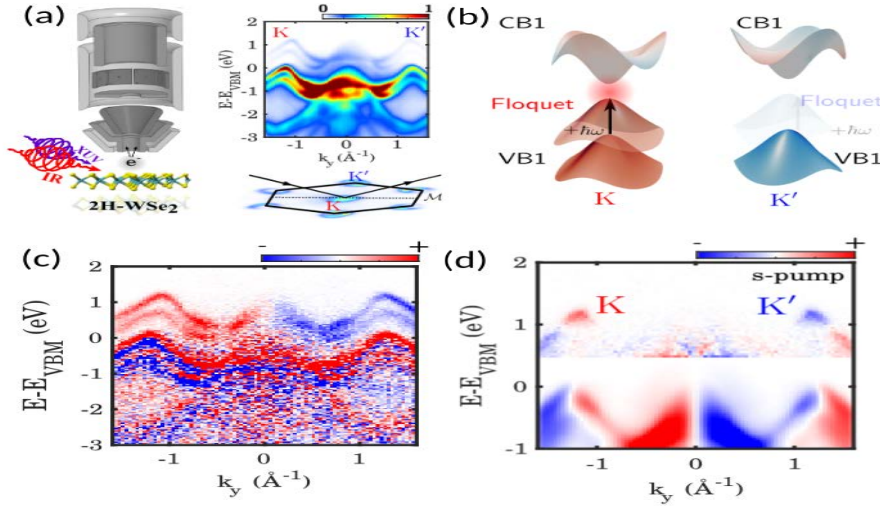
Fig. 1. Floquet-Bloch Valleytronics.
(a) Experimental scheme with polarization tunable infrared pump and XUV probe pulses. The energy-momentum cut recorded at pump-probe overlap, shows the emergence of sidebands.
(b) Schematic of the Floquet-engineered electronic structure of $2H\text{-}WSe_2$ around K and K' valleys.
(c) Valley-Polarized Floquet-Bloch States in $2H\text{-}WSe_2$.
(d) XUV circular dichroism revealing the orbital texture of the Floquet-Bloch states.

These findings link Floquet engineering and quantum geometric light-matter coupling in two-dimensional materials. They can serve as a guideline for reaching novel out-of-equilibrium phases of matter by dynamically breaking symmetries through coherent dressing of winding Bloch electrons with tailored light pulses.

References
[1] T. Rohwer, S. Hellmann, M.Wiesenmayer, C. Sohrt, A.Stange, B. Slomski, A. Carr, Y.Liu, L.M. Avila, M. Kalläne, S. Mathias, L. Kipp, K. Rossnagel M. Bauer, *Nature* **471**, 490 (2011).
[2] D. N.Basov, R.D. Averitt, D. Hsieh, *Nature Materials* **16**, 1077 (2017).
[3] A. de la Torre, D. M. Kennes, M. Claassen, S. Gerber, J. W. McIver, M. A. Sentef, *Review of Modern Physics* **93**, 041002 (2021).
[4] T. Oka, H. Aoki, Physical Review B **79**, 081406 (2009).
[5] J. W. McIver, B. Schulte, F.-U. Stein, T. Matsuyama, G. Jotzu, G. Meier, A. Cavalleri, *Nature Physics* **16**, 38 (2020).
[6] M. S. Rudner, N.H. Lindner, *Nature Reviews Physics* **2**, 229 (2020).
[7] T. Oka, S. Kitamura, *Annual Review of Condensed Matter Physics* **10**, 387 (2019).
[8] K. F. Mak, K. He, J. Shan, T.F. Heinz, *Nature Nanotechnology* **7**, 494 (2012).
[9] H. Zeng. J. Dai. W. Yao. D. Xiao. X. Cui. *Nature Nanotechnology* **7**. 490 (2012).
[10] T. Cao, G. Wang, W.Han, H.Ye, C.Zhu, J.Shi, Q. Niu, P.Tan, E. Wang, B. Liu, J. Feng, *Nature Communications* **3**, 887 (2012).
[11] J. R. Schaibley, H. Yu, G. Clark, P. Rivera, J.S. Ross, K.L. Seyler, W. Yao, X. Xu, *Nature Reviews Materials* **1**, 16055 (2016).
[12] I. Tyulnev, Á.Jiménez-Galán, J. Poborska, L. Vamos, P. St. J. Russell, F. Tani, O.Smirnova, M.Ivanov,R.E. F. Silva,J.Biegert, *Nature* **628**, 746(2024)
[13] J.- H. Park, C.H. Kim, J.-W. Rhim, J. H. Han, *Physical Review* B **85**, 195401 (2012).
[14] F. Mahmood, C.K. Chan, Z. Alpichshev, D. Gardner, Y.Lee, P.A. Lee, N. Gedik, *Nature Physics* **12**, 306 (2016).
[15] D. Choi, M. Mogi, U. De Giovannini, D. Azoury, B. Lv, Y.Su, H.Hübener, A. Rubio, N. Gedik, *arXiv 2404.14392* (2024).
[16] M. Merboldt, M. Schüler, D.Schmitt,J.P. Bange,W.Bennecke,K.Gadge,K.Pierz,H. W. Schumacher, D Momeni,D. Steil,S. R. Manmana, M. A. Sentef M. Reutzel, S.Mathias,*arXiv 2404.12791* (2024).

Generating a near perfect conductor at the transition from single to Double-well dynamics in a charge-density-wave insulator driven by an Ultrafast electric field

J. K. Freericks[1], M. Petrovic[1], M. Weber[2]
[1] Georgetown University, Washington, DC 20057, USA
[2] Max-Planck-Institut für Physik Komplexer Systeme, 01187 Dresden, Germany

We explore a transient decoupling between electrons and phonons in a one-dimensional charge-density-wave system modeled with the Holstein or Su-Schrieffer-Heeger model. In a standard pump-probe setting, the pump pulse can be fine-tuned to excite the model system so that the electron-phonon interaction briefly disappears. Switching off the electron-phonon coupling can drastically change the conducting properties of a material: an insulator can be transiently turned into a perfect conductor for a brief time. The defining characteristics of the decoupling is the dynamical slowdown, where the closer the pump gets to the critical decoupling fluence, the longer the system stays in the transient conducting state. Passing through the critical fluence is accompanied by the doubling of the phonon oscillation frequency which can be observed in the time-resolved photoemission spectrum. A schematic of the systems and the different regimes we study is given in Fig.1.
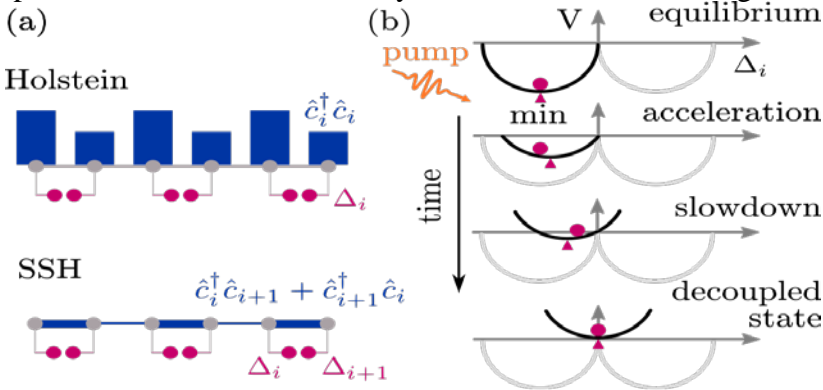
Fig.1. Schematic of the two studied models: the Holstein and the SSH model. The blue bars in the upper panel in (a) represent an onsite charge density, which is coupled to a local phonon coordinate Δi (dark red dots). In the SSH model, the local bond length $\Delta_{i+1} - \Delta_i$ is coupled to the local bond current (blue stripes in the lower panel in (a)). (b) Dynamical slowdown in the Holstein model explained in terms of a single phonon coordinate (dark red dots) moving in a local parabolic potential energy (black curve). The dark red triangles show the local potential minimum at a given time moment, while the gray parabolas show the two possible equilibrium potential profiles.

We model the electron-phonon coupling in the Holstein model as a local charge coupling, while in the Su-Schrieffer-Heeger model it is a modulation of the hopping on the lattice. In both cases, when the phonon coordinate vanishes, the electron-phonon coupling goes to zero, and the system can be described by a perfect conductor (lattice electrons with no scattering). Eventually, the metastable phase is destroyed and the system relaxes to a case where the phonons oscillate with time and conventional electron-phonon coupling returns. One needs to have fine tuning of the pump fluence to achieve this state, because it arises when the system has a transition from the phonon oscillating in one well, to oscillating in two wells. Because we model this system with semiclassical phonons, the new phase is easiest to create at T=0. But, even at nonzero T, we find the behavior remains. As an example of how the phonon coordinate is pinned to a plateau value and how the conductivity is enhanced in this region, see Fig. 2.
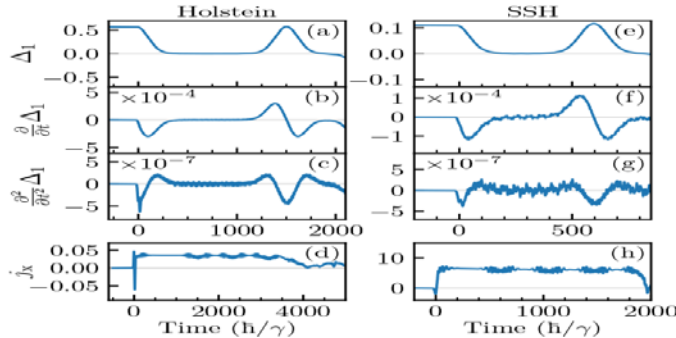
Fig. 2. Time evolution of the first phonon coordinate in the Holstein model (a), its speed (b), the force acting on it (c), and the current along the x direction. Panels (e)–(h) show the corresponding data for the SSH model. There are $L = 110$ sites in the system, $\Omega = 0.02\ \gamma/\hbar$, $\omega_p = 0.01\ \gamma/\hbar$, and $\sigma_p = 10\ \hbar/\gamma$. The critical field in the Holstein model is $E_0 = 0.4276130143995$ and for the SSH model $E_0 = 0.07022968248795$. The coupling constants are the same $\lambda = \lambda' = 0.6.$.

What one can see is by pinning the phonon coordinate near the origin, we limit the electron-phonon coupling greatly enhancing the electron lifetime and allowing for strongly enhanced electron conductivity. We have shown the result is stable (but weakened) with respect to thermal fluctuations as well. This work is being prepared for publication. The theory for this work is in [1], while an application to impulse phonons is in [2].

References
[1] M. Weber, J. K. Freericks, *Physical Review* E **105**, 025301 (2022).
[2] M. Petrovic, M, Weber, J. K. Freericks, *Physical Review* X **14**, 031052 (2024).

Giant chiral magnetoelectric oscillations in a van der Waals multiferroic

F. Y. Gao

The University of Texas at Austin, 78712 Austin, Texas, USA

The recent discovery of type-II multiferroicity in frustrated van der Waals magnets down to the single-layer limit raises prospects of unprecedented magnetoelectric couplings in two dimensions. However, the exact nature and strength of these couplings have remained unknown to date. [1,2] Here, for the first time, we perform a precision measurement of the dynamical magnetoelectric coupling in an exfoliated van der Waals multiferroic, NiI_2. We evaluate this interaction in resonance with a collective electromagnon (EM) mode, capturing the impact of its oscillations on the material's dipolar and magnetic orders. Our findings reveal a record-breaking dynamical magnetoelectric coupling strength for a single-phase multiferroic at terahertz frequencies, leading to a giant natural optical activity. State-of-the-art first principles calculations further reveal that this chiral coupling originates from a combination of spin-orbit interactions and non-collinear magnetic order, resulting in substantial enhancements over lattice-mediated couplings.
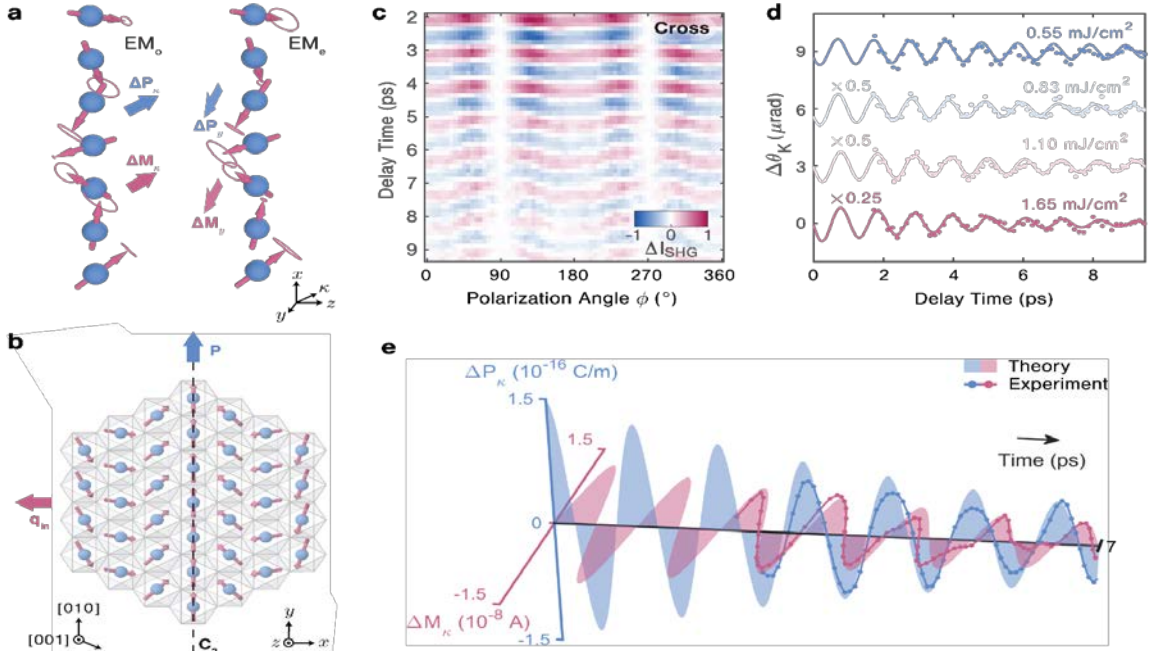
Fig. 1. a- *Eigenvector spin precessions of the two electromagnons in NiI_2, EM_o, and EM_e, shown alongside the calculated polarization, ΔP, and magnetization, ΔM, modulations for each mode. **b-** The low-temperature spin-spiral order depicted on the (001) plane with propagation vector $q = (0.138a^*, 0, 1.457c^*)$ and static electric polarization P. **c-** Anisotropic time-resolved SHG signal shown as a function of probe polarization angle ϕ in the cross-polarized configuration. **d-** Time-resolved reflective Kerr signals for several incident pump fluences. Experimental data (**circles**) is shown alongside fits to a pair of damped oscillators (**lines**). **e-** Time-dependent modulations of the two-dimensional electric polarization and magnetization extracted for EM_o from the tr-SHG (**blue dots, lines**) and tr-RKerr measurements (**red dots, lines**). Theoretical electric polarization and magnetization dynamics of the EM_o mode were obtained from DFT calculations and presented assuming a phenomenological damping rate (**filled areas**).*[3]

Our results highlight the potential for intertwined orders to enable unique functionalities in the two-dimensional limit and pave the way for the development of van der Waals magnetoelectric devices operating at terahertz speeds.

References

[1] Q. Song, C. A. Occhialini, E. Ergeçen, B. Ilyas, D. Amoroso, P. Barone, J. Kapeghian, K. Watanabe, T. Taniguchi, A. S. Botana, S. Picozzi, N. Gedik R. Comin, *Nature* **602**, 7898 (2022).

[2] T. Kurumaji, S. Seki, S. Ishiwata, H. Murakawa, Y. Kaneko, Y. Tokura, *Physical Review* B **87**, 014429 (2013).

[3] F. Y. Gao, X. Peng, X. Cheng, E. V. Boström, D. S. Kim, R. K. Jain, D. Vishnu, K. Raju, R. Sankar, S.-F. Lee, M. A Sentef, T. Kurumaji, X. Li P. Tang, A. Rubio, E. Baldini, *Nature* **632**, 273 (2024).

Ultrafast control of the superconducting condensate in cuprates Superconductors via time-resolved ARPES

N. Gauthier[1], D. Armanno[1], F. Goto[1], O. Gingras[3], J.-M. Parent[1], S. Lapointe[1], A. Longa[1], G. Jargot[1]
F. Légaré[1] B. J. Siwick[2], A.Georges[3], A.Millis[3], F.Boschini[1]

[1]*Institut National de la Recherche Scientifique, Varennes, QC J3X 1S2, Canada*
[2]*McGill University, Montreal, QC H3A 0B8, Canada*
[3]*Flatiron Institute, New York, NY 10010, USA*

Copper-based superconductors (a.k.a. cuprates) have been extensively studied using pump-probe techniques such as time- and angle-resolved photoemission (TR-ARPES) thanks to its exquisite energy, momentum and temporal resolution, with the aim of clarifying the nature and formation of their unconventional superconductivity (SC) [1]. In the broad picture of how light can be used to control the properties of the condensate in cuprates, I will address two long-standing questions: (i) how an ultrafast excitation modifies the superconducting condensate and (ii) what is the normal state on top of which unconventional superconductivity emerges. To date, there is compelling evidence that an ultrafast light excitation causes a loss of macroscopic phase coherence (without affecting the coupling strength of the Cooper pairs), resulting in a transient filling of the SC gap [2]. However, since ARPES is not sensitive to the phase of the SC gap, it is still unclear whether the microscopic mechanism responsible for this effect is light-induced pair or phase fluctuations. Here, I will present a novel experimental strategy able to directly probe essential information about the superconducting gap phase with momentum resolution. By leveraging a phase-only-sensitive hybridization gap present in Bi-based cuprates [3], we can ascribe light-induced phase fluctuation as the mechanism driving the transient filling of the SC gap. Going beyond, one of the key unresolved questions in cuprates include the nature of the low-energy density of states in the low-temperature normal state in the absence of SC. In order to experimentally probe the low-temperature normal state, the long-range SC needs to be quenched while keeping the electronic temperature below the critical temperature T_C.
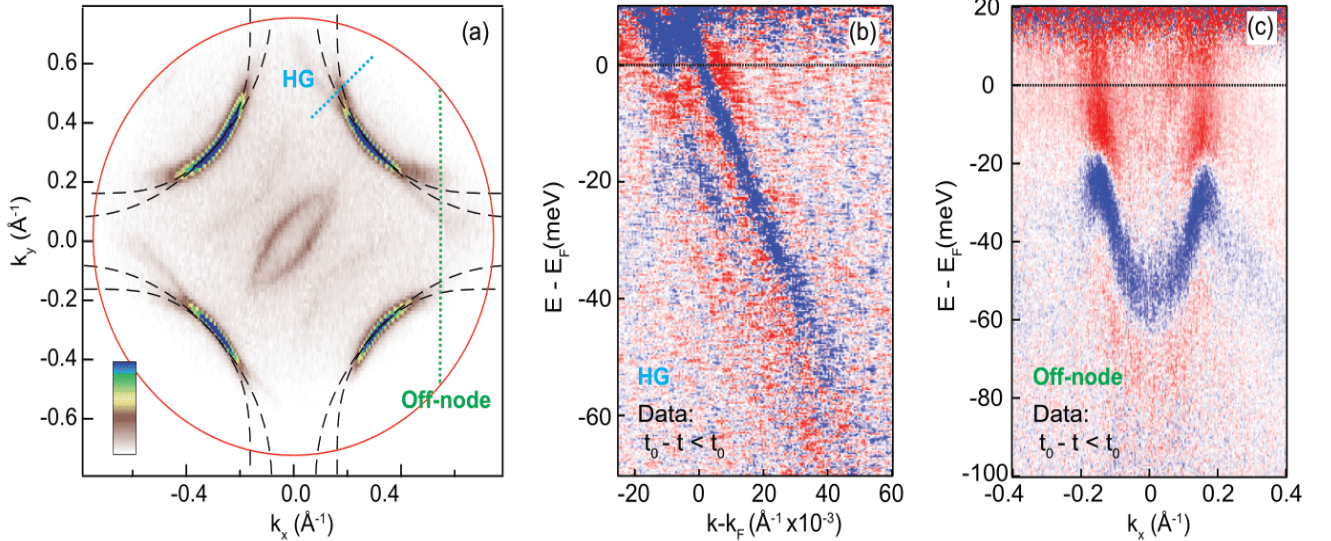
***Fig.1. a. $Bi_2Sr_2CaCu_2O_{8+\delta}$ OD91 (Bi2212) Fermi Surface integrated $\pm$ 10 meV.** The **blue** (**green**) dashed line represent the hybridization (off-node) cut. The **red circle** represents the low energy cutoff determined by the probe photon energy; **b.** Differential map (pumped-unpumped) of the hybridization gap (HG) cut in Bi2212. **c.** Differential map (pumped-unpumped) of the off-nodal cut in Bi2212.*

Specifically, I will show how mid-infrared light can be used to uncover the normal state beneath the equilibrium SC phase as well as how it connects to the pseudogap phase (a partial suppression of spectral weight at the Fermi level) by probing directly the transient spectral function of the material.

References
[1] F. Boschini, M. Zonno, A. Damascelli, *Review of Modern Physics* **96,** 015003 (2024).
[2] F. Boschini, E. H. da Silva Neto, E. Razzoli, M. Zonno, S. Peli, R. P. Day, M. Michiardi, M. Schneider, B. Zwartsenberg, P. Nigge, R. D. Zhong J. Schneeloch, G. D. Gu, S. Zhdanovich, A. K. Mills, G. Levy, D. J. Jones, C. Giannetti, A. Damascelli, *Nature Materials* **17**, 416 (2018)
[3] Q. Gao , J.M. Bok, P. Ai, J.Liu, H. Yan, X.Luo, Y.Cai, C. Li , Y. Wang, C. Yin, H. Chen, G. Gu, F. Zhang , F. Yang , S. Zhang, Q. Peng , Z. Zhu G. Liu, Z.Xu , T.Xiang, L.Zhao , H.-Y. Choi, X. J. Zhou, *Nature Communications* 15, 4538 (2024).

Correlations drive the attosecond response of Strongly-correlated insulators

R. Cazali[1], A. Alic[2], M. Guer[1], C. J. Kaplan[3], F. Lepetit[1], O. Tcherbakoff[1], S. Guizard[1], A. Rubio[4]
N. Tancogne-Dejean[5], G. S. Chiuzbăian[2], R. Géneaux[1]

[1]*Université Paris-Saclay, 91191 Gif-sur-Yvette, France*
[2]*Sorbonne Université, 75005 Paris, France*
[3]*University of California, Berkeley, CA 94720, USA*
[4]*Max-Planck-Institut für Struktur und Dynamik der Materie, 22761 Hamburg, Germany*
[5]*CFEL, DESY, 22607 Hamburg, Germany*

Strongly correlated materials present peculiar behavior of both technological and fundamental interest, due to repulsive electron-electron interactions. Yet, their response to light excitation remains unclear. The challenge is that purely electronic dynamics occur in a few femtosecond or less, requiring attosecond temporal resolution requires attosecond temporal resolution. At this timescale, do correlations enhance, screen or have no effect on the sub-optical-cycle response to an external laser field? We address this question via attosecond transient reflectivity on NiO, a prototypical strongly correlated insulator. We first benchmark our setup with MgO [1], a weakly correlated insulator. It exhibits oscillations at twice the pump laser frequency, a signature of the well-studied dynamical Franz-Keldysh effect by which the field coherently distorts the bands of the solid [2]. Strikingly, NiO does not show any sub-optical-cycle dynamics. Instead, it presents a slower and non-reversible electronic response that arises in a few femtoseconds. To understand this temporal response we conduct state-of-the-art calculations in the framework of time-dependent density-functional plus self-consistent U theory, which describes ultrafast dynamics in strongly correlated systems.
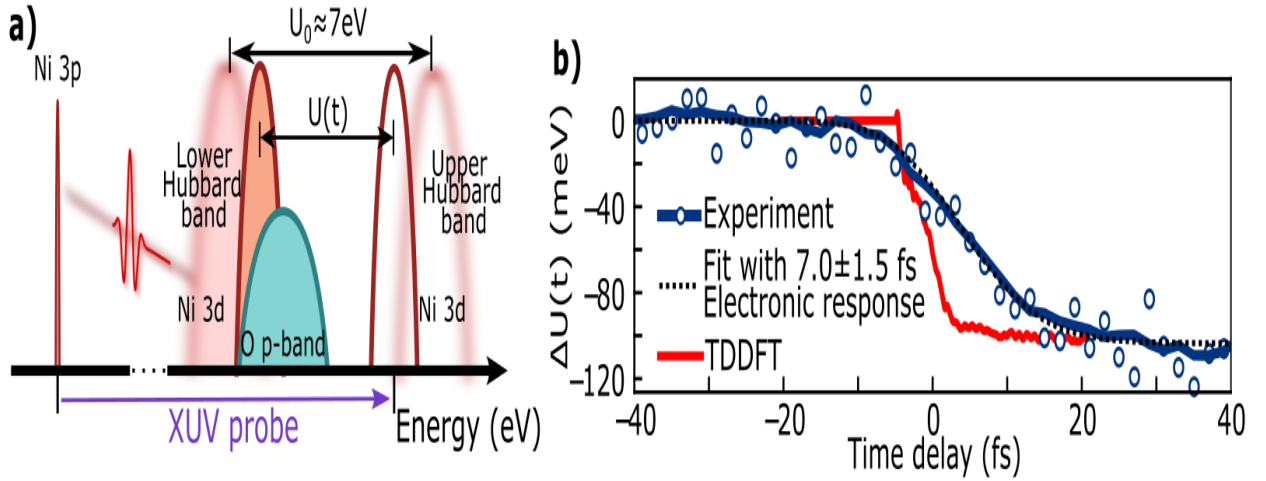
Fig.1.a.The attosecond XUV pulse probes the energy of the conduction band which is the Upper Hubbard Band, providing a direct measurement of the Hubbard U evolution as a function of time. **b.** Comparison of the measured $\Delta U(t)$ and our numerical results.

Our calculations [3], which reproduce the experiment quantitatively, explain this behavior as a light-induced renormalization of the correlation parameter U in the Hubbard model, confirming predictions made in prior theoretical work [4]. With this interpretation, the data yields direct access to the temporal evolution of the effective Hubbard U for the first time. It is found to respond in 7 fs, a system-specific timescale characterizing the dynamics of electronic screening after light excitation. The ability to measure and control the Hubbard U at its true timescale could be foundational for accessing and harnessing new non-equilibrium material states.

References
[1] R. Géneaux, C. J. Kaplan, L. Yue, A. D. Ross, J. E. Bækhøj, P. M. Kraus, H.- T. Chang, A. Guggenmos, M.- Y. Huang, M. Zürch, K. J. Schafer D. M. Neumark, M. B. Gaarde, S. R. Leone, *Physical Review Letters.* **124**, 207401 (2020).
[2] M. Lucchini, S. A.Sato, A. Ludwig, J. Herrmann, M. Volkov, L. Kasmi, Y. Shinohara, K. Yabana, L. Gallmann, U. Keller, *Science* **353**, 916(2016)
[3] R. Cazali, A. Alic, M. Guer, C. J. Kaplan, F. Lepetit, O. Tcherbakoff, S. Guizard, A. Rubio, N. Tancogne- Dejean, G. S. Chiuzbăian, R. Géneaux *to be published* (2025).
[4] N. Tancogne-Dejean, M. A. Sentef, A. Rubio, *Physical Review* B **102**, 115106 (2020).

Tracking electronic dynamics at the atomic scale with Ultrafast tunnelling spectroscopy

Ya. A. Gerasimenko, C. Roelcke, L. Z. Kastner, M. Graml, J. Wilhelm, J. Repp, R. Huber

Universität Regensburg, 93040 Regensburg, Germany

Atomic-defect-based quantum systems in monolayers and moiré heterostructures of 2D materials have attracted huge interest for their qubit and single-photon emission functionalities. Whereas time-resolved ARPES provides critical insights into the dynamics of electronic energies in momentum space, its counterpart with atomic spatial instead of momentum resolution is necessary to directly observe the interplay of electronic structure of a single defect with the microscopic excitations of the environment on the intrinsic atomic and femtosecond scales.

Here we directly resolve in space, time and energy how spin-orbit-split bound states of an individual Se vacancy – an atomic single-photon emitter – evolve under coherent lattice vibrations in moiré-distorted WSe_2 using lightwave-driven scanning tunnelling spectroscopy (LWSTS) [1] (Fig. 1a, b). We selectively launch a drum phonon mode (Fig. 1c) with a THz pulse coupled to the tip and take ultrafast snapshots of electronic spectrum on atomic scales faster than a vibration period. Such ultrafast tunnelling spectra reaching ~300 fs temporal resolution reveal transient energy shifts of the lower bound vacancy state by up to 40 meV, depending on the amplitude and phase of the coherent lattice vibration (Fig. 1d). We discuss how THz fields can couple via the Coulomb interactions to the drum mode, and how the interplay of Se-W bonds distortion and image charge renormalization due to vertical motion of the vacancy, induced by the drum mode, affect the energy levels of the vacancy.
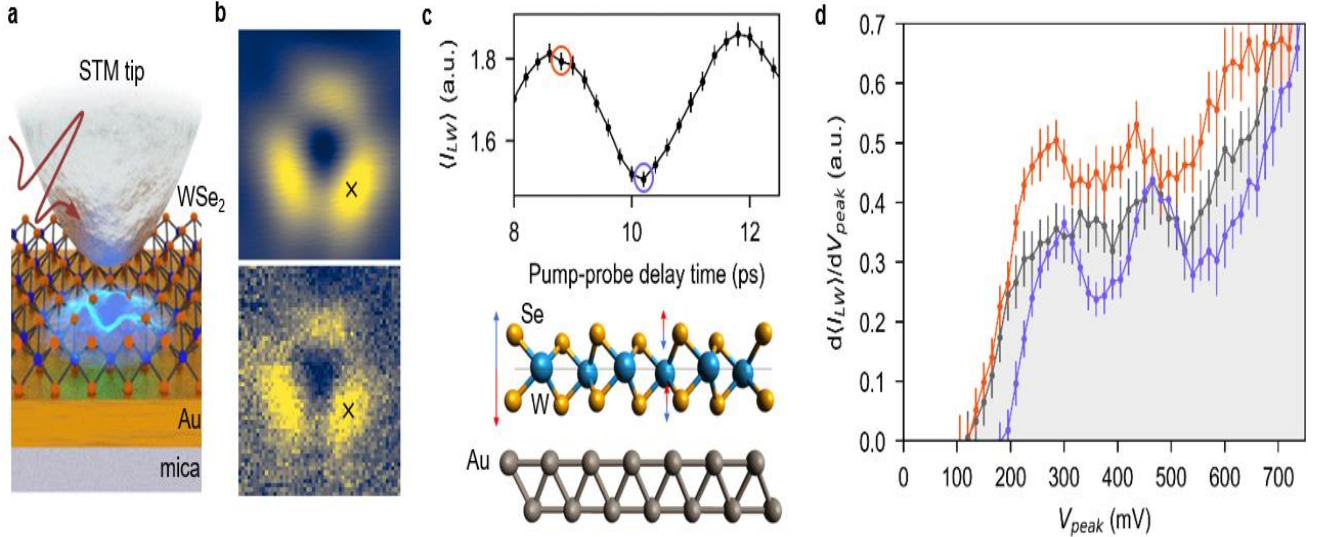
*Fig.1. **a. Schematic of LWSTS**: an ultrashort THz pulse (**red**) of variable intensity coupled to the tip transiently modulates the bias between tip and Se vacancy (**blue orbital**) in monolayer WSe_2. **b.** Constant-height images (1.5 × 1.5 nm^2) of the vacancy measured with DC (top, V_{DC} = 720 mV) and THz-driven currents (**bottom**, V_{DC} = 0, peak THz bias V_{peak} ~ 720 mV). **c,** Tunneling current driven by a THz probe pulse as a function of the delay time after local excitation by a THz pump pulse (**top**). Ball-and-stick model of the induced drum phonon mode (**bottom**), which involves a center-of-mass motion of the WSe_2 monolayer as well as out-of-phase intra-cell distortion (**red and blue arrows** mark opposite oscillation phases). **d.** Transient tunneling spectra measured at the defect lobe (**cross in (b)**) for delay times corresponding to maximum (**red**, 8.8 ps) and minimum(**blue**, 10.2 ps) distance between WSe_2 and Au in (c), **grey** – unpumped spectrum. The rising edge shows the onset of tunnelling into the lower bound state of the vacancy.*

The combination of atomic spatial, sub-picosecond temporal, and meV energy resolution marks a disruptive development towards a comprehensive understanding of complex quantum matter, paving the way to disentangling microscopic interactions one by one and tuning many-body states by transiently shifting their energetic position.

Reference

[1] C. Roelcke, L. Z. Kastner, M. Graml, A. Biereder, J. Wilhelm, J. Repp, R. Huber, Y. A. Gerasimenko, *Nature Photonics* **18**, 595 (2024).

Charge transfer excitons in correlated materials and their coupling to Magnetic excitations studied by tr-RIXS

G. Merzoni[1], L Martinelli[3], S.Dal Conte[1], L.Mercadier[2], Y.-P. Chang [2], L. P. Hoang[2], G.Mercurio[2], F. Rosa[1]
J. Schlappa[2], M.Teichmann[2], N. B.Brookes[4], R.Carley[2], G. Cerullo[1], M. Moretti Sala[1], A. Scherz[2], G.Ghiringhelli[1]

[1]*Politecnico di Milano, 20133 Milano, Italy*
[2]*European XFEL, Schenefeld, 22869, Germany*
[3]*Universität Zürich, 8057 Zürich, Switzerland*
[4]*The European Synchrotron, F-38043 Grenoble, France*

Resonant inelastic x-ray scattering (RIXS) has recently become a premier tool for the investigation of quantum materials with strong electronic correlation. The advent of high repetition rate x-ray free electron lasers (XFELs) has eventually enabled time resolved (tr) RIXS experiments with high energy and time resolution. In this context, the realization of the hRIXS instrument at the coherent scattering (SCS) beamline of the European XFEL marks a milestone towards high energy- and time-resolution ppRIXS [1]. First results on NiO and La_2CuO_4 immediately brought new insight on the photo-doped state of these archetypical charge transfer insulators. In particular, we observed that in NiO the above-gap optical excitation generates a transient charge-transfer excitonic state, whose main signature is an energy gain peak in the transient RIXS. The charge transfer exciton delocalizes within few picoseconds, leaving the system in a metastable state lasting for a much longer time [2]. Besides this clear electronic picture, the effects on the *magnetic order* due to this photo-induced transient state could not be disclosed with the data from the first experiment.Therefore, in a second run we exploited the high selectivity of trRIXS to focus on how the charge transfer excitons dynamics influences the spin waves spectrum. Although the long-range antiferromagnetic order is quickly lost after the photo-excitation, short-ranged magnons are always present in the RIXS spectra, though with smaller energy. Moreover, coherent magnon oscillations are visible for the first time in a trRIXS measurement.
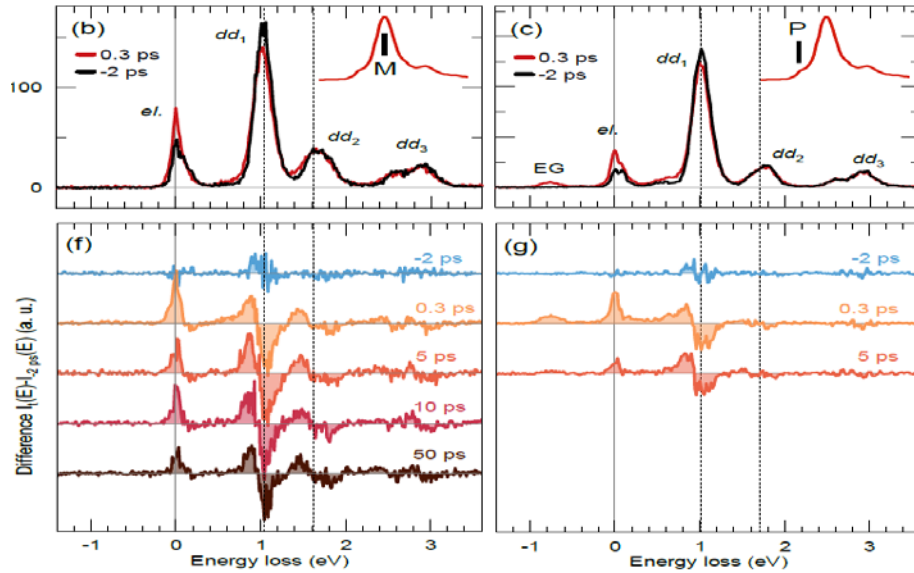
Fig 1. The trRIXS spectra of NiO at 0.3 ps delay compared to negative delay. (b, f) spectra excited at the main absorption peak, (c, g) excited at the pre-peak appearing only when the 266nm pump is on [2].

Our results suggest that the photoexcited charge transfer exciton prompts low energy coherent magnons and then moves the system in a metastable metallic state, where short range spin-spin correlation persists. Our results establish trRIXS as a superior tool to investigate transient states with unprecedented sensitivity, opening the route to innovative studies on the transient optically excited states in quantum matter.

References
[1] J. Schlappa, G. Ghiringhelli, B. E. Van Kuiken, M. Teichmann, P. S. Miedema, J. T. Delitz, N. Gerasimova, S. Molodtsov, L. Adriano B. Baranasic, C. Broers, R. Carley, P. Gessler, N. Ghodrati, D. Hickin, L. P. Hoang, M. Izquierdo, L. Mercadier, G. Mercurio S . Parchenko M. Stupar, Z.Yin, L. Martinelli, G.Merzoni,Y.Y. Peng,T.Reuss, S. S. N. Lalithambika, S. Techert, T. Laarmann, S. Huotari, C. Schroeter, B. Langer T. Giessel, J. Buchheim, G. Gwalt, A. Sokolov, F. Siewert, R. Buechner, V. Vaz da Cruz, S. Eckert, C.-Y. Liu, C. Sohrt, C. Weniger, A. Pietzsch S. Neppl, F. Senf, A. Scherza, A. Fo¨hlischet, *Journal of Synchrotron Radiation* **32**, 29 92025).
[2] G. Merzoni, L. Martinelli, S. Parchenko, S. F. R. TenHuisen, V. Lebedev, L. Adriano, R. Carley, N. Gerasimova, L. Mercadier, M. Teichmann B. E. van Kuiken, Z. Yin, A. Alic, D. R. Baykusheva, S. G. Chiuzbaian, S. Dal Conte, O. Dogadov, A. Föhlisch, M. W. Haverkort, M. Kusch T. Laarmann, W. S. Lee, M. M. Sala, Y. Y. Peng, Q. Z. Qiu, T. Schmitt, S. S. N. Lalithambika, S. Techert, G. Cerullo, M. Först, M. Mitrano M. P.M. Dean, J.Schlappa, A.Scherz, G.Ghiringhelli, *arXiv:2504.16653* (2025).

Quantum fluid dimers of hyperbolic exciton-polariton condensates

A. Gianfrate[1], D.Trypogeorgos[1], H. Sigurðsson[2 3], I. Georgakilas[4], M. De Giorgi[1], D. Ballarini[1]
D.Sanvitto[1]

[1]*Istituto di Nanotecnologia, 73100 Lecce, Italy*
[2]*University of Iceland, 107 Reykjavik, Iceland*
[3]*University of Warsaw, 02093 Warsaw, Poland*
[4]*IBM Research–Zurich, 8803 Rüschlikon, Switzerland*

Exciton-polariton Bound States in the Continuum (BiCs) are symmetry-protected from radiating in the far field. Their large quality factor, when in the strong coupling regime, enables to achieve low-threshold exciton-polariton condensation. The saddle-shaped single-particle dispersion of the BiC imparts the condensate with marked directionality. Along the BiC axis, it leads to a self-localization mechanism, offering opportunities to generate evanescently-coupled polariton chains [1]. Along the perpendicular axis, it leads to a polariton flow with a well-defined momentum, which is responsible for a time-delayed synchronization mechanism, often referred to as ballistic coupling. Consequently, on this platform, it is possible by simply adjusting the relative angle between the axis connecting the pump spots and the grating axis, to tune the BiC condensate coupling from negative-mass-evanescent to positive-mass-ballistic [2]. In this context, we investigate and characterize this interplay, exploring the potential to engineer hybrid ballistic-evanescent polariton condensate chains.
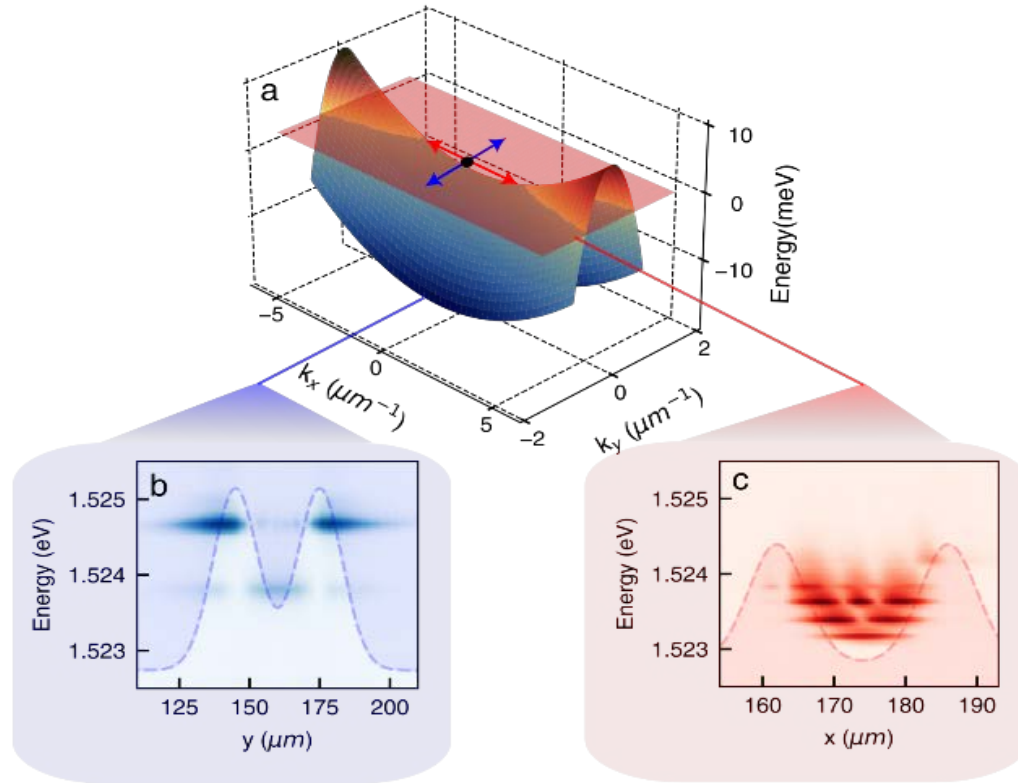
Fig. 1 a Hyperbolic dispersion *hosting the BiC condensate,* **b** *and* **c** *condensate dimer spectra in the case of evanescent and ballistic case respectively.*

These findings highlight the potential of 1D photonic crystal waveguides to engineer reconfigurable hybrid ballistic-evanescent polariton condensate chains and to study condensed matter phenomena at the interface between delay-coupled nonlinear oscillators and tight-binding physics [3].

References
[1] A. Gianfrate, H. Sigurðsson, V. Ardizzone, H. C. Nguyen, F. Riminucci, M. Efthymiou-Tsironi, K. W. Baldwin, L. N. Pfeiffer, D. Trypogeorgos M. De Giorgi, D. Ballarini, H. S. Nguyen, D. Sanvitto, *Nature Physics* **20**, 61 (2024).
[2] J. D. Töpfer, H. Sigurðsson, L. Pickup, P. G. Lagoudakis, *Communications Physics* **3**, 2 (2020).
[3] I. Georgakilas, A. Gianfrate, D. Trypogeorgos, H. Sigurðsson, F. Riminucci, K. W. Baldwin, L. N. Pfeiffer, M. De Giorgi, D. Ballarini D. Sanvitto, *arXiv 2412*.14147 (2024).

Topological plasmonics and twistronics:
Ultrafast vector movies of plasmonic skyrmions, merons, Quasicrystalline structures and skyrmion bags on the nanoscale

H. Giessen
Universität Stuttgart, 70174 Stuttgart, Germany

We utilize a new technique, time-resolved vector microscopy, that enables us to compose entire movies on a sub-femtosecond time scale and a 10 nm scale of the electric field vectors of surface plasmon polaritons. By using our vector microscopy technique, we are able to image the plasmonic spin-momentum-locking and the plasmonic skyrmion dynamics. Depending on the shape and geometrical phase, in combination with the helicity of the excitation beam, topological plasmonic quasiparticles are created: skyrmions, merons, as well as quasicrystalline excitations with 4D topology. We observe their entire field vector dynamics at subfemtosecond time resolution [1-6]. Fig. 1t depicts a snapshot of the skyrmion electric field vector arrangement with sub-10 nm resolution on a single crystalline, atomically flat gold surface.
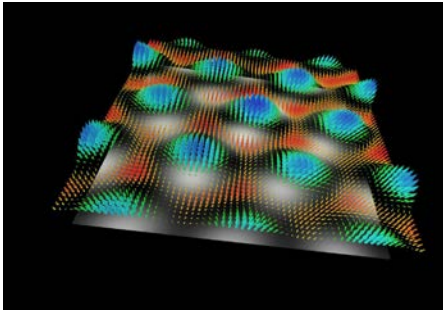
Fig. 1. Experimentally obtained snapshot of the vector components of the E-field of a plasmonic skyrmion on a monocrystalline, atomically flat gold surface [5].

When applying the concept of twistronics to plasmons, intriguing topological excitations arise, such as skyrmion bags. We find magic angles similar to twisted graphene which defines exceptional topological features. Utilizing topological plasmonics and twistronics will open the door to linear optical features on the few nm length scale [7], without the need for techniques such as STED.

References
[1] S. Tsesses E. Ostrovsky, K. Cohen, B. Gjonaj, N. H. Lindner , G. Bartal, *Science* **361**, 993 (2018).
[2] S. Tsesses , K. Cohen, E. Ostrovsky, B. Gjonaj, G.Bartal, *Nano Letters* **19**, 4010 (2019).
[3] B. Frank, P. Kahl, D. Podbiel, G. Spektor, M. Orenstein, L. Fu, T. Weiss, M. Horn - von Hoegen, T. J. Davis, F. - J. Meyer zu Heringdorf H. Giessen, *Science Advances* **3**, 1700721 (2017).
[4] G. Spektor , G. Spektor, D. Kilbane, A. K. Mahro, B. Frank, S. Ristok, L. Gal, P. Kahl, D. Podbiel, S. Mathias, H. Giessen, F.-J. Meyer zu Heringdorf M. Orenstein, M. Aeschlimann, *Science* **355**, 1187 (2017).
[5] T. Davis, D.Janoschka, P. Dreher, B.Frank, F.-J. Meyer Zu Heringdorf, H.Giessen, *Science* **367**, eaba6415 (2020).
[6] S. Tsesses, P.Dreher, D.Janoschka, A. Neuhaus, K.Cohen, T.C. Meiler, T. Bucher, S.Sapir, B.Frank T. J. Davis, F. Meyer zu Heringdorf , H. Giessen G. Bartal, *Science* **387**, 644 (2025).
[7] J. Schwab, *to be published Nature Physics* (2025).

Understanding long-lived nonequilibrium phases in Correlated electron systems

M. Eckstein,
Universität Hamburg, 20148 Hamburg, Germany

The emergence of long-lived nonequilibrium phases in strongly correlated electron systems provides new pathways to control order and symmetry through dynamical means. One prominent mechanism is photodoping, where ultrafast optical excitation injects carriers and reshapes the electronic structure [1]. I will address recent advances in a nonperturbative simulation of such photo-doped states [2]. Another mechanism to stabilize nonthermal states involves non-thermal spatial fluctuations.
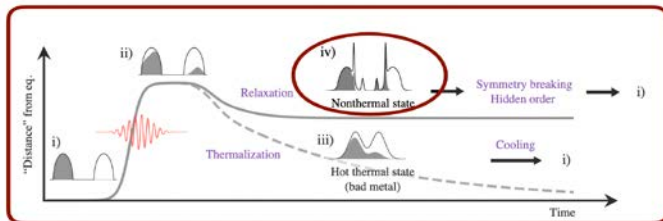
Fig. 1. Illustration of different stages in the excitation and relaxation process of photo-doped Mott system. In large-gap Mott insulators the intraband relaxation leads to distinct nonthermal quasiparticle distributions (stage iv), which we address in this talk. Figure adapted from [1].

Anisotropies in relaxation dynamics and stiffness can lead to an effective nonthermal order by nonthermal disorder scenario, where fluctuations can transiently favor ordered states not stabilized in equilibrium [3]

References
[1] Y. Murakami, D. Golež, M. Eckstein, P. Werner, *arXiv:*2310.05201 (to appear in *Review of Modern Physics*).
[2] F. Künzel, A. Erpenbeck, D. Werner, E. Arrigoni, E. Gull, G. Cohen, M. Eckstein, *Physical Review Letters* **132**, 176501 (2024).
[3] F. Grandi, A. Picano, R. Thomale, D. M. Kennes, M. Eckstein, *arXiv:*2412.02616.(2024).

Observation of Higgs modes in superconductors by non-equilibrium Anti-Stokes Raman scattering

T.E. Glier[1], S. Tian[2], M. Rerrer[1], J. Dolgner[2], S. Kaiser[3], D. Manske[2], M. Rübhausen[1]

[1] Universität Hamburg, 22761 Hamburg, Germany.
[2] Max Planck Institute for Solid State Research, 70569 Stuttgart, Germany.
[3] Technische Universität Dresden, 01062 Dresden, Germany.

Spontaneous symmetry breaking leads to massless phase modes as low-energy excitations of the Mexican-Hat potential. However, in superconductors, interaction between the charged condensate and the gauge field shifts these modes to higher energies [1], leaving the Higgs mode as the dominant low-energy excitation. The Meissner effect confirms a macroscopic quantum condensate where photons acquire mass, in analogy to high-energy physics [2]. Sooryakumar and Klein experimentally observed the Higgs mode in superconductors via Raman scattering in 1980, later confirmed in 2014 [3,4]. Due to weak light coupling, the Higgs mode remained elusive, except in $NbSe_2$ where it couples to a CDW. Over the past two decades, experimental evidence has steadily built up. In 2005, Budelmann et al. detected a distinct in-gap quasiparticle excitation via resonance Raman spectroscopy[5]. In 2009, Saichu et al. observed an in-gap feature responding to a pump on a different timescale than the pair-breaking peak, suggesting a collective excitation [6]. Subsequent studies, notably THz measurements, have reinforced evidence for the Higgs mode[7]. This talk presents Higgs-mode observations in Bi-2212 using Non-Equilibrium Anti-Stokes Raman Scattering (NEARS) [8]. A Tsunami Ti:Sapphir system with a pulse duration of 1.2 ps and a repetition rate of 80 MHz is used as laser source at a fundamental wavelength of 802 nm (pump). From a second harmonic generation (SHG) unit, a 402 nm beam is used as the Raman probe for the UT-3 spectrometer.[9] NEARS exploits the metastable nature of the Higgs particle through a soft quench of the Mexican-Hat potential, selectively populating Higgs modes with different symmetries[10], then probing them via anti-Stokes Raman scattering. The pump perturbs the potential while allowing relaxation, facilitating Higgs mode occupation (Fig. 1, left bottom).
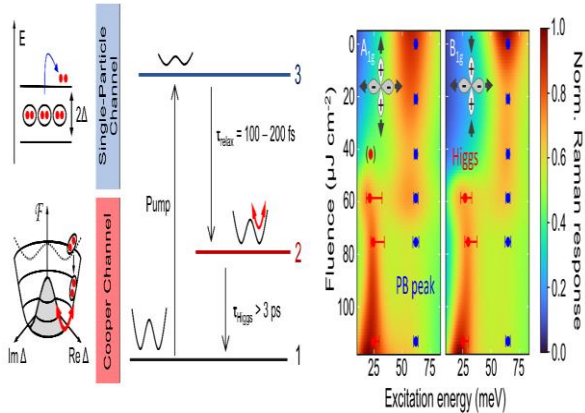
Fig. 1. Left: Cooper channel vs. single-particle channel in the NEARS experiment highlighting the specific excitation process populating the Higgs mode. The Mexican-Hat potential representing the superconducting ground state (1) is quenched upon pumping (3). Concomitantly, the reduction of the superfluid density and gap-filling occurs. On a time-scale of 100-200 fs the Mexican-Hat potentialrelaxes. The holes from the single particle channel form again bosonic Cooper pairs, which oscillate in the relaxing Mexican-Hat potential representing an excited and metastable Higgs state (2). This population inversion is probed by NEAERS. Right: Excitation spectrum of the superconductor Bi-2212. The NEARS maps of Bi-2212 show the Raman response of the Higgs particle at around 25 meV together with the PB excitation Raman susceptibility around 60 meV in A_{1g} (left) and B_{1g} (right) geometry at a time delay of 3 ps.

This population inversion (Fig. 1, left) can be tuned experimentally via soft quench fluence and characterized by comparing Stokes and anti-Stokes signals. Indeed, an additional in-gap anti-Stokes signal (Fig. 1, right, 25 meV signal) emerges with fluence, indicating Higgs mode population. The pumped Stokes side shows a suppressed pair-breaking (PB) peak (around 60 meV), confirming the superconducting state persists 3 ps after the pump. Our results, analyzed via Ginzburg-Landau theory, link Higgs mode energy to the Cooper-pair coherence length. A BCS weak-coupling model provides a coherent description of both single-particle pair-breaking and two-particle Higgs excitations. Phonon-subtracted electronic equilibrium susceptibilities align well with microscopic theory, a key result given the absence of the A_{1g} problem in our measurements at 3.1 eV photon energy [11]. This work establishes NEARS as a powerful Higgs spectroscopy tool in quantum condensates, opening new avenues for investigating Higgs physics. Beyond Higgs mode detection, NEARS offers broad applications in superconductivity research, including light-induced transient, interface, topological, and high-temperature superconductivity.

References
[1] P. Anderson, *Physical Review* **110**, 827 (1958).
[2] C. M. Varma, *Journal of Low Temperature Physics* **126**, 901 (2002).
[3] R. Sooryakumar, M. V. Klein, *Physical Review Letters* **45**, 660 (1980).

[4] P. Littlewood, P. C. Varma, *Physical Review* B **26**, 4883 (1982).
[5] D. Budelmann, B. Schulz, M. Rübhausen, M. V. Klein, M. S. Williamsen, P. Guptasarma, *Physical Review Letters* **95**, 057003 (2005)
[6] R. P Saichu, I. Mahns, A. Goos, S. Binder, P. May, S. G. Singer, B. Schultz, A. Rusidi, J. Unterhinninghofen, D. Manske, P. Guptasarma M. S. Williamsen, M. Rubhausen, *Physical Review Letters* **102**, 177004 (2009).
[7] R. Shimano, N. Tsuji, *Annual Review of Condensed Matter Physics* **11**, 103 (2020).
[8] T. E.Glier, S. Tian, M. Rerrer, L. Westphal, G. Lullau, L. Feng, J. Dolgner, R. Haenel, M. Zonno, H. Eisaki, M. Greven, A. Damascelli, S. Kaiser D. Manske, M. Rubhausen, *arXiv:2310.08162* (2023).
[9] B. Schulz, J. Bäckström, D. Budelmann, R. Maeser, M. Rübhausen, M. V. Klein, E. Schoeffel, A. Mihill, S. Yoon, *Review of Scientic Instruments* **76,** 073107 (2005).
[10] L. Schwarz, B. Fauseweh, N. Tsuji, N. Cheng, N. Bittner, H. Krull, M. Berciu, G. S. Uhrig, A. P. Schnyder, S. Kaiser, D. Manske, *Nature Communications* **11**, 287 (2020).
[11] T. P. Devereaux, D. Einzel, *Physical Review* B **51**, 16336 (1995).

How "super" is photoinduced superconductivity?

J. S. Dodge, L. Lopez
Simon Fraser University, Burnaby, BC V5T 2B2, Canada

We describe how systematic error distorts the evidence for photoinduced superconductivity. Most of this evidence has come from time-resolved terahertz (TR-THz) spectroscopy, which is sensitive to the nonequlibrium electrodynamic response of materials at the relevant frequencies and timescales [1]. However, TR-THz directly measures the complex reflection amplitude $r(\omega)$, not the local nonequilibrium complex conductivity $\sigma(\omega)$, and to relate them one needs to specify the complex photoconductivity depth profile $\Delta\sigma(\omega; z)$, which typically is not known independently [2]. We have shown previously that at the high excitation densities employed in these experiments, the photoconductivity depth profile must be distorted from the profile originally used to interpret the experiments [3]. When we correct for this distortion, we obtain nonequlibrium conductivity spectra that are qualitatively different from those originally reported. The corrected results for K_3C_{60} are consistent with a model in which photoexcitation enhances the carrier mobility but does not induce a phase transition to a superconducting state. We will show evidence that this effect compromises all previous TR-THz evidence for photoinduced superconductivity, not just in K_3C_{60}.
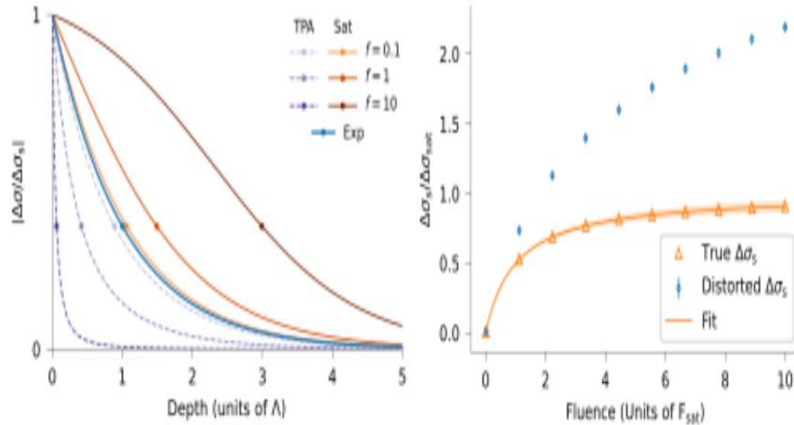
Fig.1.Left:*Normalized photoconductivity of linear and nonlinear media as a function of depth, in units of the pump penetration depth Λ. Markers on each curve indicate the $1/e$-depth. The photoexcitation profile narrows with increasing fluence $F = F_{\text{TPA}}f$ in a medium with a two-photon absorption (TPA) nonlinearity and broadens with increasing fluence $F = F_{\text{sat}}f$ in a medium with a saturable nonlinearity (Sat). The depth profile for a linear medium (Exp) is independent of fluence.*
Right*: Normalized surface conductivity estimated from the reflection amplitude using the exponential profile (blue) and the profile for a medium with combined saturation and TPA nonlinearities (**orange**).*

We will also address criticisms that Buzzi et al. (2023) [4] have raised about our reinterpretation and show how subsequent results provide further support for it [5,6].

References
[1] A. Cavalleri, *Contemporary Physics* **59**, 31 (2018).
[2] L. Lopez, D. G. Sahota, J. S. Dodge, *arXiv:2410.21496* (2024)
[3] J. S. Dodge, L. Lopez, D. G. Sahota, *Physical Review Letters* **130**, 146002 (2023).
[4] M. Buzzi, D. Nicoletti, E. Rowe, E. Wang, A. Cavalleri, *arXiv:2303.10169* (2023).
[5] E. Rowe, B. Yuan, M. Buzzi, G. Jotzu, Y. Zhu, M. Fechner, M. Först, B. Liu, D. Pontiroli , M. Riccò, A. Cavalleri, *Nature Physics* **19**,1821 (2023)
[6] E. Wang, J. D. Adelinia, M. Chavez-Cervantes, T. Matsuyama, M. Fechner, M. Buzzi, G. Meier, A. Cavalleri, *Nature Communications* **14**,1 (2023)
 * *Acknowledgements*: J. S. D. acknowledges support from NSERC.

From high-order sidebands to Bloch-wave interferometry

A. Giovannone[1], M. Jang[1], Q. Wu[1], S. D. O'Hara[2], J. B. Costello[3], M. S. Sherwin[1]

[1]*University of California, Santa Barbara, CA 93106 USA*
[2]*University of Pennsylvania, Philadelphia, PA 19104, USA*
[3]*Electrical Engineering and Computer Science- Exponent, Menlo Park, CA 94025, USA*

The 2023 Nobel Prize in Physics was awarded to scientists for generating attosecond pulses of light based on high-order harmonic generation (HHG) in atomic systems driven by strong laser fields. About a dozen years ago, HHG [1] and a related phenomenon, high-order sideband generation (HSG) [2], were discovered in crystalline solids driven by strong mid-infrared and terahertz (THz) laser fields, respectively. Both HHG and HSG in solids are highly nonlinear processes, in which strong laser fields drive the charged quasiparticles through states with energy and quasi-momentum much larger than those of the individual laser photons, presenting exciting new opportunities for optics-based energy- and momentum-resolved spectroscopies of quasiparticles in solids. While HHG is typically induced by a single laser field, HSG occurs when a semiconductor is illuminated by a relatively weak near-infrared (NIR) laser and simultaneously driven by a sufficiently strong THz field. By using two laser fields, the creation and acceleration of quasiparticles are separately controlled in HSG [2]. Owing to this distinct feature, HSG spectroscopy has evolved into a new technique for measuring electronic structures of crystalline solids. In 2017, it was shown that polarimetry of high-order sidebands can be used to discover subtle manifestations of quantum interference between the Bloch waves associated with accelerating quasiparticles, enabling new probes of Berry curvature [3]. This capability was later demonstrated in reconstruction of the Bloch wavefunctions of holes in bulk GaAs [4].
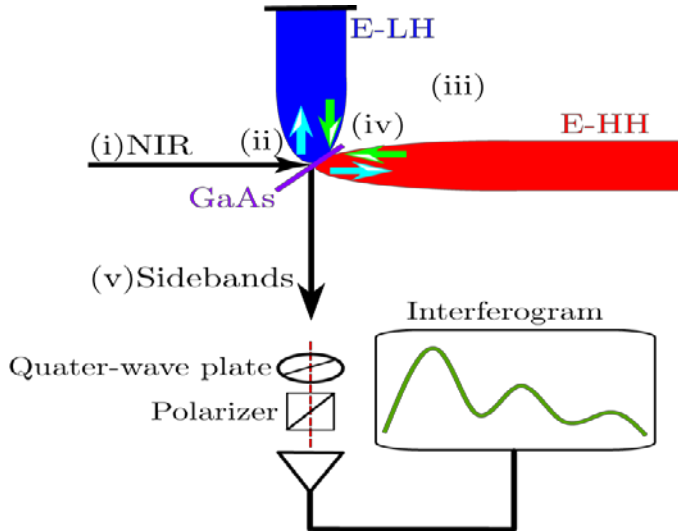
Fig. 1. A Michelson interferometer for Bloch waves in bulk GaAs. (i) A NIR laser is incident on bulk GaAs, creating an electron-hole (E-H) Bloch wave. (ii) The GaAs acts like a "beam splitter", "splitting" the E-H Bloch wave, which is a superposition of E-HH and E-LH Bloch waves, into "two arms", one for each species of Bloch wave. (iii) The THz field drives the two species of Bloch waves along different recollision pathways in their "respective arms". (iv) Upon sideband emission, the E-HH and E-LH Bloch waves "merge" at the "beam splitter" and interfere as two components of the E-H Bloch wave. (v) The Bloch-wave interferogram is "loaded" onto the sideband electric fields and recorded as sideband polarizations as functions of sideband photon energy.

We show here that the HSG in bulk GaAs can be thought of as the output of a Michelson interferometer for Bloch waves [5], enabling a probe of non-equilibrium dephasing in a strongly-driven quantum system [6]. The relevant low-energy band structure of bulk GaAs involves one conduction band and two valence bands that are degenerate at zero quasi-momentum. In the HSG process, the incident NIR laser creates both the so-called heavy-holes (HHs) and light-holes (LHs) associated with the two valence bands, resulting in two species of electron-hole pairs that are driven by the THz field along different recollision pathways and interfere with each other (Fig. 1). I will conclude with a discussion of open questions, including the opportunities for employing HSG in studies of strongly-correlated electronic materials.

References
[1] S. Ghimire, A. D. DiChiara, E. Sistrunk, P. Agostini, L. F. DiMauro, D. A. Reis, *Nature Physics* **7**, 138 (2011).
[2] B. Zaks, R.-B. Liu, M. S. Sherwin, *Nature (London)* **483**, 580 (2012).
[3] H. B. Banks, Q. Wu, D. C. Valovcin, S. Mack, A. C. Gossard, L. Pfeiffer, R.-B. Liu, M. S. Sherwin, *Physical Review* X **7**, 041042 (2017)
[4] J. B. Costello, S. D. O'Hara, Q. Wu, D. C. Valovcin, L. N. Pfeiffer, K. W. West, and M. S. Sherwin, *Nature* **599**, 57 (2021).
[5] S. O'Hara, J. Costello, Q. Wu, K. West, L. Pfeiffer, M. Sherwin, *Physical Review* B **109**, 054308 (2024).
[6] J. Costello, S. O'Hara, Q. Wu, M. Jang, L. Pfeiffer, K. West, M. Sherwin, *Physical Review* B **108**, 195205 (2023).

Optical response and superradiance in driven Excitonic condensates

D. Golež[2,], A. Osterkorn[1], Y.Murakami[3], T. Kaneko[4], Z. Sun[5], A. J. Millis[6]

[1] Jozef Stefan Institute, 1000 Ljubljana, Slovenia
[2] University of Ljubljana, 1000 Ljubljana, Slovenia
[3] RIKEN, Wako, Saitama 351-0198, Japan
[4] Osaka University, Toyonaka, Osaka 560-0043, Japan
[5] Tsinghua University, Beijing 100084, P. R. China
[6] Columbia University, New York, NY 10027, USA

Bilayer materials hosting interlayer excitons—comprising electrons in one layer and holes in the other—are a promising experimental platform for realising high-temperature condensates and studying their dynamical properties. Imposing a chemical potential bias, either through optical pumping or electrical contacts drives exciton condensates into distinct dynamical regimes, see Fig. 1. We investigate how these regimes manifest in emitted light and how they are influenced by placing the material within an optical cavity.
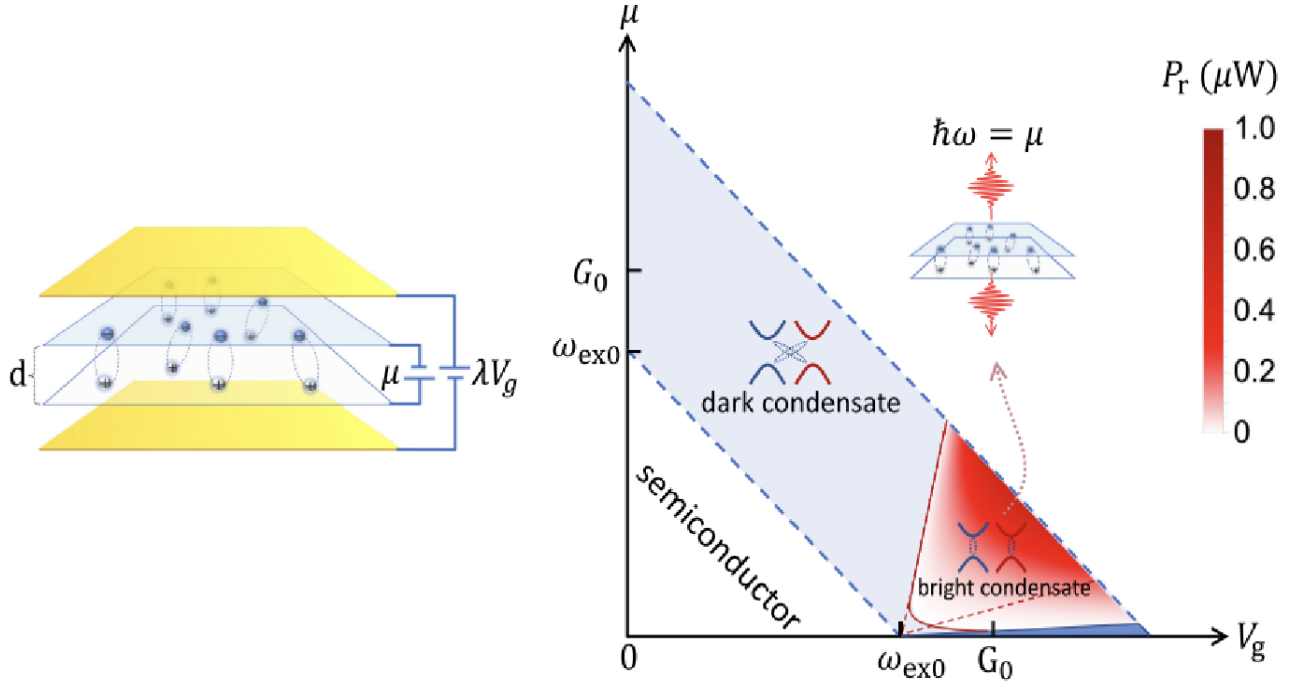
Fig.1. *Left:* Schematic of the biased transition metal dichalcogenides bilayer with biased voltage μ and the gate voltage V_g. *Right:* The phase diagram of the nonequilibrium steady states on the $\mu - V_g$ plane with blue and red regions being the dark or bright dynamical condensate, respectively.

We show that in a bilayer system where the charge can tunnel between the layers, the chemical potential bias means that an exciton condensate is in the dynamical regime of the Josephson effect. By increasing the bias voltage, the system undergoes a transition from the phase-trapped to phase-delocalized dynamical condensation. Optical spectroscopy can identify these phases, with a strong response to weak fields near the transition due to the instability in the order parameter dynamics [1]. If such a system is placed in an optical cavity within the phase-trapped regime, coupling to photons favors a super-radiant state. The phenomenon allows the device to convert DC current into coherent photons at tunable frequencies determined by the bias and material thickness. These findings highlight mechanisms to control and harness excitonic condensates for optoelectronic applications [2].

References
[1] A. Osterkorn, Y. Murakami, T. Kaneko, Z. Sun, A. J Millis, D. Golež, *arXiv:2410.22116* (2024).
[2] Z. Sun, Y. Murakami, F. Xuan, T. Kaneko, D. Golež, A. J. Millis, *Physical Review Letters* **133**, 217002 (2024).

Controlling electronic and magnetic properties of strongly-correlated Oxides via heterostructuring and ultrafast pulses

A. X. Gray

Temple University, Philadelphia, PA 19122, USA

The interplay between charge, spin, and orbital degrees of freedom at oxide interfaces gives rise to emergent electronic and magnetic states, offering pathways to novel functionalities in spintronic and electronic devices. In this talk, I will present a comprehensive investigation of the electronic and magnetic structure at buried interfaces in $LaNiO_3/CaMnO_3$, $CaMnO_3/CaRuO_3$, and $VO_2/LaAlO_3/TiO_2$ heterostructures using a suite of depth-sensitive synchrotron-based x-ray techniques, density functional calculations, and ultrafast THz-pump tr-MOKE spectroscopy.Our studies reveal that interfacial ferromagnetism can be stabilized in nonferromagnetic systems through precise interface engineering and thickness control, as demonstrated in $LaNiO_3/CaMnO_3$ and $CaMnO_3/CaRuO_3$ superlattices [1,2]. Furthermore, we demonstrate that tunable interfacial charge transfer in $VO_2/LaAlO_3/TiO_2$ enables modulation of the VO_2 metal-insulator transition temperature over a 65 K range without doping or strain [3]. Building on these findings, I will present recent standing-wave photoemission data on the $NdNiO_3/CaMnO_3$ system, where interfacial ferromagnetism and the metal-insulator transition can potentially be controlled both statically, via temperature, and dynamically, using IR or THz pulses.Beyond static control, these interfacial phenomena create opportunities for ultrafast manipulation of electronic and magnetic states using intense THz electric-field pulses. This is exemplified in $LaNiO_3/CaMnO_3$ [4], where we employ a suite of time-resolved spectroscopies to disentangle multiple interrelated electronic and magnetic processes driven by high-field THz excitation. These findings underscore the power of combining x-ray and ultrafast optical techniques to probe and manipulate interfacial phenomena, offering insights into the design of tunable correlated oxide interfaces for future electronic and spintronic applications.
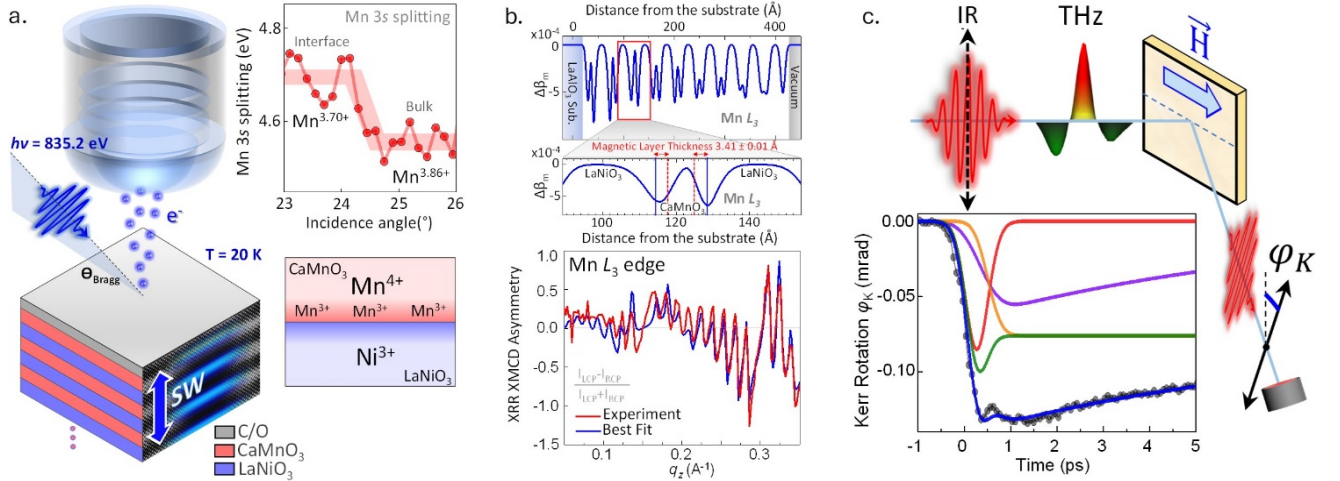
Fig. 1. A comprehensive depth- and time-resolved approach for investigating emergent electronic and magnetic phenomena at oxide interfaces *(e.g., LaNiO₃/CaMnO₃). (**a**) Standing-wave X-ray photoelectron spectroscopy provides the electronic valence-state profile at the interface, (**b**) momentum-resolved X-ray resonant magnetic reflectivity reveals a detailed magnetic profile, and (**c**) THz-pump IR tr-MOKE probes the dynamics of the electronic and magnetic structure.*

These findings underscore the power of combining x-ray and ultrafast optical techniques to probe and manipulate interfacial phenomena, offering insights into the design of tunable correlated oxide interfaces for future electronic and spintronic applications.

References
[1] J. R. Paudel, M. Terilli, T.-C. Wu, J. D. Grassi, A. M. Derrico, R. K. Sah, M. Kareev, C. Klewe, P. Shafer, A. Gloskovskii, C. Schlueter V. N. Strocov, J. Chakhalian, A. X. Gray, *Physical Review* B **108**, 054441 (2023).
[2] J. R. Paudel, A. Mansouri Tehrani, M. Terilli, M. Kareev, J. Grassi, R. K. Sah, L. Wu, V. N. Strocov, C. Klewe, P. Shafer, J. Chakhalian N. A. Spaldin, A. X. Gray, *Nano Letters* **24**, 15195 (2024).
[3] D. Mondal, S. Mahapatra, A. M. Derrico, R. Rai, J. R. Paudel, C. Schlueter, A. Gloskovskii, R. Banerjee, A. Hariki, F. M. F. DeGroot D. D. Sarma, A. Narayan, P. Nukala, A. X. Gray, and N. P. B. Aetukuri, *Nature Communications* **14**, 6210 (2023).
[4] A. M. Derrico, M. Basini, V. Unikandanunni, J. R. Paudel, T. Terilli, T.-C. Wu, A. Alostaz, C. Klewe, P. Shafer, A. Gloskovskii C. Schlueter, C. M. Schneider, J. Chakhalian, S. Bonetti, A. X. Gray, *arXiv:2402.04302* (2024).

Spatio-temporal coherence in nonequilibrium semiconductor spin dynamics

A. Greilich, N. E. Kopteva, V. L. Korenev, M. Bayer

Technische Universität Dortmund, 44227 Dortmund, Germany

This study demonstrates the realization of highly robust, non-decaying auto-oscillations under continuous excitation in a tailored semiconductor's electron-nuclear spin system. Based on the dissipative many-body system, these oscillations form a continuous time crystal (CTC) state. Our findings establish robust CTC dynamics (limit cycle), as seen in Fig. 1a, over a wide range of control parameters, including laser power, temperature, and magnetic field. The classical coherence time of the periodic oscillations, indicative of the ideal ordering of "time atoms" within the CTC, is defined by the experimental measurement time and extends to several hours. Additionally, we observe the presence of chaotic oscillations, signaling the melting of the CTC. This research provides valuable insights into the dynamic regimes of the CTC state [1].Introducing periodic modulation of the laser's polarization leads to a transition from a continuous to a discrete time crystal (DTC) behavior (Fig. 1b).
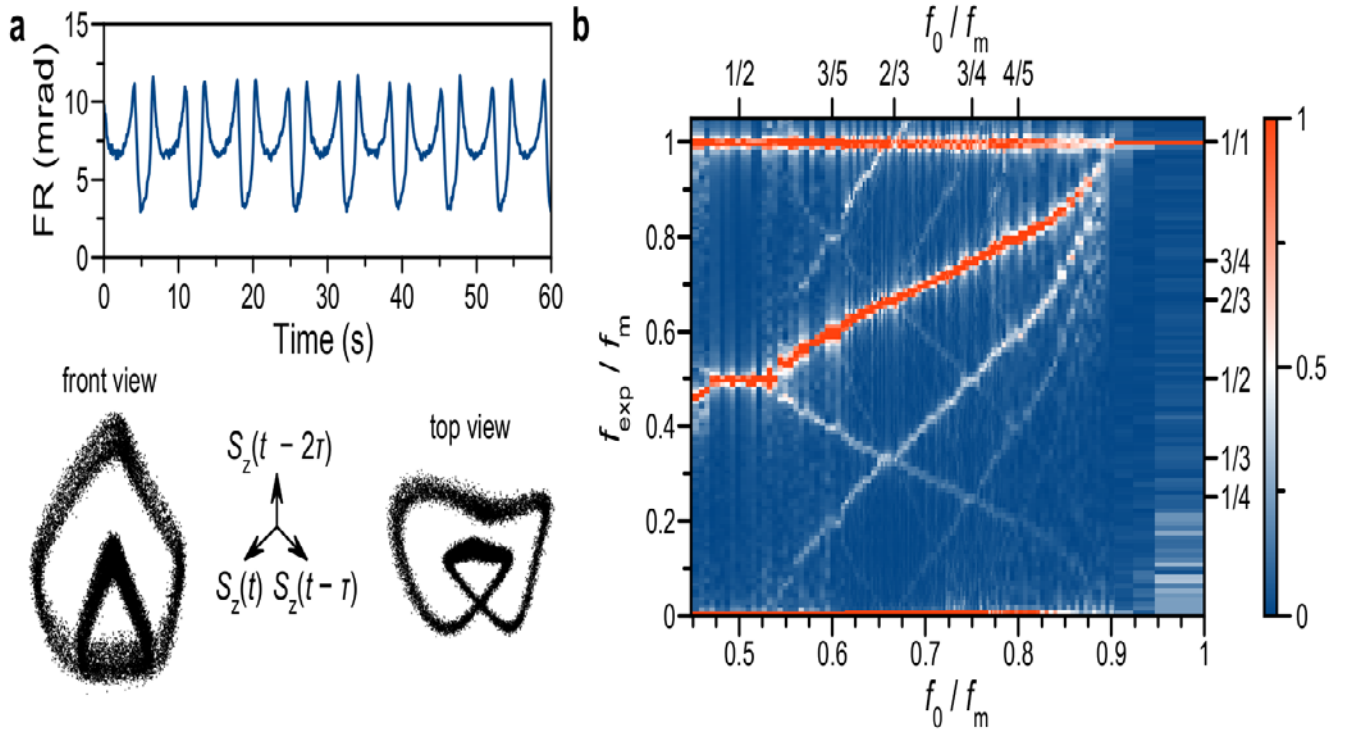
*Fig. 1. a- **Periodic oscillations of electron spin polarization**. At the bottom, different views of the 3-dimensional phase space plot on the limit cycle. **Black points** mark the recorded data. **b**- Measured contour plot of fast Fourier (FFT) spectra for the modulated version of the system as a function of the inverse modulation frequency f_m. It demonstrates different regimes, including synchronization (**horizontal plateaus**), bifurcation jets, and chaos. The color scheme on the right indicates the normalized amplitude of the Faraday rotation. f_0 – is the first own harmonics of the unmodulated oscillations. f_{exp} – observed FFT frequencies.*

The observed key phenomena include synchronization and the formation of Arnold tongues, where the system's oscillations lock onto the modulation frequency. Beyond entrainment, we observe fractional subharmonic responses organized in bifurcation jets, creating a devil's staircase structure in the frequency spectrum. Notably, as the system nears an entrainment region, it undergoes a chaotic transition, revealing the intricate boundary between synchronized and chaotic dynamics [2]. Finally, the coupling between several spatially separated CTC sites would introduce a degree of nonlocality, which can lead to spatial synchronization.

These results deepen our understanding of nonlinear systems and highlight potential applications in semiconductor technology. By bridging experimental realizations with theoretical predictions, this work offers insights into complex, synchronized phenomena in natural and technological systems.

References
[1] A. Greilich, N. E. Kopteva, A. N. Kamenskii, P. S. Sokolov, V. L. Korenev, M. Bayer, *Nature Physics* **20**, 631 (2024).
[2] A. Greilich, N. E. Kopteva, V. L. Korenev, Ph. A. Haude, M. Bayer, *Nature Communications* **16**, 2936 (2025).

Upgrade of a X-ray pump-probe arrangement by a high-energy Few-cycle OPCPA pump at 11 µm

M. Bock, P. Fuerties, U. Griebner

Max-Born- Institut für Nichtlineare Optik und Kurzzeitspektroskopie, 12489 Berlin, Germany

Ultrafast X-ray diffraction is a recognized technique for the investigation of structural dynamics on atomic length scales in the femtosecond range. The availability of compact laser-driven table-top hard X-ray sources enables time-resolved X-ray diffraction and absorption studies on a lab scale [1]. Using the idler of a midwave-IR (MWIR) OPCPA at 5 µm wavelength delivering multi-mJ, few-cycle pulses, the highest table-top hard X-ray flux of 1.5×10^{12} ph/s was demonstrated at a repetition rate of 1 kHz [2]. A pump-probe setup is required for time-resolved measurements. Initial X-ray pump-probe experiments were carried out with a small proportion of the 5 µm driver pulses as pump pulses [3].The availability of pump pulses in the longwave IR (LWIR) would enable novel excitation channels. Here we report on the addition of a LWIR channel in our MWIR OPCPA. Utilizing the residual 2-µm pump energy, a single-stage OPCPA is implemented whose idler at 11 µm provides pulses with a duration of 180 fs and 50 µJ energy. The work is based on a MWIR OPCPA [4] which operates at a repetition rate of 1 kHz. The front-end supplies the seeds for the pump and the signal at 2.05 µm and 3.4 µm wavelength, respectively. The 2.05 µm pulses are amplified to 50 mJ in a few-ps Ho:YLF CPA. The parametric amplifier consists of four stages, all containing ZGP as a nonlinear crystal. The idler pulses of the OPCPA at 5 µm wavelength used for the further experiments comprise an energy of 3.4 mJ and a duration of 85 fs.
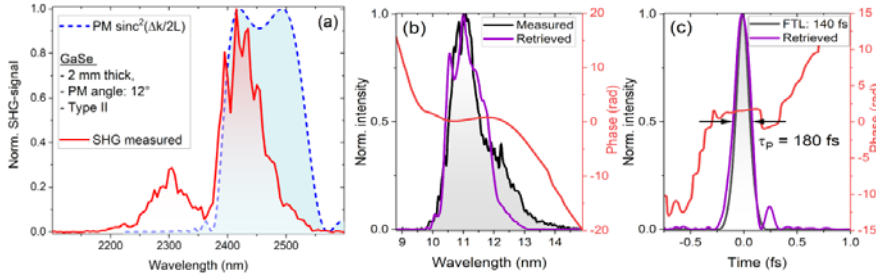
Fig. 1. LWIR OPCPA – *extension of the 5-µm-driven X-ray source. (**a**) Signal spectrum (**red**) and Type-II phase-matching (PM) curve of GaSe (**blue**). (**b,c**) SH-FROG characterization of the 11-µm idler pulses;(**b**) measured and retrieved spectral amplitude and phase; (**c**) retrieved temporal pulse amplitude and phase with its Fourier-limit.*

The multi-color OPCPA is extended into the LWIR range by adding an OPCPA stage based on GaSe. This stage is pumped with the remaining 2.05-µm pump energy after the 4th stage of the MWIR OPCPA. The signal pulses for the LWIR-OPCPA are provided by the second harmonic (SH) of the 4.9 µm MWIR-OPCPA emission. Less than 10% of the 4.9 µm pulse energy is required for this and the X-ray flux is only marginally affected. The LWIR-OPCPA signal pulses centered at 2.4 µm exhibit a FWHM-bandwidth of 100 nm (Fig. 1a, red) and an energy of 40 µJ. These are stretched to a duration of 1.5 ps in sapphire to match the pump pulse duration. The implemented LWIR-OPCPA consists of only one stage equipped with a 2 mm thick GaSe crystal for parametric amplification. It is oriented for Type-II phase matching because a broader bandwidth is supported compared to Type-I (Fig. 1a, blue). Due to damage issues of GaSe the pump intensity has to be below 30 GW/cm^2. The effective aperture of the crystal is 7 mm, which limits the 2-µm pump energy to 4 mJ. In order to generate an idler free of angular dispersion, the collinear amplification geometry is chosen which provides idler pulses centered at 11.2 µm with an energy of 70 µJ. This corresponds to an impressive pump-to-idler conversion efficiency of 1.7%. The idler spectrum has a $1/e^2$-bandwidth of 10.2 to 12.9 µm (Fig. 1b, purple), which results in a Fourier limited pulse duration of 140 fs (Fig. 1c, black). The subsequent compression is performed with bulk ZnSe, which leads to a loss of 28% despite anti-reflection coating of the ZnSe. The 11-µm idler pulses are characterized with the SH-FROG method (Fig. 1c). The retrieved pulse exhibits a duration of 180 fs (Fig. 1c, purple), so it possesses less than five optical cycles. The compressed pulse energy amounts to 50 µJ, resulting in an impressive peak power of 300 MW. In summary, an efficient single-stage LWIR OPCPA at 1 kHz repetition rate was demonstrated as an extension of a multi-mJ MWIR OPCPA. The generated 50 µJ pulses with few cycles at 11 µm wavelength deliver a record peak power of 300 MW, comparable to the value recently achieved in a three-stage LWIR OPCPA at 12 µm [5]. These pulses will serve as an additional pump wavelength for X-ray pump-probe measurements [3].

References
[1] J. Weisshaupt, V. Juvé, M. Holtz, S. A. Ku, M. Woerner, T.Elsaesser, S.Ališauskas, A.Pugžlys, A.Baltuška, *Nature Photonics* **8**, 927 (2014)
[2] A. Koç, C. Hauf, M. Woerner, L. von Grafenstein, D. Ueberschaer, M. Bock, U. Griebner, T. Elsaesser, *Optics Letters* **46**, 210 (2021)
[3] A. Koç, I. Gonzalez-Vallejo, M. Runge, A. Ghalgaoui, K. Reimann, L. Kremeyer, F. Thiemann, M. Horn - von Hoegen, K. Sokolowski - Tinten M. Woerner, T. Elsaesser, *Physics Review* B **107**, L180303 (2023).
[4] L. von Grafenstein, M. Bock, D. Ueberschaer, A. Koç, E. Escoto, K. Zawilski, P. Schunemann, U. Griebner, T. Elsaesser, *Optics Letters* **45**, 5998 (2020)
[5] P. Fuertjes, M. Bock, L. von Grafenstein, D. Ueberschaer, U. Griebner, T. Elsaesser, *Optica* **9**, 1303 (2022).

Excited charge and spin carrier dynamics in WSe_2 and molecule/WSe_2 Heterostructures

S. Hedwig[1], G. Zinke[1], B. Arnoldi[1], B. Stadtmüller[2], M. Aeschlimann[1]

[1] *Rheinland-Pfälzische Technische Universität Kaiserslautern*-Landau, *67663 Kaiserslautern, Germany*
[2]*Universität Augsburg, 86159 Augsburg, Germany*

Layered 2D Van der Waals systems are a highly intriguing class of materials with promising spin functionalities for future spintronic applications. Due to their atomic thickness and exceptional electronic properties, transition-metal dichalcogenides (TMDs) intrinsically fulfill the requirement of miniaturization, making them ideal candidates for next-generation nanoscale devices. One of the most exciting aspects of TMDs is their ability to form van der Waals heterostructures by stacking different 2D materials together without the constraints of lattice matching, giving rise to entirely new fields such as valleytronics or twistronics. This flexibility allows for the precise tuning of electronic and spin properties through interlayer interactions and is often achieved using other TMD materials. A different approach is forming heterostructures with monolayers of other molecules. In spite of all these advanced research areas involving TMDs, there are still open questions about the native materials with their rich and unique spin-related phenomena. To fully exploit the technological potential of TMDs, it is crucial to gain a deeper understanding of their spin dependent transport state properties as well as the dynamics of optically excited charge and spin carriers. Here, we present the results of spin-, time- and momentum-resolved photoemission experiments on WSe_2 and molecule/WSe_2 heterostructures in a vis-pump XUV-probe geometry, as shown in Fig. 1.
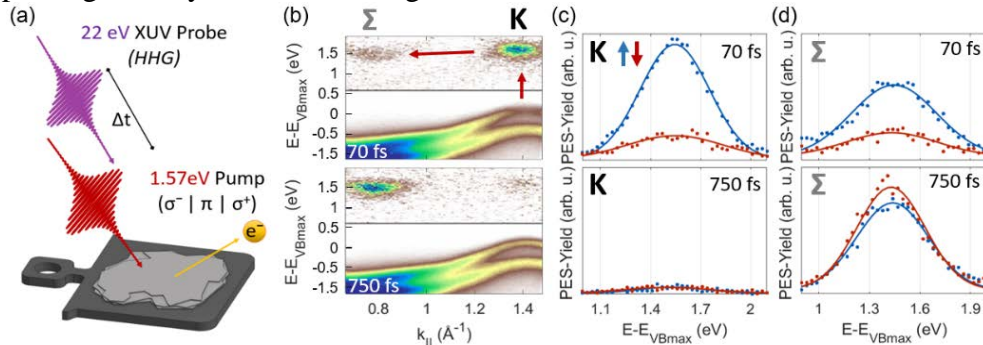
Fig. 1 Sketch of the measuring scheme :
(a).Momentum-resolved PES maps of WSe_2 along the $\Sigma - K$ direction for two time steps after optical excitation.
(b).Momentum - integrated spin signal at the K (c) and Σ point (d) for two time steps after optical excitation.

In the pristine material, the evolution of optically excited spin carriers at important key symmetry points of the Brillouin zone is investigated. In particular, after an initial spin-selective optical excitation of carriers at the K point, a subsequent intervalley scattering process to the conduction band minimum at the neighboring Σ point takes place (Fig. 1 (b)). The spin polarization of the initially excited non-equilibrium populations and their evolution during the intervalley scattering is directly traced (Fig. 1 (c) and (d)) and further disentangled from the intrinsic spin polarization of the ransport states, which do not coincide at all times during the thermalization process [1]. Furthermore, we investigate how the behavior of optically excited spin carriers is altered in a prototypical heterostructure consisting of an ultrathin CuPc layer on bulk WSe_2. The resulting band structure of the heterostructure shows contributions from both the TMD and the molecular layer, giving rise to potentially new excitation pathways at the interface. Starting from the non-dispersing CuPc HOMO, which is energetically located between the spin-split valence band branches of WSe_2, we find an additional, optically selectable excitation pathway in the CuPc/WSe_2 heterostructure compared to pristine WSe_2. This excitation pathway allows for a direct excitation of carriers at the previously momentum forbidden conduction band minimum at the Σ point of WSe_2 in a charge transfer process from the molecular HOMO. In addition, we discuss a compound of a thin layer of the spherical molecule C_{60} on a WSe_2 surface. For this C_{60}/WSe_2 heterostructure, the creation of an ultrafast spin polarization upon optical excitation in the absence of an external magnetic field is demonstrated [2]. In particular, an interlayer transfers of optically excited charge-transfer excitons from the fullerene C_{60} [3, 4] to the WSe_2 layer leads to an electric field that induces layer-dependent Stark shifts of the WSe_2 valence bands.
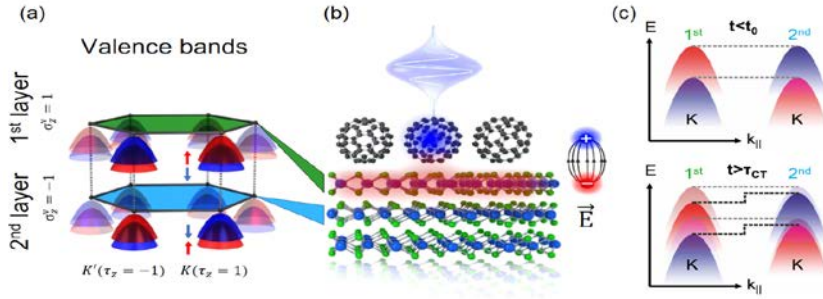
Fig. 2. (a) Layer specific spin polarization of the valence band maxima at the K point of WSe_2. (b) Optical excitation of the C_{60}/WSe_2 heterostructure leading to an interfacial charge transfer and an electrical field. (c) Layer dependent Stark shifts of the valence bands, leading to the creation of ultrafast spin polarization. [2].

These shifts transiently lift the spin degeneracy of the system, thereby revealing its "hidden" spin polarization, as shown in Fig. 2

References
[1] S. Hedwig, G. Zinke, J. Braun, B. Arnoldi, A. Pulkkinen, J. Minár, H. Ebert, M. Aeschlimann, B. Stadtmüller, *to be submitted* (2025).
[2] B. Arnoldi, S. L. Zachritz, S. Hedwig, M. Aeschlimann, O. L. A. Monti, B. Stadtmüller, *Nat. Commun.* **15**, 3573 (2024).
[3] B. Stadtmüller, S. Emmerich, D. Jungkenn, N. Haag, M. Rollinger, S. Eich, M. Mahalingam, M. Aeschlimann, M. Cinchetti, S. Mathias *Nature Communications* **10**, 1470 (2019).
[4] S. Emmerich, S. Hedwig, B. Arnoldi, J. Stöckl, F. Haag, R. Hemm, M. Cinchetti, S. Mathias, B. Stadtmüller, M. Aeschlimann *Journal of Physical Chemistry* C **124**, 43 (2020).
* *Acknowledgements*: The presented work was funded by the Deutsche Forschungsgemeinschaft (DFG, German Research Foundation) - TRR 173 –268565370 Spin+X: spin in its collective environment (Projects A02).

High-temperature superfluorescence in perovskites

K. Gundogdu
North Carolina State University, Raleigh, NC 27695 USA

The formation of coherent macroscopic states and the manipulation of their entanglement using external stimuli are essential for emerging quantum applications. However, the observation of collective quantum phenomena such as Bose–Einstein condensation, superconductivity, superfluidity and superradiance has been limited to extremely low temperatures to suppress dephasing due to random thermal agitations. In this presentation I will talk about room-temperature superfluorescence (SF) in hybrid perovskite thin films [1,2]. In SF an optically excited population of incoherent dipoles develops collective coherence spontaneously (Fig. 1a). This emergent collective state forms a giant dipole and radiates a burst of photons. Because electronic transitions dephase extremely fast, observation of SF in semiconductors is extremely rare and under high magnetic fields and at very low temperatures. Therefore, the discovery of room temperature SF in perovskites is very surprising and shows that in this material platform, there exists an extremely strong immunity to electronic dephasing due to thermal processes. To explain this observation, we propose that the formation of large polarons in hybrid perovskites provides a quantum analogue of vibration isolation to electronic excitation and protects it against dephasing even at room temperature (Fig. 1b).
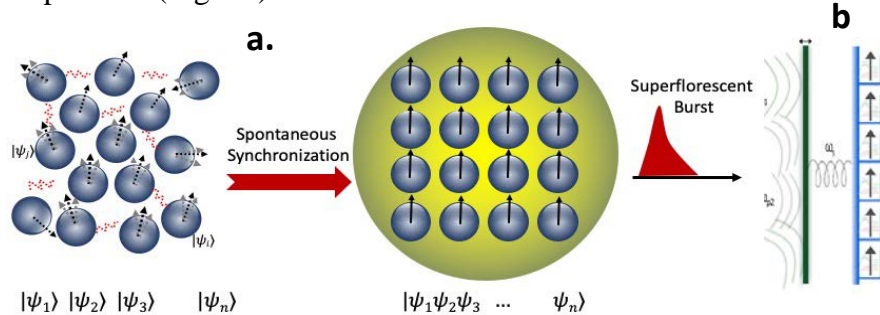
Fig. 1: a- Illustration of superfluorescence; b- Protection of dipoles with a quantum analog of vibrational isolation mechanism. Multiple boxes attached to a common lattice distortion mode that protects dipoles from dephasing. This leads to a macroscopic state even at high temperatures.

Understanding the origins of sustained quantum coherence and the superfluorescence phase transition at high temperatures can provide guidance to design systems for emerging quantum information technologies and to realize similar high-temperature macroscopic quantum phenomena in tailored materials.

References
[1] M. Biliroglu, G Findik, J. Mendes, D. Seyitliyev, L. Lei, Q. Dong, Y. Mehta, V.V. Temnov, F. So, K. Gundogdu, *Nature Photonics* **16**, 324 (2022)
[2] G. Findik, M.Biliroglu, D.Seyitliyev, J. Mendes, A. Barrette, H. Ardekani, L. Lei, Q. Dong, F. So, K. Gundogdu, *Nature Photonics* **15**, 676 (2021)
* *Acknowledgement(s)*: authors acknowledge support from DOE DE-SC0024396.

Photoinduced non-reciprocal phase transitions

R. Hanai[1], D. Ootsuki[2], R. Tazai[3]

[1] *Institute of Science Tokyo, Tokyo 152-8551, Japan*
[2] *Okayama University, Okayama 700-8530, Japan*
[3] *Kyoto University, Kyoto 606-8502, Japan*

In nonequilibrium systems where the detailed balance is broken, the free energy minimization principle does not generically apply. In such situations, interparticle interactions do not necessarily have action-reaction symmetry. Recent studies, mainly in the field of active matter, showed that non-reciprocal interactions may give rise to diverse collective phenomena. For example, an ordered state with non-reciprocal interaction may exhibit the so-called non-reciprocal phase transition [1] to a time-dependent phase where the order parameter exhibits a persistent many-body 'chase-and-runaway' dynamics. Although ubiquitous in classical active systems, implementing such non-reciprocal interactions in solid-state systems has remained challenging, as the known quantum schemes require precise control over the system on a single-site level. In this talk, we propose a novel dissipation-engineering protocol to induce non-reciprocal interactions in solid-state platforms with light [2]. Focusing on magnetic metals for concreteness, we show microscopically that a light injection that introduces the decay channel to a virtually excited state gives rise to non-reciprocal interactions between localized spins (Fig. 1). One can even realize a situation where spin A tries to align with spin B but the B tries the opposite, resulting in a chase-and-runaway dynamics.
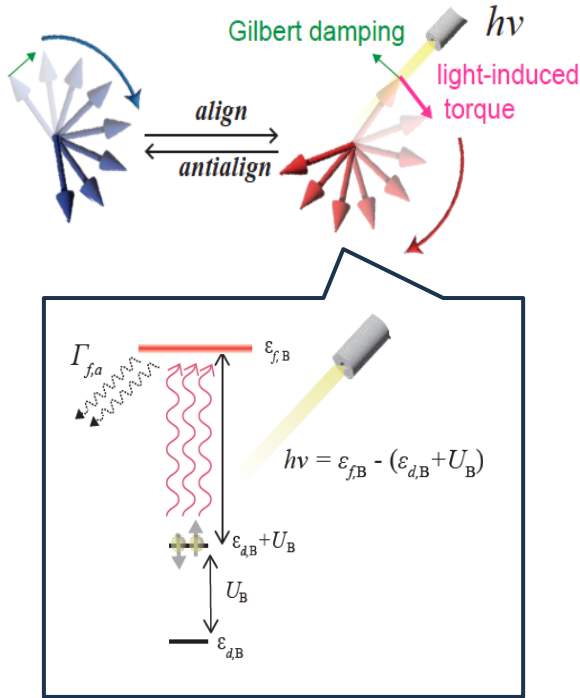
Fig. 1 Our reservoir-engineering protocol to implement non-reciprocal interactions *(interaction that breaks action-reaction symmetry) by light. By injecting light at an appropriately tuned frequency that turns om dissipation to a virtually excited state on one of the two (types of) spins, non-reciprocal interactions emerge, giving rise to a chase-and-run dynamics of electronic spins.*
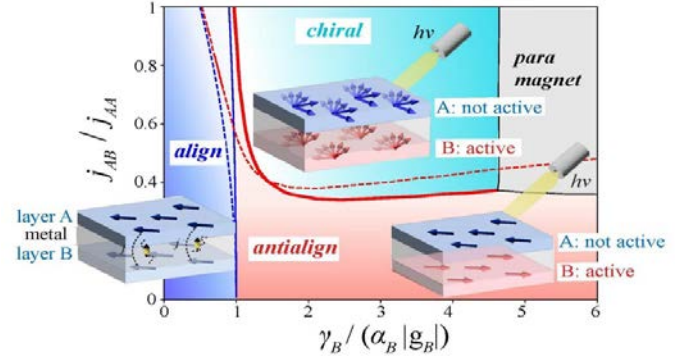
Fig. 2 Phase diagram for a layered ferromagnet as a function of photoinduced dissipation rate γ_B and interlayer interaction strength j_{AB}. *At sufficiently large dissipation rate, a non-reciprocal phase transition occurs to the chiral phase, where the magnetization of two layers exhibits a persistent chase-and-run dynamics. The solid (dashed) line is the phase boundary for temperature T=9meV (5meV)*

Applying our scheme to layered ferromagnets and noncollinear antiferromagnets, we show that a non-reciprocal phase transition from a static to a many-body time-dependent chiral phase emerges (Fig. 2). We see a signature of noise-induced symmetry breaking, which we attribute to the property that non-reciprocally interacting system has a direct analogy to geometrically frustrated systems [3]. We estimate that the required power for their emergence is within the reach of current state-of-the-art experiments. Our work paves the way to bring photo-excited solid-state platforms to the realm of non-reciprocal science.

References
[1] M. Fruchart, R. Hanai, P. B. Littlewood, V. Vitelli, *Nature* **592**, 363(2021).
[2] R. Hanai, D. Ootsuki, R. Tazai, *arXiv:2406.05957* (2024).
[3] R. Hanai, *Physical Review* X **14**, 011029 (2024).

Coherent control of electrons for ultrafast electronics
Floquet engineering, and spectroscopy

C. Heide[1], Y. Kobayashi[3], S.R.U. Haque[2], P.D. Keathley[4], M.F. Kling[2], S. Ghimire[2]

[1]University of Central Florida, Orlando, Fl 32816, USA
[2]SLAC National Accelerator Laboratory, Menlo Park, CA 94025, USA
[3]University of Michigan, Ann Arbor, MI 48109, USA
[4]Massachusetts Institute of Technology, Cambridge, MA02138, USA

Well-controlled light fields have recently been applied to coherently control electron dynamics in solids and at nanostructures [1,2,3]. In solids, this allows for femtosecond-fast current injection caused by sub-cycle-controlled interferometry[1,2], while in nanostructures, light-field-controlled electron emission allows for attosecond-fast gates to perform electric field sampling[3], the analog of a petahertz oscilloscope. More recently, it has also been demonstrated that the periodic interaction of light fields with solids enables the generation of new out-of-equilibrium states, so-called Floquet states, with novel optical and electrical properties. In this talk, I will focus on the Floquet engineering of excitons, which are quasiparticle electron-hole correlated states. We apply intense mid-infrared laser pulses below the optical bandgap to excite excitons in monolayer tungsten disulfide and track the absorption features using time-resolved transient absorption spectroscopy. Our transient absorption signal reveals a large blue shift of ~140 meV and the formation of a virtual absorption feature below the 1s-exciton resonance, which we assign to a light-dressed sideband from the dark 2p-exciton state. This feature is separated by the energy of one photon, and its location depends on the laser wavelength.
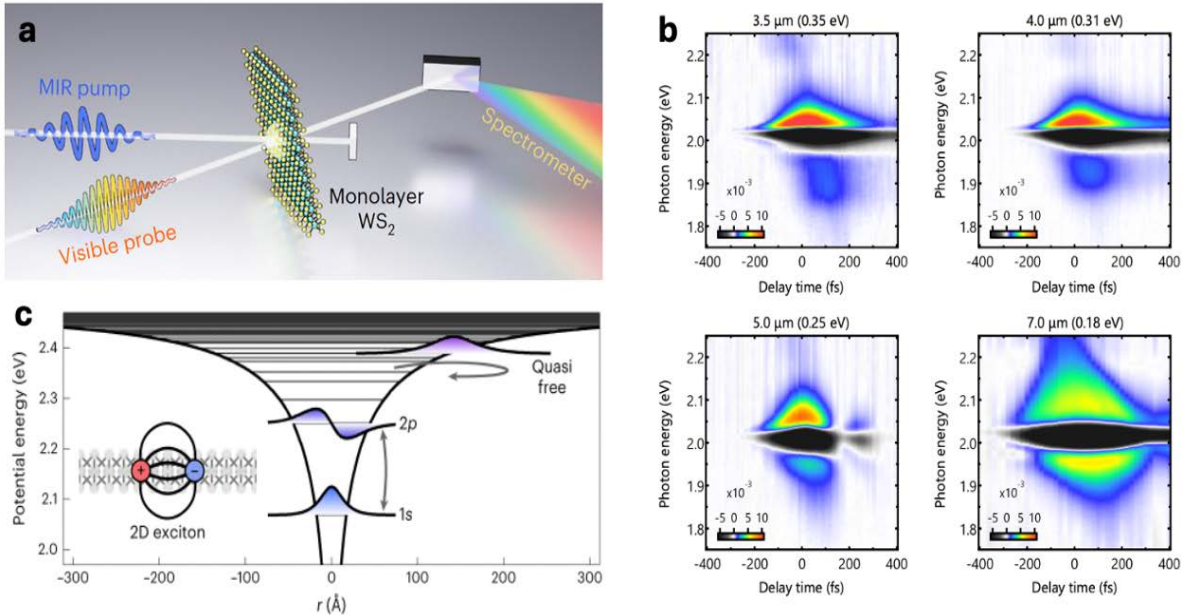
*Fig. 1 Transient absorption spectra of strongly driven excitons in monolayer WS$_2$: **a** Outline of the experiment. A mid-infrared pump pulse drives coherent exciton dynamics in monolayer WS$_2$, and a visible probe pulse records the light-dressing effects in its transmission spectrum. **b** Transient absorption spectra of monolayer WS$_2$ under various mid-infrared wavelengths. The measurements have been performed at room temperature, with a peak field strength of 1 V\nm. The positive delay corresponds to the visible probe pulse following the MIR. **c** Model simulations for Floquet engineering of excitons. An effective two-dimensional potential for excitons and the associated energy levels. An external laser field can excite internal resonances of excitons, such as the 1s-2p transition, and drive the exciton wavepacket into the quasi-free region of the potential.*

Together with quantum-mechanical simulations, supporting the experimental results, we confirm that the dressed state is a Floquet replica.

References
[1] C. Heide, P.D. Keathley, M. F. Kling, *Nature Review Physics* **6,** 648 (2024).
[2] M Borsch, M. Meierhofer, R. Huber, M. Kira, *Nature Review Materials* **8**, 668 (2023).
[3] M. R.Bionta, F.Ritzkowsky, M.Turchetti, Y. Yang, D. Mor, P. Putnman, F.X. Kärtner, K. Bereggren, P.D. Keathley, *Nature Photonics* **15**, 456 (2021)
[4] C. Heide, Y. Kobayashi, S.Rui Haue, S. Ghimire, *Nature Physics* **30**, 1546 (2024).
[5] Y. Kobayashi, C. Heide, A.C. Johnson, V. Tiwari, F. Liu, D.A. Reis, T.F. Heinz, S. Ghimire, *Nature Physics* **19**, 171 (2023).

CO_2 activation by solvated electrons at the Amorphous NH_3/Cu(111) interface

M Heine, L. Gierster, J. Stähler

Humboldt Universität zu Berlin, 12489 Berlin, Germany

Understanding CO_2 reactivity is crucial; the amount of CO_2 in the atmosphere continues to rise with no imminent peak in fossil emissions in sight [1]. Previously, solvated electrons (e_{solv}) have been suggested to activate CO_2, i.e. forming CO_2 radicals that can then lead to cascade hydrogenation steps [2]. However, the fundamental rate of CO_2 activation as well as transient reaction intermediates remain unknown. With time-resolved two-photon photoemission and the amorphous NH_3/Cu(111) interface, we can study the energetics and dynamics of e_{solv} on femtosecond timescales [3]. Here, the electrons are localised at the surface and their lifetime depends exponentially on NH_3 coverage. On an ultrafast timescale, we can now use e_{solv} to decipher the fundamental rate and steps of CO_2 activation. Figure 1b, shows the decreasing solvated electron lifetime with increasing CO_2 exposure. We observe a systematic decrease in the e_{solv} lifetime as CO_2 is added and conclude that CO_2 opens a new decay channel for e_{solv} [4], in addition to the decay back to the copper substrate. By varying the coupling to the copper substrate via the NH_3 thickness, we can then test this kinetic model and extract the fundamental rate of CO_2 activation. This allows us to determine that the rate of e_{solv} attachment to CO_2 occurs on a 10s of picoseconds timescale [4]. Additionally, increases in the work function serve as indicators of possible reactions. Both electron attachment to CO_2 or activated CO_2^- -which has a dipole moment- would lead to a surface dipole, as illustrated in Figure 1a. In fact, as shown in Figure 1c, for thick NH_3 films (i.e. with slow decay to copper) we see a much larger increase in the work function than for thin NH_3 films, where the solvated electrons are not long lived enough to react with CO_2.
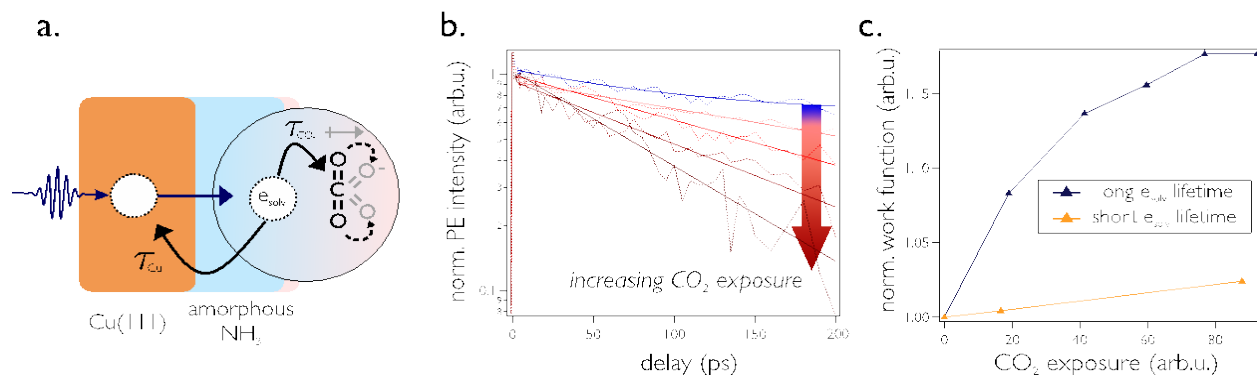
Fig. 1 (left to right). a- *schematic of the NH_3/Cu(111) system and illustration of the two proposed decay channels upon CO_2 addition. Upon electron attachment the CO_2 molecule becomes bent and has a dipole moment;* ***b**-population decay traces of the solvated electrons for increasing CO_2 exposure. Fits to the data are single exponential decays. We see quenching of the solvated electron signal with increasing CO_2 exposure;* ***c**-normalized work function with increasing CO_2 exposure for i. a solvated electron which is long lived enough to react with CO_2 and ii. a solvated electron with lifetime shorter than the proposed reaction with CO_2.*

In future work, we plan to XPS to investigate the core levels of CO_2 as this could enable us to gain temporal information about the CO_2 molecule, and possible reactions with NH_3.

References:
[1] P. Friedlingstein, M. O'Sullivan, M. W. Jones, R. M. Andrew, J. Hauck, P. Landschützer, C. Le Quéré, H. Li, I. T. Luijkx, A. Olsen, G.P. Peters W. Peters, J. Pongratz, C. Schwingshackl, S. Sitch, J. G. Canadell. P. Ciais, R. B. Jackson, S. R. Alin, A. Arneth, V. Arora. N. R. Bates M. Becker, N. Bellouin, C. F. Berghoff, H. C. Bittig, L. Bopp, P. Cadule, K. Campbell. M. A. Chamberlain, N. Chandra, F. Chevallier L. P. Chini, T. Colligan, J. Decaveux, L. M. Djeutchouang, X. Dou, C. D. Rojas, K. Enyo, W. Evans, A. R. Fay, R. A. Feely. D. J. Ford A. Foster, T.Gasser, M. Gehlen, T. Gkritzalis, G. Grassi, L. Gregor, N. Gruber, Ö. Gürses, I. Harris, M. Hefner, J. Heinke, G. C. Hurtt Y. Iida, T. Ilyina, A. R. Jacobson, A. K. Jain, T. Jarníková, A. Jersild, F. Jiang, Z. Jin, E. Kato, R. F. Keeling, K. K. Goldewijk, J. Knauer J. I. Korsbakken, X. Lan, S. K. Lauvset, N. Lefèvre, Z. Liu. J. Liu, L. Ma, S. Maksyutov, G. Marland. N. Mayot, P. C. McGuire, N. Metzl N. M. Monacci, E. J. Morgan, S. - I. Nakaoka, C. Neill, Y. Niwa. T. Nützel, L. Olivier, T. Ono. P. I. Palmer, D. Pierrot, Z. Qin L. Resplandy, A. Roobaert, T. M. Rosan, C. Rödenbeck, J. Schwinger, T. L. Smallman, S. M. Smith, R. Sospedra - Alfonso, T. Steinhoff Q. Sun, A. J. Sutton, R. Séférian. S. Takao. H.Tatebe. H. Tian, B. Tilbrook, O. Torres, E. Tourigny, H. Tsujino, F. Tubiello, G. van der Werf R. Wanninkhof, X. Wang, D. Y. X. Yang, Z. Yu, W. Yuan, X. Yue, S. Zaehle, N. Zeng, J. Zenget, *Earth System Science Data,* **17**, 965 (2024).
[2] C. Hu, Z. Jiang, Q. Wu, S. Cao, Q. Li, C. Chen, L. Yuan, Y. Wang, W. Yang, J. Yang, J. Peng, W. Shi, M. Zhai, M. Mostafavi, J. Ma, *Nature Communications* **14**, 4767 (2023)
[3] J. Stähler, M. Meyer, U. Bovensiepen, M. Wolf, *Chemical Science* **5**, 907 (2011).
[4]M. Heine, L. Gierster, J. Stähler, *to be submitted* (2025).
* *Acknowledgement(s) :Maya Heine acknowledges support by the IMPRS for Elementary Processes in Physical Chemistry*

Light control of quantum matter:
Floquet engineering and metastable states

J.-N. Herre, D. M. Kennes

RWTH Aachen University, 5206 Aachen, Germany

Engineering novel quantum states of matter and controlling them on an ultrafast timescale has become a major research area of condensed matter physics [1]. A lot is still unclear and requires novel theoretical (analytical and numerical) tools that go beyond the well-established ways of studying equilibrium quantum physics. In this talk we will discuss advances on two pathways of achieving full light control of quantum materials. First, we will show how to Floquet engineer long lived prethermal states far from equilibrium and how to efficiently simulate them assuming a classical light source [1]. Then, we will continue to discuss quantum Floquet engineering of Andreev bound states in a cavity [2]. Finally, we will present numerical progress in accessing metastable states by means of Dynamical Mean Field Theory (DMFT) [3]. In the first part, we consider a periodically driven system of spinless fermions. Performing a time-dependent gauge change we trade the time dependency for a breaking of translation invariance. This problem is known as Stark many-body localization. We simulate the dynamics of this system that shows long-term memory even at infinite temperature, allowing for a prethermal Floquet state (Fig. 1, left panel). We introduce a new variant of continuous unitary transformations called tensor-flow-equations (TFE) as a multi-purpose tool to obtain an approximated full spectrum of both translation-invariant and disordered quantum-many-body systems, enabling the study of far-from-equilibrium dynamics both in 1D and 2D. In the second part, we quantize the light field and investigate the hybridization of a superconducting chain featuring Andreev bound states at the normal-superconducting interface with a single cavity mode. Bound-state compounds are uniquely suited to form polaritons when placed in a photonic environment, e.g. a cavity. We quantum Floquet engineer the system to display several polaritonic signatures, indicating the formation of Andreev bound state polaritons. The formation of the Andreev bound state (inner peaks) together with Floquet sidebands (outer peaks) are shown in the right panel of Fig. 1.
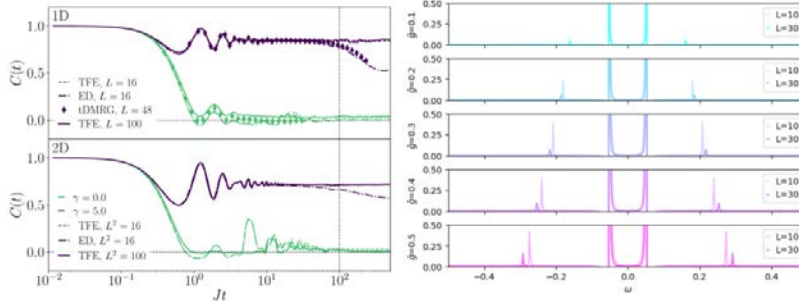
Fig. 1. Left: *Infinite temperature dynamics of prethermal stable states in one and two spatial dimensions, computed with TFE, tDMRG and exact diagonalization (ED). A non-zero value of C(t) indicates memory of the initial state. Different system sizes L and frequencies/field strengths γ are shown.* **Right**: *Andreev bound state and Floquet sidebands in the local density of states due to coupling to a cavity. Different coupling strengths g and system sizes L are shown.*

In the last part, we show how to achieve access to metastable states in correlated systems. To assess the formation of metastable states, we aim to establish a microscopic framework for equilibrium free-energy landscapes in quantum materials featuring electron-electron and electron-phonon interactions. A key ingredient are Landau functionals derived from DMFT calculations, capturing the interplay between various types of order and their coupling to external control parameters.

Fig.2. DMFT Phase Space Extension method for the single-orbital Hubbard model. **Upper panel**: *Double occupancy curve for 1/T = 64 including the unstable solution present during the Mott transition.***Lower panels**: *Landau free energy functionals calculated from the upper curve via integration of equations of state.*
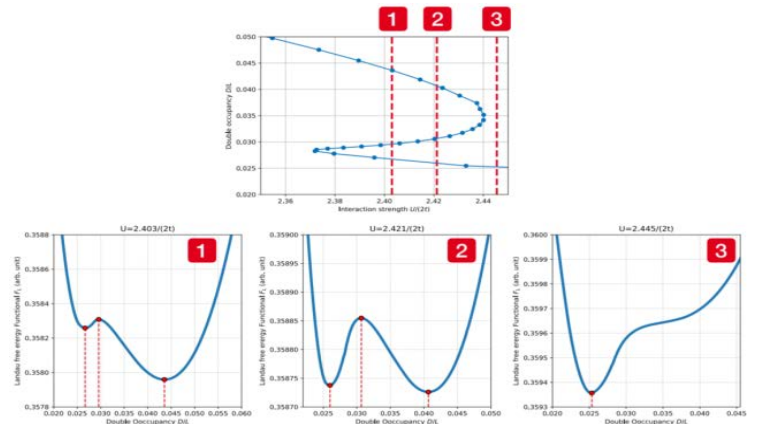
At the core of this effort is the integration of equations of state to construct free-energy landscapes. For this purpose, we extend the so-called phase space extension method [5] to multi-orbital systems. Results for the single-band Hubbard model (Fig. 2), show how one can resolve the free energy landscape at each step of a sweep through the Mott transition at half-filling.

References
[1] A. de la Torre, D. M. Kennes, M. Claassen, S. Gerber, J. W. McIver, M. A. Sentef, *Review of Modern Physics* **93**, 041002 (2021).
[2] J.- N. Herre, Q. Liyu, R. Rausch, C. Karrasch, D.M. Kennes, arxiv:2411.14527, submitted to *Physical Review Research* (2025).
[3] J. Reimann, V. Kozin, J. Klnovaja, D. Loss, A. Rubio, D. M. Kennes, *to be submitted* (2025).
[4] L. Bremer, M. Eckstein, H. U. R. Strand, T. O. Wehling, *to be submitted* (2025).
[5] H. U. R. Strand, A. Sabashvili, M. Granath, B. Hellsing, S. Östlund, *Physical Review* B **83**, 205136 (2011).

Out-of-equilibrium dynamics of the optimally doped Bi2212 Superconducting cuprate by ultrafast Time resolved Raman scattering

L. Gatuingt[1], A. Alekhin[1], N. Nilforoushan[1], S. Houver[1], A. Sacuto[1], G. Gu[2], Y. Gallais[1]
[1] Université Paris Cité, 75013 Paris, France
[2] Brookhaven National Laboratory, Upton, NY 11973, USA

Despite extensive studies of the out-of-equilibrium dynamics of cuprate superconductors [1,2], there is still no consensus on several key aspects. This includes the recombination mechanisms and whether the recovery dynamics is dominantly thermal or not. Time-resolved Raman (tr-Raman) spectroscopy is a promising technique to explore the dynamics of correlated materials. Here, we used tr-Raman on the cuprate Bi2212 to track the excitation and relaxation of both quasi-particles and superconducting (SC) condensate initiated by a 1.2eV pump with sub-picoseconds time resolution. By choosing adequate polarizations of the incident and scattered light, we access the nodal and anti-nodal regions of the Brillouin zone allowing to explore potential dichotomy in their dynamics. In the anti-nodal region, we could directly follow the destruction and recovery of the SC condensate (Fig. 1, Green curve) and compare it to the Drude response of photo-induced Bogoliubov quasi-particles (Fig. 1, Black curve). Using Raman thermometry, we show that a thermal model, which describes the transient state as a sequence of equilibrium states at a given temperature, does not apply. Instead, we find that the thermalization of Bogoliubov quasi-particles (Fig. 1, blue curve) occurs significantly faster than the SC condensate recovery.
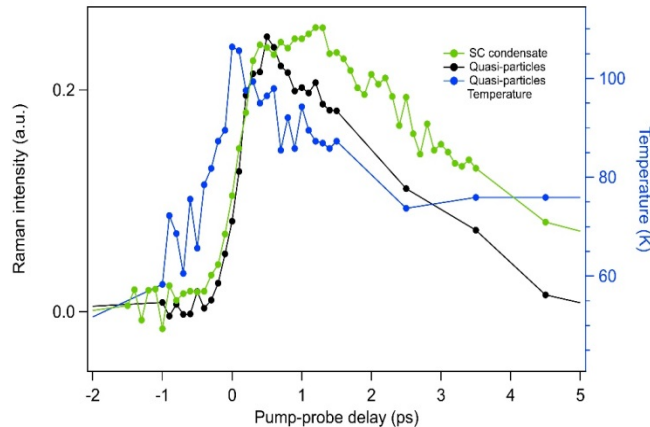
Fig. 1. Tr-Raman dynamics of the SC condensate (green), the quasi-particle Drude response (black) and the quasi-particle temperature (blue) as a function of the pump-probe delay. Right axis shows the extracted temperature of SC condensate.

Our results point to a non-thermal transient state where a depleted SC condensate coexists with a population of cold quasi-particles

References
[1] S. Parham, H. Li1, T. J. Nummy, J. A. Waugh, X. Q. Zhou, J. Griffith, J. Schneeloch, R. D. Zhong, G. D. Gu, D.S. Dessau, *Physical Review* X **7** 041013, (2017).
[2] G. Coslovich, C. Giannetti, F. Cilento, S. Dal Conte, G. Ferrini, P. Galinetto, M. Greven, H. Eisaki, M. Raichle, R. Liang, A. Damascelli F. Parmigiani, *Physical Review B* **83,** 064519, (2011). ,

Non-equilibrium energy flow among electrons and phonons in Ultrathin Pb films on Si(111) – where the heck is the energy?

C. Brand[1], M. Tajik[1], T. Witte[1], L. Rettig[2], B. Sothmann[3], U. Bovensiepen[1], M. Horn von Hoegen[1]

[1]*Universität Duisburg-Essen, 47057 Duisburg, Germany*
[2]*Fritz-Haber-Institut der Max-Planck-Gesellschaft, 14195 Berlin, Germany*
[3]*Center for Nanointegration (CENIDE), 47048 Duisburg, Germany*

The pathways of flow of energy subsequent to an impulsive optical excitation through various degrees of freedom of the electronic and lattice systems were studied for ultrathin lead films on Si substrates. The response of the electron system is determined through time-resolved photoelectron spectroscopy [1]. The lattice excitation is followed by means of the Debye-Waller effect in ultrafast reflection high-energy electron diffraction [2,3]. Both methods are highly surface sensitive and provide information on the dynamics of the Pb film only. Epitaxial 5 monolayer thick Pb films on Si(111) were grown by molecular beam epitaxy [4]. The sample is optically irradiated by fs-IR laser pulses of 80 fs duration at 1.5 eV photon energy. The Schottky barrier between Pb film and Si substrate inhibits charge transfer. The very low thermal boundary resistance $G_{Pb/Si}$ of the Pb/Si interface hinders dissipation of the structural excitation which is then confined to the Pb film [5]. The Pb films were excited at an absorbed energy density of up to $\Phi_{abs} = 100$ J/cm^3. Due to the large direct bandgap of Si the substrate gets only barely excited.
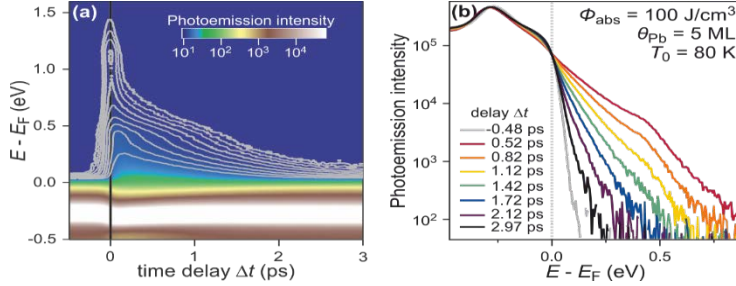
***Fig. 1. Time-resolved PES** for a 5 ML Pb film at $\Phi_{abs} = 100$ J/cm3 and $T_0 = 80$ K **Left:** Gaussian-filtered photoemission intensity as a function of energy E above E_F and of time delay Δt. **Right:** photoemission spectra and corresponding fits before and after fs laser excitation for different time delays.*

The transient temperature of the electron system in the Pb film is determined from the slope of the Fermi Dirac distribution of the excited electron system as shown in Fig. 1. We observe thermalization of the electronic excitation in less than 200 fs to a maximum temperature of 1140 K and cooling in 1.4 ps. The electronic heat ΔQ_{el} decays even faster in only 0.5 ps. The lattice exhibits a completely different temporal dynamic. The intensity of the Bragg spots decay – depending on excitation density – slowly in 3.5 to 8 ps as is shown in Fig. 2

***Fig. 2. URHEED on 5 ML Pb on Si(111). Left:** RHEED pattern at $T_0 = 19$ K. **Right:** Transient intensity drop $I(\Delta t)/I(T_0)$ of the (00) spot for different absorbed energy densities Φ_{abs}. The solid lines give exponential fits to the intensity drops, i.e., the increase in vibrational displacements. The temporal response function is shown as a cyan Gaussian.*
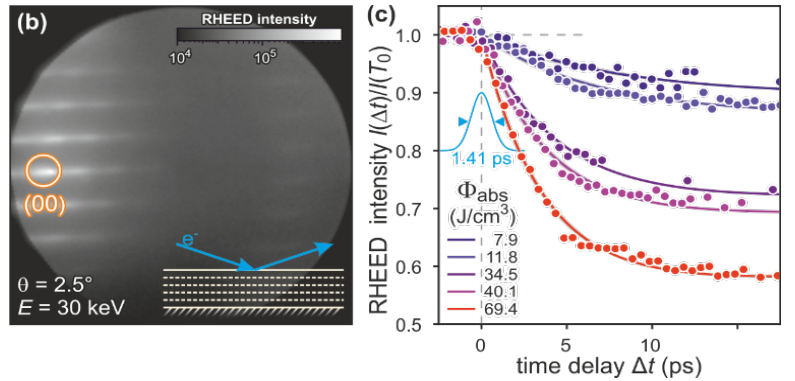
This drop of intensity can be converted through a Debye-Waller analysis to an increase in lattice temperature T by $\Delta T_{max} = 10$ K to 72 K depending on the absorbed energy density of $\Phi_{abs} = 11$ to 80 J/cm^3. The different time scales of evolution of electron temperature and lattice temperature leaves a time gap of 3 - 7 ps, where the energy is hidden to our analysis. Here, we propose that the energy is transiently stored in high-frequency phonon modes for which diffraction is insensitive [6]. These high frequency phonons are excited by strong electron phonon coupling in 0.5 ps. Within a three-temperature model as sketched in Fig. 3 we use three heat baths, namely electrons, high-frequency and low-frequency phonon modes to simulate the observations and thus providing the coupling parameters among the sub-systems. The direct excitation of low frequency phonons is strongly suppressed and only facilitated through anharmonic phonon-phonon coupling from high to low frequency phonon system.

This model is supported by the fluence dependence of the excitation time constant, since a faster excitation of the low-frequency phonons is observed for higher fluences. Quantitative experimental access to the temperature of the high frequency phonon subsystem is provided through the slow drop of temperature of the electron system on longer time scales $t > 3$ ps as shown in Fig. 3 which is strong support of the proposed model. Equilibration among the phonon system, i.e., among high and low frequency phonons, takes up to 80 ps as derived from the temporal shift of the transient minimum of diffracted intensity as function of absorbed fluences.
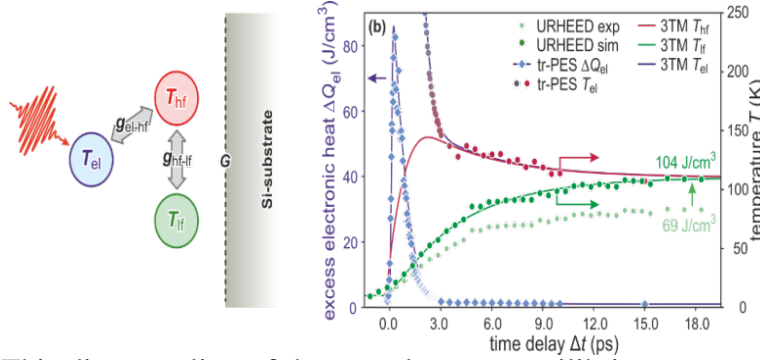
*Fig. 3. Three-temperature model fit. Left: Sketch of the energy flow between the electron and phonon subsystems and their coupling parameters. **Right:** 3TM as solid lines for transient electron temperature T_{el} (blue), and lattice temperature for high-frequency phonons T_{hf} (red) and low-frequency phonons T_{lf} (green), and excess electronic heat ΔQ_{el} (blue dashed line) as fitted to the experimental tr-PES data (bluish to reddish symbols) and corrected URHEED data (dark green dots). The transient electron temperature T_{el} at $\Delta t > 3$ ps serves as a measure of the high-frequency phonon temperature T_{hf} after thermalization of electrons and high-frequency phonons.*

This disentangling of the complex non-equilibrium energy flow through a multitude of subsystems, that go far beyond a simple two-temperature model, was only made possible by the combination of electron spectroscopy and diffraction. We are convinced that such non-equilibrium steps of energy flow through different electronic and phononic subsystems are universal for many material systems.

References
[1] L. Rettig, P.S. Kirchmann, U. Bovensiepen, *New Journal of Physics* **14**, 023047 (2012).
[2] B. Hafke, T. Witte, C. Brand, Th. Duden, M. Horn-von Hoegen, *Review of Scientific Instruments* **90**, 045119 (2019).
[3] M. Horn von Hoegen, *Structural Dynamics* **11**, 021301 (2024).
[4] M. Hupalo, M.C. Tringides, *Physical Review* B **65**, 115406 (2002).
[5] T. Witte, T. Frigge, B. Hafke, B. Krenzer, M. Horn-von Hoegen, *Applied Physics Letters* **110**, 243103 (2017).
[6] S. Schäfer, W. Liang, A.H. Zewail, *New Journal of Physics* **13**, 063030 (2011).

Ultrabroadband mid-infrared nonlinear optics driven by a Cr:ZnSe Chirped-pulse amplifier

K.-H. (Kyle) Hong
Massachusetts Institute of Technology, Lexington, MA 02420, USA

High-peak-power femtosecond laser sources with an ultrabroadband spectral span in the mid-infrared (mid-IR, ~2–15 μm) spectrum have various applications, such as spectroscopic detection of chemicals, studies of ultrafast dynamics, and driving strong-field laser-matter interactions. Transition-metal-doped II-VI materials, such as Cr:ZnSe, Cr:ZnS, and Fe:ZnSe, are found to be a suitable choice for direct lasing in the mid-IR with broad wavelength tunability and ultrashort pulse generation in the range from 2 to 5 μm of wavelength. This paper focuses on our experimental efforts in ultrabroadband nonlinear optics using a 2.4 μm, 250 fs, 1.2 mJ Cr:ZnSe chirped-pulse amplifier (CPA) at a 1 kHz repetition rate. We present 1) the high-energy mid-IR laser filamentation in solids with supercontinuum generation (SCG) [1], 2) the highly efficient, octave-spanning mid-IR optical parametric amplification (OPA) [2], and 3) a power-scaling strategy based on a multipass Cr:ZnSe amplifier and a multi-channel mid-IR coherent beam combiner concept [3]. First, we have investigated strong-field mid-IR laser beam propagation in solids and demonstrated high-energy laser filamentation with multi-octave-spanning SCG. The SCG is studied in both anomalous and normal dispersion regimes with YAG and polycrystalline ZnSe, respectively. The formation of stable and robust single filaments along with the visible-to-mid-IR SCG is obtained with a pump energy of up to record-high 100 μJ in a 6-mm-long YAG medium (Fig. 1(a)). On the other hand, the SCG and even-harmonic generation from random quasi-phase matching are

simultaneously observed from the single filaments in a 6-mm-long polycrystalline ZnSe medium with a pump energy of up to 15 µJ (Fig. 1(c)). The numerical simulations reveal the temporal structure of mid-IR filaments, such as soliton-like self-compression in YAG (Fig. 1(b)) and pulse broadening in ZnSe [1].
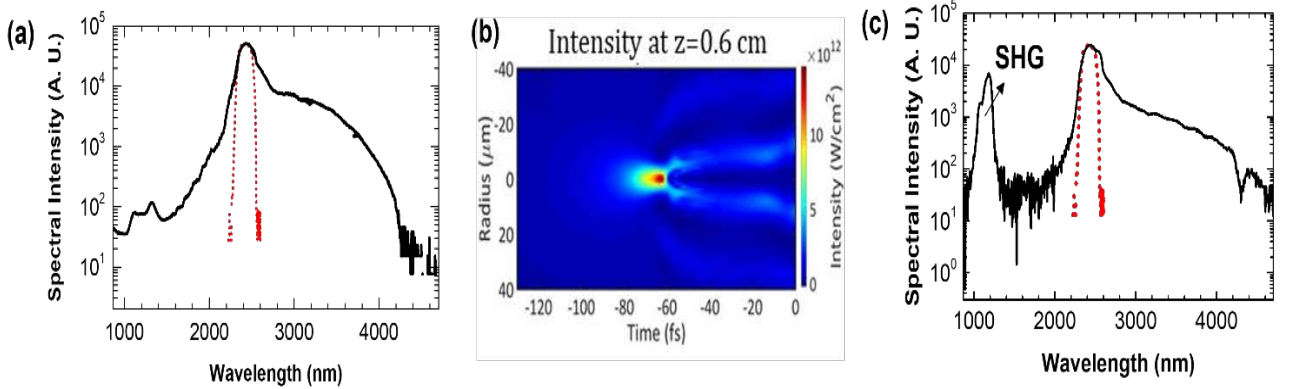
Fig. 1. SCG spectrum from mid-IR laser filament in YAG (a), the simulated temporal profile (**b**), and SCG spectrum in ZnSe (**c**); SHG: second-harmonic generation.

Second, ZnGeP$_2$ (ZGP) is suitable for high-energy mid-IR OPA pumped at ~2−3 µm wavelength due to its broad transparency range, favorable phase-matching conditions, and high damage threshold. We have built a mid-IR ZGP OPA setup, pumped by the 2.4 µm Cr:ZnSe laser. The full spectral coverage of 3−10 µm with the amplified signal and idler beams is demonstrated, as shown in Fig. 2. The signal beam in the range of ~3−5 µm is produced by either SCG in YAG (Fig. 2(a)) or optical parametric generation (OPG) in another ZGP (Fig. 2(b)) using the common 2.4 µm pump laser.
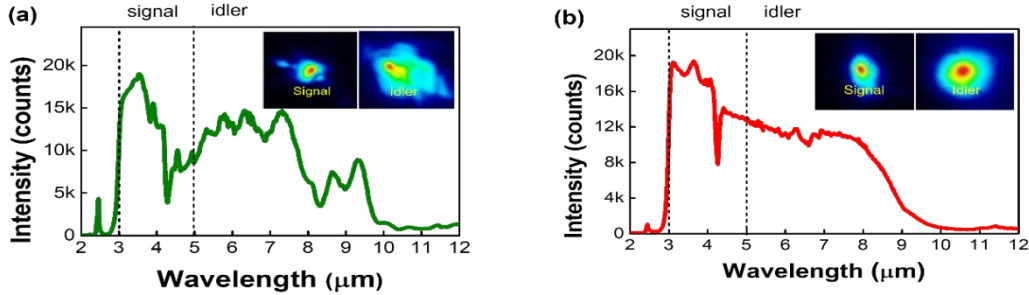
Fig. 2. Octave-spanning mid-IR spectrum from OPA in ZGP pumped at 2.4 µm.

The pulse duration of signal pule is measured to be ~330 fs for both cases. The idler pulse for OPG-seeded case is partially coherent to the pump pulse while that from SCG is fully coherent to the pump. We obtain a pump to signal and idler combined conversion efficiency of record-high 23% in this mid-IR range and the pulse energy of up to 130 µJ with ~2 µJ OPG seeding [2]. The OPA output energy is limited by the available pump pulse energy and therefore further energy scalable with multi-stage OPA and higher pump pulse energy. Addition of a multipass Cr:ZnSe amplifier chain can boost the peak power of the 2.4 µm pulses to 10 mJ, 100 GW level, which is high enough for forming mid-IR laser filaments in air. These high-energy pulses can pump OPA for generation of multi-mJ mid-IR pulses in the range of 3-10 µm. In addition, the peak power of ~5-14 µm idler pulses can be scaled to tens of GW with an OPA-based coherent waveform synthesis concept [3] if we use several nonlinear crystals, such as CdSiP$_2$, ZGP, and GaSe, in multi-channel OPA. In summary, we demonstrate and propose high-peak-power ultrabroadband mid-IR sources based on nonlinear optics pumped by a high-power femtosecond Cr:ZnSe CPA system.

References
[1] S .-H. Nam, G. C. Nagar, D. Dempsey, O. Novák, B. Shim, K.-H. Hong, *High-Power Laser Science and Engineering* **9**, e12(2021).
[2] S.- H. Nam, V. Fedorov, S. Mirov, K.-H. Hong, *Optics Express* **28**, 32403 (2020).
[3] S.- W.Huang, G. Cirmi, J. Moses, K.-H. Hong, S. Bhardwaj, J. R. Birge, L.-J. Chen, E. Li, B. Eggleton, G. Cerullo, F.X. Kärtner, *Nature Photonics* **5**, 475 (2011).

Ultrafast decoupling of polarization and strain in ferroelectric BaTiO$_3$

L. P. Hoang[2], D. Pesquera[4], G. N. Hinsley[5], R. Carley[1], L. Mercadier[1], M. Teichmann[1], S. Ganguly[4]
T. C. Asmara[1], G. Merzoni[6], S. Parchenko[1], J. Schlappa[1], Z. Yin[1], J. M. C. Roque[4], J. Santiso[4], I. Spasojevic[4]
C. Carinan[1], T. -L.Lee[7], K. Rossnagel[3], J.Zegenhagen[7], G. Catalan[8], I. A.Vartanyants[5], A. Scherz[1], G. Mercurio[1]

[1]European XFEL, 22869 Schenefeld, Germany
[2]Max-Planck-Institut für Struktur und Dynamik der Materie, 22761 Hamburg, Germany
[3]Kiel University, 24098 Kiel, Germany
[4]Universitat Autonoma de Barcelona, 08193 Barcelona, Spain
[5]Deutsches Elektronen-Synchrotron DESY, 22607 Hamburg, Germany
[6]Politecnico di Milano, 20133 Milano, Italy
[7]Diamond Light Source Ltd., Didcot, OX110DE Oxfordshire, United Kingdom
[8]Institucio Catalana de Recerca i Estudis Avancats (ICREA), 08010 Barcelona, Catalonia

The ability to switch ferroelectric polarization is crucial for technological applications, and optical control over this property could drive the development of next-generation nonvolatile memory and optoelectronic devices [1]. However, achieving stable and reversible all-optical polarization switching remains elusive [2]. Strain engineering, enabled by precise sample design [3,4], has been used to fine-tune the spontaneous polarization by leveraging its proportionality to the strain via the piezoelectric effect. However, this approach is hindered by complex sample growth and the inability to achieve ultrafast modulation. Other methods, such as photocarrier redistribution at the interface of a 2D layer and ferroelectric BaTiO$_3$, have induced polarization switching without reversibility [5], while THz light has enabled reversible switching, though only transiently and at high fluences [6]. In this study, we go beyond strain engineering and demonstrate a novel light-induced approach to polarization control using a combination of time-resolved X-ray diffraction (tr-XRD), time-resolved optical second harmonic generation (tr-SHG), and time-resolved optical reflectivity (tr-refl) [7]. Upon above-bandgap UV laser excitation of the prototypical ferroelectric BaTiO$_3$, we observe an ultrafast decoupling of polarization from strain (Fig. 1). During this process, the polarization, indicated by SHG intensity (Fig. 1a), is primarily influenced by the photoexcited electrons, as shown by the reflectivity (Fig. 1b), rather than by the strain (Fig. 1c). Additionally, we observe the softening of Ti-O bonds due to charge transfer from oxygen to titanium, which reduces the displacement between Ti and the oxygen octahedron, leading to decreased tetragonality. Fundamentally, our findings go beyond the Landau-Ginzburg-Devonshire framework by revealing an out-of-equilibrium polarization-strain decoupling and identifying its underlying physical mechanisms [7].
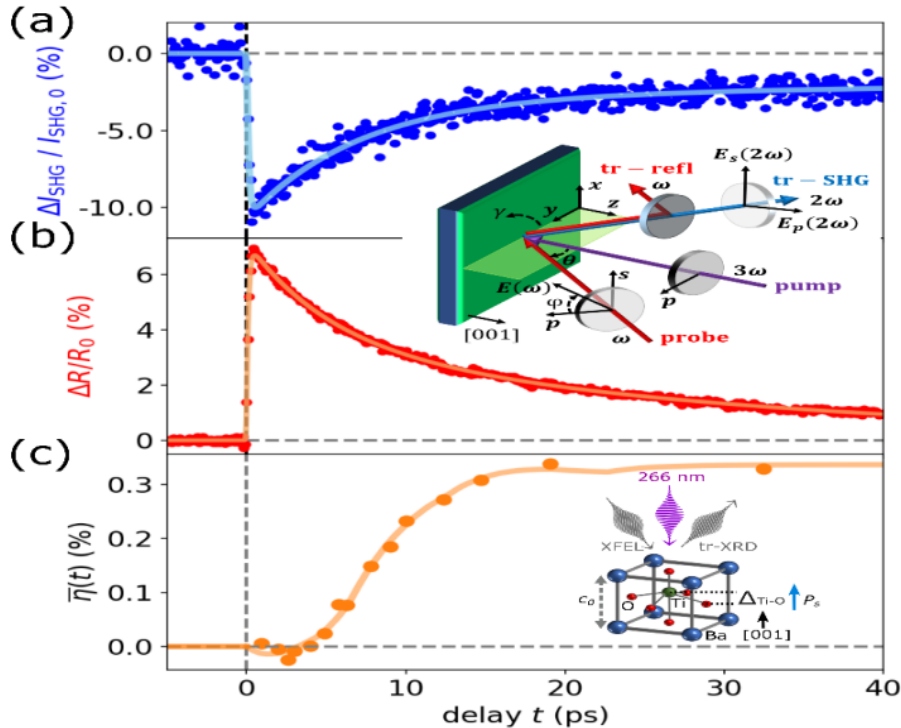
Fig.1.Photoinduced ferroelectric polarization, electron, and strain dynamics in ferroelectrics BaTiO$_3$ under 266 nm optical excitation. a) Relative change of SHG $\Delta I_{SHG}/I_{SHG,0}$ and b) reflectivity $\Delta R/R_0$ as a function of pump-probe delay t and their corresponding fit curves, with the sketch of tr-SHG and tr-refl setup in the inset. c) Relative change of the average strain $\bar{\eta}(t)$ of the BaTiO$_3$ thin film as a function of pump-probe delay t and its corresponding fit curve, with the sketch of the BaTiO$_3$ unit cell, the out-of-plane lattice parameter in the ground state c_0, the relative displacement Δ_{Ti-O} of the Ti atom from the center of the O octahedron, the spontaneous ferroelectric polarization P_s, the incident and diffracted XFEL beams as a function of pump-probe delay t.

From an application perspective, this excited state is expected to have a lower energy barrier to polarization switching, which could be stably and reversibly enabled by further excitation with THz light. Given the broader relevance of our findings, this method could extend to multiferroics, where simultaneous control of ferroelectric polarization and its decoupling from strain could facilitate optical manipulation of magnetization, paving the way for full optical control of these complex materials.

References
[1] L. W. Martin, A. M. Rappe, *Nature Review Materials* **2**, 16087 (2017).
[2] J. Guo, W. Chen, H. Chen, Y. Zhao, F. Dong, W. Liu, Y. Zhang, *Advanced Optical Materials* **9**, 2002146 (2021).
[3] K. J. Choi, M. Biegalski, Y. L. Li, A. Sharan, J. Schubert, R. Uecker, P. Reiche, Y. B. Chen, X.Q. Pan, V. Gopalan, L.-Q. Chen, D. G. Schlom
C. B. Eom, *Science* **306**, 1005 (2004).
[4] D. Pesquera, E. Parsonnet, A. Qualls, R. Xu, A. J. Gubser, J. Kim, Y. Jiang, G. Velarde, Y. - L. Huang, H. Y. Hwang, R. Ramesh
L. W. Martin, *Advanced Materials* **32**, 2003780, (2020).
[5] T. Li, A.Lipatov, H.Lu, H.Lee, J.-W. Lee, E.Torun, L.Wirtz,C. B. Eom, J. Iniguez, A. Sinitskii, A. Gruverman, *Nature Communications* **9**,3344 (2018)
[6] R. Mankowsky, A. von Hoegen, M. Först, A. Cavalleri, *Physical Review Letters* **118**, 197601 (2017).
[7] L. P. Hoang, D. Pesquera, G. N. Hinsley, R. Carley, L. Mercadier, M. Teichmann, S. Ganguly, T. C. Asmara, G. Merzoni, S. Parchenko
J. Schlappa, Z. Yin, J. M. C. Roque, J. Santiso, I. Spasojevic, C. Carinan, T. -L. Lee, K. Rossnagel, J. Zegenhagen, G. Catalan
I. A. Vartanyants, A. Scherz, G. Mercurio, *arXiv:2503.19808* (2025).

Measuring the non-equilibrium electronic structure of Phonon-driven 2D materials

N. Hofmann, I. Gierz
Universität Regensburg, 93040 Regensburg, Germany

Quasi-periodic driving of solids with tailored light fields has emerged as a promising pathway for non-equilibrium materials design. To bring this approach to the next level, tailored driving schemes targeting specific degrees of freedom need to be combined with ultrafast probes of the atomic and electronic structure. We combine pump pulses tunable all the way from the Terahertz to the visible spectral range with a time-a and angle-resolved photoemission (trARPES) probe to gain access to the transient electronic structure of driven materials. We recently implemented a narrow-band, strong-field Terahertz source [1] that allows for the selective excitation of phonon modes in materials with strong spin-orbit coupling and extreme ultraviolet probe pulses with tunable pulse duration to trace band structure dynamics on sub-cycle as well as cycle-averaged time scales.
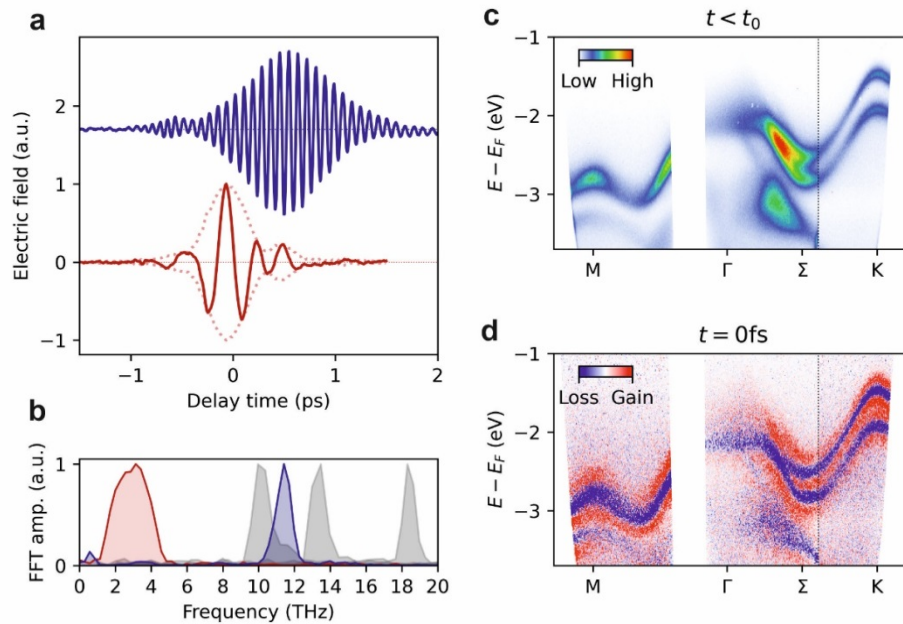
Fig. 1.a) Narrow-band transient waveform generated by chirped-pulse difference frequency generation inside of an organic crystal (blue) and transient from optical rectification (red).
b) Spectra of transients generated with the source from a), red and blue spectra correspond to the transients in a).
c) Electronic structure of WS_2 for negative pump-probe delay as obtained by HHG-driven trARPES.
d) Pump-induced changes of the photocurrent in c) upon excitation in resonance to the E_{1u} phonon mode of WS_2.

In this talk, we present proof-of-principle experiments on graphene and show the transient electronic structure of WS_2 driven at resonance to the E_{1u} phonon mode. We discuss and analyze possible changes of central features like the valence band spin splitting.

Reference
[1] B. Liu, H. Bromberger, A. Cartella, T. Gebert, M. Först, A. Cavalleri, *Optics Letters* **42**, 129 (2017).

Strong-field-induced dynamics of Harmonic dipole phase in solids

A. Husakou[1], L.-M. Koll[1], S. V. B. Jensen[2], P. J. van Essen[3], B. de Keijzer[3], E. Olsson[3], J. Cottom [3]
T. Witting[1], M. J. J.Vrakking[1], L. B. Madsen[2], P. M. Kraus[4], P. Jürgens[3]

[1]*Max-Born- Institut für Nichtlineare Optik und Kurzzeitspektroskopie, 12489 Berlin, Germany*
[2] *Aarhus University, DK-8000, Denmark*
[3]*Advanced Research Center for Nanolithography, 1098 XG Amsterdam, the Netherlands*
[4]*Vrije Universiteit, 1081 HV Amsterdam, the Netherlands*

Interferometry is a fundamental technique in physics which enables precise measurements through the interference of waves. High-harmonic generation (HHG) in solids has emerged as a powerful approachfor probing ultrafast electronic dynamics within crystalline structures. The transient change of the optical properties of transparent solids has been studied by spectral interferometry yielding information on the dynamic modification of the refractive index during ultrafast light-matter interaction. The concepts of solid-state HHG and interferometry have been merged to characterize the intensity-dependence of the dipole phase [1], i.e. the phase accumulated by an electron wavepacket during its excursion in an interband, recollision-like HHG process. Identified intensity-dependent dipole phase variations were attributed to changes in the nonlinear polarization. In another study, a Mach-Zehnder interferometer was employed to track the real-time dynamics of Floquet states in WSe_2 [2]. Here we employed extreme ultraviolet (XUV) high-harmonic interferometry with phase-locked pulse pairs to investigate excitation-induced bandgap dynamics in solids
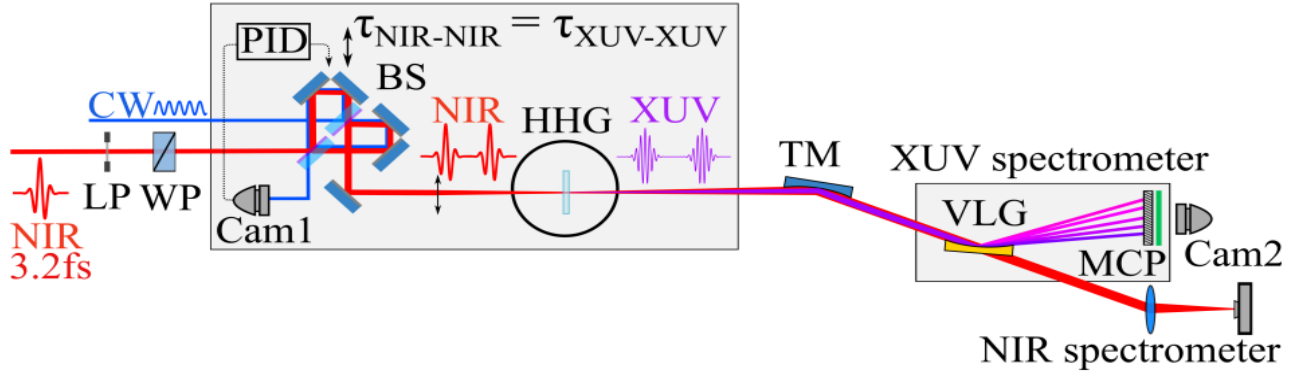
Fig. 1. Experimental Setup. *A near-infrared (NIR), few-cycle laser pulse was split into two identical copies and focused into a bulk solid sample. The resulting phase-locked extreme ultraviolet (XUV) pulse pair was analyzed with the help of an XUV spectrometer, while the fundamental near-infrared beam was analyzed with a near-infrared spectrometer. LP: Half-wave plate, WGP: Wire-grid polarizer, CW: Continuous wave stabilization laser, PID: Proportional–integral–differential controller, Cam 1: CMOS camera, BS: Beam splitters, TM: Toroidal mirror, VLG: Variable line-spacing grating, MCP: Micro-channel plate + phosphor screen, Cam2: CCD camera.*

Our experiments on amorphous SiO_2 and crystalline MgO, augmented by analytical modeling and semiconductor Bloch equation simulations, reveal a correlation between transient bandgap modifications and variations in the phase of harmonic emission. These findings suggest a potential pathway for sub-cycle, all-optical control of band structure, advancing prospects for petahertz-scale electronic applications and attosecond diagnostics of carrier dynamics.

In our experiments, we investigated the XUV spectral interferometry signal obtained from amorphous SiO_2 and crystalline MgO. For both materials, we observed odd harmonics of orders five to nine. A representative high-harmonic interferogram for fifth and seventh harmonic obtained with an NIR-NIR delay of 30 fs in MgO as a function of intensity is shown in Fig. 2 (a). A well-defined interference pattern, consisting of periodic minima and maxima, is visible for both detected harmonics (labelled H5 and H7) and for all intensities. By progressively increasing the intensity of both pulses, we aimed to assess how the interaction of the first NIR pulse with the sample influences the subsequent interaction between the second NIR pulse and the sample. This influence manifests as a shift in the minima and maxima observed in the interferometric spectra, reflecting a phase shift between the two generated phase-locked XUV fields. To quantify the phase shift for a given intensity distribution. The result of this

analysis are shown in Fig. 2(b), where the resulting phase shift is visualized as a function of the NIR peak intensity for the three observed harmonics. At high intensities above ~ 15 TWcm^{-2}, a substantial shift of the interference pattern towards higher energies (blueshift) was observed. Surprisingly, for the SiO$_2$ sample an inverse trend was observed: the interefometric fringes were shifting towards lower energies (redshift) with increasing intensity.
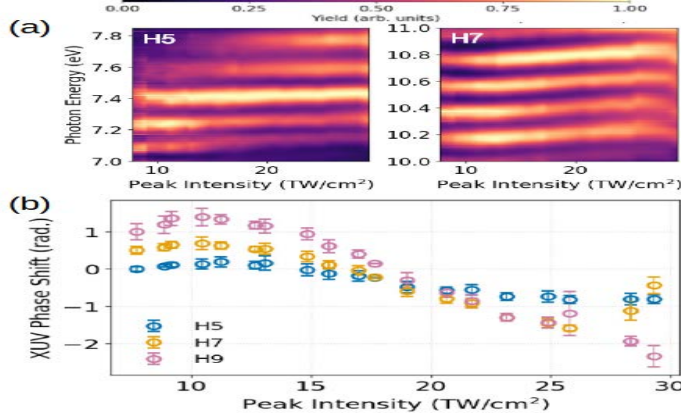
Fig. 2. Extraction of the phase shift in MgO. (*a*) 2D maps of the intensity dependence of the spectral interferometry signal of the observed high harmonics. (*b*) Extracted XUV phase shift as a function of the NIR peak intensity (Phases of H7 and H9 are offset vertically by 0.5 rad and 1 rad for visibility).

To explain the above findings, we have used two approaches: semiconductor Bloch equations (SBEs) and density function theory. We numerically solved the SBEs in a two-band tight binding approximation for cubic MgO along the Γ-X direction. In addition, we used density functional approach within the adiabatic local density approximation. The comparison of density function calculations in pristine and strongly-perturbed MgO reveals that due to state-blocking, the energy gap between the highest lying valence band state and the lowest-lying conduction band state increases steadily as a function of the carrier concentration [see Fig. 3(a) and (b)].
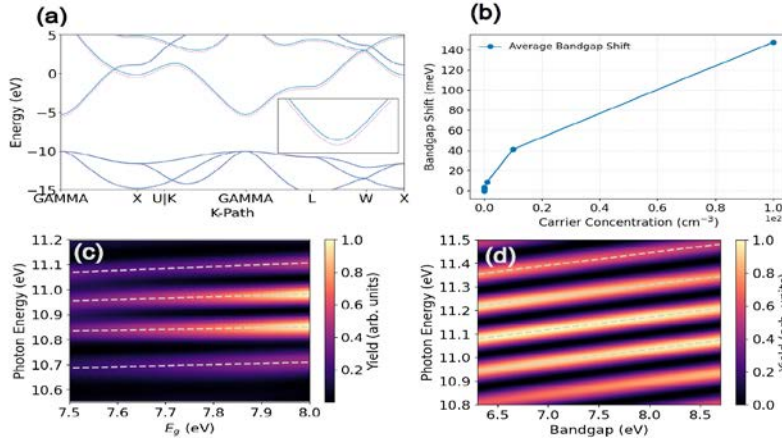
Fig. 3. (*a*) **DFT calculations of the band structure variations** due to an excited carrier population. (*b*) Averaged bandgap shift due to excitation of carriers. (*c*) Numerically simulated bandgap-dependent shift of the interference pattern of the seventh harmonic based on obtained by solving the SBEs. (*d*) Same as in (*c*) but obtained by the semi-classical analytical model.

Further, we have have employed an additional analytical, semi-classical model for the calculation of HHG in solids, calculating classical trajectories within a two-band system under the assumption of low carrier inversion. Results of this approach are presented in Fig. 3(d). A seemingly linear relationship between the shift of the interference pattern and the bandgap variation can be observed in a qualitative agreement to the experimental results shown in Fig. 2.

In conclusion, we have expanded high harmonic spectroscopy of solid-state systems to XUV spectral interferometry, a technique previously limited to gas phase and molecular systems. We analyzed the intensity-dependent variation of the high-harmonic phase using XUV spectral interferometry and correlated our experimental results with the transient alteration of the electronic structure. We observed bandgap shrinkage in the amorphous case and bandgap widening due to state blocking in the crystalline case. The experimentally observed differences were related to the distinct nature of the photoinduced bandgap dynamics and the consequent dipole phase dynamics.

References
[1] J. Lu, E. F. Cunningham, Y. S. You, D. A. Reis, S. Ghimire, *Nature Photonics* **13**, 96 (2019).
[2] K. Uchida, K. Tanaka, *Optica* **11**, 1130 (2024).

Quasiparticle generation in superconducting cuprate Captured by near infrared 6 fs pulse

Y. Taniguchi[1], R. Kato[1], T. Amano[1], H. Itoh[1], Y. Kawakami[1], Y. Nakamura[2], H. Kishida[2], T. Sasaki[1]
T. Nishizaki[3], K. Yonemitsu[4], S. Iwai[1]
[1]Tohoku University, Sendai, 980-8578, Japan
[2]Nagoya University, 464-8603, Japan
[3]Kyushu Sangyo University, Fukuoka, 813-8503. Japan
[4]Chuo University, Tokyo, 112-8551, Japan

Since the early 1990s, the relaxation dynamics of superconducting (SC) quasiparticles have been reported extensively [1]. In contrast, the generation processes have not been directly captured, despite its great importance as a driving mechanism of superconducting photo-sensors used in quantum optics. In fact, no measurements with a time window less than 100 fs have been made at $T < T_c$, although, many ultrafast (> 1 ps) measurements have been performed in the THz range near the SC gap. However, electronic phase transitions in strongly correlated systems are characterized by a broader spectral range covering several eV [2, 3]. In view of this situation, we have performed transient reflectivity ($\Delta R/R$) measurements in optimally-doped SC YBCO ($YBa_2Cu_3O_y$ ($T_C \sim 92$ K)) using a near-infrared 6 fs pulse (0.5 -1 eV) and a conventional 100 fs pulse (0.1-4 eV). Fig. 1 shows transient reflectivity spectra measured by 100 fs pulses at 11 K (Pump (0.89 eV) and probe pulses polarization parallel to the a axis ($E_{pu}\|a$, $E_{pr}\|a$), excitation intensity $I_{ex} = 0.05$ mJ/cm^2).
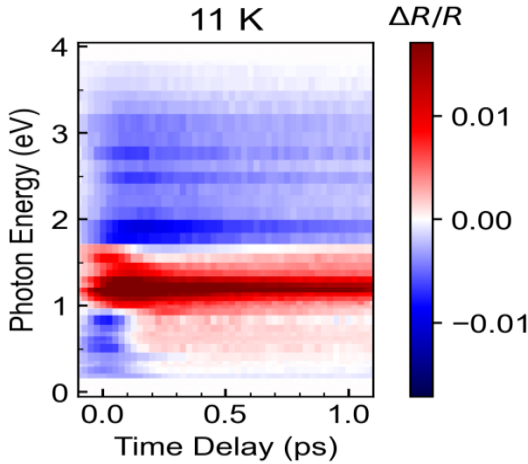
Fig. 1. Time dependent transient reflectivity ($\Delta R/R$) spectrum of YBCO measure by 100 fs pulse at 11 K. Excitation photon energy and intensity are 0.89 eV and $I_{ex}=0.05$ mJ/cm^2 ,respectively

$\Delta R/R$ spectrum is characterized by a positive (red) peak at 1.1 eV, a negative (blue) dip at 1.9 eV, and a broad negative tail toward 4 eV. These spectral features are observed only in the SC state and are different from those at 300 K. Steady state optical conductivity spectra have been analyzed by the Drude-Lorentz (DL) model [4, 5]. In the DL analysis, the Drude component, a mid-IR absorption (peaked at 0.1 eV with broad tail in the high energy side), an intraband transition (1.5 eV) and interband transitions (1.9, 2.9, 4.9, 6.07 eV) are considered to reproduce the steady state R. To reproduce the $\Delta R/R$ spectra, we have to consider the spectral weight transfer from the interband (1.9 eV and 2.9 eV) transitions mainly to the intraband (1.5 eV) and mid-IR absorption, in addition to the increase in scattering rate for all transitions. This is in contrasts to the main contribution of the increased scattering rates at room temperature. We also made $\Delta R/R$ measurements using 6 fs pulses. The spectral weight transfer and increased scattering rate were characterized on time scales of 90 fs and < 10 fs, respectively. Considering that the i) 1.9 eV band and ii) mid-IR abs. are respectively attributed to the i) Zhang-Rice singlet to nonbonding orbital and ii) spin-related bad metal [6], 90 fs is suggested to be the relaxation time of the charge-spin coherent state. On the othre hand, < 10 fs is understood as a purely electronic coherence time.

References
[1] C. Giannetti, M. Capone, D. Fausti, M. Fabrizio, F. Parmigiani, D. Mihailovic, *Advances in Physics* **65**, 58 (2016).
[2] H. J. A. Molegraaf, C. Presura, D. van der Marel, P. H. Kes, M. Li, *Science* **295**, 2239 (2002).
[3] A. V. Boris, N.N. Kovaleva, O.V. Dolgov, T. Holden, C.T. Lin, B. Keimer, C. Bernhard, *Science* **304**, 708(2004).
[4] E. Heyen, J. Kircher, M. Cardona, *Physical Review* B **45**, 3037 (1990).
[5] H. T. Romberg. N. Nucker, J. Fink, Th.Wolf, X.X. Xi, B. Koch, H. P. Geserich, M. Durrler, W. Assmus, B. Gegenheimer, *Zeitschrift für Physik* B- *Condensed Matter* **78**, 367 (1990).
[6] J. Wagner, W. Hanke, D. J. Scalapino, *Physical Review* B **43**, 10517 (1991).

Probing spin-injection in $Bi_{1-x}Sb_x$ based topological insulators in Time domain via THz-TDS spectroscopy: from Epitaxial growth to sputtered structures

H. Jaffrès[1], S. Massabeau[1], F. Miljevic[1], M. Jain[,2], M. Bibes[1], L. Moreno[1], R. Lebrun[1], J.-M. George[1]

Thales, 91767 Palaiseau France
[2]Université Paris-Saclay, 91120 Palaiseau, France

Spin-to-charge conversion (SCC) in femtosecond laser excited magnetic heterostructures may generate high efficiency and wide-bandwidth terahertz emission with a magnetically controllable polarization state [1]. The origin of this THz emission has been assigned to the generation of a spin-polarized current and subsequent conversion of the spin current to a transverse charge current [2]. Two main SCC mechanisms are generally involved: the Inverse Spin Hall Effect (ISHE) and the Inverse Rashba-Edelstein Effect (IREE). The discovery of metallic quantum states at the surface of 3D topological insulators (TIs) has opened exciting new functionalities owing to their time-reversal symmetry property and their spin-momentum locking (SML) properties. The resulting SCC combining strong spin-orbit coupling (SOC) and SML is expected to be enhanced compared to the spin Hall effect (SHE) of heavy metals. SCC has been demonstrated in a range of Bi-based TI compounds, including bismuth selenide Bi_2Se_3, bismuth telluride Bi_2Te_3, $Bi_2(Se,Te)_3$ or $Bi_{1-x}Sb_x$ (BiSb) [*Fig.1*]. To benefit fully from IREE, the charge currents should be confined in the surface states and any current flowing through the bulk states should be avoided.
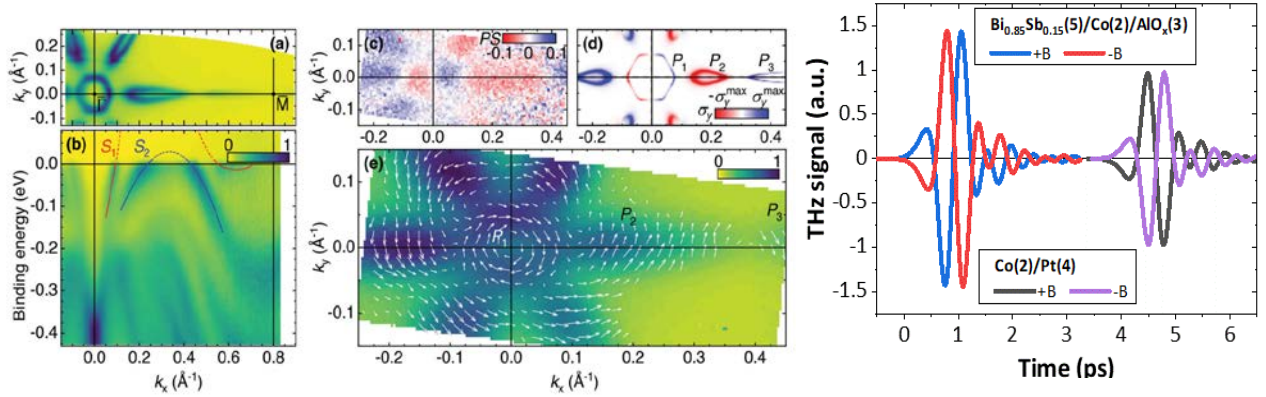
***Fig.1 (left). Electronic band structure** of $Bi_{0.85}Sb_{0.15}(5nm)$ epitaxial layer acquired by Angular Resolved Photo-Emission (ARPES) at room temperature (**a**) Fermi surface density of states (DOS) (**b**) Energy dispersion along the Γ- K line of the 2-dimensionnal Brillouin zone (**c**) spin-polarized DOS projected onto the Fermi surface showing the spin-chirality (**d**) and the two dimensional orbital projection onto the Fermi surface (**white arrow**).
(**Right**): THz-TDS emission time trace measured on $Co/Bi_{0.85}Sb_{0.15}(5nm)$ intersurface showcasing ultrafast spin-charge conversion (SCC) and compared to state of the art Co/Pt bilayers.*

In this talk, I will report particularly on our detailed investigation of the surface state SML properties of ultrathin (111)-oriented $Bi_{1-x}Sb_x$ epitaxial films. They exhibit a topological phase as recently confirmed by angular-resolved photo-emission spectroscopy (ARPES) [3] and mainly in-plane spin texture as shown by spin &angular resolved photo-emission SARPES. SCC mediated by the BiSb surface states is probed at the sub-picosecond timescale. Unprecedentedly large SCC is measured with efficiencies beyond the level of carefully optimized Co/Pt systems. I will present our more recent results dealing with the fabrication of sputtered BiSb materials giving rise to very efficient spin-charge conversion [4] in the time domain at the level of up-to-date best bilayers spintronics emitters.

The last part of my talk will be devoted to the discussion and comparison between fully epitaxial and sputtered $Bi_{1-x}Sb_x$ materials synthesized at laboratory.

References
[1]. T. Seifert, S. Jaiswal, U. Martens, J. Hannegan, L. Braun, P. Maldonado, F. Freimuth, A. Kronenberg , J. Henrizi, I. Radu, E. Beaurepaire Y. Mokrousov, P.M. Oppeneer, M. Jourdan, G. Jakob, D. Turchinovich, L.M. Hayden , M. Wolf, M. Münzenberg, M. Kläui, T. Kampfrath *Nature Photonics* **10**, 483 (2016).
[2]. T. H.Dang J. Hawecker, E. Rongione G. Baez Flores, D. Q. To, J. C. Rojas-Sanchez, H. Nong;J. Mangeney,J. Tignon,F. Godel ,S. Collin, P.Seneor M. Bibes,A. Fert, M.Anane, J.-M. George, L.Vila, M. Cosset-Cheneau, D. Dolfi, R. Lebrun, P. Bortolotti, K. Belashchenko, S. Dhillon, H. Jaffrès *Applied Physics Review* **7**, (2020).
[3]. L. Baringthon, T. H. Dang, H. Jaffrès, N. Reyren, J.-M. George, M. Morassi, G. Patriarche, A. Lemaitre, F. Bertran, P. Le Fèvre, *Physical Review Materials* **6**, 074204 (2022).
[4] E. Rongione, L. Baringthon, D. She, G. Patriarche, R Lebrun, A. Lemaître, M. Morassi, N. Reyren, M. Mi˘cica, J. Mangeney, J. Tignon, F. Bertran S. Dhillon, P. Le Févre, H. Jaffrès, J.-M. George, *Advanced Science* **10**, 2301124 (2023).

Ultrafast dynamics of strongly coupled lattice and Spin dynamics in CoF$_2$

M. Savoini[1], E. Manetti[1], A. Nag[2], R. Winkler[1], D. Soranzio[1], M. Shi[1], R. Acampora[1], E. Mashkovich[3]
T. Metzger[4], Y. Deng[2], B. Liu[2], S. Zerdane[2], H. Lemke[2], M. Sander[2], R. Mankowsky[2], D. Babich[2], E.Razzoli[2] U. Hiroki[2], P. Eugenio[2], E. Skoropata[2], E. Abreu[1], U. Staub[2], R. Pisarev[5], R. Bubrovin[5], A. Kimel[4]
S. L. Johnson[1]

[1] *ETH Zürich, 8093 Zürich, Switzerland*
[2] *Paul Scherrer Institut, 5232 Villigen PSI, Switzerland*
[3] *Universität zu Köln, 50937 Cologne, Germany*
[4] *Radboud Universitet, 6525 Nijmegen, Netherlands*
[5] *A.F. Ioffe Insittute, 194021 St. Petersburg, Russia*

Strong coupling between magnetism and structure is a feature of many important materials. In order to explore the possible opportunities this gives for new ways to manipulate material properties, we have performed experiments using ultrafast x-ray diffraction and spectroscopy to better understand how this coupling manifests in ultrafast dynamics in CoF$_2$, a model system for piezomagnetism. Cobalt difluoride (CoF$_2$) has a tetragonal rutile structure with paramagnetic properties at room temperature. On cooling below $T_N = 39$ K it becomes antiferromagnetic with strong piezomagnetism [1-4]. Recently ultrafast optical experiments have shown some unusual consequences in the response of this system to strong excitation. In one such work Disa [5] report that direct excitation of an infrared-active vibrational mode at 12 THz induces what appears to be a metastable ferroelectric phase that persists on a time scale of several hundred picoseconds. In another report Mashkovich et al. [6] drive using lower frequency THz light a magnetic-dipole-active resonance near 1 THz and observe nonlinear coupling to a B$_{1g}$ vibrational mode at 2 THz. Both of these observations indicate that the strong dynamical interaction of the magnetic order with the lattice mirrors the piezomagnetic phenomena observed in equilibrium, and are postulated to arise from dynamic modulations of the crystal field splitting of the Co 3d orbitals. By performing direct measurements of the lattice and spin dynamics of CoF$_2$ using x-ray diffraction and spectroscopy with femtosecond time resolution in response to strong THz driving, we show that the resonance near 1 THz, while driven by magnetic-dipole interaction, has in addition to a spin component a large vibrational component due to the large spin-orbit coupling in CoF$_2$.

E_g (v ≈ 1 THz)

B$_{1g}$ (v = 1.95 THz)
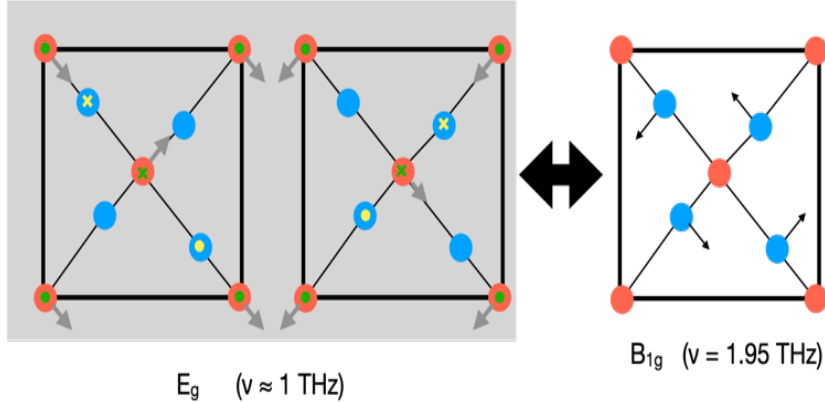
Fig. 1. Schematic description of the spin and atomic displacements of the involved modes. The unit cell of CoF$_2$ is shown in the ab plane, with red circles indicating Co and blue circles O. Green arrows indicate the direction of the Co ion spins that are in equilibrium along the c-axis. Our data indicate that the E$_g$ magnon at 1 THz (spin displacements shown by grey arrows) is hybridized with O atomic displacements atlong the c-axis with the same symmetry (yellow arrows).This hybrid mode couples to the B$_{1g}$ mode shown on the right, where displacements of the O atoms are shown by black arrows.

We also confirm using time-resolved XMCD the magnetic component of this resonance. This low-frequency excitation directly driven by the THz pulse is thus best considered as a hybrid excitation of vibrational and spin motion analogous to electromagnons, which are typically defined as electric-dipole active excitations with significant spin components. Our measurements also quantify the amplitude of the B$_{1g}$ mode that is driven indirectly, and suggest possible alternative mechanisms for the coupling to this mode.

References
[1] T. Moriha, *Journal of Physics and Chemistry of Solids* **11**, 73(1959).
[2] I. E. Dzialoshinskii, *Soviet Physics - Journal of Experimental and Theoreticsl Physics* **6**, 621(1957).
[3] A. S. Borovik-Romanov, *Soviet Physics - Journal of Experimental and Theoreticsl Physics* **11**, 786 (1960).
[4] A. S. Borovik-Romanov, *Ferroelectrics* **162**, 153(1994).
[5] A. S. Disa, M. Fechner, T. F. Nova, B. Liu, M. Först, D. Prabhakaran, P. G. Radaelli, A. Cavalleri, *Nature Physics* **16**, 937 (2020).
[6] E. Mashkovich, K. A. Grishunin, R. M. Dubrovin, A. K. Zvezdin, R.V. Pisarev, A. V. Kimel, *Science* **374**, 1608 (2021).

Dressing electronic states with photons in tunnel nanocavities

M. Varea[1], D. Mateos[2], K. Lauwaet[1], R. Miranda[2], R. Otero[2], A. Martin-Jimenez[1]

[1] IMDEA Nanociencia, 28049 Madrid, Spain
[2] Universidad Autónoma de Madrid, 28049 Madrid, Spain

In the presence of strong electromagnetic fields (in the order of TW/m^2), electronic states of matter become non-stationary, leading to energy values that vary over time, known as Floquet states. While quasi-energy levels can still be defined as the cycle-averaged energy, they often exhibit slight deviations from the original electronic levels in the absence of light, a phenomenon described by the AC Stark shift. Additionally, sidebands emerge at energy intervals corresponding to integer multiples of the photon energy, commonly referred to as Floquet bands. Floquet engineering has attracted much attention lately as reports show that new states of matter, such as Quantum Hall states in graphene can be achieved, and the topology of the band structure modified in emerging Quantum Materials. In our work (*to be submitted, 2025*) we explore how light-matter interaction influences the energy and spatial distribution of electronic states. We employ Scanning Tunnelling Microscopy (STM) and Spectroscopy (STS) under laser radiation focused within a plasmonic nanocavity formed between the STM tip and the sample surface. This approach leverages the extreme electromagnetic field enhancement occurring in plasmonic picocavities [1,2,3], particularly in the gap between an atomically sharp tip and a metallic surface [4,5], achieving field dressing effects with moderately intense (about MW/m^2) continuous-wave lasers. Combining STM with laser excitation offers the unique possibility to investigate and control light-matter interaction at the atomic scale, which is critical for the development of novel technologies from diverse branches including quantum computing, optoelectronics, sensing, or catalysis. Recent studies have invoked photon-assisted tunnelling to explain the emergence of new conductance peaks in the Field-Emission Resonance (FER) region under laser illumination in STM junctions [6]. Specifically, the first FER in Ag(111) was observed at a lower bias voltage than required in the absence of laser illumination, shifted precisely by the photon energy of the laser. In our experiments with a Ag(100) surface, we replicate these findings for the first FER but also show a crucial distinction: under laser illumination, the FER peaks corresponding to the dark condition ("dark FERs") remain visible (Fig. 1).
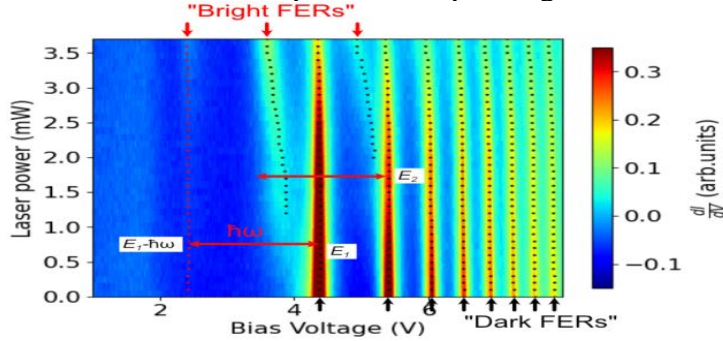
Fig. 1. Light-induced changes in the Field Emission Resonances (FERs) of an STM nanocavity comprised of a Ag tip and an Ag(100) sample. By illuminating the STM nanocavity with a continuous-wave HeNe laser a series of new peaks appear in the differential conductance, the bright-FERs. While the first light-induced FER peak appears at the photon energy below the first dark-FER, the other peaks are separated from their corresponding dark-FERs by energies that do not match the photon energy and depend on the laser power. The existence of sidebands and AC Stark shifts are characteristic of Floquet physics.

This persistence allows us to detect photocurrent-induced tip-sample modifications via the energy shifts of the dark FERs, thus providing a means to quantify DC Stark shifts arising from tip-sample distance variations during irradiation. In this respect, Figure 1 reveals that while dark FER positions exhibit minimal shifts with increasing laser intensity (indicating that the tip-sample distance changes are small), the FER peaks induced by illumination shift substantially, demonstrating a nontrivial dependence that is not strictly set by the photon energy. This behavior suggests that simple plasmon-assisted resonant tunneling cannot fully explain our observations. Instead, the intense field confinement within the STM nanocavity appears to induce strong light-matter coupling, dressing the dark FER states with the electromagnetic (plasmonic) field inside the nanocavity. Moreover, we have thoroughly investigated the evolution of the FERs under laser illumination with tunneling current, laser polarization, and photon energy. Our results show that the laser-induced FER peaks can be tuned by altering either the driving laser parameters or the nanocavity configuration. This controllability points toward the manifestation of hybrid light-matter (Floquet) states within the STM junction. We thus provide a new platform to study Floquet physics at the nanoscale, opening avenues for precise manipulation of electronic states in quantum materials.

References
[1] F. Benz, M. K. Schmidt, A. Dreismann, R. Chikkaraddy, Y. Zhang, A. Demetriadou, C. Carnegie, H. Ohadi, B. de Nijs, R. Esteban J. Aizpurua, J. J. Baumberg, *Science* **354**, 726 (2016).

[2] J. J. Baumberg, *Nano Letters* **22**, 5859 (2022).
[3] J. J. Baumberg, J. Aizpurua, M.H. Mikkelsen, D.R. Smith, *Nature Materials* **18**, 668 (2019).
[4] D. Mateos, O. Jover, M. Varea, K. Lauwaet, D. Granados, R. Miranda, A. I. Fernandez-Dominguez, A. Martin-Jimenez, R. Otero, *Science Advances* **10**, (2024).
[5] A. Martín-Jiménez, A. I. Fernández - Domínguez, K. Lauwaet, D. Granados, R. Miranda, F.J. García-Vidal, R. Otero, *Nature Communications* **11**, 1021(2020)
[6] S. Liu, M. Wolf, T. Kumagai, *Physical Review Letters* **121**, 226802 (2018).

Ultrafast coherent imaging for quantum materials

A. S. Johnson

Instituto Madrileño de Estudios Avanzados en Nanoci -IMDEA Nanoscience, 28049 Madrid, Spain

Quantum materials can exhibit a wide range of nanoscale textures, fluctuations and dynamics all of which are key to understand the emergent behavior and properties of these systems. Measuring such effects has proven to be challenging for a host of reasons, including the short-length scales involved, rapid timescales for dynamics, and non-stationary nature of the ground state dynamics. Recently ultrafast X-ray coherent diffractive imaging has emerged as a new method for resolving these dynamics, combining the high spatial resolution of X-ray imaging with the ultrafast time-resolution of femto to attosecond pulses from X-ray free electron lasers, with the first measurements of nanoscale domain dynamics during photoinduced phase transitions reported [1,2]. I will present recent progress on ultrafast imaging of nucleation and growth dynamics in vanadium dioxide on the nanosecond timescale following ultrafast photoexcitation from the monoclinic to the rutile phase (Fig. 1).
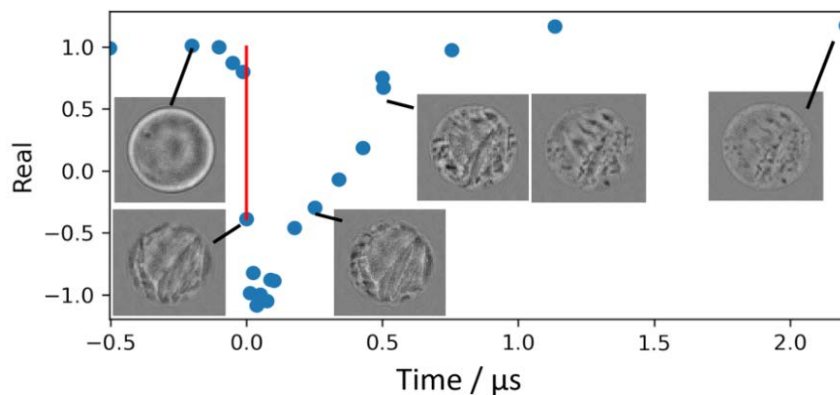
Fig. 1. Long time dynamics in vanadium dioxide measured using resonant X-ray coherent diffractive imaging at the Oxygen K-edge following ultrafast photoexcitation at the PAL XFEL, Korea. The overall change in transmission is shown in blue, with the photoexcitation moment indicated in red, while the inset images show the measured structure at indicated times. After initial excitation to a homogeneous metallic R-phase state we observe subsequent nucleation and growth of monoclinic insulating domains over the nanosecond to few microsecond timescale.

Furthermore, as coherent imaging return full-field-of-view images it is significantly more robust to both shot-to-shot and medium-time scale fluctuations than alternative scanning methods [3], but this is conventionally considered to be contingent on single-shot or near single-shot acquisition. Recently we have shown that the interferometric nature of coherent diffractive imaging can actually be leveraged to disentangle repeatable and stochastic contributions to an X-ray diffraction pattern, allowing tracking of fluctuations in quantum materials even far from the single-shot limit [4]. It can also be used to track measure nanoscale X-ray birefringence and isolate non-linear X-ray wavemixing signals enabling non-linear coherent X-ray imaging [5]. I will present these numerical results and speculate on the future of ultrafast coherent X-ray imaging for quantum materials.

References
[1] A. S Johnson,, D. Perez-Salinas, K. M. Siddiqui , S. Kim , S. Choi , K. Volckaert , P. E. Majchrzak , S.. Ulstrup , N. Agarwal , K. Hallman R. F. Haglund, Jr, C. M. Günther , B. Pfau , S. Eisebitt, D. Backes , F. Maccherozzi , A. Fitzpatrick, S. S. Dhesi, P. Gargiani , M. Valvidares N. Artrith. F. de Groot. H. Choi. D. Jang. A. Katoch. S. Kwon. S.H. Park. H. Kim, S. E. Wall,, *Nature Physics* **19**, 215 (2023).
[2] S Zayko, O. Kfir, M. Heigl, M. Lohmann, M. Sivis, M. Albrecht, C. Ropers., *Nature Communications* **12**, 6337 (2021).
[3] C. Klose, F. Büttner, W. Hu, C. Mazzoli, K. Litzius, R. Battistelli, S. Zayko, I. Lemesh, J. M. Bartell, M.Huang, C. M. Günther, M. Schneider A. Barbour, S. B. Wilkins, G. S. D. Beach, S. Eisebitt, B. Pfau, *Nature* **614**,256 (2023).
[4] A. Sarkar, A.S. Johnson, *Materials Advances* **5**, 6378 (2024).
[5] A. Sarkar A.S. Johnson, *in preparation* (2025)..

Engineering electronic states with polaritonic effects and robust Floquet drives

F. H. da Jornada

Stanford University, Stanford, CA94305, USA

First-principles formalisms based on many-body perturbation theory and interacting Green's function (*e.g.*, the Bethe-Salpeter equation) have been critical in accurately predicting the optical properties of materials. Part of this success is in their ability to accurately capture both the spectroscopic responses of various systems and their underlying excitonic wavefunctions – the latter often allowing for an intuitive rationalization of the excited-state physics in materials. However, these approaches have been largely restricted to the linear response regime and consider light-matter coupling perturbatively. Here, we present new first principles, many-body perturbation theory formalisms, and calculations that capture light-matter effects beyond these regimes. We first introduce a new formalism that captures light-matter interactions non-perturbatively and captures exciton-polaritons – hybrid states of light and matter [1]. In particular, we show how polaritonic effects qualitatively change exciton wavefunctions in materials, an effect we attribute to a change in the electron-hole exchange interactions away from its usual *repulsive* nature to an effective *attractive* interaction when retardation effects are considered. We also discuss nonlinearities we predict in the optical properties materials, and show that the presence of a large number of excitons in monolayer MoS_2, each with excitation energy E_X, leads to a time dependence of the electronic self-energy, $\delta\Sigma \sim e^{iE_x t}$. This, in turn, causes a *time-dependent coupling* between valence and conduction quasiparticle states, an effect which can be rationalized within the language of a Bloch-Floquet effect. Critically, however, this effect occurs even when the external optical pump is no longer present, and so we denote it as an exciton-driven Floquet effect [2,3]. We also present recent results from our group concerning the robustness of such Floquet effects when the driving bosic mode is not coherent [4]. The results suggest the possibility of driving out-of-equilibrium quantum states in materials using *thermalized* internal bosonic modes that may support longer-lived emergent states.
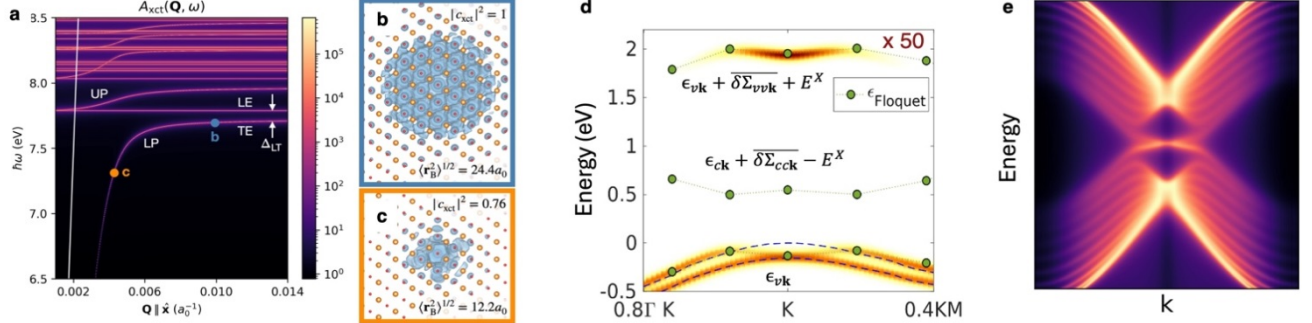
Fig. 1. *(a) Spin-singlet polariton spectral function of MgO. The lower polariton (LP) and upper polariton (UP) branches and transverse excitons (TEs) are highlighted. (b) Modulus squared of the exciton component associated with the highlighted polariton, with the hole fixed near an O atom. This state is primarily exciton-like ($|c_{xct}|^2 = 1$). (c) Same as (b) but for a photon-like LP, showing the reduction of the exciton Bohr radius and excitonic character. (d) Simulated single-particle spectral function for monolayer MoS_2 under the presence a finite number of coherent excitons. The replica of the valence band and the camel-backed dispersion of the valence band can be interpreted as an exciton-driven Floquet effect [7]. (e) Computed single-particle spectral function of a graphene nanoribbon under the presence of a partially coherent external field. Spectral features associated with the topologically protected edge state, driven by the external field, are still present even with the presence of disorder.*

We conclude by mentioning future ways to understand the coupled flow of electrons and ions and, in particular, how some of our preliminary calculations allow us to capture photoexcited nuclear dynamics and their associated optical and vibrational fingerprints [5,6].

References
[1] Z. Mauri, C. Ciccarino, J. B. Haber, D. Y. Qiu, F. H. da Jornada, *arXiv:2503.13613* (2025).
[2] Y.- H. Chan, D. Y. Qiu, F. H. da Jornada, S. G. Louie, *Proceedings of National Academy of Sciences* **118**, e1906938118 (2021).
[3] Y.- H. Chan, D. Y. Qiu, F. H. da Jornada, S. G. Louie, *Proceedings of National Academy of Sciences* **120**, e2301957120 (2023).
[4] J. Haber, C. Ciccarino, F. H. da Jornada, *to be submitted* (2025).
[5] A. R. Altman, F. H. da Jornada, *arXiv:2503.03136* (2025).
[6] A. R. Altman, A. Ramdas, J. B. Haber, F. H. da Jornada, *to be submitted* (2025).

s-d exchange: Key to ultrafast all-optical magnetization control

J. Hohlfeld

Universite de Lorraine, 54506 Vandoeuvre-les-Nancy, France

Optical excitation of thin magnetic films, multilayers and spin valve structures by ultrashort laser pulses leads to a large variety of different magnetization dynamics ranging from ultrafast demagnetization on the sub-picosecond time scale to similarly fast helicity-independent all-optical switching of magnetization (AO-HIS). For thin films, AO-HIS appears to be restricted to Gd-based ferrimagnetic materials [1,2] and MnRuGa [3]. The complexity of laser pulse-induced magnetization dynamics has hindered the development of a unified theory capable to describe these dynamics at all relevant length and time scales. Nevertheless, most of the observed dynamics can qualitatively be explained in terms of a simple model that describes a ferromagnetic metal in terms of aligned localized moments (aligned by their mutual exchange) that are exchange coupled to a bath of free electrons [4,5]. Most strikingly, this so-called *s-d-* or *s-f*-model explains the seemingly distinct processes of ultrafast demagnetization and AO-HIS to be predominated by one single microscopic mechanism - total angular momentum conserving exchange scattering between localized magnetic moments and conduction electrons. The model predicts that any non-equilibrium between (the temperatures of) the magnetic moments and of the conduction electrons leads to angular momentum transfer between both systems which creates a non-equilibrium spin-accumulation $\Delta\mu$ within the electron gas at a rate that is proportional to -dM/dt. Since the total angular momentum is conserved during this transfer, the observed magnetization dynamics is governed by the relaxation dynamics of $\Delta\mu$. Within the framework of the *s-d*-model, ultrafast demagnetization of uniformly heated ferromagnetic films is explained by the fast decay of $\Delta\mu$ due to spin-flipping electron-phonon collisions, while AO-HIS in ferrimagnetic Gd-transition metal alloys is understood in terms of exchange coupling mediated angular momentum transfer between the two antiferromagnetically coupled magnetizations that results from their distinct individual demagnetization rates. The *s-d*-model description of ultrafast magnetization dynamics is most useful to describe optically induced magnetization reversal in spin valve structures. It seamlessly explains the mutual interaction between the magnetizations of both layers as the result of angular momentum transfer via the spin currents that are emitted from both layers during their de- and remagnetization [5,6]. Moreover, since the de- and remagnetization dynamics that follow ultrashort laser pulse excitation of individual metallic magnetic layers are understood to result from transient variations of the electron temperature one expects that they can be controlled by adjacent heat sink layers [7]. In the first part of my talk, I will first demonstrate the large impact of heat sink layers for all-optical magnetization control by example of the upper limits for the duration and fluence of laser pulses that lead to AO-HIS in perpendicular GdFeCo alloys [7]. I will also show that the elimination of the need to maintain perpendicular anisotropy in the presence of strong demagnetizing fields within in-plane magnetized films significantly enhances the range of Gd-concentrations suitable for AO-HIS [8,9]. In the second part, I will focus on laser pulse induced magnetization control in various spin-valve structures. Starting from our initial time-resolved investigations of a perpendicular spin valve containing a Gd-based ferrimagnetic fixed layer [10], I will show that spin valves comprising two ferromagnetic layers allow for deterministic magnetization control via variations of the applied laser fluence [11]. While the switching from the anti-parallel (AP) to the parallel (P) configuration, observed at high laser fluences, can clearly be assigned to spin current emitted by the reference layer during its fast demagnetization, the detailed mechanism for P-to-AP switching at lower fluences remains a matter of debate [5,6,11]. Initial results indicated ultrafast magnetization reversal within a few hundreds of femtoseconds, thereby favoring a picture where the spin current emitted by the free layer reverses its polarization upon reflection at the reference layer and, by reentering the free layer, causes the switch to the AP configuration [6,11]. However, more recent data indicate a much slower switching speed with a zero crossing on the picosecond time scale. These findings indicate that the reversal of the free layer is driven by the spin current emitted by the reference layer during its remagnetization. As for the investigations on AO-HIS, the incorporation of thick heat sink layers enables to control the magnetization in ferromagnetic spin valves with much longer pulses [11] and a much wider range of materials can be used as magnetic layers within in-plane magnetized spin valves.

References
[1] T. A. Ostler, J. Barker, R. F. L. Evans, R. W. Chanterll, U. Atxitia, Q. Chubykalo-Fesenko, S. El Miussaoui, I. Le Guyander, E. Mengotti L J.Heyderman, F.Nolting, A. Tsukamoto, A. Itho, D. Afanasiev, B. A. Ivanov, A. M. Kalashnikova, K. Vahaplar, J. Mentink, A. Kirilyuk T. Rasing, A. V. Kimel, *Nature Communication*. **3**, 666 (2012).

[2] M. Beens, M. L. Lalieu, A. J. M. Deenen, R. A. Duine, B. Koopmans, *Physical Review* B **100**, 220409(R) (2019).
[3] C. Banerjee, N.Teichert, K. E. Siewierska, Z. Gercsi, G. Y. P. Atcheson, P. Stamenov, K. Rode, J. M. D. Coey, J. Besbas, *Nature Communications* **11**, 4444 (2020).
[4] V. N. Gridnev, *Physical Review* B **98**, 014427 (2018).
[5] M. Beens, R. A. Duine, B. Koopmans, *Physical Review* B **102**, 054442 (2020).
[6] Q. Remy, *Physical Review* B **107**, 174431 (2023).
[7] M. Verges, W.Zhang, Q. Remy,Y.LeGuen, J.Gorchon, G.Malinowski, S. Mangin, M. Hehn, J. Hohlfeld, *Physical Review Applied* **21**, 044003 (2024)
[8] J. Wei, B. Zhang, M. Hehn, W. Zhang, G. Malinowski, Y. Xu, W. Zhao, S. Mangin, *Physical Review Applied* **15,** 054065 (2021)
[9] J.- X. Lin, M. Hehn, T. Hauet, Y. Peng, J. Igarashi, Y. Le Guen, Q. Remy, J. Gorchon, G. Malinowski, S. Mangin, J. Hohlfeld, *Physical Review* B **108**, 220403 (2023).
[10] Q. Remy, J. Hohlfeld, M. Verges, Y. Le Guen, J. Gorchon, G. Malinowski, S. Mangin, M. Hehn, *Nature Commutations* **14**, 445 (2023)
[11] J. Igarashi, W.Zhang, Q. Remy, E. Diaz, J.-X. Lin, J. Hohlfeld, M. Hehn, S. Manging, J. Gorchon, G. Malinowski, *Nature Materials* **22**, 725 (2023)

Probing driven materials with ultrafast proximate Magnetometry at the picosecond and nanometer frontiers

G. Jotzu

École Polytechnique Fédérale de Lausanne, 1015 Lausanne, Switzerland.

Periodic driving has emerged as a new avenue to control material properties on demand and on ultrafast time scales, even allowing for the creation of quantum states with no static counterpart. A particular experimental challenge for this direction of research arises because of the fact that many of the standard observable used in materials science do not feature the (sub)picosecond time resolution which is required - for reasons both technical and fundamental - for the study of such strongly driven materials. I will introduce a method to perform ultrafast proximate magnetometry. This approach is based on using magneto-optic sensing [1] in a weakly diamagnetic material with a large Faraday effect and a fast magnetic response time in the vicinity of the sample of interest (see Fig.1a). The polarization rotation of an ultrashort laser pulse hence gives access to the time- and spatially resolved stray magnetic field.A first achievement of ultrafast proximate magnetometry was to show the ultrafast expulsion of *static* magnetic flux from $YBa_2Cu_3O_{6.48}$ [2] when the cuprate was driven (see Fig.1b) with a phonon-resonant light pulse – a condition in which the material had previously shown a superconducting-like THz conductivity [3,4] – and giving an upper limit for this effect in the organic superconductor K_3C_{60} [5] (see Fig.1c). This extension of an unbiased magnetic susceptibility probe to the sub-picosecond regime can be taken even further: One the one hand, it is not limited to static applied fields. Indeed, it can be used to study the response of a material (driven or not) to a magnetic field that varies rapidly in time. I will present a scheme that allows for the creation of magnetic field steps with a time constant of ~1ps (see Fig.1d/e), which can be kept at a high (or low) level for an arbitrarily long time. [6] This enables all-optical AC magnetometry that extends from the low-frequency limit up to almost 1THz, giving access to a broad range of magnonic modes, as demonstrated by probing the ferrimagnet $Lu_{3-x}Bi_xFe_{5-y}Ga_yO_{12}$ (see Fig.1f/g). Through the creation of eddy currents, it also allows for contactless phase-sensitive conductivity measurements in the same frequency range, giving direct access to the carrier scattering time in some regimes. On the other hand, beyond probing the bulk properties of a driven sample, spatially resolved measurements also become possible. Here I will present the implementation of a wide-field imaging scheme with a low micrometer-scale spatial resolution. Going even further, achieving simultaneous picosecond time-resolution and nanometer spatial resolution could be enabled by using nitrogen-vacancy centers in diamond. These systems, which provide excellent field resolution despite their nanometric size, are normally limited in speed by the ~3GHz resonance employed for performing qubit gates. We show that modern THz technology could enable a 1000x speedup for this process, hence bringing the time-resolution into the picosecond regime. Performing spatially-resolved ultrafast magnetometry is of particular interest in the context of superconductivity: here, creating simply connected topologies leads to the quantization of the magnetic fluxoid.
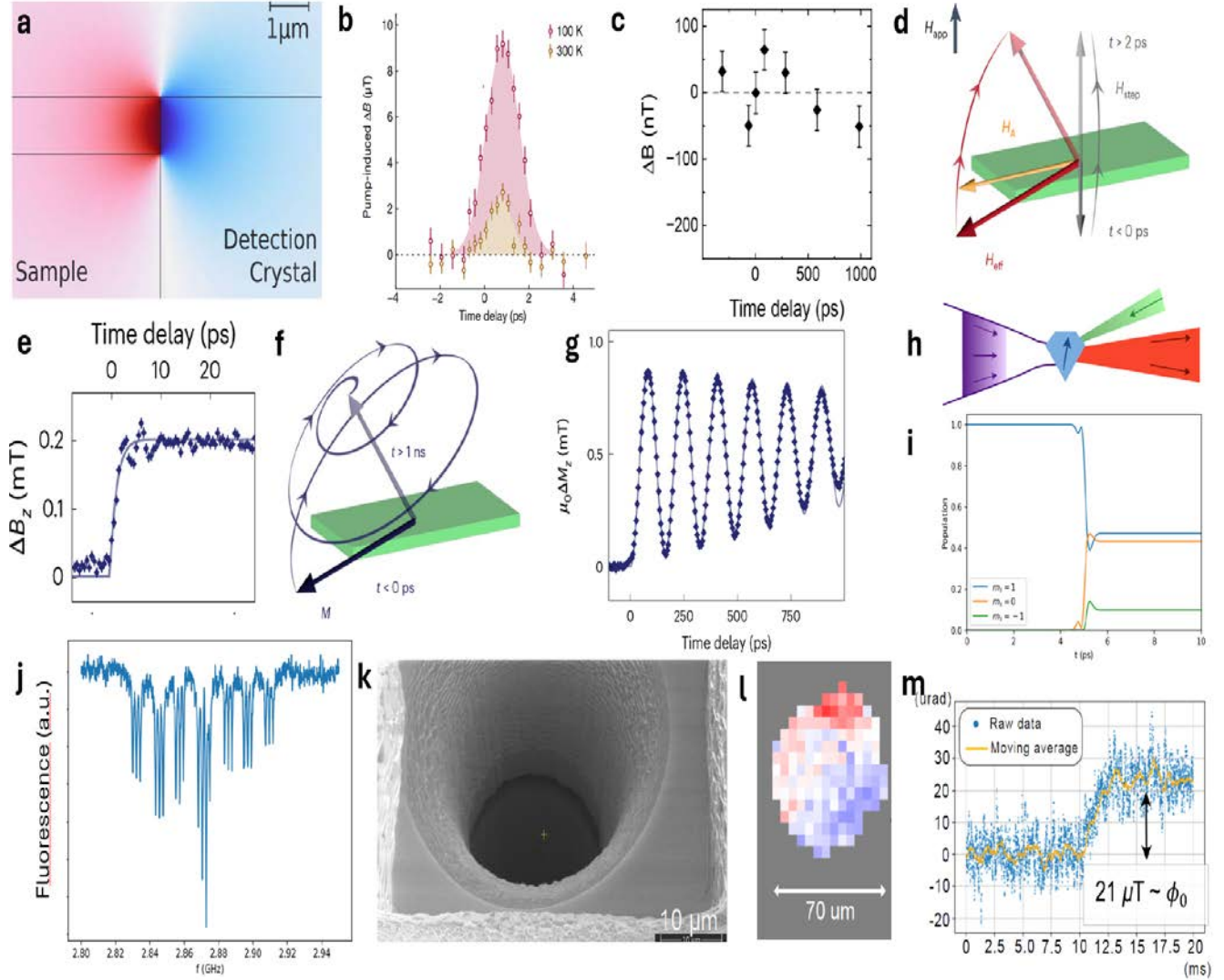
Fig. 1. Ultrafast proximate magnetometry for driven quantum materials. a) Magnetic field surrounding a magnetized sample / proximate magnetometry geometry. b) Magnetic field expulsion from phonon-driven YBCO c) Upper bound for mangetic field expulsion from driven K_3C_{60} d) Schematic of a magnetic field step e) Magnetic field step produced by a sudden destruction of superconductivity in a YBCO thin film f) Schematic of the resulting spin dynamics in a ferro/ferrimagnet g) Measured spin dynamics in $Lu_{3-x}Bi_xFe_{5-y}Ga_yO_{12}$ h) Schematic of THz-controlled diamond NV center i)Calculated population dynamics after a circularly polarized THz pulse j)Measured fluorescence (hyperfine-resolved) of an NV center ensemble k) Electron-microscopy image of a microscopic hole in a YBCO superconducting thin film and its substrate l) Detail from a wide-field magneto-optic image, showing the field distribution inside a hole in a YBCO thin film below the critical t emperature m) Magneto-optic measurement (using a CW laser) showing sensitivity to single mangetic flux quanta.

However, little is know about the time-dynamics of the process of quantization, which is linked to the establishment of a well-defined superfluid phase across a defect, and may hence be drastically different from the time-scale for pair creation. Using time-resolved optical magnetometry on microstructured superconducting thin-films now allows for studying this process directly.

References
[1] J. A. Riordan, F. G. Sun, Z. G. Lu, X.-C. Zhang, *Applied Physics Letters* **71**, 1452 (1997)
[2] S. Fava, G. de Vecchi, G. Jotzu, M. Buzzi, T. Gebert, Y. Liu, B. Keimer, A. Cavalleri, *Nature* **632**, 75 (2024).
[3] S. Kaiser, D. Nicoletti, C.R. Hunt, W. Hu, I. Gierz, H.Y. Liu, M. Le Tacon, T. Loew, D. Haug, B. Keimer, A. Cavalleri. *Physical Review* B **89**, 184516 (2014)
[4] W. Hu, S. Kaiser, D. Nicoletti, C.R. Hunt, I. Gierz, M. C. Hoffmann, M. Le Tacon, T. Loew, B.Keimer, A. Cavalleri. *Nature Materials* **13**, 705 (2014)
[5] G. de Vecchi, M. Buzzi, G. Jotzu, S. Fava, T. Gebert, G. Magnani, D. Pontiroli, M. Riccò, A. Cavalleri, *arXiv.2502.20276* (2025)
[6] G. de Vecchi, G Jotzu, M. Buzzi, S. Fava, T. Gebert, M. Fechner, A.V. Kimel, A. Cavalleri, *Nature Photonics* **1** doi:10.1038/s415661 (2025).

Multicolor-pumped ZGP NOPCPA for nonlinear optical studies in LWIR

R. Jutas[1], T. Zhou[1], J. Roman[1], I. Astrauskas[1], A. Imani[1], P. Carpeggiani[1], P. Polynkin[2], E. Kaksis[1], T. Floery[1], J. Kolenda[3], T. Bartulevičius[3], K. Michailovas[3], A. Michailovas[4], A. Baltuška[1], A. Pugžlys[1]

[1] *Technische Universität Wien, 1040 Vienna, Austria*
[2] *The University of Arizona, Tucson, AZ 85721, USA*
[3] *EKSPLA, 02300 Vilnius, Lithuania*
[4] *Center for Physical Sciences & Technology, 02300 Vilnius, Lithuania*

We report on the experimental realization of a multicolor, non-collinearly-pumped long-wave infrared (LWIR) OPCPA, based on zinc germanium phosphide (ZGP) crystals. The multicolor pump pulses above 2 µm wavelength are generated in a non-collinearly-seeded KTA-based near-infrared (NIR) OPCPA pumped by a Nd:YAG amplifier (AMP, Fig.1) operating in burst mode [1].
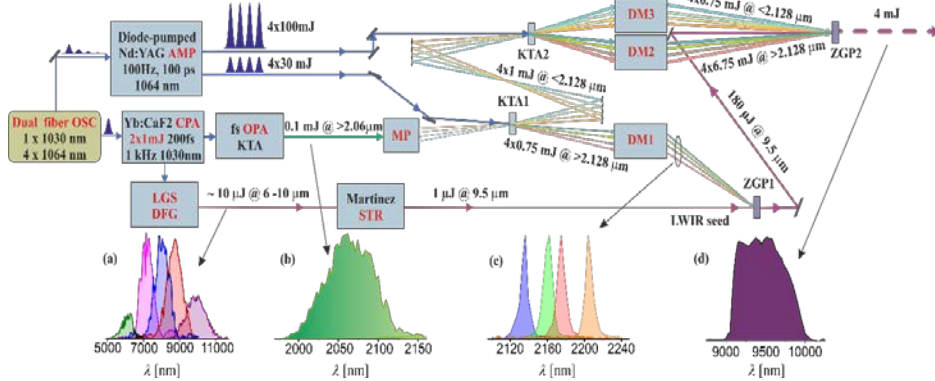
Fig. 1. *Schematics of the pulse burst pumped OPCPA; **OSC** – oscillator, **CPA** – chirped pulse amplifier, **OPA** – optical parametric amplifier, **AMP** – power amplifier; **LGS**, **KTA**, and **ZGP**, respectively, Lithium Gallium Sulfide, Potassium Titanyl Arsenate and Zinc Germanium Phosphide crystals; **DFG** – difference frequency generation; **STR** – stretcher; **MP** – multiplexer; **DM1-3** – demultiplexers. (**a**) – Measured spectra after DFG process; (**b**) – fs OPA output spectrum; (**c**) – idler spectra after KTA1 NOPCPA stage; (**d**) – spectrum of the amplified LWIR pulses.*

The frontend of the system is a femtosecond white-light-seeded KTA OPA pumped by 200-fs Yb:CaF2 laser system. The output of the OPA (Fig.1 (b)) is sent to a multiplexer (MP). The MP, which is based on a grating pair, splits the broadband pulses into four replicas with different central wavelengths, delays each replica to match the timings with the individual pulses in the 1 µm pump burst, and stretches the replicas for efficient amplification in the KTA OPCPA. After the multiplexer, the obtained spatially separated and temporally stretched replicas of different colors are individually directed at different incidence angles to seed the KTA OPCPA. The µJ-level LWIR seed pulses for the multicolor-pumped ZGP NOPCPA are generated via inter-pulse difference frequency generation (DFG) [2] in a lithium gallium sulfide (LGS) crystal between 200 fs, 1030 nm laser pulses from Yb:CaF2 CPA and their red-shifted replicas, produced via stimulated Raman scattering [3] in N_2O gas-filled capillary. This DFG approach also allows to have tunability over the LWIR output. Changing the gas pressure or input energy in the capillary, the obtained Raman shift can be tuned, thus changing the wavelengths involved in the DFG process. Some of the LWIR spectra obtained via DFG process are shown in Fig.1 (a). Before sending the LWIR seed to the ZGP1 NOPCPA stage, it is stretched in a Martinez-type stretcher. The ZGP1 NOPCPA stage is pumped by four idler pulses coming from the non-collinearly-seeded KTA1 OPCPA stage (spectra in Fig.1 (c)), while the ZGP2 NOPCPA stage is pumped by eight multicolor beams (four signal and four idler), which are generated in the KTA2 crystal. ZGP1 NOPCPA stage generates 180 µJ pulses centered at 9.5 µm. So far, 4 mJ at 9.5 µm were obtained after the ZGP2 NOPCPA stage, when it was pumped by eight pulses having combined pump energy of 54 mJ (amplified spectrum in graph (d), Fig.1). This corresponds to an energy conversion efficiency of over 7 %. The 4 mJ LWIR pulses were generated with a limited high-energy Nd:YAG output. The Nd:YAG amplifier is specified to generate two pulse bursts with energies up to 4x40 mJ and 4x300 mJ. When pumped by 4x300 mJ, eight multicolor 2 µm pulses with combined energy well exceeding 100 mJ can be generated in the KTA2 OPCPA stage. This gives potential for the amplification of broadband LWIR pulses to energies above 10 mJ. After compression, the intense LWIR pulses could serve as a unique tool for nonlinear optical studies in the LWIR, as well as intense terahertz generation due to potentially better phase matching with longer wavelength pump.

References
[1] R. Jutas, J. Roman, I. Astrauskas, P. Polynkin, E. Kaksis, T. Floery, J. Kolenda, T.Bartulevičius, K. Michailovas, A. Michailovas, A. Baltuška, A. Pugžlys *Conference on Lasers and Electro-Optics/Europe (CLEO/Europe 2023, Technical Digest Series (Munich, 2023)*, .
[2] V. Petrov, F. Rotermund, F. Noack, *J. Opt. A Pure Appl. Opt.* **3**(3), R1–R19 (2001).
[3] P. A. Carpeggiani, G. Coccia, G. Fan, E. Kaksis, A. Pugžlys, A. Baltuška, R. Piccoli, Y.-G. Jeong, A. Rovere, R. Morandotti, L. Razzari, B. E. Schmidt A. A. Voronin, A. M. Zheltikov, *Optica* **7**, 1349 (2020).

Light-induced nonlinear phonon dynamics in Bilayer nickelate superconductors

T. Kaneko, S. Kamiyama, K. Kuroki, M. Ochi

Osaka University, Toyonaka, Osaka 560-0043, Japan

Recently discovered high-temperature superconductivity in the bilayer Ruddlesden-Popper nickelate $La_3Ni_2O_7$ has attracted significant interest in the field of condensed matter physics [1]. Signatures of superconductivity have also been reported in the trilayer $La_4Ni_3O_{10}$ [2] and $La_3Ni_2O_7$ thin films [3]. Strongly correlated electrons in the Ni d orbitals mainly characterize the electronic properties of these multilayer nickelates [2,4]. Superconductivity with a maximum transition temperature of 80 K occurs in the tetragonal crystal structure [Fig. 1(b)] realized by applying pressure to $La_3Ni_2O_7$ [5], suggesting a strong relationship between the crystal structure and the emergence of superconductivity. Therefore, using light to probe phonon dynamics and associated electronic states is expected to provide important insights into elucidating the physical properties of bilayer nickelate superconductors. We theoretically investigate optically driven phonon dynamics in $La_3Ni_2O_7$ to provide a procedure for controlling the crystal structure using light [6]. In our study, we adopt the idea of nonlinear phononics, in which optical excitation of an infrared-active (IR) lattice vibration can induce a nonlinear Raman-mode displacement via anharmonic phonon-phonon coupling [7]. To discuss possible light-induced phonon dynamics in $La_3Ni_2O_7$ - Fig. 1(a), we evaluate anharmonic lattice potential based on first-principles calculations. Then, we simulate nonlinear phonon dynamics activated by optical excitation of an IR mode on the classical equations of motion. As a result, we find an appropriate IR mode that activates the Raman mode, in which the crystal structure can get slightly closer to the high-pressure structure. We expect that our study will provide a way to elucidate the relationship between the crystal structure and the mechanisms of superconductivity in bilayer nickelates.
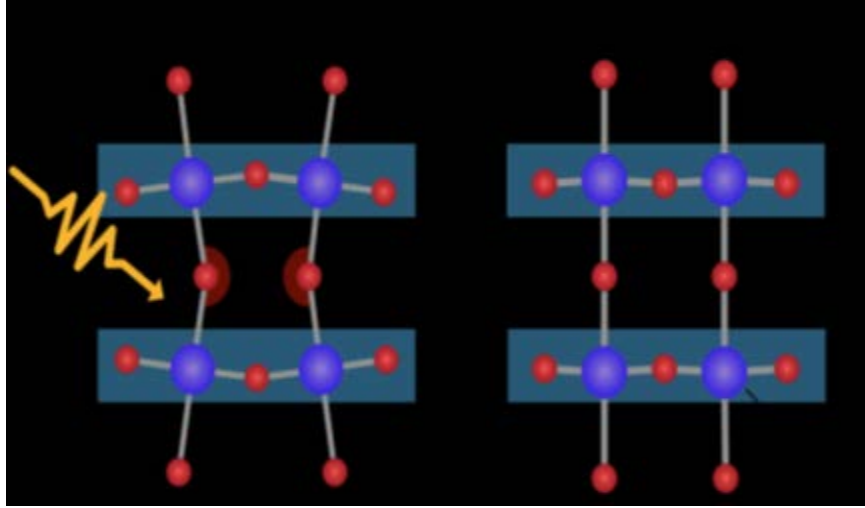
Fig. 1. *Crystal structures of $La_3Ni_2O_7$ at (a) ambient pressure and (b) high pressure. Phonon modes of the crystal structure at ambient pressure are optically excited to investigate nonlinear phonon dynamics in $La_3Ni_2O_7$ [6].*

We expect that our study will provide a way to elucidate the relationship between the crystal structure and the mechanisms of superconductivity in bilayer nickelates.

References
[1] H. Sun, M. Huo, X. Hu, J. Li, Z. Liu, Y. Han, L. Tang, Z. Mao, P. Yang, B. Wang, J. Cheng, D.-X. Yao, G.-M. Zhang, M. Wang, *Nature* **621**, 493 (2023).
[2] H. Sakakibara, M. Ochi, H. Nagata, Y. Ueki, H. Sakurai, R. Matsumoto, K. Terashima, K. Hirose, H. Ohta, M. Kato, Y. Takano, K. Kuroki *Physical Review* B **109**, 144511 (2024).
[3] E. K. Ko, Y. Yu, Y. Liu, L. Bhatt, J. Li, V. Thampy, C.-T. Kuo, B. Y. Wang, Y. Lee, K. Lee, J.-S. Lee, B. H. Goodge, D. A. Muller, H. Y. Hwang *Nature* **638**, 935 (2025).
[4] H. Sakakibara, N. Kitamine, M. Ochi, K. Kuroki, *Physical Review Letters* **132**, 106002 (2024).
[5] L. Wang, Y. Li, S.-Y. Xie, F. Liu, H. Sun, C. Huang, Y. Gao, T. Nakagawa, B. Fu, B. Dong, Z. Cao, R. Yu, S. I. Kawaguchi, H. Kadobayashi M.Wang, C. Jin, H.-K. Mao, H. Liu, *Journal of American Chemical Society* **146**, 7506 (2024).
[6] S. Kamiyama, T. Kaneko, K. Kuroki, M. Ochi, *arXiv:2501.11377* (2025)..
[7] A. S. Disa, T. F. Nova, A. Cavalleri, *Nature Physics* **17**, 1087 (2021).
 * *Acknowledgement(s):* authors acknowledge support from JSPS, KAKENHI Grants Numbers JP22K04907, JP24K06939, JP24H00191, and JP24K01333.

Shaken, not stirred:
Ultrafast magnetic switching via phononic resonances

A. Kirilyuk
Radboud University, 6525 ED Nijmegen, the Netherlands

Excitations of the crystal lattice have a significant impact on the orbital dynamics of the electrons, and through it, also on spins. Recently, ultrafast optical techniques have provided new insights into the spin-lattice coupling including angular momentum transfer from magnetization to phonons [1,2]. It should therefore be possible to realize the opposite process, by driving the lattice and thus controlling the magnetization, on the same (femtosecond) time scale. To provide resonant excitation of the optical phonon modes, we use pulses from FELIX (Free Electron Lasers for Infrared eXperiments, Nijmegen, The Netherlands). Single pulses of IR/THz light with photon energy ranging between 25 meV and 124 meV (wavelength 10-50 μm) are typically used. We have thus demonstrated that the resonant excitation of circularly-polarized optical phonons in paramagnetic substrates can permanently reverse the magnetic state of the overlayer [3]. This was shown to be the result of a phono-magnetic effect, which is a low-frequency analogue of the inverse Faraday effect. With the handedness of the phonons steering the direction of switching, such effect offers a selective and potentially universal method for ultrafast non-local control over magnetic order.

Moreover, a different and ultimately universal behaviour, characterized by displacive modification of crystal potentials, is driven by linearly-polarized excitation. The magnetic switching was shown to create very peculiar quadrupolar spatial patterns [4], confirming the mechanism. The mechanism appears to be very universal, and is shown to work in samples with very different crystallographic symmetry and magnetic properties, including weak ferromagnets and antiferromagnets, but also completely different systems such as ferroelectrics [5].
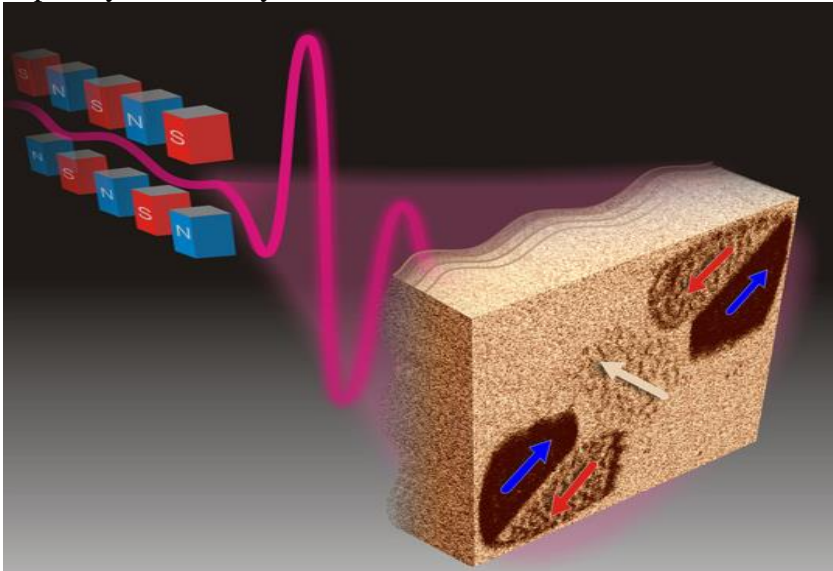
Fig. 1. A single picosecond pulse from the free electron laser FELIX in the frequency range of optical phonons creates a peculiar quadrupole pattern of reversed magnetization, which serves as a fingerprint of lattice-strain driven reversal mechanism [4].

The dynamics of the domain formation was shown to proceed via a strongly inhomogeneous magnetic state resulting in a self-organization of magnon-polarons [6] and development of magneto-elastic solitons.

References
[1] C. Dornes, Y. Acremann, M. Savoini, M . Kubli, M. J. Neugebauer, E. Abreu, L. Huber, G. Lantz, C. A. F. Vaz, H. Lemke, E. M. Bothschafter M. Porer, V. Esposito, L. Rettig, M. Buzzi, A. Alberca, Y. W. Windsor, P. Beaud , U. Staub, D. Zhu, S. Song, J. M. Glownia, S. L. Johnson *Nature* **565**, 209 (2019).
[2] S. R. Tauchert, M. Volkov, D. Ehberger, D. Kazenwadel, M. Evers, H. Lange, A. Donges, A. Book, W. Kreuzpaintner, U. Nowak, P. Baum *Nature* **602**, 73 (2022).
[3] C. S. Davies, F.G.N. Fennema, A. Tsukamoto, I. Razdolski, A.V. Kimel, A. Kirilyuk, *Nature* **628**, 540 (2024).
[4] A. Stupakiewicz, C.S. Davies, K. Szerenos, D. Afanasiev, K. S. Rabinovich, A. V. Boris, A. Caviglia, A. V. Kimel, A. Kirilyuk, *Nature Physics* **17** 489 (2021).
[5]. M. Kwaaitaal, D.G. Lourens, C.S. Davies, A. Kirilyuk, *Nature Photonics* **18**, 569 (2024).
[6] M. Gidding, T. Janssen, C.S. Davies, A. Kirilyuk, *Nature Communications* **14**, 2208 (2023).

Development and applications of IR and mid-IR ultrafast laser sources

F. Légaré

Institut national de la recherche scientifique, Varennes, J3X1P7 Canada

During the last decades, the generation of laser pulses in the infrared (IR) and mid-infrared (mid-IR) spectral range has experienced a growing interest for various applications including strong-field physics [1,2] and molecular spectroscopy [3,4]. Furthermore, the development of table-top atto- to femtosecond soft X-ray sources based on high harmonic generation (HHG) from noble gases has benefited from the development of high-power IR and mid-IR sources with keV photons being generated in compact setups [5,6]. The generation of XUV photons by means of HHG is intrinsically connected to the energy of electrons as they get accelerated by the driving field and directly linked to their ponderomotive energy [7]. Due to the quadratic scaling of the electron ponderomotive energy with the driving laser wavelength, long wavelength pulses allow to significantly increase the harmonic cutoff compared to shorter wavelength at a cost of efficiency [8,9]. While HHG in gaseous media has been studied for decades now, its counterpart in transparent solid media is rather new [10]. To drive HHG from solids, in particular from low bandgap materials such as semiconductors and quantum materials [11,12], there is a need for long wavelength (usually above 1.5 µm) and energetic (several µJ) laser pulses. Such sources allow to maintain the interaction in the tunneling regime where the system can withstand significantly stronger intensities leading to highly non-linear processes. In addition, as opposed to near-IR and visible light that typically redistributes carriers across the entire momentum space in a quasi-thermal fashion, the use of intense long-wavelength light excitation enables the selective drive of non-thermal phases in quantum materials with minimal coupling to the electronic bath [13]. Until recently, the standard approach for the generation of IR and mid-IR pulses was to start from a Titanium-Sapphire (Ti-Sa) chirped pulse amplifier, pumping an optical parametric amplifier (OPA) for generating tunable signal and idler pulses between 1.2 and 2.5 µm, followed by difference frequency generation for mid-IR radiation from 3 to 15 µm. At the Advanced Laser Light Source (ALLS) user facility, with this approach we generated 10-mJ level pulses at 1.8 micron [14] followed by pulse compression to two-cycle duration [15]. Such pulses enabled the generation of high-field THz pulses [16], water window harmonics [17], direct electron acceleration to relativistic energies [18], and the generation of high dose radiation for radiotherapy [19]. Furthermore, at low repetition rate, Ti-Sa pumped dual-chirped OPA and Frequency domain OPA have enabled the generation of multi-TW IR laser pulses [20,21]. Using optical parametric chirped pulse amplification (OPCPA), the group of A. Baltuska pioneered the development of 20 Hz high-energy mid-IR laser systems enabling record HHG cut-off with 1.6 keV photon energy [5,22]. In recent years, two approaches have allowed to further scale repetition rate and average power of IR and mid-IR laser systems. First, using IR and mid-IR gain media (Thulium, Holmium, Chromium- and Iron doped zinc selenide (Cr^{2+}/Fe^{2+}: ZnSe) with chirped pulse amplification, ultrafast (pico- to femtosecond) laser systems operating between 1.9 and 4.1 µm have been developed [23-26]. Second, based on OPA and OPCPA, using Ytterbium (Yb), Thulium, and Holmium pump lasers, tunable light sources from 1.5 to 15 µm have been achieved at high repetition rates (> kHz) and with higher conversion efficiency to the mid-IR compared to Ti-Sa pumped OPA [27-30]. In my talk, I will review these approaches followed by the recent work performed at ALLS by my team and collaborators, including the company *Few-cycle Inc.*: the development of a high repetition rate Yb pumped OPA with a DFG stage for the generation of tunable pulses from 1.5 to 8 µm, synchronized temporally to 206 nm pulses for time- and angle-resolved photoemission spectroscopy (TR-ARPES) [31]. Typical spectra for the tunable signal, idler, and mid-IR pulses (from DFG) are presented in Fig. 1. Complete temporal characterization of this OPA was performed using Frequency Resolved Optical Switching [32].
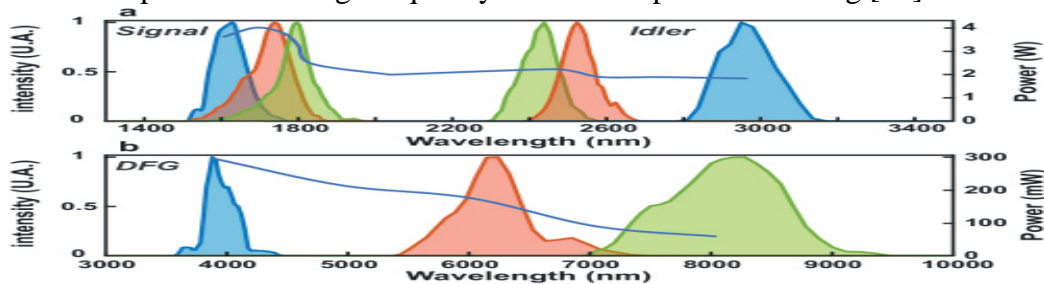
Fig. 1: **(a)** *Tunability of the OPA system for three different signal and idler couples (blue, orange and green).* **(b)** *Tunability of the DFG between 4 µm and 8 µm for the three different couples. The blue curve represents the average power [31].*

We demonstrated the efficient generation of multidimensional solitary states (MDSS) [33] using high-energy, transform-limited picosecond Yb-based lasers in hollow-core fibers (HCFs) filled with molecular gases, followed by nonlinear spectral broadening towards longer wavelength and post-compression [34]. A comprehensive series of experiments explored the generation of MDSS under varying conditions, including picosecond and sub-picosecond Yb-laser pulses, different HCF geometries, and distinct nonlinear propagation regimes. Across all conditions, MDSS generation was consistently observed, enabled by enhanced spatiotemporal nonlinear interactions when the input pulse duration exceeded the characteristic molecular response time. One set of experiments, presented in Fig. 2, involved launching 700 fs, 4 mJ pulses into a 2 bar N_2-filled HCF. The corresponding experimental and reconstructed SHG-FROG spectrograms, retrieved spectra, and compressed temporal profiles are shown. A long-pass filter with a 1050 nm cut-off was used to isolate the MDSS portion of the spectra. After accounting for dispersion from the output tube, vacuum window, collimating lens, and 5 m of air, the pulse duration was measured to be ~62 fs. To compensate for the negative chirp characteristic of MDSS, an additional 12 mm thick BaF_2 window was introduced, yielding a final compressed pulse of 24 fs, centered at 1150 nm, with 1.3 mJ energy and ~54.2 GW peak power. The total output energy was 2.1 mJ, with ~62% in the MDSS spectral region.
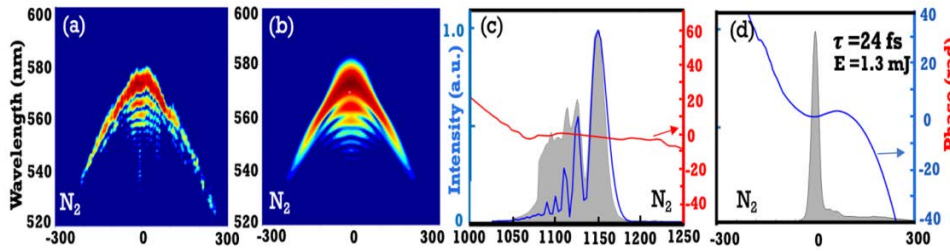
Fig. 2: (a) *Experimental and* **(b)***reconstructed spectrograms, along with* **(c)** *the corresponding experimental and reconstructed spectra and* **(d)** *the temporal intensity profiles of the compressed pulses for N_2 gas.* τ *is the pulse duration [34].*

The company *Few-cycle Inc.*, in collaboration with my group and collaborators, has advanced HCF pulse compression of Yb laser systems with hundreds of Watts of average power [35] or 100-mJ level of energy per pulse [36]. Using self-phase modulation, narrow band Yb lasers are broadened and compressed to sub-10 fs pulse duration. With the large bandwidth of these pulses and their short pulse duration, the company has developed a platform providing tunable fs pulses from 200 nm to 12 μm starting with an 80 W Ytterbium laser system (2 mJ/pulse, 300 fs, 40 kHz). This platform used resonant dispersive waves (RDW) in HCF [37], SHG, and DFG. Typical results are presented in Fig. 3.
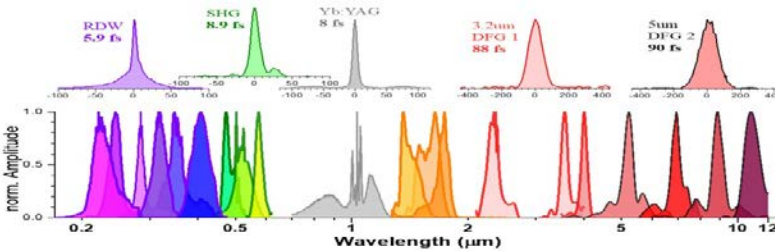
Fig. 3: Spectral tuning range (bottom) *and corresponding temporal pulse shapes of the (HYPerspectral Ultrafast Source) HYPUS.*

Using spectral broadening of laser pulses at 1.8 μm in a hollow core fiber to seed a FOPA followed by a DFG stage, we have generated tunable pulses from 5.5 to 13 μm with 20 microjoules of energy per pulse [37]. Carrier envelope phase stability of the mid-IR has been demonstrated using high harmonic generation from ZnSe. The advantages of this approach will be presented as well as how to scale this technology for direct amplification of mid-IR pulses with an Ytterbium laser system. To conclude, the development of IR and mid-IR laser sources is a very active research field. Thanks to the development of turnkey, robust and efficient pump laser systems, high pulse energy and average power are now available at long wavelength such as *10 μm … Back to the Future!* [38].

References
[1] B. Wolter, M. G. Pullen, A.- T. Le, M. Baudisch, K. Doblhoff - Dier, A. Senftleben, M. Hemmer, C. D. Schröter, J. Ullrich, T. Pfeifer , R. Moshammer, S. Gräfe, O. Vendrell, C. D. Lin, J. Biegert, *Science* **354**, 308 (2016).
[2] Z. Chang, L. Fang, V. Fedorov, C. Geiger, S. Ghimire, C. Heide, N. Ishii, J. Itatani, C. Joshi, Y. Kobayashi, P. Kumar, A. Marra, S. Mirov I. Petrushina, M. Polyanskiy, D. A. Reis, S. Tochitsky, S. Vasilyev, L. Wang, Y. Wu, F. Zhou, *Advances in Optics and Photonics* **14**, 652 (2022)
[3] A. Schliesser, N. Picqué, T. W. Hänsch, *Nature Photonics* **6**, 440 (2012).
[4] J. Haas, B. Mizaikoff, *Annual Review of Analytical Chemistry* **9**, 45 (2016).
[5] T. Popmintchev, M.- C. Chen, D. Popmintchev, D. Popmintchev, P. Arpin, S. Brown, S. Ališauskas, G. Andriukaitis, T. Balčiunas O. D. Mücke, A. Pugzlys, A. Baltuška, B. Shim, S. E. Schrauth, A. Gaeta, C. Hernández - García, L. Plaja, A. Becker, A. Jaron- Becker

M. M. Murnane, H. C. Kapteyn, *Science* **336**, 1287 (2012).

[6] J. Li, X. Ren, Y. Yin, K. Zhao, A. Chew, Y.Cheng, E. Cunningham, Y.Wang, S.Hu, Y.Wu, M. Chini, Z.Chang, *Nature Communications* **8,** 186 (2017)

[7] P. B. Corkum, *Physical Review Letters* **71**, 1994 (1993).

[8] B. Shan, Z. Chang, *Physical Review A* **65**, 011804 (2001).

[9] A. D Shiner, C. Trallero - Herrero, N. Kajumba, H - C Bandulet, D. Comtois, F. Légaré, M. Giguère, J.- C. Kieffer, P. B Corkum D. M. Villeneuve , *Physical Review Letters* **103**, 073902 (2009).

[10] S. Ghimire, A. D. DiChiara, E. Sistrunk, P. Agostini, L. F. DiMauro, D. A. Reis, *Nature Physics* **7**, 138 (2011).

[11] O. Schubert, M. Hohenleutner, F. Langer, B. Urbanek, C. Lange, U. Huttner, D. Golde, T. Meier, M. Kira, S. W. Koch, R. Huber *Nature Photonics* **8** 119 (2014).

[12] C. Heide, Y. Kobayashi, D. R. Baykusheva, D. Jain, J. A. Sobota, M. Hashimoto, P . S. Kirchmann, S. Oh, T. F. Heinz, D. A. Reis, S. Ghimire *Nature Photonics* **16**, 620 (2022).

[13] D. N. Basov, R. D. Averitt, D. Hsieh, *Nature Materials* **16**, 1077 (2017).

[14] N. Thiré, S. Beaulieu, V. Cardin, A. Laramée, V. Wanie, B. E. Schmidt, F. Légaré, *Applied Physics Letters* **106**, 091110 (2015).

[15] V. Cardin, N. Thiré, S. Beaulieu, V. Wanie, F. Légaré, B. E. Schmidt, *Applied Physics Letters* **107** , 181101 (2015).

[16] M. Clerici, M. Peccianti, B. E. Schmidt, L. Caspani, M. Shalaby, M. Giguère, A. Lotti, A. Couairon, F. Légaré, T. Ozaki, D. Faccio R. Morandotti, *Physical Review Letters* **110**, 253901 (2013).

[17] V. Cardin, B. E. Schmidt, N. Thiré, S. Beaulieu, V. Wanie, M. Negro, C. Vozzi, V. Tosa, F. Légaré, *Journal of Physics* B, **51**, 174004 (2018)

[18] J. Powell, S. W. Jolly, S. Vallières, F. Fillion - Gourdeau, S. Payeur, S. Fourmaux, M. Lytova, M. Piché, H. Ibrahim, S. McLean F. Légaré , *Physical Review Letters* **133**, 155001 (2024).

[19] S. Vallières, J. Powell, T. Connell, M. Evans, M. Lytova, F. Fillion - Gourdeau, S. Fourmaux, S. Payeur, P. Lassonde, S. McLean, F. Légaré *Laser Photonics Review* **18**, 2300078 (2024).

[20] V. Gruson, G. Ernotte, P. Lassonde, A. Laramée, M. Bionta, M. Chaker, L. Di Mauro, P. Corkum, H. Ibrahim, B. Schmidt, F. Légaré *Optics Express* **25**, 27706 (2017).

[21] L. Xu, B. Xue, N. Ishii, J. Itatani, K. Midorikawa, E. J. Takahashi, *Optics Letters* **47**, 3371 (2022).

[22] G. Andriukaitis, T. Balčiūnas, S.Ališauskas, A. Pugžlys, A. Baltuška, T. Popmintchev, M.- C. Chen, M. M. Murnane, H. C. Kapteyn, *Optics Letters* **36**, 2755 (2011).

[23] T. Heuermann, Z.Wang, M. Lenski, M.Gebhardt, C.Gaida, M.Abdelaal, J. Buldt, M. Müller, A.Klenke, J.Limpert, *Optics Letters* **47**, 3095(2022).

[24] M. Bock, D. Ueberschaer, M. Mero, T. Nagy, U. Griebner, *Optics Express* **33**, 17245 (2025).

[25] X. Ren, L. H. Mach, Y. Yin, Y. Wang, Z. Chang, *Optics Letters* **43**, 3381(2018).

[26] Z. A. Marra, Y. Wu, F. Zhou, Z. Chang, *Optics Express* **31**, 13447 (2023).

[27] T. Feng, A. Heilmann, M. Bock, L. Ehrentraut, T. Witting, H. Yu, H. Stiel, S. Eisebitt, M. Schnürer, *Optics Express* **28**, 8724 (2020).

[28] R. Budriūnas, K. Jurkus, M. Vengris, A. Varanavičius, *Optics Express* **30**, 13009 (2022).

[29] T. Kanai, P. Malevich, S. S. Kangaparambil, K. Ishida, M. Mizui, K. Yamanouchi, H. Hoogland, R. Holzwarth, A. Pugzlys, A. Baltuska *Optics Letters* **42**(4), 683 (2017).

[30] P. Fuertjes, M. Bock, L. von Grafenstein, D. Ueberschaer, U. Griebner, T. Elsaesser, *Optica* **9**, 1303 (2022).

[31] A. Longa, J-M. Parent, B. Frimpong, D. Armanno, N. Gauthier, F. Légaré, F. Boschini, G. Jargot, *Optics Express* **32**, 29549 (2024).

[32] E. Haddad, A. Longa, P. Lassonde, A. Leblanc, H. Ibrahim, F. Boschini, G. Jargot, *Optics Express* **31**, 25840 (2023).

[33] R. Safaei, G. Fan, O. Kwon, K. Légaré, P. Lassonde, B. E. Schmidt, H. Ibrahim, and F. Légaré, *Nature Photonics* **14**, 733 (2020).

[34] M. Arshadipirlar, D. Khatri, S. Londo, B. Azizi, G. Jargot, M. Kumar, C. Zhang, C. Kincaid, C. Lantigua, T.- C. Truong, H. Ibrahim P. B. Corkum, M. Chini, F. Légaré, R. Safaei, *APL Photonics* **10**, 046112 (2025).

[35] M. Ivanov, E. Doiron, M. Scaglia, P. Abdolghader, G. Tempea, F. Légaré, C. A. Trallero-Herrero, G. Vampa, B. E. Schmidt, *IEEE Journal of Selected Topics in Quantum Electronics*, **30**, 1 (2024).

[36] G. Fan, P. Carpeggiani, Z. Tao, G. Coccia, R. Safaei, E. Kaksis, A. Pugzlys, F. Légaré, B. Schmidt, A. Baltuška, *Optics Letters* **46**, 896 (2021)

[37] G. Dalla - Barba, G. Jargot, P . Lassonde, S. Tóth, E. Haddad, F. Boschini, J. Delagnes, A. Leblanc, H Ibrahim, E. Cormier, F. Légaré *Optics Express* **31**, 14954 (2023).

[38] L. Young, K. Ueda, M. Gühr, P. H. Bucksbaum, M. Simon, S. Mukamel, N. Rohringer, K. C. Prince, C. Masciovecchio, M. Meyer, A. Rudenko D. Rolles, C. Bostedt, M. Fuchs, D. A, Reis, R. Santra, H. Kapteyn, M. Murnane, H. Ibrahim, F. Légaré, M. Vrakking, M. Isinger, D. Kroon M. Gisselbrecht, A. L'Huillier, H. J. Wörner, S. R. Leone, *Journal of Physics* B. **51**, 032003 (2018).

Localizing multipartite entanglement with local and Global measurements

C. Vairogs, S. Hermes, F. Leditzky

University of Illinois Urbana-Champaign, Urbana, IL 61801, USA

The localizable entanglement (LE) is the maximal amount of entanglement that can be concentrated, on average, onto part of a multipartite system via local projective measurements on its complement [1,2]. The LE has found bountiful applications in the study of quantum phase transitions and entanglement in spin systems. Traditionally, the LE has been defined with respect to bipartite entanglement measures, such as the entanglement entropy or the two-qubit concurrence. More recent work has analyzed specific quantum states using the LE defined by multipartite entanglement measures [3]. Motivated by a GHZ state distillation problem, we study the LE given by multipartite entanglement measures known as the n-tangle [4], the GME-concurrence [5], and the concentratable entanglement (CE) [6]. For generic states, we derive a set of easily computable and experimentally accessible upper and lower bounds on the LE given by these measures in terms of either spin correlation functions or explicit functions of marginal states. To motivate this problem further, consider a scenario in which we wish to produce with nonzero probability a state that somehow resembles a GHZ state by using only a single-copy local measurement

on a larger state. Intuitively, to maximize our chances of success, we should choose our initial state so that its LE is large. This approach has an advantage over naïve strategies such as constructing a measurement to perform an exact state transformation or choosing the initial state to maximize average post-measurement fidelity. The former is not tractable in general, while the latter penalizes post-measurement states that are locally unitarily equivalent to the GHZ state, which are still of great use.

The n-tangle assumes the same value on any pair of states for which one may reversibly convert one into the other with some nonzero probability via local operations and classical communication (LOCC). In this way, the n-tangle distinguishes between different classes of entanglement. Thus, by maximizing the LE given by the n-tangle, we are decreasing our chances of obtaining a state that is inequivalent to the GHZ state under "stochastic" LOCC, such as the W state. On a different note, the GME concurrence always vanishes on bi-separable states. Thus, by maximizing the LE determined by the GME-concurrence, we diminish the likelihood of getting states that have the same value of the n-tangle as the GHZ state, yet do not exhibit genuine multipartite entanglement. The CE of a state is indexed by a collection of its subsystems and is equal to the average entanglement, as measured by the linear subsystem entropy, of the state across all bipartitions with one part contained in the given collection. Several well-known entanglement measures are recoverable from the CE, which together with its definition suggests that it gives a more fine-grained picture of entanglement, making it useful for the aforementioned distillation problem. Our analytical results are derived primarily through arguments invoking the convexity or concavity of various functions. We show that the LE of a state, when defined by the n-tangle, is upper bounded by the fidelity of its reduced density matrix and its "spin-flipped" version by refining an earlier argument regarding the related entanglement of assistance [7]. We express our bounds of the LE given by the GME-concurrence in terms of straightforward functions of the state's marginals. Furthermore, we observe that the LE of a state, when defined by the CE, is upper bounded by the original value of the CE on the given state. We also derive a lower bound on the CE in terms of spin correlation functions. Since divergence in the correlation length is an indicator of a quantum phase transition, this latter fact may open the door to the use of the localizable CE as a tool for characterizing phase transitions. On the numerical side, we compute the LE defined by our entanglement measures for a collection of weighted graph states. A weighted graph state is a quantum state associated with a graph, each of whose edges is labeled by a "weight" indicating the degree of entanglement between corresponding qubits. In this way, weighted graph states are a useful model for the study of multipartite entanglement. We show that for a collection of reasonable graphs, our bounds are reasonably tight. We compare our results to a recent protocol for generating GHZ states via local measurements on a particular weighted graph state [8]. Fig. 1 shows that the LE is near maximal in this case, giving an explicit example of our motivating GHZ state distillation scenario.
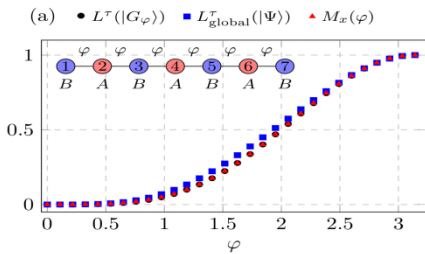
Fig. 1: Values of localizable entanglement (for local and global measurements, respectively) based on the n-tangle, evaluated on a weighted line graph state with uniform edge weight φ. The red qubits labeled by even numbers are measured out

Our ongoing work characterizes the LE in the ground states of spin-half Hamiltonians, which we anticipate will clarify the role of using multipartite entanglement measures to study quantum phase transitions

References
[1] D. P. Di Vincenzo, C. A. Fuchs, H. Mabuchi, J. A. Smolin, A. Thapliyal, A. Uhlmann, *Quantum Computing and Quantum Communications Springer, Berlin- Heidelberg*, 247 (1999).
[2] M. Popp, F. Verstraete, M. A. Martín-Delgado, J. I. Cirac, *Physical Review* A **71**, 042306 (2005).
[3] D. Sadhukhan, S. S. Roy, A. K. Pal, D. Rakshit, A. Sen(De), U. Sen, *Physical Review* A **95**, 022301 (2017).
[4] A. Wong, N. Christensen, *Physical Review* A **63**, 044301 (2001).
[5] Z.- H. Ma, Z.-H. Chen, J.-L. Chen, C.Spengler, A. Gabriel, M.Huber, *Physical Review* A **83**, 062325 (2011).
[6] J. L. Beckey, N. Gigena, Patrick J. Coles, M. Cerezo, *Physical Review Letters* **127**, 140501 (2021).
[7] T. Laustsen, F. Verstraete, S. J. van Enk, *Quantum Information and Computation* **3**, 64 (2003).
[8] R. Frantzeskakis, C. Liu, Z. Raissi, E. Barnes, S. E. Economou, *Physical Review Research* **5**, 023124 (2023).

Optical control of electrons in a Floquet topological insulator

D. M. B. Lesko[1] , T. Weitz[1], S. Wittigschlager[1], W. Li[1], C. Heide[2],O.Neufeld[3], P.Hommelhoff[1]

[1]Friedrich-Alexander-Universität Erlangen-Nürnberg, 91054 Erlangen, Germany
[2]University of Central Florida, Orlando, FL 32816, USA
[3]Technion, 3200003 Haifa, Israel

Light interaction with materials can modify their electronic band structure, creating light-dressed Floquet states with new quantum and topological properties. Transformations of trivial materials into topologically nontrivial states, called Floquet topological insulators (FTIs), by periodic driving have been observed in photonic waveguides [1] and cold atom systems [2]. These experiments in synthetic systems elucidate both time-periodic and sub-cycle physical phenomena [3,4]. While theory suggests that Floquet dressing can synthesize almost arbitrary material band structures with varying topological phenomena [5], FTI states in real materials have yet to be directly observed and controlled. Pioneering works observed Floquet-Bloch bands on a topological surface state [6] as well as engineered bands in a bulk semiconductor [7]. In a wide-bandgap semiconductor, ultrafast Floquet physics can be used to explain phenomena such as the enhancement of optical nonlinearities [8]. A differential DC anomalous Hall conductivity was shown in [9].Here, we demonstrate a new method for generating and probing these phenomena in a real material by harmonically related optical fields. The fundamental frequency laser pulse dresses bare graphene (Fig. 1), a topologically trivial material, into an FTI. Importantly, this out-of-equilibrium state exhibits multiple topological bands separated by harmonics of the dressing frequency [10].
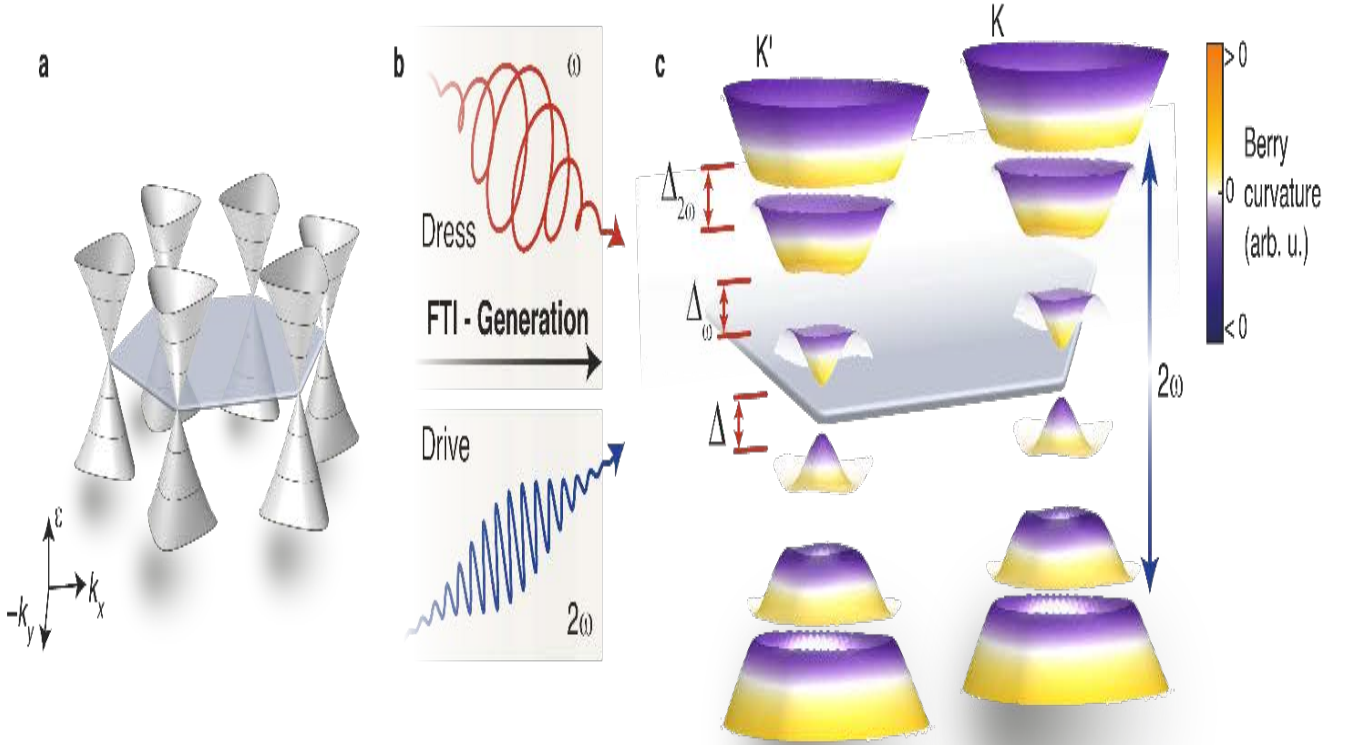
Fig. 1. Lightwave control of electrons in a Floquet topological insulator. *a–c:* ** *A Floquet topological insulator (FTI) emerges from driving the gapless, topologically trivial band structure of graphene (a**) by irradiation with a circularly polarized fundamental laser field (**b**, **red waveform**).This dressing breaks only time-reversal symmetry, giving rise to both a nonzero gap Δ at the emerging K and K' valleys and a Berry curvature (**color bar**) of the same sign in both valleys. This results in a non-zero Chern number as well as anon-trivial topological insulating phase, with avoided crossings at resonant energies ($\Delta_{n\omega}$, **c**). A second harmonic pulse (**b**, **blue waveform**) controls the motion of electrons in the FTI bands.*

While traditional measurements of transport phenomena in FTIs are done with DC or low frequency fields, here we use an all-optical driving/dressing approach, which is critical for elucidating new phenomena not seen before in solid-state FTIs. We probe a topological band resonant with the second harmonic, measuring two-color phase and helicity-dependent photocurrents. For the first time, we observe photocurrent circular dichroism (Fig 2a), the all-optical anomalous Hall effect (Fig. 2b-c), and the attosecond FTI state's micromotion [11] (observed through a dependence of the photocurrent signal on the initial state relative phase).

We compare these photocurrents with state-of-the-art time-dependent density functional theory (TDDFT) calculations. This directly connects the traditional static (periodic) Floquet picture with attosecond phenomena probed with optical fields.
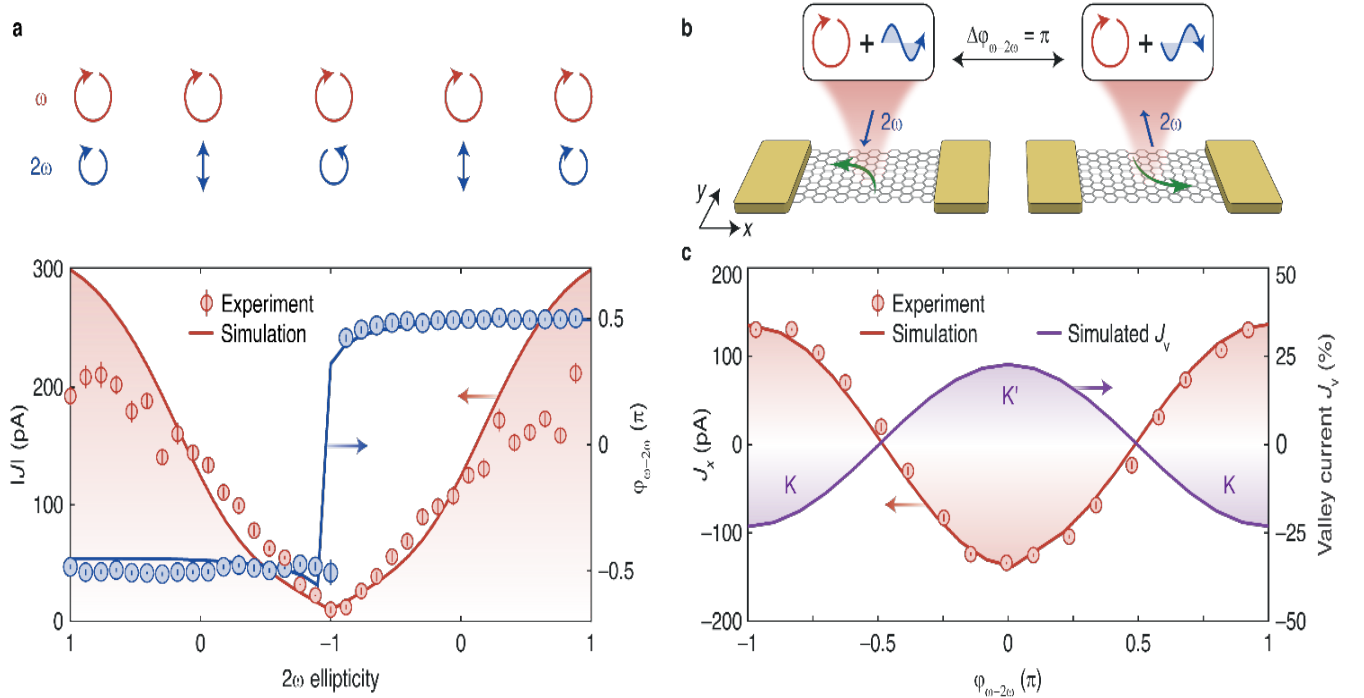
Fig. 2. Circular dichroism and all-optical anomalous Hall effect. *a*, We probe circular dichroism by keeping the helicity of ω constant, generating the FTI, and continuously sweep the ellipticity of 2ω (*above*). Below, measured current amplitude |J| (*red circles*) and phase θ (*blue circles*) as a function of the 2ω ellipticity. TDDFT simulation results (*lines*) support the dichroic generation of ballistic photocurrent for co-rotating helicities of ω and 2ω and photocurrent suppression for counter-rotating helicities. *b*, All-optical anomalous Hall currents (*green arrows*) emerge from excitation of the ω-driven FTI with the 2ω control polarized perpendicularly to the electrode axis. Shifting $\varphi_{\omega-2\omega}$ by π effectively results in a reversal of the 2ω deflection and consequently the Hall current direction. *c*, Measured current (*red circles*) as a function of $\varphi_{\omega-2\omega}$. The computed current density (*red line*) confirms the directional control of the anomalous Hall effect.

By understanding how to optically modify materials and measure their ultrafast response, we can dynamically change material properties and engineer quantum and topological phenomena in trivial materials.

References
[1]   M. Rechtsman, J. M. Zeuner, Y. Plotnik, Y. Lumer, S. Nolte, M. Segev, A. Szameit, *Nature* **496**, 196 (2013).
[2]   G. Jotzu, M. Messer, R. Desbuquois, M. Lebrat, T. Uehlinger, D. Greif, T. Esslinger, *Nature* **515,** 237 (2014).
[3]   M. S. Rudner, N. H. Lindner, *Nature Reviews Physics* **2,** 229 (2020).
[4]   R. Desbuquois, M. Messer, F. Görg, K. Sandholzer, G. Jotzu, T. Esslinger, *Physical Review* A **96**, 053602 (2017).
[5]   K. Wintersperger, C.Braun, F. Nur Unal, A. Eckardt, M. Di Liberto, N. Goldman, I. Bloch, M. Aidelsburger, *Nature Physics* **16**, 1058 (2020)
[6]   Y. H. Wang, H. Steinberg, P. Jarillo-Herrero, N. Gedik, *Science* **342**, 453 (2013).
[7]   S. Zhou, C. Bao, B. Fan, H. Zhou, O. Gao, H. Zhong, T. Lin, H. Liu, P. Yu, P. Tang, S. Meng, W. Duan, S. Zhou, *Nature* **614**, 75 (2023)
[8]   J. - Y. Shan, M. Ye, H. Chu, S. Lee, J.G. Park, L. Balents, D. Hsieh, *Nature* **600**, 235 (2021).
[9]   J. W. McIver, B. Schulte, F.U. Stein, T. Matsuyama, G. Jotzu, G. Meier, A. Cavalleri, *Nature Physics* **16**, 38 (2019).
[10] T. Kitagawa, E. Berg, M. Rudner, E. Demler, *Physical Review* B **82,** 235114 (2010).
[11] D. M. B. Lesko, T. Weitz, S. Wittigschlager, W. Li, C. Heide, O. Neufeld, P. Hommelhoff, *.arXiv:2407.17917* (2024).

Giant enhancement of optical nonlinearities in hybrid WS2/ Plasmon structures probed by ultrafast 2-D electronic spectroscopy

C. Lienau

Carl von Ossietzky Universität Oldenburg, 26129 Oldenburg, Germany

Transition metal dichalcogenide (TMDC) monolayers are quantum materials with unusual optoelectronic properties [1]. Strongly bound excitons in the material are particularly sensitive to many-body interactions in the atomically thin monolayer, dominating their optical nonlinearity [2]. Hybridization of these excitons with light-like excitations, such as surface plasmon polaritons (SPPs), allows to dramatically alter the optical response and to tailor material properties on the nano scale [3-5]. The role of excitonic many-body interactions [6] for the new hybridized polariton states is of crucial importance. The ideal tool to investigate these interactions and their coherent dynamics is ultrafast two-dimensional electronic spectroscopy (2DES). Here, we report the first ultrafast 2DES spectra of a TMDC monolayer coupled to plasmonic nanoresonator array. Here, we report ultrafast 2DES with 8 fs resolution [7] of a hybrid WS2/plasmon structure. For this, we manufacture aA silver nano-slit array (Fig. 1a) with a period of 495 nm is fabricated using focused ion beam milling. The structure is coated with a 5-nm layer of Al2O3 and then covered with an exfoliated monolayer flake of WS2. An angle-dependent reflectivity measurement (Fig. 1b) shows upper (UP) and lower (LP) polariton branches that form due to a coupling between the A exciton of WS2 and the AM[-1] mode of the SPP close to 2 eV. The deduced coupling strength of V_XP= 23 meV places the sample into the intermediate coupling regime. At around 2.3 eV, the B exciton energetically overlaps with the AM[+1] mode of the SPP.
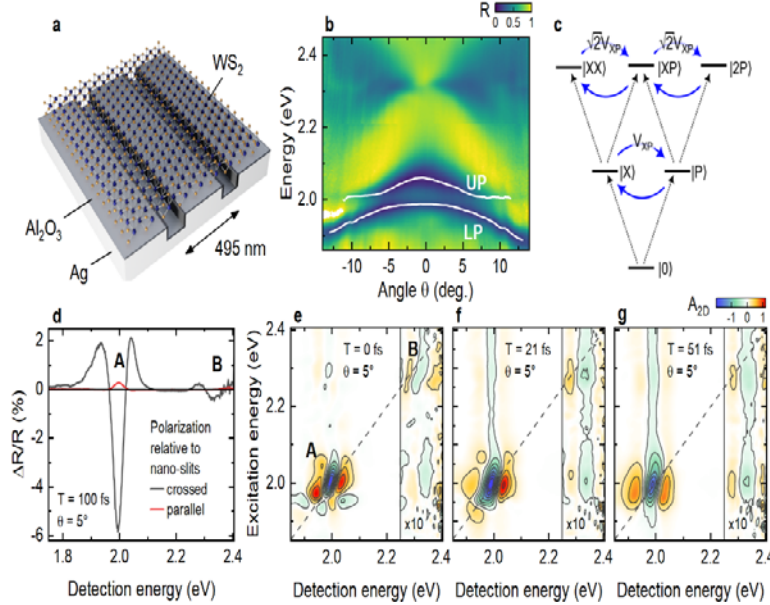
Fig. 1. a) Sketch of the hybrid sample comprising a periodic nano-slit array (20x50 µm²) milled into a silver film and coated with a 5-nm layer of Al2O3. The nanostructure is covered with an exfoliated monolayer of WS2. b) Angle-dependent linear reflectivity showing an anti-crossing at an incidence angle of θ=±5° forming upper (UP) and lower (LP) polariton branches with a coupling strength of V_XP= 23 meV. c) Level scheme of strong coupling between the A exciton |X⟩ and plasmon |P⟩ including one- and two-quantum excitations. d) Differential reflectivity at θ=5° and a waiting time of T=100 fs for pulses polarized perpendicular to the nano-slits (black) and along the slits (red). A giant enhancement of the nonlinearity by a factor of ~20 is demonstrated, arising from the hybridization between |X⟩ and |P⟩. e)-g) 2DES maps for selected waiting times. Two polariton manifolds for the A and B exciton and cross-peaks are observed. The diagonal A exciton polariton peak rapidly evolves within ~50 fs.

When focusing on the A exciton of WS2region of the sample, the exciton-plasmon coupling hybridizes both one-quantum (|X⟩ and |P⟩) as well as two-quantum (|XX⟩, |2P⟩ and the mixed |XP⟩) states, as depicted in the level scheme in Fig. 1c. We can regard the plasmonic ladder as a harmonic oscillator without nonlinearity. The semiconductor exciton, however, possesses a nonlinearity that - in the case of TMDCs - is dominated by many-body interactions such as excitation-induced shifts (EIS) or dephasing (EID) [2]. One important question is whether and how these many-body interactions are transferred to the hybridized system [5]. To investigate the ultrafast nonlinear response of the hybrid structure, we employ a 2DES setup that utilizes 8-fs pulses from a home-built built non-collinear optical parametric amplifier operating at 175 kHz. For 2DES, we use an inherently phase-stable common-path interferometer and a fast and sensitive line camera in combination with fast mechanical chopping of the pump [4]. Fig. 1d depicts the differential reflectivity at a waiting time of T=100 fs at the crossing angle of θ=5° for two polarization settings of the pump and probe pulses. When pump and probe are both s-polarized along the nano-slits, the SPP is effectively "turned off". Indeed, the and the probed observed nonlinearity (red line in Fig. 1d) matches that of a WS2 monolayer on a bare silver substrate. In this

case, the weak nonlinearity in this case is Analysis of such a reference measurement shows that in the absence of the nanostructure the optical nonlinearity is dominated by EID with additional contributions from EIS. When turning the polarization of pump and probe perpendicular to the nano-slits (black line in Fig. 1d), a giant enhancement of the nonlinearity by a factor of ~20 can be observed. This enhancement arises is the distinct signature from of the hybridization between the TMDC excitons and the SPP resonances. The large magnitude of this enhancement is surprising since, iIn our previous a related study of strong couplings between molecular J-aggregates and a gold nano-slit array, we could not observe such a giant hybridization-induced enhancements of the nonlinearity were basically absent[4]. In that case, the oscillator strength of the aggregate excitons and the SPP were of similar amplitude. Now, the oscillator strength of the WS2 exciton is much weaker than that of the silver SPP. Therefore, both UP and LP are gaining oscillator strength from the SPP. The transfer of many-body effects such as EID and EIS to the polariton states then introduces the pronounced nonlinearity. 2DES maps of the polaritonic system recorded at of $\theta = 5°$ are presented in Fig. 1e-g. They display a strong diagonal A polariton feature close to 2 eV with a lineshape along the detection energy that resembles the $\Delta R/R$ profile in Fig. 1d. Side peaks along the excitation axis point to the excitation of upper and lower polariton resonances. These peaks vanish during the first 50 fs after excitation, the decoherence time of the polariton system. Due to the broad nature of the polariton resonances and the intermediate coupling strength, no clear and spectrally distinct diagonal and cross-peaks for the UP and LP are apparent. In addition to the A exciton-polaritons, a B exciton polariton feature close to 2.3 eV can be seen. Clear cross peaks between the A and B exciton polariton manifolds point to an additional, coherent coupling between the hybridized subsystems. Since such cross-peaks are also seen in the reference measurement of the isolated WS2 system, they likely are caused by an intrinsic intra- and intervalley exchange interactions coupling in the TMDC monolayer, enhanced in amplitude by . They may also reflect the individual coupling of the A and B excitons to the polariton modes of the grating. coupled AM[-1] and AM[+1] SPP modes, respectively. The B exciton polariton peaks show a similar lineshape as the A exciton polariton, also pointing to many-body interactions as the main cause for their nonlinearity. Pronounced vertical stripes, usually a feature for EID or EIS by free carriers, also point towards such many-body effects in the polariton system. Preliminary simulations of the optical nonlinearities show that the spectral peak pattern at T=51 fs the key observations of our experiments (Fig. 1g) can be reproduced rationalized by in terms of the effective Hamiltonian outlined in Fig. 1c, when introducing EID and a Pauli blocking of the $|X\rangle \rightarrow |XX\rangle$ transition as the dominant microscopic origin of the optical nonlinearity of the hybrid system. Pauli blocking upon optical excitation transiently reduces the phase space available for radiative coupling between excitons and plasmons and, therefore, effectively closes the Rabi gap. This results in bright and highly nonlinear hybrid polariton resonances. With realistic model parameters, the Hamiltonian in Fig. 1c can quantitatively reproduce the observed 20-fold enhancement in nonlinearity of the hybrid systems, and most of the lineshape dynamics seen in the 2DES spectra in Fig 1. Angle-resolved 2DES experiments will be reported at the meeting that address open questions. A more quantitative analysis using a more refined model is currently underway. In summary, we use 2DES with 8 fs resolution to investigate a hybrid WS2/plasmon structure. Hybridization of the plasmon with the semiconductor exciton results in a giant enhancement of the optical nonlinearity. In essence, the nonlinearity of the weakly absorbing and atomically thin WS2 monolayer can be enhanced via coupling to a linear harmonic oscillator - the SPP mode - with large oscillator strength. The transfer of excitonic Pauli blocking and many-body effects to the hybrid system results in strongly interacting bright and highly nonlinear polaritons. Our findings highlight the importance of two-quantum states and many-body interactions in for the nonlinearities of hybrid light-matter systems based on TMDC monolayers. They are therefore and is likely of similar relevance for strongly coupled hybrid semiconductor exciton based quantum materials in general.

References
[1] G. Wang, A. Chernikov. M. M. Glazov. T. F. Heinz. X. Marie. T. Amand, B. Urbaszek, *Review of Modern Physics* **90**, 021001 (2018)
[2] C. Trovatello, F. Katsch, Q. Li, X. Zhu, A. Knorr, G. Cerullo, S. Dal Conte, *Nano Lett*ers **22,** 5322 (2022).
[3] P. Törmä, W. L. Barnes, *Reports on Progress in Physics* **78**, 013901 (2014).
[4] D. Timmer, M. Gittinger, T. Quenzel, S. Stephan, Y. Zhang, M. F. Schumacher, A. Lützen, M. Silies, S. Tretiak, J .- H. Zhong, A. De Sio C. Lienau, *Nature Communications* **14**, 8035 (2023).
[5] Y. Tang , Y. Zhang, Q. Liu, K. Wei, X. Cheng, L. Shi, T. Jiang, *Light Science and Applications* **11**, 94 (2022).
[6] D. Timmer, A. Frederiksen, D. C. Lünemann, A. R. Thomas, J. Xu, R.Bartölke, J. Schmidt, T. Kubař, A. De Sio,I. A. Solov'yov, H. Mouritsen C. Lienau, *Nano Letters* 24, 8117 (2024).
[7] D. Timmer, D. C. Lünemann, M. Gittinger,A. De Sio,C. Manzoni,G. Cerullo,C. Lienau, *Optica* **11**, 1646 (2014).

Non-reciprocal phase transitions in correlated matter

R.Belyansky[1], X.Huang[1], R. Hanai[2], S. Liu[1], J. Jachinowski[1], C. Weis[1], A. Clerk[1], P. Littlewood[1]

[1]*University of Chicago, Chicago, IL 60637, USA*
[2]*Institute of Science Tokyo, Tokyo, 52-8551, Japan*

Driven dissipative light-matter-coupled systems such as polariton condensates and lasers possess non-equilibrium steady states that show similarities to thermodynamically ordered phases with corresponding broken symmetries. However, as non-equilibrium dynamical systems they also can exhibit states with dynamical order (e.g. limit cycles, pattern formation) that cannot exist as ground states in a thermodynamic system. Transitions between different stationary states emerge via dynamical instabilities, and one novelty of non-equilibrium systems is the existence of transitions marked by critical exceptional points, where two (or more) collective modes merge with identical eigenvalues and eigenvectors. These states can in principle exist as steady states of a pumped system, but they are also evidenced by ultrafast probes that occur on a time scale faster than the thermalization time. Such phenomena are generic for multicomponent non-Hermitian (and non-reciprocal) states and there is a ready classification for both classical and quantum active systems at the mean field level [1].An example is shown in Fig [1] for a model of two species with non-reciprocal interactions. Beyond mean field, these transitions are described by new universality classes as shown in the right panel of the figure [2].
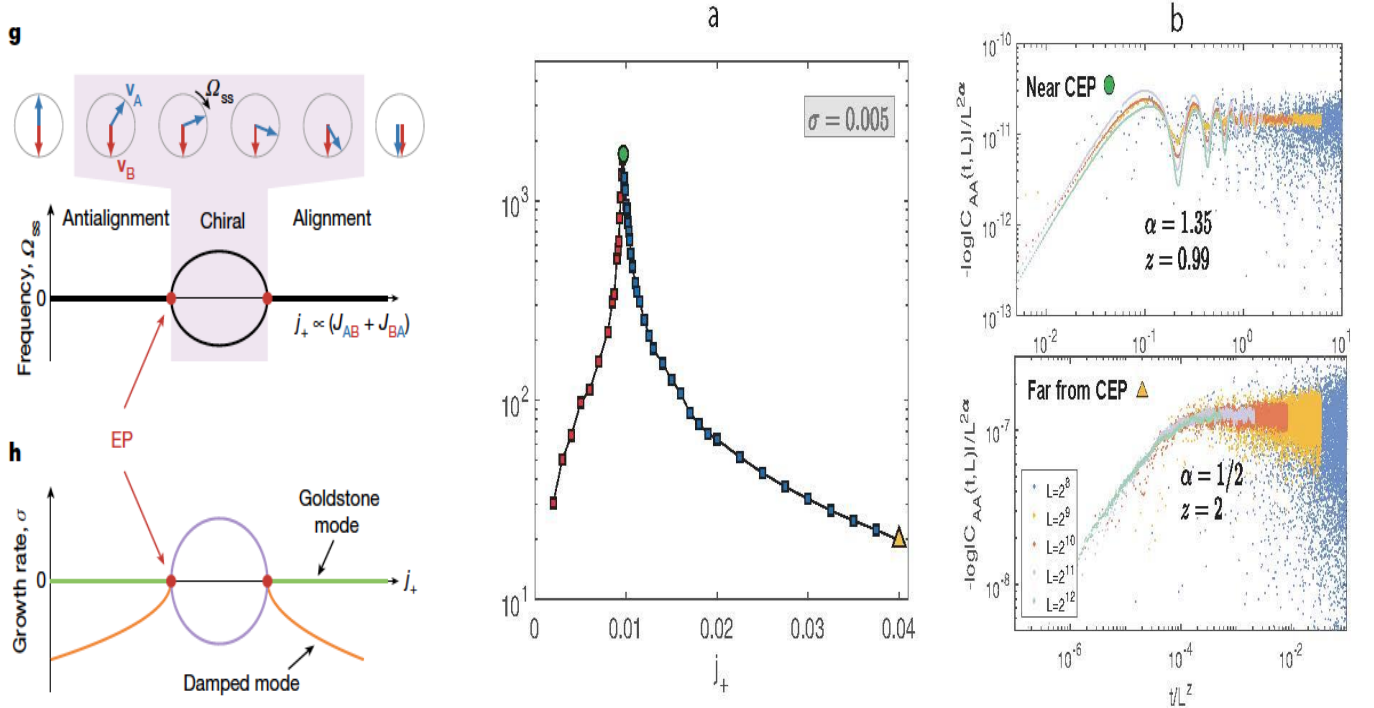
Fig. 1. Left. Schematic diagram to show the transition between two stationary phases via a chiral phase with broken symmetry [1]. Right.. Finite size scaling behavior of the correlation function of the order parameter under weak noise of a one-dimensional model. Long range order is destroyed by the noise, as expected, but the fluctuations near the CEP are much larger than away from the CEP, which shows conventional scaling of a diffusive model. [2]

There is an opportunity to construct explicitly 'active' quantum matter by building non-reciprocal terms into an effective equation of motion, as in the non-reciprocal Dicke model [3] and driven quantum chains [4].

References
[1] M. Fruchart, R. Hanai. P. B. Littlewood , V. Vitelli, *Nature* **592**, 363 (2021).
[2] S Liu , R Hanai, P. B. Littlewood, *arXiv:2503.14384* (2025).
[3] E. I. Rodr´ıguez Chiacchio, A.Nunnenkamp, M. Brunelli, *Physics Review Letters* **131**, 113602 (2023)
[4] R Belyansky, C Weis, R. Hanai, P.B. Littlewood, A.A. Clerk, *arXiv:2502.05267* (2025).

Nanoscale IR and THz dynamics of polaritons in Low-dimensional materials

M. Liu

State University of New York Stony Brook, Stony Brook, NY 11794, USA

In contemporary condensed matter physics and photonics, four key length scales play an essential role in shaping the behavior of quantum materials: *1)* the polaritonic wavelength (λ) in the infrared (IR) and terahertz (THz) frequency range, which governs light confinement and light-matter interactions; *2)* the magnetic lengths $l_B = \sqrt{\hbar/eB} = 257\text{Å}/\sqrt{B[T]}$ determined by the magnetic field B, which constrains electron motion; *3)* the diffusion length D of the hot carriers at interfaces and the edges, which dictates energy relaxation, and *4)* the periodicities of superlattices induced by moiré engineering, which defines the energy scale of emerging quantum phases. In this talk, I will present cutting-edge optical nanoscopy experiments capable of simultaneously probing all four critical length scales in a single experiment. Using a combination of terahertz scattering-type scanning near-field optical microscopy[1] (THz s-SNOM) and infrared near-field photocurrent imaging[2, 3], we report spatially resolved THz dynamics and hot carrier diffusion in 2D materials at the nanoscale (Fig.1). We find that the substrate-induced charge gradient leads to spontaneous phase separation[4] of the two-dimensional electron gas (2DEG) in a magnetic field, forming compressible regions with different Landau level occupations. The edges between these regions constitute wide, tunable incompressible quantum Hall stripes, which can be manipulated in real space by adjusting the magnetic field and gate voltage.
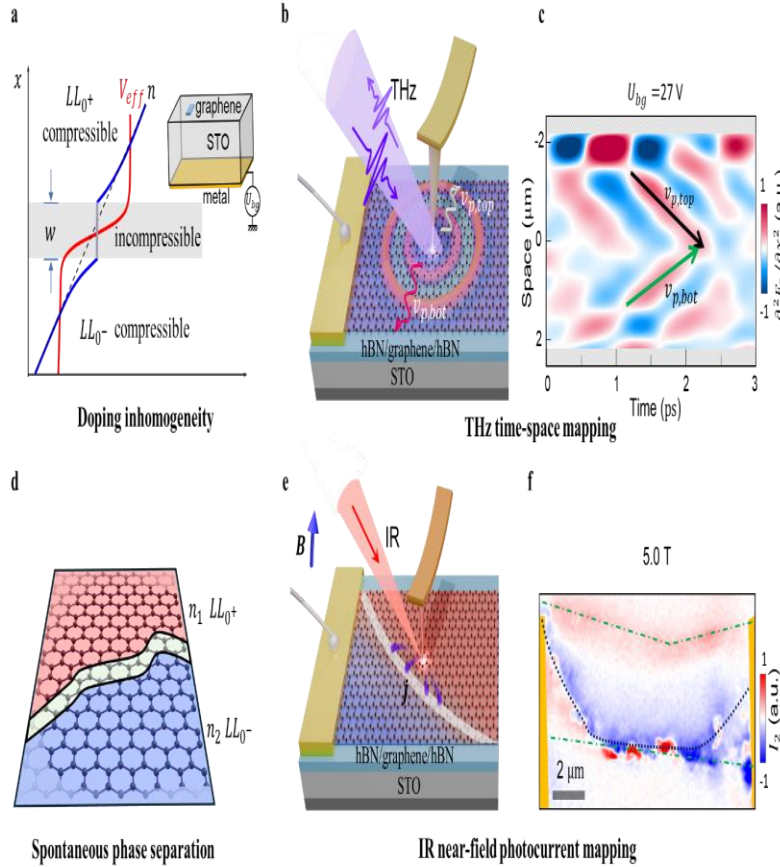
*Fig. 1 Nanoimaging of spontaneously formed compressible and incompressible phases in a gateable graphene cavity. a, carrier density n and effective electrostatic potential V_{eff} as a function of distance x. Inset shows a schematic of the graphene nanoribbon positioned off-center on a thick STO substrate; b, schematics of the nano-THz experimental setup. A monolayer graphene encapsulated with hBN resides on the high dielectric constant STO substrate and illuminated with broadband THz pluses (0.5~1.5 THz); c, THz Spacetime maps of plasmon polaritons measured across the graphene ribbon when applying back-gate voltages $U_{bg} = 27\,V$ at room temperature. The **arrows** mark the slopes of the polariton's world lines, which correspond to the phase velocity of polaritons; d, schematic illustration of the incompressible region in graphene with a magnetic field. When Fermi level crosses a Landau level, a compressible region is formed, separated by incompressible region **(gray area)** that emerges due to the LL energy transitions. e, The schematic illustrates the near-field photocurrent generation in graphene when illuminated with mid-infrared incident beam at wavelengths corresponding to 600 - 900 cm^{-1}; f, near-field photocurrent images of hBN-encapsulated graphene heterostructure on STO near the CNP, with frequency $\sim 840\,cm^{-1}$ and T = 25 K. The **green dash-dotted lines** outline the boundaries of graphene, and the dotted lines visualize the locations of charge inhomogeneity boundaries.*

Our approach establishes magneto IR and THz nanoscopy as a versatile platform for investigating magneto-optical effects and many-body interactions with unprecedented spatial resolutions. Our preliminary results also set the stage for future spectroscopic explorations of topological and chiral photonic phenomena in complex quantum materials using low-energy photons.

References

[1] S. Xu, Y. Li, R.A. Vitalone, R. Jing, A. J. Sternbach, S.Zhang, J. Ingham, M Delor, J.W. McIver, M. Yankowitz, R. Queiroz, A.J. Mills, M.M. Fogler C. R. Dean, A.N. Pasupoathy, J. Hone, M. Liu, D.N. Basov, *Science Advances* **10**, eado5553 (2024).

[2] J. C. Song, M.S. Rudner. C.M. Marcus. L.S. Levitov. *Nano Letters* **11**, 4688 (2011).

[3] Q. Ma, R. Krishna Kumar, S.Y. Xu, F.H.L. Koppens, J.C.W. Song, *Nature Review Physics* **5**, 170 (2023).

[4] D. B. Chklovskii, B.I. Shklovskii, L.I Glazman, *Physical Review* B **46**, 4026 (1992).

Attosecond electron dynamics in atomic-scale Lightwave-scanning tunneling microscopy

S. Maier[1], R. Spachtholz[1], K. Glöckl[1], C. Bustamante[2], M. Maczejka[1]
J. Schön[1], K. Pürckhauer[1], F. Gießibl[1], F. Bonafé[2], M. A. Huber[1]
A. Rubio[2], J. Repp[1], R. Huber[1]

[1]*Universität Regensburg, 93040 Regensburg, Germany*
[2]*Max-Planck-Institut für Struktur und Dynamik der Materie, 22761 Hamburg, Germany*

Understanding and controlling ultrafast dynamics in quantum materials in real space is essential for both fundamental research and future technologies. Lightwave-driven scanning tunneling microscopy enables atomic-scale slow-motion imaging of molecular orbitals and defect states with intrinsic spatio-temporal resolution [1, 2, 3, 4]. In this technique, the oscillating carrier field of terahertz pulses replaces the conventional DC bias voltage across the tip-sample junction. However, the current time resolution of approximately 100 fs remains insufficient to resolve the dynamics of intra-atomic electron motion. This requires a single-digit fs or even attosecond time resolution, calling to push the time resolution of lightwave-driven tunneling microscopy. Yet, simply scaling the carrier wave frequency by two orders of magnitude presents fundamental challenges: First, it is a priori unclear whether quasi-adiabatic sub-cycle field-controlled tunnelling is still possible as multi-photon excitation processes and photon-mediated tunnelling become increasingly likely.Literature on field-driven sub-fs charge transfer in nanostructures and attosecond field emission from metallic tips clearly proves that single-cycle pulses centered at 200 THz can act as an ultrafast bias transient [5,6]. The combination of attosecond time resolution and true atomic spatial resolution in STM has not yet been realized. Second, maintaining picometer stability in the tunneling junction is crucial in STM and becomes particularly challenging under illumination, due to the thermal load. Even subatomic variations of the tip-sample distance cause measurement artifacts. At higher carrier frequencies, the absorption coefficients of metals typically increase, therefore the problem of thermal expansion induced by fluctuations in laser power becomes more prevalent. Here, we introduce an attosecond STM concept that avoids thermal artifacts via precise waveform modulation and enables atomic resolution [7]. To this end, we derive two spectrally distinct near-infrared pulses from a femtosecond Er:fiber laser system and couple them into the STM junction (Fig. 1a).
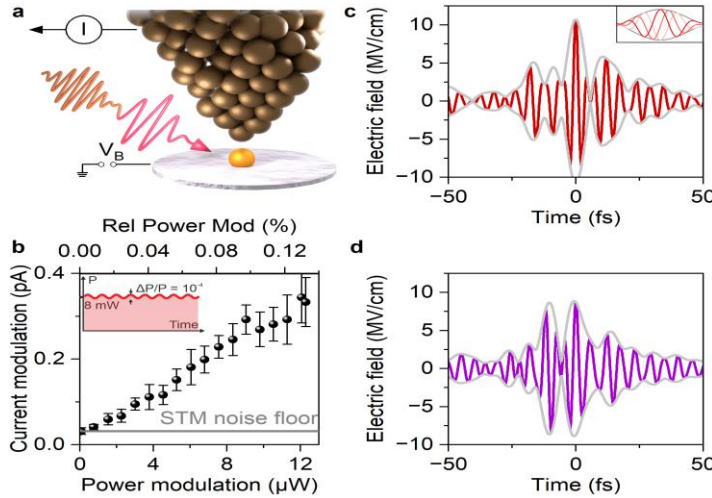
Fig. 1. Attosecond lightwave-STM. a, *Experimental setup. Two spectrally distinct NIR light pulses couple to a STM tunnel junction, inducing a CEP-dependent tunneling current I_{CEO}. **b**, Sensitivity of the STM junction to laser power modulations: The laser power on the junction is modulated on the microwatt-level (average power of 8.5 mW) which corresponds to a relative modulation depth of ~10^{-4} (Inset). This modulation of the thermal load induces picoampere-scale current modulations (at a set point current of 100 pA), well above the STM noise floor of 30 fA. **c**, Reconstructed single cycle waveform (FWHM = 5.2 fs) synthesized at optimal temporal overlap of the two NIR pulses, with controllable CEP (inset), corresponding to a maximum in the current (Fig. 2 a). **d**, Reconstructed electric field corresponding to a current minimum.*

We first quantify the effects of thermal expansion (Fig. 1b): even relative changes as small as 10^{-4} (~µW level) cause picoampere-scale current modulations showcasing the sensitivity of the tunneling junction to power variations. Such a thermally induced current modulation can overwhelmingly dominate the lightwave-induced signal, excluding usual modulation schemes of pump-probe spectroscopy such as beam chopping. Therefore, we refrain from modulating the optical power and solely manipulate the waveform of the bias pulses. At temporal overlap, the pulses synthesize a single-cycle waveform (Fig. 1c) [8]. The delay time t controls the exact field shape and allows to switch between symmetric (Fig. 1d) and asymmetric field envelopes (Fig. 1c). Note that t only changes the waveform and leaves the average power on the junction untouched, because the two original pulses (Fig. 1a) are spectrally disjunct. For a given delay time t, we periodically vary the carrier-envelope phase (CEP) at a modulation frequency $f_{CEO} = 917$ Hz. Tracing the fraction of the tunneling current demodulated at f_{CEO} shows a strong

dependence on t, i.e. on the synthesized waveform (Fig. 2a). I_{CEO} occurs only when the two pulses overlap in time, is maximal for asymmetric waveforms (Fig. 1c) and decreases for more symmetric field transients (Fig. 1d), confirming its sensitivity to the field direction. Most remarkably, the light-induced current exhibits pronounced sub-cycle features (Fig. 2a) indicating field-driven charge transfer processes on attosecond timescales. Crucially, this field-resolved response is not driven by a modulation of the optical power. The sub-cycle signatures agree with TDDFT simulations (Fig. 2b), which reveal ultrafast redistribution of electrons in tip and sample: states below the Fermi level are depleted, while those above are populated, forming a non-thermal distribution. These excited electrons, with reduced tunneling barriers and extended wavefunctions finally cross the barrier in the lightwave-driven tunneling regime – very distinct from photon-driven above threshold ionization.

This intriguing mechanism of photon-assisted lightwave-driven tunneling, bridging different regimes of light-matter interaction, calls for an assessment of its spatial resolution. To this end, we first measure the decay of I_{CEO} with tip-sample distance at $t = 0$ (Fig. 2c). At the highest tested pulse energy (171 pJ), the decay length of ~10 Å reflects contributions from extended wavefunctions. For pulse energies below 100 pJ, the decay becomes much steeper (<5 Å). To put the spatial resolution to its ultimate test, we image a single Cu adatom on Ag(111) with attosecond currents (Fig. 2d). The measurement shows clear atomic contrast, and a line profile confirms lateral confinement of I_{CEO}, demonstrating that attosecond tunneling can sustain atomic-resolution imaging.
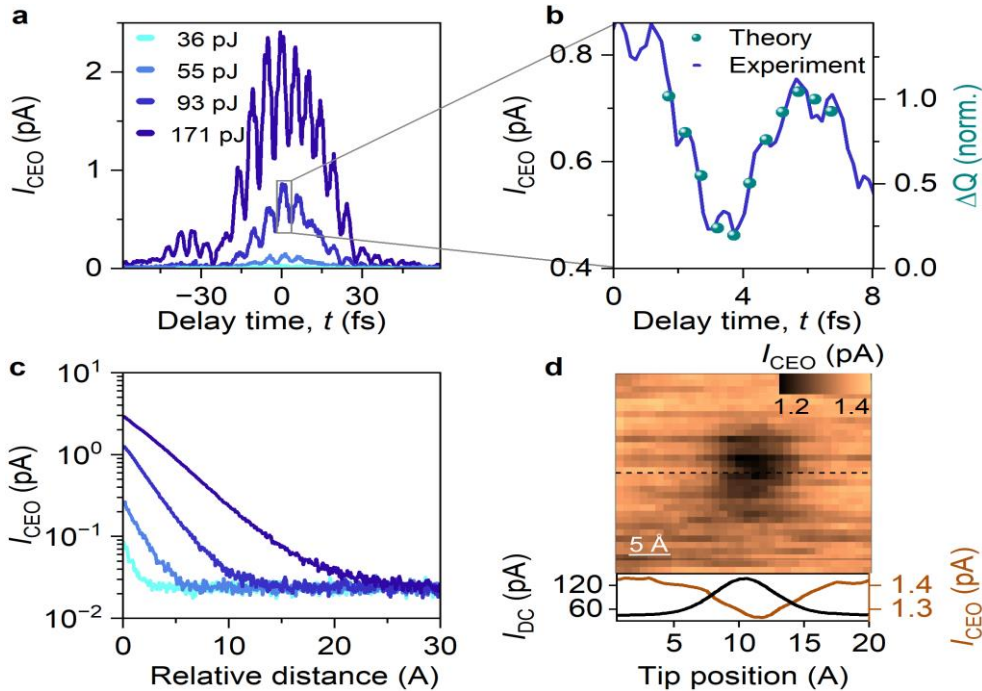
Fig. 2. Atomically resolved sub-cycle currents. a, *CEP modulated tunneling current as a function of delay time for different pulse energies (dark blue to light blue).* **b,** *TDDFT simulations confirm that such sub-cycle signatures are to be expected for lightwave-driven electron dynamics in a tip-sample junction.* **c,** *Retraction curves of I_{CEO} for different pulse energies. Below 100 pJ we find atomic confinement with a decay length of ~5 Å.* **d,** *Map of the lightwave-induced tunneling current on a single Cu adatom on Ag (111), showing atomic resolution. Below: line cut through* **d** *(dashed line) proving similar widths for DC and lightwave-modulated currents.*

In summary, we achieve attosecond STM at atomic resolution with waveform-controlled near-infrared bias pulses. Using two-color pulse synthesis of CEP controlled waveforms makes instantaneous electric field effects accessible and keeps the thermal load on the junction constant, avoiding thermal artifacts. Our measurements and simulations reveal sub-cycle tunneling of an excited non-thermal electron distribution with reduced barrier height. Imaging of individual Cu adatoms confirms atomic spatial resolution, comparable to conventional STM. Our results pave the way for attosecond STM to enable real-time studies of ultrafast electron dynamics with atomic spatial and sub-fs temporal precision.

References
[1] T. L. Cocker, D. Peller, P. Yu, J. Repp, R. Huber, *Nature* **539**, 263 (2016).
[2] D. Peller, L. Z. Kastner, T. Buchner, C. Roelcke, F. Albrecht, N. Moll, R. Huber, J. Repp, *Nature* **585**, 58 (2020).
[3] D. Peller, C. Roelcke, L. Z. Kastner, T. Buchner, A. Neef, J. Hayes, F. Bonafé, D. Sidler, M. Ruggenthaler, A. Rubio, R. Huber, J. Repp *Nature Photonics* **15**, 143 (2021).
[4] C. Roelcke, L. Z. Kastner, M. Graml, A. Biereder, J. Wilhelm, J. Repp, R. Huber, Y. A. Gerasimenko, *Nature Photonics* **18**, 595 (2024).
[5] P. Dienstbier, L. Seiffert, T. Paschen, A. Liehl, A. Leitenstorfer, T. Fennel, P. Hommelhoff, *Nature* **616**, 702 (2023).
[6] T. Rybka, M. Ludwig, M. F. Schmalz, V. Knittel, D. Brida, A. Leitenstorfer, *Nature Photonics* **10**, 667 (2016).
[7] S. Maier, *to be sumitted* (2025).
[8] G. Krauss, S. Lohss, T. Hanke, A. Sell, S. Eggert, R. Huber, A. Leitenstorfer, *Nature Photonics* **4**, 33 (2010).

Recent progress on Higgs spectroscopy of superconductors

D. Manske

Max Planck Institute for Solid State Research, 70569 Stuttgart, Germany

Higgs spectroscopy is a new and emergent field [1,2,3] that allows to classify and determine the superconducting order parameter by means of ultra-fast optical spectroscopy. There are two ways to activate the Higgs mode in superconductors, namely a single-cycle 'quench' or an adiabatic, multicycle 'drive' pulse, both illustrated in Figure 1. In the talk I will review and report on the latest progress on Higgs spectroscopy, in particular on the role of the third-harmonic-generation (THG) [4,5,6] and the possible IR-activation of the Higgs mode by impurities or external dc current [7,8]. I also provide new predictions for time-resolved ARPES experiments in which, after a quench, a continuum of Higgs mode is observable and a phase information of the superconducting gap function would be possible to extract [9]. As a recent milestone, I discuss recent results on Non-Equilibrium Anti-Stokes Raman Scattering (NEARS) [10] and on two-dimensional coherent spectroscopy [11] where the Higgs mode has been observed experimentally.
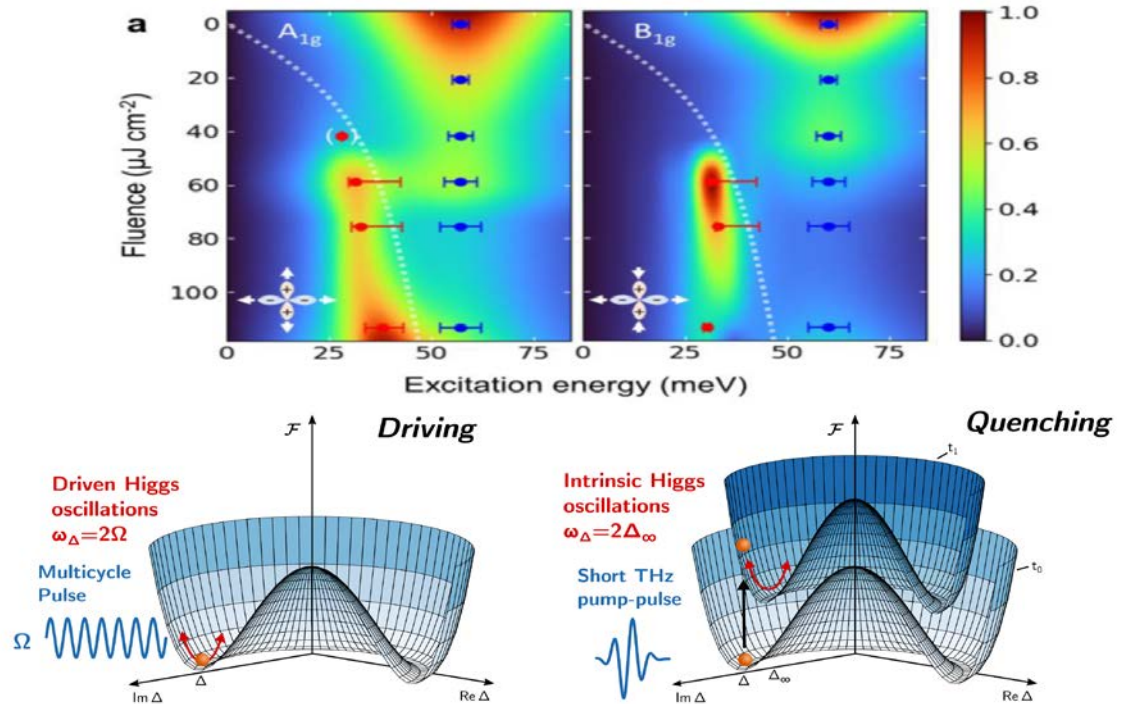
Fig. 1. ***Top panel*** *Higgs mode in the NEARS spectrum of optimally doped BISSCO for A_{1g} and B_{1g} polarization, respectively. Taken from [10.]* ***Bottom panel:*** *two ways for activation of the Higgs mode by light* ***(left)*** *Illustration of multi-cycle driving the Higgs mode: (**right**): Illustration of single-cycle quenching of the free energy potential.*

Finally, we have extended our approach to time-reversal superconductors [12] and find a variety of new possible Higgs modes.

References
[1] L. Schwarz, B. Fauseweh, N. Tsuji, N. Cheng, N. Bittner, H. Krull, M. Berciu, G. S. Uhrig, A. P. Schnyder, S. Kaiser, D. Manske, *Nature Communicatons* **11**, 287 (2020).
[2] L. Schwarz, D. Manske, *Physical Review* B **101**, 184519 (2020).
[3] H. Chu, M.- J. Kim, K. Katsumi, S. Kovalev, R. D. Dawson, L. Schwarz, N. Yoshikawa, G. Kim, D. Putzky, Z. Z. Li, H. Raffy, S. Germanskiy J.-C. Deinert, N. Awari, I. Ilyakov, B. Green, M. Chen, M. Bawatna, G. Cristiani, G. Logvenov, Y.Gallais, A. V. Boris, B. Keimer, A.P. Schnyder D. Manske, M. Gensch, Z.Wang, R. Shimano, S. KaiserS, Nature Communications **11**, 1793 (2020).
[4] L. Schwarz. R. Haenel, D. Manske, *Physical Review* B **104**, 174508 (2021).
[5] H. Chu, S. Kovalev, Z. X. Wang, L. Schwarz, T. Dong, L. Feng, R. Haenel, M.- J. Kim, P. Shabestari, L. P. Hoang, K. Honasoge, R. D. Dawson D. Putzky, G. Kim, M. Puviani, M. Chen, N. Awari, A. N. Ponomaryov, I. Ilyakov, M. Bluschke, F. Boschini, M. Zonno, S. Zhdanovich, M.X. Na G. Christiani , G. Logvenov, D. J. Jones, A. Damascelli, M. Minola, B. Keimer, D. Manske, N. Wang, J.- C. Deinert, S. Kaiser, *Nature Communications* **14**, 1343 (2023).
[6] M- J. Kim, S. Kovalev, M. Udina, R. Haenel, G. Kim, M. Puviani, G. Cristiani, I. Ilyakov, T. V. A. G. de Oliveira, A. Ponomaryov, J.- C. Deinert G. Logvenov, B. Keimer , D. Manske, L.Benfatto, S. Kaiser, *Science Advances* **10**, 3adi7598 (2024).
[7] M. Puviani, L. Schwarz, X.-X. Zhang, S. Kaiser, D. Manske, *Physical Review* B **101**, 220507 (2020).
[8] R. Haenel, P. Froese, D. Manske, L. Schwarz, *Physical Review* B **104**, 134504 (2021).
[9] L. Schwarz, B. Fauseweh, D. Manske, *Physical Review* B **101**, 224510 (2020).
[10] T. Glier, D. Manske, *to be published, Nature Communications* **16** (2025).
[11]M. Puviani, R. Haenel, D. Manske, *Physical Review* B **107**, 094501 (2023).
[12] S. Neri, W. Metzner, D. Manske, *arXiv 2503.0890* (2025).

Dynamics and control of non-equilibrium quantum systems

I. Marvian

Duke University, Durham, NC 27708, USA

In this talk, I will present an overview of an ongoing theoretical and experimental project aimed at understanding the dynamics and control of quantum systems evolving under Hamiltonians that respect a global symmetry. We approach this problem from both the perspective of continuous-time Hamiltonian dynamics and the discrete framework of quantum circuits. Recent studies have shown that, in the presence of symmetries, the locality of interactions can severely restrict the set of realizable unitaries [1-4]. In particular, generic symmetric unitaries on a composite system cannot be implemented, even approximately, using local symmetric unitaries on the subsystems [1]. This has motivated the design of new types of experiments [5] intended to probe the locality of interactions in quantum systems (see Fig. 1).
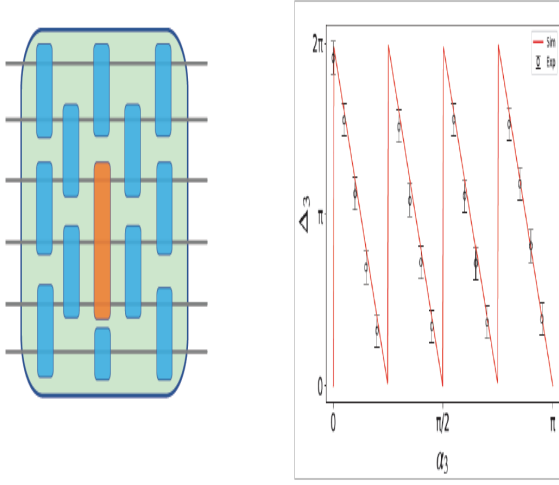
Fig. 1. Learning 3-body interactions. The recent n-go theorem of [1] revealed that, in the presence of symmetries, it is possible to directly detect 3-qubit unitaries (interactions) without any prior knowledge of existing 2-qubit unitaries. In the recent follow-up work [3], which focuses on U(1) symmetry, we showed how this detection can be achieved efficiently, without requiring full process tomography, by probing a subspace whose dimension scales linearly with the number of qubits. This scheme was experimentally demonstrated on a trapped-ion quantum computer. This experiment measures a phase, denoted as $\Delta_3 = \theta_{n-1} - \theta_1 - (n-2) \times (\theta_n - \theta_0)$ (mod 2π), where n is the number of qubits and θ_m is the phase of the determinant of the unitary in the sector with m excitations (Hamming weight m). This phase is insensitive to 2-qubit U(1)-invariant unitaries and enables the direct detection of 3-qubit unitaries. For instance, in a circuit of the form shown in the figure on the left, which includes an arbitrary number of qubits and a single 3-qubit unitary $exp(-i\alpha_3 Z^{\otimes 3})$ along with arbitrary unknown 2-qubit U(1)-invariant unitaries, we find $\Delta_3 = -8\alpha_3$ (mod 2π), as experimentally verified in the plot on the right (see[3] for details)

Interestingly, the nature of these restrictions depends significantly on the properties of the symmetry. As an example, we show that when a system evolves under Hamiltonians consisting only of two-body interactions that respect an SU(d) symmetry with d>2, the dynamics within certain subspaces can be mapped to those of a free fermionic system. This mapping leads to new conservation laws that impose strong restrictions on the system's dynamics (See Fig. 2).
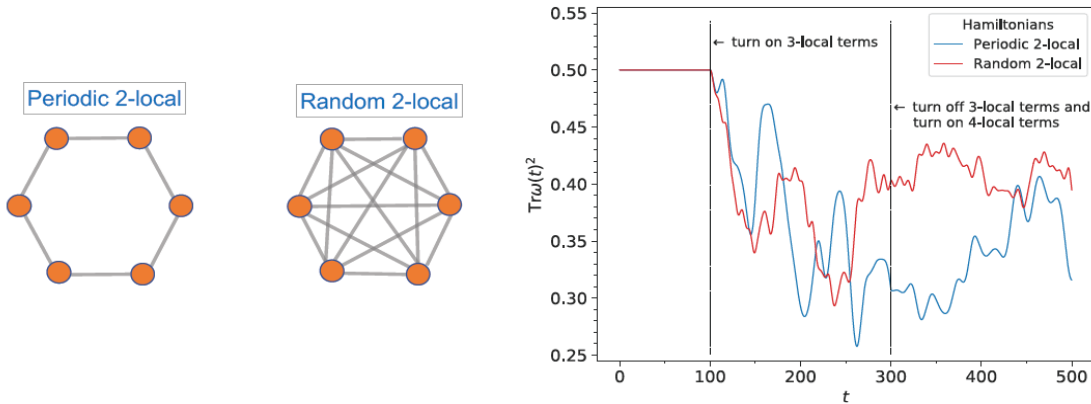
Fig. 2: An example of new conservation laws imposed by locality and symmetry: In [2], we introduced new conservation laws for qudit systems that evolve under 2-qudit SU(d)- invariant Hamiltonians. A family of such conservation laws is found by mapping the dynamics in certain irreducible invariant subspaces of qudits to the dynamics of free fermionic systems. In this example, we consider 6 qutrits with the total Hilbert space $(C^3)^{\otimes 6}$ in an initial state that is restricted to a sector with one irreducible representation of SU(3). From t = 0 to t = 100, they evolve under periodic 2-body SU(3)-invariant interactions (blue curve) and random all-to-all 2-body SU(3)-invariant interactions (red curve). We observe that the function under considerationremains conserved. At t = 100, we turn on a 3-body interaction that respects the symmetry, causing the function to start changing. Then, at t = 300, we turn off the 3-body interaction and introduce a 4-body interaction that also respects the symmetry, and again observe that the function is not conserved.

For instance, one consequence is that random circuits composed of SU(d)-invariant gates do not form approximate 2-designs for the Haar measure over the group of all SU(d)-invariant unitaries. Furthermore, I will discuss novel techniques [7] for synthesizing U(1)-invariant quantum circuits, focusing in particular on constructions based on XY interactions (see Fig. 3).
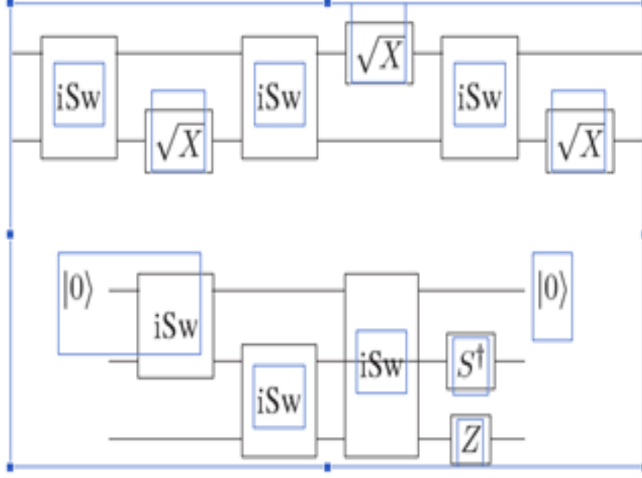
Fig. 3. SWAP via XY interaction. A SWAP gate exchanges the states of a pair of qubits and is one of the most commonly used operations in quantum computing. The top circuit is the standard way [5] of implementing this gate using three iSWAP = exp(iRπ/2) gates, where R = (X ⊗ X + Y ⊗ Y)/2 is the XY interaction, which is the native X gates, which are not interaction in some platforms, such as superconducting qubits. This circuit requires three three √X gates, which break the U(1) symmetry. We show that although SWAP is U(1)-invariant, unless one uses ancilla qubits, it can not be realized with XY interaction and U(1)-invariant single-qubit gates [1, 6]. The bottom circuit introduced in [6] realizes SWAP using three iSWAP gates, together with two U(1)-invariant single-qubit gates, namely S† and Z, and one ancillary qubit. The absence of symmetry-breaking unitary transformations makes the bottom circuit more resilient against certain types of noise, such as fluctuations in the master clock that controls the timing of pulses

References
[1] I. Marvian, *Nature Physics* **18**, 283 (2022).
[2] I. Marvian, H. Liu, A. Hulse, *Physical Review Letters* **132**, 130201 (2024).
[3] I. Marvian, H. Liu, A. Hulse, *arXiv:2105.12877* (2021).
[4] I. Marvian, *Physical Review Research* **6**, 043292 (2024).
[5] L. A. Zhukas, Q. Wang, O. Katz, C. Monroe, I. Marvian, *arXiv:2408.10475* (2024).
[6] N. Schuch, J. Siewert, *Physical Review* A, **67**, 032301 (2003).
[7] G. Bai, I. Marvian, *arxiv:2309.1105*1 (2024).

Floquet topological insulator

W. Li[1], D. M. B. Lesko[1], T. Weitz[1], O. Neufeld[2], P. Hommelhoff[1]
[1]Friedrich-Alexander-Universität Erlangen-Nürnber, 91054 Erlangen, Germany
[2]Technion, 3200003 Haifa, Israel

Light-dressed materials, based on Floquet engineering, offer unique opportunities to design transient band structures with quantum and topological phenomena from trivial materials [1]. Graphene, a topologically trivial semimetal, becomes a Floquet topological insulator (FTI) when dressed with a circularly polarized laser field, due to the broken time reversal symmetry [2,3,4]. While Floquet physics has been shown to exist on an ultrafast timescale [5,6,7], the control of Floquet engineered topological properties has not been demonstrated on a similar timescale. We will report on our ongoing experiment along these lines. While Floquet physics has been shown to exist on an ultrafast timescale [5,6,7], the control of Floquet engineered topological properties has not been demonstrated on a similar timescale. We will report on our ongoing experiment along these lines.

Fig. 1. Epitaxial graphene sample attached to gold electrodes, from where the photocurrent is measured.

References
[1] M. S. Rudner, N. H. Lindner, *Nature Reviews Physics* **2**, 229 (2020).
[2] T. Oka, H. Aoki, *Physical Review* B **79**, 169901 (2009).
[3] J. McIver, B. Schulte, F. Stein, T. Matsuyama, G. Jotzu, G. Meier, A. Cavalleri, *Nature Physics* **16**, 38 (2020).
[4] D. M. B. Lesko, T. Weitz, S. Wittigschlager, W. Li, C. Heide, O. Neufeld, P. Hommelhoff, *arXiv:2407.17917v2* (2025).
[5] J. Reimann, S. Schlauderer, C. P. Schmid, F. Langer , S. Baierl, K. A. Kokh, O. E. Tereshchenko, A. Kimura, C. Lange, J. Güdde, U. Höfer
      R. Huber, *Nature* **562**, 396 (2018).
[6] S. Ito, M. Schüler, M. Meierhofer, S. Schlauderer, J. Freudenstein, J. Reimann, D. Afanasiev, K. A. Kokh, O. E. Tereshchenko , J. Güdde
      M. A. Sentef, U. Höfer, R. Huber, *Nature* **616**, 696 (2023).
[7] J. Shan, M. Ye, H. Chu, S. Lee, J. Park, L. Balents, D. Hsieh, *Nature* **600**, 235 (2021).

Theory of ultrafast nanomagnetism

J.H. Mentink

Radboud Universiteit,6525 ED Nijmegen, The Netherlands

Despite decades of downscaling of magnetic bits, magnetism at length scales below ~10 nanometer and time scales below ~1 nanosecond is a poorly understood regime. This regime of "ultrafast nanomagnetism" is only recently becoming accessible experimentally thanks to new magnetic imaging methods based on femtosecond x-ray and electron pulses. Interestingly, results obtained with such experimental techniques [1,2,3] disclose counter-intuitive results for which established theories do not provide an adequate explanation. In this talk, we review recent progress in ultrafast nanomagnetism from the perspective of theory and simulations. We showcase examples where atomistic spin models greatly assisted in corroborating key experimental observations concerning the ultrafast nucleation of skyrmions in ferromagnetic multilayers. For example, it was found that the nucleation proceeds by transiently passing through a topological fluctuations state, leading to picosecond nucleation times, much faster than accessible with external fields [1]. To obtain a more intuitive understanding of the fluctuations and predict general trends for dependencies on external field and temperature, we developed an effective phenomenological theory [4]. This theory is derived from the observation that on ultrafast timescales the skyrmion position $\mathbf{X}$~const, since motion of spin textures in space is bound by the highest magnon group velocity. Therefore, in the ultrafast regime, illustrated in Figure 1, skyrmions are essentially localized in space and their dynamics can occur only due to nucleation or annihilation by thermal activation over energy barriers. We show that evaluating these two processes during a heat pulse shows good agreement with atomistic spin dynamics simulations and experiments. Since on short time scales there is no time for the skyrmions to interact, the skyrmions can be treated independently to very good approximation, resulting in a remarkably simple and computationally efficient theory.
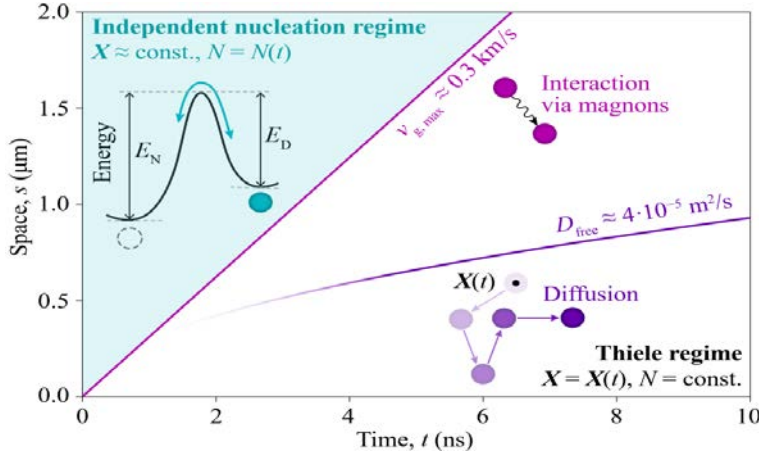
Fig 1. Space-time diagram of skyrmion dynamics. Slow dynamics results changes in the position $X(t)$ governed by the Thiele equation and preserves the skyrmion number N. Long-range interactions between skyrmions are limited by the maximum group velocity $v_{g,max}$ of the magnons that can efficiently scatter with skyrmions. Outside of the magnon "light cone", ultrafast dynamics occurs where the positions $X \approx$ const. and nucleation/decay events and a dynamic N(t).

The theory furthermore provides a direct guide for experimentally optimizing the number of nucleated skyrmions by tuning magnetic field and heat dissipation and even predicts a novel pathway for ultrafast annihilation of skyrmions, which is confirmed with atomistic simulations. Moreover, we show that our theory can be applied as well beyond non-interacting skyrmions, including laser-induced generation of skyrmion lattices as well as the nucleation and helicity-dependent control of stochastic domain structures [2]. Moreover, we show that the same analysis can be applied to domain-wall dynamics during ultrafast demagnetization, displaying a counter-intuitive stability in the low fluence regime [3]. The systematic approach combining simulations and phenomenological theory provides a new path to the development of a general theory of ultrafast nano-magnetism. This has not only great relevance to stimulate and support experiments but is also capable of identifying conceptually new pathways to challenge the limits for the fastest, smallest and most energy-efficient writing of magnetic bits.

References
[1] F. Büttner, B. Pfau, M. Böttcher, M. Schneider, G. Mercurio, C. M. Günther, P. Hessing, C. Klose, A. Wittmann, K. Gerlinger, L.- M. Kern C. Strüber, C. von Korff Schmising, J. Fuchs, D. Engel, A.Churikova, S. Huang, D. Suzuki, I. Lemesh, M. Huang, L. Caretta, D. Weder, J. H. Gaida M. Möller, T. R. Harvey, S. Zayko, K. Bagschik, R. Carley, L. Mercadier, J. Schlappa, A. Yaroslavtsev, L. Le Guyarder, N. Gerasimova, A. Scherz C. Deiter, R. Gort, D. Hickin, J. Zhu, M. Turcato, D. Lomidze, F. Erdinger, A. Castoldi, S. Maffessanti, M. Porro, A. Samartsev, J. Sinova C. Ropers, J. H. Mentink, B. Dupé, G. S. D. Beach, S. Eisebitt, *Nature Materials* **20**, 30 (2021).
[2] D. Khusyainov, R. Liefferink, M. X. Na, K. Fabian, R. Frömter, M. Kläui, D. Kozodaev, N. Vovk, R. Mikhaylovskiy, D. Afanasiev, A. Kimel J. H. Mentink, T.Rasing, *arXiv:2412.1170* (2024)
[3] H.-T. Chang, S. Zayko, T.Schmidt, O. Kfir, M.Sivis, J.H. Mentink, M. Albrecht, C. Ropers, *arXiv:2504.17917*(2025).
[4] R. Liefferink, L. Körber, K. Gerlinger, B. Pfau, F. Büttner, J.H. Mentink, *arXiv:2504.11013* (2025).

Ultrafast dynamics with surface plasmon polaritons

F.-J. Meyer zu Heringdorf

Universität Duisburg-Essen, 47048 Duisburg, Germany

The coherent coupling of surface plasmon polaritons (SPPs) to distinct electronic states in the band structure of a solid has so far only been little investigated. Experimentally, this requires (i) precise control over the SPP's electric field and (ii) electron spectroscopy on the nanoscale. Fig. 1 shows results from a measurement that satisfies both requirements. An Archimedean spiral was structured into a self-organized Au platelet using a focused ion beam (Fig. 1a). The gap-size of the spiral is one SPP wavelength ($l = 1$), i.e., if the spiral is excited by circularly polarized femtosecond laser pulses with the proper wavelength and helicity, concentric SPP phase fronts can be created that propagate to the center of the spiral to form a SPP focus. Figure 1b shows example images from a reconstruction of the electromagnetic field of the SPP using a pump-probe experiment [1] in which the polarization of pump- and probe pulses can be independently adjusted [2]. The SPP, excited by the circularly polarized pump pulse, is subsequently probed with several probe pulses of different polarization. Using Fourier-techniques, the longitudinal **E**-field vector of the SPP can be triangulated from the dataset, and its transverse component can be calculated from the divergence-free nature of the evanescent SPP field in the vacuum. At a pump-probe delay of 70 fs the (red) **E**-field vectors in the center of the top panel of Fig. 1b point away from the surface, and this central focus is surrounded by a ring where (blue) field vectors point towards the surface. Since the temporal dependence of the **E**-field vectors is known from the reconstruction, the magnetic **H**-field vectors at the bottom of Fig. 1b can be derived using the induction law. The **H**-field vectors lie within the surface plane and form closed rings of opposite orientation around the central **E**-field maximum. Both **E**- and **H**- field vectors oscillate in time.
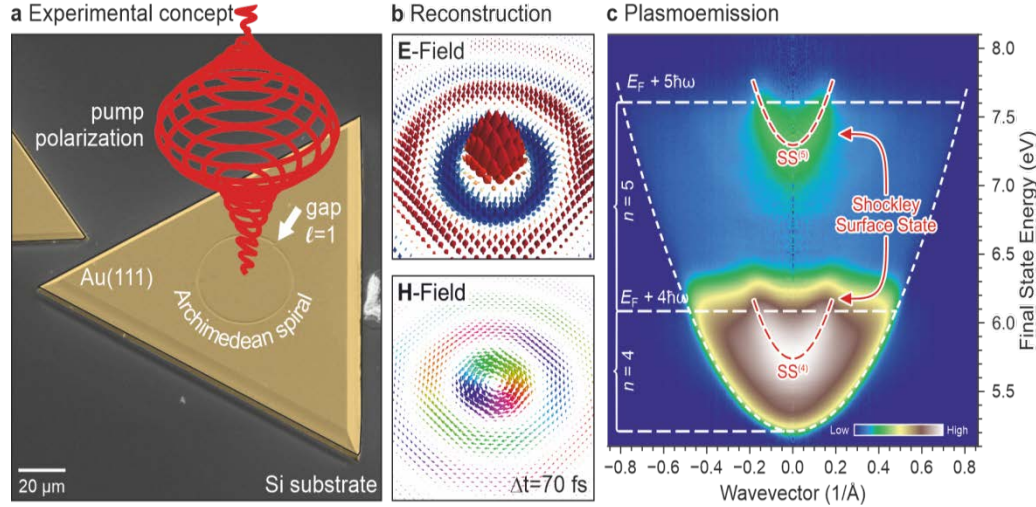
Fig. 1: (a) Sample design and excitation. (b) Electric and magnetic field vectors reconstructed from a polarimetric pump-probe experiment at a delay time of 70 fs. (c) Angle-resolved electron emission spectrum from the SPP focus.

Using optimized coupling structures, maximum SPP field strengths of >4 V/nm have been demonstrated in the center of Archimedean spirals [3]. Accordingly, electron emission from the central emission spot, shown in Fig. 1c, is expected to be highly non-linear. Since at least 4 SPP quanta with $\hbar\omega$=1.52 eV are required to overcome the work function of the clean Au(111) surface, the electron emission from the SPP focus is dominated by a 4th order process. The spectral feature at the Γ-Point that disperses parabolically to the Fermi edge represents 4th order emission from the Au Shockley surface state. All spectral features are replicated at higher final state energies, indicating the presence of 5th order emission and above-threshold ionization [4]. Since at the time of electron emission no light was present at the surface, the electron emission is unambiguously caused by the SPP – a process that was coined 'plasmoemission' to distinguish it from the well-known photoemission. The presentation will focus on the experimental measurement of the electric field and the (coherent) emission path of the electrons from the nanofocus into the vacuum.

References

[1] T. J. Davis, D. Janoschka, P. Dreher, B. Frank, F. Meyer zu Heringdorf, H. Giessen, *Science* **368**, eaba6415 (2020).

[2] P. Dreher, A. Neuhaus, D. Janoschka, A. Rödl, T. Meiler, B. Frank, T.J. Davis, H. Giessen, F. Meyer zu Heringdorf, *Advanced Photonics* **6** 66007 (2024).

[3] P. Dreher, D. Janoschka, A. Neuhaus, B. Frank, H. Giessen, M. Horn-von Hoegen, F. Meyer zu Heringdorf, *Nanophotonics* **11**, 3687 (2022)

[4] P. Dreher, D. Janoschka, B. Frank, H. Giessen, F. Meyer zu Heringdorf, *Communication Physics* **6**, 15 (2023)

Terahertz coherent magnonics in canted antiferromagnets

R. A. Leemnders[1], D. Afanasiev[2], A. V. Kimel[2], R. V. Mikhaylovskiy[1]

[1] *Lancaster University, Lancaster LA1 4YW, United Kingdom*
[2] *Radboud Universiteit,6525 ED Nijmegen, the Netherlands*

Magnonics aims to employ quanta of spin waves, magnons, to carry, transport and process information, avoiding the dissipation of energy inherent to electronics. Experiments on magnons in regular (ferro)magnets have yielded demonstrations of basic logic devices, albeit macroscopic (mm-scale) in size and operating at GHz frequencies. Recently, the spotlight has shifted towards the use of antiferromagnets, in which neighbouring spins are aligned antiparallel to each other. This alternating order leads to significantly higher spin wave propagation velocities and might enable devices operating at terahertz (trillion of hertz) clock-rates. However, the absence of the net magnetisation also makes antiferromagnets magnetically 'invisible': it is very hard to detect and influence the antiferromagnetic order. Yet, in some antiferromagnets strong spin–orbit coupling results in canting of the spins, thereby producing net magnetization. The canted antiferromagnets combine antiferromagnetic order with phenomena typical for ferromagnets and hold a great potential for spintronics and magnonics. In my talk I will discuss a new functionality of canted antiferromagnets and altermagnets for magnonics and show that these materials facilitate mechanisms allowing to generate, detect and convert propagating magnons at the nanoscale.
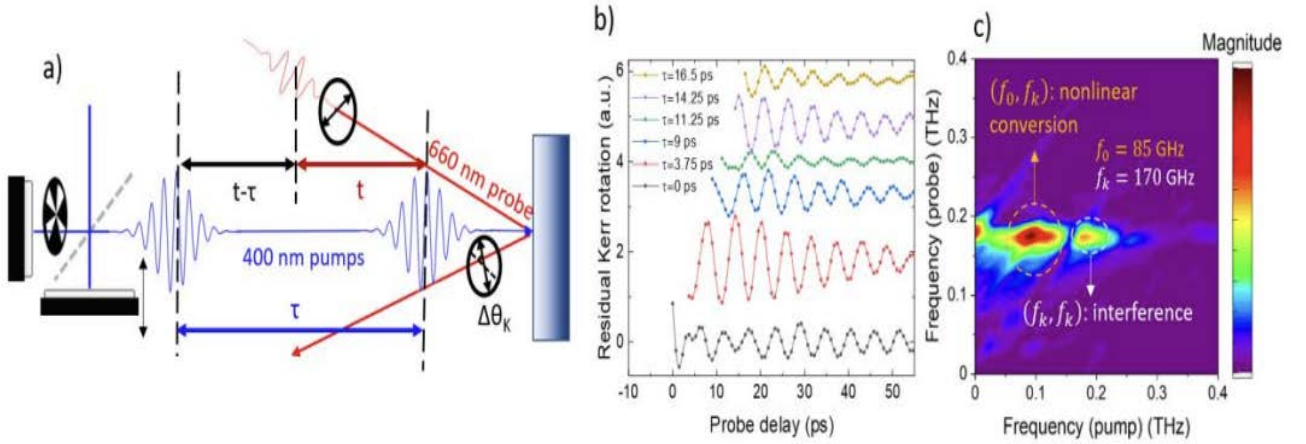
Fig. 1. a) *Experimental scheme. The spin dynamics is excited by the first 400 nm pump pulse and then controlled with a second 400 nm pump pulse. The ultrafast dynamics is probed magneto-optically, using a 660 nm pulse.* ***b)*** *Detected spin dynamics as a function of the delay τ between the two pumps.* ***c)*** *2-dimensional Fourier transfor3m of the data in* ***b).***

The breakthrough is based on using nanoscale confinement of the laser pump pulse to excite magnons, while selectively detecting them by scattering of another probe pulse [1,2]. Then we demonstrated strong nonlinear coupling between magnons and realized the ultrafast conversion of quasi-uniform spin precession into propagating magnons with higher frequencies (energies) and wavenumbers (momenta) [3]. We demonstrated suppressing or amplifying of THz propagating magnons, mimicking the operation of a transistor. To this end, we performed a double pump - probe experiment illustrated in figure 1. The first pump pulse launches spin dynamics, which are modulated and transformed by the second pump. The dynamics are probed magneto-optically, using the detection mechanism reported in [1,2]. We find that the amplitude of the detected spin wave can be controlled by the delay between the pumps (figure 1b). This amplitude modulation is intrinsically nonlinear, as we observe features at (f_k, f_k) frequencies (interference), and (f_0, f_k) frequencies (nonlinear conversion) (figure 1c), where f_k is the finite-k component of the freely propagating spin wave, and f_0 is the frequency of the uniform spin precession. Using the Lagrangian formalism for describing nonlinear spin dynamics [2], we can show that our experiment can be interpreted as conversion of the quasi-uniform spin precession to the finite-k magnon modes by a second light pulse. The converter enables ultrafast modulation of spin waves in an antiferromagnet, which is a major milestone in THz magnonics.

References
[1] J. Hortensius, D. Afanasiev, M. Matthiesen, R. Leenders, R. Citro, A.V. Kimel, R.V. Mikhaylovskiy, B. A. Ivanov, A.D. Caviglia, *Nature Physics* **17**, 1001 (2021)
[2] R. A. Leenders, R.V. Mikhaylovskiy. *Physical Review* B **107**, 094423 (2023).
[3] R .A. Leenders, D. Afanasiev, A.V. Kimel, R.V. Mikhaylovskiy. *Nature* **630**, 335 (2024).

Mid-IR Cr:ZnS/Se ultrafast lasers, power and energy amplifiers

S. Mirov

University of Alabama at Birmingham, Birmingham, AL 35233, USA

Chromium doped ZnSe and ZnS lasers have come of age due to advancements in laser design, thermal management, fabrication of low-loss polycrystalline gain media, as well as the availability of effective fiber and hybrid fiber-bulk pump lasers. Ultrafast Cr:ZnS/Se lasers attract growing attention because they provide direct access to high peak- and average-power scalable few-optical-cycle mid-IR pulses. The progress in TM:II-VI lasers has been further accelerated by the development of new methods of laser material fabrication. Specifically, the technology based on a post-grown thermal diffusion doping of ZnS and ZnSe [1] has enabled large-scale production of large-size polycrystalline gain elements with high optical quality and high dopant concentration. This, in turn, has dramatically simplified the development of ultrafast amplifiers and enabled the development of fs oscillators with unique output parameters [1-7]. The unique capabilities of polycrystalline Cr:ZnS and Cr:ZnSe for generation, amplification, and nonlinear frequency conversion of ultra-short optical pulses in the MIR range were successfully explored for the development of octave-spanning single optical cycle oscillators [5], full repetition rate MOPAs with average power above 30 W [1], and CPA multipass amplifiers with TW levels of output power [8]. Cr:ZnS combines superb ultrafast laser capabilities with broad IR transparency and high nonlinearity of wide-bandgap II-VI semiconductors. It supports all mode-locking regimes, from active to passive to Kerr-lens mode-locking. The key advantage of Cr:ZnS Kerr lens-based ultrafast laser and frequency comb technology is high efficiency: 20 – 25% optical-to-optical conversion from low-cost CW EDFL light to 2-cycle MIR pulses and 10 – 12% conversion of 2-cycle pulses at 2.4 µm to single-cycle electromagnetic transients in the longwave IR. Cr:ZnS MOPA architecture supports direct amplification of few-optical-cycle pulses at MHz repetition rates to multi-Watt levels using a simple and reliable single-pass configuration without additional pulse stretcher and compressor. Further, the system's complexity is significantly reduced because all the optical signals required for stabilizing the MIR comb with the large lever arm are generated directly inside the polycrystalline Cr:ZnS gain medium of a single-pass amplifier. One can equip the system with an additional optical rectification stage to enhance the optical power in the offset-free longwave IR spectral band. For instance, ZGP crystal allows the record-breaking efficiency of optical rectification. It generates super-octave longwave (4-12 µm) IR combs with Watt-level power [7]. Those advantages, in turn, allowed the implementation of shoe-box-sized, lightweight fs frequency combs with the brightness exceeding the brightness of a synchrotron by orders of magnitude in a broad spectral range [9].
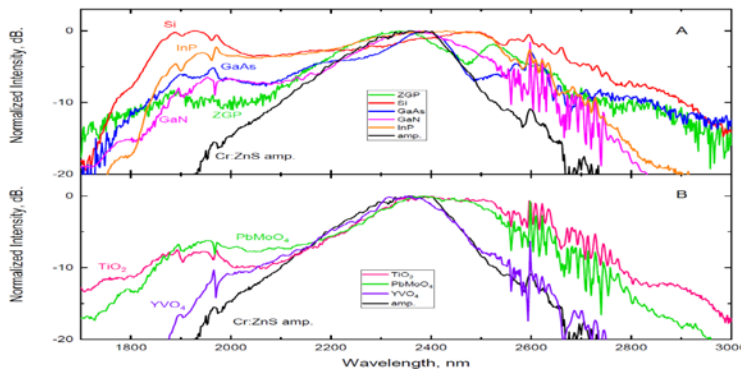
Fig. 1. Broadening of Cr:ZnS MOPA radiation in different materials: (A) semiconductors: ZGP, Si, GaAs, GaN, InP. (B) oxides: TiO_2, PbMoO4, YVO_4. [11].

The developed MIR frequency combs open new avenues in imaging, sensing, and spectroscopy [10]. Generation of supercontinuum radiation in several bulk materials, including InP, Si, GaN, GaAs, $PbMoO_4$, ZGP, YVO_4, and TiO_2, using Cr:ZnS femtosecond MOPA pump radiation will be also discussed at the conference. Some of the materials investigated, as shown in Fig. 1, have excellent potential as effective media for mid-IR supercontinuum generation, providing a robust approach to producing ultra-broadband and single-cycle pulses. In our opinion, supercontinuum generation at MHz repetition rates in bulk materials has several advantages over commonly used approaches based on integrated guided optics: versatility, simplicity of implementation, and power scalability [11]. Radiation of Cr:ZnS ultrafast master was used as a seed for a sequence of single pass Cr:ZnS and multipass Cr:ZnSe energy amplifiers pumped by radiation of nanosecond 1645 nm Er:YAG lasers (ELPN series, IPG Photonics corporation). The maximum single-pass amplification gain of ~ 2400 was demonstrated in a 3.5 cm long Cr:ZnS gain element with a chromium concentration of 9.8×10^{18} cm^{-3} under 12 mJ pump energy from Q-switched Er:YAG. As seed radiation, 6 nJ fs pulses from a femtosecond Cr:ZnS

Kerr-lens mode-locked laser operating at 1 kHz were used. The 30-fs seed pulses were not stretched other than due to the dispersion of the optical elements. The maximum output energy after single-pass amplification was measured to be 14.4 µJ. Pulses from a single pass Cr:ZnS energy amplifier stretched to 150 ps were used as a seed for a 5-pass Cr:ZnSe amplifier pumped by a 18 mJ radiation of 1645 nm Er:YAG resulting in 5 mJ output at 2350 nm. Further scaling of mid-IR Cr:ZnS/Se CPA to TW-class system will be discussed for high energy physics applications.

References
[1] S. Mirov, I. Moskalev, S. Vasilyev, V. Smolski, V. Fedorov, D. Martyshkin, J. Peppers, M. Mirov, A. Dergachev, V. Gapontsev, *IEEE Journal of Selected Topics Quantum Electronics* **24**, 1601829 (2018).
[2] S. Vasilyev, I. Moskalev, M. Mirov, S. Mirov, V. Gapontsev, *Optics Express* **24**, 1616 (2016).
[3] S. Vasilyev, M. Y. Sander, J. Gu, V. Smolski, I. Moskalev, M. Mirov, Y. Barnakov, J. Peppers, M. Kolesik, S. Mirov, V. Gapontsev, *Journal of Optical Society of America* B **38,** 1625 (2021).
[4] S. Vasilyev, V. Smolski, J. Peppers, I. Moskalev, M. Mirov, Y. Barnakov, S. Mirov, V. Gapontsev, *Optics Express* **27**, 35079 (2019).
[5] S. Vasilyev, I. Moskalev, V. Smolski, J. Peppers, M. Mirov, Y. Barnakov, V. Fedorov, D. Martyshkin, S. Mirov, V. Gapontsev, *Optics Express* **29,** 2458 (2021).
[6] S. Vasilyev, I. Moskalev, V. Smolski, J. Peppers, M. Mirov, V. Fedorov, D. Martyshkin, S. Mirov, V. Gapontsev, *Optica* **6,** 126 (2019).
[7] S. Vasilyev, I. S. Moskalev, .O. Smolski, J. M. Peppers, M. Mirov, A. V. Muraviev, K. Zawilski, P. G. Schunemann, S. B. Mirov K. L. Vodopyanov, V. P. Gapontsev, *Optica,* **6,** 111 (2019).
[8] X. Lu, X. Wang, J. Fan, R. Xu, J. Chen, L. Zhang, Y. Leng, *Optica* **10,** 1567 (2023).
[9] S. Vasilyev, M. Mirov, S. Mirov, *Laser Focus World*, 21 (2022).
[10] S. Vasilyev, A. Muraviev, D. Konnov, M. Mirov, V. Smolski, I. Moskalev, S. Mirov, K.L. Vodopyanov, *Optics Letters* **48,** 2273 (2023).
[11] R. Danilin, S. Vasilyev, D. Danilin, D. Martyshkin, V. Fedorov, S. Mirov, Proceedings of SPIE 13347, PC133470K (2025).
* *Acknowledgement:* S.M. acknowledges support from IPG Photonics Corporation, DARPA (grant W31P4Q-15-1-0008), DOE (grant DE-SC0018378) NIEHS grant (P42ES027723) and University of Rochester subcontract SUB00000793/GR534355. I would like to thank collaborators Rem Danilin, Daniil Danilin, Dmitry Martyshkin, Vladimir Fedorov (University of Alabama at Birmingham), Sergey Vasiliev (IPG Photonics Corporation), and Jeremy Pigeon (Laboratory for Laser Energetics, University of Rochester) for great input and useful discussions.

Verification of Floquet states in graphene using Ultrafast momentum microscopy

S. Mathias
Georg-August-Universität Göttingen, 37073 Göttingen, Germany

Recent advances in the field of condensed-matter physics have unlocked the potential to realize and control emergent material phases that do not exist in thermal equilibrium. One of the most powerful approaches to study such non-equilibrium phases is femtosecond time- and angle-resolved photoelectron spectroscopy. In this regard, we recently developed a combined micro-ARPES electronic structure and real-space photoelectron system that we use to access electronic and excitonic dynamics in space and time [1,2,3]. We further employ this method to test one of the most promising concepts to create light-matter coupled phases, namely Floquet engineering, which is the coherent dressing of matter via time-periodic perturbations. In this field of research, the broad applicability of Floquet engineering to quantum materials is still unclear, because, for the paradigmatic case of monolayer graphene, the theoretically predicted Floquet-induced effects have been put into question. We overcome this problem by using our advanced photoemission setup to provide direct experimental evidence of Floquet engineering in graphene. We report light-matter dressed Dirac bands by measuring the contribution of Floquet sidebands, Volkov sidebands, and their quantum path interference to graphene's photoemission spectral function [4].
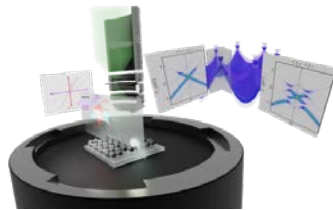
Fig. 1. Artistic scheme of Floquet engineering in graphene and its verification using time - resolved momentum microscopy

Our results finally demonstrate that Floquet engineering in graphene is possible, paving the way for the experimental realization of the many theoretical proposals on Floquet-engineered band structures and topological phases.

References
[1] D. Schmitt, J. P. Bange, W. Bennecke, A. A. Al-Mutairi, G. Meneghini, K. Watanabe, T. Taniguchi, D. Steil, D. R. Luke, R. T. Weitz, S. Steil G. S. M. Jansen, S.Brem, E.Malic,S. Hofmann, M. Reutzel, S.Mathias, *Nature* **608**, 499 (2022)
[2] J. P. Bange, D. Schmitt, W. Bennecke, G. Meneghini, A. A Al Mutairi, K. Watanabe, T. Taniguchi, D. Steil, S. Steil, R. T. Weitz, G. S. M. Jansen S. Hofmann, S. Brem, E. Malic, M. Reutzel, S. Mathias, *Science Advances* **10**, eadi1323 (2024)
[3] D. Schmitt, J. P.Bange, W. Bennecke, G. Meneghini, A. A. Al-Mutairi, M. Merboldt, J. Pöhls, K. Watanabe, T. Taniguchi, S. Steil, D. Steil R. T. Weitz, S. Hofmann, S. Brem, G. S. M. Jansen, E.Malic, S. Mathias, M. Reutzel, *Nature Photonics* **19**, 187 (2025)
[4] M. Merboldt, M. Schüler, D. Schmitt, J. P. Bange, W. Bennecke, K. Gadge, K. Pierz, H. W. Schumacher, D. Momeni, D. Steil S. R. Manmana, M.A. Sentef, M.Reutzel, S. Mathias, *Nature Physics*, accepted, (2025).

Symmetry-protected electronic metastability in an Optically-excited cuprate ladder

H. Padma[1], F.Glerean[1], S. F. R. TenHuisen[1], Z.Shen[2], H.Wang[3], L.Xu[2], J. D. Elliott[4], C. C. Homes[5]
E. Skoropata[6], H.Ueda[6], B.Liu[6], E. Paris[6],A. Romaguera[6], B. Lee[7], W. He[5], Y. Wang[8],S. H. Lee[8]
H. Choi[7], S.-Y. Park[7], Z. Mao[8], M. Calandra[9], H. Jang[7], E. Razzoli[6], M. P. M. Dean[5], Y.Wang[2], M. Mitrano[1]

[1] *Harvard University, Cambridge, MA02138, USA*
[2] *Emory University, Atlanta, GA30322, USA*
[3] *The Chinese University of Hong Kong, Hong Kong, China*
[4] *Diamond Light Source, Didcot OX11 0DE, UK*
.[5] *Brookhaven National Laboratory, Upton, NY, USA*
[6] *Paul Scherrer Institut, 5232 Villigen, Switzerland*
[7] *Pohang University of Science and Technology, Pohang, Korea*
[8] *Pennsylvania State University, University Park, PA16802, USA*
[9] *University of Trento, 38123 Povo, Italy.*

Optically excited quantum materials exhibit nonequilibrium states with remarkable emergent properties [1], but these phenomena are usually short-lived, decaying on picosecond timescales and limiting practical applications. In rare instances, photoexcited solids become trapped in metastable states due to material-specific relaxation bottlenecks [2-16]. Advancing the design and control of nonequilibrium metastable phases requires a microscopic understanding of their underlying mechanisms and the development of targeted excitation strategies. Here, we report the observation of photo-induced metastability in a prototypical one-dimensional cuprate ladder $Sr_{14}Cu_{24}O_{41}$ [17].
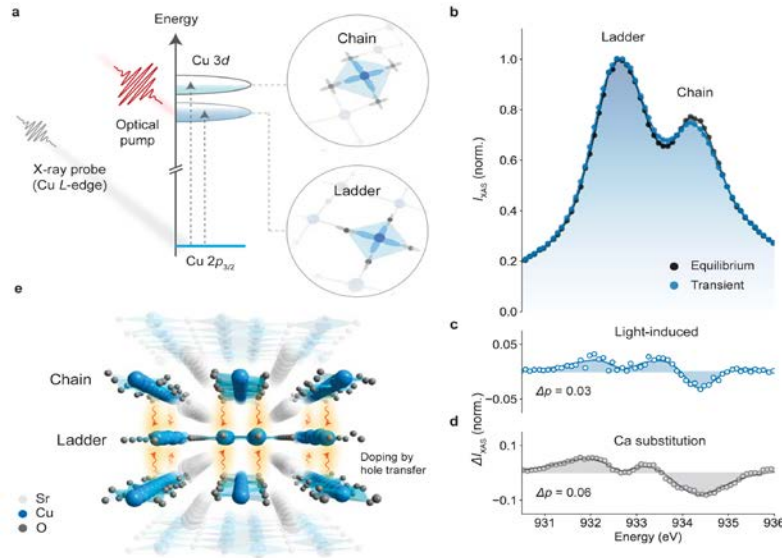
Fig. 1. a, *Schematic of the Cu L-edge time-resolved x-ray absorption spectroscopy experiment. The different chemical environments of the Cu atoms on the corner-sharing ladder and edge-sharing chain result in a double-peaked spectrum.* **b,** *Equilibrium (**black**) and transient (**blue**) Cu L3- edge x-ray absorption spectra (XAS) at pump-probe delay t = 3 ps. The two peaks correspond to the ladder (**left**) and chain (**right**).* **c,** *Differential XAS intensity of light - driven $Sr_{14}Cu_{24}O_{41}$ [$I_{XAS}(t = 3\ ps)$ - $I_{XAS}(t < 0)$]. The pump is polarized along the legs with E_{pump} ~7.7 MV/cm.* **d,** *Equilibrium XAS intensity change due to the chain - to- ladder hole transfer induced by Ca substitution in $Sr_{14-x}Ca_xCu_{24}O_{41}$. We take the difference between the x = 0 and x=11.5 compositions, corresponding to a charge transfer of $\Delta p = 0.06$ holes/CuL. (CuL: on ladder Cu site).* **e,** *Sketch of the pump-induced chain-to-ladder hole transfer.*

Using femtosecond resonant x-ray scattering and spectroscopy, we show that this metastability involves a transfer of holes from chain-like charge reservoirs [18, 19] into the ladders. The nonequilibrium charge redistribution originates from the optical dressing and activation of a hopping pathway that is forbidden by symmetry at equilibrium. Relaxation back to the ground state is then suppressed after the pump coherence dissipates. These findings highlight how dressing materials with electromagnetic fields can dynamically activate terms in the electronic Hamiltonian and provide a rational design strategy for nonequilibrium phases of matter.

References
[1] D. N. Basov, R. Averitt, D. Hsieh, *Nature Materials* **16**, 1077 (2017).
[2] S. Koshihara, Y. Tokura, T. Mitani, G. Saito,T. Koda, *Physical Review* B **42**, 6853 (1990).
[3] V. Kiryukhin, D. Casa, J.P. Hill, B. Keimer, A. Vigliante, Y. Tomioka, Y. TokuraV, *Nature* **386**, 813 (1997).
[4] M. Fiebig, K. Miyano, Y. Tomioka, Y. Tokura, *Science* **280**, 1925 (1998).
[5] J. Zhang, X. Tan, M. Liu, S. W. Teitelbaum, K.W. Post, F. Jin, K. A. Nelson, D. N. Basov, W. Wu, R. D. Averitt *Nature Materials* **15**, 956 (2016).
[6] L. Stojchevska, I. Vaskivskyi, T. Mertelj, P. Kusar, D.Svetin, S. Brazovskii, D. Mihailovic. *Science* **344**, 177 (2014).
[7] V. A. Stoica, N. Laanait, C. Dai, Z. Hong, Y. Yuan, Z. Zhang, S. Lei, M. R. McCarter, A. Yadav, A. R. Damodaran, S. Das, G. A. Stone J. Karapetova, D.A. Walko, X. Zhang, L.W. Martin, R. Ramesh, L.-O. Chen, H. Wen.V. Gopalan. J.W. Freeland, *Nature Materials* **18**, 377 (2019).
[8] K. A. Cremin, J.Zhang, C. C. Homes, G.D. Gu, Z. Sun, M. M. Fogler, A. J. Millis, D. N. Basov, R. D. Averitt *Proceedings of the National Academy of Sciences* **116**, 19875 (2019).
[9] T. F. Nova, A.S. Disa, M. Fechner, A. Cavalleri, *Science* **364**, 1075 (2019).
[10] E. J. Sie, C. M. Nyby, C. D. Pemmaraju, S. J. Park, X. Shen, J. Yang, M. C. Hoffmann, B. K. Ofori - Okai, R. Li , A. H. Reid, S. Weathersby E. Mannebach, N. Finney, D. Rhodes, D. Chenet, A. Antony, L. Balicas, J. Hone, T. P. Devereaux, T. F. Heinz, X. Wang, A. M. Lindenberg *Nature* **565**, 61 (2019).

[11] A. S. Disa, J. Curtis, M. Fechner, A. Liu, A. von Hoegen, M. Först, T. F. Nova, P. Narang, A. Maljuk, A. V. Boris, B. Keimer, A. Cavalleri *Nature* **617**, 73(2023).

[12] M. Budden, T. Gebert, M. Buzzi, G. Jotzu, E. Wang, T. Matsuyama, G. Meier, Y. Laplace, D. ontiroli, M. Riccò, F. Schlawin, D. Jaksch A. Cavalleri, *Nature Physics* **17**. 611 (2021).

[13] S. Vogelgesang, G. Storeck, J.G. Horstmann, T. Diekmann, M. Sivis, S. Schramm, K. Rossnagel, S.Schäfer . C.Ropers, *Nature Physics* **14**, 184 (2018)

[14] A. Zong, A. Kogar, Y. Q. Bie, T. Rohwer, C. Lee, E. Baldini, E. Ergeçen, M. B. Yilmaz, B. Freelon, E. J. Sie, H. Zhou, J. Straquadine P. Walmsley, P. E. Dolgirev. A. V. Rozhkov. I.R. Fisher. P. Jarillo-Herrero. B. V. Fine. N. Gedik. *Nature Physics* **15**, 27 (2019).

[15] Y. A. Gerasimenko, I. Vaskivskyi, M. Litskevich, J. Ravnik, J. Vodeb, M. Diego, V. Kabanov, D. Mihailovic, *Nature Materials* **18**, 1078 (2019)

[16] D. von der Linde, A.M. Glass, K.F. Rodgers, *Applied Physics Letters* **25**, 155 (1974).

[17] H. Padma, *Nature Materials*, accepted (2025).

[18] T. Osafune, N. Motoyama, H. Eisaki, S. Uchida, *Physical Review Letters* **78**, 1980 (1997).

[19] N. Nücker, M.Merz, C.A. Kuntscher, S. Gerhold, S. Schuppler, R. Neudert, M. S. Golden, J. Fink, D. Schild, S, Stadler, V. Chakarian, J. Freeland Y Udzerda, K. Conder, M. Uehara, T. Nagata, J. Goto, J. Akimitsu, N. Motoyama, H. Eisaki, S. Uchida, U. Amerahl, A. Reskolevschi *Physical Review B* **62**, 14384 (2000).

Exciton-Bloch-equation approach to intervalley coupling and the Competition of exciton-exciton and exciton-light interaction

A. Knorr, H.Mittenzwey

Technische Universität Berlin, 10623 Berlin, Germany

In-plane quantum confined electron-hole excitations in semiconductors constitute a remarkable playground for many-body physics in two dimensions. This involves optically accessible (bright) as well as spin- and momentum-forbidden (dark) excitonic states for intra- and intervalley excitations. In this talk, we apply a set of excitonic Bloch equations to address the following topics: *(a)Temporal dynamics of intervalley depolarization:* for atomically thin semiconductors we discuss the interplay of momentum-dark exciton-phonon scattering and intervalley exchange after optical excitation to establish the equilibration between different valleys (valley depolarization). We find different activation processes for the intervalley exchange to establish depolarization, depending on whether the energetically lowest excitonic state is spin-bright or spin-dark, cp. Fig. 1(a-d).
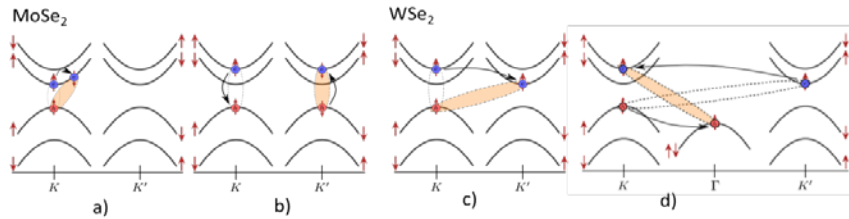
*Fig1. Shows that due to spin conserving exciton-phonon scattering, for spin bright ground states (**a**) intervalley exchange is activated (**b**), whereas the direct exchange channel is suppressed for spin dark ground states (**c**), and requires the assistance of additional valleys (**d**).*

(b) Competition of exciton light and exciton-exciton interaction: due to the different dielectric screening of the Coulomb potential in semiconductor quantum wells and atomically semiconductors, the binding energies of excitons differ by more than an order of magnitude. This situation allows to compare the competition of exciton-exciton and exciton-light interaction in different regimes: For typical field strengths in non-linear optical experiments, exciton-exciton interaction dominates the dynamics in atomically thin semiconductors whereas exciton-light interaction is more pronounced in conventional quantum well structures. We study excitonic Bloch equations as an approach to theoretically describe resonant and ultrafast non-linear optical phenomena such as biexciton formation and Rabi-oscillations and -splitting in an interacting exciton gas. Differences in the optical response, are traced back to the different strength of exciton-to-biexciton transitions at different ratios of Rabi- and binding energy. Throughout the talk, a discussion of the theory with respect to recent experiments will be provided.

Reference

[1] H. Mittenzwey, A. M Kumar, R. Dhingra, K. Watanabe, T. Taniguchi, C. Gahl, K. I Bolotin, M. Selig, A. Knor, *Physical Review Letters* **134** 026901 (2025).

Superlattice design at 2D interfaces for inversion-symmetry breaking

J. Park[1], R. Hemm[2], W. In[3], S. Hus[3], A. Baddorf[3], B. Stadtmüller[4], T. Fritz[5], A.-P. Li[3], O. L.A. Monti[1]

[1] *University of Arizona, Tucson, AZ 85721, USA*
[2] *Rheinland-Pfälzische Technische Universität Kaiserslautern-Landshut, 67663 Kaiserslautern, Germany*
[3] *Oak Ridge National Laboratory, Oak Ridge, TN 37831, USA*
[4] *Universität Augsburg, 86159 Augsburg, Germany*
[5] *Friedrich-Schiller Universität Jena, 07737 Jena, Germany*

Heterostructures of 2D materials have enabled extraordinary possibilities for designing materials that host novel photonic properties and correlated states. The ability to stack the same or different materials with different lattice arrangements and twist angles make it possible to tailor materials properties with extraordinary precision. Furthermore, many 2D materials support strong spin-orbit coupling which enables activating spin degrees of freedom in transport and optical responses. While the investigation of 2D / 2D heterostructures has drawn the most attention, there are promising advances made in making organic / 2D material heterostructures. A useful perspective is to consider the organic layer as a possibly functional layer that "proximitizes" the 2D or layered material, thereby imparting new functionality [1]. Over the past few years, we have shown that this can drive Lifshitz transitions [2], induce strong spin-orbit coupling and hence generate spin texture [3], generate hybrid excitons [4], or create layer-dependent ultrafast spin polarization [5].

Fig. 1. Left: *ARPES of* WTe_2*.* **Right:** *ARPES of 1 ML* C_{60} *on* WTe_2*.*
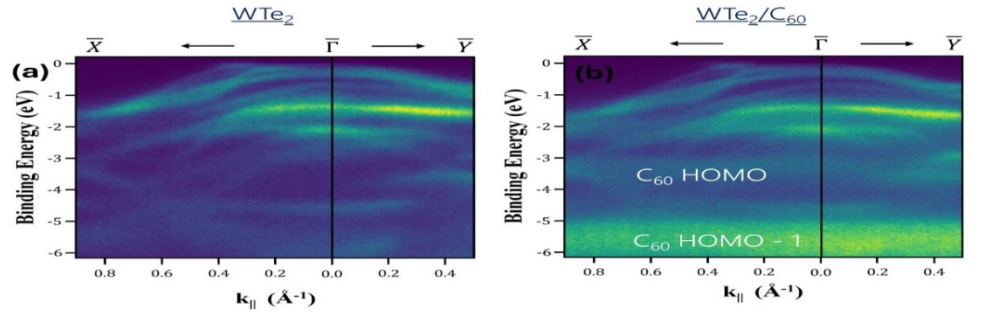
Here we show that phenomena of the sort found in 2D / 2D heterostructures can also be found in organic / layered material heterostructures, with the added dimension that molecules support additional degrees of freedom [6]. In particular, we show that long-wavelength moiré superstructures can be created, with significant potential modulations approaching many tens of meV. We show in the case of C_{60} on WTe_2 that the combination of a rectangular and a hexagonal lattice leads to emergence of a moiré superlattice with a wavelength in excess of 5 nm. We show by ARPES that this heterostructure is weakly interacting, a precondition for the incommensurate growth of the C_{60} superlattice. A detailed structural analysis by low-temperature STM reveals how static distortion waves play an important role in establishing the epitaxy. Beyond the ability to create a moiré lattice, the molecular adsorbate carries additional degrees of freedom. In the case of C_{60}, we show how the moiré potential controls the rotational orientation of the C_{60} molecule on the surface. The resulting rotational supercell, periodic over the whole surface, introduces an additional potential corrugation.

Fig. 2: STM of 1 ML C60 on WTe2. LUMO, $V_s = 1$ V, $I_T = 10$ pA

The importance of our findings lies in the ability to create spatially varying and controllable interfacial potentials that establish large electric fields. In the case of WTe_2, these fields can couple to the ferroelectricity originating from the orthorhombic crystal structure, which in turn are coupled to a complex canted spin texture. The C_{60}/WTe_2 heterostructure offers therefore the possibility to manipulate spin texture on ultrafast timescales by generating time-varying fields at the interface, and modulated over many nanometers.

References
[1] J. Park, A. N. Batyrkhanov, J. R. Schaibley, O. L. Monti, *Applied Physics Letters* **124**, 140502 (2024).
[2] J. Park, A. N. Batyrkhanov, J. Brandhoff, F. Otto, M. Gruenewald, M. Schaal, S. Hus, T. Fritz, F. Göltl, A. Li, O. L. A Monti, *Journal of Physical Chemistry* C **129,** 5065 (2025)
[3] S. Jakobs, A. Narayan, B. Stadtmueller, A. Droghetti, I. Rungger, Y. S. Hor, S. Klyatskaya, D. Jungkenn, J. Stoeckl, M. Laux, O. L. A. Monti M. Aeschlimann, R.J. Cava, M. Ruben, S. Mathias, S. Sanvito, M. Cinchetti, *Nano Letters* **15**, 6022 (2015).
[4] C. Muccianti, S. L. Zachritz, A. Garlant, C. N. Eads, B. H. Badada, A. Alfrey, M. R. Koehler, D. G. Mandrus, R. Binder, B. J. LeRoy, O. L. A. Monti J. R. Schaibley, *Journal Physical Chemistry* C **124,** 27637 (2020).
[5] B. Arnoldi, S.L. Zachritz, S. Hedwig, M. Aeschlimann, O.L.A. Monti, B. Stadtmüller, *Nature Communications* **15,** 3573 (2024)
[6] J. Park, R. Hemm, W. In, S. Hus, A. Baddorf, B. Stadtmüller, T. Fritz, A.-P. Li, O.L.A Monti, *submitted ACS Nano* (2025).
* *Acknowledgment:* we gratefully acknowledge support from the Air Force Office of Scientific Research under grant #FA9550-21-1-0219.

Mid-infrared- and THz-resonant polarizabilities as a route to Material control: science and sources

J. Moses

Cornell University, Ithaca, NY 14853, United States

Light-driven coherent phonon coupling via the lattice anharmonicity has been used as a tool to investigate lattice-dependent materials physics for over a decade [1], making use of the recent advent of intense, ultrafast, mid-infrared and THz sources for driving infrared-active phonons resonantly. Recently, another pathway for inducing structural change via infrared resonances was identified. Rather than relying on coupling of infrared- and Raman-active phonons through the lattice anharmonicity, it instead relies on an optical hyperpolarizability that is jointly dependent on infrared- and Raman-active phonon displacements (Fig. 1(b)) [2]. The resulting optical scattering effect is a third-order polarizability and is a form of Raman scattering. Unlike conventional Raman scattering in crystals, the light-matter interaction is due to the dependence of an infrared-active phonon's dipole moment on the simultaneous displacement of a Raman phonon. We found this can produce giant refractive index shifts for a secondary laser beam when a first laser is resonant with the infrared phonon, and we therefore refer to it as *Infrared Resonant Raman Scattering* (IRRS). In $SrTiO_3$, we have predicted third-order nonlinear susceptibilities seven orders of magnitude larger than the optical Kerr effect in fused quartz [2,3]. This prediction, together with the recent measurement of similarly large third-order nonlinearity in quartz crystal attributed to the quartic anharmonic potential of THz-frequency infrared-active modes [4], strongly motivates the exploration of ultrafast nonlinear optics in the mid-infrared and THz range due to coherent phonon effects. Recently, we have also predicted that quasi-static lattice displacements can be created through the IRRS mechanism, adding another tool, in addition to optical rectification through the lattice anharmonicity [5], for investigating lattice-dependent materials physics. The lattice anharmonicity allows a driving force on a Raman-active phonon mode quadratically dependent on an infrared-active phonon displacement, $Q_R \propto Q_{IR}^2$. In contrast, IRRS, through the nonlinear polarizability that is jointly dependent on the infrared and Raman mode displacements, allows a driving force linearly dependent on an infrared-active phonon displacement and a secondary laser field, $Q_R \propto \ddot{Q}_{IR} E_{laser}$. This provides several new opportunities for structural control through the use of two laser pulse sequence [6], including control of the sign of a fully symmetric Raman mode and the duration of the quasi-static lattice displacement (Fig. 1e-h).
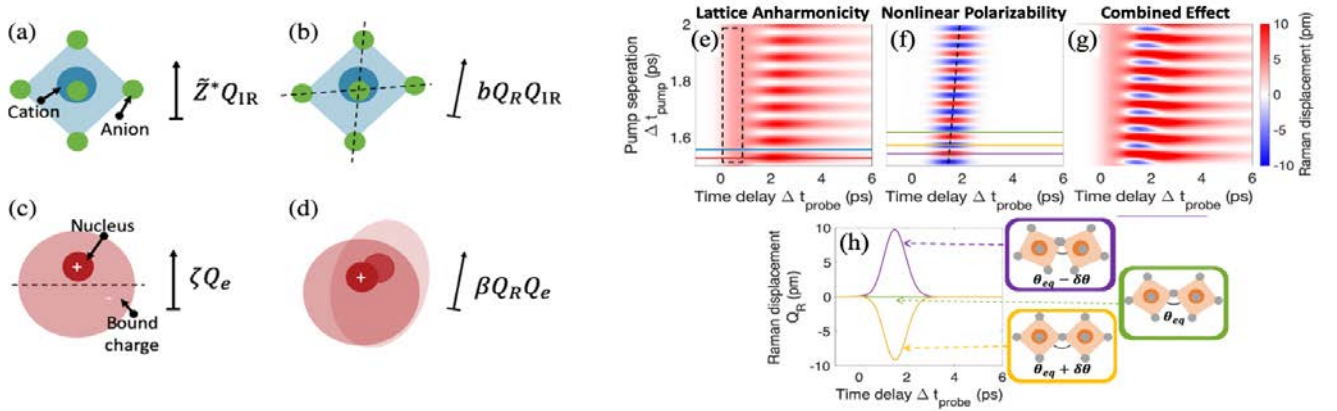
Fig. 1. Left: *from [2], (**a**) a dipole moment is created by the relative displacement of cations relative to anions as an infrared-active phonon is excited. (**b**) This dipole moment can be enhanced or reduced by the simultaneous displacement of a Raman-active phonon, leading to a hyperpolarizability jointly dependent on infrared and Raman phonons. This is analogous to the conventional Raman scattering effect, in which the dipole induced by shifting an electronic distribution (**c**) is modified due to the displacement of a Raman phonon (**d**).*
Right: *from [6], two THz-pulse-driven lattice dynamics for a model system involving an infrared mode coupled to a fully symmetric Raman mode with both pulses resonant with the infrared-active mode. Both the lattice anharmonicity (**e**) and the nonlinear polarizability (**f**) allow quasi-static Raman mode displacements. However, the nonlinear polarizability can be used to control both the sign and the duration of the lattice displacement by tuning the pulse separation and the pulse durations, respectively. (**g**) The combined effects of lattice anharmonicity and nonlinear polarizability. (**h**) Line-outs from (**f**), showing how the nonlinear polarizability can be used to control the sign of the Raman mode displacement.*

These observations motivate new study of light-driven coherent phonon coupling with intense, ultrafast, mid-infrared and THz sources. In addition to summarizing the scientific opportunities described above, we will present several developments in our investigations of new concepts for efficiently down-converting Yb-laser sources to the mid-infrared and THz ranges to generate pulses with high field strength and few-picosecond duration. One method involves overcoming the usual quantum-efficiency limitation of a parametric amplifier through the hybridization of multiple phase-matched nonlinear optical processes. Using idler second-harmonic generation as an idler elimination method in parametric amplification [7], we have so far been able to down-convert ultrashort pulses to the mid-infrared with 68% quantum efficiency [8], a several-fold improvement compared to the efficiency of conventional parametric amplification with bell-shaped Yb-laser beams.

References
[1] A. S. Disa, T. F. Nova, and A. Cavalleri, *Nature Physics* **17**, 1087 (2021).
[2] G. Khalsa, N. A. Benedek, and J. Moses, *Physical Review* X **11**, 021067 (2021).
[3] G. Khalsa, N. A. Benedek, J. Moses, *Proceedings of the International Conference on Ultrafast Phenomena* (UP), W3A.1 (2022).
[4] M. Först, C. Manzoni, S. Kaiser, Y. Tomioka, Y. Tokura, R. Merlin, A. Cavalleri, *Nature Physics* **7**, 854 (2011).
[5] S. Zibod, P. Rasekh, M.Yildrim, W.Cui, R. Bhardwaj, J.-M. Ménard, R. W. Boyd, K. Dolgaleva, *Advanced Optical Materials* **11**, 2202343(2023)
[6] J. Zheng, G. Khalsa, N. A. Benedek, J. Moses, *Proceedings of the International Conference on Ultrafast Phenomena* (UP), W4A.20 (2022)
[7] N. Flemens, N. Swenson, J. Moses, *Optics Express* **29**, 30590 (2021).
[8] N. Flemens, D. Heberle, J. Zheng, D. J. Dean, C. Davis, K. Zawilski, P. G. Schunemann, J. Moses, *arXiv:2207.04147* (2022).
 * *Acknowledgement(s)*: J. M. acknowledges support from NSF, (grants DMR-1719875 and ECCS-1944653) and ONR, (grant N00014-19-1-2592).

Time resolved spontaneous Raman scattering in Materials with electronic order

T. E. Glier[1], M. Rerrer[1], J. Dolgner[2], P. Klein[1], M. von Heek[1], C. Arlt,[1] S. Kaiser[3], D. Manske[2], K. Burch[4]
M.Rübhausen[1]
[1]Universität Hamburg, 22761 Hamburg,Germany.
[2] Max Planck Institute for Solid State Research,70569 Stuttgart, Germany.
[3]Technische Universität Dresden, 01062 Dresden, , Germany.
[4] Boston College, Chestnut Hill, MA 02467, USA

Electronic phase transitions can be studied by time-resolved Raman scattering out of equilibrium in a very sensitive manner adding the pump as an additional tunable experimental tool to understand the low-energy excitation spectrum. The pump can address electronic and structural degrees of freedom depending on wavelength and pulse duration. Two of the most interesting phase transitions resulting in a gapped single-particle excitation spectrum are the transition into a charge-density wave (CDW) and into a superconductor. Even though related, these transitions result into quite different quasi-particle excitations of the electronically ordered phases and the associated coupled degrees of freedom.
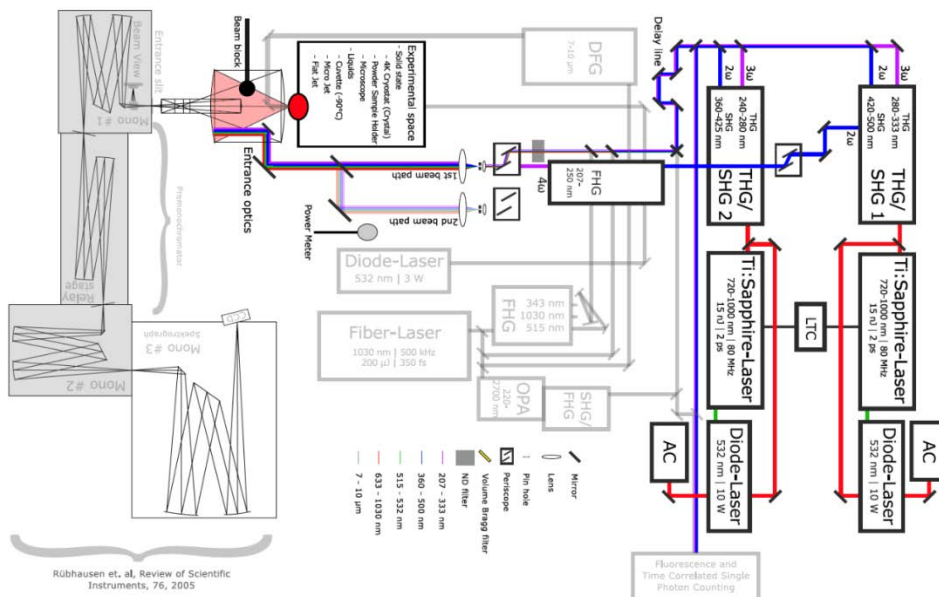
Fig. 1: Time resolved Raman with a 82 MHz laser in the "CW" limit. Pulse durations are typically 1 ps for probe and pump and the pulse energy is limited to the nJ range. Intracavity flexible harmonic generation allows to tune pump and probe wavelength between 200 nm and 1000 nm. The fully reflective design of this custom-made Raman setup allows for collinear pump/probe spectroscopy.

The aim of this presentation is to discuss the similarities and differences in phase an amplitude modes between these two types of transitions and how to detect them in a time resolved spontaneous Raman experiment. We will showcase two different materials systems namely the high temperature superconductor Bi-2212 and the CDW system LaTe$_3$. The time resolved custom-made Raman setup is shown in Fig. 1. I will discuss the setup up its technical realization and our approach to meta data acquisition within the FAIR data framework. Two main laser sources are being used in the setup. Firstly, a set of coupled 82 MHz TiSa oscillators provide pump and probe wavelengths for the fully achromatic and reflective design of our focusing optics. This is the range relevant for selected excitations of charge gaps in CDW systems and phonons in e.g. graphene enabling the selective pumping of structural and charge degrees of freedom. The different experimental conditions allow to discriminate between drive and quench like excitation schemes.

Fig.2: Time resolved Raman with a fiber laser *typically run around 500 kHz with pulse energies of several tenth of uJ. Pulse durations are typically 300 fs. The higher peak power facilitates the use of an OPA with subsequent FHG or a DFG to generate IR pulses to structurally pump the sample.*

In my talk I will discuss the time resolved investigation of electronic order in superconductors and charge density wave systems. Electronic order is typically studied subsequently to a quench of the order parameter which is different to a structural drive. High temperature superconductors show excitations in the single particle and two-particle channel quite different to the excitations of phonons coupling to amplitude modes in CDW systems.

References:
[1] B. Schulz, J. Bäckström, D. Budelmann, R. Maeser, M. Rübhausen, M. V. Klein, E. Schoeffel, A. Mihill,S. Yoon, *Review of. Scientofic Instruments* **76** 073107 (2005).
[2] R. Saichu, I. Mahns, A. Goos, S. Binder, P. May, S. G. Singer, B. Schulz, A. Rusydi, J. Unterhinninghofen, D. Manske, P. Guptasarma M. S Williamsen, M. Rübhausen,. *Physical Review Letters* **102**, 177004 (2009).
[3] S. Buchenau, B. Grimm - Lebsanft , F. Biebl , T. Glier, L. Westphal, J. Reichstetter, D. Manske, M. Fechner, A. Cavalleri, S. Herres - Pawlis M. Rübhausen,. *Physical Review*. B **108**, 075419 (2023).
[4] T. E.Glier, S. Tian, M. Rerrer, L. Westphal, G. Lullau, L. Feng, J. Dolgner, R. Haenel, M. Zonno, H. Eisaki, M. Greven, A. Damascelli, S. Kaiser D. Manske, M. Rubhausen, *arXiv:2310.08162* (2023)
[5] I. Wang, I. Petrides, , G. McNamara. M. M. Hosen, S. Lei, Y.-C. Wu, J. L. Hart, H. Lv, J. Yan, D. Xiao, J. J. Cha, P. Narang, L. M. Schoop K. S. Burch, *Nature* **606**, 896 (2022).

Quasiclassical theory of tunneling induced by pulses of Classical and quantum light

S. Kim, S. Ahn, A. S. Moskalenko
Korea *Advanced Institute of Science and Technology- KAIST, Daejeon 34141, Korea*

Firstly, we present a general quasiclassical theory of tunneling through time-dependent barriers induced by ultrashort light pulses [1]. The theory is based on the Lagrangian formulation of the imaginary time method, extending the classical motion into the complex domain by allowing for the complex time, trajectories and resulting action. Calculating the complex action, we determine the quasi-classical wave function and then the tunneling probability. This is important in the context of the recent studies of the charge transport through nanogaps driven by ultrashort light pulses [2]. We apply our theory to the situation when the tunneling through the nanogap is driven by an ideal half-cycle pulse (Fig. 1).
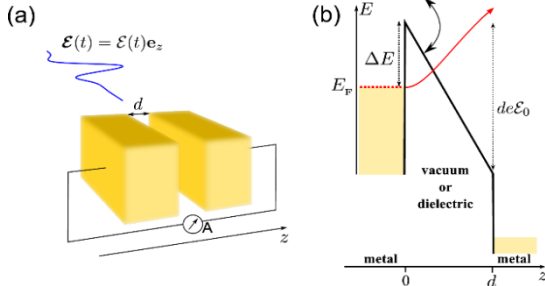
Fig. 1. Left: *geometry of the nano-gap formed by two metallic nano-contacts and the driving few -cycle femtosecond light pulse.*
Right: *the corresponding energy diagram for the electron travelling between the nanocontacts Through the field-influenced time- dependent barrier.*

Among the numerous solutions that contribute to the tunneling probability, we choose two main solution branches with the largest contributions: The 1st solution exhibits the "tunneling" behavior of a wave packet whereas the 2nd solution exhibits the "evanescent-wave" behavior (Fig. 2).

Fig. 2. Tunneling probability density *with respect to the time and position of two solutions branches* **Left**: *1st solution.* **Right**: *2nd solution.*
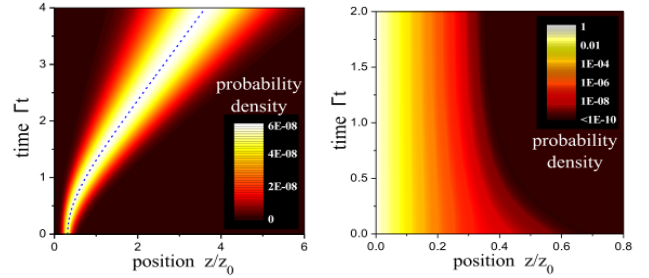
We investigate also the dependence of the tunneling probability on the generalized Keldysh parameter [3] γ and various intercontact distances (Fig. 3).
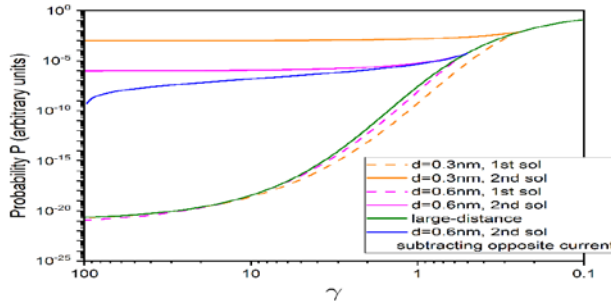
Fig. 3. Tunneling probabilities *in dependence on the Keldysh parameter γ, shown for both solution types and several intercontact distances.*

Then we analyze a situation when the tunneling is driven by realistic few-cycle pulses, finding that the direction of the electron transport in the nanocontacts may be altered in dependence on the carrier-envelope phase of the driving pulse (Fig. 4),

Fig. 4. Tunneling direction controlled by the CEP ϕ. *Positive (**negative**) values of the probability difference, shown by the blue curve, correspond to the **left** (**right**) to **right** (**left**) direction of the resulting current flow. The red curve depicts the result of the quasi-static approximation*
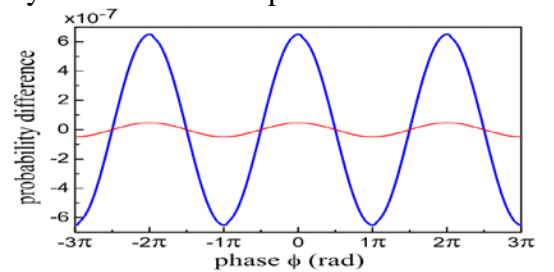
similar to the experiment and DFT simulations for larger values of intercontact distance [2], performed in the direct tunneling regime $\gamma \ll 1$. Recent experiments [5,6,7] reported the generation of quantum light, called bright squeezed vacuum, with very high intensities on the order of 10^{12} W/cm^2 imposed on matter within few femtoseconds in form of an ultrashort pulse. This poses a question how to appropriately describe electron tunneling induced by such pulses and, especially, if it is possible to combine such a description with the quasiclassical formalism for the electron dynamics. We find that this is indeed, maybe surprisingly, possible by resorting to the method of Bohmian trajectories [8], applied to describe the quantum light. Since these light-related trajectories are classical, the method is nicely combinable with the electron-related complex classical trajectories of the quasi-classical description [9]. Notice that in this approach, opposite to the common semi-classical approach, we treat light actually as quantum (the Bohmian description is here equivalent to the Copenhagen interpretation) whereas we treat the matter almost classically (quasi-classically). We apply our theory to study tunneling in the driven between the metallic tip and the metallic surface in the tunneling microscope configuration (Fig. 5).
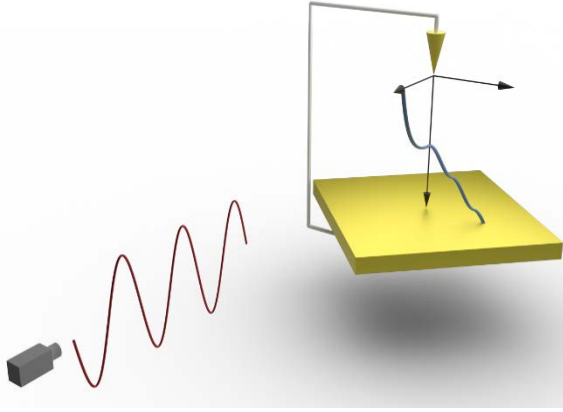
Fig. 5. Schematic diagram of the setup. *Pulse is shot from the laser to the system of metallic tip and surface. Blue curves in between them visualize the complex and real parts of the trajectory of the tunneling electron under the action of a field trajectory corresponding to a single Bohmian realization contributing to the state of the applied quantum light.*

We calculate the tunneling probability and demonstrate that it exhibits a transition from the direct tunneling to the multiphoton regime in dependence on the effective Keldysh-like parameter, which is in this case determined by the squeezing strength (Fig. 6).
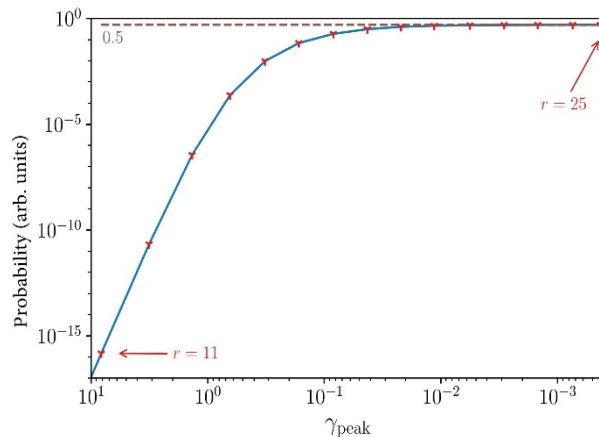
Fig. 6. *Tunneling probability in dependence on the effective Keldysh-like parameter γ_{peak}. From **left** to **right**, the squeezing factor increases from r = 11 to r = 25.*

References
[1] S. Kim, T. Schmude, G. Burkard, A.S. Moskalenko, *New Journal of Physics* **23**, 083006 (2021).
[2] M. Ludwig, G. Aguirregabiria, F. Ritzkowsky, T. Rybka, D. C. Marinica, J..Aizpurua, A. G. Borisov, A. Leitenstorfer, D. Brida, *Nature Physics* **16**, 341 (2020).
[3] L. V. Keldysh, *Soviet Physics- Journal of Experimental and Theoretical Physics* **20**, 1307 (1965).
[4] M. Garg, K. Kern, *Science* **367**, 411 (2020).
[5] K. Y. Spasibko, D.A. Kopylov, V.L. Krutyanskiy, T.V. Murzina, G. Leuchs, M.V. Chekhova, *Physical Review Letters* **119**, 223603 (2017).
[6] M. Manceau, K.Y. Spasibko, G.Leuchs, R. Filip, M.V. Chekhova, *Physical Review Letters* **123**, 123606 (2019).
[7] A. Rasputnyi, Z. Chen, M. Birk, O. Cohen, I. Kaminer, M.Krüger, D. Seletskiy, M. Chekhova, F. Tani., *Nature Physics* **20**, 1960 (2024).
[8] D. Bohm *Physical Review* **85**, 166 (1952).
[9] S. Kim, *in preparation* (2025).

Shaping high-harmonic spatial structures via Dynamical symmetry in anisotropic crystals

K. Nagai, T. Okamoto, Y. Shinohara, H. Sanada, K. Oguri

NTT Corporation, 243-0198 Kanagawa, Japan

Symmetry in nonlinear light–matter interactions provides essential guidelines for controlling photon conversion processes in solid-state materials. In particular, dynamical symmetry (DS) has significantly advanced our understanding of nonperturbative interactions under strong fields [1]. This framework has enabled the formulation of selection rules for polarization-dependent high-harmonic generation (HHG), including unique conservation rules of spin angular momentum (SAM, associated with circular polarization), which reflect the discrete symmetries of crystals [2]. In addition to SAM, the rich symmetry properties of anisotropic solids are also promising for controlling orbital angular momentum (OAM, associated with twisted wavefronts), which provides a basis for describing the spatial degrees of freedom of light. While the generation of spatially structured light has been successfully demonstrated in gas-phase HHG by controlling light-field symmetries [3,4], no such demonstration has been achieved in solids by exploiting their intrinsic crystal symmetries.

Here, we experimentally demonstrate the generation of vectorially structured high harmonics governed by discrete crystal symmetry through the preservation of dynamical symmetry in an anisotropic crystal [5]. We induce HHG in the extreme nonlinear regime using a Gaussian-shaped driving beam at a wavelength of 2.4 μm focused into a 2 mm-thick GaSe semiconductor crystal (Fig. 1). By exploiting the spin–orbit interaction of light, which arises from tight focusing onto a thick uniaxial crystal (e.g., GaSe), we generate OAM components that interact with the crystal [6]. The resulting light–crystal system is described within a multiscale dynamical symmetry framework, which governs not only microscopic light–matter interactions but also macroscopic beam profiles [4]. We measured polarization-resolved spatial profiles of the generated harmonics and observed spatial structures that directly reflect the crystal symmetry. By decomposing the OAM components of the harmonics, we identified that the generated spin–orbit states are selected by total angular momentum conservation in the solid, which arises from the dynamical symmetry.
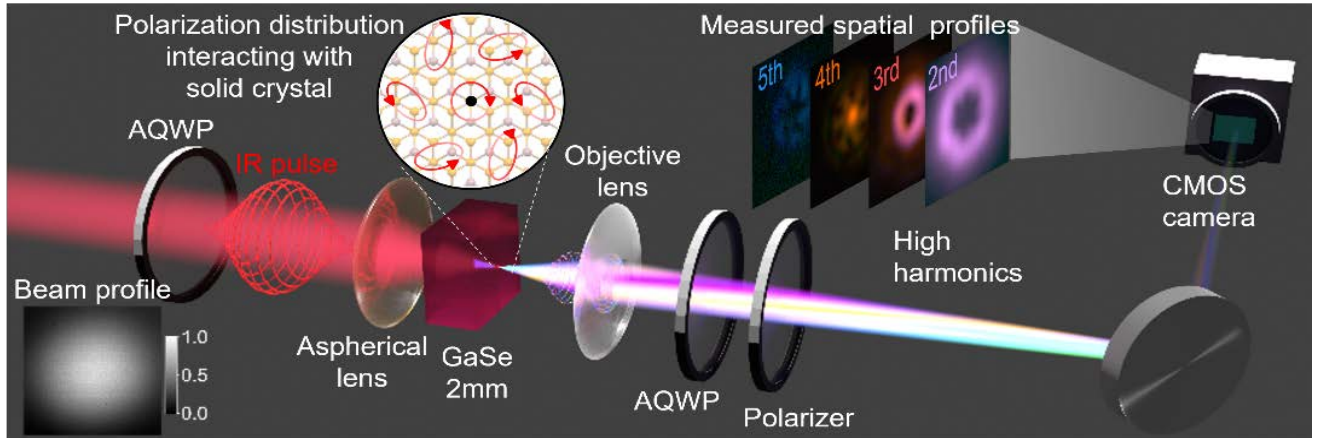
*Fig. 1. Experimental configuration for high harmonic optical angular momentum generation in 2mm-thick GaSe crystal. The **bottom left** inset is the beam profile of the fundamental beam and top right insets are those of high harmonics measured at the camera by inserting color filters.*

These results demonstrate that preserving dynamical symmetry in solids provides a powerful approach for using electronic structures to control the spatial properties of light through photon conversion processes.

References
[1] O. Neufeld, D. Podolsky, O. Cohen, *Nature Communications* **10**, 405 (2019).
[2] N. Saito, P. Xia, F. Lu, T. Kanai, J. Itatani, N. Ishii, *Optica* **4**, 1333 (2017).
[3] M. Luttmann, M. Vimal, M. Guer, J.-F. Hergott, A. Z. Khoury, C. Hernández-García, E. Pisanty, T. Ruchon, *Science Advances* **9**, 486 (2023)
[4] G. Lerner, O. Neufeld, L. Hareli, G. Shoulga, E. Bordo, A. Fleischer, D. Podolsky, A. Bahabad, O. Cohen, *Science Advances* **9**, 953 (2023)
[5] K. Nagai, T. Okamoto, Y. Shinohara, H. Sanada, K. Oguri, *Science Advances* **10**, 7315 (2024).
[6] K. Y. Bliokh, F. J. Rodríguez-Fortuño, F. Nori, A. V. Zayats, *Nature Photonics* **9**, 796 (2015).

Coherent phonon-driven modification of orbital-specific Local field dynamics in Ti$_3$C$_2$T$_x$ (MXene)

S. Neb[1], D. Shin[2], F. Burri[1], M. Hollm[1], E. W. de Vos[1], D. A. Kuznetsov[1], C. R. Müller[1], A. Fedorov[1]
S. A. Sato[4], A. Rubio[3], L. Gallmann[1], U. Keller[1]
[1]*ETH Zürich, 8093 Zürich, Switzerland*
[2]*Gwangju Institute of Science and Technology -GIST, Gwangju 61005, Korea*
[3]*Max-Planck-Institut für Struktur und Dynamik der Materie,22761 Hamburg, Germany*
[4]*Tohoku University, Sendai 980-8578, Japan*

In a recent study by attosecond transient absorption spectroscopy (ATAS), we demonstrated the ability to probe collective electromagnetic interactions—local field effects (LFEs)—with element specificity [1]. Here, we take a decisive step further, revealing the role of LFEs in the strongly coupled dynamics of charge carriers and phonons. We combine ATAS with advanced theoretical modeling to reveal how phonon-driven modifications of anisotropic LFEs govern electron localization and energy transfer at the microscopic level. We demonstrate orbital-specific LFEs and their modulation by the coherent A_{1g} phonon mode in functionalized MXene Ti$_3$C$_2$T$_x$ (T: O, OH, F). Achieving full agreement with the experiment requires going beyond both the Born-Oppenheimer and the independent particle approximation (IPA), as these frameworks fundamentally fail to capture collective effects. Our ATAS scan (Fig. 1a) directly captures the Ti d-orbital fingerprint as probed via the Ti $3p$ shallow-core level. Below the Fermi level, the spectrum reflects mixed d_{z^2} and d_{xz} character, while higher-energy states exhibit nearly pure d_{z^2} character, transitioning to fully pure d_{xz} above 40 eV (Fig. 1b). Solving the Bethe-Salpeter Equation (BSE) for hot electrons, while incorporating lattice elongations from Ehrenfest dynamics within time-dependent density functional theory, yields an accurate agreement with measurement. However, agreement with experiment is only achieved when LFEs are included, whereas the IPA completely fails to capture the observed behavior (Fig. 1c).
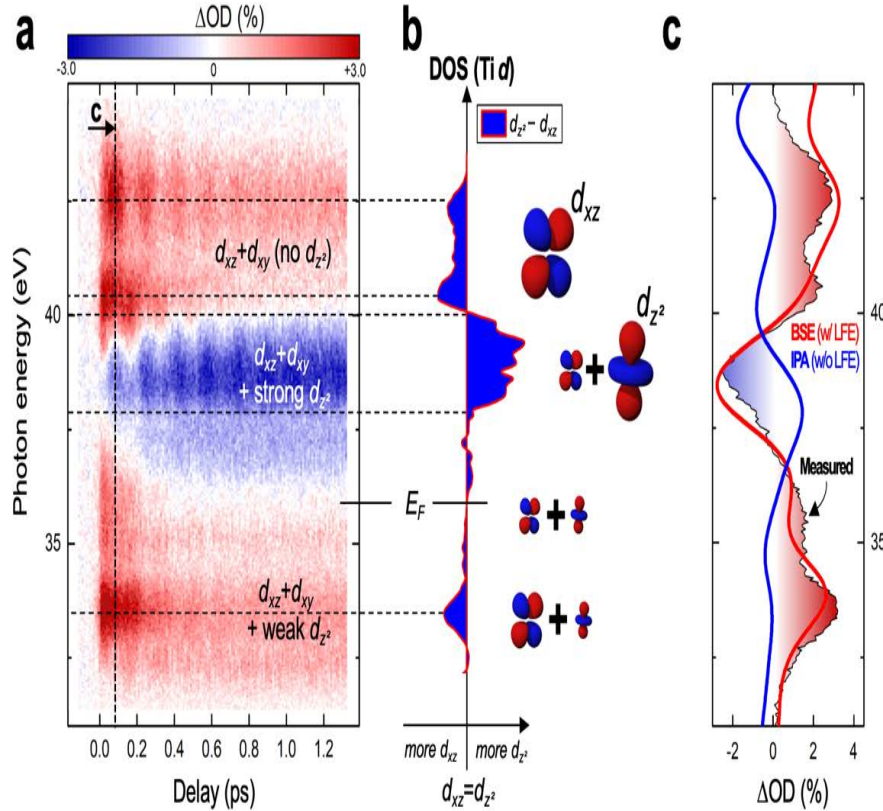
Fig 1. a) Measured ΔOD in Ti$_3$C$_2$T$_x$ after background subtraction.
b) Orbital-resolved Ti DOS for T: O, showing d_{z^2} − d_{xz} difference.
c) BSE/IPA for T: O compared with measured ΔOD at 90 fs delay (label c in sub figure a).

Our study not only establishes ATAS as a powerful probe of element-specific LFEs but also unveils the pronounced sensitivity of LFEs to phononic fingerprints at the individual d-orbital level. The proper incorporation of these effects into theory yields excellent agreement with experiment.

Reference
[1] Z. Schumacher, S. A. Sato, S. Neb, A. Niedermayr, L. Gallmann, A. Rubio, U. Keller, *Proceedings of National Academy of Sciences.* **120** 15 (2023).

All-optical atomic-scale detection of the subcycle Quantum flow of tunnelling electrons

S. Nerreter, T. Siday, J. Hayes, F. Schiegl, F. Sandner, P. Menden, V. Bergbauer, M. Zizlsperger,
S. Lingl, J. Repp, J. Wilhelm, M. A. Huber, Y. A. Gerasimenko, R. Huber
Universität Regensburg, 93040 Regensburg, Germany

Advancing optical microscopy to the shortest length and time scales has been a key prerequisite to establish a causal link between nanoscopic elementary dynamics and macroscopic functionalities of condensed matter. Super-resolution microscopy has bypassed the diffraction limit by harnessing optical nonlinearities [1]. By utilizing linear light-matter interaction with evanescent fields at metallic tips, yet higher resolution has been enabled with scanning near-field optical microscopy (SNOM). While this approach has been combined with simultaneous femtosecond time resolution [2,3], facilitating insights into the nanocosm in motion, the spatial resolution in near-field microscopy has been limited by the mesoscopic tip apex (~10 nm) [3], preventing access to the atomic scale. Here, we exploit an extreme nonlinearity within the near field of an atomically sharp tip to bring all-optical microscopy to combined subcycle and atomic resolution [4]. This is based on the intriguing discovery of a novel near-field response where the subcycle AC tunnelling of electrons acts as a quantum source for electromagnetic radiation. Our approach relies on integrating SNOM with an ultra-high vacuum and cryogenic environment, enabling picometre control over the tip-sample distance – which is a first in SNOM, to the best of our knowledge. We couple phase stable THz pulses to the apex of a sharp tungsten tip positioned in close proximity to an Au(111) surface (Fig. 1a), polarizing the tip and consequently the sample. The tip then acts as an antenna to scatter the light into the far field where the waveforms, imprinted with information on the nanoscale dielectric function of the sample, are detected via electro-optic sampling (EOS). To suppress any far-field background, we tap the tip and capture the electric field demodulated at harmonics of the tapping frequency. When approaching the tip to the sample, we initially observe the typical increase in the scattered near-field signal on length scales comparable to the tip's radius of curvature [3] (Fig. 1b, tip-tapping amplitude $A = 25$ nm).
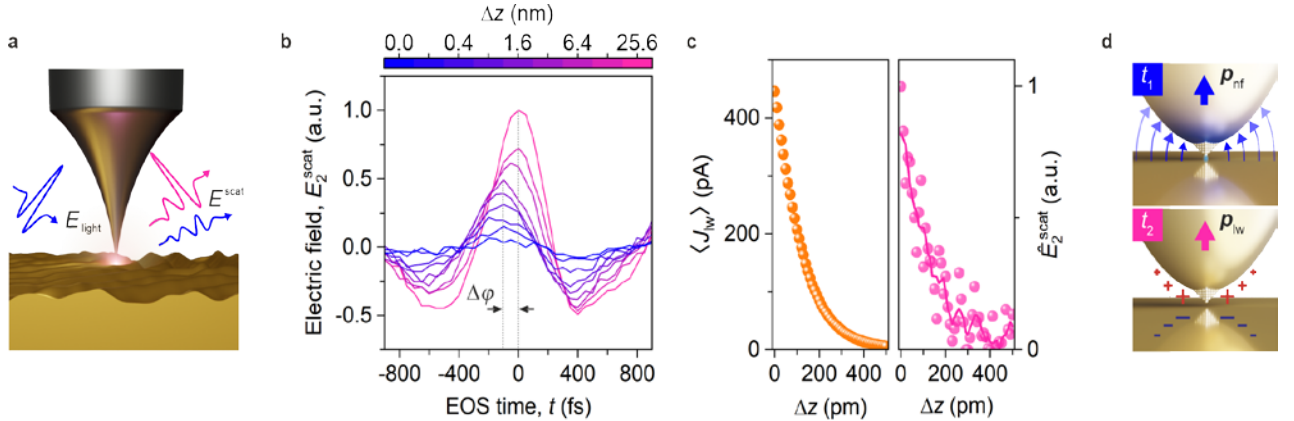
Fig. 1. *(**a**) A THz light pulse (E_{light}) is coupled to the apex of a sharp tungsten tip positioned close to the surface of Au(111). The scattered light (E^{scat}) is detected using EOS. Modulating the height of the STM tip and measuring at harmonics n of the tip-tapping frequency, we isolate the harmonics E_n^{scat} from the far-field background. (**b**) E_2^{scat} at varying relative tip-sample distances Δz ($A = 25$ nm). For the shortest Δz, the transient is markedly transformed, accruing a phase shift $\Delta\varphi$, and dramatic increase in peak amplitude. (**c**) Peak of the scattered THz transients $\hat{E}_2^{scat}$ ($A = 200$ pm), alongside the time-integrated lightwave tunnelling current $\langle J_{lw}\rangle$ measured for increasing Δz. (**d**) Top: Formation of a mesoscopic near-field dipole p_{nf} at the tip apex, driven by E_{light} at time t_1 where E_{light} is maximal. Atomically confined tunnelling currents J_{lw} flow in response to p_{nf}. **Bottom**: At time t_2 there is no p_{nf} as E_{light} crosses zero, but p_{lw} is at its maximum.*

Surprisingly, at distances $\lesssim 1$ nm, the amplitude of the scattered near-field waveform rises much more rapidly with decreasing tip-sample distance accompanied by a phase shift of $\sim\pi/2$. These observations indicate the emergence of a fundamentally new contribution to the scattered fields. Since the large tapping amplitude mixes atomic-scale with classical near-field signals, we reduce A to the atomic scale ($A = 200$ pm), which is more than two orders of magnitude smaller than typical tapping amplitudes used in SNOM, to isolate this new contribution. At such small distances where wavefunction overlap between tip and sample is retained over the entire tapping cycle, lightwave-driven tunnelling currents rectified by

the nonlinearity of the tunnelling junction start to occur. Remarkably, under these extreme conditions we still manage to observe a near-field signal which even decays on the same length scale as the time-averaged lightwave-driven tunnelling currents (Fig. 1c), indicating the origin of the atomically confined near fields: a polarization stemming from subcycle quantum mechanical AC tunnelling currents. Typically, the classical mesoscopic near-field interaction can be described by a near-field dipole p_{nf} that follows the electric field in phase, reaching its maximum at time t_1 in Fig. 1d, top. Yet, in our conditions, atomically confined tunnelling currents can flow in response to p_{nf}. These tunnelled electrons transiently charge the tip and form a second dipole p_{lw}. At time t_2 where the electric field crosses zero, the accumulated tunnelled charge and thus p_{lw} is maximal (Fig. 1d, bottom), leading to the observed phase shift of $\pi/2$, which we confirm with ab initio quantum simulations. As this new near-field optical tunnelling emission (NOTE) signal originates from tunnelling currents, we expect the achievable spatial resolution to be on the atomic scale. We assess this by using nanometre-sized packing defects on Au(111)hidden to atomic force microscopy but revealed by scanning tunnelling microscopySTM, Fig.2a
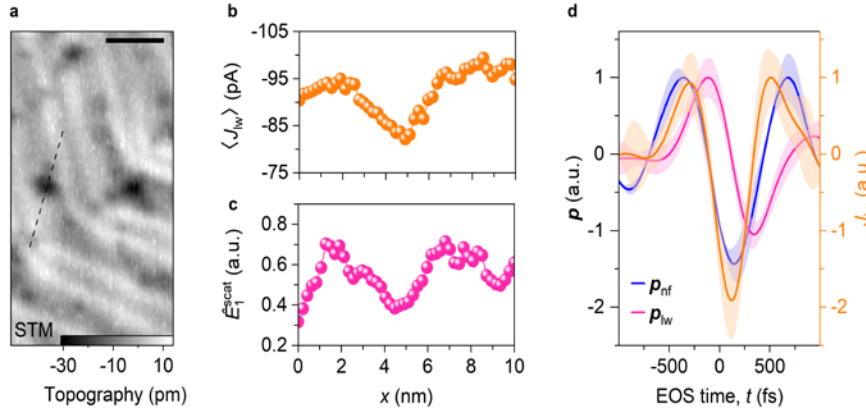
Fig. 2. (a) Constant-current STM image of the Au(111) surface, showing a herringbone reconstruction and nanometre-sized lattice defects. Scale bar: 5 nm. *(b) Quasi-constant height lightwave-STM line scan along the dashed line in a. (c) Simultaneously measured NOTE line scan. (d) Subcycle tunnelling currents on a WSe$_2$ trilayer. Shown are the near-field dipole at the tip apex (blue), the NOTE dipole p_{lw} (pink) and the retrieved ultrafast tunnelling currents (orange), sampled directly in the time domain. All error bars represent one standard deviation*

When performing line scans over such a defect with both lightwave-driven STM (Fig. 2b) and the instantaneous NOTE signal measured at the peak of the scattered transient (Fig. 2c), we find that the spatial resolution of NOTE follows the same rules as STM: It emerges from the orbital overlap between the frontier atom of the tip and the sample. Moreover, NOTE offers insights into the tunnelling dynamics during the oscillation cycle of the driving light field. In most material systems the ultrafast quantum flow of tunnelling electrons is unlikely to align with DC measurements. To showcase this, we investigate the NOTE signal on a native trilayer of WSe$_2$ exfoliated on Au(111). The multiple layers add ultrafast tunnelling pathways hidden from time-integrated measurements. By measuring the NOTE and near-field transients on the trilayer and inverting the tip-transfer function, we retrieve the NOTE and near-field dipoles in the tunnelling junction as a function of time (Fig. 2d). Taking the time derivative of the NOTE dipole enables us to directly trace the subcycle tunnelling current (Fig. 2d, orange), revealing that, intriguingly, electrons appear to enter the trilayer for voltages inside the DC bandgap. Here, field-induced band bending and subcycle distortion of atomic orbitals in the top WSe$_2$ layer, owing to charges which remain confined within the trilayer itself over the entire THz pulse, may contribute to the signal. This subcycle separation of charges without a time-averaged current would be invisible to time-integrated probing of lightwave-driven currents [5 6,7,8]. In summary, our study reveals a novel atomic-scale near-field signal formed by lightwave-tunnelling currents. Via EOS, NOTE microscopy enables subcycle tracking of the quantum flow of tunnelling electrons in angstrom-scale tunnelling junctions, even on insulating materials.

References
[1] S. W. Hell. *Science* **316**. 1153 (2007).
[2] T. Jiang, V. Kravtsov, M. Tokman, A. Belyanin, M.B. Raschke, *Nature Nanotechnology* **14**, 838 (2019).
[3] M. Plankl , M. Plankl, P. E. Faria Jr. , F. Mooshammer, T. Siday, M. Zizlsperger, F. Sandner, F. Schiegl, S. Maier , M. A. Huber, M. Gmitra J. Fabian, J. L. Boland, T. L. Cocker, R. Huber, *Nature Photonics* **15**, 594 (2021).
[4] T. Siday, J.Hayes, F. Schiegl, F. Sandner, P. Menden, V. Bergbauer, M. Zizlsperger, S. Nerreter, S. Lingl , J. Repp, J. Wilhelm, M. A. Huber Y. A. Gerasimenko, R. Huber, *Nature* **629**, 329 (2024).
[5] T. L. Cocker, V. Jelic, M. Gupta, S. J. Molesky, J. A. J. Burgess, G. De Los Reyes, L. V. Titova, Y. Y. Tsui, M. R. Freeman, F. A. Hegmann *Nature Photonics* 7. 620 (2013).
[6] T. L. Cocker, D. Peller, P. Yu, J. Repp, R. Huber, *Nature* **539**, 263 (2016).
[7] V. Jelic, K. Iwaszczuk, P.H. Nguyen, C. Rathje, G. J. Hornig, H. M. Sharum, J. R. Hoffman, M. R. Freeman, F. A. Hegmann, *Nature Physics* **13** 591 (2017).
[8]   D. Peller, L.Z. Kastner, T. Buchner, C. Roelcke, F. Albrecht, N. Moll, R. Huber, J. Repp, *Nature* **585**, 58 (2020).

Optical control of superconductivity

D. Nicoletti[1], M. Rosenberg[1], M. Buzzi[1], A. Ribak[1], N. Taherian[1], M. Nishida[1], M. Först[1], M. Fechner[1]
Y. Liu[2], B. Keimer[2], G. D. Gu[3], M. H. Michael[1], E. Demler[4], A. Cavalleri[5]

[1] Max-Planck-Institut für Struktur und Dynamik der Materie,22761 Hamburg, Germany
[2] Max Planck Institute for Solid State Research, 70569 Stuttgart, Germany
[3] Brookhaven National Laboratory, Upton, NY 11973, USA
[4]ETH Zurich, 8092 Zurich, Switzerland
[5]University of Oxford, Oxford OX1 3PU, UK

Tailored optical excitation in certain high-T_C cuprates has been shown to induce superconducting-like coherence at temperatures far above T_C, as evidenced by the terahertz-frequency optical properties in the nonequilibrium state [1]. In single-layer cuprates of the 214 family, signatures of transiently enhanced interlayer Josephson tunneling were observed both by resonant driving of phonon modes [2] and upon non-resonant high-energy charge excitation in the near infrared [3]. These responses were associated with the perturbation of the charge stripe phase, which coexists and competes with superconductivity at equilibrium. Here, we discuss the results on 214 cuprates by combining data taken on $La_{2-x}Ba_xCuO_4$, for various temperatures, doping levels, and applied DC magnetic fields [3, 4], with those recently reported for $La_{1.6-x}Nd_{0.4}Sr_xCuO_4$ and $La_{2-x}Sr_xCuO_4$ [5]. We show how the degree of coherence of the photoinduced THz response appears to be positively affected by a preexisting stripe phase with longer correlation length at equilibrium. We interpret these results as an indication that optically-enhanced interlayer coupling in this class of materials does not originate from a simple optical melting of charge stripes, as previously hypothesized. Rather, we speculate that the photoinduced state may emerge from activated tunneling between optically-excited stripes in adjacent planes [4].Different from 214 cuprates, in bi-layer $YBa_2Cu_3O_{6+x}$, optically-enhanced superconductivity [6, 7] was initially attributed to the nonlinear excitation of certain lattice modes in the mid infrared and the creation of new crystal structures [8]. More recent work, however, has associated this phenomenon to a parametric excitation and amplification of Josephson plasma polaritons, which are overdamped above T_C but are made coherent by the phonon drive [9, 10].Here we discuss a study of the photoinduced dynamics in $YBa_2Cu_3O_{6.48}$ at T > T_C upon resonant drive of apical oxygen phonons by systematically tuning the duration and energy of the mid-infrared excitation pulses. We show how the lifetime of the superconducting-like response can be extended to several picoseconds (see Fig. 1), thus removing possible ambiguities in the low-frequency terahertz properties [11].

Fig. 1. a- Schematic of the mid-infrared (MIR) pump–THz probe experiment in $YBa_2Cu_3O_{6.48}$. The sample is excited by a MIR pump pulse (yellow) polarized along the crystal c-axis, resonantly driving apical oxygen phonon modes as indicated inside the yellow shading. The subsequent changes in the low-frequency optical properties are sampled by a broadband THz probe pulse (grey). b- Dynamical evolution of the transient spectral weight (top),indicative of dissipation, and of the coherent superconductinglike response (bottom) as a function of pump-probe time delay, for short (0.15 ps) pulse excitation. c- Same as in (b), but for long (3 ps) excitation pulses. The dashed lines in the top panels are fits to the data with a finite rise time and an exponential decay. The horizontal lines in the bottom panels indicate the 10 K equilibrium value of the superfluid density, while the shaded blue areas represent the time delay windows for which a finite coherent response was detected [11].
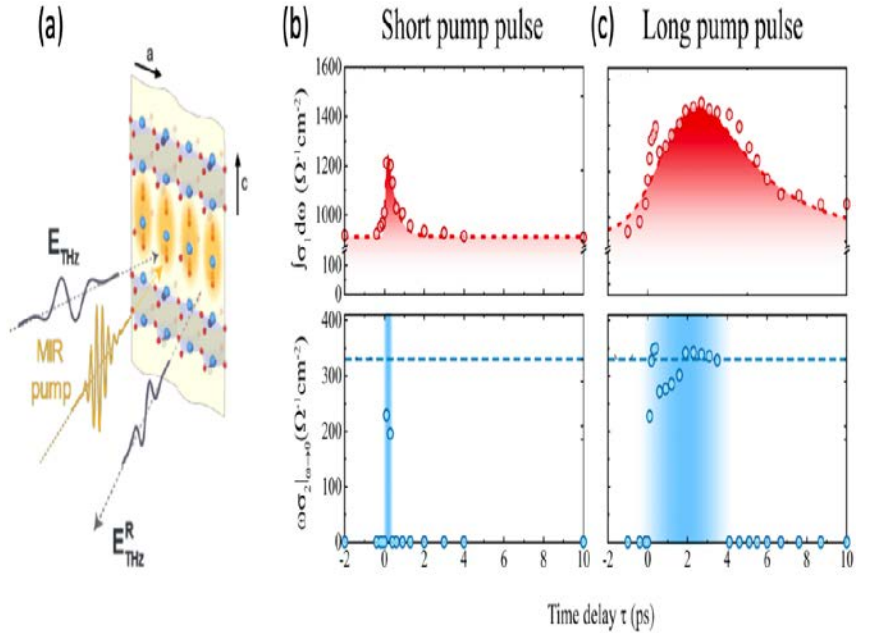
We also report a comparison with the transient optical properties measured along the Cu-O layers [12]. These show, as the out-of-plane response, signatures of nonequilibrium superconductivity, with the opening of a gap in $\sigma_1(\omega)$ and a low-frequency divergence in $\sigma_2(\omega)$, albeit of a different magnitude with

respect to the equilibrium properties below T_C. By fitting the complex optical conductivity with two-fluid superconducting models throughout its dynamic evolution, we were able to extract relevant parameters and study their behavior along the different crystallographic directions. This experiment provides a complete characterization of the transient optical response in apical-oxygen-driven $YBa_2Cu_3O_{6.48}$ to be combined with the recent observation of a Meissner-like magnetic field expulsion in the same material [13].

References
[1] D. Nicoletti, A. Cavalleri, *Advances in Optics and Photonics* **8**, 401(2016).
[2] D. Fausti, R. I. Tobey, N.Dean, S. Kaiser, A. Dienst, M. C. Hoffmann, S. Pyon, T. Takayama, H. Takagi, A. Cavalleri, *Science* **331**, 189 (2011)
[3] D. Nicoletti, E. Casandruc, Y. Laplace, V. Khanna, C. R. Hunt, S. Kaiser, S. S. Dhesi, G. D. Gu, J. P. Hill, A. Cavalleri, *Physical Review B* **90** 100503(R) (2014).
[4] D. Nicoletti, D. Fu, O. Mehio, S. Moore, A. S. Disa, G. D. Gu, A. Cavalleri, *Physical Review Letters* **121**, 267003 (2018).
[5] M. Nishida, D. J. Song, A. M. Hallas, H. Eisaki, and R. Shimano, *Physical Review* B **110**, 224515 (2024).
[6] W. Hu, S.Kaiser, D. Nicoletti, C. R.Hunt, I.Gierz, M. C.Hoffmann, M. Le Tacon, T. Loew, B. Keimer, A. Cavalleri, *Nature Materials* **13,** 705(2014)
[7] B. Liu, M. Först, M. Fechner, D. Nicoletti, J. Porras, B. Keimer, A. Cavalleri, *Physical Review* X **10**, 011053, (2020).
[8] R. Mankowsky, A.Subedi, M. Först, S. O. Mariager, M. Chollet, H. Lemke, J. Robinson, J. Glownia, M. Minitti, A. Frano, M. Fechner N. A. Spaldin, T. Loew, B. Keimer, A. Georges,A. Cavalleri, *Nature* **516,** 71 (2014).
[9] A. von Hoegen, M.Fechner, M.Först, N. Taherian, E. Rowe, A. Ribak, J. Porras, B. Keimer, M. Michael, E. Demler, A. Cavalleri, *Physical Review* X **13**, 031008 (2022)..
[10] N. Taherian, M. Först, A. Liu, M. Fechner, D. Pavicevic, A. von Hoegen, E. Rowe, Y. Liu, S. Nakata, B. Keimer, E. Demler, M. H. Michael A. Cavalleri, *arXiv:2401.01115* (2024).
[11] A. Ribak, M. Buzzi, D. Nicoletti, R. Singla, Y. Liu, S. Nakata, B. Keimer, A. Cavalleri, *Physical Review* B **107,** 104508 (2023).
[12] M. Rosenberg, D. Nicoletti, Y. Liu, B. Keimer, A. Cavalleri, *to be submitted* (2025).
[13] S. Fava, G. De Vecchi, G. Jotzu, M. Buzzi, T. Gebert, Y. Liu., B. Keimer, A. Cavalleri, *Nature* **632,** 75 (2024).

Engineering orbitally-driven spin dynamics in van der Waals antiferromagnets

M. X. Na[1], V. Radovskaiia[1], D. Khusyainov[1], V. Bilyk[1], P. Kim[1], J. Groefsema[1]E. Kochetkova[2], A. Isaeva[3] A. de Visser[2], K. Mukhuti[4], P. C, M. Christianen[4], S. Archarya[5], B. A. Ivanov[1], A. Chatuverdi[6]A. V. Kimel[1] T. H. Rasing[1], D. Afanasiev[1]

[1]*Radboud Universiteit. 6525 Nijmegen, the Netherlands*
[2]*Universiteit van Amsterdam, Amsterdam 1098 XH, the Netherlands*
[3]*Technische Universität Dortmund, 44227 Dortmund, Germany*
[4]*High Field Magnet Laboratory (HFML—EMFL) 6525 ED Nijmegen, the Netherlands*
[5]*National Renewable Energy Laboratory, Golden, CO 80401, USA*
[6]*Nanyang Technological University, Singapore 639798*

Femtosecond laser pulses have emerged as a versatile tool for studying and controlling magnetic materials [1, 2]. The resonant coupling of light to electronic, orbital, spin, and lattice degrees of freedom is particularly crucial for controlling the abundant yet elusive antiferromagnets (AFM), which have zero net magnetization and do not respond to external magnetic fields. Since the shape and occupation of electron orbitals significantly affect superexchange and anisotropy, photoexcitation of orbital resonances with ultrafast laser pulses is a promising route for manipulating antiferromagnetic order. However, to date, orbitally-driven spin dynamics have only been demonstrated on a handful of systems [3,4,5,6]. In this work, we engineer orbitally-driven spin dynamics on the platform of mixed transition-metal thiophosphates $Mn_{1-x}Ni_xPS_3$. For this, there are two key considerations: First, the magnetic anisotropy must be "stiff" enough to distinguish between AFM ground states, yet "soft" enough that spins can respond to the small change induced by the orbital excitation. Second, the photoexcited state must demonstrate high quantum efficiency and possess significant coupling to spins to ensure the transient effects are substantial. Here, we achieve selectivity over both the AFM ground state and the orbital-driver by creating a mixed TM-thiophosphate system. Specifically, we mix $MnPS_3$ – a zero-orbital angular momentum AFM with low magnetic anisotropy – with $NiPS_3$, an AFM in a competing ground-state configuration with a large single-ion anisotropy. Despite their structural similarities, the magnetic properties of Mn and $NiPS_3$ differ due to the distinct spin configurations of the TM ions. $MnPS_3$ adopts a Néel (N)-type AFM order while $NiPS_3$ exhibits a zigzag (ZZ)-type AFM order, as shown in Fig.1a. Furthermore, the Mn^{2+} ion, with a $3d^5$ configuration, has zero orbital angular momentum, negligible spin-orbit coupling, and a singlet ground state that is insensitive to the D_{3d} distortion of the sulfur octahedra. In contrast, the Ni^{2+} ion, with a $3d^8$ configuration, has a larger orbital moment that contributes

to a significantly stronger in-plane anisotropy favoring alignment of spins orthogonal to that in $MnPS_3$. The trigonal distortion in $NiPS_3$ leads to a visible splitting of the $^3T_{2g}$ orbital resonance at low temperature [7,8]. In Fig.1b, we combine mSHG (teal) and mLB (purple) measurements to generate an AFM phase diagram for mixed $Mn_{1-x}Ni_xPS_3$ compounds.
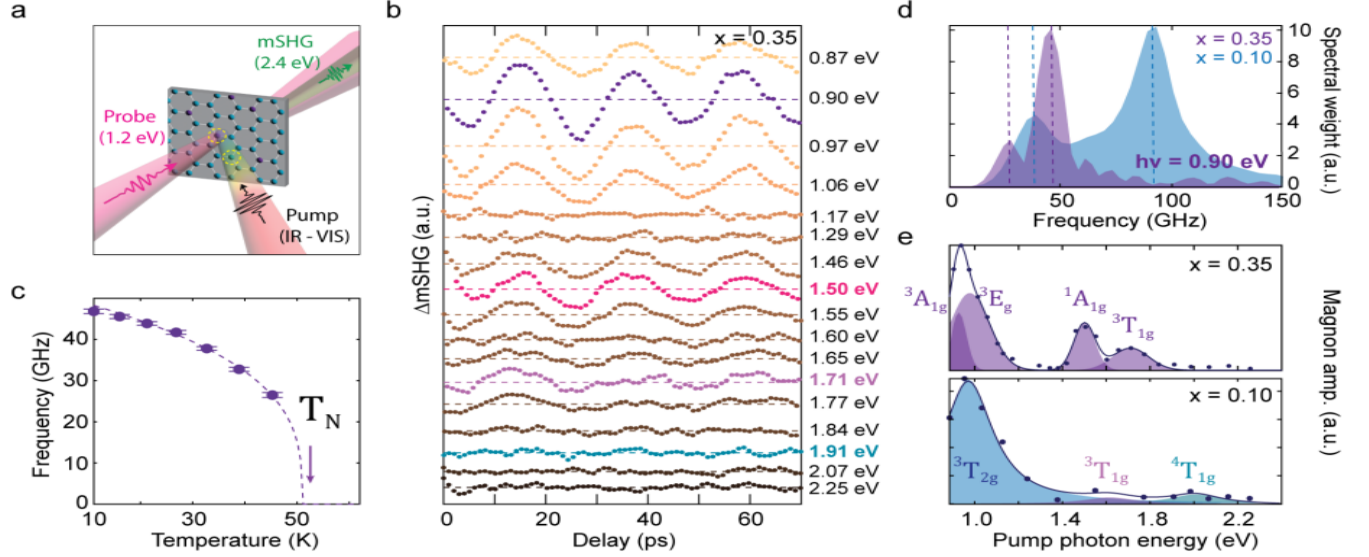
Fig. 1 The crystal and magnetic structure of $Mn_{1-x}Ni_xPS_3$. *(a) The transition metal (TM) ions form a hexagonal lattice and are surrounded by S^6 octahedral cages. The orbital configurations for Mn^{2+} and Ni^{2+} ions in the octahedral (O_h) crystal field, accompanied by a trigonal (D_{3d}) distortion is shown in the center. The high-spin $^6A_{1g}$ ground state of Mn^{2+} (**left**) has zero orbital momentum and favors a Néel (N)-type antiferromagnetic (AFM) order, with weak out-of-plane anisotropy given by magnetic dipolar interactions. In contrast, the significantly higher trigonal distortion and spin-orbit coupling leads to an in-plane anisotropy for Ni^{2+} (**right**), which has an zig-zag (ZZ) AFM order. (b) The AFM ground state of $Mn_{1-x}Ni_xPS_3$. The Mn (Ni)-rich compounds have a N (ZZ)-type AFM ground state reflective of the pure compound. A spatial inversion symmetry breaking in the N-type order gives magnetic second-harmonic generation (mSHG), which is used to determine the onset of the AFM order at the Néel temperature (T_N). Similarly, the ZZ AFM gives rise to magnetic linear birefringence (mLB), which is used to probe the onset of the AFM order In the Ni-rich compounds.*

First, we observe that Mn-rich samples (x < 0.5) exhibit mSHG, while mLB only occurs in Ni-rich samples (x > 0.5); this indicates that the AFM ground state is primarily dictated by the quantitatively dominant TM ion, such that the Mn (Ni)-rich side of the phase diagram shows a N (ZZ)-type order. Secondly, we observe a suppression of T_N – relative to pure Mn and $NiPS_3$ – upon mixing; this suppression is reflective of the competition between N and ZZ-type orders. At half-mixing (x = 0.5), the frustration suppresses long-range magnetic order, resulting in a spin-glass state and the absence of mLB and mSHG [9]. Having established our ground state, we now evaluate the efficacy of orbital resonances in driving coherent spin dynamics. The experimental schematic is depicted in Fig. 2a. We start with the Mn-rich side of the phase diagram and use mSHG to probe the spin dynamics. The pump photon energy is continuously varied from 0.8 to 2.4 eV across the orbital resonances of both Ni and Mn ions. The incident pump fluence is constant at 1 mJ/cm^2. The probe pulse is 1.2 eV, off the orbital resonances in both Mn and Ni ions, with the mSHG signal measured in the transmission geometry. The pump-induced change in the mSHG signal for the x = 0.35 sample ($Mn_{0.65}Ni_{0.35}PS_3$) as a function pump-probe delay is shown in Fig. 2b. To highlight coherent oscillations, we subtract a contribution from the signal with the functional form of a bi-exponential decay arising from electron and lattice relaxation dynamics. What is immediately striking from the photon-energy dependence of Fig. 2b is the large amplitude dynamics with a driven by the 0.94 eV pump (purple), and nominally corresponds to the $^3A_{2g} \rightarrow ^3T_{2g}$ Ni d-d orbital excitation. Here, the amplitude of ΔmSHG is nearly 1% of the equilibrium value. At higher photon energies, smaller resonances are highlighted in magenta, violet and turquoise at 1.50, 1.71 and 1.91 eV, respectively, and are in nominal agreement with previously identified Mn and Ni d-d orbital resonances. Specifically, the Ni excitations $^3A_{2g} \rightarrow ^1A_{1g}$ is a Zhang-Rice singlet exciton centered at 1.5 eV, $^3A_{2g} \rightarrow ^3T_{1g}$ is an Ni d-d orbital excitation centered at 1.7 eV, and the Mn $^6A_{1g} \rightarrow ^4T_{1g}$ orbital excitation is centered at 1.9 eV [8, 10]. To verify the magnetic origin of these coherent oscillations, we show the temperature dependence of the dynamics measured with the 0.94 eV excitation in Fig.2c; the frequency

of the dynamics is 45 GHz and softens directly towards the Néel temperature at $T_N = 52$ K, characteristic of an antiferromagnetic magnon. Remarkably, even though the sample is Mn-rich, the resonances associated with Ni *d-d* orbital resonances are the most efficient at at magnon generation. To further establish the efficacy of the Ni orbital driver, we replicate the experiment on the x = 0.1 sample ($Mn_{0.9}Ni_{0.1}PS_3$). A look at the Fourier transform of the measured dynamics in x = 0.1 and 0.35 samples are shown in Fig. 2d.
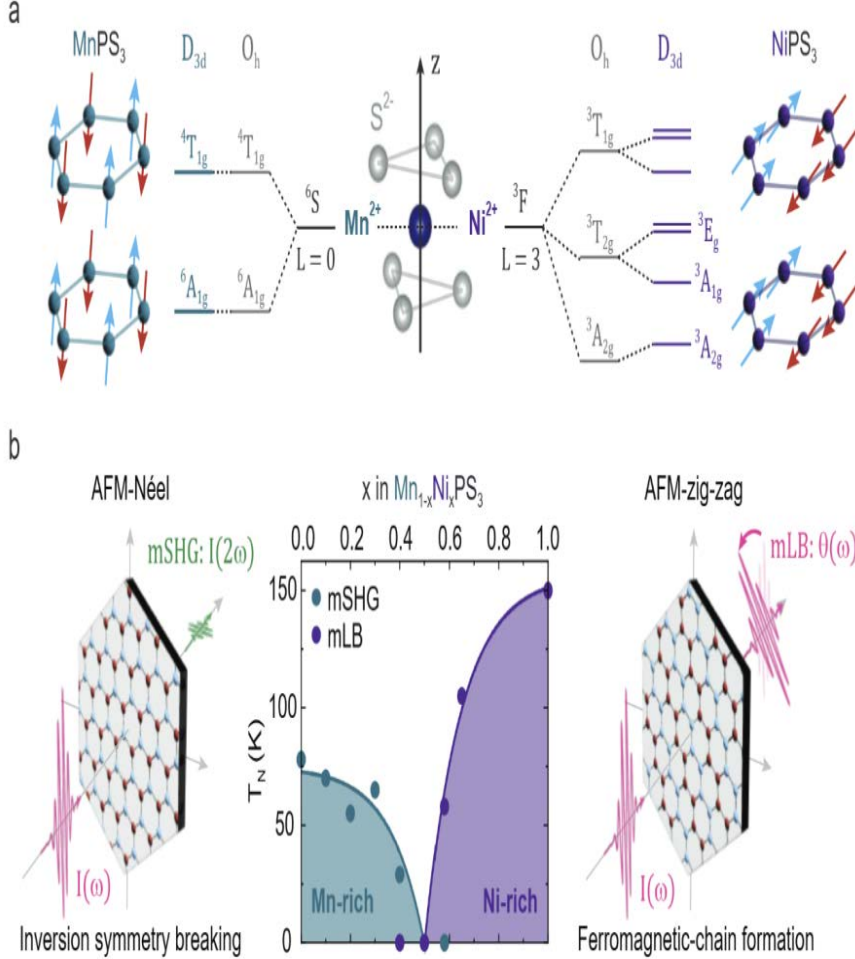
Fig. .2 Excitation of coherent dynamics via onant orbital excitations in $Mn_{1-x}Ni_xPS_3$. *(a)* The experimental configuration. Bulk $Mn_{1-x}Ni_xPS_3$ of approximately 10 um are measured at 10 K. The mSHG is used as a probe, with the fundamental (1.2 eV) detuned from the orbital resonances. The pump pulse, with an incident fluence of 1 mJ/cm², is tuned from 0.8 to 2.4 eV. *(b)* The change of the magnetic second harmonic signal (ΔmSHG) as a function of pump-probe delay measured in the transmission geometry. The traces at 0.94, 1.50, 1.71 and 1.91 eV are highlighted. *(c)* The temperature dependence of the 45 GHz oscillation in (b) is shown to have a softening towards the Néel temperature, characteristic of a magnon. *(d)* The Fourier transform spectra of the 0.9 eV excitation. The purple *(blue)* spectra corresponds to the magnon excitation in the x = 0.35 (0.1) sample, showing two modes at 45 (92) GHz and 39 (25) GHz. *(e)* Top: The amplitude of the 45 (90) GHz mode is plotted as a function of the photon energy in the x = 0.35 (0.1) sample, and is fitted with three (four) Gaussian peaks. In the x = 0.35 sample, clear resonances are observed at E_{Ni} = [0.925, 0.97, 1.498, 1.708] eV, corresponding to orbital resonances in Ni^{2+} in the trigonally distorted octahedra. For the x = 0.1 sample, a large resonance is observed at 0.95 eV *(blue)*, and smaller resonances near 1.55, and 1.98 eV are highlighted, corresponding to orbital excitations in Ni^{2+} *(purple)* and Mn^{2+} *(turquoise)*.

In pure MnPS₃, the two zone center modes are degenerate with a frequency of 120 GHz. In the x = 0.1 mixture, we see two modes at 92 and 39 GHz, which are further renormalized to 45 and 25 GHz in the x = 0.35 mixture. The decrease in the magnon frequency is reflective of the quench of the exchange interaction by Ni-doping in the Mn-rich side of the phase diagram, which is also reflected in the Néel temperature (see Fig.1b). In addition, a small in-plane anisotropy is introduced, which splits the degeneracy of the zone-center magnons. We show the amplitude of the 45 (92) GHz modes as a function of pump photon energy in the x = 0.35 (0.1) sample in the top (bottom) panel of Fig. 2d. The Ni orbital resonances are clearly visible in the x = 0.35 sample. Here, the line shape is best fit with four Gaussians, which peak at E_{Ni} = [0.925, 0.975, 1.498, 1.708] eV, consistent with the resonances given by a splitting of the excited $^3T_{2g}$ triplet state due to a trigonal distortion D_{3d} of the NiS_6 octahedra (see Fig. 1a). Even in the x=0.1 composition, we see that the 0.94 eV excitation *still* dominates in terms of magnon generation efficiency. Since the data here is less dense, we can only tentatively identify the small orbital resonances of Ni and Mn at 1.55 and 1.98 eV. While these higher energy orbital-driving efficiencies are suppressed, the large amplitude precession driven by the $^3T_{2g}$ Ni orbital excitation remains surprisingly robust. We briefly note that this observation is also consistent in simultaneous measurements of ΔmSHG in the reflection geometry and ΔmLB in transmission. To better understand the spin-wave symmetry in the mixed compounds, we study their pump-polarization and helicity dependence, again using the $^3T_{2g}$ orbital resonance as the driver. Spin-wave dynamics measured at 10K for x=0.1 sample is shown Fig. 3a.
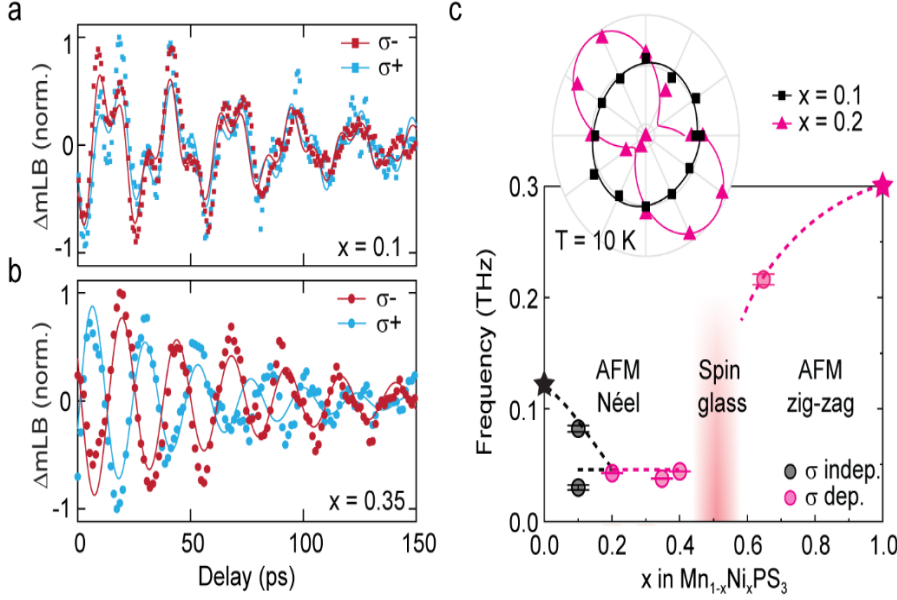
Fig. 3. Phase control of orbitally-driven spin dynamics in $Mn_{1-x}Ni_xPS_3$. (a, b) Helicity dependence of the magnon excitation for the x = 0.1 and x = 0.35 sample at 10 K. **(c)** Frequency of the magnons driven by the Ni $^3A_{1g}$ orbital excitation as a function of Ni fraction, measured with magnetic linear birefringence. Black (**magenta**) colors indicate the lack (presence) of phase-flip, as seen in panel a. The star marker for x = 0 indicates magnons generated via pumping of the Mn orbital resonance at 1.9 eV from literature. The inset shows the linear pump polarization dependence for the 92 GHz mode in x = 0.1 and the 48 GHz mode in x = 0.2 samples.

It is readily apparent that the magnon phase is independent of pump helicity, like pure $MnPS_3$ [6]; however, increasing the Ni fraction to 0.35, the modes acquire helicity dependence, like behavior observed in pure $NiPS_3$ [11]. This observation indicates that the symmetry of the magnons fundamentally changes from the x = 0.1 mixture to the x = 0.35 mixture. This change is not tied to the type of AFM order in the ground state – the symmetry selective magneto-optical probes shown in Fig. 1b unambiguously identifies the N-type AFM ground state for x < 0.5, like that of pure $MnPS_3$. The helicity dependence therefore comes from a change in the magnetic anisotropy and a reorientation of the Néel vector from out-of-plane to in-plane upon mixing. Such a reorientation would be within our expectations, as the single-ion anisotropy of Mn is intrinsically low. When mixed with TM ions of higher single-ion anisotropy, such as Fe and Ni, the Mn ions are prone to spin-orientation [12, 13, 14]. To confirm our hypothesis, we use the 0.95 eV pump excitation to drive coherent spin-precession across the entire composition spectrum of $Mn_{1-x}Ni_xPS_3$. The results are summarized in Fig. 3e; we observe that while the frequency of the magnon changes with the parameters of the AFM ground state, the helicity dependence is maintained for the compositions where x ≥ 0.2. In the inset, we show the linear pump-polarization dependence at 10 K. We see that the 92 GHz mode in x = 0.1 samples is largely isotropic, while the 48 GHz mode in x = 0.2 is anisotropic much like the magnon behavior seen in pure $NiPS_3$. In this work, we have outlined a new strategy for orbital control of antiferromagnetic coherent spin dynamics. Specifically, we demonstrate that the chemical substitution of TM ions in isostructural compounds is an effective method for tuning the AFM ground state and enhancing spin precession amplitudes. By introducing 10% of Ni ions into $MnPS_3$ – a material characterized by minimal orbital momentum and inherently weak anisotropy – we show that we can enhance the response of spins to orbital excitation by an order of magnitude. Further tuning the chemical composition, we show that we can change the very nature of the spin-wave excitation: From Neel-type out-of-plane (x = 0.1) like that in $MnPS_3$, to Neel-type in-plane (x = 0.35), to ZZ in-plane (x > 0.5) like that in $NiPS_3$.

References
[1] A. Kirilyuk, A. V. Kimel, T. Rasing, *Reviews of Modern Physics* **82**, 2731 (2010).
[2] N. Wu, S. Zhang, Y. Wang, S. Meng, *Progress in Surface Science* 98, 100709 (2023).
[3] R. V. Mikhaylovskiy, T. J. Huisman, V. A. Gavrichkov, S. I. Polukeev, S. G. Ovchinnikov, D. Afanasiev, R. V. Pisarev, Th. Rasing, A. V. Kimel *Physical Review Letters* **125**, 157201 (2020).
[4] S. Baierl, M. Hohenleutner, T. Kampfrath, A. K. Zvezdin, A. V. Kimel, R. Huber, R. V. Mikhaylovskiy, *Nature Photonics* **10**, 715 (2016).
[5] D. Afanasiev, J. R. Hortensius, M. Matthiesen, S. Mañas-Valero, M. Šiškins, M. Lee, E. Lesne, H. S. J. van der Zant, P. G. Steeneken, B. A. Ivanov E. Coronado, A. D. Caviglia, *Science Advances* **7**, eabf3096 (2021).
[6] M. Matthiesen, J. R. Hortensius, S. Manas-Valero, I. Kapon, D. Dumcenco, E. Giannini, M. Siskins, B. A. Ivanov, H. S. J. van der Zant, E. Coronado A. B. Kuzmenko, D. Afanasiev, and A. D. Caviglia, *Physical Review Letters* **130**, 076702 (2023).
[7] E. J. K. B. Banda, *Journal of Physics* C: *Solid State Physics* **19**, 7329 (1986).
[8] J. Kim, J. Kim, B. H. Kim, J.-G. Park, J. H. Kim, *Physical Review* B **110**, L180406 (2024).
[9] Z. Lu, X. Yang, L. Huang, X. Chen, M. Liu, J. Peng, S. Dong, and J.-M. Liu, Journal of Physics: Condensed Matter 34, 354005 (2022).
[10] S. Kang, K. Kim, B. H. Kim, J. Kim, K. I. Sim, J.-U. Lee, S. Lee, K. Park, S. Yun, T. Kim, A. Nag, A. Walters, M. Garcia-Fernandez, J. Li, L. Chapon K.-J. Zhou, Y.-W. Son, J. H. Kim, H. Cheong, J.-G. Park, *Nature* **583**, 785 (2020).
[11] S. Toyoda, J. Kruppe, K. Yamakawa, J. Analytis, J. Orenstein, *Physical Review* B **109**, 064408 (2024).
[12] T. Masubuchi, H. Hoya, T. Watanabe, Y. Takahashi, S. Ban, N. Ohkubo, K. Takase, Y. Takano, *Journal of Alloys and Compounds* **460**, 668 (2008)
[13] R. Basnet, A. Wegner, K. Pandey, S. Storment, J. Hu, *Physical Review Materials* **5**, 064413 (2021).
[14] Y. Shemerliuk, Y. Zhou, Z. Yang, G. Cao, A. U. B. Wolter, B. Büchner, S. Aswartham, *Electronic Materials* **2**, 284 (2021).

Tailored-light photocurrent spectroscopy

S. Nöcker[1], D. M. B. Lesko[1], T. Weitz[1], S. Wittigschlager[1], W. Li[1], O. Neufeld[2], P. Hommelhoff[3]

[1]*Friedrich-Alexander-Universität Erlangen-Nürnberg, 91054 Erlangen, Germany*
[2]*Technion - Israel Institute of Technology, Haifa 3200003, Israel*
[3]*Ludwig-Maximilians-Universität, 80539 München, Germany*

Symmetry breaking phenomena are crucial for many nonlinear physical phenomena [1,2,3,4]. Tailored-light field interaction with graphene, a highly symmetric two-dimensional material, allows for probing specific symmetry breaking phenomena by means of photocurrent spectroscopy. With two linearly polarized harmonic light fields, where we can independently control polarization angle and delay, we map out the photocurrent selection rules for the combined electric field and material symmetries [2,5,6]. We benchmark these results with state-of-the-art time-dependent density functional theory (TDDFT) simulations, apply this technique to samples with inherent broken time-reversal symmetry (TRS) and predict this broken symmetry's effect on the two-color photocurrent response.
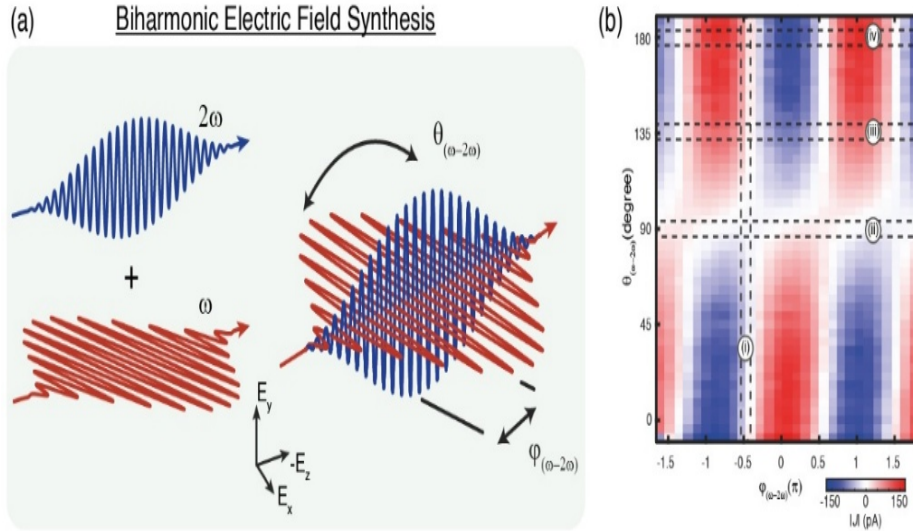
Fig. 1. a) Electric field components. *Two linearly polarized fields at frequencies ω and 2ω are combined to create a biharmonic light field. We vary the relative polarization axis between the two beams ($\theta_{\omega-2\omega}$) and the two-color phase delay ($\varphi_{\omega-2\omega}$).*
b) Mapped photocurrent *for the variation of the two-color phase delay ($\varphi_{\omega-2\omega}$) and the angle between the dressing (ω) and driving (2ω) light pulse ($\theta_{\omega-2\omega}$).*

Two-color photocurrents in graphene, an inversion-symmetric material, primarily stem from asymmetric carrier distributions in the conduction bands, known as injection currents. TRS dictates that excitation probabilities must be equal for conjugate momenta, leading to a suppression of this injection current for TRS-maintaining light-matter systems. Here, we investigate symmetry-protected injection current suppression by biharmonic field synthesis (Fig. 1a) to probe TRS breaking. We combine two linearly polarized harmonics with control over the two-color phase ($\varphi_{\omega-2\omega}$) and polarization angle ($\theta_{\omega-2\omega}$). With this technique, we individually break mirror symmetry (with respect to the graphene/electrode axis) and TRS to measure the symmetry-dependent injection current suppression (Fig. 1b). The photocurrent map (Fig. 1b) highlights unique suppressions of the injection current for symmetry-maintained field-material combinations. When $\varphi_{\omega-2\omega} = 0.5\pi$ ((i), vertical), TRS is strictly maintained, leading to a strong suppression of the injection current. When $\theta_{\omega-2\omega} = 90°$ ((ii), horizontal), mirror symmetry is maintained leading to a suppression of the injection current. Finally, characteristic two-color phase dependent injection currents are measured for fields that break mirror and TRS (iii-iv). We apply this new photocurrent spectroscopy to TRS-broken systems such as CrI_3 and an inversion-symmetric Floquet topological insulator. We show that simulated two-color-phase-dependent photocurrent responses behave starkly differently, allowing these tailored fields to be used for probing broken symmetries. Our work shows the potential of using linearly polarized short laser pulses to probe symmetry-broken phases of matter, with precise control over the symmetry-breaking [7]. This method is ultrafast, in nature, and does not require the use of magnetic fields or circularly polarized electric fields.

References
[1] D. Ayuso, O. Neufeld, A. F. Ordonez, P. Decleva, G. Lerner, O. Cohen, M. Ivanov, O. Smirnova, *Nature Photonics* **13**, 866(2019).
[2] O. Neufeld, N .Tancogne-Dejean, U. De Giovannini, H.Hübener, A. Rubio, *Physical Review Letters* **127**, 126601 (2021).
[3] D. Habibović, K. R. Hamilton, O. Neufeld, L. Rego, *Nature Review Physics* **6**, 663 (2024).
[4] O. Neufeld, *ACS Photonics* **12**, 2151 (2025).
[5] I. Franco, P. Brumer, *Journal of Physics* B **41**, 074003 (2008).
[6] M. Shapiro, P. Brumer, *Quantum Control of Molecular Processes* (Wiley, 2012).
[7] D. M. B. Lesko, *in preparation* (2025).

Ultrafast demagnetization:
Magnon excitation vs fast spin transport

M. Weißenhofer[2], M. S. Mrudul[1], P. M. Oppeneer[2]
[1]Uppsala University, 75120 Uppsala, Sweden
[2]Freie Universität Berlin, 14195 Berlin, Germany

Laser induced ultrafast demagnetization was first observed in 1996 [1]. Excitation with a short, femtosecond laser pulse was found to demagnetize a ferromagnetic Ni film within less than 0.5 picoseconds. The mechanism that could cause such fast dissipation of spin angular momentum has been intensively debated during the last two decades, but consensus on the dominant mechanism that drives the demagnetization has not yet emerged [2]. We discuss here recent theory developements for two possible scenarios, (1) demagnetization in ferro-magnetic films through ultrafast magnon generation [3], and (2) ultrafast demagnetization through non-local spin transport. The latter may occur through superdiffusive spin transport in metallic heterostructures [4]. An alternative mechanism is called OISTR, in which the optical excitation transfers spin from one atom to a neighboring atom in a compound [5,6,7].

For scenario (1), we developed *ab initio* parameterized out-of-equilibrium theory based on a quantum kinetic approach to describe magnon occupation dynamics due to electron-magnon scattering [8]. We performed quantitative simulations of the ultrafast generation of magnons in iron and find that the magnon distribution is highly non-thermal. Our *ab initio* calculations show that ultrafast generation of non-thermal magnons provides a sizable demagnetization within 200 fs in excellent comparison with experiment [3], see Fig. 1. This finding emphasizes the importance of non-thermal magnon excitations for the ultrafast demagnetization process in single ferromagnetic films.
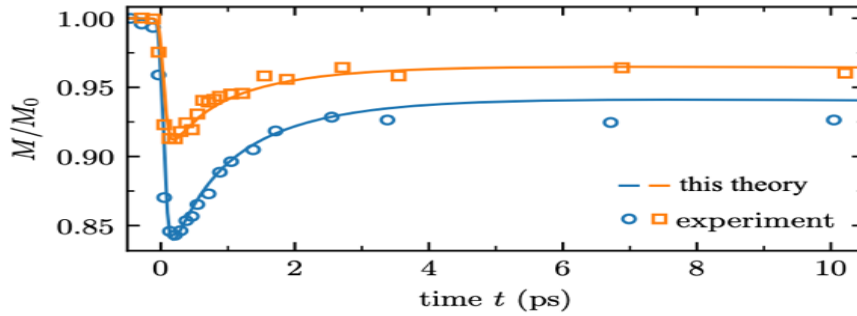
Fig. 1. Comparison between experiment and theory for the ultrafast demagnetization of an iron film. The theory is based on ultrafast excitation of non-thermal magnons due to electron-magnon scattering. The experimental data (symbols) are those of Ref. [3].

For case (2) we performed *ab initio* calculations for ferromagnetic FePt to investigate through which mechanism ultrafast demagnetization occurs in TDDFT. We find that fs demagnetization in TDDFT is a longitudinal magnetization reduction (spin flip) and results from a nonlinear opto-magnetic effect, akin to the inverse Faraday effect [9]. The demagnetization scales quadratically with the electric field E in the perturbative limit, i.e., $\Delta M_z \propto E^2$. Moreover, the magnetization dynamics happens dominantly at even multiples $n\omega_0$, (n = 0, 2, $\cdots$) of the pump-laser frequency ω_0. The main contribution to the demagnetization occurs at $\omega \sim 0$, consistent with the inverse Faraday effect mechanism. Our results imply that magnetization modulation coherent with the light-wave frequency ω [6] is not possible. We furthermore establish that electronic coherence plays a dominant role in the demagnetization process, whereas interpretations based on occupation numbers poorly describe the ultrafast demagnetization on the femtosecond timescale [9].

References
[1] E. Beaurepaire, J.-C. Merle, A. Daunois, J.-Y. Bigot, *Physical Review Letters* **76**, 4250 (1996).
[2] K. Carva, P. Baláž, I. Radu, *Handbook of Magnetic Materials* **26**, 291 (2017).
[3] E. Carpene, E. Mancini, C. Dallera, M. Brenna, E. Puppin, S. De Silvestri, *Physical Review* B **78**, 174422 (2008).
[4] M. Battiato, K. Carva, P.M. Oppeneer, *Physical Review Letters* **105**, 027203 (2010).
[5] J.K. Dewhurst, P. Elliott, S. Shallcross, E.K.U. Gross, S. Sharma, *Nano Letters* **18**, 1842 (2018).
[6] F. Siegrist, J. A. Gessner, M. Ossiander, C. Denker, Y.- P. Chang, M. C. Schröder, A. Guggenmos, Y. Cui, J. Walowski, U. Martens, J. K. Dewhurst U. Kleineberg, M. Münzenberg, S.Sharma, M.Schultze, *Nature* **571**, 240 (2019).
[7] F. Willems, C. von Korff Schmising, C. Strüber, D. Shick, D. W. Engel, J. K. Dewhurst, S. Sharma, S. Eisebitt, *Nature Communications* **11**, 871 (2020)
[8] M. Weißenhofer, P.M. Oppeneer, *Advanced Physics Research*, 2300103 (2024).
[9] M.S. Mrudul, P.M. Oppeneer, *Physical Review* B **109**, 144418 (2024).

Enhanced spin-to-charge conversion at graded Ferromagnetic/non-magnetic interfaces

E. Th. Papaioannou[1], G. Torosyan[3], O. Crisan[2], C. Locovei[2], U. Arnalds[4], V. Kapaklis[5], R. Beigang[3]

[1]*Aristotle University of Thessaloniki, 54124 Thessaloniki, Greece*
[2]*National Institute of Materials Physics, 077125 Magurele-Bukarest, Romania*
[3]*Rheinland-Pfälzische Technische Universität Kaiserslautern-Landau, 67663 Kaiserslautern, Germany*
[4]*University of Iceland, Reykjavik 107, Iceland*
[5]*Uppsala Universitet, 75120 Uppsala, Sweden*

The spin-to-charge conversion (SCC) on ultrafast timescales enabled by spin Hall effect (SHE) and the inverse spin Hall effect (ISHE) is an emerging research topic in nanomagnetism and spintronics that can have a great impact on THz physics, ultrafast-magnetism and ultrafast photonics [1,2]. In this presentation we investigate the SCC conversion at ferromagnetic (FM) / non-magnetic (NM) multilayers utilizing the THz emission of the thin layers. In particular, we deal with the generation and the transport of an ultrafast spin current after femtosecond (fs) laser pulse excitation of FM/NM structures. The fs-laser excites spin current in the FM layer that diffuses into the NM layer where it is then converted by the ISHE to an ultrafast charge current that is able to emit THz radiation. The THz emission from these structures can cover a frequency range from 0.1 to 30 THz and moreover without any phonon absorption. The latter renders them superior to all the current solid emitters and subsequently makes them candidates to further develop THz technology and to be applied in various applications spanning from chemistry and material sciences to medicine and security [1,2,3]. In details, we use the THz emission to quantify the SCC from structural and compositional gradient FM/NM multilayers. We induce during growth process the tetragonal $L1_0$-FePt crystal phase at the interface. We show that a graded structure of Fe/$L1_0$-FePt/Pt boosts the THz emission (Fig. 1).
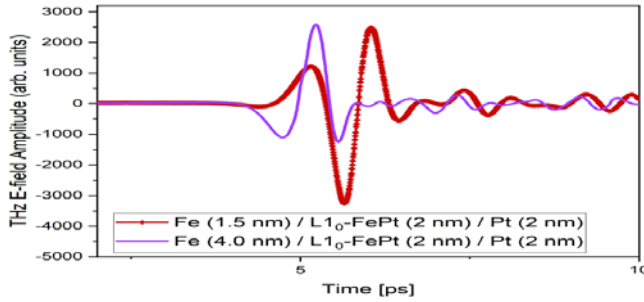
Fig. 1. THz E-field amplitude emission from a series of Fe / $L1_0$-FePt / Pt samples. *The presence at the Fe/Pt interface of alternate layers of Fe and Pt in the $L1_0$ phase creates a graded structure that enhances the spin-to-charge conversion as the enhanced THz signal shows. The effect is sensitive to the thicknesses of the Fe layers and the chemical gradient that the $L1_0$-phase provides.*

We present the dependence of the THz emission with respect to the thickness of the induced $L1_0$-phase and the thicknesses of Fe and Pt layers. We further engineering the alloy-interface by changing the stoichiometry of the lattice without modifying the tetragonal $L1_0$ crystal symmetry. Practically, by maintaining the crystal structure we only modify the chemical composition achieving a compositional graded structure. We reveal that the graded interface has a large influence on the magnetization reversal that we attribute to the different values of exchange stiffness of Fe atoms. The stoichiometrically graded tetragonal structure modifies further the THz emission. Finally, SCC, interface transparency and subsequent Terahertz emission efficiency are correlated to investigations of the magnetization profile in the $L1_0$-FePt phase and the Pt layers. The profile is determined using x-ray resonant magnetic reflectivity measurements (XRMS). The measurements were performed at the European Synchrotron Radiation Facility (ESRF) with x-ray energy corresponding to the L3 resonant edge of Pt. XRMS allowed us to extract the element-specific polarization profile and assess the interplay between structural and magnetic interfaces of the multilayers (Fig.2).
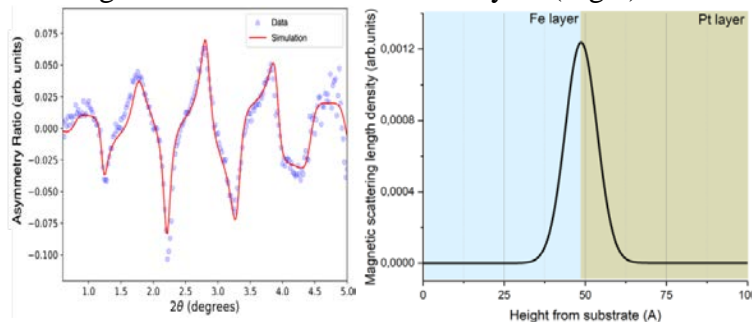
Fig. 2: (Left) Asymmetry ratio and simulation recorded at the Pt-L3 edge *at 300 K for Fe (5 nm) / Pt (6nm) sample. The magnetic information is obtained from the asymmetry ratio (AR), defined as $(I^L - I^R)/(I^L + I^R)$, where I^L and I^R are the intensities measured with left and right circularly polarized light, respectively.(**Right**) Extracted magnetic scattering length density (mSLD) corresponding to the bilayer composition. An enhanced magnetic polarization is observed for Pt that occurs at interface. The induced magnetic polarization of Pt influences the SCC conversion and the THz emission*

Our results shed light on the structure-property relationship of the SCC effect. We use Fe/Pt as a starting model system to induce a compositional grading (chemical stoichiometry) or a structural gradient at the interface. We utilize the THz emission to probe without electrical contacts the ultrafast SCC mechanism and to quantify the FM/NM interface transparency of spin current and the spin-to-charge efficiency of such gradient nanostructures. The ability of the $L1_0$ phase to transfer spin current and to emit THz radiation reveals the potential of graded structures as efficient spintronic THz sources [4].

References
[1] E. Th. Papaioannou. R. Beigang. *Nanophotonics* **10**. 1243 (2021).
[2] T. S. Seifert, L. Cheng, Z. Wei, T. Kampfrath, J. Qi, *Applied Physics Letters* **120**, 180401 (2022).
[3] B. Das-Mohapatra , R. Rouzegar, E. Th. Papaioannou, T. Kampfrath, G. Schmidt, *Physical Review Applied* **23**, 014024 (2025).
[4] L. Scheuer,M. Ruhwedel, D.Karfaridis, I.G.Vasileiadis, D Sokoluk, G. Torosyan, G. Vourlias, G. P. Dimitrakopoulos, M. Rahm, B. Hillebrands T. Kehagias, R. Beigang, E. T. Papaioannou, *iScience* **25**, 104319 (2022).

Real-time time-dependent DFT investigation of the ultrafast Laser-induced carrier and Magnetization dynamics in SrTiO$_3$

A. Darmawan, M. E. Gruner, R. Pentcheva
Universität Duisburg-Essen, 47057 Duisburg, Germany

Recent experimental studies indicate electric-field-driven ferroelectricity [1] and multiferroicity [2] in the paradigmatic nonmagnetic band insulator SrTiO$_3$ in the terahertz regime. Following a comprehensive study of the optical [3] and x-ray absorption [4] spectra including quasiparticle and excitonic effects, here we explore the response of SrTiO$_3$ to optical laser excitation. Using real-time time-dependent density functional theory (RT-TDDFT) as implemented in the elk code [5] we investigate both linear and circular polarized laser pulses and vary systematically the laser frequency and fluence. A complex site- and orbital-dependent temporal dynamics is observed with opposite sign of fluctuations at O and Ti sites and charge transfer from O *2p* to Ti *3d* states for linearly polarized light, that breaks dynamically inversion symmetry. Notably, circularly polarized pulses induce a finite transient magnetic moment of up to $0.1\mu_B$ at the Ti sites which is absent for linearly polarized pulses. We assess the origin of the induced magnetization.

Fig. 1. *Electron density redistribution* at 20 fs upon *laser excitation of SrTiO$_3$ with circularly polarized light.*
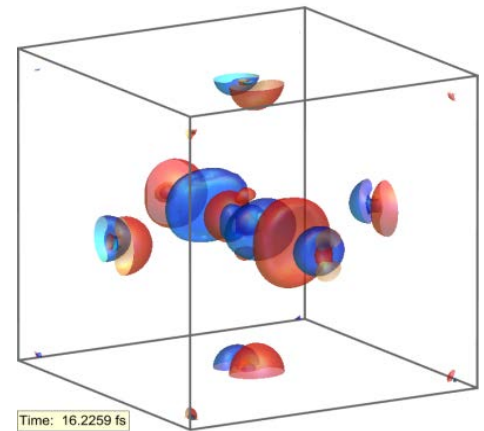
Notably, circularly polarized pulses induce a finite transient magnetic moment of up to $0.1\mu_B$ at the Ti sites which is absent for linearly polarized pulses. We assess the origin of the induced magnetization.

References
[1] T. F. Nova A.S. Disa, M. Fechner, A. Cavalleri, *Science* **364**, 1075 (2019)
[2] M. Basini,M. Pancaldi, B. Wehinger, M. Udina, V. Unikandanunni, T. Tadano, M. C. Hoffmann, A. V. Balatsky, S. Bonetti, *Nature* **628**, 534 (2024)
[3] V. Begum, M.E. Gruner, R. Pentcheva, *Physical Review Materials* **3**, 065004 (2019),
[4] V. Begum-Hudde, V. Begum - Hudde, T. Lojewski, N. Rothenbach, B. Eggert, A. Eschenlohr, K. Ollefs, M. E. Gruner, R. Pentcheva, *Physical Review Research* **5**, 013199 (2023).
[5]   J. K. Dewhurst, S. Sharma, Development of the Elk LAPW Code. *Max Planck Institute of Microstructure Physics* (2011).

Terahertz two-dimensional spectroscopy of superconductivity: Deciphering nonlinear quantum dynamics and interference

M. Mootz[2], J. Wang , I.E. Perakis
Ames National Laboratory, Ames, IA 50011, USA
[2]Iowa State University, Ames, IA 50011, USA
[3]University of Alabama at Birmingham, Birmingham, AL35294, USA

Two-dimensional Coherent Terahertz (THz-2DCS) spectroscopy allows the study and control of quantum materials with an unprecedented resolution by using a pair of phase-locked, intense Terahertz (THz) laser pulses to capture both amplitude and phase dynamics. It adds a second frequency dimension that provides a strategy and advanced resolution to distinguish between multiple quantum pathways contributing at the same frequency in the one-dimensional (1D) spectra obtained by conventional ultrafast spectroscopies. Beyond characterizing equilibrium states, THz-2DCS provides advanced measurements of coherence, symmetry, correlations, couplings, and non-perturbative responses of light-induced non-equilibrium states of quantum materials—thus offering capabilities that conventional materials characterization techniques cannot. For instance, multiple electromagnetic field pulses with precisely tailored phases and amplitudes can be used to achieve nonlinear modulation of equilibrium quantum material properties in time and thus reveal emergent quantum phases. Starting from our theoretical predictions of new THz-2DCS spectral features arising from time-modulation of superconducting order parameters by a pair of electromagnetic field pulses with controlled relative phases [1,2,3], key milestones of our experiment-theory team's work presented in this talk include: *1. First-ever THz-2DCS measurements in superconductors,* uncovering a THz-light-induced transition from hybrid-Higgs modes to Floquet-driven states with phase-amplitude collective modes in iron pnictides [4,5]. *2. Discovery of THz-2DCS responses in infinite-layer nickelates* consistent with d-wave symmetry akin to cuprates [6,7]. *3. Demonstration of THz-light-induced persistent anisotropic DC supercurrents* that break inversion symmetry and activate forbidden Higgs and second-harmonic forbidden responses—laying the groundwork for quantum control through collective modes [8,9]. As a result, Higgs collective modes dominate THz 2DCS at *distinct* 2D frequencies, even in the absence of disorder, which allows their separation from quasiparticle excitations and enhances disorder mechanisms. In the first part of the talk, we will discuss *Dicke-superradiant-like coherent nonlinear emission* in periodically driven superconductor soliton states. Such superradiance-like nonlinear coherent emission behavior can be generated and controlled by designing THz excitation protocols involving single- and multi-cycle pulses. The Dicke model of soliton states describes the coupling of an ensemble of two-level quantum systems by a bosonic mode, such as the electromagnetic mode inside an optical cavity. A transition from the normal state, where the emitters/two level systems behave independently, to the superradiant state, characterized by cooperative "giant spin" soliton behavior, occurs as the coupling increases. It manifests as enhanced coherence and intensity of emitted radiation (Dicke superradiance). Here, synchronization of pseudo-spins is driven self-consistently by undamped order parameter oscillations. Fig.1 shows our simulations for a homogeneous FeAs superconductor with low-energy gap 2Δ=6.8 meV, which is excited by a $\omega_0 = 1$ THz multi-cycle pulse, which reveals that: *1. Weak excitation results in second-harmonic oscillations at $2\omega_0$ (grey line); 2. Above a critical excitation, soliton oscillations emerge at a distinct frequency ω_{sol} (magenta line), producing characteristic sidebands at $2\omega_{0-}\omega_{sol}$ in the 2D THz spectrum (white lines);3.Rabi flopping manifests as additional sidebands in THz-2DCS along the ω_τ-axis.*
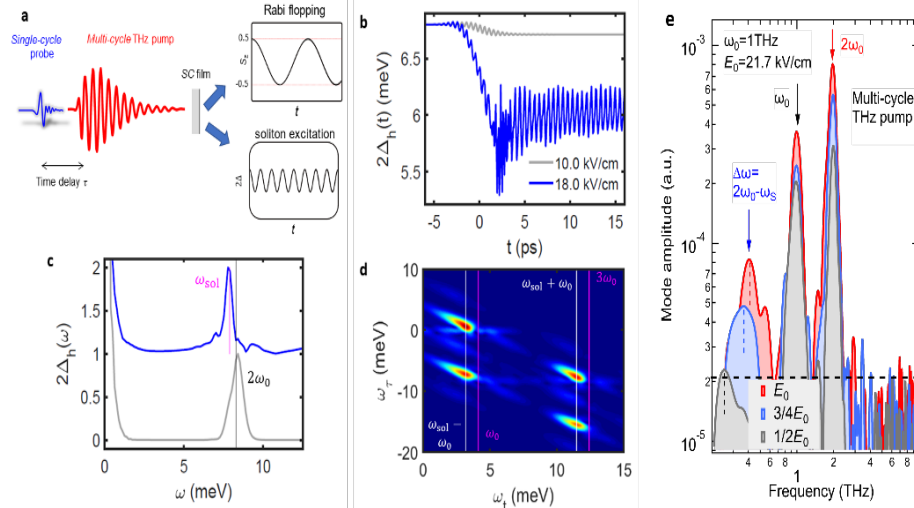
Fig. 1 (a) Schematics of THz-2DCS to drive and detect the pseudo-spin soliton state. *(b), (c) Superconductor order parameter dynamics for a weak and a strong THz electric field strength (b) and the corresponding spectra (c).* Traces are offset for clarity. *(d)* $E_{NL}(\omega_t, \omega_\tau)$ *spectrum for a pump electric field strength of 18.0 kV/cm.* White (magenta) linesindicate soliton sidebands at $\omega_t = \omega_{sol} \pm \omega_0$ *(the conventional third-order nonlinear signals are at $\omega_t = 2\omega_0 \pm \omega_{sol}$*

(e) Experimental data to detect pseudo-spin soliton nonlinear emission peaks at $2\omega_{0-}\omega_{sol}$, well below the SC energy gap

.

In the second part of the talk, we will discuss quantum echo signals made possible through Higgs collective modes and the retrieval of phase coherence stored in *multiple collective modes and quasiparticle excitations.* We reveal distinct rephasing and two-quantum pathways associated with unconventional broadening and Higgs-quasiparticle anharmonic couplings, including re-phasing and two-quantum coherence dynamics leading to echo signals with characteristic temporal profiles. By generating, preserving, and retrieving phase coherence, a pulse of light propagating through a medium with inhomogeneously broadened excitations and small homogeneous linewidth can be forced to re-emerge later as a *photon echo.* Here we compare echo signals involving collective modes in superconductors with those arising from uncorrelated two-level excitations as in atomic/spin systems, and with those from exciton or Josephson plasmon bosonic excitations, where the echo signal temporal profile is affected significantly by the scattering of bosonic excitations with momenta **Q** and **-Q**. For instance, exciton-exciton two-quantum coherences are known to introduce new wave mixing signals for negative time delays, absent in two-level systems. Here we show that superconducting echoes can arise from a "time grating" resulting coherence imprinted in the order parameter by the frequency-difference Raman process of excitation and deexcitation by two different THz pulses [1,2,3]. This order parameter modulation depends on the relative phase (time delay) between the two pulses. Unlike for bosonic excitations, where scattering affects the nonlinear effects, superconductor collective modes exhibit nonlinear coupling to other excitations via anharmonicity rather than direct interaction.
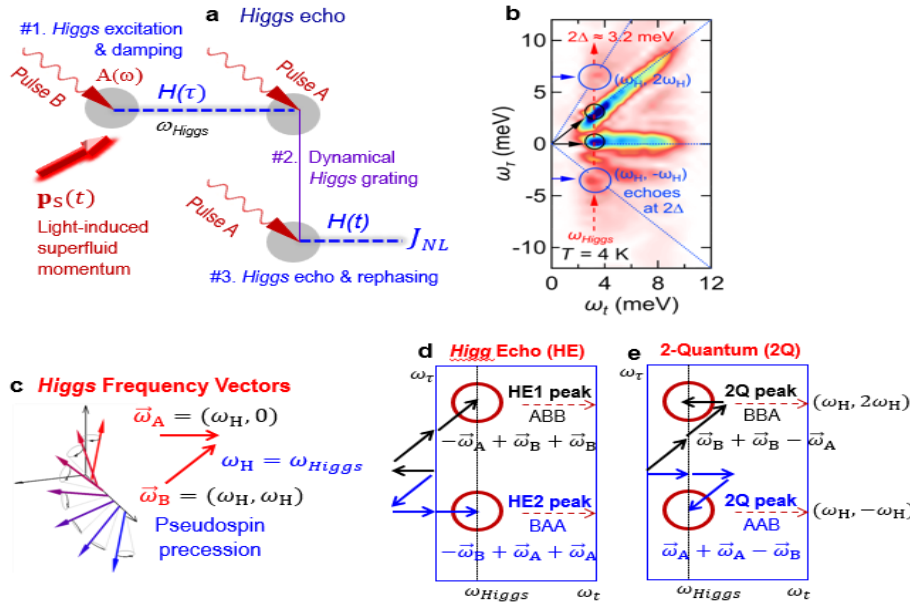
Fig. 2. Higgs Collective Mode Echo Signals. *(a) Illustration of Higgs Echo process where coherence is stored in a temporal grating of the order parameter. (b) Preliminary THz-2DCS experimental results showing a series of echo and pump-probe different peaks at the symmetry-forbidden Higgs frequency, separated along the vertical axis. (c) Higgs Wave Mixing. (d) Analysis of different processes leading to the observed Higgs Echo and Two-Quantum peaks.*

We will discuss the unconventional quantum echo signal arising from Higgs coherence in a niobium superconductor, and identify distinct experimental signatures attributed such anharmonicity. Notable differences from conventional behaviors include: 1.*Negative time delay signals* absent in uncorrelated two-level systems, arising from two-quantum processes involving Higgs (amplitude) modes coupled by anharmonicity; 2. *Rephasing signal contributions* exhibiting time-delayed photon echoes with distinct τ-dependence, i.e., with time profile differing from echoes in disordered two-level systems; 3. *Anharmonic effects in superconductors,* which contrast with interaction-induced echo features in excitonic systems and Josephson plasmons, where finite center-of-mass momentum *(Q,-Q)* continuum states dominate; 4.*Echo signals at the Higgs frequency* $\omega_H=2\Delta_{SC}$ distinct from conventional signals at laser frequencies $\sim\omega_0$ observed in earlier THz-2DCS semiconductor and superconductor studies. 5.*Higgs echo peaks in THz- 2DCS spectra* appearing at unique 2D frequencies $(2\Delta_{SC}, -2\Delta_{SC})$ and $(2\Delta_{SC}, 4\Delta_{SC})$ displaced along the phase-sensitive vertical axis, revealing unconventional broadening and Higgs-QP anharmonic coupling.

References
[1] M. Mootz, L.Luo, C. Huang, J. Wang, l. E. Perakis, P*hysical Review* B **109**, 014515 (2024).
[2] M. Mootz, J. Wang, I. E. Perakis, *Physical Review* B **102**, 054517 (2020).
[3] M. Mootz, L. Luo, J. Wang, l. E. Perakis, *Communications Physics* **5**, 47 (2022).
[4] L. Luo, M. Mootz, J.H. Kang, C. Huang, K. Eom, J.W. Lee, C. Vaswani, Y.G. Collantes, E.E. Hellstrom, I. E. Perakis, C. B. Eom, J. Wang , *Nature Physics* **19**, 201 (2022).
[5] C. Vaswani, J. H. Kang, M. Mootz, L. Luo, X. Yang, C. Sundahl, D. Cheng, C. Huang, R. H. J. Kim, Z. Liu, Y. G. Collantes, E. E. Hellstrom I. E. Perakis, C. B. Eom and J. Wang, *Nature Communications* **12**, 258 (2021).
[6] B. Chen , D. Cheng, K.Lee , L.Luo, Z.Chen, Y.Lee, B. Y.Wang, M.Mootz, I.E. Perakis, Z.-X.Shen, H. Y. Hwang, J. Wang, *Nature Materials* **23,** 775 (2024)
[7] B. Chen, D. Cheng, K. Lee, M. Mootz, C. Huang, L.Luo, Z. **Chen**, Y.Lee, B.Y. Wang, I.E. Perakis, *Physical Review* B **111**, 014519 (2025).
[8] X. Yang, C. Vaswani, C. Sundahl, M. Mootz, L. Luo, J. H. Kang, I. E. Perakis, C. B. Eom, J. Wang, *Nature Photonics* **13**, 707 (2019).
[9] C. Vaswani, C. Sundahl, M. Mootz, D. H. Mudiyanselage, J. H. Kang, X. Yang, D. Cheng, C. Huang, R. H. J. Kim, Z. Liu, L. Luo, I. E. Perakis C. B. Eom, J. Wang, *Physical Review Letters* **124**, 207003 (2020).

Quantum thermalization via travelling waves

A. Picano[1], G. Biroli[2], M.Schirò[1]

[1]Collège de France, PSL Research University, 75321 Paris, France
[2] Université Paris Cité, 75005 Paris, France

Isolated quantum many-body systems which thermalize under their own dynamics are expected to act as their own thermal baths [1], thereby losing memory of initial conditions and bringing their local subsystems to thermal equilibrium. Here [2], we show that the infinite-dimensional limit of a quantum lattice model, as described by dynamical mean-field theory (DMFT), provides a natural framework to understand this self-consistent thermalization process [3, 4]. Using the Fermi-Hubbard model as a working example, we demonstrate that the emergence of a self-consistent bath occurs via a sharp thermalization front, moving ballistically and separating the initial condition from the long time thermal fixed point (Fig. 1). We characterize the full DMFT dynamics through an effective temperature for which we derive a traveling wave equation of the Fisher-Kolmogorov-Petrovsky-Piskunov type [5]. This equation allows for predicting the asymptotic shape of the front and its velocity, which match perfectly the full DMFT numerics. Our results provide a new angle to understand the onset of quantum thermalization in closed isolated systems.
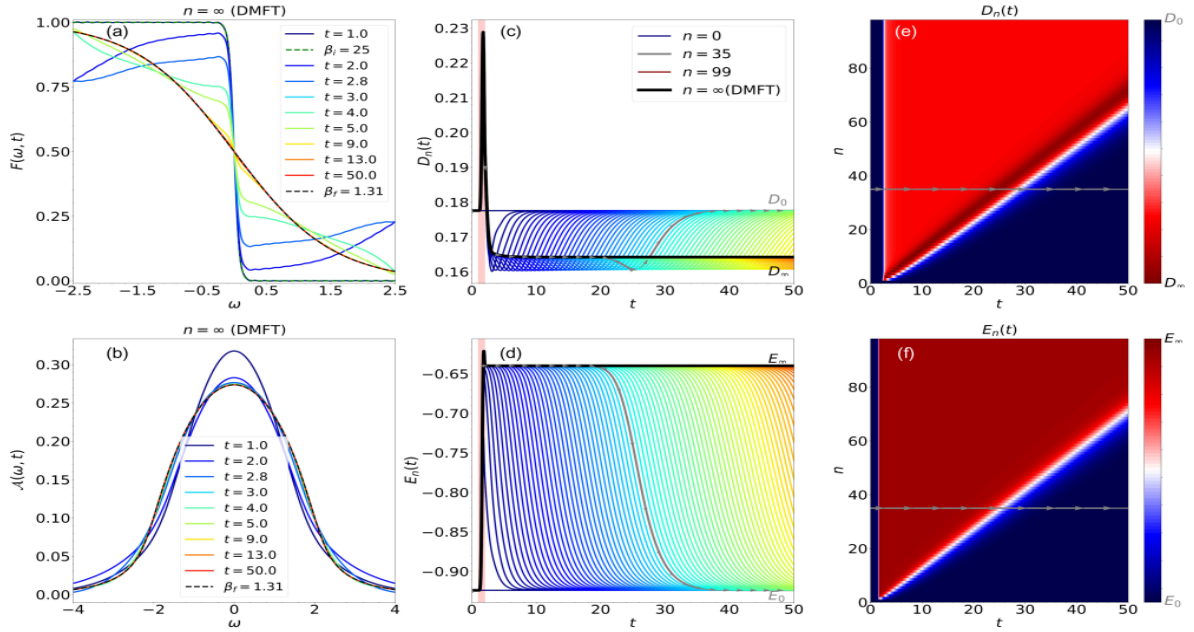
Fig. 1. Thermalization in infinite dimensions with DMFT. *Time evolution of the distribution function (a) and spectral function (b) after an energy excitation, for $U = 2$ (initial inverse temperature $\beta_i = 25$), leading to a thermal equilibrium fixed point. Full self-consistent DMFT solution [$n = \infty$ in the notation of panels (c),(d)]. Thermalization front: time evolution of the total energy (c) and double occupation (d) after an energy excitation, for different DMFT iteration numbers (**colored lines from blue to red** as a function of the DMFT iteration number $n \in [0, 99]$ and compared to the full self-consistent DMFT solution (**black line**). Emergence of a thermalization front in both energy and double occupation, panels (e), (f).*

A natural avenue for future applications of this methodology is the case of disordered quantum many-body systems, using statistical DMFT [6]. We can expect that, in an Anderson localized phase, the ballistic front would give way to a localized one, which never loses memory of the initial condition. In the presence of disorder and interactions, we argue a competition between thermalizing fronts and pinning due to disorder, which could shed new light on the stability of many-body localization.

References
[1] R. Nandkishore, D. A. Huse, *Annual Review of Condensed Matter Physics* **6**, 15 (2015).
[2] A. Picano, G. Biroli, M. Schiro, *Physical Review Letters* **134,** 116503, (2025).
[3] A. Georges, G. Kotliar, W. Krauth, M. J. Rozenberg, *Review of Modern Physics* **68**, 13 (1996).
[4] H. Aoki, N. Tsuji, M. Eckstein, M. Kollar, T. Oka, P. Werner, *Review of Modern Physics* **86**, 779 (2014).
[5] É. Brunet, B. Derrida, *Journal of Statistical Physics* **161**, 801 (2015).
[6] E. Miranda, V. Dobrosavljević, *Reports on Progress in Physics* **68**, 2337 (2005).

Controlling quantum material properties via artificial structures

R. P. Prasankumar
Los Alamos National Laboratory, Los Alamos NM 87545, USA

Quantum materials display a host of fascinating phenomena, including high-T_c superconductivity, novel topological phenomena, and excitonic condensates [1], [2], [3] These materials are exquisitely sensitive to external perturbations including pressure, light, and magnetic fields, allowing one to readily tune their properties for a given phenomenon or application. More recently, substantial attention has been devoted to the use of artificial structures (e.g., cavities, metamaterials, and heterostructures) to control and even enhance the intrinsic properties of quantum materials. Here, some examples in which artificial structures are used to modify novel phenomena in different quantum materials will be discussed. Recently, broken symmetries in quantum materials have garnered substantial interest, as they lead to nonlinear responses including terahertz (THz) emission and second harmonic generation (SHG) under optical excitation [4]. By tailoring the driving optical field, one can control the degree of symmetry breaking in a given material, which in turn influences linked properties like topology and magnetic order. One example was shown in the topological semimetal TaAs, where optically driven transient photocurrents emit THz radiation [5] and drive transient symmetry breaking, observed with SHG [6] The photoexcited carriers drive coherent shear and longitudinal phonons that can be observed with time-resolved X-ray diffraction [7]. However, these responses are governed by the intrinsic properties of TaAs; instead, could one artificially structure a quantum material for greater control over its response? One approach is to use metasurfaces, which have been extensively explored in conjunction with conventional metals, semiconductors, and insulators [8], [9], [10], but rarely combined with quantum materials.[11], [12], [13], [14], [15], [16], [17], [18] By designing a metasurface that explicitly breaks symmetry, photocurrents can be generated and controlled in a normally centrosymmetric material like graphene[19]We designed optoelectronic metasurfaces composed of arrays of teardrop-shaped gold nanoantennas with resonances at 800 nm that were fabricated on graphene monolayers (Fig. 1).
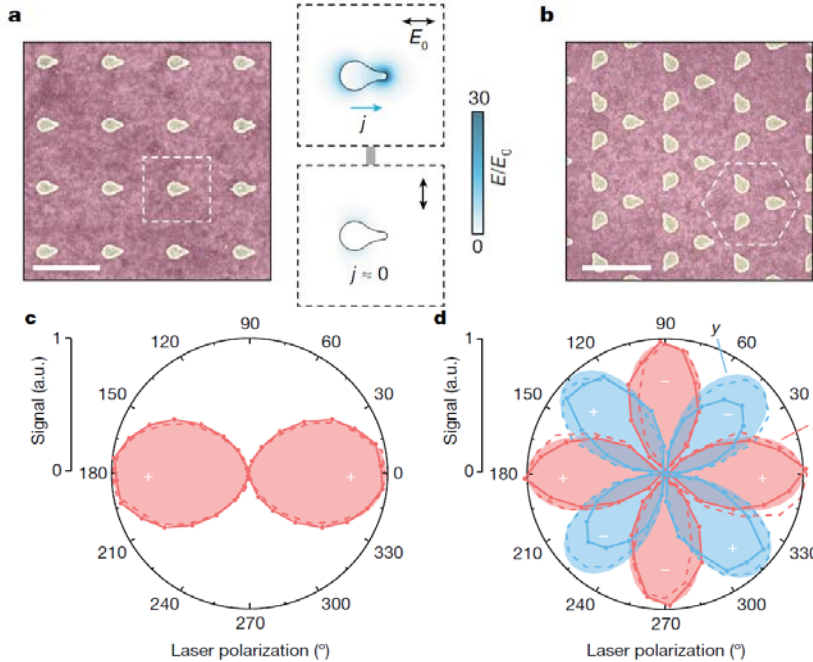
Fig. 1. SEM images of (a) uniformly oriented and (b) Kagome metasurfaces consisting of teardrop Au nanoantennas on graphene. (c, d) Measured x (red) and y (blue) components of the emitted THz field from the metasurfaces in (a,b), respectively, as a function of the incident polarization angle.[19]

Femtosecond excitation of the uniformly oriented metasurface (Fig. 1(a)) at 800 nm yields a directional THz emission pattern (Fig. 1(c)), demonstrating the ability of appropriately designed metasurfaces to generate directional photocurrents in a centrosymmetric quantum material. Furthermore, when orienting the nanoantennas in a Kagome pattern with threefold rotational symmetry (Fig. 1(b)), control of the incident light polarization gives additional control over the directionality of the emitted photocurrents (Fig. 1(d)). Finally, with nonuniform spatial patterning we were able to generate radially and azimuthally polarized THz fields, providing a new degree of control over THz fields that could lead to a host of new phenomena and applications [19].

Another approach for modifying quantum material properties relies on external cavities. This has already been shown to modify the insulator-metal transition in 1T-TaS2 [15], but to the best of our knowledge has never experimentally been shown to modify superconductivity, despite several theoretical studies [20], [21], [22], [23], [24], [25], [26], [27]. Notably, an appropriately designed cavity could make it possible to modify superconducting properties in equilibrium, without an external driving electromagnetic field. Two-dimensional (2D) van der Waals materials can naturally act as high-quality cavities, making it possible to experimentally test these concepts.
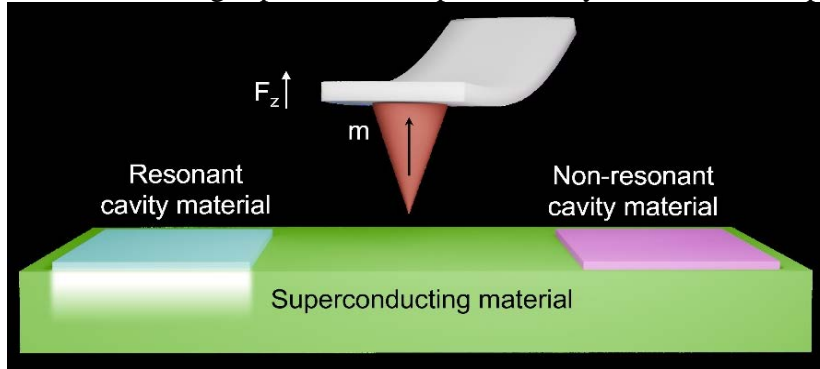
Fig. 2. Schematic of SNOM and MFM measurements on resonant and non-resonant cavities placed on top of a superconducting material.

Here, we placed 2D materials on the surface of a superconductor and used scanning near-field optical microscopy (SNOM) to demonstrate coupling between phonon-polaritons in the 2D material to phonons in the superconductor that have previously been linked to superconductivity. We then used magnetic force microscopy (MFM) to measure the influence of the 2D cavity material on the superfluid density, observing a reduction near the 2D material/superconductor interface. The influence of the cavity on superconductivity was further supported by comparison to a cavity formed with a non-resonant material as well as to the bare superconducting material, neither of which showed a suppression of the superfluid density. To the best of our knowledge, this is the first experimental demonstration of cavity-modified superconductivity, setting the stage for future enhancements in the critical temperature with an optimal cavity design.

References
[1] D. N. Basov, R. D. Averitt, D. Hsieh, *Nature Materials* **16**, 1077 (2017).
[2] B. Keimer, J. E. Moore, *Nature Physics* **13,** 1045 (2017).
[3] Y. Tokura, M. Kawasaki, N. Nagaosa, *Nature Physics* **13**, 1056 (2017).
[4] J. Pettine, P. Padmanabhan, N. Sirica, R. P. Prasankumar, A. J. Taylor, H. T. Chen, *Nature Light Science and Applications*, (2023).
[5] N. Sirica, R. I. Tobey, L. X. Zhao, G. F. Chen, B. Xu, R. Yang, B. Shen, D. A. Yarotski, P. Bowlan, S. A. Trugman, J.-X. Zhu, Y. M. Dai A. K. Azad, N. Ni, X. G. Qiu, A. J. Taylor, R. P. Prasankumar, *Physical Review Letters* **122**, 197401 (2019).
[6] N. Sirica, P. P. Orth, M. S. Scheurer, Y.M. Dai, M.-C. Lee, P. Padmanabhan, L.T. Mix, S. W. Teitelbaum, M. Trigo, L.X. Zhao, G.F. Chen, B. Xu R. Yang, B. Shen, C. Hu, C.-C. Lee, H. Lin, T.A. Cochran, S.A. Trugman, J.-X. Zhu, M. Z. Hasan, N. Ni, X.G. Qiu, A.J. Taylor, D.A. Yarotski R. P. Prasankumar, *Nature Materials* **21**, 62 (2022).
[7] M.-C. Lee, N.S. Sirica, S. W. Teitelbaum, A. Maznev, T. Pezeril, R. M. Tutchton, V. Krapivin, G. A. de la Pena, Y. Huang, L. X. Zhao, G. F. Chen B. Xu, R. Yang, J. Shi, J. Zhu, D.A. Yarotski, X. G. Qiu, K. A. Nelson, M. Trigo, D. A. Reis, R.P. Prasankumar, *Physical Review Letters* **128** 155301 (2022).
[8] H. Chen, A. J. Taylor, N. Yu, *Reports on Progress in Physics*. **79**, 76401 (2015).
[9] K. Fan, W. J. Padilla, *Materials Today* **18**, 39 (2015).
[10] M. Lapine, I. V Shadrivov, Y. S. Kivshar, *Review of Modern Physics*. **86**, 1093 (2014).
[11] L. Yuan, J. Jeong, K. W. C. Kwock, E. S. Yanev, M. Grandel, D. Rhodes, T. S. Luk, P. J. Schuck, D. Yarotski, J. C. Hone, I. Brener R. P. Prasankumar. *Nano Letters* **21**. 9930 (2021).
[12] S. Rajabali, S. Markmann, E. Jöchl, M. Beck, C.A. Lehner, W. Wegscheider, J. Faist, G. Scalari, *Nature Communications* **13**, 2528(2022).
[13] I. I. Smolyaninov, V. N. Smolyaninova, *Nanophotonics* **7**, 795 (2018).
[14] H. Chen, H. Yang, R. Singh, J.F. O'Hara, A.K. Azad, S.A. Trugman, Q.X. Jia, A.J. Taylor, *Physical Review Letters* . **105**, 247402 (2010).
[15] G. Jarc,S. Y. Mathengattil, A. Montanaro, F. Giusti, E. M. Rigoni, R. Sergo, F. Fassioli, S. Winnerl , S. D. Zilio, D. Mihailovic , P. Prelovšek M. Eckstein, D. Fausti, *Nature* **622**, 487(2023).
[16] J. van de Groep, J. H. Song, U. Celano, O. Li, P. G. Kik, M. L. Brongersma, *Nature Photonics* **14**, 426 (2020).
[17] W. Liu, Z. Ji, Y. Wang, G. Modi, M. Hwang, B. Zheng, V.J.Sorger, A. Pan, R. Agarwal, *Science* **370**, 600 (2020).
[18] F. Schlawin, D. M. Kennes, M. A. Sentef, *Applied Physics Review* **9**, 011312 (2022).
[19] J. Pettine, P. Padmanabhan, T. Shi, L. Gingras, L. McClintock, C.-C. Chang , K. W. C. Kwock, L. Yuan, Y. Huang, J. Nogan , J. K. Baldwin P. Adel, R. Holzwarth, A. K. Azad, F. Ronning, A. J. Taylor, R. P. Prasankumar, S.-Z. Lin, H.-T. Chen, *Nature* **626**, 984 (2024).
[20] F. Schlawin, A. Cavalleri, D. Jaksch, *Physical Review Letters* **122**, 133602 (2019).
[21] I.-T. Lu, D. Shin, M. K. Svendsen, H. Hübener, U. De Giovannini, S. Latini, M. Ruggenthaler, A. Rubio, *Proceedings of National Academy of Science USA* **121**, e2415061121 (2024).
[22] M. E. Berkowitz, B. S. Y. Kim, G. Ni, A. S. McLeod, L. Lo, G. Gu, K. Watanabe, T. Taniguchi, J. Hone, M. M. Fogler, R. A. Averitt D. N. Basov, *Nano Letters* **21**, 308 (2021).
[23] M. A. Sentef, M. Ruggenthaler, A. Rubio, *Science Advances* **4** , 2018.
[24] J. B. Curtis, A. Grankin, N. R. Poniatowski, V. M. Galitski, P. Narang, E. Demler, *Physical Review Research* **4**, 013101 (2022).
[25] H. Gao, F. Schlawin, M. Buzzi, A. Cavalleri, D. Jaksch, *Physical Review Letters* **125**, 053602 (2020).
[26] J. B. Curtis, Z. M. Raines, A. A. Allocca, M. Hafezi, V. M. Galitski, *Physical Review Letters* **122**, 167002 (2018).
[27] M. A. Sentef, M. Ruggenthaler, A. Rubio, *Science Adv*ances **4**, 1 (2018).

Entropy production in ultrafast classical and Quantum stochastic dynamics

Y. Qiao, R. M. Geilhufe

Chalmers University of Technology, 41296 Gothenburg, Sweden

Thanks to advancements in femtosecond and attosecond laser technology, thermodynamics has entered the ultrafast era. Ultrafast dynamics provide a unique way to probe the transient properties of materials. Specifically, the nonequilibrium dynamics induced by external fields, such as ultrashort THz pulses, are accompanied by heat and mass transfer, which are further characterized by entropy production. In [1], ultrafast stochastic thermodynamics based on X-ray scattering experiments [2] was developed and has been successfully applied to the study of entropy production in collective excitations, such as phonons (see schematic diagram Fig. 1). However, developing unified stochastic thermodynamics for both classical and quantum systems remain an open challenge [3].
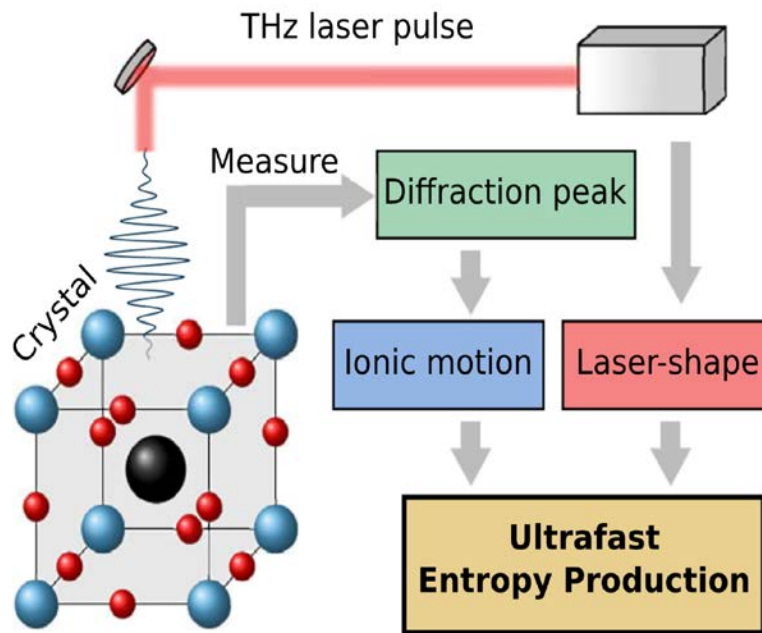
Fig. 1. Schematic representation of a crystal (SrTiO3 or KTaO3) excited by a THz laser pulse [1].

In this talk, I will discuss how to develop ultrafast stochastic thermodynamics in both classical and quantum phonon systems. Modeling stochastic thermodynamics requires exploring microscopic details, particularly the interactions between systems and their environments. In the classical part, we consider a phonon-phonon coupling model, from which we derive a non-Markovian Langevin equation for a laser-driven phonon mode. The thermal fluctuations from the environment modes are treated as correlated stochastic forces acting on the system. With the spectral data of the noise correlation function, we calculate the entropy production using the path integral method and compare our result with those of advanced numerical simulations. In the quantum realm, fluctuations arising from the uncertainty principle are inevitable even in a vacuum. Consequently, in quantum analogues of the Langevin equations, classical stochastic forces are replaced by quantum operators characterized by their expectation values and correlation functions. In the second part of this talk, I will discuss how to investigate ultrafast stochastic dynamics in the framework of open quantum systems. I will present how the corresponding entropy production in the quantum phonon-phonon coupling model is quantized when quantum effects are taken into account.

References
[1] L. Caprini, H. Löwen, R. M. Geilhufe, *Nature. Communication.* **15**, 94 (2024).
[2] M. Kozina, M. Fechner, P. Marsik, T. van Driel, J. M. Glownia, C. Bernhard, M. Radovic, D. Zhu, S. Bonetti, U. Staub M. C. Hoffmann *Nature. Physics.* **15**, 387 (2019).
[3] G. T. Landi, M. Paternostro, *Revies of Modern Physics* **93**, 035008 (2021).

Ultrafast nano-imaging and tip-enhanced control of Electronic coherence in 2D semiconductors

M. B. Raschke

University of Colorado, Boulder, CO 80309, USA

Understanding and ultimately controlling the properties of quantum materials and their coupled degrees of freedom will require counteracting the effects of dissipation and dephasing. This necessitates imaging the elementary excitations on their natural time and length scales. To achieve this goal, we developed scanning probe microscopies with ultrafast and shaped laser pulses for multiscale coherent spatio-temporal optical nano-imaging. In corresponding ultrafast movies, we resolve the fundamental quantum dynamics down to the few-femtosecond regime with nanometer spatial resolution. Specifically, in 2D materials and their heterostructures, the emergent electronic, spin, and other quantum properties are controlled by the underlying interlayer coupling and associated charge and energy transfer dynamics. These processes are sensitive to interlayer distance and crystallographic orientation, which are in turn affected by defects, grain boundaries, and other nanoscale heterogeneities. In this talk, I will present the use of adiabatic plasmonic nanofocused four-wave mixing (FWM) [1] to image the coherent electron dynamics in monolayer WSe_2 resolving nanoscale heterogeneities in dephasing ranging from $T_2 < 5$ fs to $T_2 > 60$ fs on length scales of 50-100 nm [2]. Further, in combination with Purcell-enhanced nano-cavity clock spectroscopy [3] in WSe_2/graphene heterostructures we identify interlayer energy transfer dynamics at times scales of 350 fs [4].
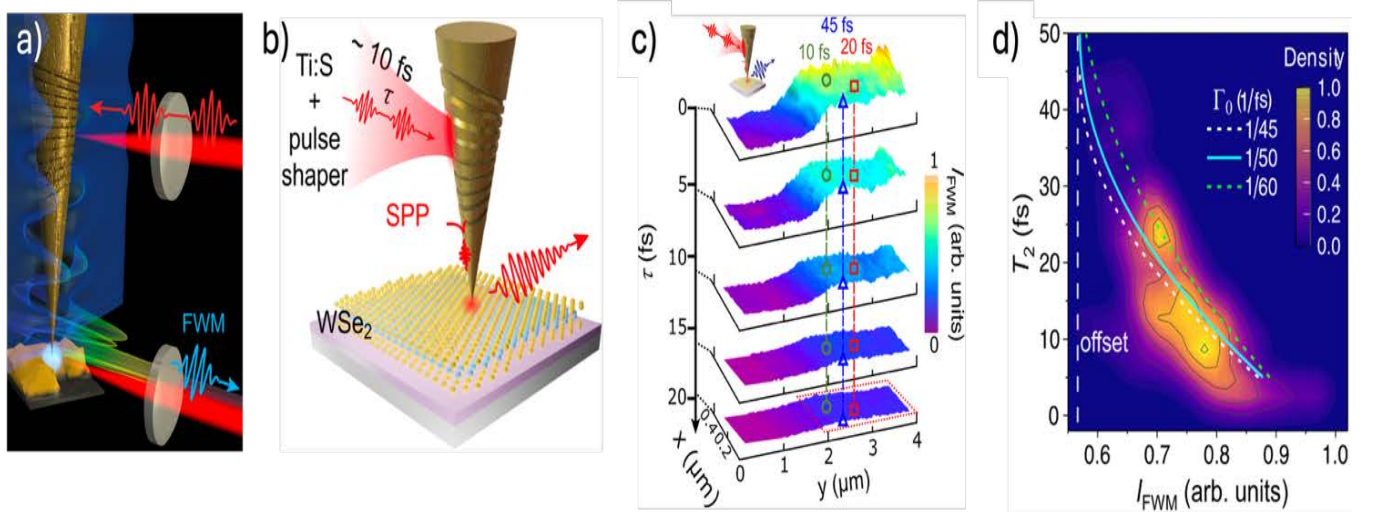
Fig. 1 : a-illustration of adiabatic nano-focusing of few-fs pulses with pulse-shaper and MIIPS controlled pulse replica for interferometric nano-localized FWM spatio-temporal coherent spectroscopy; **b**-application to 2D semiconductors probing exciton coherence, its spatial heterogeneity, and relation to local defects and strain; **c**- spatio - temporal variation of dephasing time ranging from < 5fs to >60 fs on length scales of 50-100 nm;**d**- unusual anti-correlation of coherence time T_2 with FWM signal intensity as a result of defect induced decoherence within the coherence area defined by spatial extent of the tip-confined optical near-field defining a new regime of nonlinear nano-optics.

Beyond the fundamental understanding to the competition between intrinsic and extrinsic effects on excitation lifetimes and coherence, we discover a new regime of nonlinear nano-optics at the interplay of spatial coherence and disorder-induced scattering.

References
[1] T. Jiang, V. Kravtsov, M.Tokman, A. Belvanin, M.B. Raschke, *Nature Nanotechnology* **14**, 838 (2019).
[2] W. Luo, W. Luo, B.G. Whetten, V. Kravtsov, A. Singh, Y. Yang, A. Belvanin, M. Raschke, *Nano Letters* **23**, 1767 (2023).
[3] M. A. May, T. Jiang, C. Du, K.D. Park, X. Xu, A. Belvanin, M.B. Raschke *Nano Letters* **21**, 522 (2020).
[4] W. Luo, R Song, B. G Whetten, D. Huang, X. Cheng, A .Belyanin, T. Jiang, M.B. Raschke, *Small* **20**, 2307345 (2024).

A femtosecond time- and momentum-resolved journey through the Exciton landscape of 2D, organic and hybrid 2D/organic semiconductors

M. Reutzel

Georg-August-Universität Göttingen,37077 Göttingen, Germany

Transition metal dichalcogenides (TMDs) are an exciting model system to study ultrafast energy dissipation pathways, and to create and tailor emergent quantum phases. The versatility of TMDs results from the confinement of optical excitations in two-dimensions and the concomitant strong Coulomb interaction that leads to excitonic quasiparticles with binding energies in the range of several 100 meV. In TMD stacks consisting of at least two layers, the interlayer interaction can be precisely controlled by manipulating the twist angle: The misalignment of the crystallographic directions leads to a momentum mismatch between the high symmetry points of the hexagonal Brillouin zones. This strongly impacts the interlayer wavefunction hybridization, and, moreover, adds an additional moiré potential. Crucially, in this emergent energy landscape, dark intra- and interlayer excitons dominate the energy dissipation pathways. While these dark excitonic features are hard to access in all-optical experiments, time-resolved momentum microscopy [1] can provide unprecedented insight on these quasiparticles [2].

In the first part of my talk, I will present our results on the ultrafast formation dynamics of interlayer excitons in twisted WSe_2/MoS_2 heterostructures [3-6]. First, I will report on the identification of a hallmark signature of the moiré superlattice that is imprinted onto the momentum-resolved interlayer exciton photoemission signal. With this data, we reconstruct the electronic part of the exciton wavefunction, and relate its extension to the moiré wavelength of the heterostructure. Second, I will show that interlayer excitons are effectively formed via exciton-phonon scattering, and subsequent interlayer tunneling at the interlayer hybridized Σ valleys on the sub-50 fs timescale. Third, I will discuss our efforts to monitor the interlayer exciton formation dynamics with spatiotemporal resolution using femtosecond photoelectron dark-field microscopy.
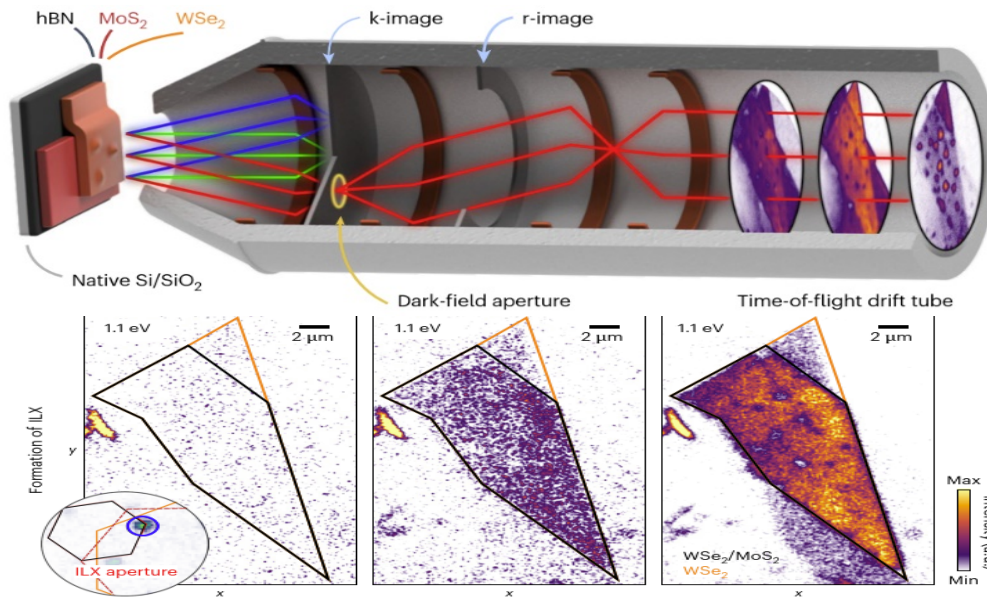
Fig. 1. Working principle of the femtosecond photoelectron dark -field microscope. By placing the dark field aperture on the energy - momentum photoemission signature of the dark interlayer excitons, their formation dynamics can be probed with 50 fs time- and 500 nm spatial resolution. Figs. adopted from Ref. [6].

Finally, I will show how ultrafast momentum microscopy experiments are not limited to 2D TMD heterostructures, but can also be employed to study the ultrafast formation of hybrid Frenkel-Wannier excitons in organic/inorganic heterostructures (i.e., PTCDA/WSe_2) [7].

References
[1] M. Keunecke, C. Möller, D. Schmitt, H. Nolte, G. S. M. Jansen, M. Reutzel, M. Gutberlet, G. Halasi, D. Steil, S. Steil, S. Mathias, *Review of Scientific Instruments* **91**, 063905 (2020).
[2] M. Reutzel, G.S.M. Jansen, S. Mathias, *Advances in Physics* X **9**, 2378722 (2024).
[3] D. Schmitt. J. P. Bange, W. Bennecke, A. A. Al-Mutairi, K. Watanabe, T. Taniguchi, D. Steil, D. R. Luke, R. T. Weitz, S. Steil G. S. M. Jansen, S. Hofmann, M. Reutzel, S. Mathias, *Nature* **608**, 499 (2022).
[4] J. P. Bange, P. Werner, D. Schmitt, W. Bennecke, G. Meneghini, A. A. Al-Mutairi, M. Merboldt, K. Watanabe, T Taniguchi, S. Steil D. Steil, R T. Weitz, S. Hofmann, G. S. M. Jansen, S. Brem, E. Malic, M. Reutzel, S.Mathias, *2D Materials* **10**, 035039 (2023).
[5] J. P. Bange, D. Schmitt, W. Bennecke, G. Meneghini , A. A. Al-Mutairi K. Watanabe, T. Taniguchi , D. Steil, S. Steil , R. T. Weitz G. S. M. Jansen, S. Hofmann , S. Brem , E.Malic, M. Reutzel, S. Mathias , *Science Advances* **10**, eadi1323 (2024).
[6] D. Schmitt, J.P. Bange. W. Bennecke. G. Meneghini. A.A. Al-Mutairi. M. Merboldt. J. Pöhlset al.. *Nature Photonics* 19, 187 (2025).
[7] W. Bennecke, I.G. Oliva, J.P. Bange, P. Werner, D. Schmitt, M.Merboldt, A.M. Seiler, K. Watanabe, *arXiv:2411.14993* (2024).

Coherent control through phonon anharmonicity

G.Scharf, T. Hasharoni, L. Donva, L. Ben Gur, A. Ron

Tel Aviv University, Tel Aviv, 6997801 Israel

Anharmonic lattice vibrations play a key role in many physical phenomena. They govern the heat conductivity of solids, strongly affect the phonon spectra, play a prominent role in soft mode phase transitions, allow ultrafast engineering of material properties and more. The most direct evidence for anharmonicity is to measure the oscillation frequency changing as a function of the oscillation amplitude. For lattice vibrations, this is not a trivial task, and anharmonicity is probed indirectly through its effects on thermodynamic properties and spectral features or through coherent decay of one mode to another. However, measurement of the anharmonicity of a single Raman mode is still lacking. We show that ultrafast double pump-probe spectroscopy could be used to directly observe frequency shifts of Raman phonons as a function of the oscillation amplitude and disentangle the coherent contributions from quasi-harmonic sources such as temperature and changes to the carrier density in the thermoelectric materials SnTe and SnSe [1]. Our results have dramatic implications for the material engineering of future thermoelectrics. Moreover, our methodology could be used to isolate the basic mechanisms driving optically induced phase transitions and other nonlinear phenomena based on their unique timestamps. Fig. 1 shows a summary of the single pump-probe measurements taken on SnTe.
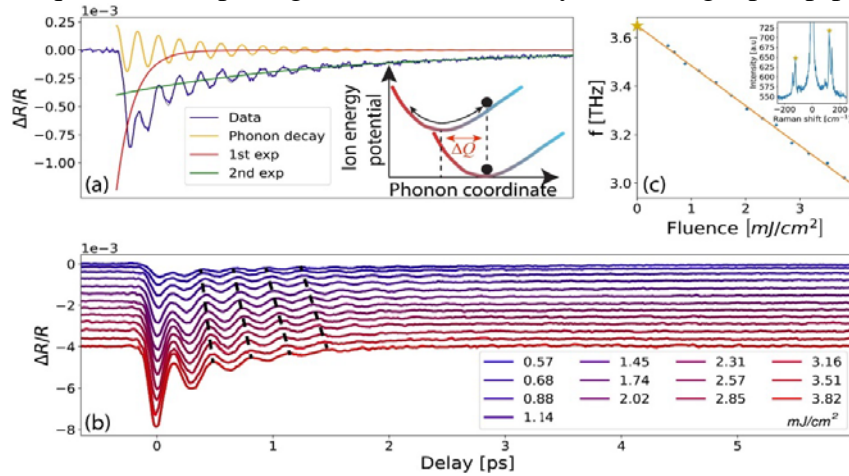
Fig.1. a) typical transient reflectivity measurement at a fluence of 0.57mJ/cm². The signal could be fit to two exponentially decaying components and a damped oscillatory component; b) fluence dependence of the signal. Apart from the expected changes to the amplitude of the signal a change in the positions of the oscillatory peaks shows the change in the oscillation frequency as a function of the pump fluence indicating of the mode anharmonicity; c)extracted frequencies from the data in (b) as a function of the fluence. The frequency extrapolates to the known frequency of an A_g mode of SnTe as also measured by Raman spectroscopy (inset).

Fig. 2 shows the results of a double pump experiment done to separate the different contributions to anharmonicity.

Fig.2 a) the transient reflectivity (color) as a function of the pump-pump delay (vertical axis) and trailing pump-probe delay (horizontal axis). Shifts in the oscillatory peak positions as a function of pump-pump delay are visible in the raw data and are indications of the phonon anharmonicity; b) is extracted frequency as a function of pump-pump delay. At short times the signal shows an oscillatory behavior (inset) while at longer timescales decaying bi-exponential behavior is observed; c) compares the frequency shifts to the transient reflectivity measured only by the leading pump.
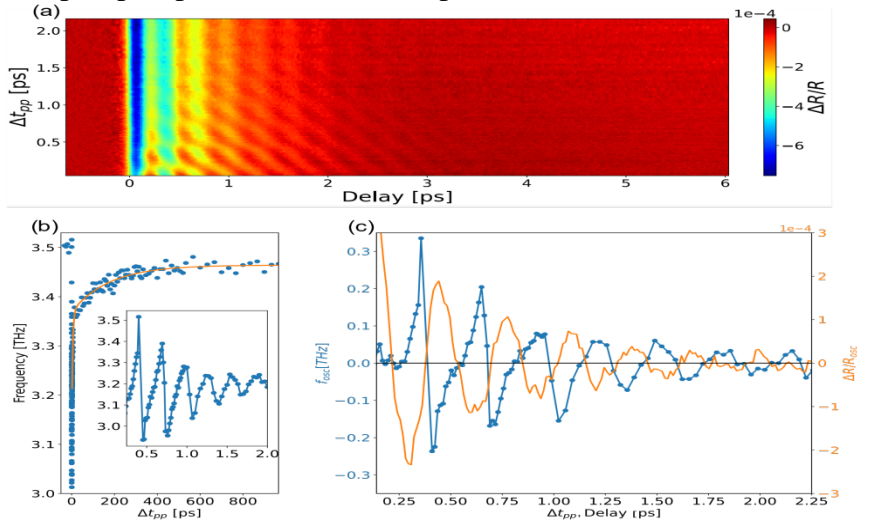
This indicates that the frequency shifts result from three different physical origins, thermal and electronic detected as the bi-exponential components and a pure anharmonic signal manifested as the oscillations at short timescales

References

[1] G. Scharf, T. Hasharoni, L. Donval, L.B. Gur, A. Ron, *arXiv preprint arXiv:2503.10757* (2025).

Advanced 2.1µm femtosecond laser technology for improved Conversion to the THz region

S.Tomilov, M. Redkin, Y. Wang, W. Yao, A. O. Suzuki, C. J. Saraceno

Ruhr-Universität Bochum, 44801 Bochum, Germany

Ultrafast lasers are ubiquitous front-end systems for generating short Terahertz transients and are thus essential tools in progressing THz science and technology. However, so far, most driving lasers have concentrated on commercially available technologies, most dominant ones being Ti:Sapphire lasers and Er-doped fiber lasers, with their well-known limitations in average power. More recently Yb-lasers emitting at around 1030nm with high average power have emerged also as an alternative for increasing the average power of pulsed THz sources, with sources currently approaching the watt level [1]. In this context, many Terahertz generation schemes could greatly benefit from longer driving wavelengths with comparable performance to the more well-established laser systems. For example, they allow in many $c^{(2)}$ materials to reduce the impact of multi-photon absorption, as well as enable to reach high conversion efficiencies in two-color plasma sources, thanks to increase ponderomotive energy [1,2]. More generally, long-wavelength lasers are also desired for reaching high photon energies up to soft X-rays in high harmonic generation and for reaching mid-IR light using various oxide nonlinear crystals that are not transparent at the traditionally used wavelengths. In this goal of improving the performance and coverage of secondary sources, the 2-3µm wavelength region is being currently heavily explored in the laser community. Traditionally, high-power ultrafast sources in this wavelength region are restricted to complex and inefficient parametric conversion stages, allowing to reach tens of watts of average power, using pumps with several hundreds of watts based on Yb systems in most latest state-of-the-art lab developments. A much more elegant and simple approach is to use gain media directly emitting in this wavelength range for high-power oscillators and amplifiers. As shown in Fig. 1, many advances have been realized in bulk and fiber-based amplifier systems in this wavelength range. Some remarkable achievements in the wider area of high-power 2 µm ultrafast lasers are the demonstration of a Tm-fiber based chirped pulse amplifier systems, with an average power of 1060 W at 80-MHz pulse repetition frequency, corresponding to a pulse energy of 13.2 µJ [4]. Nevertheless, compared with ultrafast lasers in the 1-µm wavelength range, the average power of 2 µm ultrafast lasers are at least one order of magnitude lower as show in Fig. 1, showing large potential for further progress.
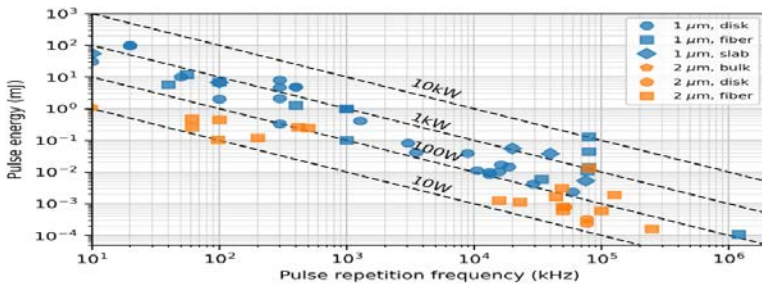
Fig. 1. Comparison of state-of-the art of ultrafast lasers at 1µm and 2µm, including oscillators and amplifiers

In the context of the different emerging laser technologies for accessing this wavelength region, Holmium lasers are particularly attractive for power and energy scaling because they operate in a window of atmospheric transmission at 2.1µm; furthermore, Holmium operates as a three-level laser with very comparable thermal advantages to Ytterbium. In this presentation, we will discuss the development of high-power 2 µm disk and bulk lasers, based on Holmium-doped materials and current challenges and application possibilities, with a focus towards THz generation using these sources. We will present a novel broadband regenerative amplifier based on the new gain material Ho:CALGO, 100µJ pulse energy with femtosecond pulse durations at 100 kHz and pulse compression to sub-100 fs. We will discuss the different THz generation schemes where these novel sources are promising to enable high average power, high repetition rate THz sources operating with very high conversion efficiency.

References

[1] T. Vogel, S. Mansourzadeh, C. J. Saraceno, *Optics Letters*. **49**, 4517 (2024).
[2] A. D Koulouklidis, C. Gollner, V. Shumakova, V.Y. Fedorov, A. Pugžlys, A. Baltuška, S. Tzortzakis, *Nature Communications* **11**, 292 (2020)
[3] C. Gollner, M. Shalaby, C. Brodeur, I. Astrauskas, R. Jutas, E. Constable, L. Bergen, A. Baltuška, A. Pugžlys; *APL Photonics* **6**, 046105 (2021)
[4] C. Gaida, M. Gebhardt, T. Heuermann, F. Stutzki, C. Jauregui, J. Limpert, *Optics Letters* **43**, 5853 (2018).

Nonlinear terahertz spectroscopy of phonon-polaritons

N.Sellati[1], M.Udina[3], J.Fiore[1], S.P.Villani[4], R.Acampora[5], M.F.Nielson[6], E.Abreu[5], S.Johnson[5], J.A.Johnson[6], L.Benfatto[1]

[1]*Sapienza University of Rome, 00185 Rome, Italy*
[2]*Université de Strasbourg, Strasbourg, 67200, France*
[3]*Université Paris Cité, 75205 Paris, France*
[4]*University of Chicago, Chicago, Illinois 60637, USA*
[5]*ETH Zurich, 8093 Zurich, Switzerland*
[6]*Brigham Young University, Provo, UT 84602, USA*

The latest experimental advances in time-resolved spectroscopic techniques, based on the generation of intense and phase-stable THz pulses, have paved intriguing new ways for the investigation, resonant excitation and control of ultrafast low-energy collective modes in many complex systems. Among these, charged modes are of particular interest as they can directly couple to light and form hybrid modes, the so-called polaritons [1]. As a prototypical example, phonon-polaritons are associated with the coupling of infrared-active optical phonons with the electromagnetic field in polar insulators. The highly dispersive behaviour of these modes, for the small momenta comparable to those of electromagnetic waves in the THz region, encases important information on the coupling of matter with light. In non-centrosymmetric materials, in which modes can be both infrared- and Raman-active, the dispersion of phonon-polaritons in the hybrid region can be accessed through nonlinear protocols, either in three-wave mixing [2,3] or four-wave mixing [4] interaction schemes. Despite the great interest and the huge experimental progress, a comprehensive general framework able to describe the ultrafast excitation and Raman-like detection of polaritons is still lacking, opening to possible misinterpretations of the spectral features of the experimental response. In this talk we will discuss a theoretical approach able to capture the different roles played by phonon-polaritons in different experimental protocols. In particular, we combine a many-body derivation of the nonlinear current involved in multiwave mixing processes with a perturbative solution of Maxwell's equations in the presence of a nonlinear source current, in order to correctly describe propagation effects given by the light travelling through the material and at its interfaces.
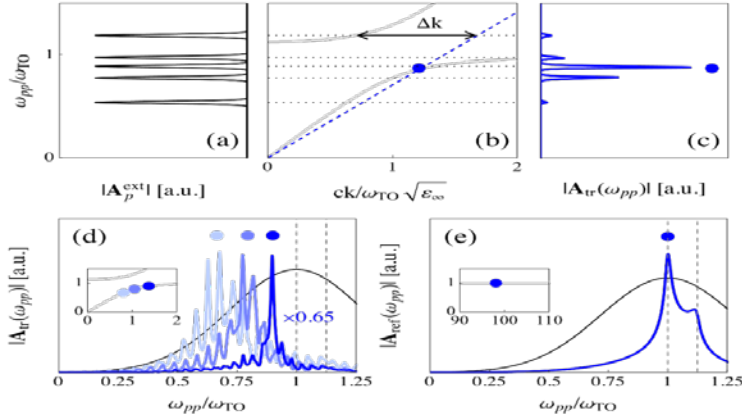
Fig. 1. THz pump-optical probe response on a thick sample with different pump spectra. (a) Spectral content of narrowband pump pulses with different central frequencies pump pulses (b) Phase-matched point along the phonon-polariton dispersion. (c) Transmitted signal for the different pump pulses shown in panel (a). The signal is maximized at the phase-matched frequency, but nonlinear signal is also observed for finite momentum mismatch Δk. (d) Transmitted signal induced by a broadband Gaussian THz pump. The signal is maximized at the phase-matched frequency, that can be tuned by changing the frequency of the probe, allowing for a direct measurement of the phonon-polariton dispersion relation (inset). (e) Reflected signal induced by a broadband Gaussian THz pump. The phase-matching condition is realized at high momenta, far from the hybrid light-matter region, allowing one to probe the bare phonon.

We show that in Raman-like pump and probe four-wave mixing schemes, such as impulsive stimulated Raman scattering, one can directly access the phonon component of the polariton, while in THz pump-visible probe three-wave mixing protocols the polariton affects the response at the level of the propagation effects only. We discuss how one can make use of these coherent techniques in a transmission geometry to probe the dispersion of the mode in the hybrid light-matter region, taking advantage of the fact that the response is dominated by the phase-matched frequency in thick samples. We thus highlight the advantages of exploiting a broadband THz pump to enlarge the phase-space of phonon-polaritons accessible within a single experiment [5]. Finally, we comment on the generalization of our theoretical framework to two-dimensional THz-THz pump-optical probe spectroscopy, comparing with recent experimental results [6]. We discuss the complex spectral features given solely by propagation and screening effects, and how this technique could be employed in quantum materials to eventually resolve complex processes like nonlinear couplings between phonons as opposed to simpler non-resonant electronic excitations.

References
[1] D. N. Basov, M.M. Fogler, F.J. Garcìa de Abajo, *Science* **354**, 6309 (2016).
[2] W. L. Faust, C.H. Henry, *Physical Review Letters* **17**, 1265 (1966).
[3] B. S. Dastrup, J. R. Hall, J. A. Johnson, *Applied Physics Letters* **110**, 162901 (2017).
[4] J. K. Wahlstrand, R. Merlin, *Physical Review* B **68**, 054301 (2003).
[5] N. Sellati, J. Fiore, S.P. Villani, L. Benfatto, M. Udina, *arXiv:2411.10160* (2024).
[6] R. Acampora, N. Sellati, M. Nielson, M. Udina, E. Abreu, L. Benfatto, S. Johnson, J.A. Johnson, *to be submitted* (2025).

Continuous-wave and pulsed operation of Tm-doped and Tm,Ho-doped Fluoride crystal waveguide lasers near 2 mm and 2.3 mm

A.Sennaroglu[1], Y. Morova[2], B. Ayevi[1], D. Faik Ince[3], B. Morova[2], E. Damiano[4], M. Tonelli[4]

[1]Koç University, Istanbul 34450, Türkiye
[2]Istanbul Technical University,34367 Istanbul, Türkiye
[3]Rutgers University, Piscataway, NJ 08854, USA
[5]Università di Pisa, 56127 Pisa Italy

This presentation focuses on the development of two new rare-earth ion-doped mid-infrared channeled waveguide lasers: $Tm^{3+},Ho^{3+}:YLiF_4$ (Tm,Ho:YLF) at 2050 nm [1, 2] and $Tm^{3+}:KY_3F_{10}$ (Tm:KYF) at 1.9 µm and 2.3 µm [3]. In both cases, femtosecond laser writing was used to inscribe depressed circular waveguides inside the fluoride hosts. Important advantages of the fluoride host include high optical quality and wide transparency in the mid infrared spectral region. Fig. 1(a) shows a confocal microscope image of the channeled waveguides fabricated inside (Tm,Ho:YLF) crystal with a diameter of 70 µm and measured waveguide loss of 0.14 dB/cm. The waveguide laser was pumped at 780 nm with a Ti:sapphire laser and lasing was obtained at 2053 nm, as can be seen from the spectrum in Fig. 1(b). With a 20% output coupler, up to 2W of continuous-wave (CW) output power was obtained near 2050 nm. By using a Cr:ZnSe saturable absorber, passively Q switched operation was further obtained, resulting in the generation of pulses as short as 19.6 ns. The temporal profile of the output pulse is shown in Fig. 1(c).
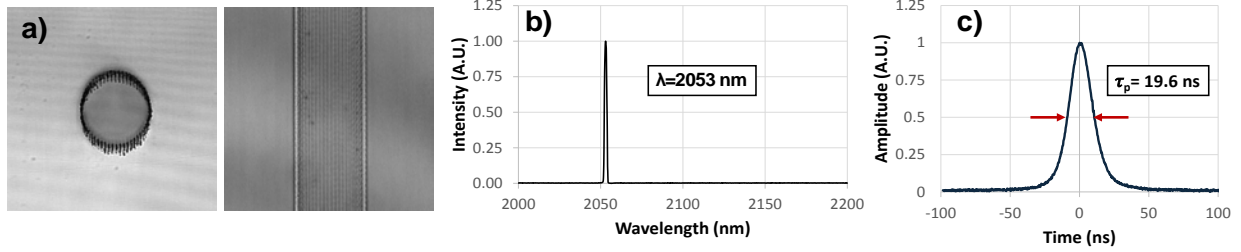
Fig. 1. *(a) Confocal microscope image of the (Tm,Ho:YLF) waveguide, (b) output spectrum of the waveguide laser at 2053 nm, and (c) temporal profile of the waveguide output laser pulses during passively Q-switched operation.*

In other studies, channeled waveguides were inscribed inside a Tm:KYF crystal. In this case, upconversion pumping was employed at 1064 nm and CW lasing was obtained at 1.9 µm and 2.3 µm with maximum output powers of 303 mW, and 70 mW, respectively, by using 2W of 1064-nm pump power. The output spectra at 2.3 µm and 1.9 µm are shown in Figs. 2(a) and (b).
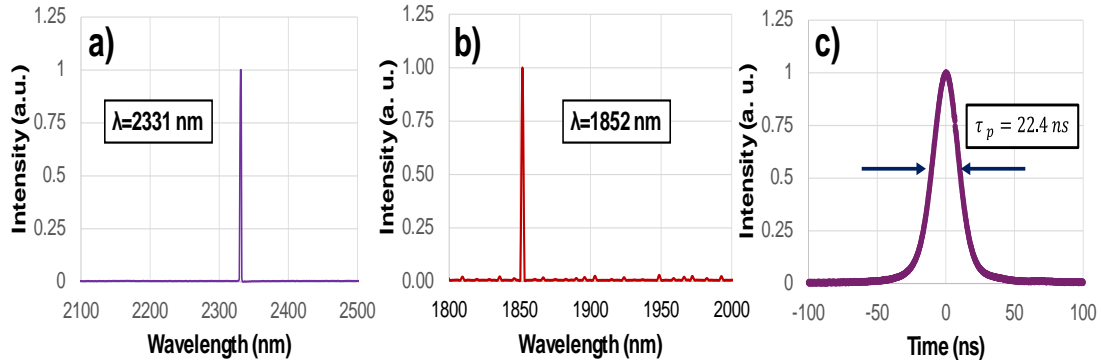
Fig. 2. *Optical spectra near (a) 1.9 µm and (b) 2.3 µm, generated with a channeled waveguide laser inside Tm:KYF crystal. (c) Pulse profile obtained with the Tm:KYF waveguide laser during passively Q-switched operation.*

In addition, passive Q switching was demonstrated near 1.9 µm, yielding 22-ns pulses at 11 kHz repetition rate. The obtained pulse profile is shown in Fig. 2(c).

References
[1] B. Ayevi, Y. Morova, E. Damiano, M. Tonelli, A. Sennaroglu, *Laser Congress -ASSL, LAC, LS&C*, Osaka (2024) paper JW2A.4,
[2] B. Ayevi, Y. Morova, B. Morova, E. Damiano, M. Tonelli, A. Sennaroglu, *Optics Letters* **49**, 6968 (2024).
[3] F. D. Ince, Y. Morova, M. Tonelli, A. Sennaroglu, *Laser Congress -ASSL, LAC, LS&C,*Osaka (2024) paper AW6A.3.

Designing quantum materials with light

M. A. Sentef

Bremen Universität, 28359 Bremen, Germany

In recent years, light-driven quantum materials science has undergone a fundamental transformation. What was once a theoretical vision—the ability to control and manipulate emergent properties of materials on ultrafast timescales—has now become a reality [1]. This progress has been enabled by rapid advancements in shaping laser pulses, probing nonequilibrium dynamics with femtosecond resolution, and developing sophisticated theoretical approaches to describe light-driven many-body systems [2]. As a result, we are now entering an era in which quantum materials can be actively "designed" and controlled using tailored light fields. A cornerstone of this approach is Floquet engineering, which exploits periodic driving to coherently modify electronic states and induce novel phases of matter. I will briefly review key experimental and theoretical developments in realizing Floquet states in quantum materials and discuss their implications for controlling competing orders. However, despite its promise, Floquet engineering also faces intrinsic limitations, particularly due to heating effects and decoherence, which can constrain its applicability as a general tuning mechanism. Moving beyond conventional Floquet approaches, a new frontier is emerging: cavity quantum materials [3]. By embedding materials in tailored quantum-electrodynamical environments, such as optical cavities, it is possible to enhance light-matter interactions and create hybrid light-matter states with fundamentally new properties. Unlike classical laser-driven schemes, cavity-mediated interactions can modify quantum fluctuations and collective excitations even in thermal equilibrium, offering a novel route to control material properties without direct external driving. I will highlight recent advances in this field, both from theoretical [4] and experimental [5,6] perspectives, and specifically discuss how strong correlations in cavity quantum materials provide new opportunities for engineering competing electronic orders through light-matter hybridization.
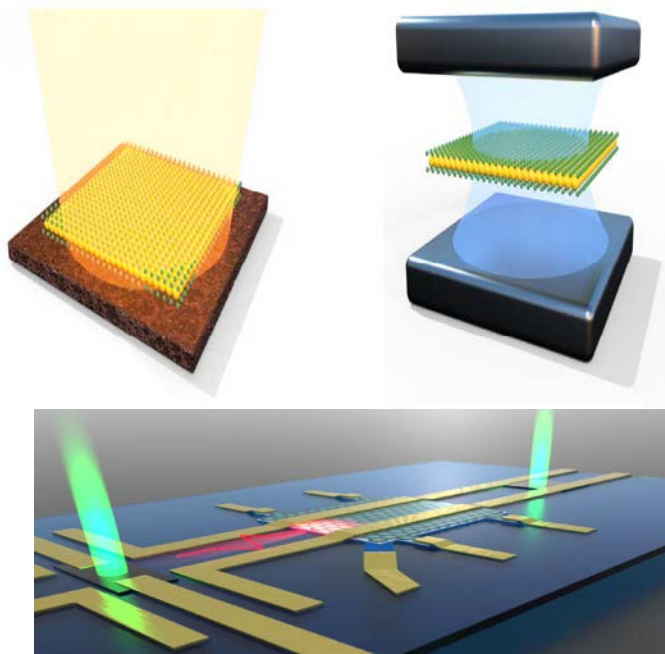
Fig. 1. **Top left** – *illustration of a quantum material driven by a classical laser drive.*
Top right – *cavity-embedded quantum material, opening the possibility to use vacuum fluctuations of light to control emergent properties.*
Bottom – *setup of the McIver lab for on-chip THz spectroscopy of quantum materials in a plasmonic cavity [5].*

This emerging paradigm may open pathways toward controlling superconductivity, charge density waves, and other ordered phases in a fundamentally new way.

References
[1] A. de la Torre, D.M Kennes, M. Claassen, S. Gerber, J.W. McIver, M.A. Sentef, *Review of Modern Physics* **93**, 041002 (2021)
[2] F. Caruso, M. A. Sentef, C.Attaccalite, M.Bonitz, C.Draxl, U. DeGiovannini, M. Eckstein, R. Ernstorfer, M. Fechner, M. Grüning, H. Hübener J.- P. Joost, D. M. Juraschek, C. Karrasch, D. M. Kennes, S. Latini, I - T. Lu, O. Neufeld, E. Perfetto, L. Rettig, R. R. Pela, A. Rubio J. F. Rudzinski, M. Ruggenthaler, D. Sangalli, M. Schüler, S. Shallcross, S. Sharma, G. Stefanucci, P. Werner, *arXiv:2501.06752* (2025).
[3] F. Schlawin F Schlawin, DM Kennes, MA Sentef, *Applied Physics Reviews* **9**, 011312 (2022)
[4] M. A. Sentef, J. Li, F. Kunzel, M. Eckstein, *Physical Review Research* **2**, 033033 (2020)
[5] G. Kipp, H. Bretscher, B. Schulte, D. Herrmann, K. Kusyak, S. Kesavan, T. Matsuyama, X. Li , S. M. Langner, J. Hagelstein, F. Sturm, A. M Potts C. J Eckhardt, Y. Huang, K. Watanabe, T. Taniguchi, A. Rubio, D. M Kennes, M.. A Sentef, E Baudin, J W McIver, *arXiv:2403.19745* (2024).
[6] B. Le Dé, CJ Eckhardt, DM Kennes, MA Sentef et al., Journal of Physics: Materials 5, 024006 (2022);
[7]   I. Keren, T. Webb, D. Basov, *to be submitted* (2025).

Ultrafast control of magnetism thru strongly non-equilibrium states

T. Rasing

Radboud Universiteit, 6525 ED Nijmegen, the Netherlands

Since our demonstration of magnetization reversal by a single 40 femtosecond laser pulse, the manipulation of spins by ultra-short laser pulses has developed into an alternative and energy efficient approach to magnetic recording [1,2]. Though originally thought to be due to an optically induced effective magnetic field, later studies demonstrated that the switching occurred via a strongly non-equilibrium state, exploiting the exchange interaction between the spins [3,4,5]. Recent work also show how magnetic textures like skyrmions are generated via a strongly non-equilibrium phase [6]. While for a long time, all-optical switching (AOS) was exclusively observed in ferrimagnetic alloys, more recent work demonstrated AOS in a broad range of ferromagnetic multilayer materials, albeit that in those examples a large number of pulses were required [7]. By studying the dynamics of this switching process, we have discovered that this switching is a 2-step process of nucleation and switching, which has led to the subsequent demonstration that highly efficient AOS can be achieved by using pairs of femto/pico-second laser pulses, that are separated by a precisely tuned delay time [8]. By combining optical laser excitation with in situ magnetic force microscopy, we recently found that the nucleation and switching process evolves via a stochastic network of domains.   In this talk, I will discuss the state of the art in ultrafast manipulation of magnetization and present some new ideas to implement brain-inspired computing concepts in magnetic materials [9,10].
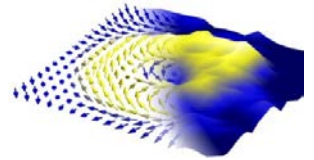
References
[1]   A. Kirilyuk, A.V. Kimel, Th. Rasing, *Review of Modern Physics* 82, 2731 (2010).
[2]   A. V. Kimel, M. Li, *Nature Reviews Materials* **4**, 189 (2019) .
[3]   I.   Radu, K. Vahaplar, C. Stamm, T. Kachel, N. Pontius, H. A. Dürr, T. A. Ostler, J. Barker, R. F. L. Evans, R. W. Chantrell, A. Tsukamoto
      A. Itoh, A. Kirilyuk, Th. Rasing, A. V. Kimel, *Nature* 472, 205 (2011),
[4]   T. Ostler, J. Barker, R. F. L. Evans, R. W. Chantrell, U. Atxitia, O. Chubykalo-Fesenko, S. El Moussaoui, L. Le Guyader, E. Mengotti
      L. J. Heyderman, F. Nolting, A. Tsukamoto, A. Itoh, D. Afanasiev, B. A. Ivanov, A. M. Kalashnikova, K. Vahaplar, J. Mentink, A. Kirilyuk
      Th. Rasing, A.V. Kimel, *Nature Communications* **3**, 666 (2012),
[5]   J.   Mentink, J.Hellsvik,D.V.Afanasiev,B. A. Ivanov,A. Kirilyuk, A.V. Kimel, O.Eriksson,M. I. Katsnelson,Th. Rasing, *Physical Review Letters* **108**
      057202 (2012)
[6]   F.   Büttner, B. Pfau, M. Böttcher, M. Schneider, G. Mercurio, C. M. Günther, P. Hessing, C. Klose, A. Wittmann, K. Gerlinger, L-M. Kern
      C. Strüber, C. von Korff Schmising, J. Fuchs, D. Engel, A. Churikova, S. Huang, D. Suzuki, I. Lemesh, M. Huang, L. Caretta, D. Weder
      J. H. Gaida, M. Möller, T. R. Harvey, S. Zayko, K. Bagschik, R. Carley, L. Mercadier, J. Schlappa, A. Yaroslavtsev, L. Le Guyarder
      N. Gerasimova, A. Scherz, C. Deiter, R. Gort, D. Hickin, J. Zhu, M. Turcato, D. Lomidze, F. Erdinger, A. Castoldi, S. Maffessanti, M. Porro
      A. Samartsev, J. Sinova, C. Ropers, J. H. Mentink, B. Dupé , G. S. D. Beach, S. Eisebitt, *Nature Materials* **20**, 30 (2021)
[7]   C.- H. Lambert, S. Mangin,   B. S. D. Ch. S. Varaprasad , Y. K. Takahashi , M. Hehn, M. Cinchetti , G. Malinowski , K. Hono, Y. Fainman
      M. Aeschlimann,   E.E. Fullerton, *Science* **345,** 1337 (2014)
[8]   K.   T. Yamada, A. V. Kimel, K.H. Prabhakara, S.Ruta, T. Li , F. Ando, S. Semin, T. Ono, A. Kirilyuk, T. Rasing, *Frontiers in Nanotechnolgy* **4**
      765848(2022).
[9]   A. Chakravarty, J.H. Mentink, S. Semin, A.V. Kimel, Th. Rasing, *Applied Physics Letters* **120**, 022403 (2022)
[10] K. Raab, M. A. Brems, G.Beneke, T.Dohi, J. Rothörl, F. Kammerbauer, J.H. Mentink, M. Kläui, *Nature Communications* **13**, 6982 (2022)

Femtosecond dynamics of quantum materials: femto- phono- magnetism

S. Sharma

Max-Born- Institut für Nichtlineare Optik und Kurzzeitspektroskopie*, 12489 Berlin, Germany*

From the outset of research into femtomagnetism, the field in which spins are manipulated by light on femtosecond or faster time scales, several questions have arisen and remain highly debated: How does the light interact with spin moments? How is the angular momentum conserved between the nuclei, spin, and angular momentum during this interaction? What causes the ultrafast optical switching of magnetic structures? What is the ultimate time limit on the speed of spin manipulation? What is the impact of nuclear dynamics on the light-spin interaction? In my talk I will advocate a parameter free *ab-initio* approach to treating ultrafast light-matter interactions, and discuss how this approach has led both to new answers to these old questions but also to the uncovering of novel and hitherto unsuspected spin dynamics phenomena [1,2]. In particular I will highlight following aspects
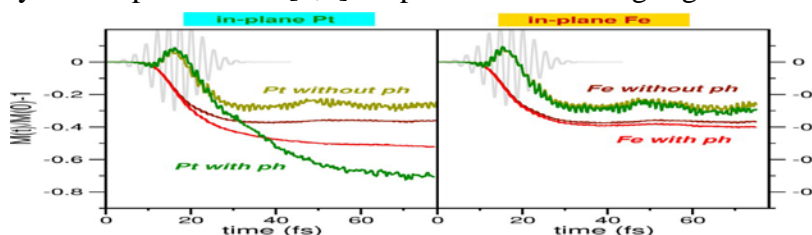

*Fig.1 Normalized spin moment as a function of ti*me *(in fs)* **in laser pumped FePt.** *The moment is calculated in presence of phonon modes as well as in absence of any nuclear motion.*

of ultrafast dynamics: (a) Femto- phono- magnetism: an extra degree of control over spin dynamics can be obtained by selective excitation of phonon modes [3].(b) Pulse design: control of spin- valley- tronics via pulse shaping [4,5]. (c) Spin vacuum switching: full reversible switching using spin-currents[6].(e) Exciton dynamics: strong correlations between excitons and free carriers. I will show that OISTR is one of the fastest ways to control spins by light and I will make a case for femto- phono- magnetism by demonstrating that selective excitation of optical phonon modes exert a strong influence on femtosecond demagnetisation, generating an additional loss of moment [3] in laser pumped materials (see Fig.1). In the second part of the talk I address the question of valley control in2d transition metal dichalcogenides (TMDC), with current understanding that it couples exclusively via circularly polarized light. In our work we show that on femtosecond time scales valley coupling is a much more general effect. We find that two time separated linearly polarized pulses allow almost complete control over valley excitation.

References
[1] J. K. Dewhurst, P. Elliott, S. Shallcross, E.K.U. Gross, S. Sharma, *Nano Letters* **18**, 1842 (2018).
[2] F. Siegrist, J. A Gessner, M. Ossiander, C. Denker, Y.- P. Chang, M. C. Schröder, A. Guggenmos, Y. Cui, J. Walowski, U. Martens
     J. K. Dewhurst, U.Kleineberg, M. Münzenberg, S. Sharma, M. Schultze, *Nature* 571, **240** (2019)
[3] S. Sharma. S. Shallcross. P. Elliott, J. K. Dewhurst, *Science Advances* **8**, eabq2021 (2022)
[4] S. Sharma, P. Elliott, S. Shallcross, *Optica* **9**, 947(2022)
[5] S. Sharma, P.Elliott, S. Shallcross, *Science Advances* **9**, eadf3673 (2023)
[6] E. I. Harris-Lee, J. K. Dewhurst, S. Shallcross, S. Sharma. *Science* **10,** 6390(2024).

Optically induced electronic spin polarizations in altermagnets: Theory and experiment

H. C. Schneider

Rheinland-Pfälzische Technische Universität Kaiserslautern-Landau, 67663 Kaiserslautern, Germany

Altermagnets combine aspects of ferromagnetism and antiferromagnetism but also give rise to properties that cannot be realized with either of the known magnetic material classes [1,2]. We present theoretical and experimental results on the optically excited electron dynamics in different altermagnetic candidate materials. The altermagnetic symmetries, in particular time-reversal symmetry breaking, allow for the excitation of an electronic spin polarization by linearly polarized optical fields. Using an ab-initio based approach for a prototypical planar d-wave altermagnets, we show how the optically excited non-equilibrium spin polarization depends on the direction of the exciting E-field vector. The theoretical prediction of a controlled, optically excited spin polarization is rooted in the altermagnetic symmetries and was observed using magneto-optical measurements on ultrathin films of the planar d-wave altermagnetic candidate material RuO_2 [3]. We will also present results on the optically excited spin polarization in the bulk g-wave system MnTe [4], which has been demonstrated to be altermagnetic by ARPES measurements [5]. An example of the angle dependence of the optically driven spin polarization is presented in Fig. 1, where the angles refer to the direction of the exciting laser pulse with respect to the crystal axes.
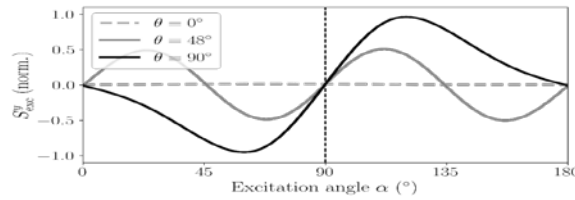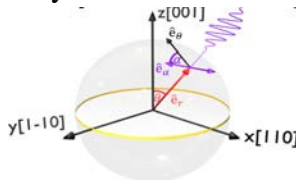
Fig.1. Right: *Dependence of the excited spin polarization S_{exc}^y on the polarization angle α of the linear polarized laser pulse for different incident angles θ in MnTe.* **Left**: *Definition of the angles used in the plot[6].*

Optically excited electronic spin polarizations can decay by electronic spin-flip scattering due to the influence of spin-orbit coupling. In planar d-wave altermagnets, however, the anisotropic spin splitting in the band structure restricts the phase space for such electronic spin-flip transitions compared to ferromagnetic metals. We present microscopic calculations of electron-electron and electron-phonon scattering processes for altermagnetic KRu_4O_8 that show how non-thermalized, anisotropic electronic distributions survive on times long compared to the typical momentum relaxation-times and thus give rise to a long-lived spin polarization [6].

References
[1] L. Šmejkal, J. Sinova, T. Jungwirth., *Physical. Review* X **12**, 040501(2022)..
[2] L. Šmejkal, J. Sinova, T. Jungwirth, *Physical. Review* X **12**, 031042 (2022).
[3] M. Weber, S.Wust, L. Haag, A.Akashdeep, K. Leckron, C. Schmitt, R. Ramos, T. Kikkawa,, *arXiv: 2408.05187* (2024).
[4] L. Haag, *to be submitted* (2025).
[5] J. Krempaský, J. Krempaský, L. Šmejkal, S. W. D'Souza, M. Hajlaoui, G. Springholz, K. Uhlířová, F. Alarab, P. C. Constantinou, V. Strocov
     D. Usanov, W.R.Pudelko, R. González-Hernández, A. Birk Hellenes, Z. Jansa, H. Reichlová, Z. Šobáň, R. D. Gonzalez Betancourt, P. Wadley
     J. Sinova, D. Kriegner, J. Minár, J. H. Dil.T. Jungwirth, *Nature* **626***, 517 (2024).
[6] M. Weber, K. Leckron, L. Haag, R. Jaeschke-Ubiergo, L. Šmejkal, J. Sinova, H.C. Schneider, *arXiv:2411.08160* (2024).
 *   *Acknoledgement*: funded by the Deutsche Forschungsgemeinschaft TRR 173 *Spin + X*.

Charged bosonic states in 2D bilayer structures

Q. Wan[1], D. Vaz[1], L. Xiang[2], A. Ramavath[1], B. Vargo[1], J. Ye[1], J. Beaumariage[1], K. Watanabe[3], T. Taniguchi[3] Z. Sun[4], D. Smirnov[2], N. Youngblood[1], I.V. Bondarev[5], D.W. Snoke[1]
[1] University of Pittsburgh, Pittsburg, PA 15260, USA
[2] Florida State University, Tallahassee, FL 32310, USA
[3] National Institute for Materials Science, Tsukuba, Ibaraki 305-0044, Japan
[4] East China Normal University, Shanghai 2000062, China
[5] North Carolina Central University, Durham, NC27707, USA

Many higher-order excitonic bound states have been seen in 2D semiconducting layers, including trions, biexcitons, charged biexcitons, and spatially indirect excitons and trions in bilayer systems. We have now demonstrated the existence of a four-fermion state, namely three electrons bound to one hole, or three holes bound to one electron, in specially designed bilayer structures with transition metal dichalcogenide (TMD) layers.
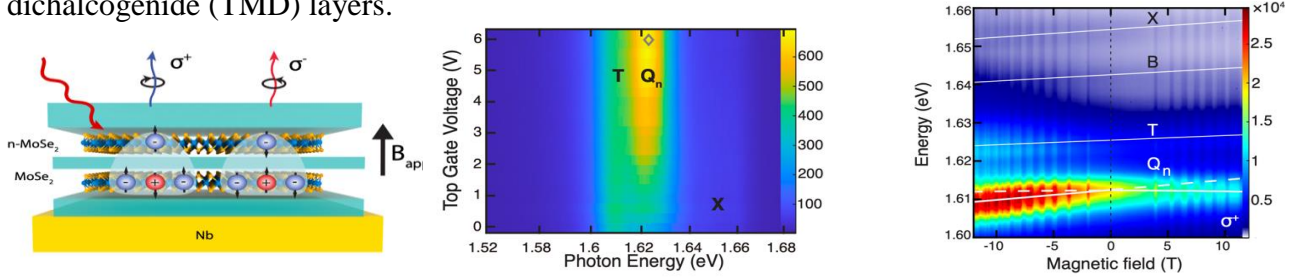
Fig. 1. Left. *Designed structure showing the stable four-particle states, consisting of a trion in one layer bound to a free charge in the adjacent layer. The green layers are hexaginal boron nitride (hBN).* **Middle:** *Photoluminescence (PL) spectrum as the free charge density is increased by electric gating. The negative quaternion (Q_n) increases in intensity relative to the trion, indicating it has extra charge.* **Right:** *Circularly-polarized PL spectrum as a function of vertical magnetic field, showing that the exciton (X), biexciton (B), and trion (T) each have only two allowed PL emitting states, while the quaternion (Q_n) has three, in agreement with the selection rules for the TMD structure [1]. The relative energy of the trion and quaternion varies depending on the thickness of the hBN layer between the bottom TMD and the thick metal layer, in agreement with the prediction of the theory for the bound states [2].*

This is exciting because these complexes (dubbed "quaternions") are charged bosons, and therefore can undergo Bose-Einstein condensation, in which case they would also be a superconductor carrying charge current. I will present evidence for these states and prospects for the future.

References
[1] Q. Wan, D. Vaz, L. Xiang, A. Ramavath, B. Vargo, J. Ye, J. Beaumariage, K. Watanabe, T. Taniguchi, Z. Sun, D. Smirnov, N. Youngblood I. V. Bondarev, D. W. Snoke, *arXiv:2412.06941* (2024).
[2] Z. Sun, J. Beaumariage, Q. Wan, H. Alnatah, N. Hougland, J.Chisholm, Q.Cao, K.Watanabe, T. Taniguchi, B. M. Hunt, I. V Bondarev, D. Snoke *Nano Letters* **21**, 7669 (2021).

Nonequilibrium in photovoltaics

M.K. Rafailov
Dynamics of Nonequlibrium, Vienna, VA 22180

Metastability is a critical problem especially important for technology-driven applications. Using relatively slow effects like acoustic phonons, carrier motion, etc. that in low dimensional structures propagation time is approaching ps-time scale, to "envelop" ultrafast excitation-relaxation processes in a way that may allow to extend nonequilibrium state. With sub-nm molecular size and carriers and acoustic phonon velocities the enveloping may become plausible. The approach may also help to arrange a non-ultrafast and even non-photonic excitations that may lead to some plausible technology applications. From that point here we will discuss negative photoresponse-NPR, the effect that was observed with sub-ps laser pulse excitation,Fig.1 [1]. Instead of anticipated unipolar response depended only on RC of a detector, the NPR demonstrates rapid voltage polarity change that follows extended relaxation pattern lasting up to ms that is much less dependable on detector's RC constant. One explanation comes out of increase of both carrier density and temperature, when during relaxation the system reaches a state sufficiently close to the quasi-thermal equilibrium in which the carrier density is still elevated, but smaller than the intrinsic thermal equilibrium density at the elevated temperature [2]. There are few more concepts-from piezo-effects to electronic resnance that occurs while p-n junction is i present.

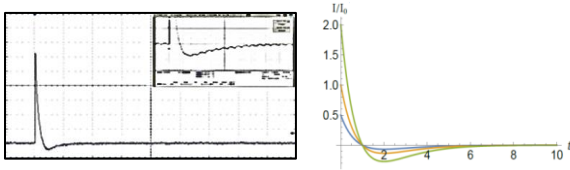*Fig.1. NPR-resulted excitation by ultrashort pulse is lasting up to ms. a. observed in Ge p-i-n diode structure:(**insert**)response coming out of a transient heterostructure formed by bleached layer of bulk material,**b**. modeling of intensity dependence with the same RC. From [1].*

While NPR opens interesting applications in remote sensing, communications etc [3]., it may have broader applications with respect to underlying related effects: the effects that appears in irradiated semiconductors, opening an opportunity for extension nonequlibrium lifetime, particularly with semiconductors arranged in a form of p-(intrinsic material)-n junctions (p-i-n). Despite the effect has been observed in bulk materials, bleaching effect in appropriate semiconductors allows to stack semiconductor structures in a way allowing maximum utilization of incoming photon flux. Eventually can be considering stacked 2D semiconductor structures may be considered.

Fig. 2. Bleaching in semiconductors. After [4].
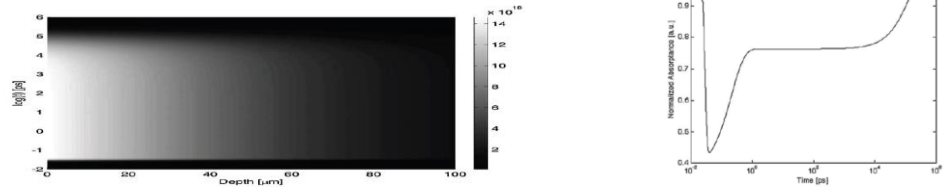
Insulated and stacked p-i-n 2D structures while utilizing NPR effect, may to build meta-material maintaining practically indefinite metastability while operating not only with ultrashort pulses. If we look at that with respect to bleaching time and pulse time of flight that it is possible to build a photovoltaic structures that can be used to maintain metastable nonequlibrium with very long excitation pulses or even with CW sources. The same principle also can be used when electric pulses are used as a pumping source for inducing nonequlibrium in solids [5,6]. In such a case the only limitations for pulse width and, thereto pumping power will be the capacitance-C which is directly depends on layer thickness and can be done infinitesimally small in low dementias structures [5]. In some cases involved we may need a potential or bias to move pulses across a layer. While results of positive response is strongly depends on RC s it will be plausible in low dimentionals semiconductor structures to see above mentioned enveloping of nonequlibrium with carrier velocity. Farther considering electronic pumping of such low dimensional structures may open unique opportunity for technology application and along with stacked structure pumping and excitation enveloping indefinitely increase lifetime of nonequlibrium. Once tested in organic light emitting diodes [5] electronic pumping that strongly depends on capacitance-size of the structure demonstrated high efficiency in maintaining of nonequlibrium even in relatively thick materials see Fig. 3.

Fig.3. Schematic of electrical pumping pulse train combining very low intensity bias, and high intensity "ultrashort"(RC permitted) pulses. From [5]
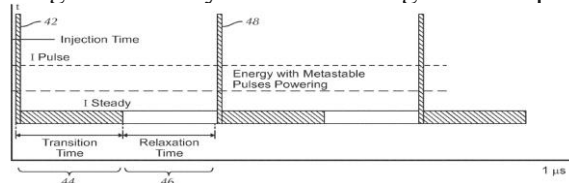
Electronic phase-transition with electric pumping was experimentally demonstrated in double pump-probe experiment [7], where phase transition were measured with respect to X-ray probe diffraction pattern while where pumped optically with 100fs laser pulse and electrically with different step-voltages applied to the structure. Switching to electronic pumping and using layered structures, like similar to twisted vdW structures, may allow using nonequlibrium in SWAP (size-weight-power) plausible technology for ultra-broadband electronics etc. Not only electric pumping in combination with layered material structures is a plausible way to induce nonequlibrium but any other non-ultrashort laser pulse pumping is a way to pump high intensity pulse into a such structured material and it makes nonequlibrium-related phenomena lausile and effects in multiple technology applications: from peta-Hz electronics to remote sensing, photovoltaics in general, including Sun-based photovoltaic conversion, high-temperature superconductivity, magnetic switches and so on.

References
[1] I. K. Zak, M.K. Rafailov, *Proceedings SPIE* **9467**, 946726-1 (2015).
[2] M. Yuan, M. K. Rafailov, R. Binder, *Journal of Applied Physics* 134, 174503 (2023).
[3] C. Huang, F. Chen, Z. Zhang, X. Tang, M. Zhu, J. Sun, Y. Chen, X. Zhang, J. Yu, Y. Zhang, *Sensors* **24,** 4226 (2024).
[4] X.-A. Dou, X. Sun, X.Li, X. Chen, *Optik* **126,** 3267 (2015).
[5] M. K. Rafailov, US Patent 10242618, *US Patent ad Trademark Office* (2019).
[6] A. Lindenberg, *Ultrafast Dynamics and Ultrafast Bandgap Photonics* **VIII**, Georgetown Washington DC, 14 (2021). .
[7] A. Sood, X.Chen,Y. Shi, S.Kumar, S. J. Park, M.Zajac,Y.Sun, L. Q.Chen,S.Ramanathan,X.Wang,W.C.Chueh,A.M.Lindenberg, *Science* **373**, 352 (2021)

Towards integrated Cr:ZnS/ZnSe waveguide lasers and amplifiers

I. T. Sorokina[1], A. Rudenkov[1], V. L. Kalashnikov[1], J. Brinkmann[1], C. Grivas[1], C. Brüne[1], E. Einmo[1]
M. di Sabatino[1], E. Sorokin[2]
[1]*Norwegian University of Science and Technology, 7034 Trondheim, Norway*
[2]*Technische Universität Wien, 1040 Vienna, Austria*

Solid-state lasers utilizing Cr^{2+}-doped II-VI semiconductor crystals [1,2,3] have matured to industrial grade femtosecond lasers, operating efficiently at room temperature and offering the broadest gain bandwidth with up to 45% of their central wavelength. They can produce output powers in the tens of watts range and generate ultrashort femtosecond pulses lasting only a few optical cycles [2,4], now achievable even with diode pumping [5]. With peak powers reaching 1 MW and pulse durations as short as 28 femtoseconds, these lasers enable the generation of carrier-envelope phase (CEP)-stable mid-infrared pulses in bulk format. Advances in power scaling have further allowed nonlinear frequency conversion to extend mid-IR coverage across the entire "molecular fingerprint" spectral range, from 4.5 to 18 µm [4,5]. Development of energetic 0.1-10 µJ ultrafast mid-IR sources would pave the way for additional interesting industrial applications such as e.g. sub wavelength 3-D sub-surface processing of silicon and other semiconductor materials [6,7]. However, all these advances have been achieved still in the bulk, complex and rather expensive format and the trend nowadays goes towards integration with photonic circuits. There are currently two platforms for integration of ultra-short pulsed lasers: based on isolators (e.g. $LiNbO_3$) and on silicon (Si). While traditional integration methods often rely on bonding prefabricated lasers onto photonic wafers, these approaches face challenges such as precise alignment requirements and limited scalability for mass production. On the other hand, monolithic integration, where the laser-active material is directly grown and fabricated on photonic platforms, offers a more scalable and cost-effective solution. In this talk we review the state-of-the art in the field with a particular emphasis on our recent advances towards the challenging goal of development of compact high-energy ultrashort-pulsed laser systems in the 2–3 µm wavelength range. We will report on our first steps towards on-chip integration of the Cr:ZnS waveguide on Si [8] and will further focus on novel approaches for generating high laser peak power and energy scaling [9] in a chirped pulse master-oscillator-amplifier (CPMOPA) waveguide system and discuss ways to achieve amplification maintaining a good quality mode in a particularly compact waveguide design compatible with the future integration steps. We also present the results of theoretical analysis of physical mechanism enabling nearly complete utilization and efficient energy extraction from the gain volume in multimode waveguide.

MBE grown thin film Cr:ZnS
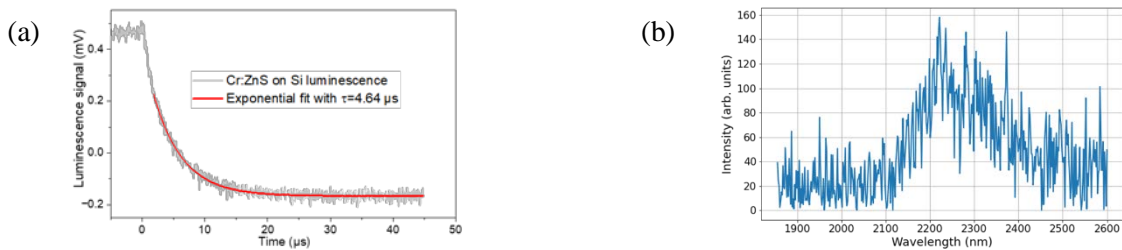
Fig. 1. Lifetime (a) and emission spectra of the MBE-grown Cr:ZnS layer on Si.

To enable on-chip integration, good optical quality thin films of chromium-doped ZnS (Cr:ZnS) were fabricated using molecular beam epitaxy (MBE). This study marks the first successful incorporation of Cr^{2+} ions into thin film form, as verified by luminescence lifetime measurements. that yielded a value of 4.6 µs (Fig. 1 a), which is comparable to that observed in bulk material (5.5 µs). Emission spectra from patterned waveguides in these films revealed a peak near 2.2 µm (Fig. 1 b), signifying the first demonstration of mid-infrared optical activity in MBE-grown Cr^{2+}:ZnS thin films and confirming their promise for laser applications. Dry-etched silicon waveguides exhibited optical losses of 1.16 dB/cm, while ZnS waveguides showed higher losses at 7.8 dB/cm, because of mode leaking into the higher-index substrate, which can be supressed by a low-index layer. These first results demonstrate that Cr:ZnS films are a viable candidate for integration into mid-infrared photonic platforms. For more details please, see the upcoming article [8].

*Waveguide amplifier:w*e demonstrate a waveguide Watt-level single-mode Cr:ZnS amplifier, capable to operate in both, chirped-pulse and femtosecond regimes. Schematic of experiment is shown Fig.2.
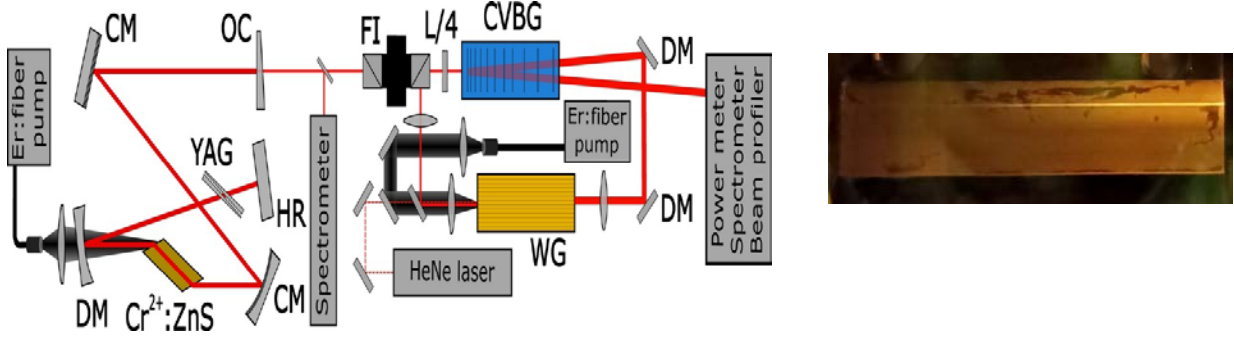
Fig. 2. Experimental setup: *CM-chirped mirror, OC-output coupler, FI-Faraday isolator, L/4-quarter wave plate, CBG-chirped Bragg grating, YAG-wedges for dispersion adjustment, HR-highly reflective mirror, DM-dichroic mirror, WG- Cr^{2+}:ZnS polycrystalline active element with inscribed waveguides.*

As a seed pulse source, we used the Kerr-lens mode-locked Cr^{2+}:ZnS laser, similar to the initial 70 MHz laser described in [10]. The FWHM spectral width of 106 nm at a central wavelength of 2336 nm corresponds to a sub-60 fs pulse duration. In the chirpd-pulse regime the chirped volume Bragg grating (CVBG) with 100 nm width acted as stretcher (~500 ps) and compressor. The waveguides were directly laser writtten by a picosecond Ho:YAG MOPA laser system (ATLA Lasers AS) operating at 2090 nm central wavelength. We fabricated circular waveguides with diameters of 20–50 μm that were inscribed in a 34-mm long polycrystalline Cr^{2+}:ZnS (Cr^{2+} concentration of $2.9 \cdot 10^{18}$ cm^{-3}) sample using a NA=0.85 objective [11]. Pump radiation was completely absorbed in the first half of the crystal. The experimental results are shown in Fig. 3. The maximum output power of 2.35 W and gain factor of 75 was obtained for 50-µm waveguide WG#1 with a power-added optical efficiency of 16.2% under 14.3 W incident pump power. Waveguide WG#28 demonstrated similar results (2.11/12.9 W output/incident power, gain factor of 57 and 16.1% opt. eff.), with M^2 factor of 1.13x1.25 (Fig. 3a). The interferometric autocorrelation trace of the amplified pulses is shown in Fig. 3c illustrating the compressed pulse duration of about 204 fs assuming sech^2 pulse temporal shape
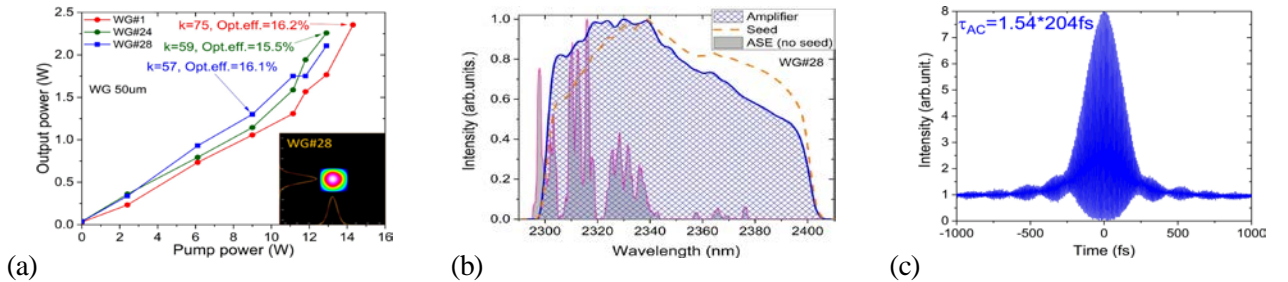
Fig. 3. Output power characteristics (*a*) *seed, ASE and amplified pulse spectra (**b**), and amplified recompressed pulse autocorrelation trace (**c**) of the 50 µm waveguides.*

In the stretcher-free (femtosecond) regime we reached the gain factors up to 29 at 2.05 W of average output power with 13.8% power added optical efficiency. The random quasi-phase matching in the ceramic Cr:ZnS material caused generation of up to the 4th spectral harmonics, propagating in the waveguide (Fig. 1, Fig. 4).
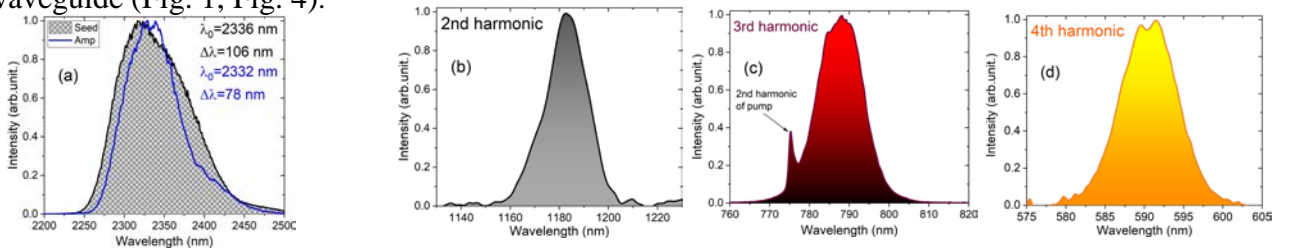
Fig. 4. Waveguide amplifier *in sub-ps regime: seed, amplified pulse spectra (a) and harmonics spectra: 2nd harmonic (**b**), 3rd harmonic (**c**), 4th harmonic (**d**).*

To our knowledge, this is the first demonstration of the Watt-level waveguide amplifier in the crystalline active medium operating with high spatial quality of output beam and generating multiple harmonics in the waveguide amplifier. The demonstrated gain factors of >29 over 17 mm correspond to >8 dB/cm, which is already more than the loss in the MBE waveguide even without the low-index layer. With proper dispersion precompensation we expect to observe also pulse spectral extra-broadening, eliminating the need for additional bandwidth-enhancing elements. *Mode synthesis in compact waveguide amplifier: o*ne of the most remarkable results is the efficient amplification in a multimode waveguide while maintaining single-mode beam quality. Both, experiment and modelling indicate a cooperative action between non-dissipative confinement (transverse refractive-index grading) and dissipative confinement (graded gain), which induces higher-order modes to merge into lower-order ones—an effect of spatial-mode synthesis, or "mode condensation" [16]. This mechanism enables nearly complete utilization of the gain volume and efficient energy extraction in compact multimode waveguides, which are similar to large-mode-area photonic-crystal waveguides (Fig. 5).
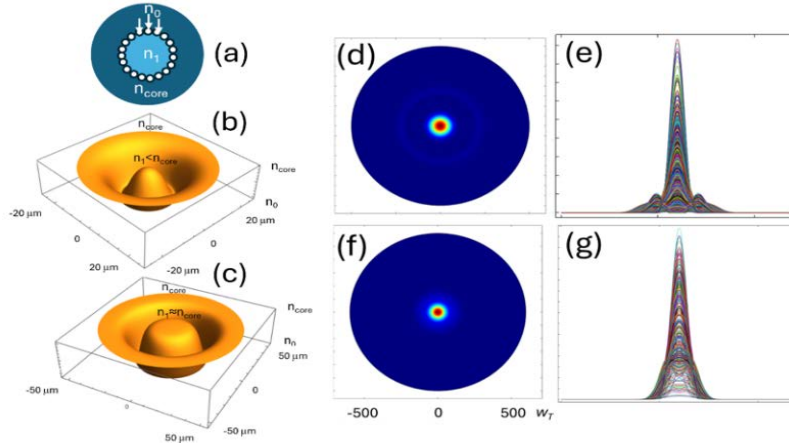
Fig. 5. Schematic presentation of the waveguide structure (a) and refractive index profiles for the thin (b) and thick (c) waveguides. The contour plots of the output mode profiles (d,f) and the corresponding mode profiles averaged on the in-waveguide propagation distance (e,g) for the waveguide sizes w_0=20 (d,e) and 50 (f,g) μm, δn = 0.003 (d,e) and 0.021 (f,g),The colored filling in (e,g) corresponds to mode profiles at different distances inside a waveguide.

Their modal content hinges on macro- (b,c) and micro-scale (a) geometries, permitting mode-area scaling and synthesis. Increasing thickness, δn-growth and "smoothening" of the $n(r)$-potential drives a thin- to thick-guide transition from (b) to (c). Simulations (Fig. 5) show higher-order modes vanishing and $M^2 \rightarrow 1$ under such a transition ((d,e) vs. (f,g)).

This work marks significant initial steps toward integrating Cr:ZnS ultrafast pulse lasers on a silicon platform, demonstrating proof of concept for what appears to be the first chirped-pulse Cr:ZnS waveguide amplifier with gain factor over 8 dB/cm, making the MBE-grown on Si Cr:ZnS waveguides feasible. We believe our present work does not only lay the foundation of the future integrated femtosecond lasers and frequency combs for sensing applications but also provides a route to the energy-scalable waveguide lasers that can have wide applications in fine material processing.

References
[1] I. T. Sorokina, *Optical Materials* **26**, 395 (2004)
[2] I. T. Sorokina, E. Sorokin, *IEEE Journal of Selected Topics on Quantum Electronics* **21**, 1601519 (2015).
[3] S. B. Mirov, S. Mirov, V. Fedorov, D. Martyshkin, I. Moskalev, M. Mirov, S. Vasilyev, *IEEE Journal of Selected Topics Quantum Electronics* **21**,292 (2015).
[4] S. Mirov, I. Moskalev, S. Vasilyev, V. Smolski, V. Fedorov, D. Martyshkin, J. Peppers, M. Mirov, A. Dergachev, V. Gapontsev, *IEEE Journal of Selected Topics Quantum Electronics* **24**, 1601829 (2018).
[5] N. Nagl, *PhD thesis*, Springer (2021).
[6] N. Tolstik, E. Sorokin, J.C. Mac-Cragh, R.Richter, I.T. Sorokina, *CLEO: Applications and Technology,* AM41.8(**2022**).
[7] I. T. Sorokina, *OPIC'2022*, Yokohama, Japan (2022).
[8] C. Brüne, to be published (2025).
[9] A. Rudenkov A Rudenkov, VL Kalashnikov, E Sorokin, M Demesh, IT Sorokina, *arxiv.org/abs/2212.00626* (2022).
[10] A. Rudenkov, V. L. Kalashnikov, E. Sorokin, M. Demesh, & I. T. Sorokina, *Optics Express* **31**, 17820 (2023)
[11] M. Demesh, E. Sorokin, E. Einmo, C. Grivas, N. Tolstik, A. G. Okhrimchuk, M. P. Smayev, V. V. Likhov, V. L. Kalashnikov, C. Brüne M. Di Sabatino, I. T. Sorokina, *High - Brightness Sources and Light- Driven Interactions Congress*, paper JW4A.4 Technical Digest Series (Optica Publishing Group, 2024), .
[12] S. Vasilyev, V. Smolski, J. Peppers, I. Moskalev, M.Mirov, Y. Barnakov, S. Mirov, V. Gapontsev, *Optics Express* **27**, 35079 (2019).
[13] A. Rudenkov,.V.L..Kalashnikov,M.Demesh, N. Tolstik, E. Sorokin, I. Sorokina, DOI:10.1364/opticaopen.27909126.v1 (2024).
[14] S. Ramachandran, J.M. Fini, M. Mermelstein, J.W. Nicholson, S. Ghalmi, M.F. Yan, *Laser & Photonics Reviews* **2**, 429 (2008).
[15] M Demesh, V.L. Kalashnikov, E. Sorokin, N. Gusakova, A. Rudenkov, I.T. Sorokina, *JOSA B* **40,** 1717 (2023).
[16] K. Krupa, A. Tonello, B.M.Shalaby, M. Fabert, A. Barthélémy, G. Millot, S. Wabnitz, V. Couderc, *Nature Photonics* **11**, 237 (2017).

X-rays to study ultrafast lattice and magnetisation dynamics

U. Staub

Paul Scherrer Institute, 5232 Villigen PSI, Switzerland

An introduction will be given to x-ray techniques that are used to investigate ultrafast dynamics of the lattice and the magnetic properties based on ultra short x-ray pulses mainly created by an x-ray free electron laser. I will present the basics of ultrafast x-ray diffraction for the study of lattice motions, showing how one can directly quantify phonons in real time. This will be exemplified on a case of an optically excited displacive phonon excitation in a manganite with the detection of a coherent phonon [1] and the case of a coherently driven mode by a THz pulse.[2] Then I will discuss x-ray absorption methods to study ion selective magnetic properties for ferromagnetic systems (x-ray magnetic circular dichroism (XMCD)) and for antiferromagnets (x-ray magnetic linear dichroism (XMLD)), which show the importance of the polarization state of the x-rays for such experiments This plays a crucial role in the extraction of the electronic and magnetic degrees of freedom of the material. In particular, I will show an example showing the difference demagnetization time scales of $3d$ and $4f$ elements, [3] which is of strong importance for all optical ultrafast magnetization switching.

Finally, the principle for ultrafast resonant x-ray scattering, both elastically and inelastically will be explained. These methods are particularly strong in detecting localized antiferromagnetic magnetic moments or their magnetic excitations. Again, due to the tuning of the x-ray energies to an absorption edge of the elements of interest, ion selectivity is obtained. These resonant x-ray techniques can also be sensitive to the different shells of ions, e.g. can have a view of the valence shell of a $4f$ electron system by choosing $M_{4,5}$ absorption edges or being sensitive to the $5d$ electrons (by choosing $L_{2,3}$ edges) relevant for the magnetic exchange interaction in Lanthanide metallic systems or using a quadrupole transition, at the $L_{2,3}$ edge as exemplified on resonant magnetic diffraction testing the demagnetization of the spiral order of elemental Ho [4].
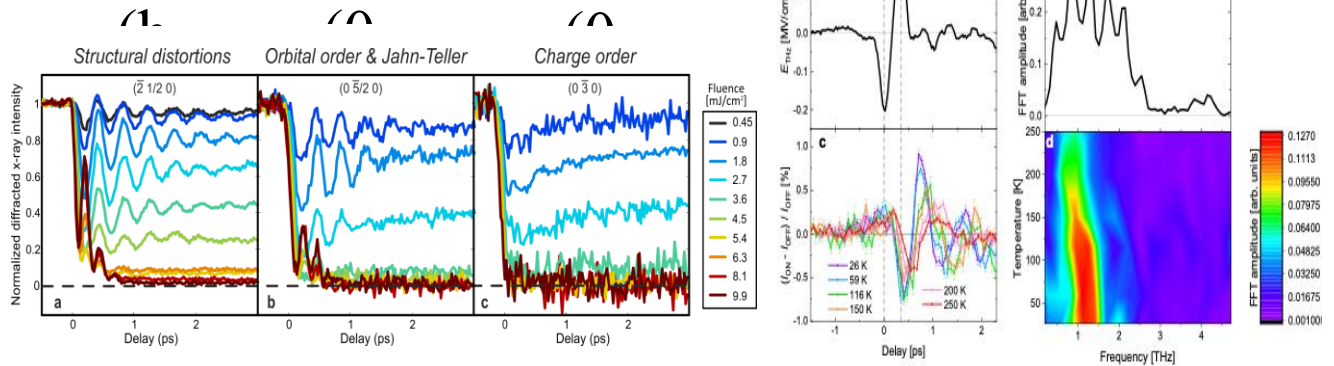
Fig.1. Left: displacive phonon observed in ultrafast x-ray diffraction *and its electronic response in a half doped manganite [1].* ***Right:*** *coherent driven electromagnon with driving field **a**) FFT of it **b**) the magnetic response **c**) and its FFT. [7]*

Also an example of a displacive magnon excitation [5] and a coherent driving of magnons and probing with x-rays will be shown [6,7].

References
[1] P. Beaud, A. Caviezel, S. O. Mariager, L. Rettig, G. Ingold, C. Dornes, S-W. Huang, J. A. Johnson, M. Radovic, T. Huber, T. Kubacka, A. Ferrer H. T. Lemke, M. Chollet, D. Zhu, J. M. Glownia, M. Sikorski, A. Robert, H. Wadati, M. Nakamura, M. Kawasaki, Y. Tokura, S. L. Johnson U. Staub, *Nature Materials* **13**, 923 (2014).
[2] M. Kozina, M. Fechner, P. Marsik, T. van Driel, J. M. Glownia, C. Bernhard, M. Radovic, D. Zhu, S. Bonetti, U. Staub, M. C. Hoffmann, *Nature Physics* **15**, 387 (2019).
[3] I. Radu, K. Vahaplar, C. Stamm, T. Kachel, N. Pontius, H. A. Durr, T. A. Ostler, J. Barker, R. F. L. Evans, R. W. Chantrell, A. Tsukamoto A. Itoh, A. Kirilyuk, Th. Rasing, A. V. Kimel, *Nature* **472**, 211 (2011).
[4] L. Rettig, C. Dornes, N. Thielemann - Kühn, N. Pontius, H. Zabel, D. L. Schlagel, T. A. Lograsso, M. Chollet, A. Robert, M. Sikorski, S. Song J. M. Glownia, C. Schüßler-Langeheine, S. L. Johnson, and *U. Staub*, Phys. Rev. Lett. **116**, 257202 (2016).
[5] Y. Windsor, A. Ernst, K. Kummer, K. Kliemt, C. Schuessler-Langeheine, N. Pontius, U. Staub, E. Chulkov, C. Krellner, D. Vyalikh, L. Rettig *Communications Physics* **3**, 139 (2020).
[6] T. Kubacka, J. A. Johnson, M.C. Hoffmann, C. Vicario, S. de Jong, P. Beaud, S. Grübel, S - W. Huang, L. Huber, L. Patthey, Y - D. Chuang J. J. Turner, G.L. Dakovski, W-S. Lee, M.P. Minitti, W. Schlotter, R. G. Moore, C. P. Hauri, S. M. Koohpayeh, V. Scagnoli, G.Ingold, S.L. Johnson U. Staub, *Science* **343**,1333 (2014).
[7] H. Ueda, R. Mankowsky, E. Paris, M.Sander, Y.Deng, B.Liu, L.Leroy, A.Nag, E.Skoropata, C. Wang, V. Ukleev, G. S. Perren, J. Dössegger, S. Gurung C. Svetina, E. Abreu, M. Savoini, T. Kimura, L. Patthey, E. Razzoli, H. T. Lemke, S. L. Johnson, U. Staub, *Nature Communications* **14**, 7778 (2023)

Cooperative optoelectronic properties of Multiexcitons in quantum dot solids

H. Tahara

Yokohama National University, Yokohama 240-8501, Japan

Chemically synthesized semiconductor quantum dots (QDs) are excellent materials for studying photodynamics of exciton complexes, e.g., biexcitons, triexcitons, and trions. These exciton complexes exhibit unique optoelectronic functionalities: multiexcitons increase photon-to-current conversion efficiencies via carrier multiplication processes in QD solar cells and trions reduce optical gain thresholds in QD lasers. Multiexcitons additionally show unique nonlinear optical responses: the high-frequency coherent oscillations with integer multiples of the exciton resonance frequency. The coherent responses, called harmonic quantum coherence, play important roles in the resonant multiphoton absorption [1,2,3]. Furthermore, cooperative optoelectronic dynamics of QDs, i.e., synchronous responses of QD ensembles, are expected to boost optoelectronic device performances, since QD devices are composed of a large number of QDs. Therefore, the understanding of ultrafast coherent dynamics and cooperative properties of exciton complexes is required to generate advanced functionalities. Here, we report on recent investigations of cooperative optoelectronic properties of QD solids. In this study, we focus on ultrafast coherent responses of multiexcitons to understand cooperative properties generated by coherent electronic coupling between QDs. The cooperative processes via electronic coupling are different from those via radiative coupling, which have been observed as superfluorescence from QD superlattices [4]. To investigate the cooperativities of QDs, inter-QD distance should be controlled precisely. Then, we fabricated PbS QD solid films by using a ligand exchange method. Since we used alkanedithiol molecules as ligands on the QD surfaces, the inter-QD distance was precisely tuned in increments of the length of carbon chain. We performed the photocurrent quantum interference spectroscopy to measure the ultrafast coherent responses of QD solids. In this method, the nonlinear coherent responses within photoexcitation were measured through the interference signals by scanning the phase-locked excitation pulse pair [5]. We observed that the nonlinear photocurrent signals increase with increasing excitation photon fluence. This shows that the nonlinear coherent signals originate from photogenerated multiexcitons. Furthermore, we found that the nonlinear signals are strongly enhanced in the short-ligand QD solids [6]. The enhancement ratio increases monotonically with the decrease of the inter-QD distance. This is the evidence that the enhancement is generated by the cooperative behavior of QDs via the electronic coupling.

Fig. 1. Experimental setup of photocurrent quantum interference spectroscopy [6]. Interference signals in excitation laser pulses and photocurrent signals were measured simultaneously.

These findings show that the cooperative quantum dynamics related to multiexcitons have a potential to provide advanced optoelectronic technologies.

References
[1] H. Tahara, M. Sakamoto, T. Teranishi, Y. Kanemitsu, *Physical Review Letters* **119**, 247401 (2017).
[2] H. Tahara, M. Sakamoto, T. Teranishi, Y. Kanemitsu, *Nature Communications* **9**, 3179 (2018).
[3] H. Tahara, Y. Kanemitsu, *Advanced Quantum Technologies* **3**, 1900098 (2020).
[4] G. Rainò, M. A. Becker, M. I. Bodnarchuk, R. F. Mahrt, M. V. Kovalenko, T. Stöferle, *Nature* **563**, 671 (2018).
[5] H. Tahara, M. Sakamoto, T. Teranishi, Y. Kanemitsu, *Physical Review* B **104**, L241405 (2021).
[6] H. Tahara, M. Sakamoto, T. Teranishi, Y. Kanemitsu, *Nature Nanotechnology* **19**, 744 (2024).

High harmonic generation in strongly correlated materials

K. Tanaka

Kyoto University, Kyoto, 606-8502 Japan & RIKEN, Wako, Saitama 351-0198, Japan

An intense infrared field can drive electrons into a highly non-equilibrium electronic state, leading to intriguing non-linear optical phenomena such as high harmonic generation (HHG). High harmonic generation (HHG) is the phenomenon of emitting integer multiples of the incident photon energy and was first reported in the atomic system, leading to the development of attosecond science. Recently, the scope of HHG has been extended to condensed matter systems, and researchers have succeeded in extracting physical parameters unique to solids, such as band structure, interatomic bonding, Berry curvature, and so on [1]. So far, HHGs have mainly been observed in semiconductors and insulators, and their extreme nonlinear optical properties have been interpreted within the single-electron approximation. However, many-body effects, such as cooperation and competition between multiple degrees of freedom, should be essential in solids and could have an impact on the extreme nonlinear optical process. Although several theoretical studies predict unique HHG properties due to many-body effects [2,3,4,5], the HHG properties unique to many-body systems have not been well studied experimentally. In this presentation, we report HHG spectroscopy in several materials that have ground states that cannot be explained by the single-electron approximation or excited states with many-body correlations. *First,* we present our HHG results in the Mott insulating phase of Ca_2RuO_4 [6,7]. Ca_2RuO_4 is an ideal two-dimensional Mott insulator with a metal-insulator transition temperature TMI ~ 360 K [8,9]. In Ca_2RuO_4, the Mott gap energy within the Mott insulating phase more than doubles with decreasing temperature [10]. This feature allows us to comprehensively investigate the relationship between HHG emission properties and the many-body electronic structure of Ca_2RuO_4.We used strong mid-infrared (MIR) pulses (0.26 eV, 100 fs, <300 GW/cm^2) for excitation and obtained up to the ninth harmonic as shown in Fig.1 (a). Fig. 1(b) shows the temperature dependence of HHG.
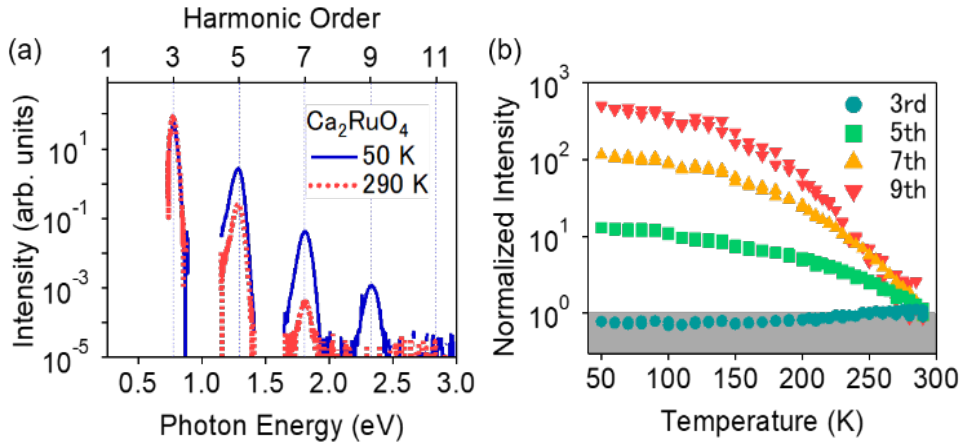

Fig. 1. (a) HHG spectra from Ca_2RuO_4 at 290 K (red-dashed line) and 50 K (blue-solid line). MIR intensity at the sample position is estimated to be 300 GW/cm^2 in air. (b) HHG intensities as a function of temperature.

High harmonic signals of order higher than the third show an enhancement of their yields by lowering the temperature. The observed enhancement of HHG yields is the opposite of what we expected because the gap opening by lowering the temperature suppresses the tunneling probability of doublon-holon pairs, which are thought to be the origin of HHG in Mott insulators [3,11]. Our theoretical calculation using the single-band Hubbard model was able to qualitatively reproduce the observations [12]. We found that the main factor for the HHG enhancement is the strong spin-charge coupling in the Mott insulator and the thermal fluctuation of the spin configuration. The thermal ensemble of doublon-holon pair dynamics, which strongly depends on the background spin configuration, should cause the destructive interference of HHG at high temperature. *Second,* we show the temperature dependence of HHG of $Pr_{0.6}Ca_{0.4}MnO_3$ in the range of 7-294 K, including the charge ordering (CO) transition and the magnetic transition temperatures [13]. The high harmonic (HH) intensity remains almost constant in the high temperature charge disordered \phase. However, as the temperature is lowered, it starts to increase near the CO transition temperature, where a CO-related optical gap appears. The anomalous gap energy dependence is similar to the result shown above for Ca_2RuO_4. We attribute the suppression of the HH intensity at high temperatures to the destructive interference between HH emissions from thermally activated multiple charge configurations. These results are unique to strongly correlated electron systems, one aspect of which can be captured by HHG spectroscopy. It should be noted that strong coupling between multiple degrees of freedom plays an important role in HHG. Our results suggest that HHG can be a spectroscopic tool to probe ultrafast nonequilibrium dynamics in strongly correlated materials.

References
[1] S. Ghimire, D. A. Reis, *Nature Physics* **15**, 10 (2019).
[2] R. E. F. Silva, I. V. Blinov, A. N. Rubtsov, O. Smirnova, M. Ivanov, *Nature Photonics* **12**, 266 (2018).
[3] Y. Murakami, M. Eckstein, P. Werner, *Physics Review Letters* **121**, 057405 (2018).
[4] N. Tancogne-Dejean, M. A. Sentef, A. Rubio, *Physical Review Letters* **121**, 097402(2018).
[5] S. Imai, A. Ono, S. Ishihara, *Physical Review Letters* **124**, 157404 (2020).
[6] K. Uchida, G. Mattoni, S. Yonezawa, F. Nakamura, Y. Maeno, K. Tanaka, *Physical Review Letters* **128**, 127401 (2022).
[7] K. Uchida, S. Kusaba, K. Nagai, T. N. Ikeda, K. Tanaka, *Science Advances* **8**, eabq7281 (2022).
[8] S. Nakatsuji, S. Ikeda, Y. Maeno, *Journal of Physical Society of Japan* **66**, 1868 (1997).
[9] G. Cao, S. McCall, M. Shephard, J. E. Crow, R. P. Guertin, *Physical Review* B **56**, 321 (1997).
[10] J. H. Jung, Z. Fang, J. P. He, Y. Kaneko, Y. Okimoto, T. Tokura, *Physical Review Letters* **91**, 056403(2003).
[11] T. Oka, H. Aoki, *Physical Review Letters* **95**, 137601 (2005).
[12] Y. Murakami, K. Uchida, A. Koga, K. Tanaka, P. Werner, *Physical Review Letters* **129**, 157401 (2022).
[13] A. Nakano, K. Uchida, Y. Tomioka, Y. Takaya, Y. Okimoto, K. Tanaka, *Physical Review Research* **6**, L042032 (2024).

Probing and manipulating effective optical responses of Quantum materials with ultrafast near field optics

A. Sternbach
University of Maryland, College Park, MD 20010, USA

Infrared radiation can selectively manipulate quantum materials and create properties that are not found in equilibrium. Terahertz frequencies are of considerable interest from the perspective of probing and manipulating non-equilibrium states. The terahertz spectral range hosts dipole active resonances associated with lattice vibrations, spin waves, orbital transitions and itinerant charge carrier acceleration. These resonances offer spectral signatures that can be used to interrogate low energy electrodynamics in non-equilibrium states. Mode selective drives of polarizable resonances can also be used to manipulate non-equilibrium order. Diffraction usually limits the ability to confine radiation to a length scale much smaller than the free space wavelength, which is on the order of 10-1,000 microns in the terahertz range. Limited spatial resolution and energy confinement presents challenges both from the perspective of probing and controlling non-equilibrium states at terahertz frequencies. I will discuss our efforts to probe and manipulate quantum materials on sub-diffraction limited length scales and femtosecond timescales. Our data, which combines around 10 nanometer spatial resolution and sub-picosecond temporal resolution provides insight into the role of inhomogeneities in non-equilibrium light-induced states [1,2]. A class of hybrid light-matter waves, known as polaritons, whose properties are distinct from far-field electromagnetic radiation will be discussed. Properties of polaritons, which can shape the electromagnetic environments of quantum materials below the diffraction limit, will be described in this talk [3].

Fig. 1. Left :*image showing negative refraction in a hyperbolic heterobicrystal. Data (**gray** colormap) and Calculation (**sky** colormap) [3]. **Right: a snapshot of a light-induced insulator to metal transition in Vanadium Dioxide** obtained with time resolved near field optical microscopy [1, 2].*

Properties of polaritons, which can shape the electromagnetic environments of quantum materials below the diffraction limit, will be described in this talk [3].
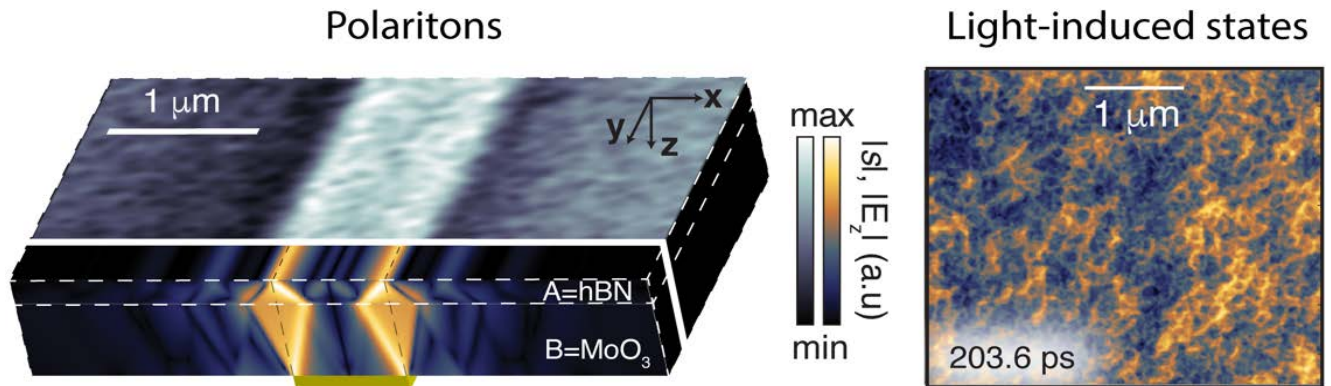
References
[1] A. J. Sternbach, T. Slusar, F. L. Ruta, S. Moore, X. Chen, M. K. Liu, H. T. Kim, A. J. Millis, R. D. Averitt, D. N. Basov, *Physical Review Letters* **132,** 186903 (2024).
[2] A. J. Sternbach, F. L. Ruta, Y. Shi, T. Slusar, J. Schalch,G. Duan,A. S.McLeod, X.Zhang, M. K.Liu, A.J.Millis, H.-T. Kim, L.- Q. Chen, R. D. Averitt D. N. Basov, *Nano Letters* **21**, 9052 (2021).
[3] A. J. Sternbach, S. Moore, A. Rikhter, S. Zhang, R. Jing, Y. Shao, B. Kim, S. Xu,   S.Liu, J. H.Edgar, A. Rubio, C.Dean, J. Hone, M. M. Fogler D. N. Basov, S*cience* **379**, 555 (2023).

Exploring nonequilibrium phenomena through laser processing simulations

M. Tani

Kansai Institute for Photon Science, 619-0215 Kyoto, Japan

The ultrafast laser material processing has been attracting increasing attention due to both broad scientific interest and industrial applications [1,2]. The process is initiated by the transfer of optical energy to electrons. Then, irreversible damage is left on the material surface when the energy is subsequently transferred to the lattice [3], the carrier density reaches the critical density at which the plasma frequency is identical to the laser frequency [4], or the interatomic forces are strongly modified owing to massive carrier creation [5]. Thus, the fundamental understanding of energy transfer from laser pulses to electrons, which drives the system into far-equilibrium states, is critical to further improve the efficiency of laser micromachining. There have been studies reporting that the use of two-color laser pulse pairs enables highly efficient laser ablation of transparent materials compared to single-color irradiation [6]. Although electron dynamics have been extensively discussed in terms of the coupling between intraband and interband transitions for single-color cases [7,8], their role under simultaneous two-color irradiation has been little studied. We investigate the energy absorption by bulk silicon under simultaneous dual-color (UV and IR) femtosecond laser fields, using numerical simulations based on the time-dependent density functional theory (TDDFT). We employ the SALMON code [9] and examine the dependence of energy absorption on the mixing ratio η of the two-color components with the total intensity (or, equivalently, fluence and energy) conserved. The calculation results are shown in Fig. 1.
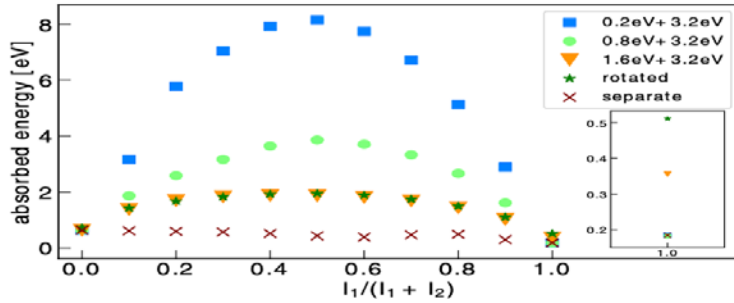

*Fig. 1. Mixing ratio η dependence of absorbed energy irradiated by various combination of two-color laser photon energies [10]: One is fixed to 3.2 eV, which is close to optical bandgap of Si, another is 0.2(**blue rectangle**) or 0.8(green circle) or 1.6 eV(**orange triangle**). Green stars are the results photon energies of 3.2eV and 1.6eV, but the polarization direction is rotated 90°. Brown crosses are the results when two color pulses are completely separated in time domain.*

Our calculations show that the absorbed energy is significantly enhanced by dual-color irradiation and maximized at $\eta \sim 0.5$. Our analyses reveal that the intraband motion of the electrons driven in the valence band by the IR field has a substantial role in increasing the valence-to-conduction interband transition induced by the UV field. These observations indicate that the strong-field electron excitation dynamics can be controlled by nonlinear coupling of a long-wavelength-driven intraband motion and a short-wavelength-driven interband transition. In this way, TDDFT is a first-principles method that strikes a good balance between accuracy and computational feasibility. However, the computational cost is still very high for performing repeatedly. Another significant challenge with TDDFT is to find an exchange-correlation functional that can properly incorporate dynamical electronic correlations such as electron-electron scattering, though no systematic improvement exists. To address these issues, we develop a semiclassical method based on the Vlasov equation as a cost-effective alternative to TDDFT for studying electron dynamics in bulk solid metals under intense laser fields [11]
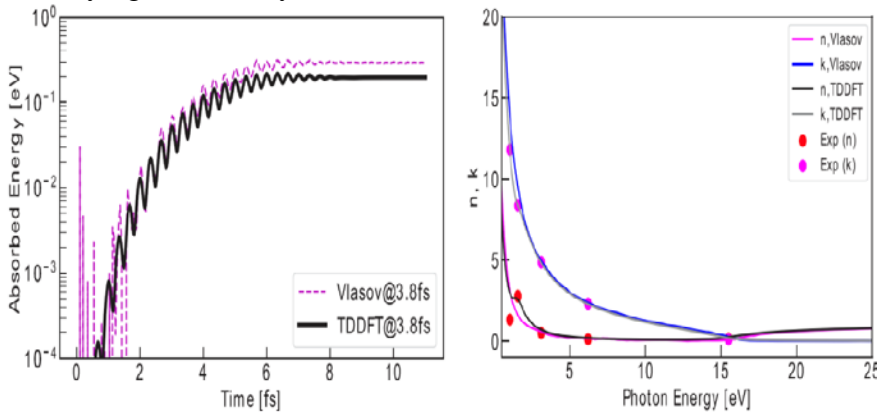

Fig. 2. Left: refractive index n and extinction coefficient k of bulk aluminum calculated with the Vlasov simulation and TDDFT as well as reported in experimental reference [12]. The experimental values are plotted at 1.03 eV (1200 nm), 1.2 eV (1030 nm), 1.55 eV (800 nm), 3.1 eV (400 nm), 6.2 eV (200 nm), and 15.5 eV (80 nm). Right: time-dependent electron energy absorption of bulk aluminum under a femtosecond laser pulse whose duration is 3.8 fs in FWHM. Pink dashed lines: Vlasov; black solid lines: TDDFT.

Starting from ground state distribution obtained by solving Thomas-Fermi model, time evolution is calculated by pseudoparticle method. On bulk aluminum, the optical spectra, including optical conductivity, dielectric function, complex refractive index (Fig.2 left), and reflectivity are evaluated by linear response calculation using impulse response, have been shown to agree well with TDDFT and experimental data. The absorbed energy, which has been evaluated as work done by laser field, has shown a linear dependence on the incident laser intensity. This trend agrees with TDDFT results in a certain laser fluence region. The time evolution of the absorbed energy is in good agreement with TDDFT calculation (Fig. 2 right). We further extend the Vlasov-based approach in two ways [13]. First, we include dynamical electron-electron scattering, which is recognized as a vital process in metallic nanoclusters [14, 15] and induces avalanche ionization in dielectrics and semiconductors in the context of laser material processing. Second, we consider the propagation effect of electromagnetic waves, which is crucial due to the fact that laser pulses typically used for laser machining can only penetrate the skin of metals. In Fig. 3, we show the comparison of Maxwell-Vlasov simulation results with and without electron-electron scattering on kinetic energy gain distribution after laser pulse irradiation on a thin aluminum film, and on kinetic energy current density along the optical axis (x) and the surface (y). These results indicate that electron energy is penetrating in deep region over optical energy, and that electron-electron scattering suppresses this effect.
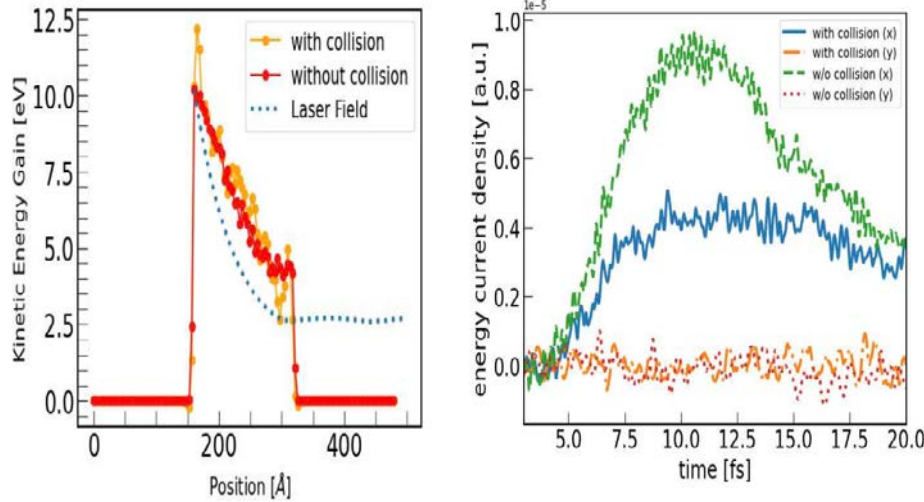

Fig. 3. Left: Kinetic energy gain distribution calculated by *collisionless simulation in red line and by collisional simulation in orange and scaled maximum laser field intensity along optical axis in blue dashed line.* **Right: Time evolution of energy current density** *in x- and y-direction. Blue solid and green dashed lines indicate x-component with and without electron-electron scattering, orange dash-dotted and red dotted lines does y-component with and without electron-electron scattering.*

The two extensions allow the investigation of electron dynamics in metals under ultrashort intense laser pulses while incorporating the effects of electron-electron scattering as well as laser pulse propagation. The former extension offers an advantage over TDDFT, since the description of electron-electron collisions in TDDFT is limited. The latter extension overcomes the limitation of our bare Vlasov simulator [11], since laser propagation is potentially important when the object size is not sufficiently smaller than the laser wavelength.

References
[1] K. K. Ostrikov, F. Beg, A. Ng, *Review of Modern Physics* **88**, 011001 (2016).
[2] K. Sugioka, Y. Cheng, *Light: Science and Applications* **3**, e149 (2014).
[3] R. R. Gattass, E. Mazur, *Nature Photonics* **2**, 219 (2008).
[4] P. P Pronko, Z. Zhang, P.A. VanRompay, *Applied Surface Science* **208**, 492 (2003).
[5] J. Thorstensen, S. E. Foss, *Journal Applied Physics* **112**, 103514 (2012).
[6] A. Rousse, C. Rischel, S. Fourmaux, I. Uschmann, S. Sebban, G. Grillon, P. Balcou, E. Förster, J. P. Geindre, P. Audebert, J. C. Gauthier D. Hulin, *Nature* 410, 65 (2001).
[7] T. Ikemachi, Y. Shinohara, T. Sato, J. Yumoto, M. KuwataGonokami, K. L. Ishikawa, *Physical Review* A 95, 043416 (2017).
[8] S. Ghimire, A. D. DiChiara, E. Sistrunk, P. Agostini, L. F. DiMauro, D. A. Reis, *Nature Physics* **7**, 138 (2011).
[9] M. Noda, S.A. Sato, Y. Hirokawa, M. Uemoto, T. Takeuchi, S. Yamada, A. Yamada, Y. Shinohara, M. Yamaguchi, K. Iida, I. Floss, T. Otobe K.- M. Lee, K. Ishimura, T. Boku, G. F. Bertsch, K. Nobusada, K. Yabana, *Computer Physics Communication* **235**, 356 (2019).
[10] M. Tani, K. Sasaki, Y. Shinohara, K. L. Ishikawa, *Physical Review* B **106**, 195141 (2022).
[11] M. Tani, T. Otobe, Y. Shinohara, K. L. Ishikawa, *Physical Review* B **104**, 075157 (2021).
[12] A. D. Rakic, *Applied Optics* **34**, 4755 (1995).
[13] M. Tani, T. Otobe, Y. Shinohara, K. L. Ishikawa, *arXiv:2502.02865* (2025).
[14] J. Kohn, R. Redmer, K.-H. Meiwes-Broer, T. Fennel, *Physical Review* A **77**, 033202 (2008).
[15] J. Heraud, M. Vincendon, P.-G. Reinhard, P. M. Dinh, E. Suraud, *The European Physical Journal* D **75** (2021).

Optical absorption activated by an ultrashort half-cycle pulse in Metallic and superconducting states of the Hubbard model

T. Tohyama

Tokyo University of Science, Tokyo 125-8585, Japan

The development of strong ultrashort pulse lasers has enabled the observation of non-equilibrium electron dynamics on femtosecond and even attosecond timescales. A novel technique called subcycle-pulse engineering has been proposed, involving the application of a subcycle pulse with less than one cycle oscillation within a pulse envelope. This approach aims to generate electronic states that cannot be accessed using conventional multicycle pulses. It has been suggested that applying ultrashort subcycle pulses to metallic or superconducting states can induce current with inversion symmetry breaking, which is detectable by second-harmonic generations [1,2].

We investigate how ultrashort halfcycle pulses, which can induce a current with an inversion symmetry breaking, contribute to transient absorption spectra of the Hubbard model that describes strongly correlated electron systems. Using the time-dependent density-matrix renormalization group method, we demonstrate that the halfcycle pump pulse leads to the enhancement of optical absorptions in metallic and superconducting states of the Hubbard model [3,4]. In the one-dimensional (1D) and two-dimensional (2D) Hubbard models with attractive on-site interactions ($U < 0$), we find the enhancement of absorptions at energies corresponding to amplitude modes associated with superconducting and charge-density-wave (CDW) orders (see Fig.1).
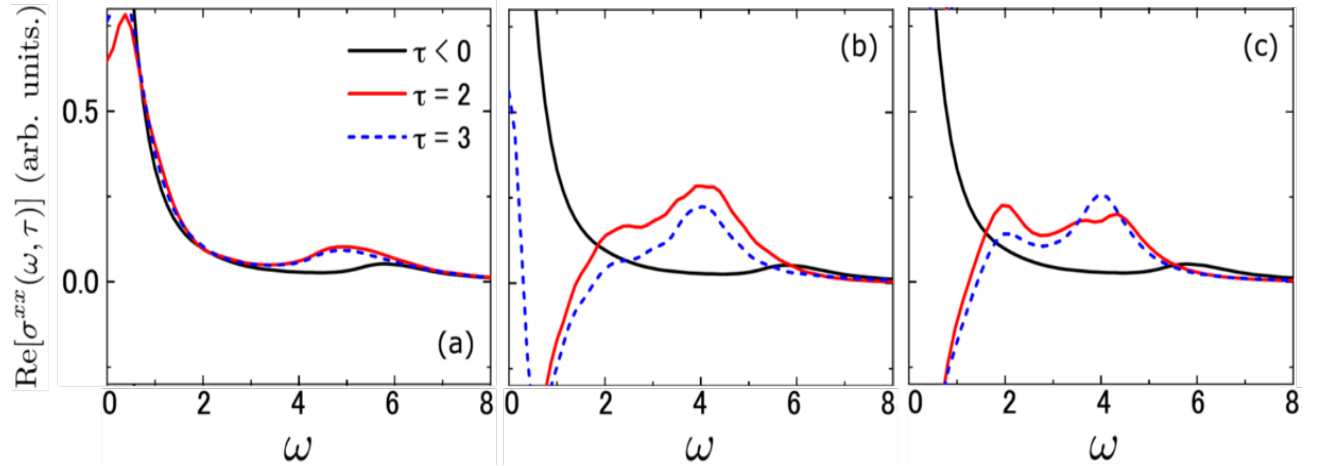

Fig. 1. Real part of time-dependent optical conductivity excited by an ultrashort half-cycle pump pulse for a 12.5% electron doped 1D Hubbard chain with 32 sites and on-site Coulomb interaction U=-4 in the unit of hopping energy. The black lines are for the delay time between pump and probe pulses with τ < 0 (i.e., before pumping) and the red solid and blue dashed lines are for τ = 2 and 3, respectively, with pumping amplitude of the vector potential 0.1π (**a**), 0.4π (**b**), and 0.5π (**c**). In (**b**) and (**c**) with large pumping amplitude, a two-peak structure appears for τ = 2 and 3, where a peak around the energy w=2 (w=|U|=4) is related to an amplitude mode of superconducting (CDW) order

This behavior is the manifestation of a current-induced activation of absorptions at amplitude modes in a clean superconducting state. In a 2D system, we find that the amplitude-mode absorptions emerge in both parallel and perpendicular directions to the pump pulse for $U= -4$ (in the unit of the electron hopping), but only in parallel for $U = -8$. This U dependence comes from the difference in the localized nature of superconducting pairing at weak and strong couplings. In a metallic state of the 2D Hubbard model at nearly half filling with repulsive $U > 0$ on-site interactions, we find another type of absorption enhancement broadly distributed in the Mott gap. The mid-gap absorptions appear in both directions parallel and perpendicular to the pump pulse, who senonlocal nature can be attributed to the effect of magnetic excitations.

References
[1] K. Shinjo, S. Sota, S. Yunoki, T. Tohyama, *Physical Review* B **107**, 195103 (2023).
[2] Y. Kawakami, T. Amano, H. Ohashi, H. Itoh, Y. Nakamura, H. Kishida, T. Sasaki, G. Kawaguchi, H. M. Yamamoto, K. Yamamoto, S. Ishihara K. Yonemitsu, S. Iwai, *Nature Communications* **11**, 4138 (2020).
[3] K. Shinjo, S. Sota, S. Yunoki, T. Tohyama, *arXiv*:2411.00313 (2024).
[4] S. Chandra, K. Shinjo, S. Sota, T. Tohyama, *to be submitted,* (2025).
 * *Acknowledgment*: this work was done in collaboration with Sumal Chandra, Kazuya Shinjo, and Shigetoshi Sota.

Room-temperature memristive switching of Charge density wave states in EuTe$_4$

R. Venturini[,2], M. Rupnik[1], J. Gašperlin[1], J. Lipič[1], P. Šutar[1], Y. Vaskivskyi[1], F. Ščepanović[1], D. Grabnar[1]
D. Golež[1], D. Mihailovic[1]

[1]*Jozef Stefan Institute, 1000 Ljubljana, Slovenia*
[2]*Paul Scherrer Institute, 5232 Villigen, Switzerland*

Control over the novel quantum states that emerge from non-equilibrium conditions is of both fundamental and technological importance. Metastable charge density wave (CDW) states are particularly interesting as their electrical manipulation could lead to novel memory devices [1]. However, the ability to use electrical pulses for non-volatile resistance switching involving CDW states is exceedingly rare and has been limited to cryogenic temperatures.In this presentation, I will focus on a recently discovered van der Waals semiconductor EuTe$_4$ that exhibits the coexistence of distinct CDW orders [2, 3], which give rise to a giant hysteresis loop. The slight difference in colinear CDW wavevectors in Te monolayers and bilayers creates a unique incommensurate Moiré superlattice [4], which was shown to be susceptible to optical manipulation [5]. We have recently discovered that electrical pulses can be used for excitation to hidden, yet stable electronic states over a broad temperature range between 6 K and 400 K [6] (Fig. 1). We find that switching occurs through a non-thermal pathway and is reversible via a thermal erase procedure. As the change in electronic order is accompanied by a change in the material resistance, the electronic device acts as a memristor. The CDW switching appears to be driven by an electric field with only low voltage needed to perturb the pristine state.
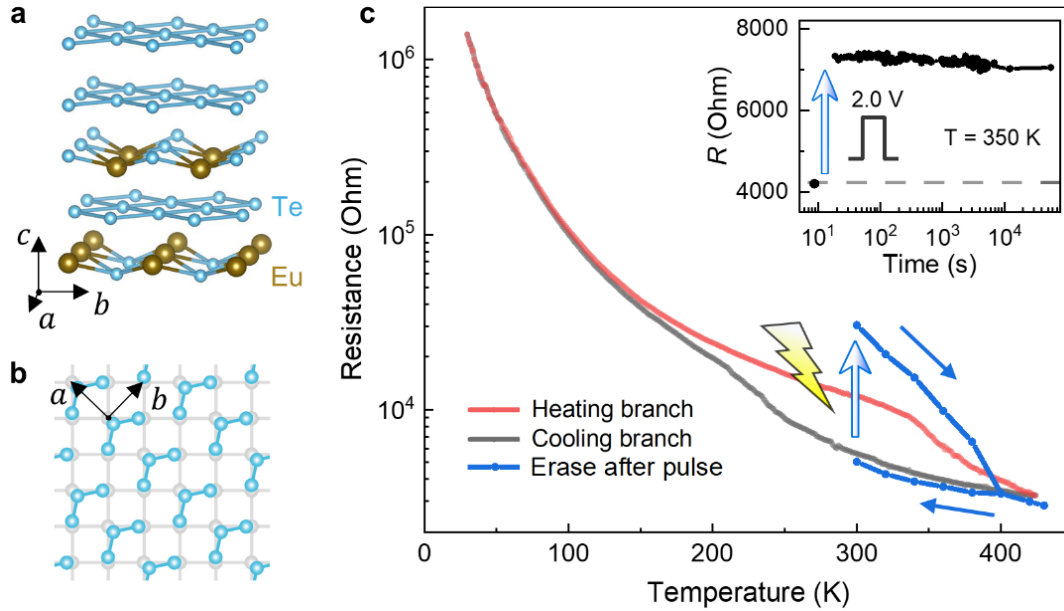

***Fig. 1. a**, crystal structure of EuTe$_4$; **b**, A square lattice of Te atoms (**gray**) and a distorted lattice hosting the CDW state (**blue**); **c**, thermal erase cycle (**blue**) after 2.7 V pulse is applied at 300 K. The **inset** shows the stability of the switched state at 350 K after applying a 2.0 V pulse.*

We demonstrate that non-volatile control of the CDW order via electrical pulses is possible up to, and even above room temperature. Low-voltage, fast, and energy-efficient CDW switching observed in EuTe$_4$ holds great promise for novel memory devices and neuromorphic computing applications.

References
[1] A. Mraz, R. Venturini, D. Svetin, V. Sever, I. A. Mihailovic, I. Vaskivskyi, B. Ambrozic, G. Drazic, M. D´ ʼAntuono, D. Stornaiuolo, F. Tafuri D. Kazazis, J. Ravnik, Y. Ekinci, D. Mihailovic, *Nano Letters* **12**, 4814 (2022).
[2] D. Wu, S. L. Chen, G.Y. Zhong, J. Su, L.Y. Shi, L. Tong, G. Xu, P. Gao, N.L. Wang, *Physical Review Materials* **3**, 024002 (2019).
[3] B. Q. Lv, A. Zong, D. Wu, A. V. Rozhkov, B. V. Fine, S.-D. Chen, M. Hashimoto, D.-H. Lu, M. Li, Y.-B. Huang, J . P. C. Ruff, D. A. Walko Z. H. Chen, I. Hwang, Y. Su, X. Shen, X. Wang, F. Han, H. C. Po, Y. Wang, P . Jarillo - Herrero, X. Wang, H. Zhou, C.- J. Sun, H. Wen Z.- X. Shen,N. L. Wang, N. Gedik, *Physical Review Letters* **128**, 036401 (2022).
[4] B. Q. Lv, Y. Su, A. Zong, Q. Liu, D. Wu, N.F.Q.Yuan, Z. Nie, J. Li, S. Sarker, S. Meng, J. P. C. Ruff, N. L. Wang, N. Gedik *arXiv:2501.09715* (2025)
[5] Q. Liu, D. Wu, T. Wu, S. Han, Y. Peng, Z. Yuan, Y. Cheng, B. Li, T. Hu, L. Yue, S. Xu, R. Ding, M. Lu, R. Li, S. Zhang, B. Lv, A. Zong Y. Su, N. Gedik, Z. Yin, T. Dong, N. Wang, *Nature Communications* **15**, 8937 (2024).
[6] R. Venturini, M.Rupnik, J.Gašperlin, J.Lipič, P. Šutar, Y.Vaskivskyi, F.Ščepanović, D.Grabnar, D.Golež, D.Mihailovic, *arXiv:2412.13094*(2024)

Interatomic spin transfer

C. von Korff Schmisng

Max-Born- Institut für Nichtlineare Optik und Kurzzeitspektroskopie, 12489 Berlin, Germany

Ultrafast magnetization dynamics can be categorized as being induced either by a direct interaction with the optical light field or by an indirect interaction via excitation of the electronic system, which only couples to the magnetization subsequently. However, to date most microscopic mechanisms in femtomagnetism in metallic systems have been identified to be secondary processes driven by an excess of energy in the electronic system gained after optical excitation.

Only with the seminal work of Dewhurst et al. [1], the concept that the light field itself can directly manipulate the magnetization was revived: time-resolved density-of-state calculations predicted that in multicomponent magnetic systems optical excitation can efficiently redistribute spin-polarized carriers between the different sublattices, leading to a local change of the magnetic moment within the temporal duration of the light pulse. The process is called optical intersite spin transfer (OISTR) and within a few years several experiments reported evidence for such direct spin manipulation by light [2,3,4,5,6,7,8,9].

In this tutorial, I will review the current understanding of OISTR and critically examine the experimental observables currently associated with direct light-matter interaction. I will explain why recent work [10,11,12] suggests alternative explanations beyond OISTR and partially challenges the significance of previous results.
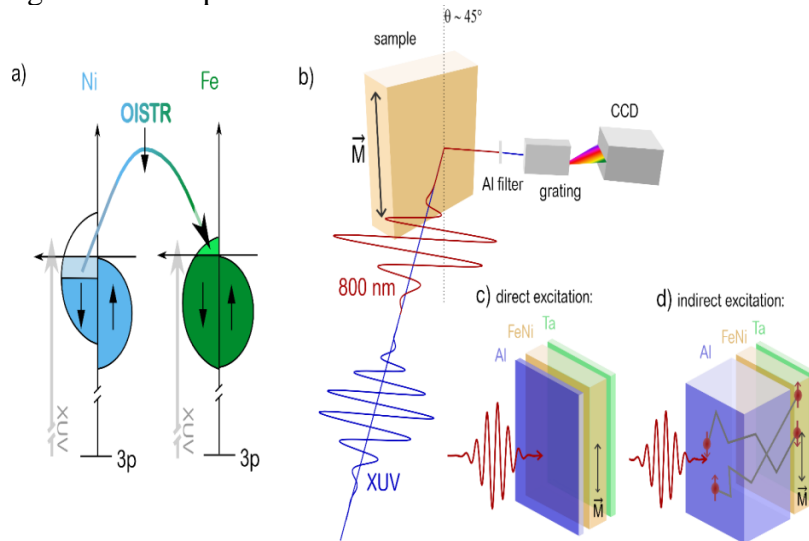

Fig. 1. a) Concept of the OISTR process.
*In an FeNi alloy minority spins are transferred via an optical `excitation from Ni to available states in Fe. This would imply an ultrafast loss of magnetization in Fe and a concomitant increase of magnetization in Ni. Changes in the transient density of states is probed by 3p core hole transitions using XUV radiation. **b)** Typical experimental geometry in ultrafast high harmonic generation spectroscopy called T-MOKE (transverse magneto-optical Kerr Effect). The magnetization is probed by a broad XUV spectrum covering the 3p core-hole transition of the magnetic sublattices, e.g. Fe and Ni. **c)** Geometry where the light can directly interact with the magnetic layer and d) geometry where only hot electrons generated in an Al layer interact with the magnetic layer. In the latter case OISTR cannot take place. Adapted from [10].*

By focusing on element-specific experiments based on laser-driven high harmonic generation sources in the extreme ultraviolet (XUV) spectral range, I will show how the complexity of the experimental observables opens up new opportunities in ultrafast magnetization research.

References
[1] J. K. Dewhurst, P. Elliott, S. Shallcross, E.K.U. Gross, S. Sharma *Nano Letters* **18**, 1842, (2018).
[2] J. Chen, U.Bovensiepen, A. Eschenlohr, T.M¨uller, P. Elliott, E.K.U. Gross, J. K. Dewhurst, S. Sharma *Physical. Review Letters* **122**, 067202 (2019)
[3] F. Siegrist, J. A. Gessner, M.Ossiander, C. Denker, Y.- P. Chang, M. C. Schröder, A. Guggenmos, Y. Cui, J. Walowski, U. Martens, J. K. Dewhurst U. Kleineberg, M. Münzenberg, S.Sharma, M.Schultze, *Nature* **571**, 240 (2019).
[4] F. Willems, C.von Korff Schmising, C.Strüber, D.Schick, D. W. Engel, J. K. Dewhurst, P.Elliott, S. Sharma, S. Eisebitt, *Nature Comunications* **11** 871 (2020).
[5] M. Hofherr, S. Häuser, J. K. Dewhurst, P. Tengdin, S. Sakshath, H. T. Nembach, S. T. Weber, J. M. Shaw, T. J. Silva, H. C. Kapteyn M. Cinchetti, B. Rethfeld, M. M.Murnane, D.Steil, B.Stadtmüller, S. Sharma, M. Aeschlimann, S. Mathias, *Science Advances* **6**, eaay8717 (2020)
[6] P. Tengdin C.Gentry, A. Blonsky, D. Zusin, M. Gerrity, L. Hellbrück, M. Hofherr, J. Shaw, Y. Kvashnin, E. K. Delczeg - Czirjak, M. Arora H. Nembach, T. J.Silva, S.Mathias, M. Aeschlimann, H.C. Kapteyn, D.Thonig, K. Koumpouras , O.Eriksson, M. M. Murnane, *Science Advances* **6** eaaz1100, (2020).
[7] S. A. Ryan, P. C. Johnsen, M. F. Elhanoty, A. Grafov, N. Li , A. Delin, A. Markou, E. Lesne, C. Felser, O. Eriksson, H. C. Kapteyn, O. Grånäs M. M. Murnane, *Science Advances* **9**, eadi1428 (2023).
[8] C. Möller , H. Probst, G. S. M. Jansen, M. Schumacher, M. Brede, J. K. Dewhurst, M. Reutzel, D. Steil, S. Sharma, S. Mathias *Communications Physics* **7**, 24, (2024).
[9] R. Géneaux H.-T. Chang, A. Guggenmos, R. Delaunay, F. Légaré, K. Légaré, J. Lüning, T. Parpiiev, I. J. P. Molesky, B. R de Roulet, M. W Zuerch S. Sharma, M. Schultze. S. R Leone. *Physical Review Letters* **133**, 106902 (2024).
[10] C. von Korff Schmising, S. Jana, O. Zulich, D.Sommer, S. Eisebitt, *Physical Review Reearch*. 6, 013270, (2024).
[11] S. Jana, R.Knut,P.Singh, K.Yao, C.Tzschaschel, J. Richter, D. Schick, D. Sommer, D. Engel, O. Karis, C. von Korff Schmising, S. Eisebitt1 , *arXiv. 2503.08811* (2025).
[12] S. A. Ryan, M. F. Elhanoty, A. Grafov, P. C. Johnsen, N. Li, J.M. Shaw, A.Delin, A. Markou, E. Lesne, C. Felser , O. Eriksson, E. K. Delczeg-Czirjak D. Karmakar, H.C. Kapteyn, O. Grånäs , M. M. Murnane, *arXiv. 2501.12416* (2025).

Visualizing terahertz light-matter coupling in a Two-dimensional superconductor

A. von Hoegen[1], T.Tai[1], C. Allington[1], M. Yeung[1], A. Cui[2], K. Torres[2], M. Michael[3], E. Viñas Boström[3]
A. Kosak[1], B. Lee[1], G. Beach[1], P. Kim[2], A. Rubio[3], N. Gedik[1]

[1] *Massachusetts Institute of Technology, Cambridge, MA 02139, USA*
[2] *Harvard University, Cambridge, MA 02138, USA*
[3] *Max-Planck-Institut für Struktur und Dynamik der Materie,22761 Hamburg, Germany*

Many fundamental excitations in solids, such as lattice vibrations, collective electron motion, and spin dynamics, naturally evolve on picosecond timescales and meV energy scales. As such, terahertz (THz) spectroscopy, which matches these intrinsic time and energy scales, has emerged as a powerful tool [1]. The current frontier of this field explores how geometrical confinement shapes these phenomena in 'low-dimensional' (e.g., atomic-width) quantum dots, wires, and sheets. However, THz spectroscopy is plagued by poor spatial resolution, and features smaller than $\sim$ 100 µm wavelength scales cannot be resolved, impeding access to the rapidly evolving field of low-dimensional materials. These limitations can be overcome by utilizing "near-field" methods, where a far-field THz beam is confined to nano-tip cavities, transmission lines, or small apertures [2,3]. In our work, we choose a different avenue, and bring the sample in direct contact with a microscopically small spintronic THz source [4]. The THz emission is stimulated by a tightly focused ultrashort near-infrared laser beam, which determines the spatial extant of the THz source. In this geometry (see Fig. 1 a), the confined THz light interacts with the sample still within the nearfield of the spintronic source before diverging into the far-field
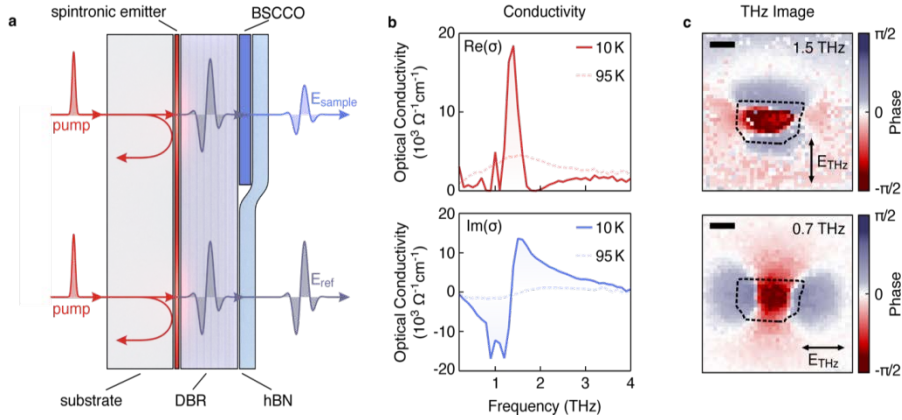

*Fig. 1. a.. Schematic of the experimental configuration. The spintronic emitter acts as a confined THz source when locally excited by the tightly focused ($\sim$ µm) NIR pump beam. The stack consists of the spintronic emitters, a distributed Bragg reflector (DBR), $Bi_2Sr_2CaCu_2O_8$ (BSCCO) and hexagonal boron nitride (hBN) **b** THz conductivity of a small flake of few-layer $Bi_2Sr_2CaCu_2O_8$ above and below the critical temperature. **c** THz images for a frequency of 1.5 THz showing the phase of the transmitted radiation for two polarizations: **top: vertical, bottom: horizontal**).*

.

Using this approach, we investigated how engineering THz light-matter coupling through the sample's geometry and dielectric environment gives rise to distinctive resonances that confine electromagnetic waves to deeply sub-wavelength scales. We observe clear spectroscopic evidence of an artificial resonance in the two-dimensional superconductor $Bi_2Sr_2CaCu_2O_8$, that only appears in the superconducting state of below T_c = 87 K (see Fig. 1, b). To visualize this resonance, we raster scan the confined THz source across the sample to locally resolve and image the THz electrodynamics. We find that resonance is associated with a clear wave-like spatial pattern, which aligns with the polarization of our THz light; a hallmark feature of a plasmon (see Fig. 1, c). We further track this mode as a function of temperature and find a clear crossover from geometry-dominated behavior below T_c to a scattering-dominated regime in the normal state of $Bi_2Sr_2CaCu_2O_8$.. These results show a clear avenue to deterministically control the THz light-matter coupling in 2D quantum materials through geometrical confinement to design systems that more effectively couple to light. This offers a promising venture point to explore the cross section of cavity quantum electrodynamics and low-dimensional quantum materials.

References
[1] A., Leitenstorfer, A. S Moskalenko, T. Kampfrath, J. Kono, E. Castro-Camus, K. Peng, N. Qureshi, D. Turchinovich, K. Tanaka, A. G. Markelz M. Havenith, C. Hough, H. J. Joyce, W. J. Padilla, B. Zhou, K.-Y. Kim, X.- C. Zhang, P. U. Jepsen, S. Dhillon, M. Vitiello, E. Linfield A. G. Davies, M. C. Hoffmann, R. Lewis, M. Tonouchi, P. Klarskov, T .S. Seifert, Y. A. Gerasimenko, D. Mihailovic, R. Huber, J. L. Boland O. Mitrofanov, P. Dean, B. N. Ellison, P. G. Huggard, S. P. Rea, C. Walker, D. T. Leisawitz, J. R. Gao, C. Li, Q. Chen, G. Valušis, V. P. Wallace E. Pickwell-MacPherson, X. Shang, J. Hesler, N. Ridler, C. C. Renaud, I. Kallfass, T. Nagatsuma, J. A. l. Zeitler, D. Arnone, M. B. Johnston J. Cunningham, *Journal of Physics* D **56,** 223001 (2023).
[2] J. W. McIver, B. Schulte, F.-U. Stein, T. Matsuyama, G. Jotzu, G. Meier, A. Cavalleri, *Nature Physics* **16**, 38 (2020).
[3] T. L. Cocker, V. Jelic, R. Hillenbrand, F. A. Hegmann, *Nature Photonics* **15**, 558 (2021).
[4] T. Seifert, S. Jaiswal, U. Martens, J. Hannegan, L. Braun, P. Maldonado, F. Freimuth, A. Kronenberg, J. Henrizi, I. Radu, E. Beaurepaire Y. Mokrousov, P. M. Oppeneer, M. Jourdan, G. Jakob, D. Turchinovich, L. M. Hayden, M. Wolf, M. Münzenberg, M. Kläui, T. Kampfrath *Nature Photonics* **10**, 483 (2016).

Selective excitation of Higgs and Leggett modes in two-band Superconductor MgB$_2$

N.-L. Wang

Peking University, Beijing 100871, China

Recent developments in nonequilibrium and nonlinear terahertz (THz) spectroscopies have significantly advanced our understanding of collective excitations in superconductors. However, there is still debate surrounding the identification of Higgs or Leggett modes, as well as BCS charge fluctuations, in the well-known two-band superconductor MgB$_2$. Here, we utilized both multi-cycle and single-cycle THz pump-broadband THz probe techniques to investigate the THz nonlinear response of MgB$_2$. Through multicycle THz pump-THz probe experiments on MgB$_2$ (Fig. 1), we observed distinct nonlinear signals at both the fundamental frequency (ω) and the second harmonic frequency (2ω) of the pump pulses, which exhibited resonant enhancement at temperatures where their frequencies respectively match $2\Delta_\pi(T)$. They are mainly attributed to the π-band Higgs mode response. By adjusting the THz pump pulse to a single-cycle waveform that satisfies non-adiabatic excitation criteria, we observed an over-damped oscillation corresponding to the Leggett mode.
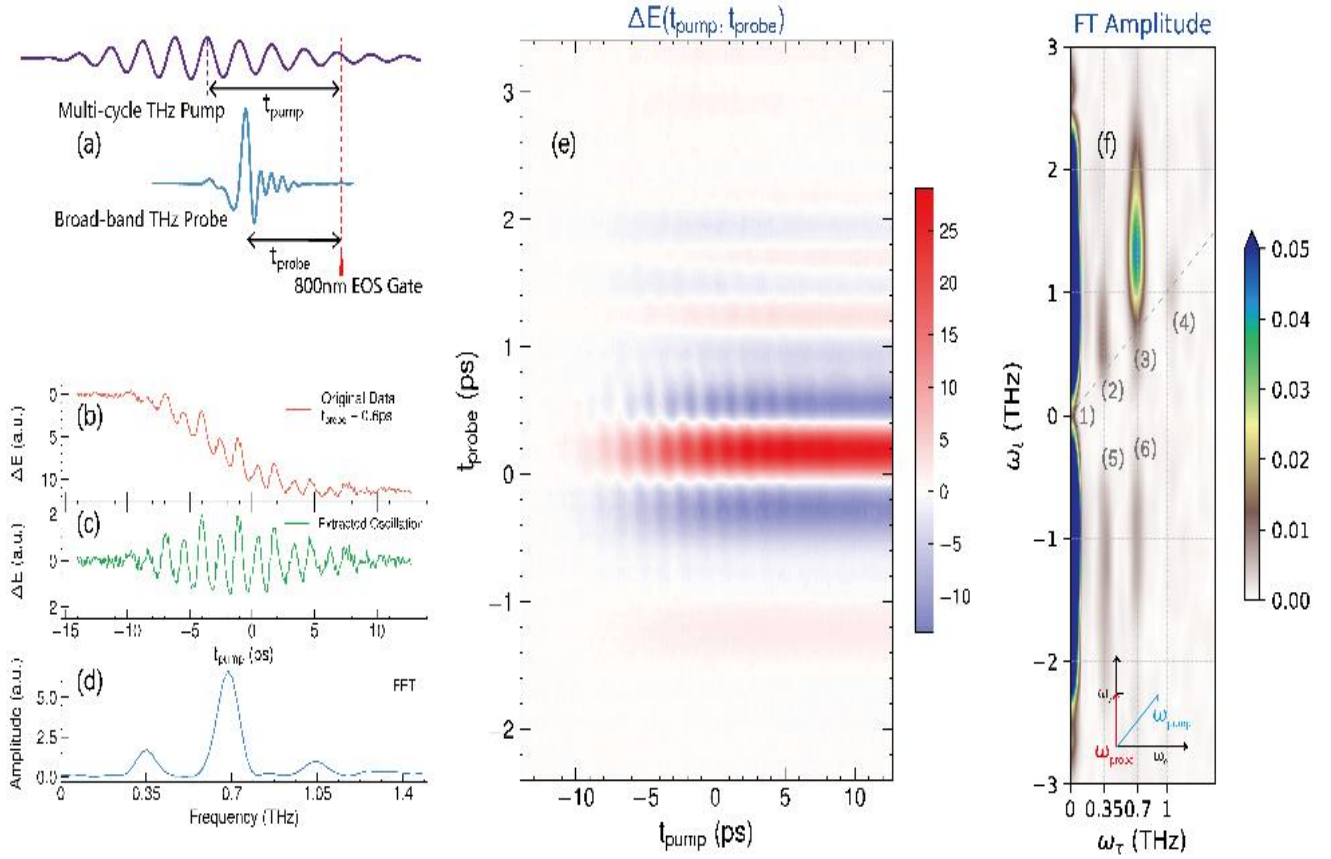

***Fig. 1. 0.35~THz multi-cycle pump-probe experiment results at 6~K.** (**a**): Definition of t_{pump} and t_{probe} in time-domain. (**b**): Time-domain waveform of the nonlinear signal, cut at t_{probe} = 0.6 ps. (**c**) and (**d**): Time- and frequency-domain waveforms of the extracted oscillation, cut at t_{probe} = 0.6 ps. (**e**): Time-domain waveform of the nonlinear signal concerning t_{pump} and t_{probe}. (**f**): Frequency-domain waveform of the nonlinear signal ΔE ($\tau = t_{pump} - t_{probe}$). The elongated signal peaks labeled from (1) to (6) could be well explained from the frequency vector analysis of pump and probe pulses (mostly arising from four wave mixing of third order nonlinear processes).*

Our findings contribute to solving the ongoing debates and demonstrate the selective excitation of collective modes in multiband superconductors, offering new insights into the interaction between Higgs and Leggett modes.

Reference
[1] J. Yuan, L. Shi, T. Xu, Y. Wang, Z. Gan, H. Wang, T. Wu, D. Wu, T. Dong, N. Wang, *arXiv:2412.13830* (2024).

Ultrafast control of entanglement and ppin-triplet pairing in Correlated materials

Y. Wang

Emory University, Atlanta, GA 30322, USA

The rapid progress in quantum science necessitates precise and predictive control over collective electronic phenomena that extend beyond classical capabilities. Among the available strategies, ultrafast laser pumping stands out for its rich parameter space and its ability to dynamically reshape electronic structures in real time. By leveraging Floquet engineering with tailored ultrafast pulses, we achieve transient control of many-body interactions and quantum states in strongly correlated systems. In this talk, I will discuss the ultrafast control of magnetic, entanglement, and superconducting properties in quantum materials. I will begin by demonstrating how paramagnon excitations in doped Mott insulators with short-range magnetic order can be precisely manipulated using an ultrafast laser pulse, following Floquet theory at the center of the pulse [see Figs. 1(a) and 1(b)]. Notably, this Floquet control is absent in undoped Mott insulators, underscoring the critical role of doping and short-range correlations.
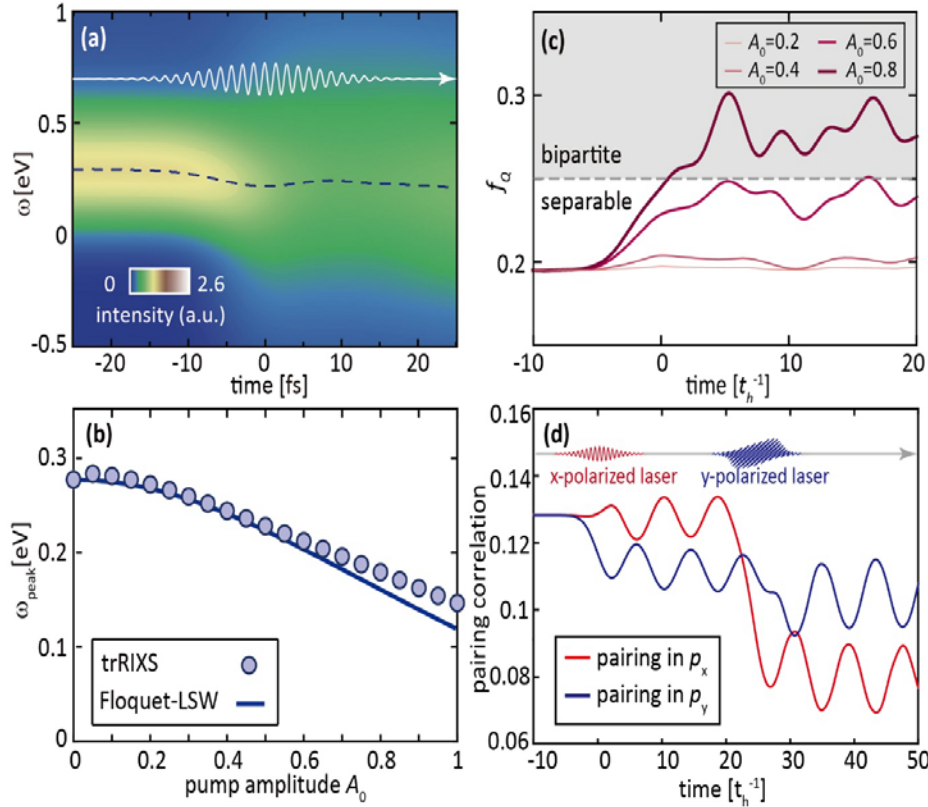

Fig. 1. (**a**) *Collective spin excitations measured by trRIXS in a two-dimensional doped Mott insulator, showing light-induced softening of paramagnons. The dashed line traces the evolution of the peak position over time, following the pump pulse (white line).* (**b**) *Transient paramagnon energy (circles) at the center of the pump pulse compared with predictions from Floquet linear spin-wave theory (solid line).* (**c**) *Dynamics of the quantum Fisher information extracted from trRIXS, witnessing a laser-induced bipartite-entangled state.* (**d**) *Evolution of p-wave pairing correlations in a quarter-filled extended Hubbard model, sequentially driven by x- and y-polarized laser pulses.*

Building on this, I will present two key applications of Floquet-engineered quantum materials. First, we show that spin entanglement in a cuprate chain can be transiently enhanced by laser pumping [see Fig. 1(c)]. This increase in entanglement depth can be quantitatively witnessed through a self-consistent analysis of time-resolved resonant inelastic x-ray scattering (trRIXS) data. Second, I will demonstrate that Floquet engineering can induce a transient sign reversal in the magnetic exchange interaction, creating favorable conditions for spin-triplet superconductivity. Leveraging this mechanism, we further show that a single polarized optical pulse can directly switch on p-wave pairing correlations [see Fig. 1(d)].

References
[1] Y. Wang, Y. Chen, T.P. Devereaux, B. Moritz, M. Mitrano, *Communications Physics* **4**, 212 (2021).
[2] J. Hales, U. Bajpai, T. Liu, D.R. Baykusheva, M. Li, M. Mitrano, Y. Wang, *Nature Communications* **14**, 3512 (2023).
[3] W.- C. Chen, Y. Wang, C.-C. Chen, *Physical Review* B **108**, 064514 (2023)
[4] Z. Shen, C. Xie, W.-C. Chen, Y. Wang, *arXiv:2503.02294* (2025)

Hidden states and dynamics in twisted moiré structures

Y. Wang, X.-Y. Zhu

Columbia University, New York, NY 10025, USA

Over decades, the search for and understanding emergent quantum phases has posed significant challenged for physicist. Moiré systems, with their tunable superlattices, provide a powerful platform to investigate quantum phases, such as correlated insulators, superconductivity, magnetism and beyond. Particularly, twisted $MoTe_2$ bilayers have recently revealed exotic fractional quantum anomalous Hall (FQAH) and fractional topological insulators (FTI), which have never been observed in conventional quantum materials. In this abstract, we introduce a non-equilibrium approach to detect equilibrium state. Using transient optical spectroscopy, we uncovered nearly 20 hidden states at fractional fillings absent in static measurements.
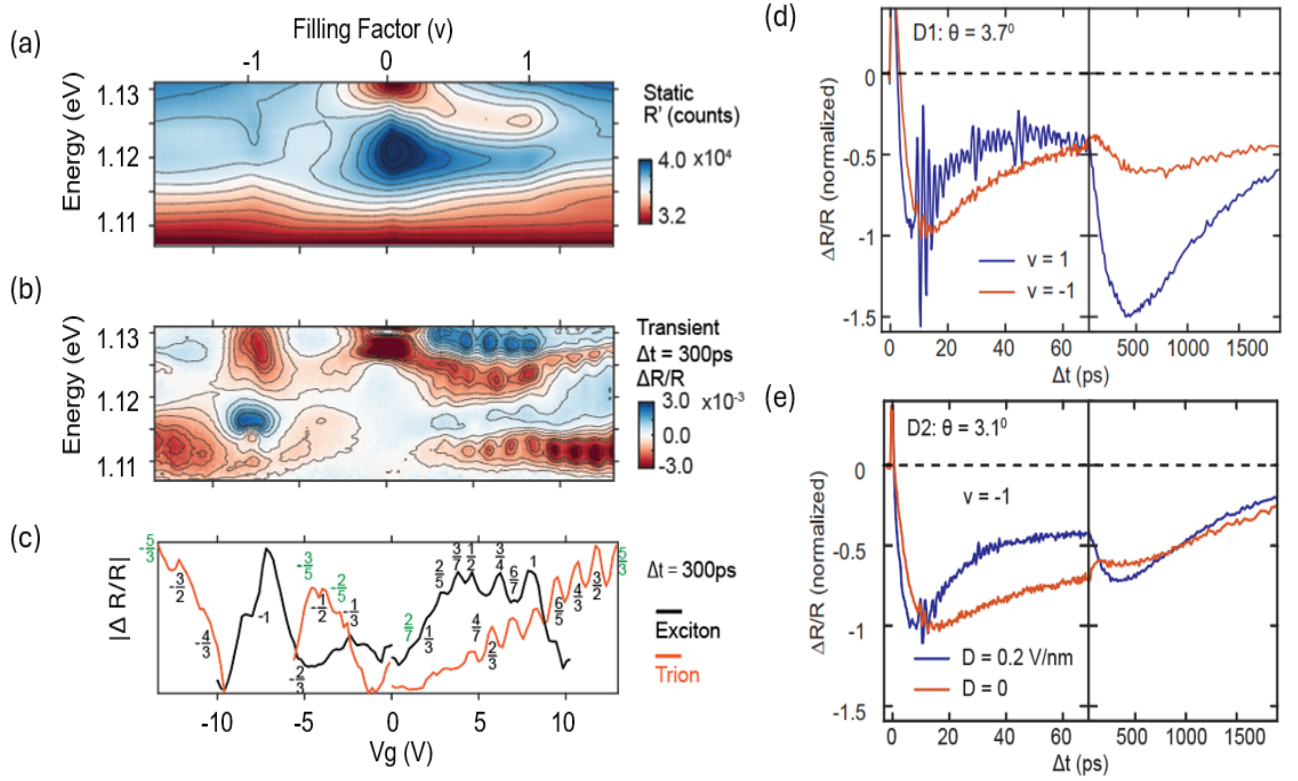
Fig. 1. Transient gate map and time profile: *(a) Static reflection spectrum (R) as a function of gate bias (Vg) and probe photon energy ($\hbar\omega$); (b) Transient reflection spectra, $\Delta R/R$ (pseudo color), where $\Delta R = R(\Delta t) - R$, as a function of Vg and $\hbar\omega2$ for delay times of $\Delta t = 300$ ps; (c) Line cuts from the spectral maps at exciton (**black**) and trion (**red**) energies. The calibrated filling factors (v) are indicated on the line cuts. All experiments carried are out at a sample temperature of T = 2.0 K; (d) Time profiles of transient reflection ($\Delta R/R$) for: a $v = \pm1$; (d) Time profiles of the $v = -1$ state in device D2 ($\theta = 3.1o$) at two displacement fields, D = 0.0 (**red**) and 0.2 V/nm (**blue**). Each profile is obtained at the probe photon energy where $\Delta R/R$ reaches minimum, integrated over a small spectral window (±2 meV). Note that each panel is divided into two scales (0-75 ps and 75 – 1875 ps).*

Beyond known states, we identified new fractional fillings, including v = -4/3, -3/2, -5/3, -7/3, -5/2, and -8/3, potential candidates for predicted topological phases. Additionally, we will discuss the differing dynamics of the electron and hole doped states. These findings not only reveal hidden states but also highlight the dynamic role of topological protection, motivating further experimental and theoretical exploration of exotic quantum phases.

References

[1] Y. Wang. J. Choe. E. Anderson. W. Li. J. Ingham, E. A. Arsenault, Y. Li, X. Hu, T. Taniguchi, K. Watanabe, X. Roy, D. Basov, D. Xiao R. Queiroz, J.C. Hone, X. Xu, X.-Y. Zhu,. *arXiv:2502.21153* (2025) .

Ultrafast dynamics and light-matter coupling at the atomic scale

M. Wolf

Fritz-Haber-Institut der Max-Planck-Gesellschaft, 14195 Berlin, Germany

Light-induced control of quantum materials has opened new frontiers in condensed matter physics, enabling the manipulation of electronic and structural phases on ultrafast timescales. While time-resolved pump-probe techniques provide insights into the ultrafast dynamics of solid-state quantum systems, they generally lack the spatial resolution required to probe atomic-scale variations arising from defects, heterogeneity, or domain boundaries. Recent advances in ultrafast scanning tunnelling microscopy (STM) [1, 2] and plasmonic nanocavities have enabled the imaging of ultrafast dynamics with angstrom-scale spatial resolution. In particular, THz-lightwave-driven tunnelling in an STM junction (THz-STM) has emerged as a powerful tool for probing ultrafast carrier dynamics, molecular vibrations, and collective excitations with sub-nanometer precision. Imaging of single molecular vibrations or coherent phonon modes in a crystal lattice has been demonstrated in real time (femtoseconds), with spatial resolution ranging from angstroms to a few nanometers. Coherent phonons can provide microscopic insight into ultrafast lattice dynamics and coupling to other degrees of freedom. Excitation and relaxation of coherent phonons may be susceptible to the local nanoscale environment, calling for real-space observation of lattice dynamics. Here we demonstrate nanoscale local coherent phonon spectroscopy employing time-resolved STM in a plasmonic junction, and unveil spatial inhomogeneities of coherent phonon dynamics in ultrathin zinc oxide (ZnO) films with nanometer spatial and femtosecond temporal resolution [3]. Scanning tunneling spectroscopy (STS) and wavelength dependent excitation allows to correlate the local electronic structure with the coherent phonon dynamics. Applying THz-STM to study the ultrafast local response of macroscopically ordered quantum phases remains a challenge, as it requires STM operation under intense local THz fields that can strongly modify sample properties. This is particularly critical for materials such as $1T\text{-}TaS_2$, where strong electron-phonon coupling, electronic correlations, and stacking-dependent electronic order render the system inherently sensitive to external perturbations and metastability. Here, we employ THz-STM combined with ultrafast photoexcitation to investigate the local ultrafast dynamics of a THz-induced metastable state in $1T\text{-}TaS_2$ (see Fig. 1).
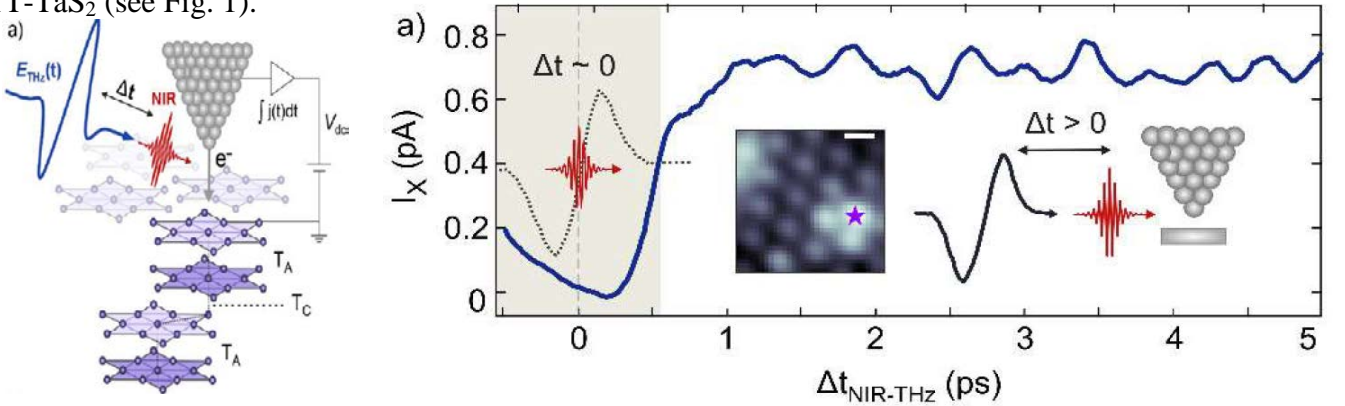

*Fig. 1. Left : Experimental scheme for measuring local ultrafast photoinduced dynamics at the surface of $1T\text{-}TaS_2$ by time-resolved THz-STM. The system is excited by a train of 35 fs NIR and THz pulses separated by time delay Δt. **Right**: Ultrafast photoinduced change of the THz-induced current on a local CDW defect (**star in inset**) induced by the NIR pulses. After pulse overlap (**shaded area**), a constant baseline with a long-lived coherent modulation is observed exhibiting two oscillation frequencies at 2.45 and 1.36 THz.*

We demonstrate that THz excitation not only enables probing of ultrafast photoinduced charge density wave dynamics via THz-lightwave-driven tunnelling, but also drives $1T\text{-}TaS_2$ into a long-lived metastable CDW phase with a locally modified quasi-stationary insulating gap (Fig. 2). In particular, coherent oscillations in the THz-driven tunnelling current reveal the well-known 2.4 THz amplitude mode of the CDW, which persists in the metastable state state. In addition, we find a previously unobserved 1.3 THz mode that emerges near local defects. Our results demonstrate the dual role of the tip-enhanced THz field in THz-STM, both as a driver of metastability and as a probe of local ultrafast dynamics, and highlight the influence of defects on the local dynamics of charge order [4].
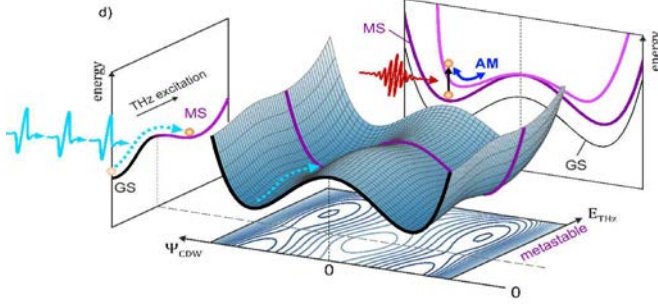
Fig. 2. Two-dimensional potential energy surface (PES) of the comensurate CDW phase of 1T-TaS2 excited by the tip-enhanced THz field. *Along the CDW order parameter Ψ_{CDW}, in the ground state (GS), the PES is described by the known double-well Mexican hat potential (at fixed CDW phase, black curve). An increasing THz field drives the system into a metastable state (MS, see left projection) with an energetically lifted C-CDW potential (purple double-well potential). Optical excitation induces coherent amplitude mode (AM) oscillations in this metastable C-CDW phase [4].*

Our results establish THz-STM as a powerful tool for unveiling the spatially varying ultrafast response of correlated quantum phases, paving the way for new insights into light-driven phase transitions at the atomic scale.

References
[1] T. Cocker, V. Jelic, R. Hillenbrand, F. Hegmann. *Nature Photonics* **15**, 558 (2021).
[2] M. Müller, *Progress in Surface Science* **99**, 100727 (2024).
[3] S. Liu, A. Hammud, I. Hamada, M. Wolf, M. Müller, T. Kumagai, *Science Advances* **8**, eabq5682 (2022).
[4] L. S. P. Lopez, A. Vaitsi, Vivien Sleziona, H. Wiedenhaupt, M. Wolf, M. Müller, *to be published* (2025).
 * *Acknowledgements:* this work was performed in collaboration with Luis S. Parra Lopez, Henrik Wiedenhaupt, Alkisti Vaitsi, , Vivien Sleziona Fabian and Melanie Müller (FHI Berlin), Schulz (NanoGUNE, Spain) and Takashi Kumagai (IMS, Japan)

Light control of quantum matter

M. Schiro
Coll`ege de France, F-75321 Paris, France

The increased control over light-matter interactions, both at the classical level as well as in the genuine quantum regime, has turned the electromagnetic radiation from a traditional spectroscopic probe to an invaluable tool to control and manipulate complex quantum many body systems. An exciting new frontier is to take advantage of the quantum nature of light in solid state experiments to enhance transport or to dress, cool and control selected collective excitations of solids. In this talk I will review our work on prototype models of electrons coupled to quantum fluctuations of a cavity mode. First I will discuss the role of gauge invariance in constraining the form of light-matter interaction and how coupling to cavity modes can allow to control the topological properties of a material [1,2,3] (Fig. 1 left). In the second part of the talk I present a theoretical framework for the quantum electrodynamics of graphene Landau levels embedded in a deep subwavelength hyperbolic cavity, where light is confined into ultrasmall mode volumes. By studying the spectrum, we discuss the emergence of polaritons, and disentangle the contributions of resonant quantum vacuum effects from those of purely electrostatic interactions.

Fig. 1. Left*: **top**-SSH Model Coupled to a Cavity mode; **bottom**-Phase Diagram.*

Right*:.**top** - Graphene in a deep sub wavelength cavity; **bottom:** Non-Local light-matter vacuum Rabi Coupling*

.
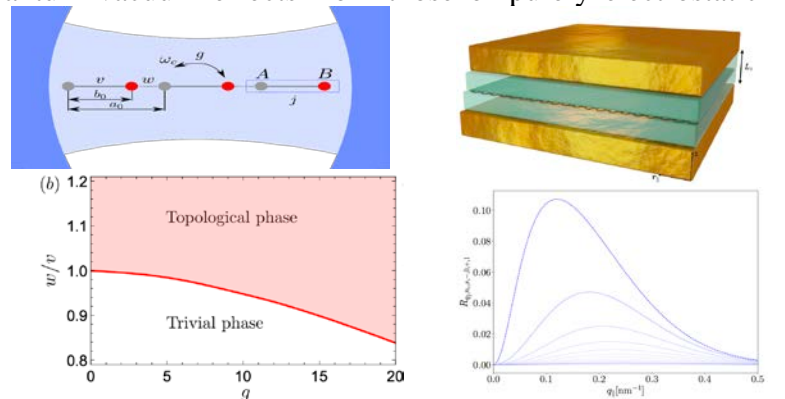
Finally, we study the hybridization between magnetoplasmons and the cavity's electromagnetic modes[4] due to the highly non-local Vacuum Rabi coupling (Fig.1 right)

References
[1] O. Dmytruk, M. Schiro, *Physical Review* B **103**, 075131(2021).
[2] O. Dmytruk, M. Schiro, *Communication Physics* **5**, 271 (2022).
[3] J. Sueiro, G. M. Andolina, M. Schiro, *to be published* (2025).
[3] G. M. Andolina,, M. Ceccanti, B. Turini, R. Riolo, M. Polini, M. Schiró, F.H.L. Koppens, *arXiv:2501.04133*(2025).
 * *Acknowledgment:* M.S. acknowledge funding from the European Research Council (ERC) under the European Union's Horizon 2020 research and innovation programme (Grant agreement No. 101002955 – CONQUER).

Nanophotonic lithium niobate waveguides for ultrafast Frequency comb generation UV to Mid-IR

T.-H. Wu[1], S. A. Diddams[2]
[1]University of Colorado, Boulder, CO 80309, USA
[2]National Institute of Standards and Technology, Boulder, CO 80305, USA

Thin-film lithium niobate integrated nanophotonics offer transformative opportunities for the development of broadband frequency combs spanning from the ultraviolet to the mid-infrared on a compact, robust, and scalable platform. By harnessing both geometric dispersion engineering and periodic poling techniques, these devices simultaneously phase-match second- and third-order nonlinear processes $\chi^{(2)}$ and $\chi^{(3)}$, enabling highly efficient harmonic generation and supercontinuum generation across lithium niobate's wide transparency window (350 to 5000 nm) [1]. In this work, we demonstrate that such spectral versatility can be achieved using straightforward and fabrication-friendly waveguide designs, which are driven by reliable and commercially available frequency comb lasers operating in the 1550 nm telecom band with only 100 picojoule-level pulse energies.This integrated approach not only simplifies the system architecture but also significantly reduces both power consumption and physical footprint, eliminating the need for complex bulk optics and high-energy pump sources. The resulting frequency comb spans a broad spectral range from 350 nm to 2800 nm, operating with pulse energies as low as 100 pJ (equivalent to 10 mW at a 100 MHz repetition rate). Leveraging highly nonlinear processes within a nanophotonic platform, the system reduces total power consumption from 50 W—typical for bulk-crystal-based amplifiers—to just 5 W. The ability to engineer dispersion and tailor nonlinear responses in thin-film lithium niobate waveguides enables the design of highly efficient, broadband sources optimized for diverse applications, including precision timing, astronomical spectrograph calibration, quantum photonics, and broadband molecular sensing. Ultimately, this work sets the foundation for the realization of fully integrated, hand-sized ultrafast laser systems and portable frequency combs. These systems will usher in a new era of field-deployable comb-based technologies, unlocking capabilities in real-time environmental monitoring, mobile atomic clocks, space-based spectroscopy, and next-generation quantum sensors. Figure 1 (a) and (b) illustrates a simplified frequency comb spectrum spanning from 350 nm to 1200 nm, effectively covering the key optical transitions for Yb and Sr atomic clocks [2]. Figure 1(c) shows the lithium niobate chip enabling f-2f measurement and integration into a self-referenced frequency comb, resulting in a compact frequency comb laser.
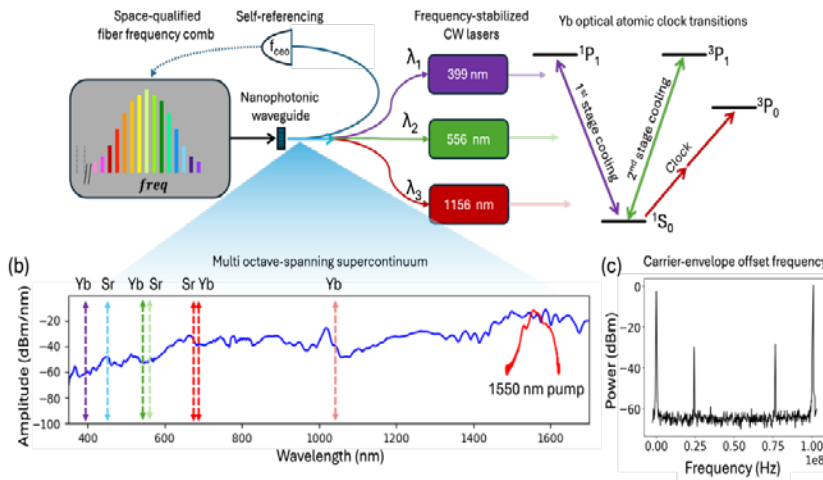

Fig. 1. Overview of space-qualified optical frequency comb (OFC) and nanophotonic module. (**a**) *A space-qualified, fiber-based IR mode-locked oscillator constructed using radiation-free components is coupled to a TFLN nanophotonic device to generate a multi-octave-spanning spectrum, which can be used to stabilize the cooling and clock lasers essential for optical atomic clock operation.* (**b**) *experimental spectra demonstrated by CU/Scott Diddams' group using the TFLN platform, including the input pump spectrum (red) that is centered around 1550 nm, and the muti-octave broadened spectrum (**blue**) generated by the TFLN nanophotonic device, and (**c**) the carrier-envelope offset frequency (f_{ceo}) with a signal-to-noise ratio (S/N) of approximately 35 dB, detected in the 2f-3f spectrum overlap range.*

This low-SWaP frequency comb light source represents a significant innovation, paving the way for compact and space-qualified atomic clocks in the near future [3]

References
[1] T.-H. Wu, L. Ledezma, C. Fredrick, P. Sekhar, R. Sekine, Q. Guo, R. Briggs, A. Marandi, S. Diddams, *Nature Photonics* **18**, 218 (2024).
[2] M. Lezius, T. Wilken, C. Deutsch, M. Giunta, O. Mandel, A. Thaller, V. Schkolnik, M.Schiemangk, *Optica* **3**, 1381 (2016).
[3] A. Derevianko, K. Gibble, L. Hollberg, N. R. Newbury, C. Oates, M. S. Safronova, L. C Sinclair, N. Yu, *Quantum cience and Technology* **7** 044002(2022).

Spin transfer dynamics in hetero-bilayer of graphene and TMDC: A first-principle computational study

S. Yamada[1], A.Hashmi[2], T. Otobe[1]

[1] *Kyushu Institute of Technology, Kyoto, 619-0215, Japan*
[2] *The University of Tokyo, Tokyo, 113-8656, Japan*

Two-dimensional materials such as transition metal dichalcogenides (TMDCs) and graphene have attracted much attention as promising materials in the field of spintronics, where spins are used as information carriers. TMDC monolayer can generate spin-polarized electronic excitations with a circularly polarized laser pulse due to the valley selection rule and strong spin-orbit interaction (SOI). On the other hand, graphene cannot generate spins due to the absence of SOI but has high electron mobility. Therefore, if we can efficiently transfer spins from TMDC layer to graphene layer in a stacked heterostructure of TMDC and graphene, we can realize an ideal optical device that can efficiently generate and transfer spins. In fact, it has been reported that spin injection with circularly polarized light pulses has been achieved in a heterostructure of MoS_2 and graphene [1]. However, the microscopic mechanism behind the spin transfer is still unclear. The aim of this study is to elucidate the microscopic mechanism of spin dynamics in TMDC-graphene hetero-bilayer by first-principles calculations based on the time-dependent density functional theory (TDDFT). Using SALMON-TDDFT code [2], we calculated the electron dynamics in a hetero-bilayer of WSe_2 and graphene irradiated with circularly polarized light pulses and analyzed the transfer process of the spin magnetization generated in WSe_2 to graphene. Figure 1(a) shows the calculated spin magnetization density after the pulse ends. It can be seen that the spin magnetization around WSe_2 is transferred to graphene. In Fig. 1(b), the distribution of the spin-polarized excited carrier density, $n_{ex}(\uparrow) - n_{ex}(\downarrow)$, after the pulse irradiation is depicted as a function of the z coordinate and orbital energy. Fig. 1(c) shows the same as (b) but for the respective isolated layers. The photon energy, peak intensity, and pulse duration of the laser pulse are set to 1.5 eV, 10^{12} W/cm^2, and 20 fs, respectively.
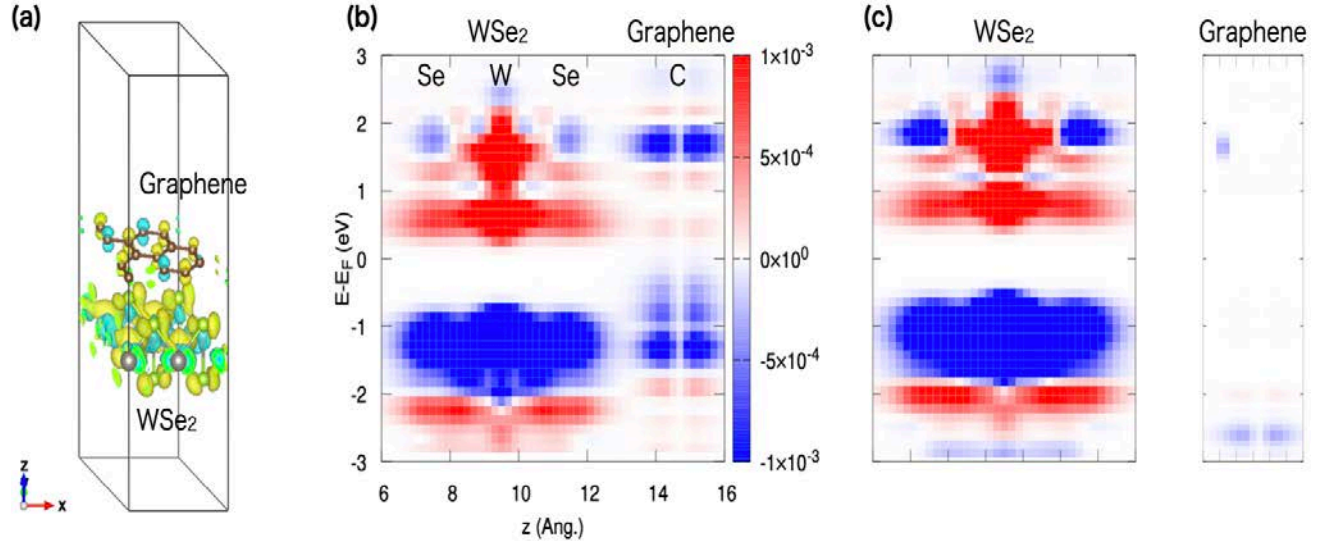

Fig. 1: (a). Spin magnetization density in the WSe_2-graphene hetero-bilayer after the pulse irradiation.
(b, c).Distribution of the spin-polarized excited carrier density as a function of the z coordinate and orbital energy for the hetero-bilayer and respective isolated layers, respectively.

We can see that the spin around the Se layer at the side of the graphene layer transfers to the graphene layer. In this presentation, we will discuss the results of our analysis for the laser intensity and pulse duration dependences of the spin transfer and its time scale.

References
[1] Y. K. Luo, J. Xu, T. Zhu, G. Wu, E. J. McCormick, W. Zhan, M. R. Neupane, R.K. Kawakami., *Nano Letters* **17**, 3877 (2017).
[2] *https://salmon-tddft.jp*

Ultrafast intrinsic optical-to-electrical conversion dynamics in 2D semiconductor proved by THz electronics

K. Yoshioka

NTT Corporation, 243-0198 Atsugi, Japan

Photodetectors based on two-dimensional materials have been extensively studied due to their high design flexibility, which offers the potential to surpass conventional semiconductor devices. However, the detailed mechanisms of the optical-to-electrical (O-E) conversion process remain unclear, and a definitive design guideline has yet to be established. Black phosphorus (BP) is a semiconductor with anisotropic properties and a tunable bandgap depending on the number of layers. Compared to transition metal dichalcogenides (TMDs), BP exhibits a higher carrier mobility, making it a particularly intriguing material. In fact, it has been reported that BP enables the fabrication of photodetectors that achieve both high sensitivity and fast operation speeds [1], and it serves as a parent material for shift current generation [2]. Understanding the fundamental properties of BP is therefore crucial from both basic science and application perspectives. Here, we investigate the ultrafast dynamics of the O-E conversion process by reading out the photocurrent with sub-picosecond time resolution using on-chip terahertz spectroscopy [3,4].The schematic diagram of the experimental setup is shown in the inset of Fig.1a
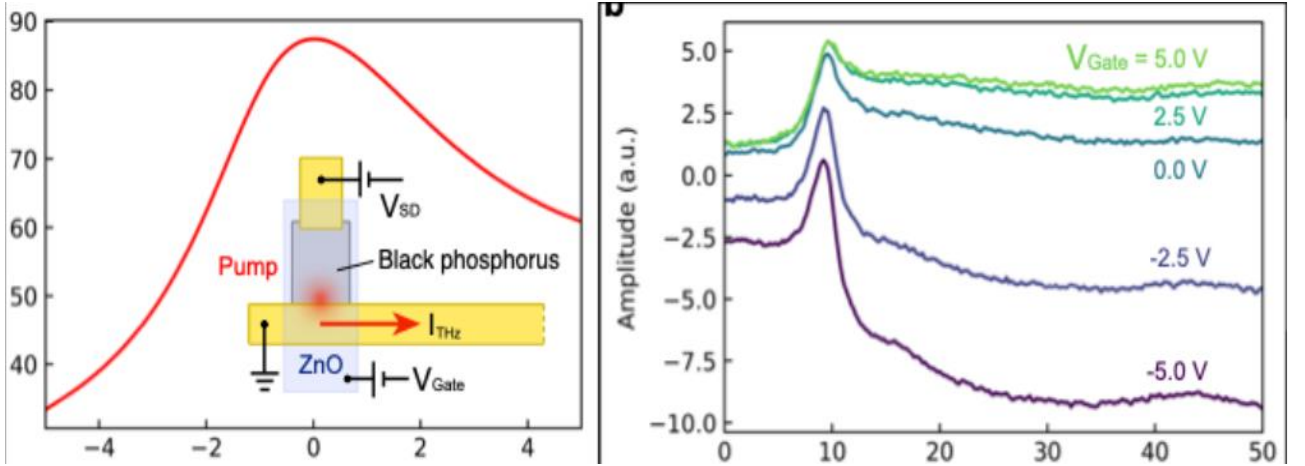

Fig. 1. a. Gate voltage dependence of the resistance in black phosphorus. *The inset shows the device structure near the black phosphorus region.* ***b****. Gate voltage dependence of the photocurrent measured at $V_{SD} = 0$ V.*

The BP sample is connected to source and drain electrodes, with the drain electrode structured as a Goubau line, enabling the readout of ultrafast currents in the THz regime. The top-gate electrode is made of zinc oxide (ZnO), which is transparent to high-frequency signals above the GHz range. This allows us to modulate the carrier density of BP without being limited by the device's RC time constant for photocurrent readout. The pump light is focused at the BP–drain electrode interface. Figure 1(a) shows the gate voltage (V_{Gate}) dependence of the BP resistance, confirming that the charge neutrality point is located near $V_{Gate} = 0$ V. Fig. 1(b) presents the V_{Gate} dependence of the real-time photocurrent waveforms measured at a source-drain bias voltage of $V_{SD} = 0$ V. We focus on the sharp peak signal observed around 10 ps. Previously, we demonstrated that ultrafast photocurrents due to the photothermoelectric effect (PTE) occur under similar experimental conditions in graphene [4]. However, in the present measurements, the sign of the photocurrent peak is independent of the carrier type, indicating that the PTE cannot account for the observed photocurrent. Instead, we interpret this response as the first direct observation of hot-carrier super-diffusion at a semiconductor-metal interface, captured as an electrical current. Further analysis revealed that the intrinsic 3 dB bandwidth of the response reaches up to 600 GHz [5].

References
[1] C. Liu, J. Guo, L. Yu, Y. Xiang, H. Xiang, J. Li, D. Dai, *ACS Photonics* **9**, 1764 (2022).
[2] T. Akamatsu, T. Ideue, L. Zhou, Y. Dong, S. Kitamura, M. Yoshii, D. Yang, M. Onga, Y. Nakagawa., *Science* **372**, 68 (2021).
[3] K. Yoshioka, T. Wakamura, M. Hashisaka, K. Watanabe, T. Taniguchi, N. Kumada, *Nature Photonics* **16**, 718 (2022).
[4] K. Yoshioka, G.Bernard, T. Wakamura, M. Hashisaka, K. Sasaki, S. Sasaki, K. Watanabe, T.Taniguchi, N. Kumada, *Nature Electronics* **7**,537 (2024)
[5] K. Yoshioka, T. Okamoto, T. Wakamura, N. Kumada, *to be submitted* (2025).

Optical control of ferroaxial order via circular phonon excitation

Z. Zeng[1], M. Först[1], M. Fechner[1], M. Buzzi[1], D.Prabhakaran[2], P. G. Radaelli[2]
A. Cavalleri[2]

[1]*Max-Planck-Institut für Struktur und Dynamik der Materie,22761 Hamburg, Germany*
[2]*University of Oxford, Oxford OX1 3PU, UK*

Ferroaxial order refers to a distinct ferroic order in crystal systems characterized by a rotational texture of electric-dipoles (Fig. 1a [1]). Recent studies have shown the potential of ferroaxially ordered materials in multiferroic applications [2,3]. However, its unique symmetry prevents direct coupling to stress or static electric fields, limiting conventional control methods. Here, we propose and demonstrate an alternative approach: resonant excitation of optical phonons with circularly polarized light. The prototypical ferroaxial material $RbFe(MoO_4)_2$, with a transition temperature at ~190 K, serves as an ideal platform for study. The transition lowers the point group symmetry from $\bar{3}m$ to $\bar{3}$, enabling second-harmonic generation circular dichroism (SHG-CD) as a sensitive probe of the ferroaxial order (Fig. 1b) [4].
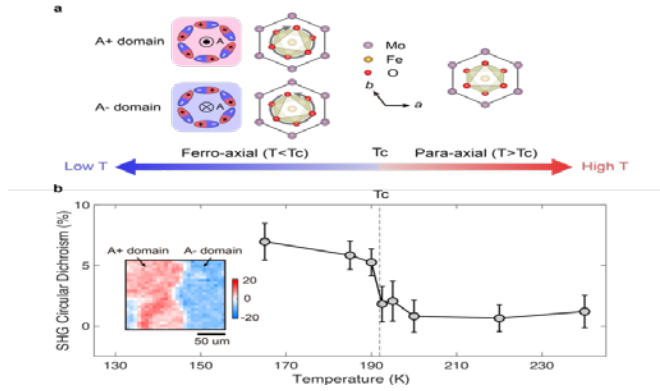

***Fig. 1. Ferroaxial Order in RbFe(MoO₄)₂. a)** Crystal structure of RbFe(MoO₄)₂ in the ferroaxial and paraxial states, respectively. **b)** Ferroaxial order characterized by second harmonic generation circular dichroism (SHG-CD). Inset: Mapping of ferroaxial domains below Tc.*

Symmetry analysis identifies the coupling between ferroaxial order in $RbFe(MoO_4)_2$ and circularly driven Eu-symmetry phonon modes, which can be excited by circularly polarized mid-infrared light. Experimentally, SHG-CD measurements show a reversible switching behavior under single-shot excitation, confirming deterministic control of the ferroaxial order (Fig. 2). This work establishes a new mechanism for manipulating ferroaxial order via light-driven phonons, enabling dynamic control of ferroic properties in complex materials.

***Fig. 2. Ferroaxial domain switching by circurlarly polarized light. a)** A left circularly polarized mid-infrared pulse drives circular phonons in RbFe(MoO₄)₂, switching the ferroaxial state from A- domain to A+ domain above a threshold fluence. **b)** A right circularly polarized mid-infrared pulse switches the ferroaxial state from A+ domain to A- domain.*

This work establishes a new mechanism for manipulating ferroaxial order via light-driven phonons, enabling dynamic control of ferroic properties in complex materials.
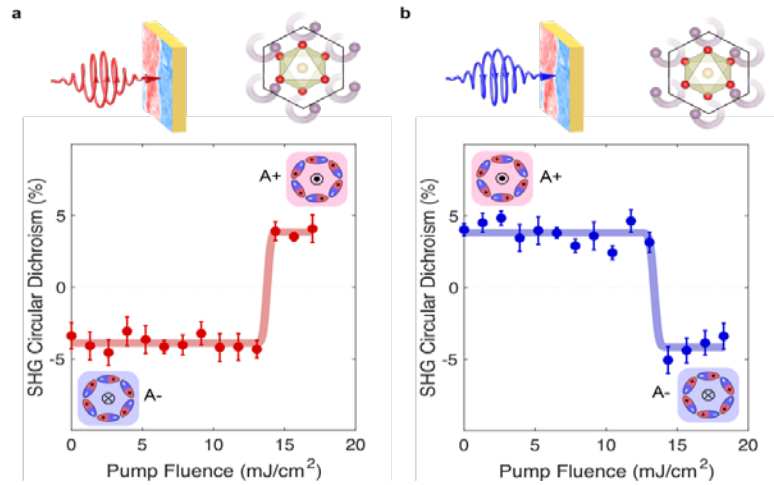
References
[1] W. Jin, E. Drueke, S. Li, A. Admasu, R. Owen, M. Day, K. Sun, S.W. Cheong, L. Zhao, *Nature Physics* **16**, 42 (2020).
[2] A. J. Hearmon, F. Fabrizi, L.C. Chapon, R.D. Johnson, D. Prabhakaran, S.V. Streltsov, P. J. Brown, P. Radaelli, *Physical Review letters* **108** 237201 (2012).
[3] S. Hayami, R. Oiwa, H.Kusunose, *Journal of the Physical Society of Japan* **91**, 113702 (2022).
[4] T. Hayashida, Y. Uemura, K. Kimura, S. Matsuoka, D. Morikawa, S. Hirose, K. Tsuda, T. Hasegawa, T. Kimura, *Nature Communications* **11** 4582 (2020).

High pressure ultrafast dynamics of superconductors

J. Zhao

Institute of Physics, Chinese Academy of Sciences, Beijing 100190, China

Both ultrafast spectroscopy and high-pressure physics is important fields of condensed matter physics. Combining the two is non-trivial, because conventional efforts cannot fully remove potential artifacts caused by repositioning fluctuations. In conventional ways, the DAC is usually taken out of the light path to tune and calibrate pressure and then put back, which often introduces sample motion and rotation (i.e. repositioning fluctuation). We successfully innovated and constructed an *on-site in situ* low-temperature high pressure pump-probe ultrafast spectroscopy instrument [1,2], for which the DACs and samples remain within the light path, thus successfully removing repositioning fluctuation. This innovation allows for precise measurements in both the amplitude and lifetime.
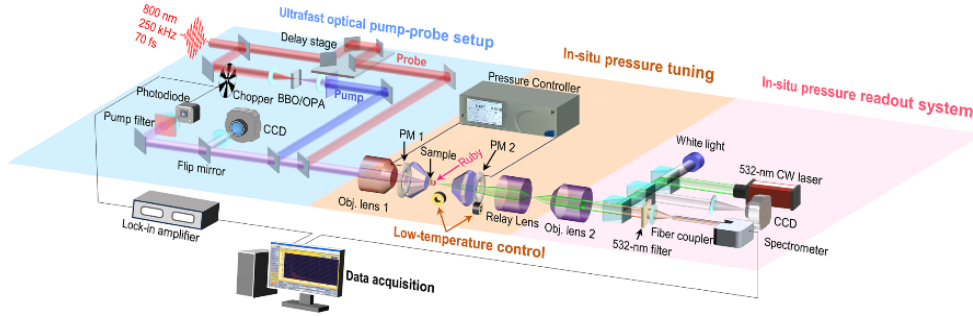

Fig. 1. On-site in situ low-temperature high-pressure ultrafast spectroscopy [1]

Using this instrument, we studied strongly correlated iridate Sr_2IrO_4 under high pressure. For the first time we found pressure-induced phonon-bottleneck effect [3]. More significantly, we have successfully conducted the first ultrafast dynamics investigation of hydrogen-rich superconductors [4]. We investigated the high-pressure ultrafast dynamics of $LaH_{10\pm\delta}$ (Fig. 2) at different temperatures. Simultaneously, we detected the phonon-bottleneck effect [5]. Through the temperature-dependent and fluence-dependent experimental data, we obtained the EPC strength of $LaH_{10\pm\delta}$ $\lambda=2.58\pm0.11$, the superconducting gap $\Delta(0) =53\pm5meV$, the gap ratio $2\Delta(0)/k_BT_c=5.6$, and the gap parameter $\vartheta=1.95$. This direct experimental evidence, especially the value of λ, points to strong EPC in the superconductivity of a clathrate superhydride [4].

Fig.2 The first "high-pressure ultrafast dynamics" of a hydrogen-rich superconductor $LaH_{10\pm\delta}$ [4].
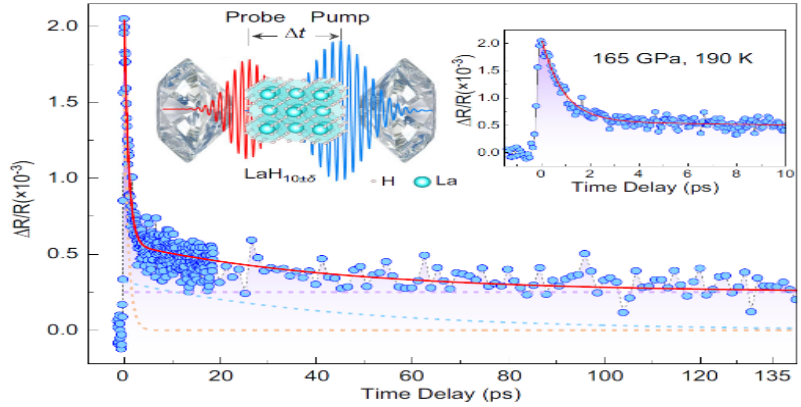
These achievements critically help the inauguration of "high-pressure ultrafast dynamics" to become a new cutting-edge frontier of condensed matter physics. Time permits, I will also address a little bit on our recent progress.

References
[1] J. Hasaien, P. F. Shan, F. R. Zhou, J. Zhao, *Review of Scientific Instruments* **96**, 013004 (2025).
[2] Y. L. Wu, X. Yin, J. Z. L. Hasaien, Z. Y. Tian, Y. Ding, J. Zhao, *Review of Scientific Instruments* **92**, 113002 (2021).
[3] Y. L. Wu, X. Yin, J. Z. L. Hasaien, Y. Ding*, J. Zhao, *Chinese Physics Letters (Express Letter)* **37**, 047801 (2020).
[4] Y. L. Wu, X. H. Yu, J. Z. L. Hasaien, F. Hong, P. F. Shan, Z. Y. Tian, Y. N. Zhai, J. P. Hu, J. G. Cheng, J. Zhao, *Nature Communications* **15** 9683 (2024).
[5] X. N. Lin, S. H. Fu, Y. N. Zhai, W. H. Wang*, H. C. Li, R. Z. Zhang, S. Meng*, Jimin Zhao*, *The Innovation* **5**, 100614 (2024).

Ab initio study of laser-induced ultrafast spin Dynamics in magnet systems

Z. Zhou, J. He

Charles University, Prague 12843, Czech Republic

The ultrafast manipulation of magnetization dynamics via laser pulses has emerged as a focal point within the realm of opto-spintronics in recent years, owing to its rapidity and low energy consumption. This talk focuses on our recent research investigating the interaction among spin, charge and phonon within magnetic systems. First, I will discuss how pre-excited coherent phonons alter the local spin moment of Fe_3GeTe_2 [1]. We observe that selective pre-excitation of coherent phonons under ultrafast laser irradiation significantly induces additional spin moment loss, which is attributed to the nuclear motion-induced asymmetric interatomic charge transfer. After the laser disappears, the excited spin-resolved charge undergoes a bidirectional spin-flip between spin-down and spin-up states, characterized by a subtle change in the spin moment within approximately 100fs, followed by unidirectional spin-flip, which will further contribute to the spin moment loss of FGT within tens of picoseconds.
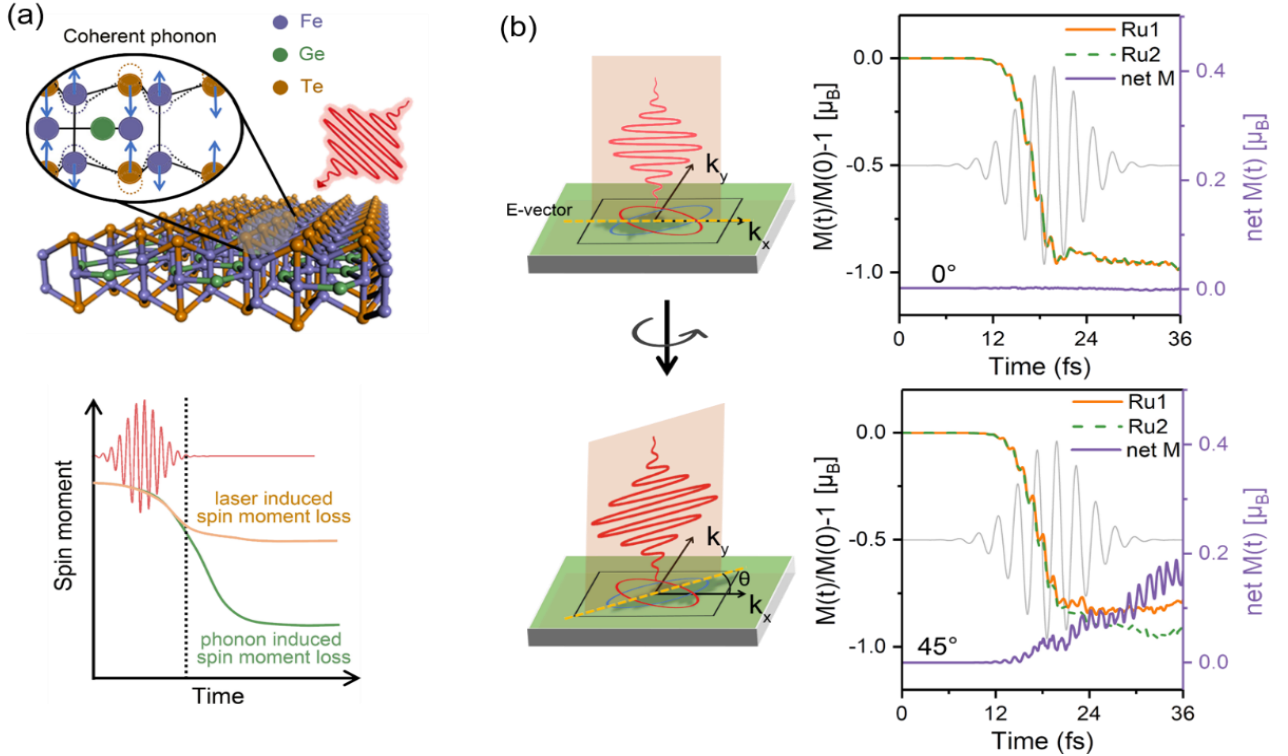

Fig. 1. (a) Schematic of pre-excited coherent phonons (Top) and corresponding phonon-assistant spin moment loss (bottom) of Fe_3GeTe_2 [1]; (b) Schematic of the laser irradiation along the k_x axis and rotated with an angle θ in Brillouin zone (left); The corresponding spin moment loss and net magnetic moment (right) [2].

Furthermore, I will discuss our recent investigation on ultrafast spin dynamics in altermagnet [2]. We demonstrate that laser pulses can drive asymmetric demagnetization dynamics of identical sublattices in the *d*-wave altermagnet RuO_2, resulting in a photo-induced ferrimagnetic state with a net moment of ~0.2 µB per unit cell. This polarization arises from the momentum-dependent spin splitting, which is unique to altermagnets, and which induces a momentum-dependent optical intersite spin transfer effect. Furthermore, ferrimagnetic polarization is highly controllable; it depends on the polarization direction of a linear polarized laser. The underlying physics of this effect comes due to excitation along the spin-polarized planes which break the symmetry of the momentum-space magnetization distribution, leading to inequivalent spin-resolved charge transfer between sublattices across both momentum and real space.

References
[1] Z. Zhou, M. Li, T. Frauenheim, J. He, *Nano Letters* **24**, 12062 (2024).
[2] Z. Zhou, S. Sharma, J. K. Dewhurst, J. He, *arXiv preprint arXiv:2502.01258* (2025).

Coherent ferrons

X. Zhu

Columbia University, New York, NY 10027, USA

Excitation of ordered phases produces quasiparticles and collective modes, as exemplified by magnons that emerge from magnetic order. Coherent magnons, also called spin waves, are finding applications in information transmission and quantum interconnects. Extending this paradigm to ferroelectric materials suggests the existence of ferrons, i.e. fundamental quanta of the collective excitation of ferroelectric order [1]. While coherent magnons are observed in a broad range of experiments, coherent ferrons have eluded experimental detection. This discrepancy is particularly intriguing given that electric dipole interactions (F_E) are inherently stronger than their magnetic counterparts (F_M), $F_E/F_M = (\alpha^2 \cdot \varepsilon_r) \gg 1$, where α (= 1/137) is the fine structure constant and ε_r the high frequency relative dielectric constant. Recently, we discovered that the 2D vdW in-plane ferroelectric $NbOI_2$ (Fig. 1a) emits intense THz radiation from optical rectification [2], with efficiency 20-50x higher than that of the current standard, ZnTe (Fig. 1b).
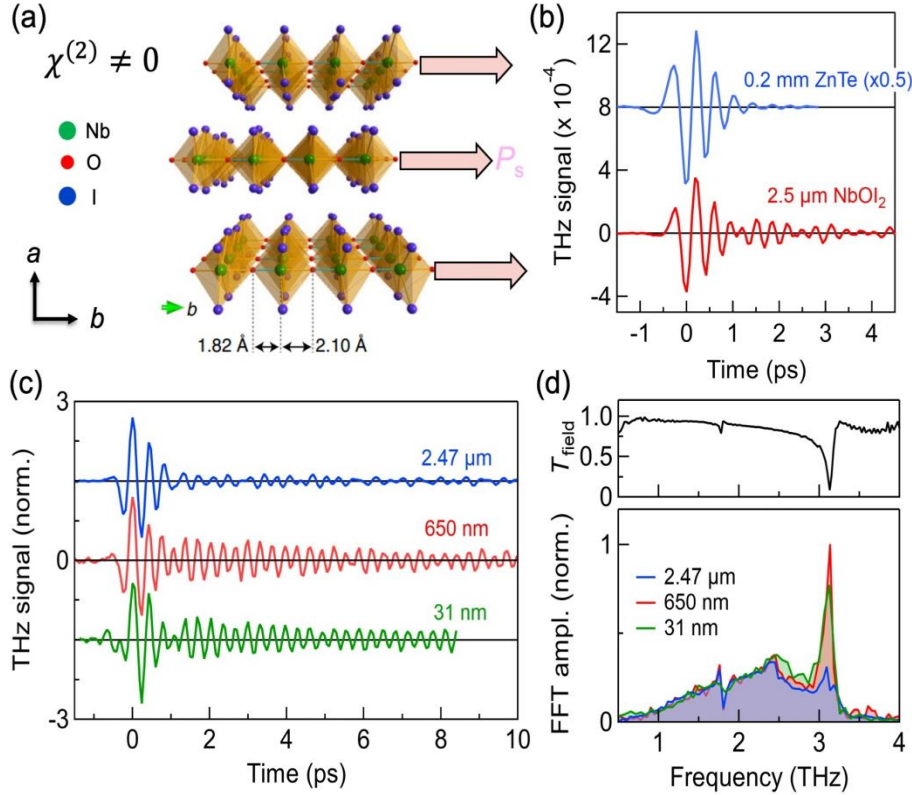

Fig. 1. THz emission from the 2D van der Waal ferroelectric semiconductor, NbOI2. (a) Structure of the 2D ferroelectric semiconductor with in plane ferroelectric polarization. (b) A comparison of THz emission from a 2.5 µm thick $NbOI_2$ and a 200 µm thick ZnTe. The efficiency of THz emission from $NbOI_2$ is 50x that from ZnTe. (c) Normalized THz field as a function of thickness of the $NbOI_2$ crystal. (d) Top: THz time domain spectroscopy from NbOI2, showing the 3.13 TO mode. Bottom: Fourier transform from (c) showing THz frequency domain spectra. The relative intensity of the 3.13 TO mode increases as the thickness decreases. All data obtained at room temperature.

In addition to broadband THz emission, we observed intense and extremely narrowband THz radiation from $NbOI_2$ at the ferroelectric transverse optical (TO) phonon frequency of 3.13 THz (Fig. 1c & 1d). The TO phonon is found to couple strongly to excitonic transition of this 2D semiconductor [3], thus allowing us to track this THz mode conveniently with visible light [3]. This 3.13 THz mode is the coherent ferron predicted theoretically [1]. Its emission is a second-order nonlinear process that requires ferroelectric order [4]. Moreover, we observe their propagations along the polar direction at extremely hypersonic velocities exceeding 10^5 m/s [4]. The discovery of coherent ferrons paves the way for numerous applications, including narrow-band THz emission, ferronic information processing, and quantum interconnects.

References
[1]   G. E. W. Bauer, P. Tang, R. Iguchi, K. Uchida, *Journal of Magnetism and Magnetic Materials* **541**, 168468 (2022).
[2]   T. Handa, C.-Y. Huang, Y. Li, N. Olsen, D. G Chica, D. D Xu, F. Sturm, J. W McIver, X. Roy, X.-Y. Zhu, *Nature Materials* **24**, (2025) .
[3]   C. - Y. Huang, D. G. Chica, Z.-H. Cui, T. Handa, M. Thinel, N. Olsen, Y. Liu, M. E Ziebel, G. He, Y. Shao, C. A Occhialini, J. Pelliciari D. N Basov, M. Sfeir, A. Pasupathy, V. Bisogni, D. R Reichman, X. Roy, X.-Y. Zhu, *Nature Communications* **16**, 1896 (2025).
[4]   J. Choe, T. Handa, C.-Y. Huang, A. K. Liston, J. Cox, J. Stensberg, Y. Hong, D. G.Chica, D. Xu, E. A. Arsenault, J. McIver, M. Delor, X. Roy X.- Y. Zhu, *to be published* (2025).

Valley polarized exciton dynamics in momentum space

X. Zhu [1], D. R. Bacon[1], V. Pareek[1], J.Madéo[1], K. Watanabe[2], T. Taniguchi[2], M. K. L. Man[1], K. M. Dani[1]
[1]Okinawa Institute of Science and Technology, Onna, Okinawa, Japan 904 0495
[2]National Institute for Materials Science,1-1 Namiki, Tsukuba, Ibaraki, Japan305-0044

In monolayer transitional metal dichalcogenides (TMDCs), due to lack of inversion symmetry, the valley index of excitonic states can be manipulated through circular polarization of light [1-2]. However, with the complex landscape of exciton species in TMDCs, such as spin- or momentum- dark excitons, the dynamics of valley polarized excitons, which are crucial for valleytronic applications, lacks clear understanding. Few experimental techniques can provide measurements that directly access the momentum and energy coordinate of constituent electrons and holes of excitons. Meanwhile, time- and angle- resolved photoemission spectroscopy (TR-ARPES) has become a powerful tool to study excitons of 2D semiconductors in energy-momentum space [3-6]. In this talk, we will discuss our momentum-resolved study on the valley-polarized excitons in monolayer WS_2 by TR-ARPES.
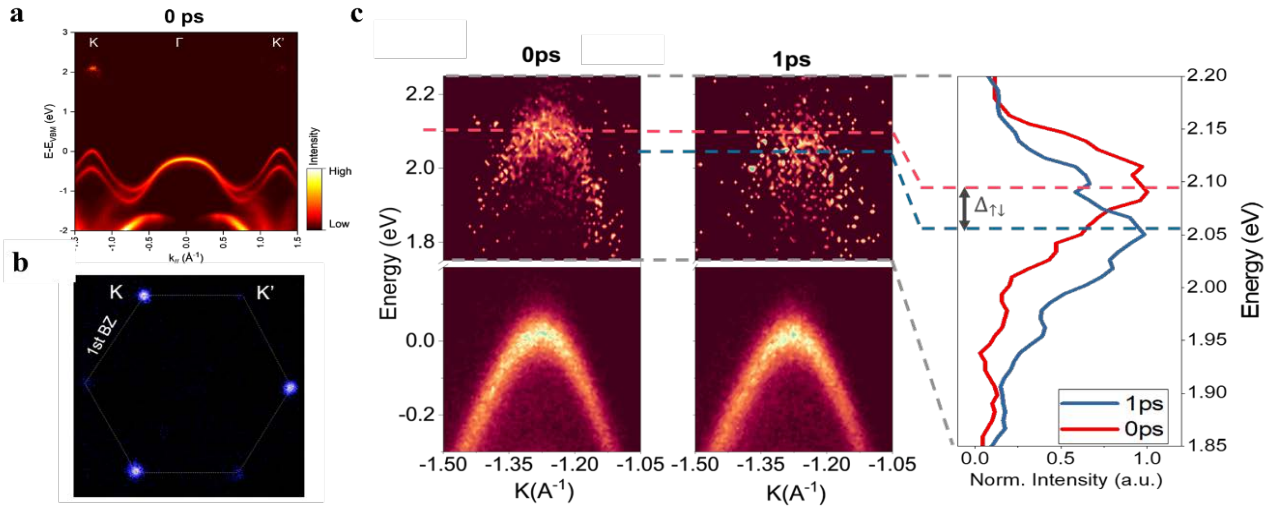

Fig. 1: (**a**). **At photoexcitation with circularly polarized light**, *the initiated bright excitons are highly polarized in K valley as in a K-Γ-K' energy-momentum cut or in (**b**) exciton-electrons distribution across the 1ˢᵗ BZ. (**c**) Energy-momentum cut along the Γ-K-M axis showing an exciton-electrons with negative dispersion. At 0 ps the exciton-electrons are located 2.1 eV above the valence band. By 1 ps, in the same valley, the exciton-electrons relax to a state at lower energy. The corresponding energy distribution curves on the right clearly shows the energy difference between the bright exciton state at 0ps and lower energy states at 1ps.*

We selectively photoexcite the bright A-excitons in the K valley by a resonant circularly polarized pump at 2.1 eV, showing an initial high degree of valley polarization as in (Fig. 1a, b). Benefiting from the high energy resolution of our TR-APRES, we resolve the spin-split states (Fig. 1c) and access the constituent electrons and holes of the various spin- and momentum- dark excitonic states after photoexcitation. By doing so, we provide a holistic view of the absolute population dynamics of dark excitons over the entire Brillouin Zone. In particular, at low temperature, low density and resonant excitation, we find that the excitonic landscape is largely dominated by valley polarized K'-K momentum-dark states, and that at long time delays, spin-dark states ultimately dominate. Accessing the absolute populations of valley-polarized dark excitons is key to taking advantage of the properties of dark excitons for quantum technologies with their long lifetime and protection against decoherence.

References
[1] W. Yao, D. Xiao, Q. Niu, *Physical Review* B **77**, 235406 (2008).
[2] D. Xiao, G. B. Liu, W. Feng, X. Xu, W. Yao, *Physical Review Letters* **108**, 196802 (2012).
[3] J. Madéo, M. K. L. Man, C. Sahoo, M. Campbell, V. Pareek, E. L. Wong, A. Al Mahboob, N. S. Chan, A. Karmakar, B. M. K. Mariserla, X. Li T. F. Heinz, T. Cao, K. M. Dani, *Science* **370**, 1199 (2020).
[4] M. K. L. Man, J. Madéo, C. Sahoo, K. Xie, M. Campbell, V. Pareek, A. Karmakar, E. L. Wong, A. Al Mahboob, N. S. Chan, D. R. Bacon X. Zhu, M. M. M. Abdelrasoul, X. Li, T. F. Heinz, F. H. da Jornada, T. Cao and K. M. Dani, *Science Advances* **7**, eabg0192 (2021).
[5] O. Karni, E. Barré, V. Pareek, J. D. Georgaras, M. K. L. Man, C. Sahoo, D. R. Bacon, X. Zhu, H. B. Ribeiro, A. L. O'Beirne, J. Hu A. Al Mahboob, M. M. M. Abdelrasoul, N. S. Chan, A. Karmakar, A. J. Winchester, B. Kim, K. Watanabe, T. Taniguchi, K. Barmak, J. Madéo F. H. da Jornada, T. F. Heinz and K. M. Dani, *Nature* **603**, 247 (2022).
[6] D. Schmitt, J. P. Bange, W. Bennecke, A. Al-Mutairi, G. Meneghini, K. Watanabe, T. Taniguchi, D. Steil, D. R. Luke, R. T. Weitz, S. Steil G. S. M. Jansen, S. Brem, E. Malic, S. Hofmann, M. Reutzel and S. Mathias, *Nature* **608**, 499 (2022).

Probing density-wave order and excitonic correlations with Attosecond core-level XUV spectroscopy

M. W. Zuerch

University of California at Berkeley, Berkeley, CA 94720, USA

The charge-density-wave (CDW) transition in $1T$-TiSe$_2$ is believed to be accompanied by exciton condensation due to strong electron-hole interactions [1], yet the signature of such excitonic effect in equilibrium is still under debate to date [2]. Theoretical and experimental advances in nonequilibrium techniques have provided an alternative route to understanding the nature of the ground state in $1T$-TiSe$_2$ [3–5], and in the past, we have shown that the melting of excitonic correlations in this compound is governed by photoinduced 3D-to-2D dimension crossover of the CDW order [6]. Here, using state-of-the-art ultrafast electron diffraction and attosecond transient XUV absorption spectroscopy, we closely examine the structural and electronic responses after photoexcitation, unveiling a transient state with proliferation of 1D topological defects as well as a fluence-dependent response that is consistent with an interpretation of transient melting of excitonic correlations. *Mechanism of ultrafast formation of topological defects.* Right above the CDW transition temperature $T_c \approx 200$ K, $1T$-TiSe$_2$ features a 2×2 short-range CDW state [6,7]. Following photoexcitation, besides the transiently suppressed intensity of the diffuse CDW peak, the most dramatic change to the CDW order is an anisotropic reduction of its correlation length, highlighted by the anisotropic broadening of the CDW peak width in Fig. 1a recorded by ultrafast electron diffraction. We observed that the CDW peak width parallel to the CDW wavevector ($\parallel\mathbf{q}$) increases much more than the perpendicular direction ($\perp\mathbf{q}$) (see Fig. 1b), suggesting the formation of 1D domain walls that disrupt the CDW phase coherence.
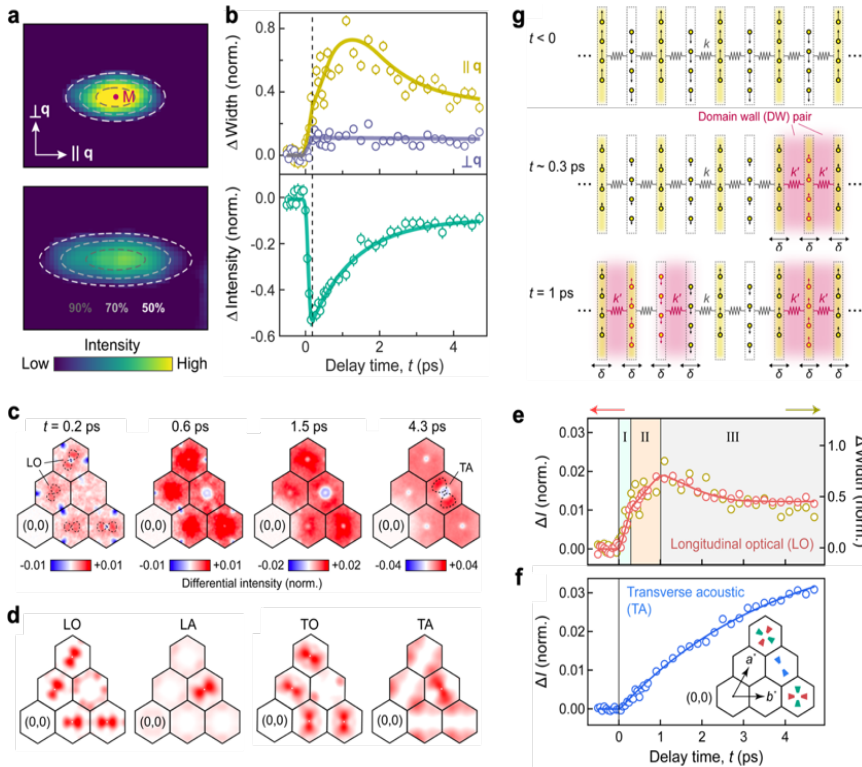

Fig. 1. Ultrafast formation of CDW domain walls mediated by LO phonons. a, comparison of the 2D CDW diffuse peak measured in ultrafast electron diffraction before and 1 ps after excitation. b, time evolution of the change in peak width (upper panel) and intensity (lower panel) of the 2D CDW peak. Vertical dashed line marks the minimum of the transient intensity, after which the peak continues to broaden. c, change in diffraction patterns at selected time delays with respect to the equilibrium value, featuring the six Brillouin zones near the undiffracted beam at (0, 0). d, calculated one-phonon structure factor for longitudinal (L) and transverse (T) phonons from optical (O) and acoustic (A) branches. e,f, Time evolution of diffuse intensities for different phonon branches, taken from color-coded regions of interests in the inset of f. Intensities from symmetry-equivalent Brillouin zones are averaged. In e, the time trace of the 2D CDW peak width parallel to the CDW wavevector is overlaid (yellow circles, reproduced from b), which shows identical temporal evolution as the LO phonon population. g, Schematic of dual-stage formation of CDW domain walls illustrated for a particular CDW wavevector. Only Ti atoms are shown (circles), where arrows denote CDW displacements.

Notably, the peak broadening dynamics does not follow the CDW amplitude dynamics encoded in the peak intensity (Fig. 1b), but rather follows the nonthermal population of longitudinal optical phonons (Fig. 1e), whose dynamics can be isolated from that of other phonon branches by examining specific order and region of the Brillouin zones, as verified by our phonon structure factor calculations (Fig. 1d). The simultaneous measurements of both 2D CDW peaks and diffuse phonon signals offer a detailed picture of how topological defects develop in two stages in the sub-picosecond regime, as summarized in Fig. 1g. This work provides the missing time axis in the sub-picosecond scale for describing a defect-driven transition, highlighting the role of longitudinal phonons in mediating the domain wall generation that is expected to find applications in

other symmetry-broken states [8]. *Signatures of excitonic melting in attosecond transient XUV absorption spectroscopy.* The superior temporal resolution, element-specificity, and broadband nature of attosecond transient XUV absorption spectroscopy (ATAS) has made it an indispensable tool in the study of quantum materials [9]. However, on the first sight, it is unclear how a low-energy phase transition such as CDW formation and excitonic condensation in $1T$-TiSe$_2$ manifests in the XUV spectrum at the energy scale over tens of eV. A previous ATAS study resorted to using the type of excited coherent mode to determine the ground state [10], whereas direct evidence of the excitonic condensation and structural change in the XUV spectrum is lacking. To this end, we systematically mapped the temperature-dependent XUV absorption spectra at the Ti $M_{2,3}$ and Se $M_{4,5}$ edges with meV energy resolution over a 300 K temperature window (Fig. 2a), and found that specific absorption peaks (such as peak 2 in Fig. 2b) exhibit a kink in peak position at T_c. Given such sensitivity to the phase transition in equilibrium, we further examined the transient response after photoexcitation (Fig. 2c,d). Besides the pronounced A_{1g} coherent phonons, we found that peak 2 also exhibits a faster quench at an increasing incident fluence (Fig. 2e,f), which scales as $1/\sqrt{n}$ where n is the number of excited carriers proportional to the fluence.
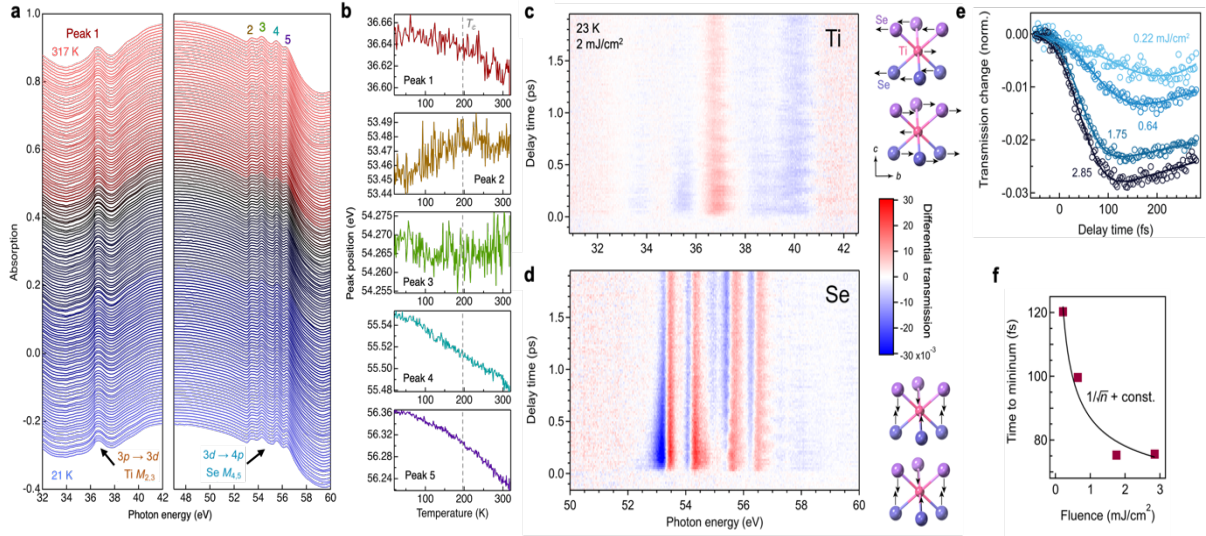

*Fig. 2. Static and transient XUV spectroscopy of 1T-TiSe$_2$. a, static absorption of 1T-TiSe$_2$ at different temperatures from 21 K (**blue**) to 317 K (**red**), featuring the Ti M$_{2,3}$ edges and the Se M$_{4,5}$ edges. The CDW transition temperature is approximately 200 K. Except for the top curve, each curve is vertically displaced for clarity. b, position of peaks 1–5 labeled in panel a, where peak 1 belongs to the Ti M$_{2,3}$ edges and peaks 2–4 belong to the Se M$_{4,5}$ edges. Vertical dashed line marks T$_c$. c,d, XUV transmission changes near the Ti M$_{2,3}$ edge and Se M$_{4,5}$ edge recorded in the CDW phase. Schematics on the right show the CDW soft phonon (c) and the A$_{1g}$ phonon (d) in the undistorted lattice. e, time-dependent changes of the Se absorption edge probed around peak 2 (**labeled in panel a**) depending on the pump fluence. f, the initial response time in panel e as a function of fluence. The delayed response for a lower number of photoexcited carriers is consistent with exciton melting.*

This observation is consistent with a picture where a larger number of excited electrons will lead to faster breaking of the exciton correlations due to carrier screening [3]. This combined temperature-dependent equilibrium spectra and fluence-dependent nonequilibrium response showcase the sensitivity of XUV absorption in detecting low-energy processes that play a dominant role in the properties of most quantum materials [11].

References

[1] A. Kogar, M.S. Rak, S. Vig, A. A. Husain, F.Flicker, Y.I.Joe, L. Venema, G. J. MacDougall, T. C. Chiang, E. Fradkin, J. van Wezel, P. Abbamonte *Science* **358**, 1314 (2017).

[2] Z. Lin, C.Wang, A. Balassis, J. P. Echeverry ,A. S. Vasenko, V. M. Silkin, E. V. Chulkov, Y. Shi, J. Zhang,1 J. Guo, X. Zhu, *Physical Review Letters* **129**, 187601 (2022)

[3] T. Rohwer, S.Hellmann, M.Wiesenmayer, C. Sohrt, A.Stange, B. Slomski, A. Carr, Y.Liu, L.M. Avila, M. Kalläne, S. Mathias, L. Kipp, K. Rossnagel M. Bauer, *Nature* 471, 490 (2011).

[4] M. Porer, U.Leierseder, J.-M. Ménard, H. Dachraoui, L. Mouchliadis, I. E. Perakis, U. Heinzmann, J. Demsar, K. Rossnagel, R. Huber, *Nature Materials* **13**, 857 (2014).

[5] C. Lian, S.-J. Zhang, S.-Q. Hu, M.-X. Guan, S. Meng, *Nature Communications* **11**, 43 (2020).

[6] Y. Cheng, A. Zong, J. Li, W. Xia, S. Duan, W. Zhao, Y. Li, F. Qi, J. Wu, L. Zhao, P. Zhu, X. Zou, T. Jiang, Y. Guo, L. Yang, D. Qian, W. Zhang A. Kogar, M. W. Zuerch, D. Xiang, J. Zhang, *Nature Communications* **13**, 963 (2022).

[7] P. Chen, Y.-H. Chan, X.-Y. Fang, S.-K. Mo, Z. Hussain, A.-V. Fedorov, M. Y. Chou, T.- C. Chiang, *Scientific Reports* **6**, 37910 (2016).

[8] Y. Cheng, A. Zong, L.Wu, Q. Meng, W. Xia, F. Qi, P. Zhu, X. Zou, T. Jiang, Y. Guo, J. van Wezel, A. Kogar, M. W. Zuerch, J.Zhang, Y. Zhu, D. Xiang *Nature Physics* **20**, 54 (2024).

[9] A. Zong, B. R. Nebgen, S.-C. Lin, J. A. Spies, M. Zuerch, *Nature Review Materials* **8**, 224 (2023).

[10] T. Heinrich, H.-T. Chang, S. Zayko, K. Rossnagel, M. Sivis, C. Ropers, *Physical Review* X **13**, 021033 (2023).

[11] A. Zong, S.-C. Lin, S. A. Sato, E. Berger, B. R. Nebgen, M. Hui, B.Q. Lv, Y. Cheng, W.Xia,Y.Guo,D.Xiang, M. W. Zuerch, *arXiv:2407.00772* (2024).

MILESTONES 2016-2025
Ultrafast Dynamics and Metastability
Ultrafast Bandgap Photonics
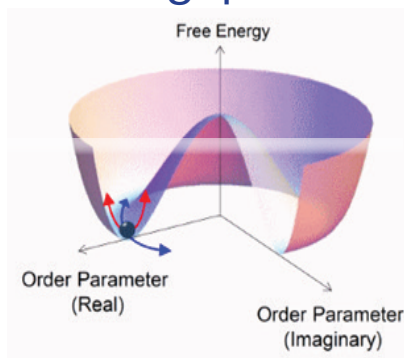
Physica Scripta
Guest Editors: Michael K. Rafailov and Luca Perfetti, 2017
http://iopscience.iop.org/journal/1402-4896/page/Focus-issue-on-Ultrafast-Bandgap-Photonics

Ultrafast Bandgap Photonics I-III
Baltimore, 2016
http://spie.org/Publications/Proceedings/Volume/9835
Anaheim, 2017
http://spie.org/Publications/Proceedings/Volume/10193
Orlando, 2018
https://spie.org/Publications/Proceedings/Volume/10638

Ultrafast Dynamics and Metastability IV
Washigton, DC 2017 *https://sites.google.com/a/georgetown.edu/ultrafast-dynamics-and-metastability-archive-2017/*

Ultrafast Dynamics and Metastability-Ultrafast Bandgap Photonics V
Washington, DC 2019 https://sites.google.com/georgetown.edu/udmandubp2019/home-page

Ultrafast Dynamics and Ultrafast Bandgap Photonics VI
International Conference St. Petersburg, 2019http://www.ioffe.ru/optics/UBGP2019/

Ultrafast Dynamics & Ultrafast Bandgap Photonics VIII
Crete June 2022 https://udm-ubp20.physics.uoc.gr/#!/up

Ultrafast Bandgap Photonics: Dynamics and Metastability of Transient States IX
Washington, DC, 2022 https://udm.georgetown.edu/home-page

Ultrafast Dynamics & Ultrafast Bandgap Photonics X
Crete, June 2023: https://udm-ubp2023.eventsadmin.com/i/AbstractProceedings

Ultrafast Dynamics & Ultrafast Bandgap Photonics XI
Crete, June 2024: https://udm-ubp2024.eventsadmin.com/Home/Welcome

Ultrafast Dynamics & Metastability : Ultrafast Bandgap Photonics XII
Tucson, AZ October 2024: https://wp.optics.arizona.edu/XII-UDM-UBP-Conference/

Dynamics of Nonequilibrium: Ultrafast Dynamics & Ultrafast Bandgap Photonics XIII Symposium and Summer School
Crete, June 2025: https://udm-ubp2025.eventsadmin.com/Home/Welcome

Dynamics of Nonequilibrium: Ultrafast Dynamics & Ultrafast Bandgap Photonics XIV Conference and Summer School
2025-2026 USA

Dynamics of Nonequilibrium: Ultrafast Dynamics & Ultrafast Bandgap Photonics XV Symposium and Summer School
2026